In this Issue

Highlights from this issue of *A&R* | By Lara C. Pullen, PhD

Association of Myocardial Inflammation With Disease Activity in Rheumatoid Arthritis

In this issue, Amigues et al (p. 496) report the results of the first study to evaluate and quantify subclinical myocardial inflammation in patients with rheumatoid arthritis (RA) using 18-fluorodeoxyglucose (FDG) positron emission tomography with computed tomography (PET-CT). The authors found that myocardial inflammation is common in patients with RA. The study included 119 patients, with FDG uptake visually observed in 39% of patients and an abnormal, quantitatively assessed myocardial FDG uptake shown in 18% of patients.

p. 496

Using the Clinical Disease Activity Index (CDAI) score to distinguish between patients with moderate-to-high disease activity (score of ≥10) and lower disease activity or remission (score of <10), the researchers found that the mean of the mean standardized uptake value (SUV_{mean}) was 31% higher in patients with moderate-to-high disease activity than it was in patients with low disease activity or remission. The adjusted SUV_{mean} was 26% lower among those treated with a non–tumor necrosis factor–targeted biologic agent than those treated with conventional disease-modifying antirheumatic drugs.

In the longitudinal substudy, the myocardial SUV_{mean} decreased from 4.50 units to 2.30 units over 6 months, which paralleled the decrease in the mean CDAI score from a score of 23 to a score of 12. The authors concluded that subclinical myocardial inflammation is related to disease activity and may improve with RA therapy.

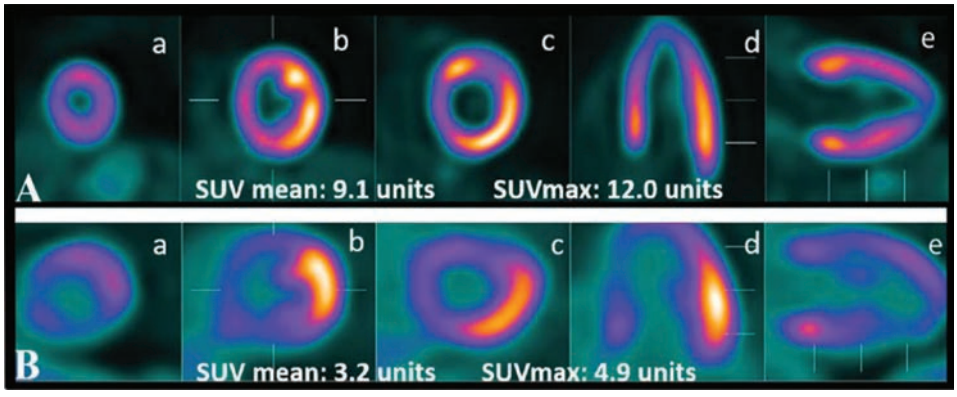

Figure 1. Examples of diffuse (**A**) and focal (**B**) myocardial FDG uptake, as measured using cardiac FDG PET-CT, in 2 patients with RA. Panels **a**, **b**, and **c** represent the short axis, panel **d** represents the horizontal axis, and panel **e** represents the vertical long axis. SUV_{mean} = mean of the mean standardized uptake value; SUV_{max} = mean of the maximum standardized uptake value.

Autoreactive T Cells in Patients With RA May Target Citrullinated Aggrecan Epitopes

Patients with rheumatoid arthritis (RA) often mount an immune response to citrullinated antigens such as vimentin, fibrinogen, and α-enolase. Newer data suggest that the matrix protein aggrecan can also be citrullinated and recognized as an autoantigen. More importantly, T cell and antibody responses to citrullinated aggrecan (Cit-aggrecan) appear to contribute to the loss of peripheral tolerance in patients with RA. In this issue, Rims et al (p. 518) report the results of their study designed to directly visualize and characterize Cit-aggrecan–specific T cells in this patient group.

p. 518

The investigators found that patients with RA not only have T cells that recognize Cit-aggrecan, but they also have significantly higher frequencies of Cit-aggrecan–specific T cells than healthy controls. Moreover, the frequencies of these T cells correlated with the presence of antibodies that target the same antigen. The authors identified 6 immunogenic peptides, 2 of which were the predominant T cell targets in peripheral blood. The 2 epitopes were citrullinated at HLA binding residues and shared homologous sequences. These results are consistent with the hypothesis that CD4+ T cells selectively recognize citrullinated aggrecan epitopes in the context of the high-risk DRB1*04:01 haplotype. Aggrecan-specific T cells and antibodies may be relevant markers for monitoring patients with RA and/or at-risk subjects.

A New Understanding of Pain in Patients With Knee Osteoarthritis

In general, studies on symptomatic knee osteoarthritis (OA) have phenotyped pain based upon Quantitative Sensory Testing (QST) measures or psychosocial factors.

p. 542

Two articles in this issue approach the issue of pain in patients with knee OA from novel perspectives. Carlesso et al (p. 542) identified 4 pain susceptibility phenotypes (PSPs); 3 were predominated by QST evidence of sensitization and 1 was associated with developing persistent knee pain 2 years later. Soni et al (p. 550) report psychophysical and neuroimaging data suggesting that a subset of patients with OA have centrally mediated pain sensitization that was likely due to supraspinally mediated reductions in inhibition, as well as increases in facilitation of nociceptive signaling.

Carlesso and colleagues evaluated 852 individuals who were free from persistent knee pain and who were differentiated into 4 distinct PSPs using measures indicative of sensitization. The 4 PSPs were primarily characterized by varying proportions (low/absent, moderate, or high) of the presence of pressure pain sensitivity and of facilitated temporal summation (TS). Patients in the PSP with a high proportion of pain sensitivity and a moderate proportion of facilitated TS were twice as likely to develop incident persistent knee pain over 2 years when compared to subjects in the PSP having a lower proportion of sensitization by both measures.

Soni and colleagues examined patients who were awaiting arthroplasty for knee OA and had features of neuropathic pain as identified using PainDETECT. Patients with neuropathic-like pain before surgery reported significantly higher pain in response to punctate stimuli and cold stimuli near the affected joint. When neural activity during punctate stimulation in these patients was compared to that seen in patients without neuropathic-like pain, it was found that the activity was significantly lower in the rostral anterior cingulate cortex and higher in the rostral ventromedial medulla (RVM). The authors found significant functional connectivity between those 2 areas of the brain. Moreover, preoperative neuropathic-like pain and higher neural activity in the RVM were associated with moderate-to-severe long-term pain after arthroplasty. These patients also tended toward worse outcomes after knee replacement surgery.

Both studies present neurobiologic confirmation of central sensitization in patients with features of neuropathic pain. The results suggest that prevention or amelioration of sensitization may be a novel approach to the prevention of persistent knee pain onset in patients with OA. The studies support further investigation of bedside measures for patient stratification in an effort to better predict postsurgical outcomes.

Sacroiliac Joint Ankylosis in Young Patients With Spondyloarthritis

The spondyloarthritides include a range of disease phenotypes that vary in disease severity, presence of structural damage, and age at presentation. In this issue, Bray et al (p. 594) report that while tumor necrosis factor inhibitor (TNFi) therapy did reduce inflammation in

p. 594

a cohort of young patients (ages 12–23 years) with spondyloarthritis, it failed to prevent the eventual development of joint ankylosis. The study included 29 patients with enthesitis-related arthritis or nonradiographic axial spondyloarthritis who were undergoing TNFi therapy. The investigators noted that inflammation scores were significantly lower in patients receiving TNFi treatment, but there was no significant effect of time from TNFi initiation on inflammation.

Moreover, while fusion scores in the cohort significantly increased with time from TNFi initiation, there was no significant effect of active TNFi treatment on fusion scores. Fusion scores did not change in the first year after the start of TNFi therapy, but they were significantly increased at all subsequent time points. The researchers also found a positive relationship between the time elapsed since biologic initiation and fat metaplasia scores.

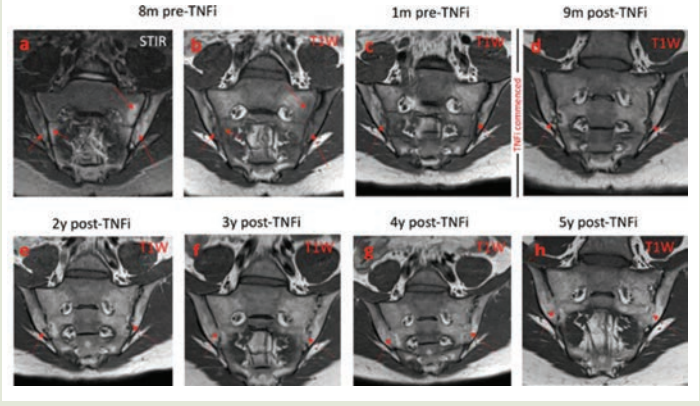

Figure 1. Magnetic resonance images from a representative patient showing the progression of ankyloses over a 5-year period. **a–c**, Before the initiation of tumor necrosis factor inhibitor (TNFi) therapy, bilateral bone marrow edema is evident on the STIR image (**a**) and T1-weighted (T1W) images (**b** and **c**). **d–h**, After TNFi therapy, the joint erosions gradually become less distinct, and the joints ultimately fuse in anatomic locations similar to those in which the initial edema was found. **Arrows** indicate the areas of involvement.

Clinical Connections

Affinity Maturation of the Anti–Citrullinated Protein Antibody Paratope Drives Epitope Spreading and Polyreactivity in Rheumatoid Arthritis

Kongpachith et al, *Arthritis Rheumatol* 2019;71:507–517.

CORRESPONDENCE
William H. Robinson, MD, PhD: w.robinson@stanford.edu.

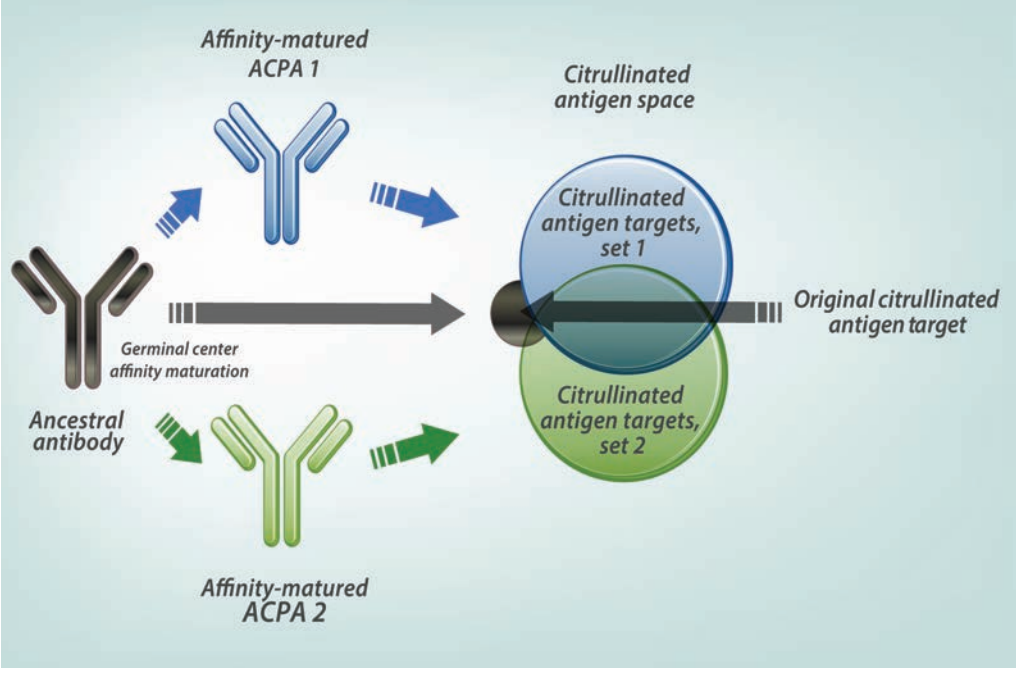

KEY POINTS

- Affinity maturation leads to epitope spreading.
- Individual ACPAs within a clonal family exhibit distinct polyreactive binding to citrullinated epitopes.
- Affinity-matured ACPAs bind greater numbers of citrullinated epitopes compared to ancestral antibodies.
- Residues within CDRs and framework regions of ACPA paratopes contribute to the specificity of ACPA reactivity.

SUMMARY

Anti–citrullinated protein antibodies (ACPAs) are a hallmark of rheumatoid arthritis (RA). The number and diversity of ACPA reactivities increase prior to clinical onset of RA and are associated with disease severity. Kongpachith et al investigated the mechanisms underlying epitope spreading of the ACPA response that lead to the presence of increased reactivities. Sequencing the blood plasmablast antibody repertoire in patients with RA revealed clonal families of affinity-matured ACPAs. Recombinant expression of these ACPAs demonstrated that unique somatic hypermutations enabled individual ACPAs from the same clonal families to bind different sets of citrullinated epitopes. Further, affinity-matured ACPAs frequently bound greater numbers of citrullinated epitopes relative to predicted ancestral family members. Molecular modeling identified key amino acid residues within the complementarity-determining regions (CDRs) and framework regions of ACPAs that mediate binding to citrullinated epitopes. Mutation of these residues within the antigen-binding site led to altered epitope specificity. These findings demonstrate that affinity maturation contributes to epitope spreading and can increase the polyreactivity of ACPAs.

Interleukin-17A Inhibition Diminishes Inflammation and New Bone Formation in Experimental Spondyloarthritis

van Tok et al, *Arthritis Rheumatol* 2019;71:612–625.

CORRESPONDENCE
Dominique L. Baeten, MD, PhD: d.l.baeten@amc.uva.nl.

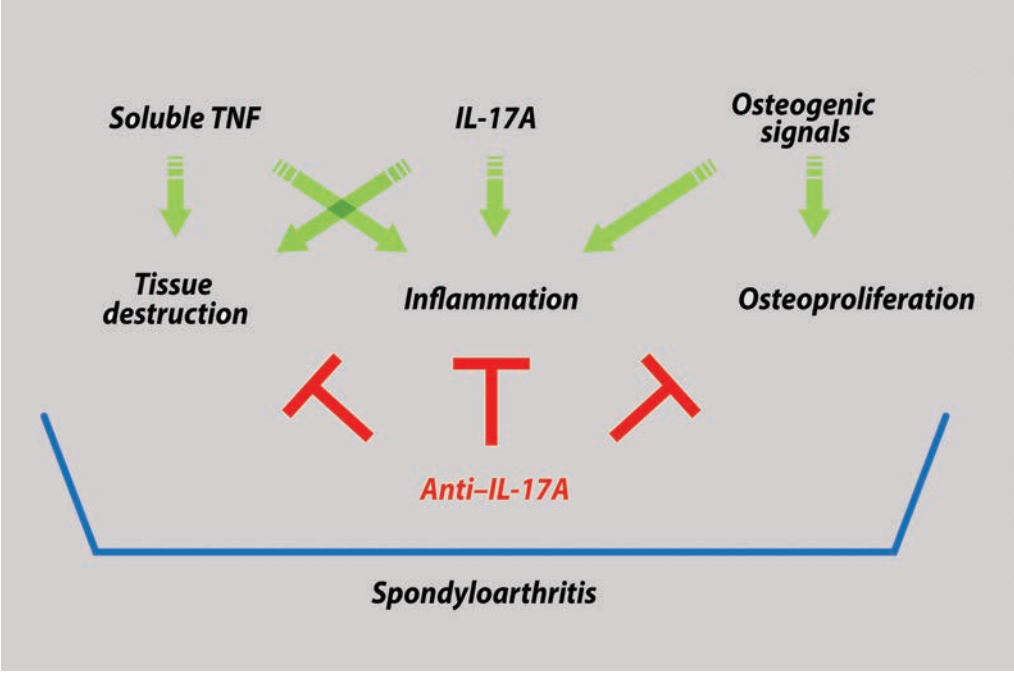

KEY POINTS

- New bone formation in experimental SpA occurs only in the presence of tissue inflammation.
- Treatment of established inflammation by anti–IL-17A inhibits the progression of new bone formation in experimental SpA.
- IL-17A promotes osteoblast differentiation of human SpA fibroblast-like synoviocytes.
- IL-17A links inflammation and new bone formation in experimental SpA.

SUMMARY

Spondyloarthritis (SpA) is characterized by tissue inflammation, cartilage and bone destruction, and new bone formation in axial and peripheral joints. Inflammation directly drives cartilage and bone destruction, and both tumor necrosis factor (TNF) and interleukin-17A (IL-17A) play a crucial role in these processes. The link between inflammation and pathologic new bone formation, however, remains less well understood, as anti-TNF therapy has minimal impact on progression of new bone formation in SpA.

It has been hypothesized that new bone formation is either 1) a derailed repair process triggered by tissue damage and occurring after resolution of tissue inflammation or 2) that inflammation and new bone formation are parallel but uncoupled processes. Using the HLA–B27–transgenic rat model of SpA, van Tok et al demonstrated that both hypotheses are likely incorrect. Prevention of inflammation with an anti–IL-17A antibody prevented new bone formation. Moreover, treatment of ongoing inflammation with anti–IL-17A did not augment reparative new bone formation (hypothesis 1) or affect stable, ongoing new bone formation (hypothesis 2). On the contrary, anti–IL-17A inhibited further progression of osteoproliferation. These observations, supported by data showing that IL-17A accelerates osteoblastic differentiation of human SpA fibroblast-like synoviocytes, indicate that IL-17A links the 3 cardinal pathologic features of SpA: inflammation, tissue destruction, and new bone formation.

Arthritis & Rheumatology

An Official Journal of the American College of Rheumatology
www.arthritisrheum.org and wileyonlinelibrary.com

Cover design: Todd Machen

This journal is printed on acid-free paper.

Arthritis & Rheumatology

An Official Journal of the American College of Rheumatology
www.arthritisrheum.org and wileyonlinelibrary.com

VOLUME 71 • April 2019 • NO. 4

Cover image: The figure on the cover (from van Tok et al, page 612) shows a 3-dimensional micro–computed tomography image of the hind paws of an HLA–B27–transgenic rat immunized with heat-inactivated *Mycobacterium tuberculosis*, with severe experimental spondyloarthritis treated with IgG2a control antibody. The remodeling bone tissue is color-coded according to material bone mineral density, with newly formed low-density bone (400–750 mg hydroxyapatite/cm^3) colored in red and normal mature-density bone tissue (>800 mg hydroxyapatite/cm^3) visualized in white.

Arthritis & Rheumatology
Vol. 71, No. 4, April 2019, pp 483–485
DOI 10.1002/art.40817

AMERICAN COLLEGE OF RHEUMATOLOGY
EDUCATION • TREATMENT • RESEARCH

EDITORIAL

Interleukin-17A and Pathologic New Bone Formation: The Myth of Prometheus Revisited

Iannis E. Adamopoulos

Inflammation has been linked with tissue regeneration going back as far as references made in ancient Greek mythology. However, despite recent advances, the cellular and molecular pathways that govern the regenerative process remain elusive. Recent findings from the study by van Tok et al, published in this issue of *Arthritis & Rheumatology*, shed new light on the complex phenomenon of bone regeneration as it pertains to inflammatory arthritis (1). In an ancient Greek myth, Prometheus upsets the gods by offering them bones wrapped in fat instead of a proper sacrificial offering and by stealing fire to return it to humankind. As an eternal punishment for his actions, it is said that Prometheus was chained to a rock and forced to endure an eagle feeding on his liver each day while it regenerated at night. Although Prometheus is a mythical character, modern science has confirmed that within this myth is the fascinating scientific fact of tissue regeneration. Liver regeneration occurs after injury, and many other tissues, including bone, have also been shown to exhibit regenerative abilities.

Bone repair after injury involves multiple events starting with the formation of a hematoma due to the rupture of blood vessels at the injury site. Injury to the soft tissues and degranulation of platelets results in the release of proinflammatory cytokines, which leads to the accumulation of an inflammatory infiltrate consisting mainly of neutrophils, macrophages, and lymphocytes. The hematoma is gradually replaced by granulation tissue, before the repair process continues with the formation of new blood vessels (neovascularization) and the recruitment of specialized cells, depending on the nature of regenerative tissue. Despite cellular differences in the local tissue, a well-orchestrated immune response regulated by proinflammatory mediators precedes the repair process. Indeed, the molecular mechanisms are so aligned that hepatocyte growth factor (HGF), which regulates liver regeneration (2), has been shown to act as a coupling factor for osteoclasts and osteoblasts (3). Similarly, tumor necrosis factor (TNF), which also participates in liver regeneration (2), is critical in bone repair, as evidenced by impaired fracture healing exhibited in TNF-deficient mice (4).

The link between inflammation and pathologic new bone formation is also demonstrated in spondyloarthropathies, a group of chronic inflammatory diseases of the skeleton and associated soft tissues, which include ankylosing spondylitis, psoriatic arthritis, inflammatory bowel disease–associated arthritis, reactive arthritis, juvenile spondyloarthritis (SpA), and undifferentiated SpA. The precise cellular and molecular pathways and the role of proinflammatory cytokines in regulating inflammatory bone remodeling remain elusive. Undoubtedly, HGF and TNF are not the only factors that contribute to pathologic new bone formation. In the report by van Tok et al, the fundamental question raised by the Prometheus myth is addressed by investigating the role of the proinflammatory cytokine interleukin-17A (IL-17A) in the coupling of inflammation and new bone formation (1).

The role of IL-17A in inflammatory arthritis and bone remodeling has been extensively studied. Multiple studies have demonstrated that cortical and trabecular bone in the femurs of IL-17A–deficient and wild-type mice exhibit similar bone mineral density, establishing an overall consensus that IL-17A does not significantly alter normal skeletal development (5,6). This finding is merely due to the fact that IL-17A expression is highly restricted under noninflammatory conditions. However, under inflammatory conditions in which IL-17A is expressed at high concentrations, multiple observations have confirmed that IL-17A exhibits pro-osteoclastogenic effects in vitro and in vivo by up-regulating RANKL expression in stromal cells and RANK expression in osteoclast precursors, thereby disturbing the RANKL/RANK/osteoprotegerin axis (5,6). The role of IL-17A in inflammatory bone formation is complex. IL-17A deficiency and/or blockade promotes periosteal bone formation in the K/BxN serum–transfer model of inflammatory arthritis (7), whereas other studies using the drill-hole injury animal model have demonstrated that enhanced bone regeneration is

Supported by the NIH (National Institute of Arthritis and Musculoskeletal and Skin Diseases grant R01-AR-062173) and the National Psoriasis Foundation.

Iannis E. Adamopoulos, MPhil, DPhil: University of California at Davis, Shriners Hospitals for Children Northern California, Sacramento.

Dr. Adamopoulos has received consulting fees from Pfizer, Merck/Schering-Plough, Tanabe Research Labs, and Novartis (less than $10,000 each) and research support from those companies.

Address correspondence to Iannis E. Adamopoulos, MPhil, DPhil, Division of Rheumatology, Allergy and Clinical Immunology, University of California at Davis, Institute for Pediatric Regenerative Medicine, Shriners Hospitals for Children Northern California, 2425 Stockton Boulevard, Sacramento, CA 95817. E-mail: iannis@ucdavis.edu.

Submitted for publication October 16, 2018; accepted in revised form December 18, 2018.

dependent on IL-17A (8). Differing observations on the effects of IL-17A on osteoblasts using different animal models likely result from variation in experimental parameters and the multiple signaling pathways that orchestrate outcomes of IL-17A in inflammatory bone remodeling, and further research is required.

Van Tok et al investigated the osteogenic capacity of IL-17A by performing in vitro osteoblast differentiation assays in primary human fibroblast-like synoviocyte cultures isolated from synovial biopsy specimens from SpA patients, to effectively demonstrate that IL-17A promotes the differentiation of osteoblasts and mineralization in SpA stromal cells. Moreover, the research team performed a series of in vivo experiments using the HLA–B27/human β_2-microglobulin (hβ_2m)–transgenic rat model of SpA, in which IL-17A was inhibited by administration of a neutralizing antibody to IL-17A either before (prophylactic) or after (therapeutic) the observed clinical onset of disease. This set of experiments demonstrated that anti–IL-17A–treated rats experienced a reduction of inflammation and bone destruction, as evidenced by histologic examination and micro–computed tomography analysis, which correlated with reduced bone formation in the spine and ankles (1).

Although IL-17A interference with RANKL/RANK signaling regulates a number of transcription factors to enhance osteoclastogenesis and bone loss, the same transcriptional regulatory elements also exert dramatic effects on osteoblastogenesis and bone formation. One such transcription factor is NFATc1, which induces osteoclastogenesis. In NFATc1-deficient mice, generation of osteoclasts does not occur, leading to reduced bone resorption. Surprisingly, it has been demonstrated that mice expressing a constitutively nuclear NFATc1 variant (NFATc1nuc) exhibited massive osteoblast overgrowth and enhanced osteoblast proliferation (9). Therefore, while it seems that transcriptional activation of NFATc1 in osteoclasts induces bone loss, the same pathways in osteoblasts have the potential to induce bone formation. These findings and the notion that TNF superfamily members (including RANKL and TNF) act as bidirectional signaling molecules that generate intracellular reverse signaling suggest that the transcriptional regulation under inflammatory conditions in osteoblasts may have dual effects, both promoting and inhibiting bone formation. Although the precise mechanisms of pathologic bone formation have yet to be determined, the potential of proinflammatory mediators to hijack cellular and molecular processes in order to activate osteogenesis is nothing short of fascinating.

In support of the notion that reverse RANKL signaling is involved in these dual effects, findings from a recent study suggest that RANKL reverse signaling couples bone resorption and bone formation (10). Specifically, the study demonstrates that vesicular RANK, secreted from terminally differentiated osteoclasts, activates the expression of *Col1a1*, *Runx2*, and *Osx* to promote osteoblast differentiation, leading to mineralization and new bone formation both in vitro and in vivo (10). Since IL-17A can induce RANK expression in osteoclast precursors and expand the RANK+ osteoclast precursor population (6), it is plausible that

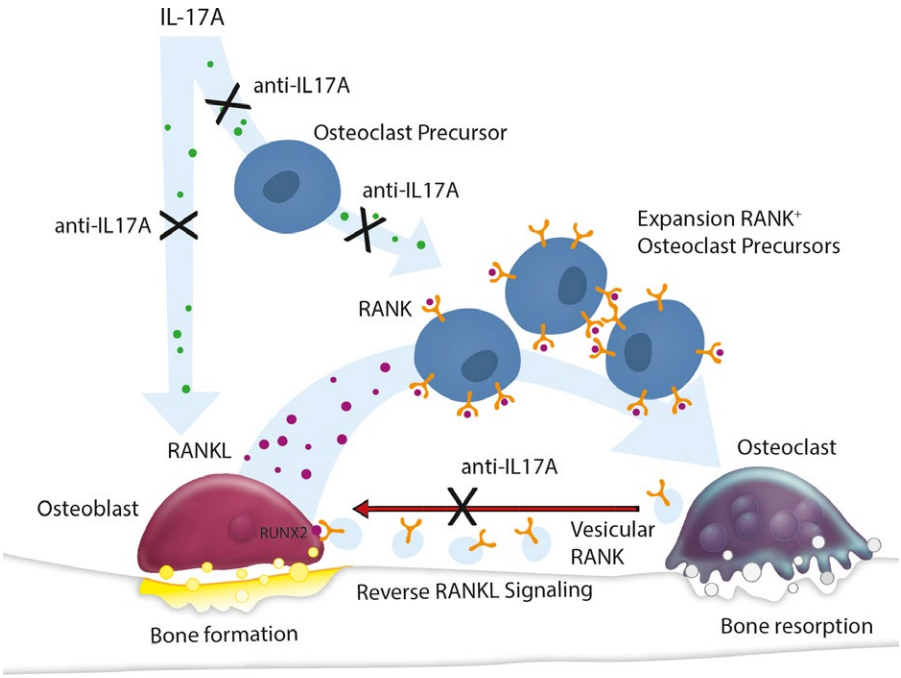

Figure 1. Interleukin-17A (IL-17A) in pathologic bone formation. Schematic representation shows the pro-osteoclastogenic roles of IL-17A (green dots), induction of RANKL secretion (magenta dots) by stromal cells, and expansion of RANK+ osteoclast precursors, which leads to an increase in vesicular RANK (yellow) that can potentiate RANKL reverse signaling and lead to *RUNX2* activation and bone formation. IL-17A–induced RANKL and RANK expression is neutralized during IL-17A inhibition and therefore may arrest pathologic bone remodeling.

excess RANK availability in terminally differentiated osteoclasts may be one of the mechanisms by which IL-17A can induce bone formation (Figure 1).

One of the most important mechanistic findings in the report by van Tok et al is that the inhibition of IL-17A and the observed changes in new bone formation correlate with a reduction of myeloid-related genes such as defensins, myeloperoxidase, and neutrophil elastase. While some studies have failed to reveal the prominent role of IL-17A when using an IL-17A minicircle overexpression model, others have used the same model and demonstrated that IL-17A expands distinct myeloid populations including neutrophils (11), as was also observed by van Tok. This finding is of primary importance, as an expansion of neutrophils (particularly neutrophil elastase, which plays a significant role in NETosis) is critical in the development of IL-17A–mediated epidermal hyperplasia and skin inflammation (11). Similarly, other groups have observed that neutrophils are important effector cells in entheseal inflammation by augmenting the inflammatory response through the release of proteases and reactive oxygen species, and the activation state of neutrophils is critical in determining the development of enthesitis (12). Collectively, these new data illustrate not only the effects of IL-17A on new bone formation but also the contribution of neutrophils, which may help us achieve a more complete understanding of the pathogenesis of enthesitis and skin inflammation, hallmark pathologic features of SpA.

With the demonstration that, at least in the HLA–B27/Hβ2m–transgenic rat model of spondyloarthritis, new bone formation is not observed without inflammation, we can conclude that in this animal model, tissue remodeling of bone recapitulates the myth of Prometheus in which tissue regeneration is closely linked to inflammation. In the absence of concrete experimental evidence that describes the exact mechanisms governing IL-17A–mediated bone formation, one can only speculate that the answer may lie within the Greek myth and the regenerating liver of Prometheus. Interestingly, findings from a previous study that used a model of reversible liver injury (in which the injury and recovery phases were distinct), combined with CD11b+ depletion strategies using CD11b–DTR–transgenic mice, provided the first clear evidence that functionally distinct myeloid subpopulations exist in the same tissue and play critical roles in both liver injury and repair (13). Based on the common features observed in liver and bone, it is certainly plausible that heterogeneity in innate immune pathways may underlie the sequential interplay of inflammation and repair (14). New evidence provided by van Tok et al elegantly demonstrates and confirms the role of the proinflammatory mediator IL-17A in bone formation, in addition to highlighting the importance of myeloid cells and neutrophils in SpA, which warrants further investigation.

ACKNOWLEDGMENTS

The author would like to thank Dr. Chris Ritchlin for critical reading of the manuscript and Thanh Nguyen for assistance with graphic design.

AUTHOR CONTRIBUTIONS

Dr. Adamopoulos drafted the article, revised it critically for important intellectual content, and approved the final version to be published.

REFERENCES

1. Van Tok MN, van Duivenvoorde LM, Kramer I, Ingold P, Pfister S, Roth L, et al. Interleukin-17A inhibition diminishes inflammation and new bone formation in experimental spondyloarthritis. Arthiris Rheumatol 2019;71:612–25.
2. Michalopoulos GK, DeFrances MC. Liver regeneration. Science 1997;276:60–6.
3. Grano M, Galimi F, Zambonin G, Colucci S, Cottone E, Zallone AZ, et al. Hepatocyte growth factor is a coupling factor for osteoclasts and osteoblasts in vitro. Proc Natl Acad Sci U S A 1996;93:7644–8.
4. Gerstenfeld LC, Cho TJ, Kon T, Aizawa T, Tsay A, Fitch J, et al. Impaired fracture healing in the absence of TNF-α signaling: the role of TNF-α in endochondral cartilage resorption. J Bone Miner Res 2003;18:1584–92.
5. Sato K, Suematsu A, Okamoto K, Yamaguchi A, Morishita Y, Kadono Y, et al. Th17 functions as an osteoclastogenic helper T cell subset that links T cell activation and bone destruction. J Exp Med 2006;203:2673–82.
6. Adamopoulos IE, Chao CC, Geissler R, Laface D, Blumenschein W, Iwakura Y, et al. Interleukin-17A upregulates receptor activator of NF-κB on osteoclast precursors. Arthritis Res Ther 2010;12:R29.
7. Shaw AT, Maeda Y, Gravallese EM. IL-17A deficiency promotes periosteal bone formation in a model of inflammatory arthritis. Arthritis Res Ther 2016;18:104.
8. Ono T, Okamoto K, Nakashima T, Nitta T, Hori S, Iwakura Y, et al. IL-17- producing γδ T cells enhance bone regeneration. Nat Commun 2016;7:10928.
9. Winslow MM, Pan M, Starbuck M, Gallo EM, Deng L, Karsenty G, et al. Calcineurin/NFAT signaling in osteoblasts regulates bone mass. Dev Cell 2006;10:771–82.
10. Ikebuchi Y, Aoki S, Honma M, Hayashi M, Sugamori Y, Khan M, et al. Coupling of bone resorption and formation by RANKL reverse signalling. Nature 2018;561:195–200.
11. Suzuki E, Maverakis E, Sarin R, Bouchareychas L, Kuchroo VK, Nestle FO, et al. T cell-independent mechanisms associated with neutrophil extracellular trap formation and selective autophagy in IL-17A-mediated epidermal hyperplasia. J Immunol 2016;197:4403–12.
12. Schett G, Lories RJ, D'Agostino MA, Elewaut D, Kirkham B, Soriano ER, et al. Enthesitis: from pathophysiology to treatment. Nature Rev Rheumatol 2017;13:731–41.
13. Duffield JS, Forbes SJ, Constandinou CM, Clay S, Partolina M, Vuthoori S, et al. Selective depletion of macrophages reveals distinct, opposing roles during liver injury and repair. J Clin Invest 2005;115:56–65.
14. Adamopoulos IE, Xia Z, Lau YS, Athanasou NA. Hepatocyte growth factor can substitute for M-CSF to support osteoclastogenesis. Biochem Biophys Res Commun 2006;350:478–83.

AMERICAN COLLEGE OF RHEUMATOLOGY
EDUCATION • TREATMENT • RESEARCH

Arthritis & Rheumatology
Vol. 71, No. 4, April 2019, pp 486–495
DOI 10.1002/art.40790

ADVANCES IN DISEASE MECHANISMS AND TRANSLATIONAL TECHNOLOGIES

The Contribution of *PTPN22* to Rheumatic Disease

Tomas Mustelin,[1] Nunzio Bottini,[2] and Stephanie M. Stanford[2]

One of the unresolved questions in modern medicine is why certain individuals develop a disorder such as rheumatoid arthritis (RA) or lupus, while others do not. Contemporary science indicates that genetics is partly responsible for disease development, while environmental and stochastic factors also play a role. Among the many genes that increase the risk of autoimmune conditions, the risk allele encoding the W620 variant of protein tyrosine phosphatase N22 (PTPN22) is shared between multiple rheumatic diseases, suggesting that it plays a fundamental role in the development of immune dysfunction. Herein, we discuss how the presence of the *PTPN*22 risk allele may shape the signs and symptoms of these diseases. Besides the emerging clarity regarding how PTPN22 tunes T and B cell antigen receptor signaling, we discuss recent discoveries of important functions of PTPN22 in myeloid cell lineages. Taken together, these new insights reveal important clues to the molecular mechanisms of prevalent diseases like RA and lupus and may open new avenues for the development of personalized therapies that spare the normal function of the immune system.

Introduction

In 2004, we and others reported the discovery that a single-nucleotide polymorphism (SNP) C1858T (rs2476601) in the *PTPN22* gene is associated with type 1 diabetes (1), rheumatoid arthritis (RA) (2), and systemic lupus erythematosus (SLE) (3). These initial findings have been extensively replicated, and today there are close to 1,000 published papers confirming and refining the genetic association of *PTPN22* with numerous autoimmune diseases. Indeed, *PTPN22* is now recognized as the most influential non–major histocompatibility complex (non-MHC) gene in the development of autoimmunity, including most rheumatic conditions. Herein we summarize the progress in our understanding of the role of protein tyrosine phosphatase N22 (PTPN22) in rheumatic diseases, highlighting how PTPN22 likely operates through multiple mechanisms of action. The varying strength and direction of the association between PTPN22 and various diseases (Figure 1) reflect the differential contribution of these mechanisms and introduce a potential novel method of pathogenetic disease classification.

PTPN22 in RA and juvenile idiopathic arthritis (JIA)

A statistically significant association of the *PTPN22* 1858T allele (encoding the W620 variant) with RA was first reported by Begovich and coworkers in 2004 (2). The odds ratio was 1.65 in their discovery cohort (n = 475 patients with RA and 475 controls) and as high as 2.63 for the homozygous TT genotype versus CC in their replication cohort (n = 840 subjects from 463 white families). Rheumatoid factor (RF)–positive RA patients had a higher odds ratio than RF-negative patients. Numerous studies have validated these findings (4) and documented an association of *PTPN22* with anti–citrullinated protein antibodies (5–9) as well as smoking (10,11), erosive disease (12), and earlier disease onset (8,13). However, the presence of the *PTPN22* risk allele 1858T did not correlate with response to anti–tumor necrosis factor (anti-TNF) agents (9) or methotrexate (14).

Despite the now well-established geographic gradient in T allele frequency, with the highest prevalence in Caucasians of northern European descent and considerably lower frequencies in southern Europeans (15) and Hispanics, particularly low frequencies (<1%) in Asians, and near absence in people of Afri-

Dr. Bottini's work was supported by the NIH (grants R01-AI-070544 and R01-AR-066053).

[1]Tomas Mustelin, MD, PhD: University of Washington, Seattle; [2]Nunzio Bottini, MD, PhD, Stephanie M. Stanford, PhD: University of California San Diego, La Jolla.

Drs. Mustelin, Bottini, and Stanford contributed equally to this work.

No potential conflicts of interest relevant to this article were reported.

Address correspondence to Nunzio Bottini, MD, PhD, Department of Medicine, University of California San Diego, 9500 Gilman Drive, MC0656, La Jolla, CA 92093-0656. E-mail: nbottini@ucsd.edu.

Submitted for publication August 15, 2018; accepted in revised form November 27, 2018.

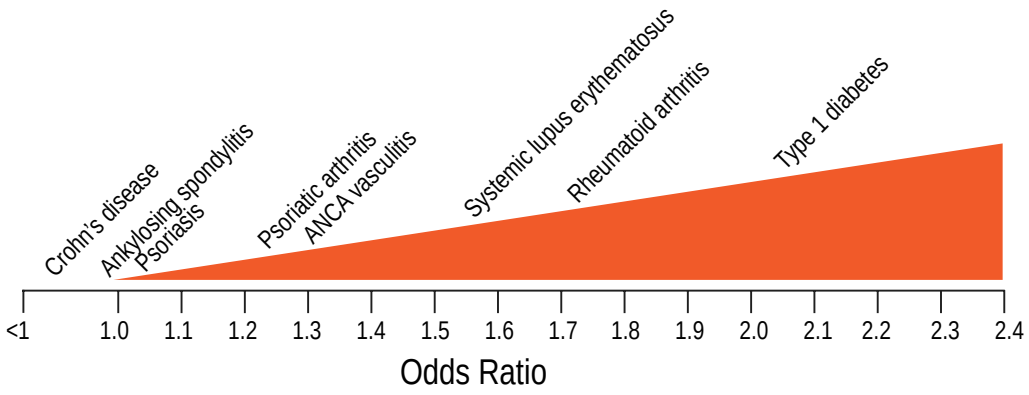

Figure 1. The spectrum of *PTPN22* 1858T–associated diseases by magnitude of risk. The x-axis shows the odds ratio, with 1.0 indicating no association and <1 indicating a protective effect. Disease names are shown above the approximate average odds ratio for heterozygotic carriers from all published studies and meta-analyses. ANCA = antineutrophil cytoplasmic antibody.

can origin, a significant association of the T allele with RA has been documented in populations worldwide, including RA patients from South Asia (16), Tunisia (17), and Turkey (18). However, in some populations the T allele frequency is too low (<1%) for a meaningful analysis (19). Interestingly, another polymorphism (rs2488457) located in the promoter region of *PTPN22* is instead associated with RA in a Chinese population (20).

The *PTPN22* 1858T allele is also associated with juvenile idiopathic arthritis (JIA) (4,21) with a somewhat lower odds ratio of ~1.3 in a meta-analysis that included >4,000 patients and 6,000 controls (22), as well as in a more recent meta-analysis (23), in which RF-positive polyarticular JIA had a stronger odds ratio of 2.12. Interestingly, this subtype of JIA is most similar to RA. Other association studies have treated all 7 recognized forms of JIA as a single entity.

PTPN22 in spondyloarthritides

While most susceptibility loci identified in psoriasis tend to be associated with both skin psoriasis and psoriatic arthritis (PsA), *PTPN22* is an exception: the association of the 1858T allele with general skin psoriasis is weak or absent, whereas its association with PsA is highly statistically significant, with odds ratios of up to 1.32 (24,25). This suggests that PsA has additional components in its pathogenesis compared to skin-restricted disease and more involvement of cells and pathways influenced by PTPN22. Also somewhat surprising considering the partially shared pathogenic mechanisms between PsA and ankylosing spondylitis (AS), the latter is not associated with *PTPN22*. The known roles of PTPN22 in CD8 memory T cell function (26) and interleukin-17 (IL-17)–producing Th17 cell differentiation (27) suggest the possibility that the differential association of PTPN22-W620 with PsA versus psoriasis or AS depends on alterations in the function of CD8 T cells—which are thought to play a more prominent role in PsA than in psoriasis or AS (28)—or that PTPN22-W620 contributes to differential phenotypes of Th17 in PsA versus psoriasis or AS (29).

PTPN22 in SLE

In the first study to show an association of the *PTPN22* 1858T allele with SLE, Kyogoku and coworkers (3) found that a single copy of the T allele increased the risk of SLE with an odds ratio of 1.37 (95% confidence interval 1.07–1.75), while TT homozygotes had a much higher odds ratio of 4.37 (95% confidence interval 1.98–9.65). The association with SLE has now been replicated in nearly 20 studies, and 2 recent meta-analyses showed an overall odds ratio of ~1.5 (30,31). SLE patients with an 1858T allele were noted in different studies to have higher interferon-α (IFNα) levels and lower TNF levels (32), somewhat more prevalent nephritis (33), and a higher incidence of antiphospholipid syndrome with anticardiolipin autoantibodies (34).

PTPN22 in vasculitides

The rs2476601 *PTPN22* polymorphism is also positively associated with antineutrophil cytoplasmic antibody (ANCA)–associated vasculitis (AAV) (35–38). Specifically, *PTPN22* 1858T is associated with 2 of the 3 distinct autoimmune vasculitides associated with ANCAs (39), microscopic polyangiitis and granulomatosis with polyangiitis, but has not been reported in eosinophilic granulomatosis with polyangiitis. PTPN22 association was equal in patients with the anti–proteinase 3 serotype and those with the antimyeloperoxidase serotype. Although an initial study (40) showed a lack of association, several later studies have documented and replicated a significant association of 1858T with biopsy-proven giant cell arteritis (GCA) (41,42) with an odds ratio of 1.62 (95% confidence interval 1.29–2.04). These findings have been replicated in Spanish, Scandinavian, British, American, and Australian patient samples. There was no difference in risk between patients with and those without polymyalgia rheumatica or visual ischemic manifestations (42,43). In contrast, PTPN22 was not associated with Takayasu arteritis, Behçet's disease, or IgA vasculitis (44,45).

PTPN22 in other rheumatic and autoimmune conditions

PTPN22 1858T is also strongly associated with type 1 diabetes, autoimmune thrombocytopenia, vitiligo, idiopathic inflammatory myopathies, Graves' disease, myasthenia gravis, and Addison's disease (44). On the other hand, the association with systemic sclerosis (SSc) is weaker and has only been found in larger cohorts and meta-analyses (46). Other diseases that lack an association with *PTPN22* 1858T include multiple sclerosis, pemphigus vulgaris, ulcerative colitis (UC), primary sclerosing cholangitis, primary biliary cholangitis (formerly known as primary biliary cirrhosis), and acute anterior uveitis, all of which represent diseases in epithelial, mucosal, or immune-privileged organs (47). Intriguingly, in Crohn's disease the direction of association is reversed, and *PTPN22* 1858T plays a protective role. Figure 1 summarizes the spectrum of association between PTPN22 and various rheumatic or autoimmune diseases. The observed variability likely reflects fundamental differences in disease pathogenesis, although it is possible that in some diseases *PTPN22* 1858T promotes both pathogenic and disease-protective pathways, ultimately attenuating the strength of the association.

Other polymorphisms in *PTPN22*

Besides the C1858T polymorphism, 2 additional PTPN22 SNPs have been found to be associated with various diseases, particularly in populations with a low frequency of the 1858T allele. The G1123C polymorphism (rs2488457) is located in the 5′-promoter region of *PTPN22* and is associated with RA (20), JIA (48), and UC (49) in Chinese populations, in which the rs2476601 SNP is not associated with autoimmunity. The impact of this noncoding SNP on the transcription, stability, or translation of the messenger RNA (mRNA) remains to be fully clarified. Interestingly, both SNPs rs2476601 and rs2488457 were recently reported as potential *cis*-expression quantitative trait loci in whole blood from Spanish RA patients (50), and another study demonstrated that PTPN22 expression is significantly decreased in whole blood from RA patients carrying the risk alleles of SNPs rs2476601 and rs2488457 compared to healthy controls (51).

The second SNP (rs33996649) is a missense G788A mutation that encodes an R263Q substitution in the catalytic domain of the protein. This variant changes the conformation of the PTPN22 active site, and therefore, unlike the 1858T allele, results in reduced catalytic activity of PTPN22 (52). It is therefore interesting that in European populations, the 788A allele displays a pattern of association with autoimmune diseases that is distinct from the 1858T allele. In contrast to 1858T, the 788A allele protects against both SLE and RA (53). The 788A allele also protects against UC, which 1858T is not associated with, and the 788A allele is not associated with Crohn's disease, which 1858T is protective against (53,54). Single studies have so far shown no association of the 788A allele with SSc, GCA, IgA vasculitis, uveitis, or Graves' disease (53).

Structure and molecular functions of PTPN22

The *PTPN22* gene encodes a 110-kd protein (Figure 2) known as lymphoid tyrosine phosphatase (55), although now more commonly referred to simply as PTPN22. It is found in all leukocyte lineages, and its mRNA is particularly abundant in neutrophils, natural killer cells, and B cells. The PTPN22 protein has a classic and strictly phosphotyrosine-specific PTP domain in its N-terminus followed by a linker region and a long C-terminus of unknown structure. Within the last 200 residues of PTPN22, there are 4 proline-rich sequence motifs, termed P1–P4, the first of which (PPPLPERTPESFIVV) binds with high affinity to the SH3 domain of C-terminal Src family kinase (CSK) (56). While CSK phosphorylates the negative regulatory C-terminus of Lck (57) and other Src family kinases that mediate signaling from a variety of immune receptors, including the T cell receptor (TCR) and B cell antigen receptors and Fc receptors (58), PTPN22, in a complementary manner, dephosphorylates the same kinases at their activation loop tyrosines (59) (Figure 2). This gives PTPN22 a strong inhibitory function in the TCR and Fc receptor signaling pathways, while the role of PTPN22 in B cell receptor (BCR) signaling remains less defined. In the context of TCR signaling, PTPN22 can also dephosphorylate subunits of the receptor (e.g., CD3ε) and other proximal signaling molecules, such as Vav, ZAP-70, and valosin-containing protein.

The elimination of PTPN22 in the mouse results in the accumulation of effector memory T cells later in life (60). These cells show enhanced responsiveness to TCR engagement. PTPN22-knockout mice also display enhanced numbers of follicular helper T cells and germinal centers, and knockout CD4+ T cells provide increased T cell help to B cells (61). Additionally, PTPN22 deletion in mice results in the expansion of CD4+CD25+FoxP3+ Treg cells, which display enhanced suppressive and adhesive functions (62). No effects on BCR signaling or B cell development were reported (60).

The C1858T polymorphism switches amino acid residue 620 in PTPN22 from Arg (R) to Trp (W) (1), changing the P1 motif to PPPLPE**W**TPESFIVV. This change is significant because R620 is a key residue for binding the CSK SH3 domain. Indeed, the PTPN22-W620 protein no longer binds CSK (1). We previously reported that PTPN22-W620 isolated from primary T cells from healthy subjects or patients with diabetes had higher catalytic activity than PTPN22-R620 (63). The consequences of increased catalytic activity, lost CSK binding, and other mechanisms (described below) are likely different and potentially all important for increasing the risk of autoimmunity. Chemical biology approaches—for example, generation of chemical activators of PTPN22 catalytic activity or probes that would disrupt the interaction between

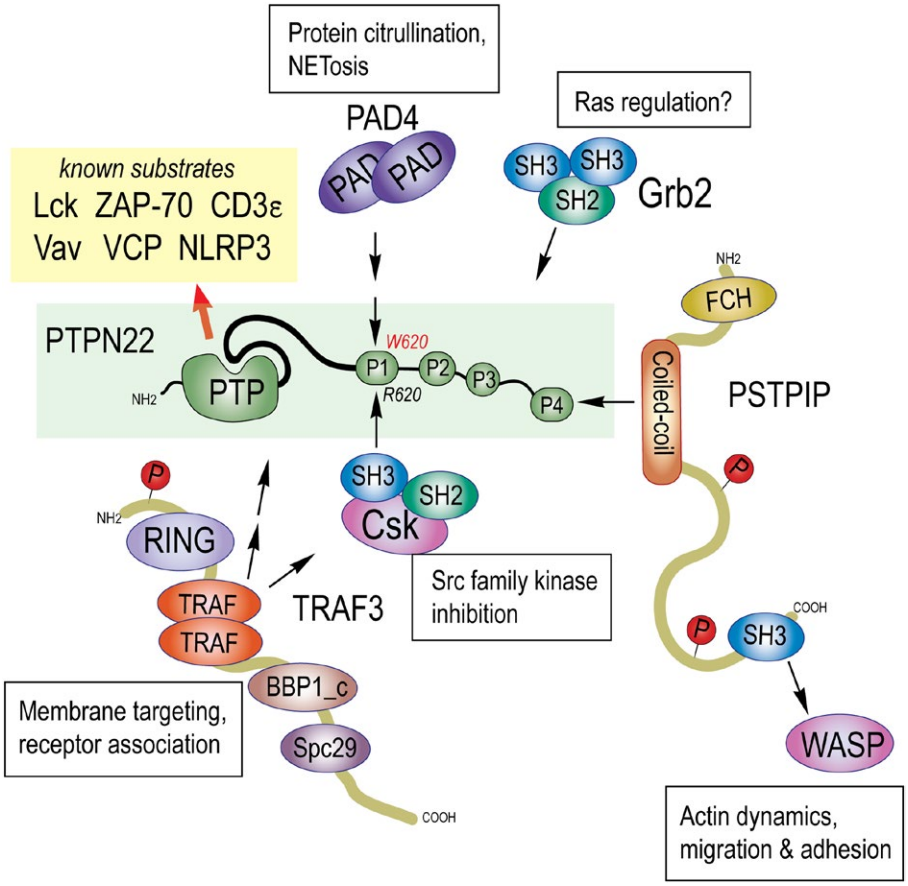

Figure 2. Structure, interactors, and substrates of protein tyrosine phosphatase N22 (PTPN22). PTPN22 (green box) contains a catalytic protein tyrosine phosphatase (PTP) domain, a linker (thick black line), and 4 proline-rich regions (P1–P4). The location of the R620W (C1858T) missense mutation in the P1 motif is indicated. Protein domains of interacting proteins are peptidylarginine deiminase (PAD), SH2 domain, SH3 domain, RING zinc finger domain, tumor necrosis factor receptor–associated factor (TRAF) domain, Brf1 binding protein, C-terminal (BBP1_c) homology, Spindle pole component 29 (Spc29) homology, Fes-CIP (FCH) homology domain, and Wiskott-Aldrich syndrome protein (WASP). VCP = valosin-containing protein; PSTPIP = proline/serine/threonine phosphatase–interacting protein. Encircled P indicates a phosphorylation site.

PTPN22 and CSK—would aid in the dissection of the impact of these mechanisms on PTPN22 function.

Indicative of even more complexity (Figure 2), PTPN22 has also been reported to associate with the TNF receptor–associated protein TNF receptor–associated factor 3 (TRAF3) (64), the adapter protein Grb2 (65), the cytoskeletal protein proline/serine/threonine phosphatase–interacting protein 1 (PSTPIP-1) (66), and the citrullinating enzyme protein peptidylarginine deiminase 4 (PAD4) (67). The physiologic relevance of these interactions remains to be fully elucidated, but binding to TRAF3 has been shown to restrict the physical location of PTPN22 and CSK to enhance signaling from the T cell antigen receptor (64) and the IL-6 receptor (68). The binding of PTPN22 to PSTPIP-1, the gene for which is mutated in familial recurrent arthritis (69,70) and pyogenic sterile arthritis, pyoderma gangrenosum, and acne syndrome (71), may direct PTPN22 to its recently recognized role in dephosphorylating the inflammasome subunit NLRP3 (72). This dephosphorylation was found to stimulate inflammasome activation and subsequent IL-1β production (72). Importantly, PTPN22-W620 also bound NLRP3, but was more effective in dephosphorylating it, leading to increased IL-1β production. Finally, the binding of PTPN22 to PAD4 reportedly only involved the major allele PTPN22-R620, while the disease-predisposing variant did not bind (67). The authors propose that this difference may result in increased protein citrullination in RA patients carrying the 1858T allele.

Another likely important aspect of the biology of PTPN22 is its regulation by mechanisms that modulate T cell function, such as its direct transcriptional suppression by the Treg cell transcription factor FoxP3 (73) and by inhibition of translation of its mRNA by the T cell–modulating microRNA-181a (74). These findings emphasize the importance of PTPN22 fine-tuning in the complex, but important, regulation of T cell immunity.

T and B cell mechanisms by which PTPN22-W620 may drive autoimmunity

The scientific community has not yet reached a consensus on exactly how PTPN22-W620 increases the risk of autoimmunity. Most investigators have focused on T cells. Some have proposed that PTPN22-W620 alters T cell antigen receptor signaling during thymic selection to promote the survival of autoreactive T cells that later participate in self-reactivity (75,76). One study suggested that Treg cells are less effective at suppressing activation of effector T cells in 1858T carriers (27) (Figure 3). Several in vitro studies with human T cells have shown that PTPN22-W620 decreases TCR signaling, as a gain-of-function effect would predict (63,77). This was seen as diminished tyrosine phosphorylation of early signaling molecules and reduced calcium mobilization (63). In contrast, experiments in mouse T cells largely led to the opposite conclusion (78). Despite these differences in TCR signaling effects between the two species, the disease-predisposing allele causes many of the same perturbations in T and B cell immunity in both species (78). In addition, other pathways activated by TCR signaling in human T cells (including the ERK and protein kinase B/Akt pathways) were found to be enhanced in 1858T carriers. This suggests that the mechanism of action of PTPN22-W620 in T cells and the consequent immunopathogenic effects are complex. Indeed, inhibition of autoimmune-protective IL-10 release, enhancement of IL-2 and IFNγ release, and expansion of the memory T cell compartment have been variably reported in studies of W620 in human T cells (63,77,79,80).

Intriguingly, while loss of PTPN22 in B cells does not seem to impact BCR signaling (81), multiple reports suggest that the W620 variation results in inhibition of human B cell activation. Although the underlying molecular mechanism remains to be further clarified, these observations suggest that PTPN22-W620 can impinge on the pathogenesis of autoimmunity by impairing the elimination of autoreactive B cells (81–83). This conclusion is also supported by experiments in humanized mice (82). Furthermore, overexpression of Ptpn22-W619 only in B cells was sufficient to cause spontaneous features of autoimmunity in mice with a mixed C57BL/6J-129/Sv background (84).

Cell type–specific contributions of PTPN22 to disease

Since PTPN22 is expressed in all leukocyte lineages, it is plausible that PTPN22-W620 contributes to the pathogenesis of different rheumatic conditions through a mix of effects on different immune cell lineages, but perhaps with a different weight of each lineage in each disease. We extrapolate this assumption from the varying roles that different immune cell lineages

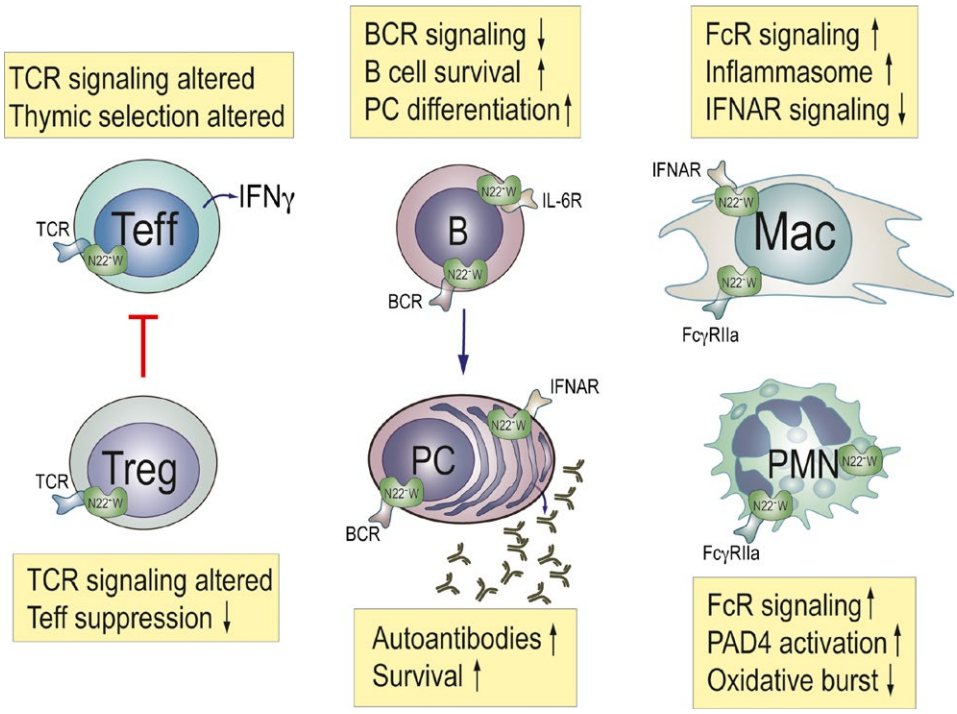

Figure 3. Effects of the *PTPN22* risk allele on the function of important immune cells. Effects on effector T (Teff) cells, Treg cells, B cells (B), plasma cells (PC), macrophages (Mac), and neutrophils (polymorphonuclear cells [PMNs]) are shown. N22-W denotes the disease-associated PTPN22-W620 variant. TCR = T cell receptor; IFNγ = interferon-γ; BCR = B cell receptor; IL-6R = interleukin-6 receptor; FcR = Fc receptor; IFNAR = interferon-α/β/ω receptor 1; FcγRIIa = Fcγ receptor IIa; PAD4 = peptidylarginine deiminase 4.

are thought to play in the pathogenesis of each disease. For example, in diseases where autoantibodies are recognized to be particularly important (e.g., SLE), dysfunction of PTPN22-W620–expressing B cells is likely to play a larger role. Similarly, in diseases where a primary dysfunction of neutrophils is considered instrumental for pathogenesis (e.g., AAV or RA), PTPN22-W620 is more likely to contribute to pathogenesis through neutrophils. However, in AAV, antineutrophil autoantibodies are also important, suggesting that PTPN22-W620 may also contribute to this disease through B cell dysfunction. As we learn more about the effects of PTPN22-W620 in other immune cells, such as myeloid or plasmacytoid dendritic cells, macrophages, monocytes, or eosinophils, we will be able to hypothesize how dysfunction of these cell lineages may contribute to diseases where they are critically involved in the pathogenesis. These concepts will require lineage-specific knockout or knockin mice for a deeper mechanistic analysis.

How PTPN22-W620 may corrupt myeloid cells in rheumatic diseases

Macrophages, dendritic cells, and neutrophils are emerging as key players in many autoimmune conditions, for example, in disposition of apoptotic or necrotic cells and immune complexes in SLE (85), protein citrullination in RA, autoantigen exposure through neutrophil extracellular traps (NETs) (86), nucleic acid sensing, and type I IFN production (87). All of these cells express PTPN22, but there are relatively few studies addressing its role in these cells.

PTPN22 selectively promotes type I IFN responses after activation of myeloid cell pattern-recognition receptors. In contrast to TCR signaling, this function of PTPN22 is not mediated by PTPN22 catalytic activity; rather PTPN22 binds to the E3 ubiquitin ligase TRAF3 and selectively promotes its Lys^{63}-linked autoubiquitination in myeloid cells after engagement of Toll-like receptors (TLRs). This leads to the production of type I IFN without an effect on the expression of proinflammatory cytokines such as IL-1β and TNF. PTPN22-W620 displays reduced binding to TRAF3, and myeloid cells carrying this variant display deficient type I IFN production following TLR stimulation. Other studies carried out in mice suggest that macrophages carrying PTPN22-W620 have hyperreactive phagocytic and proinflammatory abilities and/or skewed polarization (88,89).

In neutrophils, PTPN22-W620 appears to play a remarkably different role than in T cells. Vermeren and coworkers (90) found that loss of PTPN22 impaired (rather than augmented) Fcγ receptor II (FcγRII) signaling. They measured receptor-triggered Ca^{2+} mobilization, oxidative burst, and NETosis, all of which were reduced in $PTPN22^{-/-}$ neutrophils. Bayley and coworkers (91) went a bit further and isolated neutrophils from genotyped RA patients or healthy volunteers and measured neutrophil activation in heterozygous (W/R) and homozygous (R/R) individuals; there was only 1 homozygous carrier of the disease-predisposing allele (W/W) in the control group and 2 in the RA group, precluding much experimentation with neutrophils of this genotype. They found that PTPN22-W620 enhanced neutrophil activation, oxidative burst, and NETosis in RA donors (91). In contrast, Cao et al (92) reported that leukocytes (peripheral blood mononuclear cells) from AAV patients with PTPN22-W620 had reduced Erk activity and *IL10* transcription. However, they observed elevated activity of p38 kinase (92). It should be noted that many experiments in that study used mixed leukocytes—hence a difference between neutrophils and lymphocytes may have gone unnoticed.

Perhaps the rheumatic condition with the most likely manifestation of neutrophil dysfunction potentially caused by PTPN22-W620 is AAV. It is clear that ANCAs play a key role in driving disease by activating neutrophils to degranulate (93), produce reactive oxygen species (93), and extrude NETs (94). In patients (95), vasculitis begins with local accumulation and activation of neutrophils, which rapidly undergo NETosis, apoptosis, or necrosis while driving a necrotizing inflammation that results in endothelial cell death, vascular leakage, fibrin deposition, and a subsequent monocyte and macrophage recruitment (39). This phase eventually evolves into a fibrin and collagen–rich lesion, which may resolve if the initial inflammation was limited, or become permanent scar tissue with lingering chronic mononuclear cell infiltrates with B and T cells in ectopic germinal center–like structures. In these instances, the inflamed artery may be permanently occluded. The events leading to the formation of a nonvascular granuloma are less understood but appear to be similar. The margins of a granuloma consist of monocytes and epithelioid macrophages that wall off a center of necrotic neutrophil-derived and fibrinous debris.

PTPN22 is involved in several steps of this pathogenesis and may influence: 1) ANCA-mediated neutrophil activation via regulation of FcγRIIa signaling, 2) neutrophil priming by IL-6 via TRAF3 association, 3) NET extrusion via regulation of PAD4, and 4) inflammasome-mediated production of IL-1β and IL-18 and activation of gasdermin D, leading to neutrophil cell death by pyroptosis. All of these possible points of influence may synergize with each other and with the increased numbers of autoreactive T and B cells that produce ANCA in a vicious circle of disease propagation.

Remaining key questions

While it is intellectually gratifying that a risk allele such as that of *PTPN22* is associated with so many different autoimmune diseases, it is also thought-provoking that the risk it confers varies from strong (second only to MHC) to weak or nonexistent between different diseases. What can we learn from this? Are there patterns of disease manifestations that segregate the *PTPN22*-associated diseases from those that are not associated?

Why do subjects who carry one or two risk alleles develop a very specific autoimmune disease instead of another one? Clearly, other genetic and external factors must play a role, some of them in concert with *PTPN22* and some independently.

By examining the spectrum of diseases on a scale of their magnitude of association (e.g., by odds ratio) (Figure 1), one can draw a few tentative conclusions. First, patients with diseases that are strongly associated with *PTPN22* tend to have autoantibodies, the presence or titer of which correlate with the presence of the 1858T allele (e.g., RA, type 1 diabetes, and AAV). Second, diseases that are strongly associated with *PTPN22* tend to have a prominent role of autoreactive T and B cells (RA, SLE, and AAV). Third, diseases with a central role of neutrophils tend to be strongly associated with *PTPN22* (RA and AAV). Fourth, diseases with a key role of Th17 cells, but little involvement of autoantibodies, tend to have a poor association with *PTPN22* (AS and psoriasis). Finally, perhaps related to the previous point, diseases of mucosal sites tend to have a poor association with *PTPN22*, or even be protected against by the 1858T allele.

Another curious observation is that arthritis is strongly associated with the 1858T allele in 2 diseases, RA and PsA, but not in AS. The association is weaker in seronegative RA, suggesting that it is not the manifestation of joint disease per se that correlates with PTPN22, but the underlying immune dysfunction, which is indicated by the presence of autoantibodies.

Possible therapeutic implications

If indeed the degree of *PTPN22* association with a disease, or a subset of patients with the disease, tells us more about the critical mechanisms of pathogenesis, then these insights should be helpful for the selection of new drug targets, perhaps even PTPN22 itself. One can envision using PTPN22 expression or genetic variation as a biomarker for disease predisposition or responsiveness to specific therapeutic agents. Therapeutic targeting of PTPN22 might also be useful in the prevention or control of rheumatic diseases. For example, "molecular glue" compounds that re-establish the interaction between CSK and PTPN22-W620 might be able to rescue most of the immune abnormalities induced by the PTPN22 risk allele. A simpler approach using small-molecule inhibitors of PTPN22 might be sufficient to correct key pathogenic mechanisms and still exert sufficient preventive or therapeutic action. For example, inhibition of PTPN22 activity with the small-molecule compound LTV-1 was effective at rescuing B cell selection and preventing the development of autoreactive W620 B cells in a humanized mouse model (82). Considering that in the SKG mouse model of RA, PTPN22 promoted Th17 cell differentiation (96), a PTPN22 inhibitor might also be useful in the treatment of the large spectrum of diseases characterized by enhanced Th17 cell presence or activation.

AUTHOR CONTRIBUTIONS

All authors drafted the article, revised it critically for important intellectual content, approved the final version to be published, and take responsibility for the integrity of the data and the accuracy of the data analysis.

REFERENCES

1. Bottini N, Musumeci L, Alonso A, Rahmouni S, Nika K, Rostamkhani M, et al. A functional variant of lymphoid tyrosine phosphatase is associated with type I diabetes. Nat Genet 2004;36:337–8.
2. Begovich AB, Carlton VE, Honigberg LA, Schrodi SJ, Chokkalingam AP, Alexander HC, et al. A missense single-nucleotide polymorphism in a gene encoding a protein tyrosine phosphatase (PTPN22) is associated with rheumatoid arthritis. Am J Hum Genet 2004;75:330–7.
3. Kyogoku C, Langefeld CD, Ortmann WA, Lee A, Selby S, Carlton VE, et al. Genetic association of the R620W polymorphism of protein tyrosine phosphatase PTPN22 with human SLE. Am J Hum Genet 2004;75:504–7.
4. Hinks A, Barton A, John S, Bruce I, Hawkins C, Griffiths CE, et al. Association between the PTPN22 gene and rheumatoid arthritis and juvenile idiopathic arthritis in a UK population: further support that PTPN22 is an autoimmunity gene. Arthritis Rheum 2005;52:1694–9.
5. Johansson M, Arlestig L, Hallmans G, Rantapaa-Dahlqvist S. PTPN22 polymorphism and anti-cyclic citrullinated peptide antibodies in combination strongly predicts future onset of rheumatoid arthritis and has a specificity of 100% for the disease. Arthritis Res Ther 2006;8:R19.
6. Feitsma AL, Toes RE, Begovich AB, Chokkalingam AP, de Vries RR, Huizinga TW, et al. Risk of progression from undifferentiated arthritis to rheumatoid arthritis: the effect of the PTPN22 1858T-allele in anti-citrullinated peptide antibody positive patients. Rheumatology (Oxford) 2007;46:1092–5.
7. Kokkonen H, Johansson M, Innala L, Jidell E, Rantapaa-Dahlqvist S. The PTPN22 1858C/T polymorphism is associated with anti-cyclic citrullinated peptide antibody-positive early rheumatoid arthritis in northern Sweden. Arthritis Res Ther 2007;9:R56.
8. Goeb V, Dieude P, Daveau R, Thomas-L'otellier M, Jouen F, Hau F, et al. Contribution of PTPN22 1858T, TNFRII 196R and HLA-shared epitope alleles with rheumatoid factor and anti-citrullinated protein antibodies to very early rheumatoid arthritis diagnosis. Rheumatology (Oxford) 2008;47:1208–12.
9. Potter C, Hyrich KL, Tracey A, Lunt M, Plant D, Symmons DP, et al. Association of rheumatoid factor and anti-cyclic citrullinated peptide positivity, but not carriage of shared epitope or PTPN22 susceptibility variants, with anti-tumour necrosis factor response in rheumatoid arthritis. Ann Rheum Dis 2009;68:69–74.
10. Kallberg H, Padyukov L, Plenge RM, Ronnelid J, Gregersen PK, van der Helm-van Mil AH, et al. Gene-gene and gene-environment interactions involving HLA-DRB1, PTPN22, and smoking in two subsets of rheumatoid arthritis. Am J Hum Genet 2007;80:867–75.
11. Costenbader KH, Chang SC, De Vivo I, Plenge R, Karlson EW. Genetic polymorphisms in PTPN22, PADI-4, and CTLA-4 and risk for rheumatoid arthritis in two longitudinal cohort studies: evidence of gene-environment interactions with heavy cigarette smoking. Arthritis Res Ther 2008;10:R52.
12. Lie BA, Viken MK, Odegard S, van der Heijde D, Landewe R, Uhlig T, et al. Associations between the PTPN22 1858C->T polymorphism and radiographic joint destruction in patients with rheumatoid arthritis: results from a 10-year longitudinal study. Ann Rheum Dis 2007;66:1604–9.
13. Karlson EW, Chibnik LB, Cui J, Plenge RM, Glass RJ, Maher NE, et al. Associations between human leukocyte antigen, PTPN22, CTLA4 genotypes and rheumatoid arthritis phenotypes of autoan-

tibody status, age at diagnosis and erosions in a large cohort study. Ann Rheum Dis 2008;67:358–63.

14. Majorczyk E, Pawlik A, Kusnierczyk P. PTPN22 1858C>T polymorphism is strongly associated with rheumatoid arthritis but not with a response to methotrexate therapy. Int Immunopharmacol 2010;10:1626–9.
15. Totaro MC, Tolusso B, Napolioni V, Faustini F, Canestri S, Mannocci A, et al. PTPN22 1858C>T polymorphism distribution in Europe and association with rheumatoid arthritis: case-control study and meta-analysis. PLoS One 2011;6:e24292.
16. Mastana S, Gilmour A, Ghelani A, Smith H, Samanta A. Association of PTPN22 with rheumatoid arthritis among South Asians in the UK. J Rheumatol 2007;34:1984–6.
17. Sfar I, Dhaouadi T, Habibi I, Abdelmoula L, Makhlouf M, Ben Romdhane T, et al. Functional polymorphisms of PTPN22 and FcgR genes in Tunisian patients with rheumatoid arthritis. Arch Inst Pasteur Tunis 2009;86:51–62.
18. Ates A, Karaaslan Y, Karatayli E, Ertugrul E, Aksaray S, Turkyilmaz A, et al. Association of the PTPN22 gene polymorphism with autoantibody positivity in Turkish rheumatoid arthritis patients. Tissue Antigens 2011;78:56–9.
19. Lee HS, Korman BD, Le JM, Kastner DL, Remmers EF, Gregersen PK, et al. Genetic risk factors for rheumatoid arthritis differ in Caucasian and Korean populations. Arthritis Rheum 2009;60:364–71.
20. Feng X, Li YZ, Zhang Y, Bao SM, Tong DW, Zhang SL, et al. Association of the PTPN22 gene (–1123G > C) polymorphism with rheumatoid arthritis in Chinese patients. Tissue Antigens 2010;76:297–300.
21. Viken MK, Amundsen SS, Kvien TK, Boberg KM, Gilboe IM, Lilleby V, et al. Association analysis of the 1858C>T polymorphism in the PTPN22 gene in juvenile idiopathic arthritis and other autoimmune diseases. Genes Immun 2005;6:271–3.
22. Lee YH, Bae SC, Song GG. The association between the functional PTPN22 1858 C/T and MIF –173 C/G polymorphisms and juvenile idiopathic arthritis: a meta-analysis. Inflamm Res 2012;61:411–5.
23. Kaalla MJ, Broadaway KA, Rohani-Pichavant M, Conneely KN, Whiting A, Ponder L, et al. Meta-analysis confirms association between TNFA-G238A variant and JIA, and between PTPN22-C1858T variant and oligoarticular, RF-polyarticular and RF-positive polyarticular JIA. Pediatr Rheumatol Online J 2013;11:40.
24. Bowes J, Loehr S, Budu-Aggrey A, Uebe S, Bruce IN, Feletar M, et al. PTPN22 is associated with susceptibility to psoriatic arthritis but not psoriasis: evidence for a further PsA-specific risk locus. Ann Rheum Dis 2015;74:1882–5.
25. Chen YF, Chang JS. PTPN22 C1858T and the risk of psoriasis: a meta-analysis. Mol Biol Rep 2012;39:7861–70.
26. Mehlhop-Williams ER, Bevan MJ. Memory CD8+ T cells exhibit increased antigen threshold requirements for recall proliferation. J Exp Med 2014;211:345–56.
27. Vang T, Landskron J, Viken MK, Oberprieler N, Torgersen KM, Mustelin T, et al. The autoimmune-predisposing variant of lymphoid tyrosine phosphatase favors T helper 1 responses. Hum Immunol 2013;74:574–85.
28. Bowes J, Budu-Aggrey A, Huffmeier U, Uebe S, Steel K, Hebert HL, et al. Dense genotyping of immune-related susceptibility loci reveals new insights into the genetics of psoriatic arthritis. Nat Commun 2015;6:6046.
29. Benham H, Norris P, Goodall J, Wechalekar MD, FitzGerald O, Szentpetery A, et al. Th17 and Th22 cells in psoriatic arthritis and psoriasis. Arthritis Res Ther 2013;15:R136.
30. De Lima SC, Adelino JE, Crovella S, de Azevedo Silva J, Sandrin-Garcia P. PTPN22 1858C > T polymorphism and susceptibility to systemic lupus erythematosus: a meta-analysis update. Autoimmunity 2017;50:428–34.
31. Hu LY, Cheng Z, Zhang B, Yin Q, Zhu XW, Zhao PP, et al. Associations between PTPN22 and TLR9 polymorphisms and systemic lupus erythematosus: a comprehensive meta-analysis. Arch Dermatol Res 2017;309:461–77.
32. Kariuki SN, Crow MK, Niewold TB. The PTPN22 C1858T polymorphism is associated with skewing of cytokine profiles toward high interferon-α activity and low tumor necrosis factor α levels in patients with lupus. Arthritis Rheum 2008;58:2818–23.
33. Reddy MV, Johansson M, Sturfelt G, Jonsen A, Gunnarsson I, Svenungsson E, et al. The R620W C/T polymorphism of the gene PTPN22 is associated with SLE independently of the association of PDCD1. Genes Immun 2005;6:658–62.
34. Ostanek L, Ostanek-Panka M, Bobrowska-Snarska D, Binczak-Kuleta A, Fischer K, Kaczmarczyk M, et al. PTPN22 1858C>T gene polymorphism in patients with SLE: association with serological and clinical results. Mol Biol Rep 2014;41:6195–200.
35. Jagiello P, Aries P, Arning L, Wagenleiter SE, Csernok E, Hellmich B, et al. The PTPN22 620W allele is a risk factor for Wegener's granulomatosis. Arthritis Rheum 2005;52:4039–43.
36. Carr EJ, Niederer HA, Williams J, Harper L, Watts RA, Lyons PA, et al. Confirmation of the genetic association of CTLA4 and PTPN22 with ANCA-associated vasculitis. BMC Med Genet 2009;10:121.
37. Martorana D, Maritati F, Malerba G, Bonatti F, Alberici F, Oliva E, et al. PTPN22 R620W polymorphism in the ANCA-associated vasculitides. Rheumatology (Oxford) 2012;51:805–12.
38. Cao Y, Liu K, Tian Z, Hogan SL, Yang J, Poulton CJ, et al. PTPN22 R620W polymorphism and ANCA disease risk in white populations: a metaanalysis. J Rheumatol 2015;42:292–9.
39. Jennette JC, Falk RJ. Pathogenesis of antineutrophil cytoplasmic autoantibody-mediated disease. Nat Rev Rheumatol 2014;10:463–73.
40. Gonzalez-Gay MA, Oliver J, Orozco G, Garcia-Porrua C, Lopez-Nevot MA, Martin J. Lack of association of a functional single nucleotide polymorphism of PTPN22, encoding lymphoid protein phosphatase, with susceptibility to biopsy-proven giant cell arteritis. J Rheumatol 2005;32:1510–2.
41. Serrano A, Marquez A, Mackie SL, Carmona FD, Solans R, Miranda-Filloy JA, et al. Identification of the PTPN22 functional variant R620W as susceptibility genetic factor for giant cell arteritis. Ann Rheum Dis 2013;72:1882–6.
42. Lester S, Hewitt AW, Ruediger CD, Bradbury L, De Smit E, Wiese MD, et al. PTPN22 R620W minor allele is a genetic risk factor for giant cell arteritis. RMD Open 2016;2:e000246.
43. Carmona FD, Mackie SL, Martín JE, Taylor JC, Vaglio A, Eyre S, et al. A large-scale genetic analysis reveals a strong contribution of the HLA class II region to giant cell arteritis susceptibility. Am J Hum Genet 2015;96:565–80.
44. Stanford SM, Bottini N. PTPN22: the archetypal non-HLA autoimmunity gene. Nat Rev Rheumatol 2014;10:602–11.
45. Ortiz-Fernández L, Montes-Cano MA, García-Lozano JR, Conde-Jaldón M, Ortego-Centeno N, González-Leon R, et al. PTPN22 is not associated with Behçet's disease. Study spanning the complete gene region in the Spanish population and meta-analysis of the functional variant R620W. Clin Exp Rheumatol 2016;34(6 Suppl 102):S41–5.
46. Dieudé P, Guedj M, Wipff J, Avouac J, Hachulla E, Diot E, et al. The PTPN22 620W allele confers susceptibility to systemic sclerosis: findings of a large case–control study of European Caucasians and a meta-analysis. Arthritis Rheum 2008;58:2183–8.
47. Zheng J, Ibrahim S, Petersen F, Yu X. Meta-analysis reveals an association of PTPN22 C1858T with autoimmune diseases, which depends on the localization of the affected tissue. Genes Immun 2012;13:641–52.

48. Fan ZD, Wang FF, Huang H, Huang N, Ma HH, Guo YH, et al. STAT4 rs7574865 G/T and PTPN22 rs2488457 G/C polymorphisms influence the risk of developing juvenile idiopathic arthritis in Han Chinese patients. PLoS One 2015;10:e0117389.
49. Chen Z, Zhang H, Xia B, Wang P, Jiang T, Song M, et al. Association of PTPN22 gene (rs2488457) polymorphism with ulcerative colitis and high levels of PTPN22 mRNA in ulcerative colitis. Int J Colorectal Dis 2013;28:1351–8.
50. Walsh AM, Whitaker JW, Huang CC, Cherkas Y, Lamberth SL, Brodmerkel C, et al. Integrative genomic deconvolution of rheumatoid arthritis GWAS loci into gene and cell type associations. Genome Biol 2016;17:79.
51. Remuzgo-Martinez S, Genre F, Castaneda S, Corrales A, Moreno-Fresneda P, Ubilla B, et al. Protein tyrosine phosphatase nonreceptor 22 and C-Src tyrosine kinase genes are down-regulated in patients with rheumatoid arthritis. Sci Rep 2017;7:10525.
52. Orru V, Tsai SJ, Rueda B, Fiorillo E, Stanford SM, Dasgupta J, et al. A loss-of-function variant of PTPN22 is associated with reduced risk of systemic lupus erythematosus. Hum Mol Genet 2009;18:569–79.
53. Bae SC, Lee YH. Association between the functional PTPN22 G788A (R263Q) polymorphism and susceptibility to autoimmune diseases: a meta-analysis. Cell Mol Biol (Noisy-le-grand) 2018;64:46–51.
54. Diaz-Gallo LM, Espino-Paisan L, Fransen K, Gomez-Garcia M, van Sommeren S, Cardena C, et al. Differential association of two PTPN22 coding variants with Crohn's disease and ulcerative colitis. Inflamm Bowel Dis 2011;17:2287–94.
55. Cohen S, Dadi H, Shaoul E, Sharfe N, Roifman CM. Cloning and characterization of a lymphoid-specific, inducible human protein tyrosine phosphatase, Lyp. Blood 1999;93:2013–24.
56. Cloutier JF, Veillette A. Association of inhibitory tyrosine protein kinase p50csk with protein tyrosine phosphatase PEP in T cells and other hemopoietic cells. EMBO J 1996;15:4909–18.
57. Bergman M, Mustelin T, Oetken C, Partanen J, Flint NA, Amrein KE, et al. The human p50csk tyrosine kinase phosphorylates p56l-ck at Tyr-505 and down regulates its catalytic activity. EMBO J 1992;11:2919–24.
58. Mustelin T, Tasken K. Positive and negative regulation of T-cell activation through kinases and phosphatases. Biochem J 2003;371:15–27.
59. Gjorloff-Wingren A, Saxena M, Williams S, Hammi D, Mustelin T. Characterization of TCR-induced receptor-proximal signaling events negatively regulated by the protein tyrosine phosphatase PEP. Eur J Immunol 1999;29:3845–54.
60. Hasegawa K, Martin F, Huang G, Tumas D, Diehl L, Chan AC. PEST domain-enriched tyrosine phosphatase (PEP) regulation of effector/memory T cells. Science 2004;303:685–9.
61. Maine CJ, Marquardt K, Cheung J, Sherman LA. PTPN22 controls the germinal center by influencing the numbers and activity of T follicular helper cells. J Immunol 2014;192:1415–24.
62. Brownlie RJ, Miosge LA, Vassilakos D, Svensson LM, Cope A, Zamoyska R. Lack of the phosphatase PTPN22 increases adhesion of murine regulatory T cells to improve their immunosuppressive function. Sci Signal 2012;5:ra87.
63. Vang T, Congia M, Macis MD, Musumeci L, Orru V, Zavattari P, et al. Autoimmune-associated lymphoid tyrosine phosphatase is a gain-of-function variant. Nat Genet 2005;37:1317–9.
64. Wallis AM, Wallace EC, Hostager BS, Yi Z, Houtman JC, Bishop GA. TRAF3 enhances TCR signaling by regulating the inhibitors Csk and PTPN22. Sci Rep 2017;7:2081.
65. Hill RJ, Zozulya S, Lu YL, Ward K, Gishizky M, Jallal B. The lymphoid protein tyrosine phosphatase Lyp interacts with the adaptor molecule Grb2 and functions as a negative regulator of T-cell activation. Exp Hematol 2002;30:237–44.
66. Spencer S, Dowbenko D, Cheng J, Li W, Brush J, Utzig S, et al. PSTPIP: a tyrosine phosphorylated cleavage furrow-associated protein that is a substrate for a PEST tyrosine phosphatase. J Cell Biol 1997;138:845–60.
67. Chang HH, Dwivedi N, Nicholas AP, Ho IC. The W620 polymorphism in PTPN22 disrupts its interaction with peptidylarginine deiminase type 4 and enhances citrullination and NETosis. Arthritis Rheumatol 2015;67:2323–34.
68. Lin WW, Yi Z, Stunz LL, Maine CJ, Sherman LA, Bishop GA. The adaptor protein TRAF3 inhibits interleukin-6 receptor signaling in B cells to limit plasma cell development. Sci Signal 2015;8:ra88.
69. Wise CA, Bennett LB, Pascual V, Gillum JD, Bowcock AM. Localization of a gene for familial recurrent arthritis. Arthritis Rheum 2000;43:2041–5.
70. Shoham NG, Centola M, Mansfield E, Hull KM, Wood G, Wise CA, et al. Pyrin binds the PSTPIP1/CD2BP1 protein, defining familial Mediterranean fever and PAPA syndrome as disorders in the same pathway. Proc Natl Acad Sci U S A 2003;100:13501–6.
71. Wise CA, Gillum JD, Seidman CE, Lindor NM, Veile R, Bashiardes S, et al. Mutations in CD2BP1 disrupt binding to PTP PEST and are responsible for PAPA syndrome, an autoinflammatory disorder. Hum Mol Genet 2002;11:961–9.
72. Spalinger MR, Kasper S, Gottier C, Lang S, Atrott K, Vavricka SR, et al. NLRP3 tyrosine phosphorylation is controlled by protein tyrosine phosphatase PTPN22. J Clin Invest 2016;126:1783–1800.
73. Marson A, Kretschmer K, Frampton GM, Jacobsen ES, Polansky JK, MacIsaac KD, et al. Foxp3 occupancy and regulation of key target genes during T-cell stimulation. Nature 2007;445:931–5.
74. Li QJ, Chau J, Ebert PJ, Sylvester G, Min H, Liu G, et al. miR-181a is an intrinsic modulator of T cell sensitivity and selection. Cell 2007;129:147–61.
75. Vang T, Miletic AV, Bottini N, Mustelin T. Protein tyrosine phosphatase PTPN22 in human autoimmunity. Autoimmunity 2007;40:453–61.
76. Bottini N, Vang T, Cucca F, Mustelin T. Role of PTPN22 in type 1 diabetes and other autoimmune diseases. Semin Immunol 2006;18:207–13.
77. Aarnisalo J, Treszl A, Svec P, Marttila J, Oling V, Simell O, et al. Reduced CD4+ T cell activation in children with type 1 diabetes carrying the PTPN22/Lyp 620Trp variant. J Autoimmun 2008;31:13–21.
78. Zheng J, Petersen F, Yu X. The role of PTPN22 in autoimmunity: learning from mice. Autoimmun Rev 2014;13:266–71.
79. Rieck M, Arechiga A, Onengut-Gumuscu S, Greenbaum C, Concannon P, Buckner JH. Genetic variation in PTPN22 corresponds to altered function of T and B lymphocytes. J Immunol 2007;179:4704–10.
80. Zhang J, Zahir N, Jiang Q, Miliotis H, Heyraud S, Meng X, et al. The autoimmune disease-associated PTPN22 variant promotes calpain-mediated Lyp/Pep degradation associated with lymphocyte and dendritic cell hyperresponsiveness. Nat Genet 2011;43:902–7.
81. Menard L, Saadoun D, Isnardi I, Ng YS, Meyers G, Massad C, et al. The PTPN22 allele encoding an R620W variant interferes with the removal of developing autoreactive B cells in humans. J Clin Invest 2011;121:3635–44.
82. Schickel JN, Kuhny M, Baldo A, Bannock JM, Massad C, Wang H, et al. PTPN22 inhibition resets defective human central B cell tolerance. Sci Immunol 2016;1:aaf7153.
83. Metzler G, Dai X, Thouvenel CD, Khim S, Habib T, Buckner JH, et al. The autoimmune risk variant PTPN22 C1858T alters B cell tolerance at discrete checkpoints and differentially shapes the naive repertoire. J Immunol 2017;199:2249–60.
84. Dai X, James RG, Habib T, Singh S, Jackson S, Khim S, et al. A disease-associated PTPN22 variant promotes systemic autoimmunity in murine models. J Clin Invest 2013;123:2024–36.

85. Elkon KB. Cell death, nucleic acids, and immunity: inflammation beyond the grave [review]. Arthritis Rheumatol 2018;70:805–16.
86. Gupta S, Kaplan MJ. The role of neutrophils and NETosis in autoimmune and renal diseases. Nat Rev Nephrol 2016;12:402–13.
87. Lood C, Blanco LP, Purmalek MM, Carmona-Rivera C, De Ravin SS, Smith CK, et al. Neutrophil extracellular traps enriched in oxidized mitochondrial DNA are interferogenic and contribute to lupus-like disease. Nat Med 2016;22:146–53.
88. Li M, Beauchemin H, Popovic N, Peterson A, d'Hennezel E, Piccirillo CA, et al. The common, autoimmunity-predisposing 620Arg > Trp variant of PTPN22 modulates macrophage function and morphology. J Autoimmun 2017;79:74–83.
89. Chang HH, Miaw SC, Tseng W, Sun YW, Liu CC, Tsao HW, et al. PTPN22 modulates macrophage polarization and susceptibility to dextran sulfate sodium-induced colitis. J Immunol 2013;191:2134–43.
90. Vermeren S, Miles K, Chu JY, Salter D, Zamoyska R, Gray M. PTPN22 is a critical regulator of fcγ receptor-mediated neutrophil activation. J Immunol 2016;197:4771–9.
91. Bayley R, Kite KA, McGettrick HM, Smith JP, Kitas GD, Buckley CD, et al. The autoimmune-associated genetic variant PTPN22 R620W enhances neutrophil activation and function in patients with rheumatoid arthritis and healthy individuals. Ann Rheum Dis 2015;74:1588–95.
92. Cao Y, Yang J, Colby K, Hogan SL, Hu Y, Jennette CE, et al. High basal activity of the PTPN22 gain-of-function variant blunts leukocyte responsiveness negatively affecting IL-10 production in ANCA vasculitis. PLoS One 2012;7:e42783.
93. Falk RJ, Terrell RS, Charles LA, Jennette JC. Anti-neutrophil cytoplasmic autoantibodies induce neutrophils to degranulate and produce oxygen radicals in vitro. Proc Natl Acad Sci U S A 1990;87:4115–9.
94. Kessenbrock K, Krumbholz M, Schonermarck U, Back W, Gross WL, Werb Z, et al. Netting neutrophils in autoimmune small-vessel vasculitis. Nat Med 2009;15:623–5.
95. Mark EJ, Matsubara O, Tan-Liu NS, Fienberg R. The pulmonary biopsy in the early diagnosis of Wegener's (pathergic) granulomatosis: a study based on 35 open lung biopsies. Hum Pathol 1988;19:1065–71.
96. Sood S, Brownlie RJ, Garcia C, Cowan G, Salmond RJ, Sakaguchi S, et al. Loss of the protein tyrosine phosphatase PTPN22 reduces mannan-induced autoimmune arthritis in SKG mice. J Immunol 2016;197:429–40.

AMERICAN COLLEGE OF RHEUMATOLOGY
EDUCATION • TREATMENT • RESEARCH

Arthritis & Rheumatology
Vol. 71, No. 4, April 2019, pp 496–506
DOI 10.1002/art.40771

Myocardial Inflammation, Measured Using 18-Fluorodeoxyglucose Positron Emission Tomography With Computed Tomography, Is Associated With Disease Activity in Rheumatoid Arthritis

Isabelle Amigues, Aylin Tugcu, Cesare Russo, Jon T. Giles, Rachelle Morgenstein, Afshin Zartoshti, Christian Schulze, Raul Flores, Sabahat Bokhari, and Joan M. Bathon

Objective. To determine the prevalence and correlates of subclinical myocardial inflammation in patients with rheumatoid arthritis (RA).

Methods. RA patients (n = 119) without known cardiovascular disease underwent cardiac 18-fluorodeoxyglucose (FDG) positron emission tomography with computed tomography (PET-CT). Myocardial FDG uptake was assessed visually and measured quantitatively as the standardized uptake value (SUV). Multivariable linear regression was used to assess the associations of patient characteristics with myocardial SUVs. A subset of RA patients who had to escalate their disease-modifying antirheumatic drug (DMARD) therapy (n = 8) underwent a second FDG PET-CT scan after 6 months, to assess treatment-associated changes in myocardial FDG uptake.

Results. Visually assessed FDG uptake was observed in 46 (39%) of the 119 RA patients, and 21 patients (18%) had abnormal quantitatively assessed myocardial FDG uptake (i.e., mean of the mean SUV [SUV_{mean}] ≥3.10 units; defined as 2 SD above the value in a reference group of 27 non-RA subjects). The SUV_{mean} was 31% higher in patients with a Clinical Disease Activity Index (CDAI) score of ≥10 (moderate-to-high disease activity) as compared with those with lower CDAI scores (low disease activity or remission) (P = 0.005), after adjustment for potential confounders. The adjusted SUV_{mean} was 26% lower among those treated with a non–tumor necrosis factor–targeted biologic agent compared with those treated with conventional (nonbiologic) DMARDs (P = 0.029). In the longitudinal substudy, the myocardial SUV_{mean} decreased from 4.50 units to 2.30 units over 6 months, which paralleled the decrease in the mean CDAI from a score of 23 to a score of 12.

Conclusion. Subclinical myocardial inflammation is frequent in patients with RA, is associated with RA disease activity, and may decrease with RA therapy. Future longitudinal studies will be required to assess whether reduction in myocardial inflammation will reduce heart failure risk in RA.

INTRODUCTION

Heart failure, a key contributor to cardiovascular disease (CVD) morbidity and mortality in rheumatoid arthritis (RA) (1,2), is associated on average with fewer symptoms and higher (preserved) ejection fraction, but higher mortality rates, when compared with the general population (1–4). In the general population, higher levels of circulating proinflammatory cytokines, such as tumor necrosis factor (TNF) and interleukin-6 (IL-6), are independent predictors of heart failure (5–9). In rodents, infusion of TNF reduced myocardial contractility (10), and cardiac-specific overexpression of a TNF transgene was associated with myocardial

The content is solely the responsibility of the authors and does not necessarily represent the official views of the National Institutes of Health.

Supported in part by the NIH (National Center for Translational Science Clinical and Translational Science Award UL1-TR000040). Dr. Bathon's work was supported by the NIH (National Institute of Arthritis and Musculoskeletal and Skin Diseases grant AR-050026) and the Rheumatology Research Foundation (RHEUMARF CU12-3892).

Isabelle Amigues, MD, Aylin Tugcu, MD (current address: Bristol-Myers Squibb, Lawrenceville, New Jersey), Cesare Russo, MD (current address: Novartis Institutes for BioMedical Research, Basel, Switzerland), Jon T. Giles, MD, MPH, Rachelle Morgenstein, MPH, Afshin Zartoshti, MSc, Christian Schulze, MD, PhD (current address: University Hospital Jena, Friedrich-Schiller-University Jena, Jena, Germany), Raul Flores, MD, Sabahat Bokhari, MD, Joan M. Bathon, MD: Columbia University College of Physicians and Surgeons, and New York Presbyterian Hospital, New York, New York.

Dr. Tugcu owns stock or stock options in Bristol-Myers Squibb. Dr. Russo owns stock or stock options in Novartis. No other disclosures relevant to this article were reported.

Address correspondence to Joan M. Bathon, MD, Division of Rheumatology, Department of Medicine, Columbia University, Vagelos College of Physicians and Surgeons, 630 West 168th Street, New York, NY 10032. E-mail: jmb2311@cumc.columbia.edu.

Submitted for publication January 9, 2018; accepted in revised form November 1, 2018.

inflammation, remodeling, fibrosis, and eventually heart failure (11–13). In RA, circulating levels of TNF and IL-6 are orders of magnitude higher than those shown to predict heart failure in the general population (14); however, little is known about inflammatory processes within the RA myocardium itself. Autopsy studies of RA hearts from the mid-twentieth century suggested that myocarditis may occur in 15–20% of RA patients (15,16). However, contemporary histologic characterization studies of the myocardium in RA patients are few, mostly limited to patients with a known history of ischemic CVD (14).

The conventional gold standard for diagnosing myocarditis is endomyocardial biopsy. However, its sensitivity is limited by the heterogeneous distribution of myocarditis (17,18). This, coupled with its invasiveness, expense, and risk of complications, has limited investigations of subclinical myocarditis in patients with RA. Cardiac magnetic resonance (CMR) with late gadolinium enhancement (LGE) has been used to identify myocardial abnormalities, but clinically approved gadolinium-based contrast agents distribute to the extracellular space (19) and are not taken up by cells. Thus, myocardial LGE reflects interstitial edema but cannot directly identify inflammatory infiltrates, nor can LGE identify diffuse myocardial involvement, only focal (20–23). CMR T2-weighted imaging (T2WI), a more sensitive method for measuring myocardial edema that is not dependent on gadolinium, may overcome the latter issue but does not solve the former limitation (24).

In recent years, 18-fluorodeoxyglucose (FDG) positron emission tomography with computed tomography (PET-CT) has been shown to have high sensitivity for detecting myocardial inflammation. Inflammatory cells are metabolically active and avidly take up FDG via glucose transporters. Moreover, areas of myocardial FDG uptake strongly correlate with the numbers of infiltrating macrophages and T cells on histologic assessment (25,26). In the current study, we assessed myocardial FDG uptake among RA patients with no known history of CVD. In a nested substudy of RA patients who experienced an inadequate response to methotrexate monotherapy, we evaluated the change in myocardial FDG uptake in response to 6 months of step-up therapy. We hypothesized that myocardial inflammation would be present in a proportion of RA patients without clinical heart failure, and its presence would be correlated with RA disease activity and with the levels of circulating inflammatory mediators, and would decrease upon up-regulation of treatment.

PATIENTS AND METHODS

Patients. RA patients enrolled in the Rheumatoid Arthritis Study of the Myocardium (RHYTHM), which has been described previously (27), were recruited for the present study. Participants were recruited from the rheumatology clinics of Columbia University Medical Center (CUMC) and by referral from local rheumatologists. Inclusion criteria were age ≥18 years and fulfillment of the American College of Rheumatology/European League Against Rheumatism 2010 classification criteria for RA (28). Exclusion criteria included the following: 1) any prior self-reported physician-diagnosed CV event or procedure, contraindication to pharmacologic stress agents, and active cancer.

The study sample consisted of 119 RA patients from the RHYTHM study who had FDG PET-CT scans that were technically adequate to evaluate myocardial FDG uptake. Eight of the 119 RA patients took part in a nested, longitudinal pilot substudy that required the presence of active disease, specifically a Clinical Disease Activity Index (CDAI) score of ≥10, despite having received methotrexate monotherapy. Therapy was escalated to either a TNF inhibitor (with continued methotrexate) or triple therapy (i.e., sulfasalazine plus hydroxychloroquine with continued methotrexate). Originally, escalation was assigned randomly; however, due to slow recruitment, the protocol was switched to an open-label TNF inhibitor (either etanercept or adalimumab), such that 2 patients received triple therapy and 6 received a TNF inhibitor. These RA patients underwent a second FDG PET-CT scan after 6 months of treatment, to evaluate change in myocardial FDG uptake with treatment.

There is no established normative cutoff value for myocardial FDG uptake. Accordingly, we assembled a control group made up of volunteers without RA who were recruited from friends of RHYTHM participants and advertisements. Additional controls without RA or other rheumatic diseases were added from the CUMC nuclear cardiology archive. These control subjects, none of whom had visible FDG uptake, underwent FDG PET-CT during the same enrollment period as the RHYTHM study (i.e., 2011–2016) to rule out myocarditis or cardiac sarcoidosis, using a similar scanning protocol as that of the RHYTHM study.

The study was approved by the CUMC, New York Presbyterian Hospital Institutional Review Board. All subjects provided written informed consent prior to enrollment.

Outcome assessments. The primary outcome was myocardial FDG uptake, as assessed by PET-CT scanning. To suppress physiologic uptake of FDG by cardiomyocytes, patients were prescribed a high-fat, no-carbohydrate diet the day before the scan, followed by a 12-hour fast prior to the scan (29,30). Dietary adherence was interrogated on the day of the scan. All patients had a blood sugar concentration of <200 mg/dl at the time of imaging.

Imaging was performed on an MCT 64 PET/CT scanner (Siemens Medical Solutions). A low-dose CT transmission scan was obtained for attenuation correction of the PET data. Patients were injected with 10 mCi of ^{18}F-FDG intravenously. A list mode 3-dimensional PET scan was acquired for 10 minutes, following a 90-minute uptake period after ^{18}F-FDG injection. Nongated attenuation-corrected images were reconstructed, yielding an effective resolution of ~3 mm.

Corridor4DM version 7.0 software (Invia Medical Imaging Solutions) was used to assess myocardial FDG uptake.

Table 1. Characteristics of the study participants according to RA status*

Characteristic	RA patients (n = 119)	Controls (n = 27)
Demographic		
Age, mean ± SD (range) years	54 ± 13 (21–80)	50 ± 12
Female	97 (82)	13 (48)
Race/ethnicity		
Non-Hispanic white	44 (37)	–
Non-Hispanic black	18 (15)	–
Hispanic	53 (44)	–
Other	4 (3.4)	–
Cardiovascular risk factor		–
Ever smoker	52 (44)	7 (26)
Current smoker	13 (11)	1 (4)
Hypertension	46 (39)	10 (37)
Diabetes	15 (13)	2 (8)
BMI, mean ± SD kg/m^2	28.5 ± 5.9	33.6 ± 4.8
Total cholesterol, mean ± SD mg/dl	191 ± 37	–
LDL-C, mean ± SD mg/dl	110 ± 32	–
HDL-C, mean ± SD mg/dl	59 ± 19	–
RA characteristic		
RA duration, median (IQR) years	6.7 (2–14.1)	–
RF or anti-CCP seropositive	91 (76)	–
DAS28-CRP, median (IQR)	3.9 (3.0–4.7)	–
CDAI, mean ± SD	18.2 ± 12.1	–
HAQ score, mean ± SD	1.7 ± 0.8	–
Morning stiffness, median (IQR) minutes	20 (5–50)	–
CRP, median (IQR) mg/liter	2.51 (1.1–6.6)	0.64 (0.45–2.94)
IL-6, median (IQR) pg/ml	2.3 (1.4–7.3)	0.94 (0.80–2.26)
Troponin I, median	Undetectable	–
BNP, median (IQR) pg/ml	15.4 (10–26.2)	–
RA medication		
No DMARD	15 (13)	–
Nonbiologic DMARD†	91 (77)	–
Methotrexate	77 (67)	–
Other‡	26 (22)	–
Biologic DMARD	45 (38)	–
TNF inhibitor	35 (29)	–
Non-TNF biologic	10 (8)	–
Abatacept	8 (7)	–
Other§	2 (2)	–
Prednisone	39 (33)	0 (0)
NSAIDs	49 (41)	0 (0)
CAC score		
CAC score null	78 (65.6)	9 (69.2)
CAC score 1–99 units	19 (16)	2 (15.4)
CAC score ≥100 units	22 (18)	2 (15.4)

Table 1. *(Cont'd)*

Characteristic	RA patients (n = 119)	Controls (n = 27)
Myocardial structure		
LVMI, mean ± SD grams/height$^{2.73}$	29.9 ± 5.41	–
EDVI, mean ± SD ml/m^2	53.8 ± 11	–
ESVI, median (IQR) ml/m^2	19.4 (16–23)	–
Myocardial function		
Ejection fraction, mean ± SD %	62.9 ± 4.5	–
E/E′, mean ± SD	8.5 ± 2.4	–
Stroke volume index, mean ± SD ml/m^2	58.6 ± 13.9	–
Cardiac index, mean ± SD liters/minute/m^2	2.29 ± 0.38	–
Diastolic dysfunction, yes versus no	49 (43)	–

* Except where indicated otherwise, values are the number (%) of rheumatoid arthritis (RA) patients or non-RA control subjects. BMI = body mass index; LDL-C = low-density lipoprotein cholesterol; HDL-C = high-density lipoprotein cholesterol; IQR = interquartile range; RF = rheumatoid factor; anti-CCP = anti–cyclic citrullinated peptide (antibody); DAS28-CRP = Disease Activity Score in 28 joints using C-reactive protein level; CDAI = Clinical Disease Activity Index; HAQ = Health Assessment Questionnaire; IL-6 = interleukin-6; BNP = brain natriuretic peptide; NSAIDs = nonsteroidal antiinflammatory drugs; CAC = coronary artery calcium; LVMI = left ventricular mass indexed to height$^{2.73}$; EDVI = end-diastolic volume index; ESVI = end-systolic volume index.
† Patients may have been taking more than 1 nonbiologic disease-modifying antirheumatic drug (DMARD).
‡ Other nonbiologics included sulfasalazine, hydroxychloroquine, or leflunomide.
§ Other non–tumor necrosis factor (TNF) biologics included rituximab and tocilizumab.

Cardiac axes were defined manually by marking the base on the vertical long axis, the apex on the horizontal long axis, and the left ventricular (LV) cavity on the sagittal axis. Qualitative and quantitative assessment of FDG uptake was performed on all scans by a nuclear cardiologist (SB) who was blinded with regard to each patient's disease status. FDG uptake was assessed quantitatively as the standardized uptake value (SUV), a measure of radiotracer uptake normalized for injected dose and patient weight. The reconstruction produced a set of transverse slices through the heart perpendicular to the long axis of the body, which was used to generate sets of sagittal and coronal slices. LV segments were defined according to the segmentation nomenclature of the American Heart Association (31). Contours were placed on the myocardial walls, and automated calculations of the SUVs, both the mean SUV and the maximum SUV, for each of the segments were derived. The mean of the mean SUV (SUV_{mean}) and the mean of the maximum SUV (SUV_{max}) were then obtained.

Other measures. *Assessment of coronary artery calcium (CAC)*. CAC was assessed from the CT scan and quantified using the Agatston method (32). The presence of CAC was defined as an Agatston score of >0.

Echocardiographic parameters. Transthoracic 2-dimensional and real-time 3-dimensional echocardiography (RT3DE) was performed using a commercially available system (iE 33; Philips) by a registered cardiac sonographer (AT or CR), according to a standardized protocol. The LV end-diastolic volume index (EDVI) and end-systolic volume index (ESVI), stroke volume, and LV ejection fraction (LVEF) were each measured by RT3DE using a commercially available software (Philips QLAB Advanced Quantification software, version 8.1) as previously described (33). LV mass was also assessed by RT3DE, using tracings of the endocardial and epicardial borders. Left atrial (LA) volume and LV diastolic function were measured by 2-dimensional echocardiography, as previously described (34). Briefly, in apical 4-chamber view, the peak early velocity of mitral inflow (E) and late velocity of mitral inflow (A) were measured by pulsed-wave Doppler. The peak early diastolic velocities (E′) of the lateral and septal mitral annulus were evaluated by pulsed-wave tissue Doppler, and mean values were calculated. The E/E′ ratio was calculated as an index of LV filling pressure. LV volumes, stroke volume, cardiac output, and LA volume were indexed by body surface area. LV mass was indexed to height$^{2.73}$. LV diastolic dysfunction was defined as an abnormality in any of the following parameters: E/A ratio (abnormal defined as either <0.8 or >2.0), E deceleration time (abnormal defined as >240 msec or <140 msec), peak E′ (abnormal defined as <8 cm/second), or E/E′ (abnormal defined as >15).

Clinical covariates. Demographic and lifestyle characteristics of the study participants and current medications were as-

sessed by structured interview. Resting blood pressure (BP) was measured 3 times, and the mean of the last 2 measurements was used. Hypertension was defined as a systolic BP of ≥140 mm Hg, diastolic BP of ≥90 mm Hg, or use of antihypertensive medications. Diabetes was defined as a fasting serum glucose level of ≥126 mg/dl or use of antidiabetic medications. Body mass index (BMI) was calculated as patient weight (in kilograms) divided by height (in square meters).

RA disease duration was calculated from the date of diagnosis. Forty-four joints were examined for swelling and tenderness. RA disease activity was calculated with the CDAI (score range <10 for remission or low disease activity to ≥10 for moderate-to-high disease activity) and the Disease Activity Score in 28 joints using C-reactive protein level (DAS28-CRP) (35–37). Disability was assessed with the Health Assessment Questionnaire (HAQ) (38). Current and past use of steroids and biologic and nonbiologic disease-modifying antirheumatic drugs (DMARDs) were determined using examiner-administered questionnaires.

Laboratory covariates. Serum and plasma samples from patients, obtained during a fasting state, were collected on the morning of the study visit. Lipid levels were measured by colormetric assay, and high-sensitivity CRP levels were determined by turbidimetric immunoassay (Roche Diagnostics). Rheumatoid factor (RF), anti–cyclic citrullinated peptide (anti-CCP) antibodies, and IL-6 were measured by enzyme-linked immunosorbent assays (ELISAs) (IBL America, Inova Diagnostics, and R&D Systems, respectively). Seropositivity for RF and for anti-CCP were defined according to cutoff levels of ≥40 units and ≥60 units, respectively. Brain naturetic peptide (BNP) and troponin I were measured using an Architect chemiluminescent microparticle immunoassay (Abbott Laboratories).

Statistical analysis. Summary statistics for continuous and categorical variables were calculated, including mean values with standard deviations, ranges, counts, and percentages. Multivariable linear regression was used to model the associations of RA patient characteristics with the natural log-transformed myocardial SUV_{mean} and SUV_{max}, being analyzed first in univariate models in which each independent variable was modeled as the only covariate in the model. Independent variables found to be associated with the myocardial SUV outcome at a significance level of $P < 0.25$ were carried into multivariable models. Extended models were reduced to more parsimonious models using Akaike's Information Criterion for nested models.

We calculated variance inflation factors to ensure that collinear variables were not co-modeled, and none were detected for any of the primary models. Linear regression was also used to model SUV_{mean} and SUV_{max} levels according to groups defined by visualized myocardial FDG uptake (i.e., none, focal, diffuse, and focal on diffuse). Statistical *t*-tests were used to compare baseline natural log-transformed SUV_{mean} and SUV_{max} levels in the RA group with baseline levels of these measures in the non-RA control group. In addition, a paired *t*-test was used to compare the baseline and follow-up myocardial SUV levels within the RA group. Throughout, a 2-tailed alpha level of 0.05 was used, and analyses were performed using Stata version 14 (StataCorp).

RESULTS

Characteristics of the study patients. Baseline characteristics of the 119 RA patients are summarized in Table 1. The mean age was 54 years, and median disease duration was 6.7 years. The majority of patients (82%) were female, and those of Hispanic or non-Hispanic white race/ethnicity made up 80% of the cohort. Among the RA patients, 44% were ever smokers and 11% were current smokers. The majority of patients were seropositive for RF and/or anti-CCP (76%), and the distribution of DAS28-CRP scores indicated that most patients were in the low or moderate range of disease activity. Remission (defined as a DAS28-CRP of <2.6) and high disease activity (defined as a DAS28-CRP of ≥5.2) were observed in 15% and 10% of

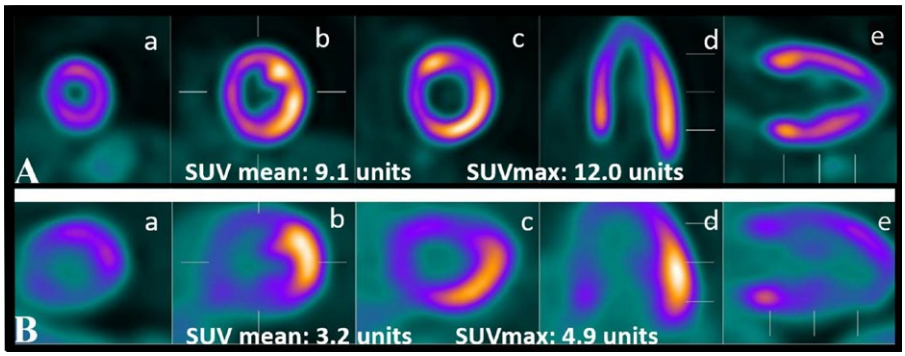

Figure 1. Examples of diffuse (**A**) and focal (**B**) myocardial 18-fluorodeoxyglucose uptake, as measured using cardiac 18-fluorodeoxyglucose positron emission tomography with computed tomography, in 2 patients with rheumatoid arthritis. Panels **a**, **b**, and **c** represent the short axis, panel **d** represents the horizontal axis, and panel **e** represents the vertical long axis. SUV_{mean} = mean of the mean standardized uptake value; SUV_{max} = mean of the maximum standardized uptake value.

patients, respectively (data not shown). The majority of patients (87%) were treated with DMARDs, with 77% being treated with nonbiologic DMARDs (the majority of whom were receiving methotrexate) and 38% being treated with biologic agents (the majority of whom were receiving TNF inhibitors). One-third were currently taking prednisone, and 41% reported taking nonsteroidal antiinflammatory drugs. More than two-thirds of the patients had signs of CAC (Agatston score >0) on CT. Troponin I was undetectable in the samples from all RA patients (data not shown). The median BNP level was in the normal range (Table 1).

Association of myocardial FDG uptake with disease activity and RA treatment. Any visually assessed myocardial FDG uptake was detected in 46 (39%) of the 119 RA patients. Of these, 25 (54%) had focal uptake only, and 21 (45%) had any diffuse uptake (n = 15 with diffuse uptake, and n = 6 with focal on diffuse uptake), examples of which are illustrated in Figures 1A and B.

Visualized myocardial FDG uptake was quantified in SUV_{mean} units, as shown in Figure 2. Patients with visualized, focal only FDG uptake had a myocardial SUV_{mean} that was 61% higher than that in patients with no visible uptake (2.80 units versus 1.74 units; $P < 0.001$). Patients with any visualized diffuse myocardial FDG uptake had a myocardial SUV_{mean} that was 124% higher than that in patients with no visible uptake (3.89 units versus 1.74 units; $P < 0.001$).

With regard to SUV_{max} values, patients with focal only FDG uptake had a myocardial SUV_{max} that was 98% higher than that in patients with no visible uptake (5.22 units versus 2.63 units; $P < 0.001$). Patients with any visible diffuse myocardial FDG uptake had a myocardial SUV_{max} that was 130% higher than that in patients with no visible uptake (6.04 units versus 2.63 units; $P < 0.001$).

We scanned a group of 27 non-RA controls to estimate a cutoff value for normal myocardial FDG uptake. Among the controls, the SUV_{mean} (1.70 units) plus 2 SD (1.70 units × 2) was 3.10 units. Using this cutoff to define normal levels, 21 (18%) of the RA patients had abnormal (high) myocardial FDG uptake (data not shown).

Univariate and multivariable associations of the demographic and clinical characteristics of the RA patients with the log-transformed myocardial SUV_{mean} values are summarized in Table 2. In univariate models, non-Hispanic black race, higher BMI, higher DAS28-CRP scores, and higher CDAI scores of disease activity were each significantly associated with a higher log SUV_{mean}, whereas current use of non–TNF inhibitor biologics was associated with a significantly lower log SUV_{mean}. However, after carrying these variables into the extended and reduced models, only higher disease activity remained significantly associated with a higher log SUV_{mean}, while use of non–TNF-targeted biologics remained inversely associated with the log SUV_{mean}, after adjustments for BMI and CAC level. Specifically,

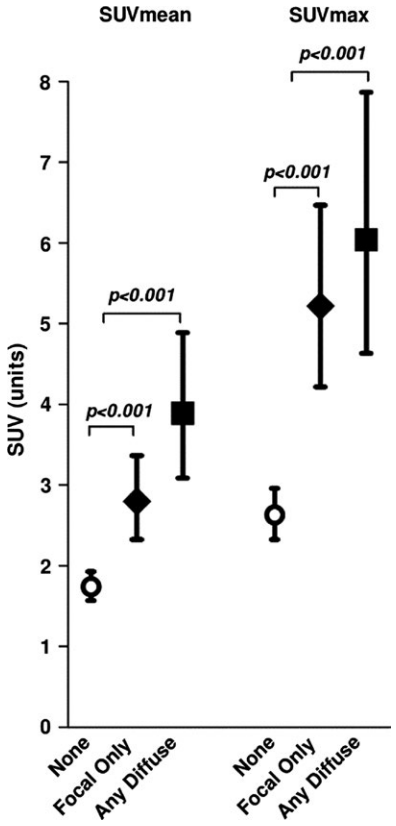

Figure 2. Quantitative mean standardized uptake values (SUVs) for myocardial 18-fluorodeoxyglucose uptake as a function of categorization by visually assessed (qualitative) SUVs in the 119 patients with rheumatoid arthritis. Results are the mean ± 95% confidence interval for the mean of the mean SUV (SUV_{mean}) and mean of the maximum SUV (SUV_{max}) according to category of visualized myocardial uptake.

patients with a CDAI score ≥10 had an adjusted SUV_{mean} that was 31% higher than that in patients with a CDAI score <10 (2.30 units versus 1.76 units; $P = 0.005$) (Figure 3A). Those treated with non–TNF-targeted biologics had an adjusted SUV_{mean} that was 26% lower than that in patients who did not receive biologic therapy (1.65 units versus 2.23 units; $P = 0.029$) (Figure 3B).

The majority of patients taking non-TNF biologic agents (8 of 10) were receiving abatacept. We did not observe any statistically significant differences in RA characteristics (RF/anti-CCP seropositivity, CDAI scores, DAS28-CRP scores, HAQ scores, CRP levels, or IL-6 levels) in the abatacept users compared with the non–TNF inhibitor/abatacept biologic users or compared with those not treated with biologics (data not shown). In contrast, the adjusted SUV_{mean} was not significantly different in those treated with TNF inhibitors compared with those not receiving biologics. A CDAI score ≥10 and current use of a non–TNF inhibitor biologic were also the only significant correlates of the SUV_{max}, after adjustment for BMI (data not shown).

Table 2. Associations of RA patient characteristics with the log-transformed myocardial SUV_{mean} values*

	Univariate models		Extended multivariate model		Reduced multivariate model	
	β	*P*	β	*P*	β	*P*
Age, per year	−0.0004	0.92	–	–	–	–
Male versus female	−0.11	0.39	–	–	–	–
Non-Hispanic white	Referent	–	Referent	–	–	–
Non-Hispanic black	0.34	0.029	0.20	0.24	–	–
Hispanic	0.17	0.14	0.064	0.63	–	–
Other race	−0.093	0.74	−0.12	0.67	–	–
Ever smoker versus never smoker	−0.023	0.82	–	–	–	–
Hypertension, yes versus no	0.0030	0.98	–	–	–	–
BMI, per kg/m^2	0.018	0.042	0.014	0.10	0.015	0.068
Diabetes, yes versus no	−0.17	0.27	–	–	–	–
Total cholesterol, per mg/dl	−0.0017	0.22	−0.0015	0.29	–	–
LDL-C, per mg/dl	−0.0010	0.55	–	–	–	–
HDL-C, per mg/dl	−0.0016	0.56	–	–	–	–
Log triglycerides, per mg/dl	−0.11	0.36	–	–	–	–
RA duration (square root), per year	0.010	0.74	–	–	–	–
RF or anti-CCP, yes versus no	0.011	0.93	–	–	–	–
DAS28-CRP >3.2	0.22	0.039	–	–	–	–
CDAI ≥10	0.31	0.006	0.25	0.047	0.28	0.012
Log CRP, per mg/liter	0.0047	0.91	–	–	–	–
Log IL-6, per pg/ml	0.015	0.74	–	–	–	–
Log BNP, per pg/ml	0.0009	0.75	–	–	–	–
Morning stiffness (square root), per minute	0.0052	0.71	–	–	–	–
HAQ score, per unit	0.11	0.099	−0.019	0.79	–	–
Methotrexate, yes versus no	0.13	0.22	0.12	0.27	–	–
No biologic	Referent	–	Referent	–	Referent	–
TNF inhibitors	−0.080	0.48	−0.029	0.80	−0.023	0.83
Non-TNF biologics	−0.38	0.043	−0.36	0.047	−0.38	0.033
Current prednisone, yes versus no	0.14	0.21	–	–	–	–
Current NSAID, yes versus no	0.067	0.52	–	–	–	–
CAC score 0	Referent	–	Referent	–	Referent	–
CAC score 1–99	0.018	0.90	0.041	0.77	0.037	0.78
CAC score ≥100	−0.22	0.10	−0.25	0.073	−0.21	0.10
Adjusted R^2			0.105	0.025	0.102	0.006

* Beta coefficients represent the average change in the log-transformed myocardial mean of the mean standardized uptake value (SUV_{mean}) per 1-unit higher value of the independent continuous variable of interest or for those with versus those without the independent dichotomous variable of interest. RA = rheumatoid arthritis; BMI = body mass index; LDL-C = low-density lipoprotein cholesterol; HDL-C = high-density lipoprotein cholesterol; RF = rheumatoid factor; anti-CCP = anti–cyclic citrullinated peptide antibody; DAS28-CRP = Disease Activity Score in 28 joints using C-reactive protein level; CDAI = Clinical Disease Activity Index; IL-6 = interleukin-6; BNP = brain natriuretic peptide; HAQ = Health Assessment Questionnaire; TNF = tumor necrosis factor; NSAID = nonsteroidal antiinflammatory drug; CAC = coronary artery calcium.

Myocardial FDG uptake after escalation of RA pharmacotherapy. Of the 8 RA patients who were assessed longitudinally for myocardial FDG uptake, the treatment was escalated to TNF inhibitors in 6 patients and to triple therapy in 2 patients. At baseline, prior to escalation of therapy, 4 RA patients had visible FDG uptake (2 focal and 2 diffuse) and the SUV_{mean} was 4.50 units, which was 165% higher than that in the group of 27 non-RA controls ($P = 0.037$).

Upon rescanning after 6 months of therapy, only 1 RA patient had visible myocardial FDG uptake, and the SUV_{mean} in the RA group numerically decreased by almost 50%, to 2.3 units, although this change was not statistically significant (P =

0.088). The myocardial SUV_{mean} at 6 months in the RA group was only 35% higher than that of the control group, but was still significantly higher (P = 0.042) (Figure 4). The reduction in myocardial FDG uptake in the RA group paralleled a decrease in the mean CDAI score, from a mean score of 23 at baseline to 12 at 6 months. A similar, but not statistically significant, trend was observed for the SUV_{max}, which decreased from 7.2 units to 3.8 units (P = 0.082) after 6 months (data not shown).

Association of myocardial FDG uptake with LV structure and function. We evaluated the association of the myocardial SUV_{mean} with echocardiographic measures of LV structure (LV mass index [LVMI], EDVI, and ESVI) and of LV function (LVEF and diastolic dysfunction [the E/E′ and diastolic dysfunction yes versus no]). Except for a high prevalence of diastolic dysfunction in the RA patients (43%), mean measures of LV structure and function were in the normal ranges (Table 1).

In univariable analyses, the SUV_{mean} was not associated with any measure of LV structure or function (results available from the corresponding author upon request). In multivariable analyses of the association of the SUV_{mean} with a selected measure of LV structure, the LVMI, and of diastolic dysfunction, the E/E′ ratio, no association of the SUV_{mean} with either measure was observed (results available from the corresponding author upon request). The SUV_{max} was also not associated with measures of LV structure or function (results of a representative multivariable analysis of association of SUV_{max} with LVMI are available from the corresponding author upon request). Furthermore, BNP levels were also not associated with the SUV_{mean} (Table 2).

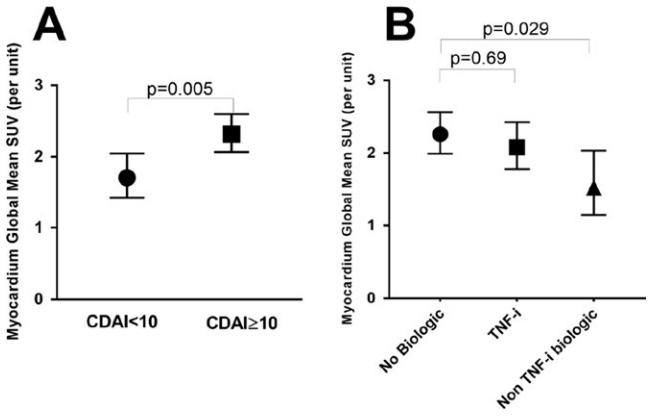

Figure 3. Adjusted global mean standardized uptake values (SUVs) for myocardial 18-fluorodeoxyglucose uptake, according to Clinical Disease Activity Index (CDAI) scores (**A**) and current use of biologic disease-modifying antirheumatic drugs (DMARDs) (**B**). Models were adjusted for CDAI disease activity level (scores <10 for low disease activity or remission versus scores ≥10 for moderate-to-high disease activity) and for DMARD treatment (no biologic versus tumor necrosis factor inhibitor [TNFi] versus non-TNFi biologic), which were the only significant covariates retained in multivariable modeling. Results are the mean ± 95% confidence interval in 119 rheumatoid arthritis patients.

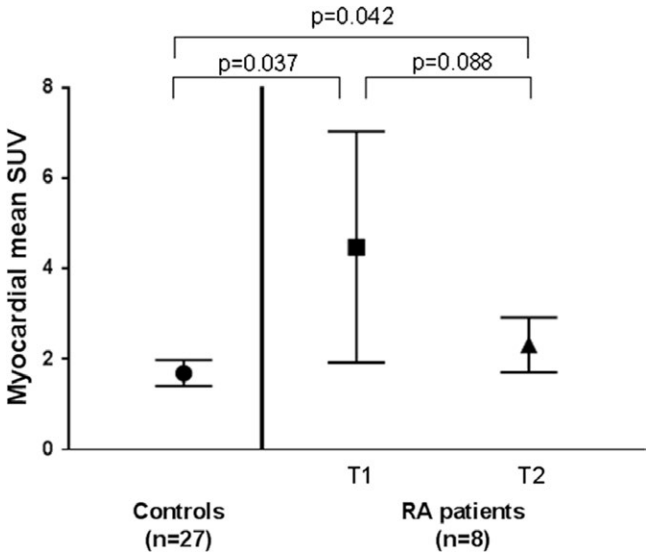

Figure 4. Global mean standardized uptake values (SUVs) for myocardial 18-fluorodeoxyglucose uptake before and after acceleration of therapy in a subset of 8 rheumatoid arthritis (RA) patients compared with 27 non-RA control subjects. Controls had only 1 scan, while RA patients had a scan before (T1) and after (T2) 6 months of step-up therapy with either tumor necrosis factor inhibitors or triple therapy with sulfasalazine and hydroxychloroquine on a background of methotrexate. Results are the mean ± 95% confidence interval.

DISCUSSION

To our knowledge, this is the first study to evaluate and quantify subclinical myocardial inflammation by FDG PET-CT in RA patients, which allowed a detailed assessment of associations of RA characteristics with FDG uptake. It is also the first study, albeit being a small pilot study, to longitudinally evaluate the effect of RA step-up therapy on myocardial inflammation. Cross-sectionally, we observed that 37% of the RA patients had visible myocardial FDG uptake, and abnormal FDG uptake, defined as an SUV_{mean} of 2 SD above that of a non-RA reference control group, was prevalent in 18% of RA patients. Furthermore, we observed that myocardial FDG uptake was strongly correlated with higher articular disease activity, and was lower in patients receiving non–TNF-targeted biologic agents. In addition, the results of the pilot longitudinal study suggested that myocardial inflammation may improve in RA patients who receive treatment with DMARDs.

Our finding of myocarditis in 18–37% of RA patients is largely comparable in magnitude to that in historical necropsy studies in which subclinical myocarditis was reported in up to 20% of RA patients (15,16). It is also in accordance with the findings of several smaller CMR studies that reported a higher prevalence of LGE in RA patients when compared with non-RA controls (39–41). However, LGE reflects extracellular edema and is therefore less specific than FDG uptake for myocarditis. Moreover, LGE

is only useful for identifying focal abnormalities. More recently, T2WI has been utilized in CMR studies as a more quantitative, non–gadolinium-dependent measure of tissue-free water content. In CMR studies in RA patients without clinical CVD, Ntusi et al reported a prevalence of myocardial LGE of 46%, compared with only 10% by T2WI (39). Similarly, in a Japanese cohort of RA patients, Kobayashi et al observed myocardial LGE in 32% of patients, but evidence of myocardial inflammation and fibrosis by T2WI was present in only 12% of patients (41). In non-RA patients with clinically suspected and histopathologically proven myocarditis, T2W1 performed better than standard CMR measures for distinguishing active from inactive myocarditis (24). A future study in RA in which quantitative myocardial FDG uptake and T2W1 CMR studies are performed in the same patients would be useful to determine whether T2W1 findings would correlate with the intensity and geographic distribution of FDG uptake.

Importantly, we observed an association of myocardial inflammation with articular disease activity in RA patients. This observation, which is consistent with that from several previous CMR studies (39–41), supports the premise that achieving low disease activity or remission of RA activity protects not only the joints, but possibly the myocardium as well. However, we did not find an association of the myocardial SUV with circulating CRP or IL-6 levels. The known effect of DMARD treatments on lowering the levels of CRP and IL-6 may have obscured any relationship with the myocardial SUV. It is also possible that systemic inflammation causing myocardial harm could be attributable to the presence of a cytokine or cytokines not measured in our study. Alternatively, in situ myocardial production of cytokines may play a greater role than systemic inflammation in mediating myocardial inflammation (42–45), but may not be robust enough to contribute to circulating levels of cytokines in this RA cohort who were without clinical heart failure and had no apparent myocardial damage (as suggested by undetectable troponin levels).

Other than BMI, we did not observe associations between myocardial FDG uptake and other traditional CVD risk factors. There was also no clear association between myocardial uptake and CAC scores. These findings suggest that myocardial uptake in RA is driven more by features unique to the RA disease state than by CVD risk factors and/or atherosclerosis that may be shared with the general population.

In our cross-sectional analyses, myocardial SUV was lower among patients treated with non–TNF-targeted biologics compared with those treated with TNF inhibitors or with a nonbiologic agent. The non–TNF-targeted biologic group comprised primarily patients receiving abatacept (soluble CTLA-4Ig). Although we did not identify any significant differences in RA characteristics between the abatacept users and the other treatment groups, channeling bias cannot be completely eliminated as an explanation for this finding, given the small number of abatacept users. Nonetheless, it is of interest that antibodies that neutralize CTLA-4, and are effective as cancer immunotherapy, have been associated with rare but potentially fatal myocarditis (46). Similarly, in experimental models, CTLA-4–deficient mice develop severe myocarditis with lymphocytic infiltration (47,48), while experimental autoimmune myocarditis in rats can be prevented by gene delivery with a plasmid encoding CTLA-4Ig (49).

Thus, while it is tantalizing to hypothesize that among the existing DMARDs for RA, abatacept may act selectively in reducing subclinical myocardial inflammation, the results of our small prospective study suggest that this effect may also be observed with escalation of therapy to nonbiologic agents and TNF inhibitors. Therefore, taken together, our findings seem to indicate that the reduction in myocardial FDG uptake is more likely dependent on a reduction in RA disease activity rather than on the specific agent used; however, understanding these interactions would require a larger cohort of longitudinally followed up patients in a study that would be appropriately powered to explore differences in effect between different treatments and treatment responses. Such studies are currently under way.

We did not observe a relationship of myocardial FDG uptake with measures of LV structure or function or with BNP levels. This may not be surprising, since we excluded patients with clinical heart failure, and BNP levels and most of the echocardiographic measures of LV structure and function in this cohort were within normal ranges.

Our study has notable strengths and limitations. Among the strengths, it is the largest study to date to evaluate and quantify the presence of subclinical myocardial inflammation in RA, and the first to utilize FDG PET-CT to do so. It is also the first to evaluate longitudinally, albeit in a small pilot study, the effect of step-up therapy on myocardial inflammation. Our cohort included patients with and those without CVD risk factors, as well as patients with early and late RA, and is thus a reflection of the typical population of RA patients managed in clinical practice.

Among the study's limitations, we assumed that FDG uptake corresponded to myocardial inflammation, as was previously shown in other studies (25,26), but, for ethical reasons, we could not verify this pathologically in this asymptomatic cohort. An additional limitation is that our final multivariable model accounted for only 10% of the variability in the SUV_{mean}, inviting a search for other possible contributory variables.

In summary, although larger longitudinal data are needed, the current study supports the hypotheses that myocardial inflammation in RA is related to disease activity, that it may contribute to the increased risk for heart failure in patients with RA compared with controls, and that it may be responsive to step-up therapy.

ACKNOWLEDGMENTS

The authors would like to thank the staff of the RHYTHM study (Janine Rose, Rachel Broderick, and Thania Perez) for their

hard work and dedication, and the participants in the RHYTHM study, who graciously agreed to participate in this research. We also thank Drs. Alice Chu, Anna Broder, Teja Kapoor, Edward Dwyer, Jane Kang, Laura Geraldino, Katherine Nickerson, Elizabeth Mayer, Amanda Sammut, Neil Gonter, and Alexandru Kimel, among others, for generously recommending their patients for this study.

AUTHOR CONTRIBUTIONS

All authors were involved in drafting the article or revising it critically for important intellectual content, and all authors approved the final version to be published. Dr. Bathon had full access to all of the data in the study and takes responsibility for the integrity of the data and the accuracy of the data analysis.

Study conception and design. Amigues, Tugcu, Russo, Giles, Morgenstein, Zartoshti, Schulze, Flores, Bokhari, Bathon.

Acquisition of data. Tugcu, Russo, Morgenstein, Zartoshti, Flores, Bokhari, Bathon.

Analysis and interpretation of data. Amigues, Tugcu, Russo, Giles, Schulze, Bokhari, Bathon.

ADDITIONAL DISCLOSURES

Author Tugcu is currently an employee of Bristol-Myers Squibb. Author Russo is currently an employee of Novartis.

REFERENCES

1. Nicola PJ, Crowson CS, Maradit-Kremers H, Ballman KV, Roger VL, Jacobsen SJ, et al. Contribution of congestive heart failure and ischemic heart disease to excess mortality in rheumatoid arthritis. Arthritis Rheum 2006;54:60–7.
2. Nicola PJ, Maradit-Kremers H, Roger VL, Jacobsen SJ, Crowson CS, Ballman KV, et al. The risk of congestive heart failure in rheumatoid arthritis: a population-based study over 46 years. Arthritis Rheum 2005;52:412–20.
3. Gonzalez A, Maradit-Kremers H, Crowson CS, Nicola PJ, Davis JM III, Therneau TM, et al. The widening mortality gap between rheumatoid arthritis patients and the general population. Arthritis Rheum 2007;56:3583–7.
4. Davis JM III, Roger VL, Crowson CS, Kremers HM, Therneau TM, Gabriel SE. The presentation and outcome of heart failure in patients with rheumatoid arthritis differs from that in the general population. Arthritis Rheum 2008;58:2603–11.
5. Kapadia SR, Yakoob K, Nader S, Thomas JD, Mann DL, Griffin BP. Elevated circulating levels of serum tumor necrosis factor-α in patients with hemodynamically significant pressure and volume overload. J Am Coll Cardiol 2000;36:208–12.
6. Matsumori A, Yamada T, Suzuki H, Matoba Y, Sasayama S. Increased circulating cytokines in patients with myocarditis and cardiomyopathy. Br Heart J 1994;72:561–6.
7. Deswal A, Petersen NJ, Feldman AM, Young JB, White BG, Mann DL. Cytokines and cytokine receptors in advanced heart failure: an analysis of the cytokine database from the Vesnarinone trial (VEST). Circulation 2001;103:2055–9.
8. Levine B, Kalman J, Mayer L, Fillit HM, Packer M. Elevated circulating levels of tumor necrosis factor in severe chronic heart failure. N Engl J Med 1990;323:236–41.
9. Rauchhaus M, Doehner W, Francis DP, Davos C, Kemp M, Liebenthal C, et al. Plasma cytokine parameters and mortality in patients with chronic heart failure. Circulation 2000;102:3060–7.
10. Goldhaber JI, Kim KH, Natterson PD, Lawrence T, Yang P, Weiss JN. Effects of TNF-α on [Ca2+]i and contractility in isolated adult rabbit ventricular myocytes. Am J Physiol 1996;271:H1449–55.
11. Krown KA, Page MT, Nguyen C, Zechner D, Gutierrez V, Comstock KL, et al. Tumor necrosis factor α-induced apoptosis in cardiac myocytes: involvement of the sphingolipid signaling cascade in cardiac cell death. J Clin Invest 1996;98:2854–65.
12. Sivasubramanian N, Coker ML, Kurrelmeyer KM, MacLellan WR, DeMayo FJ, Spinale FG, et al. Left ventricular remodeling in transgenic mice with cardiac restricted overexpression of tumor necrosis factor. Circulation 2001;104:826–31.
13. Yokoyama T, Nakano M, Bednarczyk JL, McIntyre BW, Entman M, Mann DL. Tumor necrosis factor-α provokes a hypertrophic growth response in adult cardiac myocytes. Circulation 1997;95:1247–52.
14. Grundtman C, Hollan I, Førre OT, Saatvedt K, Mikkelsen K, Lundberg IE. Cardiovascular disease in patients with inflammatory rheumatic disease is associated with up-regulation of markers of inflammation in cardiac microvessels and cardiomyocytes. Arthritis Rheum 2010;62:667–73.
15. Cathcart ES, Spodick DH. Rheumatoid heart disease: a study of the incidence and nature of cardiac lesions in rheumatoid arthritis. N Engl J Med 1962;266:959–64.
16. Sokoloff L. Cardiac involvement in rheumatoid arthritis and allied disorders: current concepts. Mod Concepts Cardiovasc Dis 1964;33:847–50.
17. Bennett MK, Gilotra NA, Harrington C, Rao S, Dunn JM, Freitag TB, et al. Evaluation of the role of endomyocardial biopsy in 851 patients with unexplained heart failure from 2000-2009. Circ Heart Fail 2013;6:676–84.
18. Uemura A, Morimoto S, Hiramitsu S, Kato Y, Ito T, Hishida H. Histologic diagnostic rate of cardiac sarcoidosis: evaluation of endomyocardial biopsies. Am Heart J 1999;138:299–302.
19. Aime S, Caravan P. Biodistribution of gadolinium-based contrast agents, including gadolinium deposition. J Magn Reson Imaging 2009;30:1259–67.
20. Bello D, Shah DJ, Farah GM, Di Luzio S, Parker M, Johnson MR, et al. Gadolinium cardiovascular magnetic resonance predicts reversible myocardial dysfunction and remodeling in patients with heart failure undergoing β-blocker therapy. Circulation 2003;108:1945–53.
21. Judd RM, Lugo-Olivieri CH, Arai M, Kondo T, Croisille P, Lima JA, et al. Physiological basis of myocardial contrast enhancement in fast magnetic resonance images of 2-day-old reperfused canine infarcts. Circulation 1995;92:1902–10.
22. Kim RJ, Wu E, Rafael A, Chen EL, Parker MA, Simonetti O, et al. The use of contrast-enhanced magnetic resonance imaging to identify reversible myocardial dysfunction. N Engl J Med 2000;343:1445–53.
23. Lima JA, Judd RM, Bazille A, Schulman SP, Atalar E, Zerhouni EA. Regional heterogeneity of human myocardial infarcts demonstrated by contrast-enhanced MRI: potential mechanisms. Circulation 1995;92:1117–25.
24. Bohnen S, Radunski UK, Lund GK, Kandolf R, Stehninh C, Schackenburg B, et al. Performance of T1 and T2 mapping cardiovascular magnetic resonance to detect active myocarditis in patients with recent-onset heart failure. Circ Cardiovasc Imaging 2015;8:e003073.
25. Lee WW, Marinelli B, van der Laan AM, Sena BF, Gorbatov R, Leuschner F, et al. PET/MRI of inflammation in myocardial infarction. J Am Coll Cardiol 2012;59:153–63.
26. Maya Y, Werner RA, Schutz C, Wakabayashi H, Samnick S, Lapa C, et al. 11C-methionine PET of myocardial inflammation in a rat model of experimental autoimmune myocarditis. J Nucl Med 2016;57:1985–90.
27. Winchester R, Giles JT, Nativ S, Downer K, Zhang HZ, Bag-Ozbek A, et al. Association of elevations of specific T cell and monocyte sub-

populations in rheumatoid arthritis with subclinical coronary artery atherosclerosis. Arthritis Rheumatol 2016;68:92–102.

28. Aletaha D, Neogi T, Silman AJ, Funovits J, Felson DT, Bingham CO III, et al. 2010 rheumatoid arthritis classification criteria: an American College of Rheumatology/European League Against Rheumatism collaborative initiative. Arthritis Rheum 2010;62: 2569–81.
29. Osborne MT, Hulten EA, Murthy VL, Skali H, Taqueti VR, Dorbala S, et al. Patient preparation for cardiac fluorine-18 fluorodeoxyglucose positron emission tomography imaging of inflammation. J Nucl Cardiol 2017;24:86–99.
30. Demeure F, Hanin FX, Bol A, Vincent MF, Pouleur AC, Gerber B, et al. A randomized trial on the optimization of 18F-FDG myocardial uptake suppression: implications for vulnerable coronary plaque imaging. J Nucl Med 2014;55:1629–35.
31. Cerqueira MD, Weissman NJ, Dilsizian V, Jacobs AK, Kaul S, Laskey WK, et al. Standardized myocardial segmentation and nomenclature for tomographic imaging of the heart: a statement for healthcare professionals from the Cardiac Imaging Committee of the Council on Clinical Cardiology of the American Heart Association. Circulation 2002;105:539–42.
32. Agatston AS, Janowitz WR, Hildner FJ, Zusmer NR, Viamonte M Jr, Detrano R. Quantification of coronary artery calcium using ultrafast computed tomography. J Am Coll Cardiol 1990;15:827–32.
33. Russo C, Jin Z, Homma S, Rundek T, Elkind MS, Sacco RL, et al. Relationship of multidirectional myocardial strain with radial thickening and ejection fraction and impact of left ventricular hypertrophy: a study in a community based cohort. Echocardiography 2013;30:794–802.
34. Russo C, Jin Z, Homma S, Rundek T, Elkind MS, Sacco RL, et al. Effect of obesity and overweight on left ventricular diastolic function: a community-based study in an elderly cohort. J Am Coll Cardiol 2011;57:1368–74.
35. Inoue E, Yamanaka H, Hara M, Tomatsu T, Kamatani N. Comparison of Disease Activity Score (DAS)28-erythrocyte sedimentation rate and DAS28-C-reactive protein threshold values. Ann Rheum Dis 2007;66:407–9.
36. Prevoo ML, van 't Hof MA, Kuper HH, van Leeuwen MA, van de Putte LB, van Riel PL. Modified disease activity scores that include twenty-eight–joint counts: development and validation in a prospective longitudinal study of patients with rheumatoid arthritis. Arthritis Rheum 1995;38:44–8.
37. Wells G, Becker JC, Teng J, Dougados M, Schiff M, Smolen J, et al. Validation of the 28-joint Disease Activity Score (DAS28) and European League Against Rheumatism response criteria based on C-reactive protein against disease progression in patients with rheumatoid arthritis, and comparison with the DAS28 based on erythrocyte sedimentation rate. Ann Rheum Dis 2009;68:954–60.
38. Fries JF, Spitz P, Kraines RG, Holman HR. Measurement of patient outcome in arthritis. Arthritis Rheum 1980;23:137–45.
39. Ntusi NA, Piechnik SK, Francis JM, Ferreira VM, Mathews PM, Robson MD, et al. Diffuse myocardial fibrosis and inflammation in rheumatoid arthritis: insights from CMR T1 mapping. JACC Cardiovas Imaging 2015;8:526–36.
40. Kobayashi Y, Giles JT, Hirano M, Yokoe I, Nakajima Y, Bathon JM, et al. Assessment of myocardial abnormalities in rheumatoid arthritis using a comprehensive cardiac magnetic resonance approach: a pilot study. Arthritis Res Ther 2010;12:R171.
41. Kobayshi H, Kobayashi Y, Yokoe I, Akashi Y, Takei M, Giles JT. Magnetic resonance imaging–detected myocardial inflammation and fibrosis in rheumatoid arthritis: associations of disease characteristics and N-terminal pr–brain natriuretic peptide levels. Arthritis Care Res (Hoboken) 2017;69:1304–11.
42. Dick SA, Epelman S. Chronic heart failure and inflammation: what do we really know? Circ Res 2016;119:159–76.
43. Andersen JK, Oma I, Prayson RA, Kvelstad IL, Almdahl S, Fagerland MW, et al. Inflammatory cell infiltrates in the heart of patients with coronary artery disease with and without inflammatory rheumatic disease: a biopsy study. Arthritis Res Ther 2016;18:232.
44. Totoson P, Maguin-Gate K, Nappey M, Wendling D, Demougeot C. Endothelial dysfunction in rheumatoid arthritis: mechanistic insights and correlation with circulating markers of systemic inflammation. PloS One 2016;11:e0146744.
45. Totoson P, Maguin-Gate K, Nappey M, Prati C, Wendling D, Demougeot C. Microvascular abnormalities in adjuvant-induced arthritis: relationship to macrovascular endothelial function and markers of endothelial activation. Arthritis Rheumatol 2015;67:1203–13.
46. Johnson DB, Balko JM, Compton ML, Chalkias S, Gorham J, Xu Y, et al. Fulminant myocarditis with combination immune checkpoint blockade. N Engl J Med 2016;375:1749–55.
47. Tivol EA, Borriello F, Schweitzer AN, Lynch WP, Bluestone JA, Sharpe AH. Loss of CTLA-4 leads to massive lymphoproliferation and fatal multiorgan tissue destruction, revealing a critical negative regulatory role of CTLA-4. Immunity 1995;3:541–7.
48. Love VA, Grabie N, Duramad P, Stavrakis G, Sharpe A, Lichtman A. CTLA-4 ablation and interleukin-12 driven differentiation synergistically augment cardiac pathogenicity of cytotoxic T lymphocytes. Circ Res 2007;101:248–57.
49. Abe S, Hanawa H, Hayashi M, Yoshida T, Komura S, Watanabe R, et al. Prevention of experimental autoimmune myocarditis by hydrodynamics-based naked plasmid DNA encoding CTLA4-Ig gene delivery. J Card Fail 2005;11:557–64.

Arthritis & Rheumatology
Vol. 71, No. 4, April 2019, pp 507–517
DOI 10.1002/art.40760

American College of Rheumatology
Education • Treatment • Research

Affinity Maturation of the Anti–Citrullinated Protein Antibody Paratope Drives Epitope Spreading and Polyreactivity in Rheumatoid Arthritis

Sarah Kongpachith, Nithya Lingampalli, Chia-Hsin Ju, Lisa K. Blum, Daniel R. Lu, Serra E. Elliott, Rong Mao, and William H. Robinson

Objective. Anti–citrullinated protein antibodies (ACPAs) are a hallmark of rheumatoid arthritis (RA). While epitope spreading of the serum ACPA response is believed to contribute to RA pathogenesis, little is understood regarding how this phenomenon occurs. This study was undertaken to analyze the antibody repertoires of individuals with RA to gain insight into the mechanisms leading to epitope spreading of the serum ACPA response in RA.

Methods. Plasmablasts from the blood of 6 RA patients were stained with citrullinated peptide tetramers to identify ACPA-producing B cells by flow cytometry. Plasmablasts were single-cell sorted and sequenced to obtain antibody repertoires. Sixty-nine antibodies were recombinantly expressed, and their anticitrulline reactivities were characterized using a cyclic citrullinated peptide enzyme-linked immuosorbent assay and synovial antigen arrays. Thirty-six mutated antibodies designed either to represent ancestral antibodies or to test paratope residues critical for binding, as determined from molecular modeling studies, were also tested for anticitrulline reactivities.

Results. Clonally related monoclonal ACPAs and their shared ancestral antibodies each exhibited differential reactivity against citrullinated antigens. Molecular modeling identified residues within the complementarity-determining region loops and framework regions predicted to be important for citrullinated antigen binding. Affinity maturation resulted in mutations of these key residues, which conferred binding to different citrullinated epitopes and/or increased polyreactivity to citrullinated epitopes.

Conclusion. These results demonstrate that the different somatic hypermutations accumulated by clonally related B cells during affinity maturation alter the antibody paratope to mediate epitope spreading and polyreactivity of the ACPA response in RA, suggesting that these may be key properties that likely contribute to the pathogenicity of ACPAs.

INTRODUCTION

Rheumatoid arthritis (RA) is a chronic autoimmune disorder of unknown etiology (1,2). A hallmark of RA is the presence of anti–citrullinated protein antibodies (ACPAs) that recognize citrullinated antigens (1,2). Citrullination is mediated by peptidylarginine deaminases and plays a role in gene regulation, organization of cell structure, apoptosis, and formation of neutrophil extracellular traps (3–5). In RA, however, citrullination of proteins in the synovial joint and other tissues, coupled with the production of ACPAs, has been hypothesized to contribute to its pathogenesis (1–4).

Increasing evidence suggests that ACPAs play an important role in the pathogenesis of RA (6). ACPAs have been detected in patients as early as 10 years prior to diagnosis, with increased titers and epitope spreading of the ACPA response preceding the onset of arthritis (7–9). The presence of ACPAs is associated with increased disease severity (10–13) and is a better predictor of erosive disease than rheumatoid factor (14). Finally, in the mouse model of collagen-induced arthritis, administration of a monoclonal ACPA exacerbated the disease, demonstrating that ACPAs can directly promote inflammatory arthritis (15).

Deciphering the mechanisms underlying the development and epitope spreading of the ACPA response could provide new

Supported by the NIH (grants R01-AR-063676, U19-AI-11049103, U01-AI-101981, and UH2-AR-067676 from the National Institute of Arthritis and Musculoskeletal and Skin Diseases).

Sarah Kongpachith, PhD, Nithya Lingampalli, BS, Chia-Hsin Ju, PhD, Lisa K. Blum, PhD, Daniel R. Lu, PhD, Serra E. Elliott, PhD, Rong Mao, PhD, William H. Robinson, MD, PhD: Stanford University, Stanford, California, and VA Palo Alto Health Care System, Palo Alto, California.

Dr. Robinson is a director of and consultant to Atreca, Inc. (consulting fees less than $10,000), and owns equity in Atreca, Inc. No other disclosures relevant to this article were reported.

Address correspondence to William H. Robinson, MD, PhD, Division of Immunology and Rheumatology, Stanford University, 269 Campus Drive, Stanford, CA 94305. E-mail: w.robinson@stanford.edu.

Submitted for publication April 25, 2018; accepted in revised form October 11, 2018.

insights into the mechanisms underlying RA. Previous studies using RA patient serum demonstrated that epitope spreading of the ACPA response occurs in the years preceding clinical disease (7–9). Of note, during the 2 years immediately preceding the onset of clinical arthritis, the number and breadth of ACPA reactivities sharply increase, correlating with an increase in proinflammatory cytokines in the blood (7). Nevertheless, the mechanisms underlying epitope spreading of ACPAs and their role in the development of clinical RA remain poorly understood.

In the present study, we used barcode-enabled single-cell sequencing to analyze ACPA plasmablast repertoires in RA. We tested the binding capabilities of 69 recombinant monoclonal antibodies (mAb) derived from the plasmablast clonal families. We found that plasmablasts within the same clonal family that possess differential somatic hypermutations encode individual ACPAs that bind different citrullinated epitopes and/or bind distinct sets of citrullinated epitopes, and thus are polyreactive (16). We also found that patient-derived, affinity-matured ACPAs frequently exhibit increased polyreactivity, in which they consistently bind a greater number of specific citrullinated epitopes as compared to predicted ancestral family members. These findings indicate that somatic hypermutations arising through affinity maturation can result in epitope spreading and increase the polyreactivity of individual ACPAs, which in turn increases the ability of the polyclonal serum ACPA repertoire to bind a multitude of citrullinated epitopes in RA. We further used molecular modeling and mutation studies to identify and characterize the key amino acid residues within the complementarity-determining regions (CDRs) and framework regions forming the paratopes within the antigen-binding sites of ACPAs that mediate binding to citrullinated epitopes.

PATIENTS AND METHODS

Collection of human blood specimens. Blood samples were collected from individuals recruited at the VA Palo Alto who met the American College of Rheumatology 1987 classification criteria for RA (17) and who were positive for anti–cyclic citrullinated peptide (anti-CCP) antibodies. The patients' demographic and clinical characteristics are provided in Supplementary Table 1 (available on the *Arthritis & Rheumatology* web site at http://onlinelibrary.wiley.com/doi/10.1002/art.40760/abstract). The samples were collected after obtaining informed consent from all patients, and the study was conducted in accordance with human subject protocols approved by the Stanford University Institutional Review Board.

Generation of fluorescent citrullinated peptide tetramers (cit-tets). Cit-tets were generated by incubating phycoerythrin (PE)–conjugated streptavidin with biotinylated citrullinated peptides (a list of the peptides used is provided in Supplementary Table 2, available on the *Arthritis & Rheumatology* web site at http://onlinelibrary.wiley.com/doi/10.1002/art.40760/abstract). These peptides were previously shown to be targeted by ACPAs in RA sera (7,18,19) (for more details, see Supplementary Methods, http://onlinelibrary.wiley.com/doi/10.1002/art.40760/abstract).

Single-cell sorting of ACPA-producing plasmablasts. Cell sorting of CD19+CD20–CD3–CD14–IgD–CD27+CD38^{high} plasmablasts, which were either IgG+ or IgA+, was performed in the same manner as used previously in our prior studies (20,21). A mix of the PE-conjugated cit-tets was included to identify ACPA-producing plasmablasts (18,19) (details in Supplementary Methods, http://onlinelibrary.wiley.com/doi/10.1002/art.40760/abstract).

Barcode-enabled antibody repertoire sequencing. Antibody repertoire sequencing was performed as previously described (20–23).

Bioinformatics pipeline and repertoire analysis. Paired-chain antibody repertoires were generated from sequencing data using a custom bioinformatics pipeline (22). Clonally related antibodies were defined as sharing heavy-chain and light-chain V–J genes and having a CDR3 nucleotide Levenshtein distance of ≤40% of the total CDR3 length for both chains (i.e., CDR3 sequences are at least 60% identical). The bimodal distribution of the nearest distances for the heavy- and light-chain CDR3 sequences was used to set the identity threshold (24). For representing individual clonal family lineages, the heavy- and light-chain sequences of each member were concatenated and analyzed using IgTree (25).

Selection and recombinant expression of mAb. The antibodies sequenced directly from RA patient blood were produced in-house, as described previously (26). Antibodies sequenced from cit-tet+ clonally expanded plasmablasts were prioritized for expression; however, a handful of cit-tet+ nonclonal and tetramer-negative (tet–) clonal plasmablast antibodies were also expressed. All other antibodies (mutation studies and predicted parent/germline antibody sequences) were commercially produced (at LakePharma).

RA planar array. RA antigen microarrays were printed and probed, and data sets were analyzed as described previously (7,27,28). Positive hits were confirmed by enzyme-linked immunosorbent assay (ELISA).

Molecular modeling. Descriptions of the methods used to model the binding of patient-derived ACPAs to citrullinated epitopes are available in the Supplementary Methods (http://onlinelibrary.wiley.com/doi/10.1002/art.40760/abstract).

ELISAs. The CCP3 and peptide ELISAs used are described in the Supplementary Methods (http://onlinelibrary.wiley.com/doi/10.1002/art.40760/abstract).

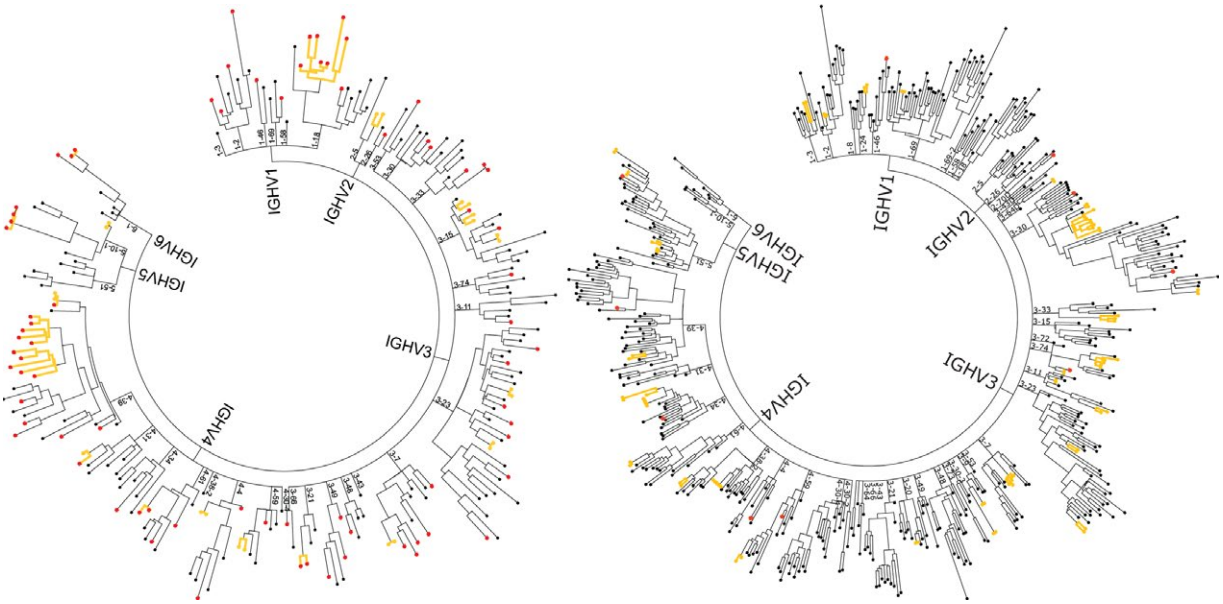

Figure 1. Representative plasmablast antibody repertoires in the blood of cyclic citrullinated peptide–positive (CCP+) rheumatoid arthritis (RA) patients. The plasmablast antibody repertoires of CCP+ RA patients were sequenced using a single-cell, barcode-based antibody repertoire capture method. Bioinformatics analyses of sequencing data sets were performed to obtain consensus sequences, pair cognate heavy-chain (HC) and light-chain (LC) sequences for individual plasmablasts, and generate phylogenetic trees. Two representative trees are presented (RA3 on left, RA11 on right) (see also Supplementary Table 3, http://onlinelibrary.wiley.com/doi/10.1002/art.40760/abstract). The tip of each branch denotes the paired HC and LC genes of an antibody expressed by a single plasmablast. Antibodies deriving from clonal families of plasmablasts are highlighted by yellow branches. Antibodies from citrullinated peptide tetramer–positive plasmablasts are colored in red.

Statistical analysis. For 2-group comparisons, the Welch's *t*-test was used. For multiple comparisons, the nonparametric Kruskal-Wallis test was used, followed by Dunn's multiple comparisons test. *P* values less than 0.05 were considered significant.

RESULTS

Sequencing the blood plasmablast antibody repertoire in RA. To study ACPA repertoires from activated, disease-relevant B cells in RA, we sequenced the antibodies expressed by plasmablasts from 6 anti-CCP+ RA patients and generated phylogenetic trees that represent the plasmablast antibody repertoires of each individual RA patient (Figure 1). A total of 2,541 antibodies were sequenced (see Supplementary Table 3, available on the *Arthritis & Rheumatology* web site at http://onlinelibrary.wiley.com/doi/10.1002/art.40760/abstract). Raw sequencing data have been deposited in the NCBI SRA database (accession no. PRJNA503739; https://www.ncbi.nlm.nih.gov/sra). In total, 182 clonal families, consisting of a total of 510 antibodies, were identified, with the remaining 2,031 antibodies representing nonclonal family "singletons." These singletons may in fact represent small clonal families that could not be captured at the current sequencing depth; therefore, our estimates of clonality are likely underestimates.

Sequenced antibodies were split nearly evenly between IgA and IgG isotypes (1,200 for IgA and 1,341 for IgG), although the ratios of IgA to IgG varied between patients. In total, 231 of the sequenced antibodies were derived from tetramer-positive (cit-tet+) plasmablasts. While this represents 9% of the total number of plasmablast antibody sequences, actual percentages of cit-tet+ plasmablasts in individual patients ranged from 1.4% to 34.7%. Of the cit-tet+ plasmablasts sequenced, 28.6% belonged to clonal families; of tet– plasmablasts, 23.8% were clonal. Heavy- and light-chain V-gene usage was comparable between the cit-tet+ plasmablasts and the entire plasmablast repertoires (see Supplementary Figures 1A–D, available on the *Arthritis & Rheumatology* web site at http://onlinelibrary.wiley.com/doi/10.1002/art.40760/abstract). Differences in mutation rates between cit-tet+ and tet– plasmablasts were nonsignificant, with the exception of that in subject RA3, whose cit-tet+ plasmablasts were significantly more mutated (see Supplementary Figures 2A–F, http://onlinelibrary.wiley.com/doi/10.1002/art.40760/abstract).

Differential binding and unique polyreactive signatures against citrullinated antigens exhibited by recombinant monoclonal ACPAs. Sixty-nine antibodies spanning samples from the 6 RA patients were selected for recombinant expression. Fifty-eight of the recombinant mAb were derived from cit-tet+ plasmablasts, the majority of which were clonally expanded. The remaining 11 were derived from tet– plasmablasts.

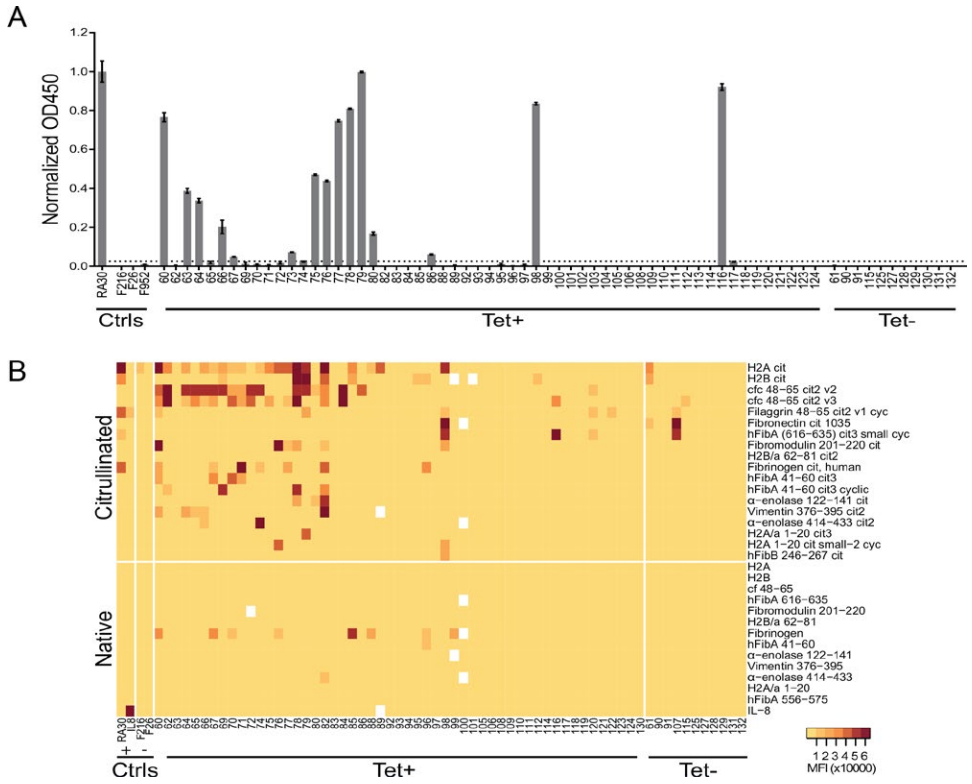

Figure 2. Recombinant monoclonal antibodies sequenced from rheumatoid arthritis (RA) patient plasmablasts exhibit distinct polyreactive binding of citrullinated antigens. **A**, Representative antibodies derived from patient plasmablasts were recombinantly expressed and tested for anti–cyclic citrullinated peptide (anti-CCP) reactivity using a commercial CCP enzyme-linked immunosorbent assay kit. Results are normalized against a monoclonal anti–citrullinated protein antibody (ACPA) control. The cutoff value for positivity was set at 3 SD above the average of the negative controls (antihemagglutinin antibodies). Data are presented as the mean ± SEM of duplicate assays, and are representative of 3 independent experiments. **B**, Antigen array analysis of recombinant antibody reactivities against RA-associated autoantigens was performed. Arrays were printed with ~300 citrullinated and native synovial peptides and proteins, including citrullinated filaggrin cyclic (cfc), a citrullinated filaggrin peptide used in first-generation CCP assays. Arrays were probed with patient-derived recombinant antibodies followed by fluorescent anti-human IgG detection antibody prior to scanning. The median mean fluorescence intensity (MFI) of 4 replicate spots for each antigen is displayed. Ctrls = controls; Tet+ = citrullinated tetramer–positive; Tet– = citrullinated tetramer–negative; H2A = histone 2A; cit = citrullinated; cyc = cyclic; hFibA = human fibrinogen α; hFibB = human fibrinogen β; cf = citrullinated filaggrin; IL-8 = interleukin-8.

The recombinant mAb were tested for citrullinated antigen specificity using a CCP assay and synovial antigen planar arrays (27). Of the 69 recombinant mAb expressed, 15 showed positive reactivity on the CCP ELISA (Figure 2A), while 34 recombinant mAb showed reactivity against citrullinated antigens contained on the synovial antigen arrays (Figure 2B). Several of the recombinant mAb exhibited low-level reactivity against native fibrinogen on the planar array.

In comparing the cit-tet+ and cit-tet– recombinant mAb, 33 (56.9%) of 58 cit-tet+ recombinant mAb showed positive reactivity to citrullinated antigens in at least 1 of the 2 assays, as compared to only 3 (27.3%) of 11 tet– recombinant mAb. Intriguingly, of the 33 cit-tet+ recombinant mAb that exhibited ACPA reactivity, 24 (72.7%) bound more than 1 citrullinated antigen, according to the findings on synovial antigen planar array. Taken together, these data indicate that we were able to successfully enrich for, express, and characterize recombinant ACPAs from RA patient plasmablast repertoires.

Differentially mutated antibodies encoded by plasmablast clonal families that exhibit differential binding to citrullinated antigens. To investigate whether epitope spreading arises from affinity maturation, we characterized, using synovial antigen arrays and with results confirmed by ELISA, the specificities of clonally related, yet differentially mutated, antibodies derived from 3 clonal families of ACPA-producing plasmablasts. Clonally related recombinant mAb exhibited distinct, but overlapping, binding specificities to citrullinated antigens (Figure 3A). For example, 5 of the 7 recombinant mAb derived from clonal family 1 bound the hFibA 41–60 cyclic (cyc) cit3 peptide (Figure 3B). Of these 5, both recombinant mAb 78 and recombinant mAb 80 bound H2A/a 1–20 cit3, but not H2B/a 62–81 cit cyc peptide. In contrast, the reverse was exhibited by recombinant mAb 60 and 76.

For both clonal family 2 and clonal family 3, 3 of the expressed recombinant mAb from each family exhibited shared binding reactivities and recognized the same set of citrullinated

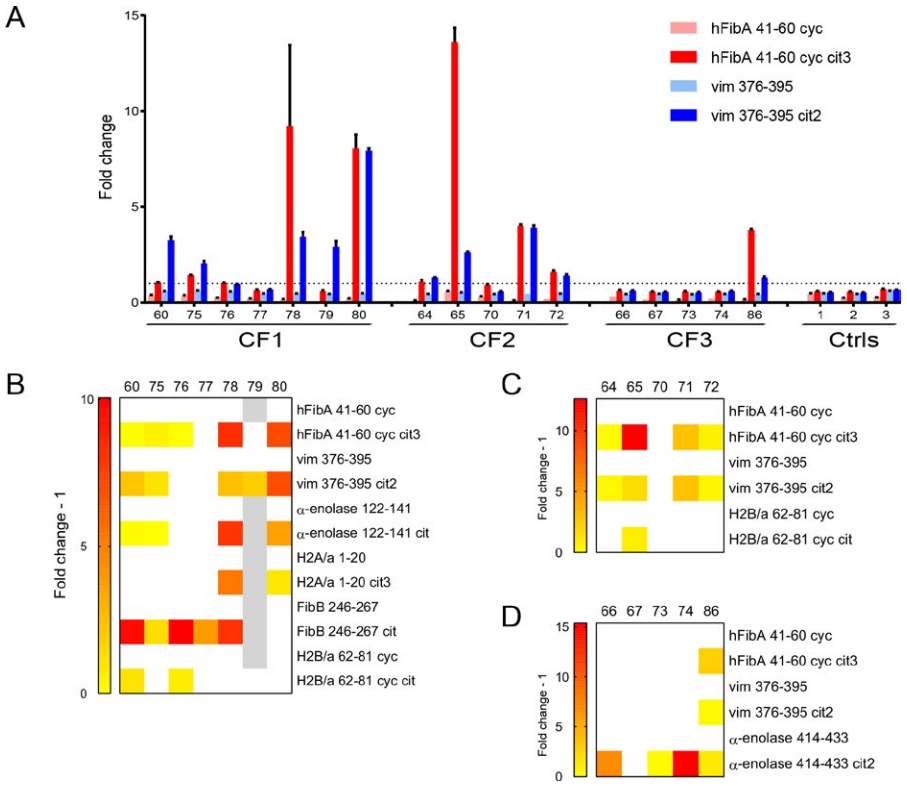

Figure 3. Identification of ACPA–producing plasmablast clonal families (CFs) containing divergent antibodies that exhibit differential polyreactive binding to citrullinated epitopes. **A**, Recombinant monoclonal antibodies (mAb) derived from the 3 ACPA clonal families were expressed and tested by enzyme-linked immunosorbent assay (ELISA) for reactivity against citrullinated peptides and their native counterparts. The cutoff value for positivity for each peptide was set at 3 SD above the average of the negative controls. The horizontal broken line represents the normalized cutoff for positive hits (fold change >1). Data are presented as the mean ± SEM fold change, and are representative of at least 3 replicated experiments. **B–D**, Heatmaps summarize the ELISA data for the binding of mAb derived from clonal families 1 (**B**), 2 (**C**), and 3 (**D**) to various citrullinated peptides. Data are representative of 3 replicated experiments. The mean reactivity of positive hits (fold change – 1 >0) are displayed in a colored gradient ranging from yellow to red. White indicates no detectable reactivity (fold change – 1 ≤0). Gray indicates data not available. vim = vimentin (see Figure 2 for other definitions).

peptides (with distinct sets of citrullinated peptides recognized by each family) (Figures 3C and D). However, each family also contained individual ACPAs that exhibited increased polyreactivity by binding additional citrullinated peptides, and 1 antibody that did not bind any peptides. None of the recombinant mAb tested bound the noncitrullinated versions of the peptides (data not shown). These findings provide evidence of overlapping, but distinct, epitope reactivity, including the generation of polyreactive ACPAs of the divergently mutated antibodies encoded within ACPA plasmablast clonal families.

Restricted binding to citrullinated antigens and reduced polyreactivity exhibited by predicted ancestral antibodies. To directly assess the effects of somatic hypermutation on antigen specificity, we reverted clonally related plasmablast ACPAs back toward their germline sequence. We used IgTree (25) to predict the shared parent antibodies for each of the 3 clonal families (Figures 4A, C, and E). All ancestral antibodies, including the inferred germline sequences, were expressed and tested by ELISA to determine their binding specificity. In cases where the germline sequence was difficult to discern, particularly for the highly variable CDR3 regions, multiple antibodies were produced.

Several of the parent sequences bound citrullinated antigens; however, in general, the ancestral recombinant mAb bound fewer antigens than the affinity-matured recombinant mAb. For example, in clonal family 1, recombinant mAb encoded by parent sequences only bound FibB 246–267 cit and H2A/a 1–20 cit3 peptides, which represent only 2 of the 6 peptides targeted by the corresponding affinity-matured antibodies (Figure 4B). Parent sequences in both clonal family 2 and clonal family 3 bound hFib 41–60 cit3 cyc and vim 376–395 cit peptides, but showed no reactivity against additional peptides bound by the affinity-matured antibodies, namely H2B/a 62–81 cit cyc or α-enolase 414–433 cit2 (Figures 4D and F). Of note, the inferred germline antibodies of 2 of the 3 clonal families did not bind to any citrullinated antigens contained on the synovial antigen arrays (Figures 4B and F). These results demonstrate that the somatic hypermutation and affinity maturation of ACPAs during clonal expansion can lead to epitope spreading of the ACPA response in individuals with RA.

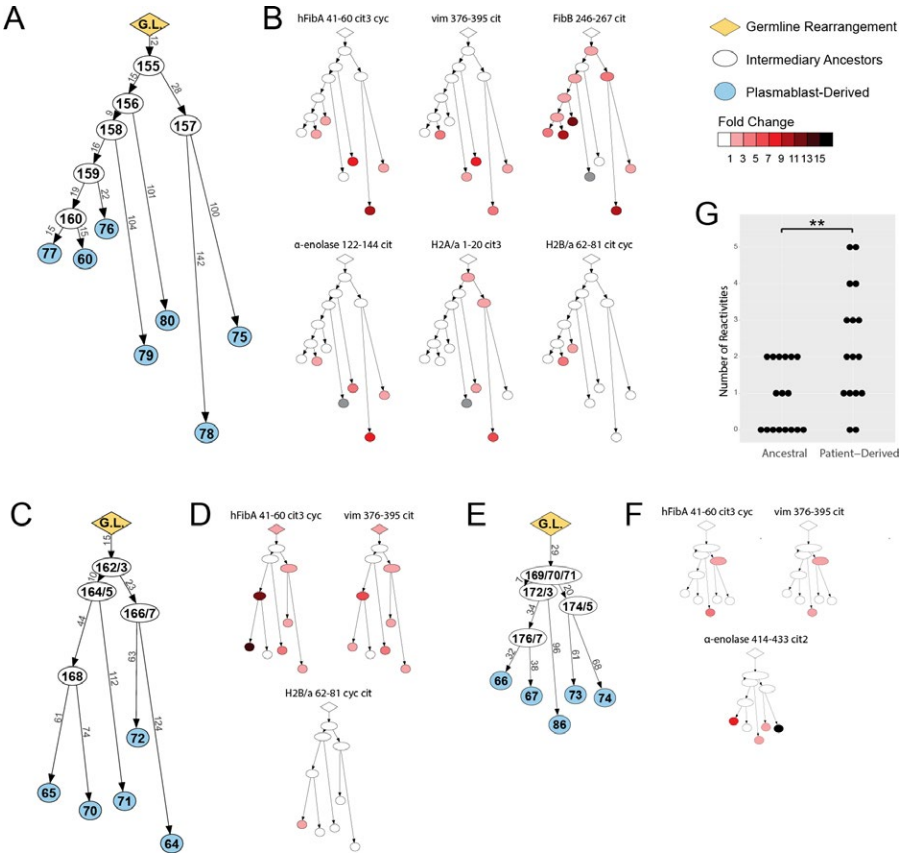

Figure 4. Ancestral antibodies of ACPAs show divergent anticitrulline reactivities and less polyreactivity. **A**, **C**, and **E**, Lineage tree analysis of the ACPA clonal families. Sequences of clonally related antibodies were analyzed with IgTree to generate lineage trees representing clonal families 1 (**A**), 2 (**C**), and 3 (**E**). The length of each branch has been adjusted to proportionally match the number of mutations present between 2 antibody nodes. **B**, **D**, and **F**, ACPA reactivity of predicted ancestral B cell antibodies. Lineage trees for clonal families 1 (**B**), 2 (**D**), and 3 (**F**) are shown in various colors based on the antigen specificity as tested by enzyme-linked immunosorbent assay (ELISA). Data are representative of at least 2 independent experiments. The color intensity indicates the mean strength of the ELISA signal. White symbols indicate no binding, and gray indicates data not available. **G**, Polyreactivity graph. The degree of polyreactivity was compared between all ancestral antibodies and all affinity-matured, patient-derived antibodies across the 3 clonal family groups. The degree of polyreactivity between the groups was compared by Welch's *t*-test. ** = $P \leq 0.01$. G. L. = germline (see Figure 2 for other definitions).

There were a few cases in which the predicted ancestral antibodies bound more citrullinated antigens than did the affinity-matured descendants. For instance, ancestral antibodies RA168, RA174, and RA175 bound hFibA 41–60 cit3 cyc and vimentin (vim) 376–395 cit, but several of their descendant antibodies, RA70, RA73, and RA74, did not (Figures 4C–F). This suggests that certain somatic hypermutations lead to loss of specific epitope recognition for some antibodies. Despite this, individual affinity-matured RA plasmablast–encoded ACPAs exhibited significantly increased polyreactivity as compared to ancestral antibodies (Figure 4G). These results demonstrate that the affinity maturation of ACPA B cells can lead to generation of individual B cell clones that encode ACPAs that bind distinct citrullinated epitopes and/or possess increased polyreactivity, which in turn contributes to the increased number of reactivities against citrullinated antigens by the polyclonal ACPA response in the serum of RA patients.

Use of molecular modeling to predict regions within the ACPA paratope involved in epitope specificity. An antibody's paratope is formed by the specific amino acid residues within the Fv domain that recognize and physically bind to its target antigen. To determine regions within the ACPA paratope responsible for citrullinated antigen binding, we performed molecular modeling using the Rosetta software package to simulate ACPA–citrullinated antigen interactions. We ran docking experiments for 28 antibody–antigen combinations and generated 2 top models for each complex, yielding a total of 56 models. A representative set of 3 docked models is presented in Figures 5A–C. Using PyMOL, we identified for each model the antibody residues predicted to be in contact with the citrullinated antigens; the cumulative results across all antibody–antigen models are shown in Figures 5D–F (29).

As expected, the majority of the contact residues were found in the CDR regions of the antibody sequences (Fig-

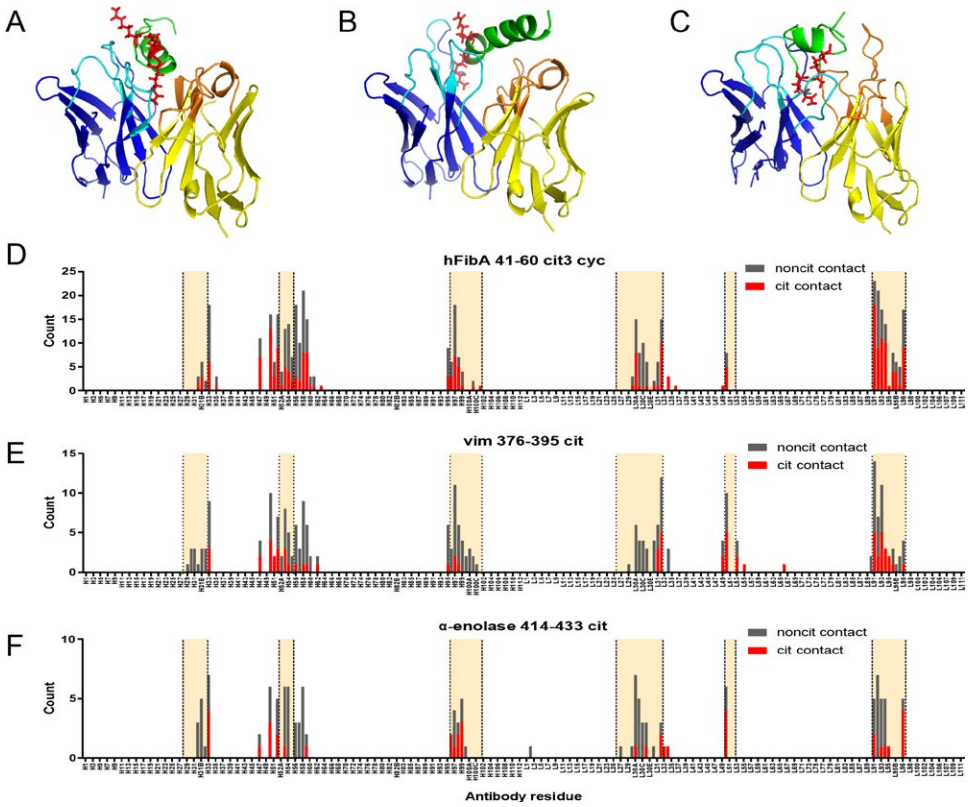

Figure 5. Predicted contact residues of ACPA clonal family antibodies based on molecular modeling. Molecular models of antibodies from clonal families 1, 2, and 3 (see Figure 4) were produced using the Rosetta software package. Three peptides, hFibA 41–60 cit3 cyc (**A** and **D**), vimentin (vim) 376–395 cit (**B** and **E**), and α-enolase 414–433 cit2 (**C** and **F**), were modeled using PEP-FOLD version 2.0 and converted to citrullinated forms using PyMOL. Antibody–antigen docking was performed using Rosetta (see Supplementary Methods, http://onlinelibrary.wiley.com/doi/10.1002/art.40760/abstract). Three representative molecular models of patient-derived monoclonal antibodies (mAb) docked with citrullinated peptides are presented: recombinant mAb 80 docked with hFibA 41–60 cit3 cyc peptide (**A**), recombinant mAb 78 with vim 376–395 cit peptide (**B**), and recombinant mAb 66 with α-enolase 414–433 cit2 peptide (**C**). The predicted contact residues for each docked model were counted and the cumulative results of all antibody–antigen combinations are presented (**D–F**). Antibody sequences are presented using the Chothia (post-1997) numbering scheme, with the heavy and light chains concatenated along the x-axis. Complementarity-determining regions are highlighted between the vertical broken lines. See Figure 2 for other definitions.

ures 5D–F). However, although contact residues are predicted in the heavy-chain CDR3 region, which is the predominant region conferring the binding specificity of most antibodies, these data indicate a stronger likelihood of involvement of the light-chain CDR3 (189 counts) than the heavy-chain CDR3 (85 counts), at least with regard to binding to hFib 41–60 cit3 cyc peptide. We also observed that a substantial number of contact residues were predicted to occur in the framework regions flanking the heavy-chain CDR2 (Figures 5D–F). Taken together, these results from our molecular modeling studies identify multiple regions within the ACPA paratopes that may be predicted to be important for citrullinated antigen binding and that confer polyreactivity against specific sets of citrullinated epitopes.

Altered specificity and epitope spreading resulting from mutagenesis of critical ACPA paratope regions. To confirm the relevant ACPA paratope regions identified from molecular modeling, we used the predicted contact residue information from the docked models to guide mutation studies on 5 pairs of clonally related ACPAs. In each pair, we compared 1 antibody with a particular anti–citrullinated antigen reactivity to a clonally related antibody without that reactivity. Residues predicted to be relevant to binding were transferred from the reactive antibody to the non-reactive antibody (see Supplementary Table 4, available on the *Arthritis & Rheumatology* web site at http://onlinelibrary.wiley.com/doi/10.1002/art.40760/abstract). Mutated antibodies along with the subject-derived recombinant plasmablast antibodies were tested using citrullinated peptide ELISAs to determine their antigen specificities (Figures 6A–E).

We were able to generate mutated antibodies that gained novel specificities against the citrullinated antigens and/or epitopes of interest. For instance, from clonal family 2, recombinant mAb 65 bound both hFib 41–60 cit3 cyc and vim 376–395 cit2, whereas recombinant mAb 70 bound neither antigen. Transferring heavy-chain residues 56–59 from recombinant mAb 65 to recombinant mAb 70 induced binding by modified recombinant mAb

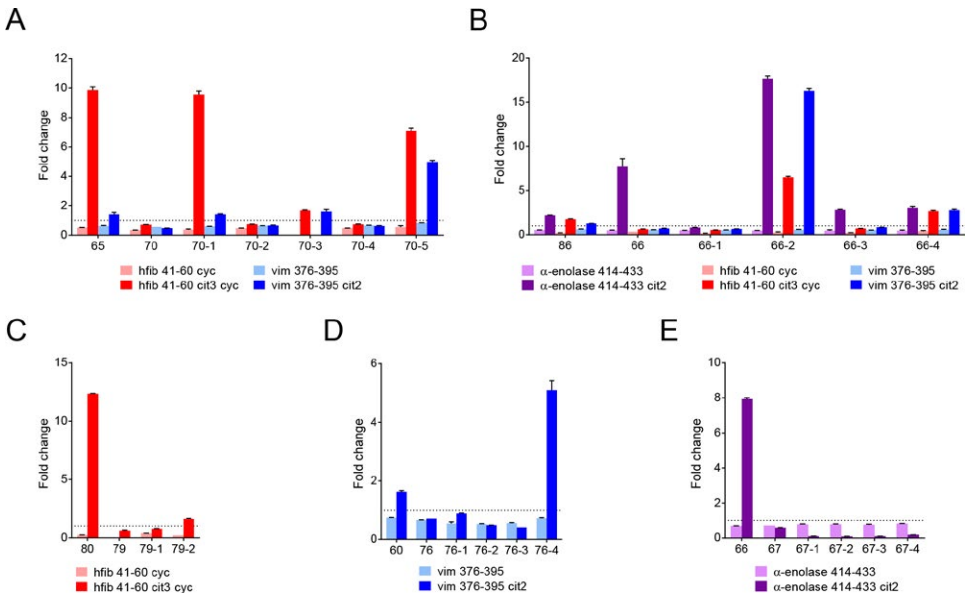

Figure 6. Paratope mutagenesis studies of clonally related ACPAs alter epitope specificity and polyreactivity. For detection of altered citrullinated antigen reactivity of mutated recombinant ACPAs, pairs of antibodies from within the ACPA-producing clonal families were selected based on having divergent reactivity against 1 or more citrullinated peptides. Specifically, recombinant monoclonal antibodies (mAb) 65 and 70 (**A**) were selected from the clonal family presented in Figure 4C. Recombinant mAb pairs 66 and 86 (**B**) and 66 and 67 (**E**) were selected from the clonal family presented in Figure 4E, and recombinant mAb pairs 79 and 80 (**C**) and 60 and 76 (**D**) were selected from the clonal family presented in Figure 4A. Mutated versions of the ACPAs were designed based on the predicted residues identified in the modeling studies that were predicted to be critical for antigen binding (see Figure 5 and Supplementary Table 4, http://onlinelibrary.wiley.com/doi/10.1002/art.40760/abstract). The original pair of recombinant antibodies and their corresponding mutated versions were then analyzed by peptide enzyme-linked immunosorbent assays for reactivity against the same antigens used in the modeling studies. Fold change values above the horizontal broken line are considered to be positive hits (fold change >1). Data are presented as the mean ± SEM, and are representative of at least 2 replicated experiments. vim = vimentin (see Figure 2 for other definitions).

70 against both peptides (recombinant mAb 70-1) (Figure 6A). Importantly, these 4 residues lie in the framework region flanking the heavy-chain CDR2 and were predicted by the modeling studies to be involved in binding. Mutating another region adjacent to the light-chain CDR1 also induced binding to both antigens, although the reactivity against hFibA 41–60 was largely abrogated (recombinant mAb 70-3). Mutating the L31 residue or light-chain CDR3 (recombinant mAb 70-2 and 70-4) did not alter binding. Interestingly, combining all the mutations together (recombinant mAb 70-5) induced not only binding to hFibA 41–60 cit3 cyc but also greater reactivity to vim 376–395 cit2, when compared to either of the original, subject-derived native recombinant mAb.

Similar results were attained for the other pairs of antibodies. Sequences from recombinant mAb 86 were transferred to recombinant mAb 66, resulting in binding activity to hFib 41–60 cit3 cyc and vim 376–395 cit2 (Figure 6B). In particular, transferring residues from the light-chain CDR1 region of recombinant mAb 86 induced strong binding reactivity against the hFib, vim, and α-enolase peptides (recombinant mAb 66-2). The heavy-chain CDR3 from recombinant mAb 80, when grafted into recombinant mAb 79, resulted in a modest amount of binding to hFib 41–60 cit3 cyc (recombinant mAb 79-2) (Figure 6C).

Finally, transferring a combination of the heavy-chain CDR2, heavy-chain CDR3, and light-chain CDR3 from recombinant mAb 60 to recombinant mAb 76 induced strong reactivity against vim 376–395 cit2 peptide (recombinant mAb 76-4) (Figure 6D). Only 1 set of mutated antibodies failed to exhibit new differential reactivities—transferring sequences from recombinant mAb 66 to recombinant mAb 67 resulted in no change in binding against α-enolase 414–433 cit (Figure 6E).

Overall, using the predicted ACPA paratope contact residues identified from the molecular models enabled mutation of clonally related antibody pairs to convey new and/or polyreactive binding to citrullinated epitopes in 4 of the 5 antibodies that had previously shown no reactivity. These mutagenesis studies mimic the somatic hypermutation process, and thus provide further evidence that affinity maturation of ACPAs during clonal expansion can lead to both binding to distinct citrullinated epitopes and/or increased polyreactivity of individual ACPAs in RA.

DISCUSSION

The phenomenon of epitope spreading of the ACPA response against citrullinated antigens is a well-established

feature of RA, but little is understood with regard to how and why it occurs. In the present study, by sequencing the plasmablast antibody repertoire, performing molecular modeling, and characterizing the encoded antibodies, we demonstrate a greater level of ACPA functional diversity at the single-cell level than has been previously reported. We additionally report data suggesting that somatic hypermutations occurring during affinity maturation confer antibody paratopes that mediate both binding to distinct citrullinated epitopes and/or increased polyreactivity, which results in epitope spreading of the serum ACPA response.

To guide our analysis of the ACPA repertoire, we developed cit-peptide tetramers as a sort reagent. This sort reagent enabled identification of ACPA-producing B cells in the blood from individuals with RA, as confirmed by positive reactivities of the encoded recombinant mAb in CCP ELISAs and against citrullinated antigens on synovial antigen arrays. Several of the expressed cit-tet+ plasmablast recombinant mAb did not bind citrullinated antigens either in the ELISA or on planar arrays. There are several potential explanations for this, including potential differences in the conformation of the peptides, which is known to be important for ACPA recognition, as they may differ in solution during flow cytometry as compared to when printed on epoxy slides. Furthermore, some cit-tet– recombinant mAb showed positive reactivity to citrullinated antigens. Since we used a cocktail of 14 citrullinated peptides to generate our tetramers—a relatively small representation of the spectrum of citrullinated antigens known to be present in RA joints—which would be expected to only enrich for a subset of ACPA-producing B cells, we likely missed some ACPA-producing B cells.

Based on the findings from the ELISAs and antigen array analyses, we determined that many of the ACPA recombinant mAb were polyreactive. This is in line with the findings from previous studies, in which ACPAs have been shown to cross-react against multiple citrullinated epitopes (21,30–32). Of note, while most of the studies were limited to analyses of the polyclonal antibodies present in RA patient blood, only a few studies characterized monoclonal ACPAs. Of these, one group identified 36 patient-derived ACPAs, 66.7% of which cross-reacted against multiple epitopes (33). This is similar to our own data, in which 72.2% of our patient-derived ACPAs bound multiple citrullinated epitopes, suggesting that the majority of ACPAs display some degree of polyreactivity. In addition, by testing for reactivity against a greater number of citrullinated antigens via synovial antigen arrays, we demonstrated distinct polyreactivity patterns between individual ACPAs, and showed that affinity maturation can increase the polyreactivity of individual ACPAs.

While the heterogeneity of ACPA reactivity is well established, it is unclear whether the epitope spreading and overall breadth of the ACPA response arises from de novo activation of ACPA B cells targeting distinct citrullinated epitopes or is the result of diversification of the citrullinated epitope binding specificity within individual clonal families. An important finding of this study is the divergence of reactivities observed among clonally related ACPAs, along with the expanded polyreactivity of individual affinity-matured ACPAs against distinct sets of citrullinated antigens.

By definition, clonal families of antibodies derive from a single, activated parent B cell. They share the same germline genes and junctional rearrangements, differing only in the somatic hypermutations that each antibody has individually accumulated over time. According to this dogma, B cells would be selected for continued clonal expansion if their somatic hypermutations increase the affinity and specificity against the original antigen. However, our data suggest that this is not the case for ACPAs, at least not in terms of their antigen specificity. We demonstrate multiple cases in which clonally related ACPAs exhibited differential binding to citrullinated epitopes. Moreover, we demonstrated differences in the ability of ancestral antibodies to bind citrullinated epitopes, often recognizing fewer targets than the affinity-matured antibodies. Finally, we utilized molecular modeling and mutagenesis to recreate somatic hypermutations, proving that they can change the antigen specificities of ACPAs. Taken together, our results reveal that somatic hypermutation alters the specific citrullinated epitopes bound by clonally related ACPAs. We propose that somatic hypermutation during clonal expansion directly causes epitope spreading of the ACPA response.

In a healthy immune response, the majority of B cells encoding autoreactive antibodies arising from affinity maturation are tolerized (34). In autoimmune diseases, these checkpoints can be disrupted, resulting in the escape of B cells encoding autoreactive antibodies. This phenomenon is not unique to RA; autoantibodies against double-stranded DNA can arise from nonautoreactive B cells undergoing somatic hypermutation in mouse models (35,36) and in patients with systemic lupus erythematosus (37). Similarly, autoantibodies against desmoglein 3 in pemphigus vulgaris can be generated through somatic hypermutation (38). Our study is the first to reveal the role of affinity maturation–mediated somatic hypermutation in the generation of ACPAs. Somatic hypermutations induced novel reactivities and/or polyreactivities against citrullinated antigens, resulting in epitope spreading within clonal families of ACPA B cells. In addition, ACPA paratopes that were artificially reverted to the inferred germline sequences lost their anticitrulline reactivity and polyreactivity, suggesting that ACPA paratopes may arise from nonautoreactive B cells.

It is important to recognize the role of citrullinated epitopes in driving the evolution of ACPAs. Based on our studies, we believe that citrulline acts as a “quasi-hapten,” increasing the antigenicity of an otherwise heterogeneous set of antigens, thereby allowing ACPAs to mutate in ways that increase their polyreactivity, so long as they retain a strong affinity for the citrulline residue itself. In this way, antibodies switching from protective reactivity against foreign citrullinated antigens, such as those arising from *Porphyromonas*

gingivalis infection or smoking, to pathogenic autoreactivity against citrullinated self antigens are easily conceivable (33,39). We hypothesize that citrulline recognition increases the likelihood of an ACPA-producing B cell receiving an activation signal because its B cell receptor is less restricted in terms of which antigens it can bind. Increased B cell activation, coupled with polyreactive ACPAs, leads to the continued expansion of B cell populations targeting multiple citrullinated antigens. Accordingly, our findings suggest that affinity maturation during clonal expansion drives epitope spreading of the ACPA response.

If citrulline is indeed acting as a quasi-hapten, elucidating the mechanisms by which ACPA B cells are generated could give rise to next-generation diagnostics and therapeutics. Conceivably, a common feature responsible for targeting citrullinated epitopes may exist among ACPAs. Identification of a conserved binding paratope could lead to treatments that selectively target ACPA-producing B cells. We characterized the ACPA paratope through molecular modeling and mutagenesis. We were able to predict and verify key contact residues important for binding to citrullinated antigens, including the framework region next to heavy-chain CDR2. This is an interesting finding given that framework regions are believed to primarily maintain loop structures and not direct antigen binding. The role of the framework regions in modulating the specificity of the ACPA paratope should be further investigated. Although our studies identified regions within the ACPA paratope important for citrullinated antigen–specific binding, crystallization studies will be necessary to confirm the critical citrulline-binding residues.

Limitations to our study include the patient population of the VA hospital, which is predominantly male, and thus the subjects utilized do not fully reflect the general RA patient population. Furthermore, at the time of our study, our technology was only optimized to sequence plasmablasts expressing IgG or IgA isotype antibodies, and therefore only B cells expressing these 2 antibody subclasses were analyzed. Additionally, given the limited number of patients analyzed, the repertoire-sequencing depth, and the number of recombinant antibodies expressed, it is difficult to estimate the extent to which affinity maturation within clonal families results in epitope spreading within individual patients and across the entire RA population. In our study, we selected the largest cit-tet+ clonal families with polyreactivity against citrullinated antigens for in depth characterization; however, these clonal families were all derived from a single donor (RA3). Therefore, although we anticipate that multiple clonal families with differentially mutated members will also exhibit epitope spreading in the repertoires of other RA patients, it is also possible that there will be families with differentially mutated members that exhibit a shared specificity without evidence of epitope expansion.

The mechanisms driving the evolution of the antibody repertoire may vary between clonal families within a patient, as well as between patients, based on the antigens targeted or may vary over the course of disease. Nevertheless, our study establishes that affinity maturation is a mechanism by which epitope spreading of ACPAs can occur. Although it is possible that our observations in the RA3 sample may represent an extreme case, given the ease with which a few mutations to the variable region of an ACPA can alter its epitope specificity, we suspect that epitope spreading via somatic hypermutation is a common occurrence. We anticipate that affinity maturation–driven epitope spreading has the potential to result in diversification of the specificity of the autoantibody response in multiple directions, depending on the specific mutations conferred in the process. Additional studies utilizing deeper sequencing in a larger cohort would help further define the extent to which this mechanism mediates epitope spreading in RA.

Taken together, our findings shed light on a mechanism mediating the pathogenesis of RA, in which somatic hypermutation and affinity maturation result in epitope spreading within lineages of ACPA-encoding B cells, as well as generation of individual ACPAs that have increased polyreactivity and that contribute to the reactivity of the overall ACPA response in RA. Further structural analysis of ACPA–citrullinated antigen interactions may help identify citrulline-specific and epitope-specific paratope regions that could inform the development of next-generation diagnostics and therapeutics. Finally, defining and characterizing the germline versions of ACPAs could reveal the key antigens involved in breaking tolerance to initiate the development of RA, and thereby open avenues for disease prevention.

ACKNOWLEDGMENTS

We thank Jeremy Sokolove for assisting in acquiring samples and for his scientific insights, and Michelle Bloom for editing and proofreading. We also thank the Stanford Functional Genomics Facility and Stanford Shared FACS Facility for advice and technical assistance.

AUTHOR CONTRIBUTIONS

All authors were involved in drafting the article or revising it critically for important intellectual content, and all authors approved the final version to be published. Dr. Robinson had full access to all of the data in the study and takes responsibility for the integrity of the data and the accuracy of the data analysis.

Study conception and design. Kongpachith, Robinson.
Acquisition of data. Kongpachith, Lingampalli, Ju, Blum, Lu.
Analysis and interpretation of data. Kongpachith, Elliott, Mao, Robinson.

REFERENCES

1. McInnes IB, Schett G. The pathogenesis of rheumatoid arthritis. N Engl J Med 2011;365:2205–19.
2. Firestein GS. Evolving concepts of rheumatoid arthritis. Nature 2003;423:356–61.
3. Schellekens GA, de Jong BA, van den Hoogen FH, van de Putte LB, van Venrooij WJ. Citrulline is an essential constituent of antigenic determinants recognized by rheumatoid arthritis-specific autoantibodies. J Clin Invest 1998;101:273–81.

4. Van Venrooij WJ, van Beers JJ, Pruijn GJ. Anti-CCP antibodies: the past, the present and the future. Nat Rev Rheumatol 2011;7:391–8.
5. Muller S, Radic M. Citrullinated autoantigens: from diagnostic markers to pathogenetic mechanisms. Clin Rev Allergy Immunol 2015;49:232–9.
6. Whiting PF, Smidt N, Sterne JA, Harbord R, Burton A, Burke M, et al. Systematic review: accuracy of anti-citrullinated peptide antibodies for diagnosing rheumatoid arthritis. Ann Intern Med 2010;152:456–64.
7. Sokolove J, Bromberg R, Deane KD, Lahey LJ, Derber LA, Chandra PE, et al. Autoantibody epitope spreading in the pre-clinical phase predicts progression to rheumatoid arthritis. PLoS One 2012;7:e35296.
8. Van de Stadt LA, de Koning MH, van de Stadt RJ, Wolbink G, Dijkmans BA, Hamann D, et al. Development of the anti–citrullinated protein antibody repertoire prior to the onset of rheumatoid arthritis. Arthritis Rheum 2011;63:3226–33.
9. Van der Woude D, Rantapaa-Dahlqvist S, Ioan-Facsinay A, Onnekink C, Schwarte CM, Verpoort KN, et al. Epitope spreading of the anti-citrullinated protein antibody response occurs before disease onset and is associated with the disease course of early arthritis. Ann Rheum Dis 2010;69:1554–61.
10. De Vries-Bouwstra JK, Goekoop-Ruiterman YP, Verpoort KN, Schreuder GM, Ewals JA, Terwiel JP, et al. Progression of joint damage in early rheumatoid arthritis: association with HLA–DRB1, rheumatoid factor, and anti–citrullinated protein antibodies in relation to different treatment strategies. Arthritis Rheum 2008;58:1293–8.
11. Lindqvist E, Eberhardt K, Bendtzen K, Heinegård D, Saxne T. Prognostic laboratory markers of joint damage in rheumatoid arthritis. Ann Rheum Dis 2005;64:196–201.
12. Meyer O, Labarre C, Dougados M, Goupille P, Cantagrel A, Dubois A, et al. Anticitrullinated protein/peptide antibody assays in early rheumatoid arthritis for predicting five year radiographic damage. Ann Rheum Dis 2003;62:120–6.
13. Rönnelid J, Wick MC, Lampa J, Lindblad S, Nordmark B, Klareskog L, et al. Longitudinal analysis of citrullinated protein/peptide antibodies (anti-CP) during 5 year follow up in early rheumatoid arthritis: anti-CP status predicts worse disease activity and greater radiological progression. Ann Rheum Dis 2005;64:1744–9.
14. Nishimura K, Sugiyama D, Kogata Y, Tsuji G, Nakazawa T, Kawano S, et al. Meta-analysis: diagnostic accuracy of anti-cyclic citrullinated peptide antibody and rheumatoid factor for rheumatoid arthritis. Ann Intern Med 2007;146:797–808.
15. Kuhn KA, Kulik L, Tomooka B, Braschler KJ, Arend WP, Robinson WH, et al. Antibodies against citrullinated proteins enhance tissue injury in experimental autoimmune arthritis. J Clin Invest 2006;116:961–73.
16. Wardemann H, Yurasov S, Schaefer A, Young JW, Meffre E, Nussenzweig MC. Predominant autoantibody production by early human B cell precursors. Science 2003;301:1374–7.
17. Arnett FC, Edworthy SM, Bloch DA, McShane DJ, Fries JF, Cooper NS, et al. The American Rheumatism Association 1987 revised criteria for the classification of rheumatoid arthritis. Arthritis Rheum 1988;31:315–24.
18. Elliott SE, Kongpachith S, Lingampalli N, Adamska JZ, Cannon BJ, Mao R, et al. Affinity maturation drives epitope spreading and generation of proinflammatory anti–citrullinated protein antibodies in rheumatoid arthritis. Arthritis Rheumatol 2018;70:1946–58.
19. Lu DR, McDavid AN, Kongpachith S, Lingampalli N, Glanville J, Ju CH, et al. T cell–dependent affinity maturation and innate immune pathways differentially drive autoreactive B cell responses in rheumatoid arthritis. Arthritis Rheumatol 2018;70:1732–44.
20. Tan YC, Blum LK, Kongpachith S, Ju CH, Cai X, Lindstrom TM, et al. High-throughput sequencing of natively paired antibody chains provides evidence for original antigenic sin shaping the antibody response to influenza vaccination. Clin Immunol 2014;151:55–65.
21. Tan YC, Kongpachith S, Blum LK, Ju CH, Lahey LJ, Lu DR, et al. Barcode-enabled sequencing of plasmablast antibody repertoires in rheumatoid arthritis. Arthritis Rheumatol 2014;66:2706–15.
22. Kinslow JD, Blum LK, Deane KD, Demoruelle MK, Okamoto Y, Parish MC, et al. Elevated IgA plasmablast levels in subjects at risk of developing rheumatoid arthritis. Arthritis Rheumatol 2016;68:2372–83.
23. Blum LK, Cao RR, Sweatt AJ, Bill M, Lahey LJ, Hsi AC, et al. Circulating plasmablasts are elevated and produce pathogenic anti-endothelial cell autoantibodies in idiopathic pulmonary arterial hypertension. Eur J Immunol 2018;48:874–84.
24. Gupta NT, Vander Heiden JA, Uduman M, Gadala-Maria D, Yaari G, Kleinstein SH. Change-O: a toolkit for analyzing large-scale B cell immunoglobulin repertoire sequencing data. Bioinformatics 2015;31:3356–8.
25. Barak M, Zuckerman NS, Edelman H, Unger R, Mehr R. IgTree: creating immunoglobulin variable region gene lineage trees. J Immunol Methods 2008;338:67–74.
26. Nair N, Feng N, Blum LK, Sanyal M, Ding S, Jiang B, et al. VP4- and VP7-specific antibodies mediate heterotypic immunity to rotavirus in humans. Sci Transl Med 2017;9:eaam5434.
27. Hueber W, Kidd BA, Tomooka BH, Lee BJ, Bruce B, Fries JF, et al. Antigen microarray profiling of autoantibodies in rheumatoid arthritis. Arthritis Rheum 2005;52:2645–55.
28. Robinson WH, DiGennaro C, Hueber W, Haab BB, Kamachi M, Dean EJ, et al. Autoantigen microarrays for multiplex characterization of autoantibody responses. Nat Med 2002;8:295–301.
29. Schrödinger, LLC. The PyMOL molecular graphics system: version 1.8. 2015.
30. Ioan-Facsinay A, el-Bannoudi H, Scherer HU, van der Woude D, Ménard HA, Lora M, et al. Anti-cyclic citrullinated peptide antibodies are a collection of anti-citrullinated protein antibodies and contain overlapping and non-overlapping reactivities. Ann Rheum Dis 2011;70:188–93.
31. Goules JD, Goules AV, Tzioufas AG. Fine specificity of anti-citrullinated peptide antibodies discloses a heterogeneous antibody population in rheumatoid arthritis. Clin Exp Immunol 2013;174:10–7.
32. Trier NH, Leth ML, Hansen PR, Houen G. Cross-reactivity of a human IgG_1 anticitrullinated fibrinogen monoclonal antibody to a citrullinated profilaggrin peptide. Protein Sci 2012;21:1929–41.
33. Li S, Yu Y, Yue Y, Liao H, Xie W, Thai J, et al. Autoantibodies from single circulating plasmablasts react with citrullinated antigens and porphyromonas gingivalis in rheumatoid arthritis. Arthritis Rheumatol 2016;68:614–26.
34. Pelanda R, Torres RM. Central B-cell tolerance: where selection begins. Cold Spring Harb Perspect Biol 2012;4:a007146.
35. Shlomchik M, Mascelli M, Shan H, Radic MZ, Pisetsky D, Marshak-Rothstein A, et al. Anti-DNA antibodies from autoimmune mice arise by clonal expansion and somatic mutation. J Exp Med 1990;171:265–92.
36. Guo W, Smith D, Aviszus K, Detanico T, Heiser RA, Wysocki LJ. Somatic hypermutation as a generator of antinuclear antibodies in a murine model of systemic autoimmunity. J Exp Med 2010;207:2225–37.
37. Wellmann U, Letz M, Herrmann M, Angermüller S, Kalden JR, Winkler TH. The evolution of human anti-double-stranded DNA autoantibodies. Proc Natl Acad Sci U S A 2005;102:9258–63.
38. Di Zenzo G, Di Lullo G, Corti D, Calabresi V, Sinistro A, Vanzetta F, et al. Pemphigus autoantibodies generated through somatic mutations target the desmoglein-3 cis-interface. J Clin Invest 2012;122:3781–90.
39. Klareskog L, Stolt P, Lundberg K, Källberg H, Bengtsson C, Grunewald J, et al. A new model for an etiology of rheumatoid arthritis: smoking may trigger HLA–DR (shared epitope)–restricted immune reactions to autoantigens modified by citrullination. Arthritis Rheum 2006;54:38–46.

AMERICAN COLLEGE OF RHEUMATOLOGY
EDUCATION • TREATMENT • RESEARCH

Arthritis & Rheumatology
Vol. 71, No. 4, Month 2019, pp 518–528
DOI 10.1002/art.40768

Citrullinated Aggrecan Epitopes as Targets of Autoreactive CD4+ T Cells in Patients With Rheumatoid Arthritis

Cliff Rims,[1] Hannes Uchtenhagen,[2] Mariana J. Kaplan,[3] Carmelo Carmona-Rivera,[3] Philip Carlucci,[3] Katalin Mikecz,[4] Adrienn Markovics,[4] Jeffrey Carlin,[5] Jane H. Buckner,[1] and Eddie A. James[1]

Objective. Recognition of citrullinated antigens such as vimentin, fibrinogen, and α-enolase is associated with rheumatoid arthritis (RA). Emerging data suggest that the matrix protein aggrecan is also recognized as a citrullinated antigen. This study was undertaken to directly visualize Cit-aggrecan–specific T cells and characterize them in patients with RA.

Methods. Citrullinated aggrecan peptides with likely DRB1*04:01 binding motifs were predicted using a previously published scanning algorithm. Peptides with detectable binding were assessed for immunogenicity by HLA tetramer staining, followed by single cell cloning. Selectivity for citrullinated peptide was assessed by tetramer staining and proliferation assays. Ex vivo tetramer staining was then performed to assess frequencies of aggrecan-specific T cells in peripheral blood. Finally, disease association was assessed by comparing T cell frequencies in RA patients and controls and correlating aggrecan-specific T cells with levels of aggrecan-specific antibodies.

Results. We identified 6 immunogenic peptides, 2 of which were the predominant T cell targets in peripheral blood. These 2 epitopes were citrullinated at HLA binding residues and shared homologous sequences. RA patients had significantly higher frequencies of Cit-aggrecan–specific T cells than healthy subjects. Furthermore, T cell frequencies were significantly correlated with antibodies against citrullinated aggrecan.

Conclusion. Our findings indicate that T cells that recognize citrullinated aggrecan are present in patients with RA and correlate with antibodies that target this same antigen. Consequently, aggrecan-specific T cells and antibodies are potentially relevant markers that could be used to monitor patients with RA or at-risk subjects.

INTRODUCTION

Rheumatoid arthritis (RA) is a chronic disease in which joints are destroyed through inflammatory processes (1). Serologic markers, including rheumatoid factor and anti–citrullinated protein antibodies (ACPAs), and a strong association with high-risk alleles such as HLA–DRB1*04:01 implicate autoreactive CD4+ T cells as an important facet of disease etiology (2,3). Detailed studies of ACPA specificity have established that vimentin, fibrinogen, and α-enolase are recognized as citrullinated antigens (4–6). These proteins are also recognized by autoreactive CD4+ T cells, supporting the notion that T cells provide help for antibody responses in RA (7). Furthermore, T cell frequency has been shown to be influenced by disease duration and therapy, suggesting that changes in T cell number and function are reflective of changes in the overall disease process (8).

Emerging data suggest that the matrix protein proteoglycan aggrecan is recognized as a citrullinated antigen (7,9). Aggrecan is an abundant component of extracellular matrix within the joints (along with proteins such as tenascin-C and type II collagen) and

All opinions, interpretations, conclusions, and recommendations are those of the authors and are not necessarily endorsed by the United States Department of Defense.

Supported in part by the NIH (National Institute of Arthritis and Musculoskeletal and Skin Diseases grants ZIA-AR-041199 and R01-AR-064206 to Drs. Kaplan and Mikecz, respectively). Dr. Uchtenhagen's work was supported by the Knut and Alice Wallenberg Foundation. Dr. Buckner's work was supported by the NIH (National Institute of Allergy and Infectious Diseases grant U01-AI-101981) and by the Office of the Assistant Secretary of Defense for Health Affairs (Peer Reviewed Medical Research Program Investigator-Initiated Research award W81XWH-15-1-0003).

[1]Cliff Rims, MHS, Jane H. Buckner, MD, Eddie A. James, PhD: Benaroya Research Institute at Virginia Mason, Seattle, Washington; [2]Hannes Uchtenhagen, PhD: Benaroya Research Institute at Virginia Mason, Seattle, Washington, and Karolinksa Institutet, Karolinska University Hospital, Stockholm, Sweden; [3]Mariana J. Kaplan, MD, Carmelo Carmona-Rivera, PhD, Philip Carlucci, BS: National Institute of Arthritis and Musculoskeletal and Skin Diseases, NIH, Bethesda, Maryland; [4]Katalin Mikecz, MD, PhD, Adrienn Markovics, MD, PhD: Rush University Medical Center, Chicago, Illinois; [5]Jeffrey Carlin, MD: Virginia Mason Medical Center, Seattle, Washington.

Mr. Rims and Dr. Uchtenhagen contributed equally to this work.

No potential conflicts of interest relevant to this article were reported.

Address correspondence to Jane H. Buckner, MD or Eddie A. James, PhD, Benaroya Research Institute, 1201 Ninth Avenue, Seattle, WA 98101. E-mail: jbuckner@benaroyaresearch.org or ejames@benaroyaresearch.org.

Submitted for publication December 22, 2017; accepted in revised form October 30, 2018.

has been conclusively shown to be citrullinated in human articular cartilage (10). The presence of aggrecan fragments has been documented within synovial fluid and is reported to increase with age (11,12). Furthermore, immunization with aggrecan was shown to induce arthritis in murine models (13). Levels of autoantibodies to citrullinated epitopes within the G1 domain are elevated in RA but not in osteoarthritis, indicating that such antibodies are specifically associated with autoimmunity rather than merely accompanying joint damage (10). Citrullinated CD4+ T cell epitopes from aggrecan have been described, and elevated responses to some were shown to be associated with RA (9,14,15). However, a systematic HLA-specific characterization of aggrecan-derived T cell epitopes has yet to be performed, and tools to directly visualize aggrecan-specific T cells have yet to be developed. The goals of our study were to define citrullinated aggrecan epitopes in the context of DRB1*04:01, to visualize and characterize Cit-aggrecan–specific T cells, and to investigate their relevance in patients with RA.

MATERIALS AND METHODS

Epitope prediction and peptide synthesis. A previously described prediction method was used to identify citrullinated aggrecan peptides with motifs likely to bind to HLA–DRB1*04:01 (henceforth DR0401) (8,16). Briefly, motif scores were calculated by multiplying coefficients corresponding to each anchor residue for all possible core 9-mers within the protein that included an internal or flanking arginine or citrulline residue. A total of 28 peptides with motif scores of 0.1 or higher were synthesized by Mimotopes. For tetramer production and further studies, selected citrullinated peptides and their corresponding native peptides were resynthesized by Sigma. All peptides were dissolved in DMSO to a stock concentration of 20 mg/ml.

Peptide binding to DR0401. The binding capacity of citrullinated aggrecan peptides to DR0401 was assessed using a previously described assay (17). Briefly, candidate peptides were plated at increasing concentrations against a fixed concentration of a biotinylated reference peptide, influenza hemagglutinin$^{306–318}$ (PKYVKQNTLKLAT) in wells coated with anti–HLA–DR antibody (clone L243, supplied by the Benaroya Research Institute [BRI] Tetramer Core). Europium-conjugated streptavidin was used to label residual HLA-bound biotinylated peptide (PerkinElmer), and the residual peptide concentration was quantified using a Wallac Victor2 Multilabel Counter. Binding curves were fitted by a sigmoidal regression model using GraphPad Prism 7.0, and 50% effective concentration values were calculated as the peptide concentration needed to displace 50% of the reference peptide.

Subject recruitment. Control and RA subjects were recruited with informed consent through the BRI healthy control and rheumatic disease registries. Sample use was approved by the BRI Institutional Review Board. All subjects had HLA–DRB1*04:01 haplotypes. Control subjects had no autoimmune disease, no first-degree relatives with RA, and ranged in age from 23 to 66 years (mean ± SD 50.2 ± 10.9 years). All RA patients were ACPA positive, ranged in age from 25 to 71 years (mean ± SD 52.5 ± 11.3 years), and met the American College of Rheumatology 1987 revised criteria for RA (1).

Isolation and preparation of peripheral blood mononuclear cells (PBMCs). PBMCs were separated from whole blood over Ficoll-Hypaque gradient, cryopreserved in heat-inactivated fetal bovine serum (FBS) supplemented with 10% DMSO, and stored in liquid nitrogen. PBMCs were subsequently thawed at 37°C, washed with RPMI media supplemented with 10% FBS and 0.001% DNase/Benzonase (Sigma-Aldrich), and resuspended in RPMI media supplemented with 10% human serum (Gemini Bio-Products).

Tetramer production. Class II tetramers were generated by the BRI Tetramer Core as previously described (18). Briefly, DR0401 monomer was purified from insect cell cultures and biotinylated at a sequence-specific site. Biotinylated monomer was loaded with 0.2 mg/ml of peptide and incubated for 72 hours at 37°C in the presence of 2.5 mg/ml n-octyl-β-D-glucopyranoside and 1 m*M* Pefabloc SC (Sigma-Aldrich). Loaded monomers were conjugated into tetramers with fluorescence-labeled streptavidin for 6–18 hours at room temperature at a molar ratio of 8:1.

In vitro PBMC expansion, HLA class II tetramer staining, and T cell clone isolation. PBMCs were cultured at 5 × 10^6 cells/well in 48-well plates in 1 ml RPMI supplemented with 10% human serum and 10 μg/ml of peptide. On day 6, cells were transferred to fresh wells and 10 units/ml of recombinant interleukin-2 (IL-2; Roche) was added. After 14 days, cultures were screened by staining a 50-μl aliquot with 0.5 μl of tetramer (final concentration 5 ng/ml) for 1 hour at 37°C. Cultures were then costained with allophycocyanin (APC)–conjugated anti-CD4 (BD Biosciences) for 30 minutes at 4°C in the dark, washed, and analyzed by flow cytometry. To isolate T cell clones, staining was repeated and tetramer-labeled cells were single-cell sorted using a BD FACSAria II into 96-well round-bottomed plates containing 150 μl of human T cell media and expanded by adding 10^5 irradiated feeders, 10 units/ml IL-2, and 2 μg/ml phytohemagglutinin (PHA; Thermo). After 10–14 days, expanded cells were transferred to 96-well flat-bottomed plates and split as needed for an additional 14 days. The resulting clones were rescreened by tetramer staining. Positive clones were further expanded by additional rounds of PHA stimulation and then cryopreserved.

Proliferation assays. To assess proliferation in response to citrullinated, partially citrullinated, or unmodified peptide, clones or cells were plated at 2.5 × 10^4 cells/well in 96-well round-bottomed plates in human T cell media with 10^5 irradiated antigen-presenting

cells from an HLA–DRB1*04:01–positive (DR0401-positive) donor plus peptide and incubated at 37°C. After 72 hours, 1 μCi of ^{3}H-thymidine was added and incubated for 24 hours. Cells were then washed and lysed in water, and DNA was collected onto glass fiber filter membranes (PerkinElmer) using a plate harvester. Each filter mat was immersed in Betaplate Scint (PerkinElmer), and counts were collected on a Wallac 1450 LSC and Luminescence Counter (PerkinElmer). The stimulation index was determined by calculating the ratio of counts of peptide-stimulated cells to counts of unstimulated cells.

Intracellular cytokine staining of T cell clones. To assess their functional profiles, T cell clones were activated with 50 ng/ml phorbol myristate acetate (PMA) and 1 μg/ml ionomycin for 30 minutes, treated with brefeldin A (eBioscience), and incubated for 3 hours at 37°C. Cells were fixed using fixation/permeabilization buffer (eBioscience), washed in permeabilization buffer (eBioscience), stained using antibodies to PerCP–Cy5.5–conjugated granulocyte–macrophage colony-stimulating factor (GM-CSF), fluorescein isothiocyanate [FITC]–conjugated granzyme B, Alexa Fluor 700–conjugated interferon-γ (IFNγ), Alexa Fluor 647–conjugated IL-4, and phycoerythrin (PE)–conjugated IL-21 (all from BioLegend), collected on an LSRII flow cytometer (BD Biosciences), and analyzed using FlowJo (Tree Star).

Activation of T cell clones by fibroblast-like synoviocytes (FLS). Human FLS were HLA typed and isolated as previously described (19), cocultured with T cell clones by plating 1 × 10^5 FLS (passage 10 for DR0401-positive FLS and passage 12 for DR0401-negative FLS) with 2 × 10^5 T cells per well, and incubated in the presence or absence of anti-DR antibody (20 μg/ml) (L243; BRI Tetramer Core) or corresponding peptide as a positive control for 5 days. Clones and FLS were also cultured individually to assess background. On day 4, 1 μCi of ^{3}H-thymidine was added to each well. Cells were harvested after 24 hours and counts were obtained on day 5 as described above.

Measurement of aggrecan gene expression in FLS. Human FLS were plated on a single 100-mm tissue culture dish (BD Biosciences). Once 80% confluent, cells were treated with 1,000 units/ml IFNγ (catalog no. 285-IF; R&D Systems) for 72 hours. Cells were then treated with trypsin, and RNA was extracted using a Qiagen RNeasy Mini kit (catalog no. 74134) according to the manufacturer's protocol. RNA was quantified using a NanoDrop spectrophotometer, and complementary DNA was synthesized using a ThermoFisher SuperScript IV reverse transcriptase kit (catalog no. 18091050) according to the manufacturer's instructions in a PTC-225 Peltier thermal cycler. Complementary DNA was probed using TaqMan Fast Advanced Master Mix (catalog no. 4444557; Applied Biosystems) in an Applied Biosystems 7500 Fast Real-Time PCR System cycler with the following Applied Biosystems TaqMan primers: VIC-MGB GAPDH Hs02786624_g1, FAM-MGB PDPN Hs00366766_m1, FAM-MGB CD3E Hs01062241_m1, FAM-MGB ACAN Hs00153936_m1, and FAM-MGB VCAN Hs00171642_m1. Gene expression levels were assessed by comparing mean C_t values to the mean C_t of GAPDH. C_t values defined as "undetermined" or assigned a default value above 35 by 7500 software version 2.3 were considered "undetectable."

Ex vivo detection of Cit-aggrecan–specific T cells. For ex vivo detection of antigen-specific T cells, 3.5 × 10^7 PBMCs were thawed and rested for 2 hours at 37°C, resuspended in 200 μl of T cell media, and treated with dasatinib for 10 minutes at 37°C to prevent internalization of T cell receptors. Cells were stained by adding 4.5 μl of each tetramer (final concentration 11 ng/ml) for 90 minutes at room temperature, with gentle manual shaking every 15 minutes. Cells were then labeled with anti-PE and anti-Myc magnetic beads (Miltenyi Biotec) for 20 minutes at 4°C, enriched on a magnetic column according to the manufacturer's protocols, reserving a 1% cell fraction before enrichment to estimate the total number of CD4+ T cells in the sample. Cells were surface-stained for 30 minutes at 4°C with CD14/CD19/FITC-conjugated annexin V (all from BioLegend), V500-conjugated CD4 (BD Biosciences), Alexa Fluor–conjugated CD45RA (BD Biosciences), and APC–Cy7–conjugated CCR7 (BioLegend). Samples were collected to completion on a BD FACSCanto II. Flow cytometry data were analyzed using FlowJo version 10 and Graph Pad Prism version 7.0. The frequency (F) of antigen-specific T cells was calculated as: F = (1,000,000 × tetramer-positive events from enriched sample)/(100 × number of CD4+ cells from the nonenriched fraction). Details of the gating strategy are available upon request from the corresponding author.

IgM depletion and serum antibody detection. IgM from serum samples from RA patients and healthy controls were depleted via immunoabsorption. Briefly, diluted sera were incubated with goat anti-human IgM (μ chain–specific) antibody conjugated to agarose beads (Millipore Sigma) for 90 minutes at 4°C on a rotary wheel. IgM depletion was verified by anti-IgM Western blotting. For enzyme-linked immunosorbent assay (ELISA), wells of 96-well ELISA plates (Nunc) were coated overnight with recombinant human aggrecan G1 or citrullinated recombinant human aggrecan G1 domain (0.2 μg/well each) in 100 μl/well of 0.15*M* sodium carbonate buffer (pH 9.6) at room temperature (10). Unbound antigen was removed by washing with horseradish peroxidase (HRP) wash buffer (Inova Diagnostics). Wells were blocked with heat-inactivated normal goat serum (R&D Systems) diluted to 1:10 in HRP sample diluent (Inova Diagnostics) for 2 hours at room temperature. IgM-depleted serum samples were diluted 1:100 in sample diluent and incubated with the antigen-coated wells (100 μl/well, duplicate wells) for 2 hours at room temperature.

Bound IgG was detected by incubation with 100 μl/well of HRP-conjugated polyclonal goat anti-human IgG (Abcam)

at a 1:3,000 dilution for 1 hour at room temperature. Unbound material was removed with HRP wash buffer between each of these steps. The color reaction was developed by incubation with 100 μl/well 3,3′,5,5′-tetramethylbenzidine (BD OptEIA TMB substrate set) for 10 minutes in the dark at room temperature and stopped with 25 μl/well stop solution (4N HCl). Absorbance at 450 nm was read in a Synergy 2 ELISA reader (BioTek Instruments). Net optical density (ΔOD) values were calculated by subtracting the OD of wells not containing samples (but coated with recombinant human G1 or Cit–recombinant human G1 and reacted with HRP secondary antibody) from the OD values of serum samples.

Anti-IgM Western blotting. Paired nondepleted and IgM-depleted serum samples (60 μg protein each) were run in a 7.5% sodium dodecyl sulfate–polyacrylamide gel electrophoresis gel under reducing conditions. The proteins were transferred to a PVDF membrane, probed with HRP-conjugated goat anti-human IgM μ chain–specific antibody (Abcam) and visualized by enhanced chemiluminescence (Amersham).

Statistical analysis. All statistical tests were performed using Prism software version 7 (GraphPad). Tests that were used (as appropriate) included unpaired *t*-tests, unpaired *t*-tests with Welch's correction, Mann-Whitney tests, analysis of variance with Sidak's multiple comparisons test, and Spearman's correlation. *P* values less than 0.05 were considered significant. Data are reported as the mean ± SEM.

RESULTS

Aggrecan peptides bind to DR0401 and are immunogenic. Using our previously described approach for identifying epitopes from joint-associated antigens (8,16), we synthesized 28 citrullinated peptides corresponding to aggrecan sequences that contain DR0401 binding motifs (data available upon request from the corresponding author). Detectable in vitro binding to recombinant DR0401 protein was confirmed for 13 of these peptides; among these, 4 peptides were preferentially bound in their citrullinated form (Table 1). To assess the immunogenicity of these arginine-containing aggrecan or citrullinated aggrecan peptides, PBMCs from DR0401-positive RA patients and healthy controls were stimulated in vitro. For Cit-aggrecan or Arg-aggrecan peptides with detectable HLA binding, expansion of epitope-specific T cells was evaluated through HLA class II tetramer staining. Possible responses to Arg-aggrecan peptides that corresponded to Cit-aggrecan peptides but lacked detectable binding were evaluated through proliferation assays, but no responses above background proliferation were observed (data available upon request from the corresponding author).

Tetramer staining indicated that aggrecan peptides display varying degrees of immunogenicity (Figure 1A). Two Arg-aggrecan peptides occasionally elicited responses (Figure 1B), but all median responses were well below our established cutoff, and consequently these peptides were not subjected to further study. In total, 7 Cit-aggrecan peptides elicited median responses in patients with RA that were above a previously established cutoff (Figure 1C). Among these, 6 were verified through isolation T cell clones (data available upon request from the corresponding author) and were included in further study. When in vitro responses to Cit-aggrecan peptides were examined, responses were also detectable in HLA-matched controls (Figure 1D) but were more frequently seen in patients with RA (Figure 1E).

In all, our approach identified 6 citrullinated aggrecan peptides that bound to DR0401 and elicited in vitro T cell responses. Two of these epitopes exhibited preferential binding to DR0401.

Table 1. Binding characteristics of aggrecan peptides chosen for further study

Peptide	Sequence	Cit, μ*M*	Arg, μ*M*
Aggrecan$^{3–20}$	TLLWVFVTL(Cit)VITAAVTV	35.30	36.06
Aggrecan$^{153–168}$*	IVFHY(Cit)AIST(Cit)YTLDF	0.98	50.96
Aggrecan$^{161–178}$	ST(Cit)YTLDFD(Cit)AQ(Cit)ACLQ	0.99	1.02
Aggrecan$^{200–215}$	DAGWLADQTV(Cit)YPIHT	2.95	2.53
Aggrecan$^{225–244}$*	DEFPGV(Cit)TYGI(Cit)DTNETYDV	2.18	>100
Aggrecan$^{298–313}$	SAGWLAD(Cit)SV(Cit)YPISK	1.90	2.94
Aggrecan^{477}*	GVVFHY(Cit)PGPT(Cit)YSLTF	14.69	>100
Aggrecan^{520}	GYEQCDAGWL(Cit)DQTV(Cit)YPIV	12.62	15.61
Aggrecan^{553}*	PGV(Cit)TYGV(Cit)PSTETYDVY	7.96	>100
Aggrecan^{568}	DVYCFVD(Cit)LEGEVFFA	23.42	3.06
Aggrecan^{579}	EVFFAT(Cit)LEQFTFQE	78.43	15.33
Aggrecan^{621}	KCYAGWLADGSL(Cit)YPIV	6.90	4.66
Aggrecan^{684}	NSPFCLE(Cit)TPLGSPDPA	0.12	0.13

* Sequences that bind better as citrullinated peptides.

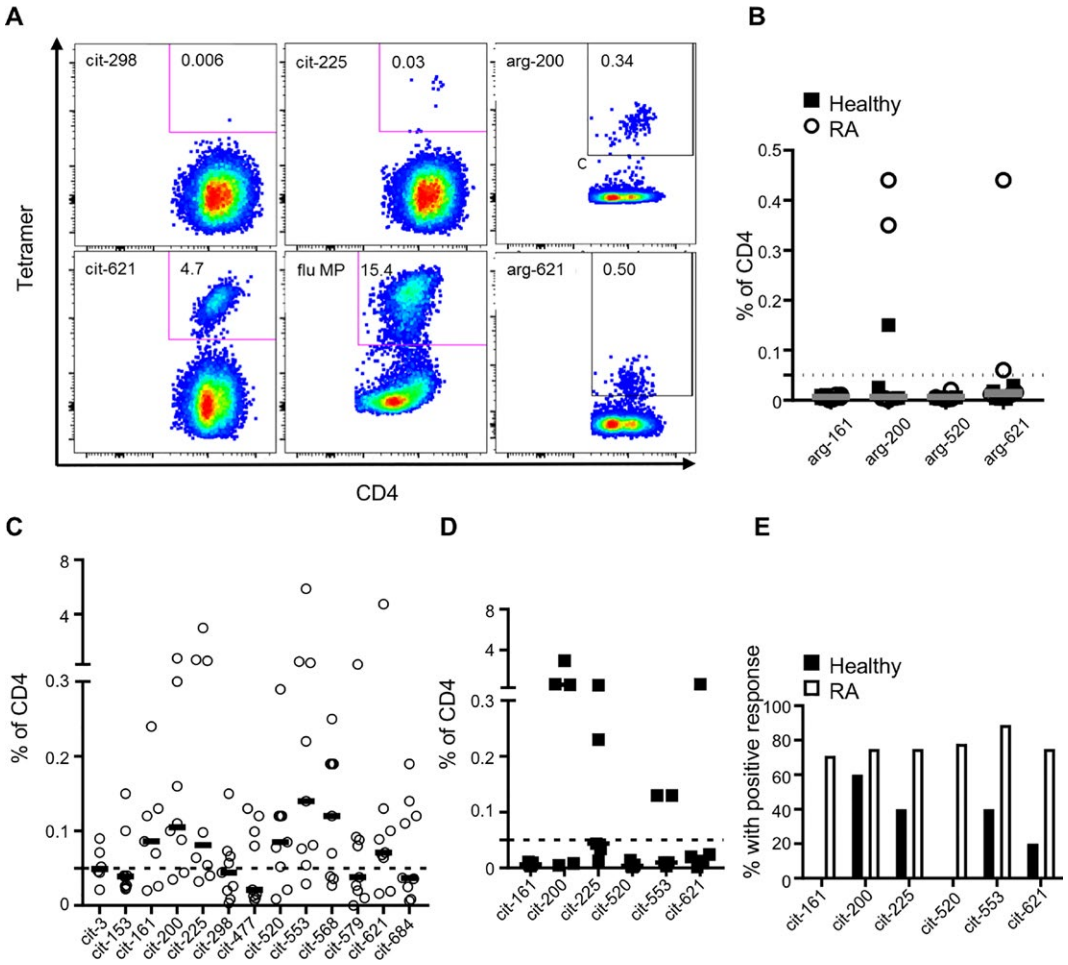

Figure 1. Assessment of the immunogenicity of aggrecan peptides. Peptides with positive binding to DR0401 were evaluated for immunogenicity by tetramer staining after 14 days of peptide stimulation. **A**, Representative fluorescence-activated cell sorting plots showing that peptides elicited diverse levels of T cell expansion that ranged from negligible expansion (top left) to modest expansion (top center) to moderate expansion (top right and bottom right) to robust expansion (bottom left). Expansion in response to an immunodominant influenza peptide (influenza matrix protein [flu MP]) was used as a reference (bottom center). Values are the percentage of cultured CD4+ T cells that were stained by DR0401 tetramer loaded with the indicated peptide. **B**, Relatively low immunogenicity of the candidate Arg-aggrecan epitopes. Median responses in healthy controls and rheumatoid arthritis (RA) patients were <0.05% of total CD4+ T cells. **C**, Immunogenicity of several candidate Cit-aggrecan epitopes. Median responses in RA patients were >0.05% of total CD4+ T cells. **D**, In vitro responses to the 6 most promising Cit-aggrecan epitopes in HLA-matched controls. Responses were observed in some controls. In **B**–**D**, symbols represent individual subjects; horizontal bars show the median. Broken lines indicate the threshold value of 0.05% that was used to define positive responses. **E**, Percentages of healthy controls (n = 5) and RA patients (n = 9) with responses to the Cit-aggrecan epitopes greater than the 0.05% cutoff. The percentages were higher for RA patients for each epitope. Differences between RA patients and controls were significant for Cit-aggrecan^{161} and Cit-aggrecan^{520} ($P = 0.028$ and $P = 0.021$, respectively) and approached significance for Cit-aggrecan^{553} and Cit-aggrecan^{621} ($P = 0.08$ and $P = 0.1$, respectively, by Fisher's exact test).

For the remaining peptides, the citrulline residues within the predicted binding register are positioned as T cell contacts (Table 2). Some of these immunogenic Cit-aggrecan peptides overlapped with previously described epitopes. In particular, our Cit-aggrecan^{200}, Cit-aggrecan^{298}, and Cit-aggrecan^{621} peptides correspond to epitopes described by Boots et al (20). The Cit-aggrecan^{298} peptide also overlaps with the p49 aggrecan sequence reported by Markovics et al (MDMCSAGWLAD(Cit)SVR) (9). Surprisingly, the Cit-aggrecan^{84} peptide (VVLLVATEG(Cit)VRVNSAYQDK) described by Law et al bound with very low affinity (21) (data not shown).

Table 2. Predicted motifs for immunogenic aggrecan peptides

Peptide	Sequence*
Aggrecan$^{161–178}$	ST(CIT)**Y**TLDFD(Cit)AQ(Cit)ACLQ
Aggrecan$^{200–215}$	DAG**W**LADQTV(Cit)YPIHT
Aggrecan$^{225–244}$	DEFPGV(Cit)T**Y**GI(Cit)DTNETYDV
Aggrecan^{520}	G**Y**EQCDAGWL(Cit)DQTV(Cit)YPIV
Aggrecan^{553}	PGV(CIT)T**Y**GV(Cit)PSTETYDVY
Aggrecan^{621}	KCYAG**W**LADGSL(Cit)YPIV

* Predicted DR0401 binding motifs are underlined with the first anchor shown in boldface.

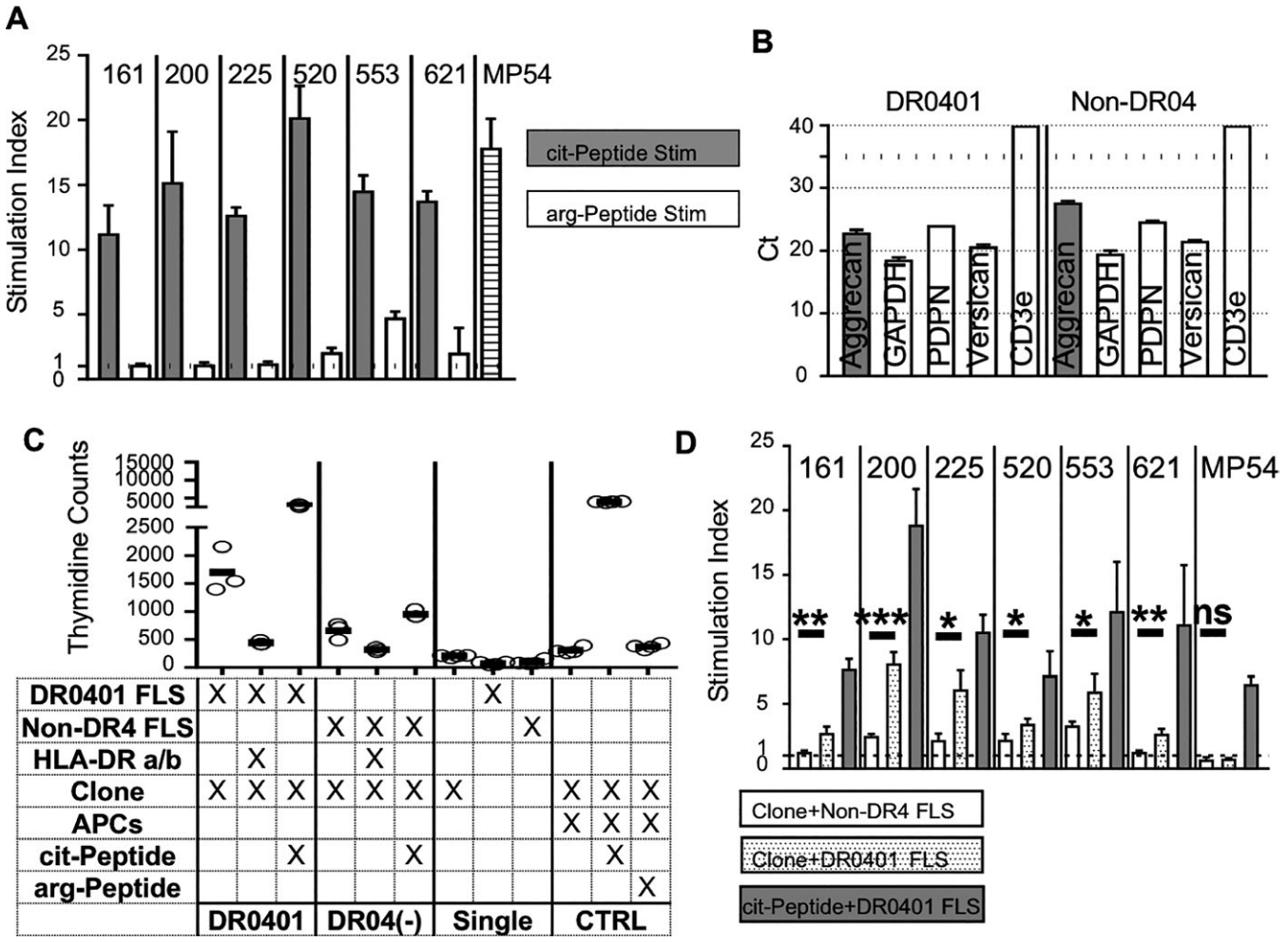

Figure 2. Aggrecan-specific T cell clones respond when cocultured with fibroblast-like synoviocytes (FLS). **A**, Stimulation index for citrullinated peptides and arginine-containing peptides. As a specificity control, each clone was stimulated with Cit-aggrecan or Arg-aggrecan peptide in the presence of HLA–DR0401–positive antigen-presenting cells (APCs). **B**, Aggrecan expression by DR0401 and non-DR04 FLS lines. Aggrecan expression was assessed by quantitative polymerase chain reaction with GAPDH (reference), podoplanin (PDPN; positive control), versican (related proteoglycan), and CD3e (negative control). The C_t value is inversely correlated with mRNA levels and values >35 (dotted line) were considered undetectable. In **A** and **B**, bars show the mean ± SEM. **C**, Representative raw proliferation results for an aggrecan-specific T cell clone cocultured with an FLS line from a DR0401-positive rheumatoid arthritis (RA) patient (columns labeled DR0401) or an FLS line from a DR0401-negative RA patient (columns labeled DR04[-]) in the presence or absence of an HLA–DR blocking antibody (row labeled anti–HLA–DR) and/or the cognate citrullinated peptide (row labeled cit-peptide). Experimental control conditions, including each cell line cultured alone (columns labeled Single) or the same T cell clone cocultured with irradiated DR0401-positive peripheral blood mononuclear cells (columns labeled CTRL) in the presence or absence of the cognate citrullinated peptide (row labeled cit-peptide) or the corresponding arginine peptide (row labeled arg-peptide) are also shown. Antigen presentation via HLA–DR0401 was required to elicit proliferation above background. Symbols represent individual subjects; horizontal bars show the median. **D**, Stimulation index for T cell clones cocultured with DR0401-negative FLS, DR0401-positive FLS, or DR0401-positive FLS plus peptide. Clones specific for Cit-aggrecan^{161}, Cit-aggrecan^{200}, Cit-aggrecan^{225}, Cit-aggrecan^{520}, Cit-aggrecan^{553}, and Cit-aggrecan^{621} showed higher expansion when cocultured with DR0401-positive FLS as compared to DR0401-negative FLS. In contrast, the influenza (matrix protein 54 [MP54])–specific clone was not activated by DR0401-positive FLS cells in the absence of peptide. Bars show the mean ± SEM (n = 3 samples per group). * = $P < 0.05$; ** = $P < 0.01$; *** = $P < 0.001$. NS = not significant.

Aggrecan-specific CD4+ T cells are citrulline selective and respond to FLS-derived antigens. To assess the selectivity of aggrecan-specific T cells, clones corresponding to each specificity were tested by proliferation assay for their responsiveness to Cit-aggrecan or the corresponding Arg-aggrecan peptide. Each clone preferentially responded to citrullinated peptide (Figure 2A). To assess their function, we characterized the cytokine profiles of aggrecan-specific T cell clones by intracellular staining. Following activation with PMA/ionomycin, the clones predominantly secreted IFNγ and GM-CSF with lesser amounts of granzyme B and IL-4 (data available upon request from the corresponding author). It is possible that a less robust antigen-specific activation of the clones would have elicited a more focused cytokine response.

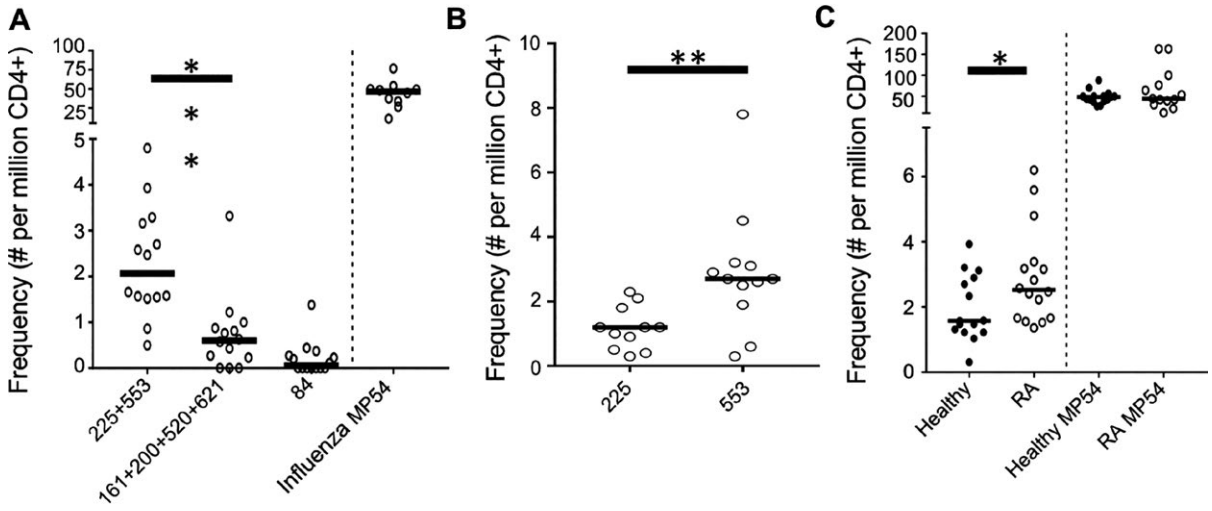

Figure 3. Greater prevalence of T cells that recognize dominant aggrecan epitopes in rheumatoid arthritis (RA) patients than in healthy subjects. **A**, Ex vivo frequencies of T cells specific for Cit-aggrecan^{225} and Cit-aggrecan^{553}, T cells specific for Cit-aggrecan^{161}, Cit-aggrecan^{200}, Cit-aggrecan^{520}, and Cit-aggrecan^{621}, and T cells specific for Cit-aggrecan^{84} in DRB1*04:01-positive RA patients. An influenza tetramer (matrix protein 54 [MP54]) was used as a positive control. **B**, Frequencies of T cells specific for Cit-aggrecan^{225} and T cells specific for Cit-aggrecan^{553} in DRB1*04:01-positive RA patients. **C**, Ex vivo frequencies of T cells specific for Cit-aggrecan^{225} and Cit-aggrecan^{553} (left) and of MP54 (right) in DRB1*04:01-positive healthy controls and DRB1*04:01-positive RA patients. Symbols represent individual subjects (n = 14 per group in **A**, except for MP54, for which only 10 subjects had sufficient cells available, n = 12 per group in **B**, and n = 15 healthy controls and 16 RA patients per group in **C**); horizontal bars show the median. * = P = 0.0395; ** = P = 0.0037; *** = P = 0.0002, by 2-tailed Mann-Whitney test.

To assess whether the Cit-aggrecan epitopes that we identified are naturally processed and presented, we performed coculture experiments with aggrecan-specific clones and human FLS cells. FLS lines isolated from DR0401-positive and DR0401-negative donors had detectable levels of aggrecan messenger RNA (mRNA) (albeit lower than versican mRNA), expressed podoplanin, and (as expected) lacked CD3e expression (Figure 2B). Each clone showed increased proliferation when cocultured with DR0401-positive FLS cells alone or pulsed with peptide or with cognate peptide presented by irradiated DR0401-positive feeder cells, and this proliferation was blocked by an anti–HLA–DR antibody (Figures 2C and D). Clones with all 6 specificities (Cit-aggrecan^{161}, Cit-aggrecan^{200}, Cit-aggrecan^{225}, Cit-aggrecan^{520}, Cit-aggrecan^{553}, and Cit-aggrecan^{621}) had significantly higher levels of proliferation in response to DR0401-positive FLS cells as compared with DR0401-negative FLS cells (Figure 2D). However, a negative control T cell clone that recognized an influenza epitope did not proliferate in response to FLS cells. These observations demonstrate that aggrecan is produced by FLS cells and that epitopes corresponding to Cit-aggrecan peptides can be processed and presented by FLS cells.

Greater frequency of T cells that recognize the dominant Cit-aggrecan epitopes in the peripheral blood in RA patients than in healthy controls. To investigate the frequency of CD4+ T cells specific for citrullinated aggrecan epitopes in the peripheral blood of RA patients, ex vivo tetramer staining was performed. As an initial screening, we performed a grouped analysis, examining the combined T cell frequencies for groups of tetramers: Cit-aggrecan^{225} and Cit-aggrecan^{553} (both of which preferentially bound in their citrullinated form); Cit-aggrecan^{161}, Cit-aggrecan^{200}, Cit-aggrecan^{520}, and Cit-aggrecan^{621} (which bound in both their citrullinated and unmodified forms), and Cit-aggrecan^{84} (which bound with very low affinity to DR0401). Previously published studies (18) and our preliminary assays (data available upon request from the corresponding author) have demonstrated that this tetramer staining approach is reliable. The observed frequencies demonstrated a hierarchy in which the Cit-aggrecan^{225} and Cit-aggrecan^{553} epitopes stood out as the dominant specificities. T cells specific for the other aggrecan epitopes were present, but at lower frequencies that in some cases were near the threshold of detection (Figure 3A). Additional ex vivo analysis of 12 HLA–DRB1*04:01–positive RA patients showed that Cit-aggrecan^{553}–specific T cells were significantly higher in frequency than Cit-aggrecan^{225}–specific cells, suggesting that the Cit-aggrecan^{553} epitope is the most prominent specificity (Figure 3B).

Previous studies have reported immunogenic aggrecan peptides and demonstrated responses to citrullinated aggrecan in samples from patients with RA (9,10,22). To corroborate the relevance of citrullinated aggrecan epitope–specific T cells, we compared the frequency of T cells specific for Cit-aggrecan^{225} and Cit-aggrecan^{553} in RA patients and healthy controls with DRB1*04:01 haplotypes. We observed that patients had significantly higher T cell frequencies than controls (Figure 3C). These differences did not merely reflect global differences between patients and controls, since no difference was observed for T cells specific for the immunodominant influenza epitope.

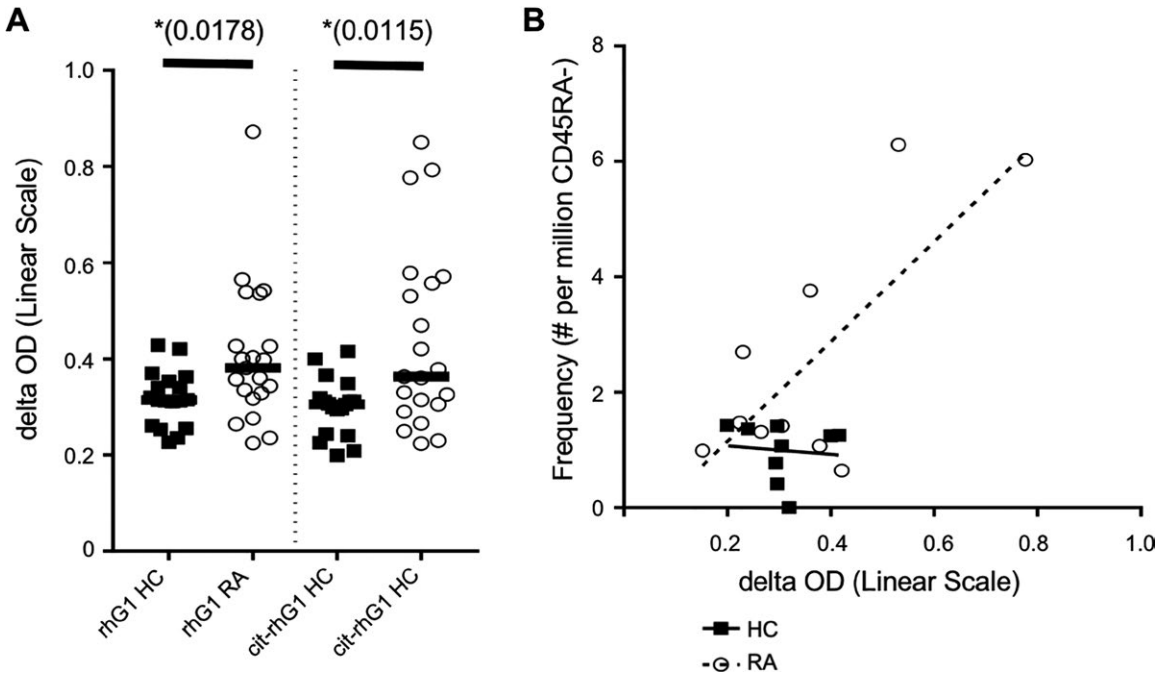

Figure 4. Elevated levels of aggrecan-specific antibodies in rheumatoid arthritis (RA) patients and positive correlation of aggrecan-specific antibodies with T cell frequency. **A**, Levels of antibodies against the native recombinant human G1 domain (rhG1) and antibodies against citrullinated aggrecan rhG1 in IgM-depleted serum from healthy controls (HC) and RA patients. Values are the background adjusted ΔOD. Symbols represent individual subjects (n = 21 RA patients and 18 healthy controls); horizontal bars show the median. * = $P < 0.05$ by 2-tailed Mann-Whitney test. **B**, Significant correlation between serum levels of aggrecan G1 domain antibodies and combined frequencies of memory (CD45RA-negative) Cit-aggrecan^{225}– and Cit-aggrecan^{553}–specific T cells in RA patients but not in healthy controls. Symbols represent individual subjects (n = 10 RA patients and 8 healthy controls). Correlation was determined by 2-tailed Pearson's correlation coefficient. $r^2 = 0.7982$, $P = 0.0128$ for RA patients and $r^2 = 0.01008$, $P = 0.5598$ for healthy controls.

The dominant citrullinated aggrecan epitopes have similar sequences but are recognized by distinct T cell clones. The Cit-aggrecan^{225} and Cit-aggrecan^{553} peptides are derived from the G1 and G2 domains, respectively, but have homologous sequences, raising the possibility that these peptides could be cross-recognized by overlapping sets of T cells. Based on binding assays and proliferation assays with variants of these 2 sequences, we identified truncated peptides that met minimum requirements for binding to DR0401 and recognition by Cit-aggrecan^{225}– or Cit-aggrecan^{553}–specific T cell clones. These results were consistent with the predicted minimal motifs: YGI(Cit)DTNET for Cit-aggrecan^{225} and YGV(Cit)PSTET for Cit-aggrecan^{553}. (Data are available upon request from the corresponding author.) Based on these results, both peptides bind to DR0401 in similar registers. These registers predict that a citrulline residue would be positioned within binding pocket 4. This supposition is further supported by the fact that citrullination of the corresponding arginine residue is required for binding. Despite sharing 10 of 14 residues within their minimal peptides (data available upon request from the corresponding author), the Cit-aggrecan^{225} and Cit-aggrecan^{553} peptides were not cross-recognized by T cell clones (data available upon request from the corresponding author). Furthermore, ex vivo tetramer staining showed no significant signs of cross-reactivity (data available upon request from the corresponding author). Therefore, these sequences appear to represent distinct epitopes, in spite of their considerable homology.

Correlation of citrullinated aggrecan–specific T cell frequency with aggrecan-specific antibody levels. A recent study demonstrated that, although ACPA-positive RA patients had increased levels of antibodies against a citrullinated aggrecan epitope, there was no clear correlation between antibody levels and T cell reactivity with the same epitope in these patients (9). Having identified 2 dominant Cit-aggrecan T cell epitopes, we were curious to explore correlations between T cell and antibody responses against aggrecan. Therefore, we measured citrullinated aggrecan antibody levels in the serum and the frequency of T cells that recognize Cit-aggrecan^{225} and Cit-aggrecan^{553} in matched samples. IgM-depleted serum samples (data available upon request from the corresponding author) from 18 healthy controls and 21 ACPA-positive RA patients were screened for the presence of IgG antibodies against the native and citrullinated G1 domain of aggrecan (an assay for G2 domain antibodies has yet to be developed). Based on either background adjusted OD (Figure 4A) or raw OD (data available

upon request from the corresponding author), RA patients had significantly higher levels of antibodies against both the native and citrullinated G1 domain of aggrecan than HLA-matched controls. Levels of antibody recognition of citrullinated and native aggrecan did not differ. Notably, we observed a positive correlation between the frequency of aggrecan-specific memory T cells and antibody levels in patients with RA (Figure 4B). This correlation was absent in controls, due at least in part to their decreased antibody levels and lower T cell frequencies.

DISCUSSION

Previous studies have indicated that T cell and antibody responses against citrullinated aggrecan contribute to the loss of peripheral tolerance in patients with RA. Of note, Boots et al assessed the HLA binding of native (noncitrullinated) aggrecan peptides to DR0401 (and also DRB1*04:04 and DRB1*01:01) and identified multiple aggrecan peptides as being immunogenic in the context of DR0401 (20). That study, which focused on unmodified (rather than citrullinated) peptides, observed proliferative responses that were lower in RA patients than in controls. Buzas et al identified the aggrecan$^{84–103}$ peptide as an immunodominant epitope recognized by BALB/c mice immunized with human aggrecan, and observed that some aggrecan peptides were "conditionally immunogenic" in that responses were only elicited in arthritic animals (15). Subsequently, Law et al examined responses to citrullinated collagen$^{1237–1249}$, vimentin$^{66–78}$, aggrecan$^{84–103}$, and fibrinogen$^{79–91}$ in RA patients and in a limited number of controls, observing that the citrullinated aggrecan peptide was the most immunogenic, eliciting IL-6 and tumor necrosis factor secretion that was not observed in response to the corresponding unmodified peptide (21). This result appears to imply that functional responses to aggrecan are citrulline selective. However, the T cell responses observed in the study by Law et al were not exclusively restricted to DR0401; 10 of the 21 RA patients sampled were not DR0401 positive and among those 4 were DR4 negative.

Our present study provides new evidence that CD4+ T cells selectively recognize citrullinated aggrecan epitopes in the context of the high-risk DRB1*04:01 haplotype. We identified 6 aggrecan peptides that are recognized by T cell clones from patients with RA when crucial arginine residues are converted to citrulline. Citrullinated residues could increase recognition by enhancing HLA binding or alter peptide recognition by modulating T cell receptor (TCR) interactions (depending on the positioning of the residue within its HLA binding motif). Indeed, 2 of the aggrecan epitopes identified in our study (Cit-aggrecan^{225} and Cit-aggrecan^{553}) bound to DR0401 and elicited T cell responses only in their citrullinated form. The remaining aggrecan epitopes (Cit-aggrecan^{161}, Cit-aggrecan^{200}, Cit-aggrecan^{520}, and Cit-aggrecan^{621}) bound comparably in their citrullinated and unmodified forms and were citrullinated at predicted TCR contact residues. Among these, aggrecan^{200} and aggrecan^{621} were able to elicit T cell responses in a limited number of subjects. Since Cit-aggrecan^{225}– and Cit-aggrecan^{553}–specific T cells were present at significantly higher frequencies in RA patients than other Cit-aggrecan specificities, it could be suggested that the poor HLA binding of the unmodified aggrecan^{225} and aggrecan^{553} peptides may lead to impaired T cell tolerance to the corresponding Cit-epitopes. In spite of sharing considerable sequence homology, the Cit-aggrecan^{225} and Cit-aggrecan^{553} peptides originate from different domains of aggrecan and T cells specific for these peptides showed no evidence of cross-reactivity.

Cit-aggrecan–specific T cells were present at elevated frequencies in RA patients in comparison with HLA–DR–matched healthy controls. The mere presence of CD4+ T cells that recognize citrullinated aggrecan does not guarantee that these cells play a role in disease. However, T cell clones that recognize citrullinated aggrecan epitopes exhibited a Th1-like phenotype that is consistent with the functional phenotype that we previously observed for more established citrullinated antigens such as vimentin, fibrinogen, and enolase (8). In addition, T cell clones specific for all 6 of the citrullinated aggrecan peptides proliferated in response to DR0401-positive FLS cells, suggesting that these epitopes can be naturally processed and presented to T cells by synovial cells. Interestingly, these same clones failed to proliferate in response to the corresponding Arg-aggrecan peptides (Figure 2A), suggesting that aggrecan is citrullinated by FLS.

A recent study documented the presence of citrullinated aggrecan in human cartilage extracts and established an ELISA to detect unmodified or citrullinated aggrecan G1 domain–specific serum autoantibodies (10). When this methodology was applied to analyze serum autoantibodies in patients and controls from our cohort, aggrecan G1 domain–specific antibodies were present at significantly higher levels in RA patients than in HLA-matched controls, but Cit-aggrecan and Arg-aggrecan were recognized at similar levels, suggesting either that G1 domain–specific antibodies cross-recognize native and citrullinated aggrecan or that there are roughly equivalent levels of antibodies that uniquely recognize native and citrullinated aggrecan, respectively. We observed a significant positive correlation between Cit-aggrecan–specific memory T cell frequency and antibody levels in RA patients (but not controls). This correlation raises the possibility that antigen-specific T cell help may contribute to antibody responses. Cumulatively, our results demonstrate that T cell responses to Cit-aggrecan are associated with RA. Such responses are of interest because aggrecan is an extracellular matrix proteoglycan that interacts with cells and extracellular molecules through its globular domains. Given that aggrecan fragments are present within synovial fluid, this protein is apparently subject to fragmentation and release in inflamed joints, where it can be presented to T cells as a citrullinated antigen by either FLS or professional APCs.

Our study does have limitations. Although we were able to demonstrate differences in the frequency of Cit-aggrecan–specific CD4+ T cells in RA patients and HLA–matched con-

trols, the characteristics of the RA patients selected for our study did not allow us to effectively examine variations with respect to disease activity or severity. In general, our patients had well-controlled disease, which may explain in part the overlap in aggrecan-specific T cell frequencies observed between controls and some patients. In addition, although it would be of considerable interest to document the presence of Cit-aggrecan–specific T cells within inflamed joints, synovial fluid and tissue samples from HLA-typed subjects were not available for our study. However, our ex vivo tetramer staining approach should be applicable to address these questions in future studies that use such samples.

Although previous studies have documented T cell responses to citrullinated aggrecan, our study represents the first HLA-controlled study to define disease-relevant citrullinated aggrecan epitopes and to characterize T cells that recognize these peptides in patients with established RA. To our knowledge, this is also the first study to demonstrate a direct correlation between T cell frequency and antibody responses against the same joint-associated antigen. Together, these results suggest that Cit-aggrecan–specific CD4+ T cells could play a role in the etiology of RA and that future studies of the frequency, phenotype, and role of Cit-aggrecan–specific T cells in various stages of disease are warranted.

ACKNOWLEDGMENT

The authors would like to thank Dr. David Fox (University of Michigan) for initially providing shared epitope–positive fibroblast-like synoviocytes for expansion.

AUTHOR CONTRIBUTIONS

All authors were involved in drafting the article or revising it critically for important intellectual content, and all authors approved the final version to be published. Dr. James had full access to all of the data in the study and takes responsibility for the integrity of the data and the accuracy of the data analysis.

Study conception and design. Rims, Uchtenhagen, Kaplan, Carmona-Rivera, Carlucci, Buckner, James.

Acquisition of data. Rims, Uchtenhagen, Carmona-Rivera, Carlucci, Mikecz, Markovics.

Analysis and interpretation of data. Rims, Uchtenhagen, Kaplan, Carmona-Rivera, Carlucci, Mikecz, Markovics, Carlin, Buckner, James.

REFERENCES

1. Arnett FC, Edworthy SM, Bloch DA, McShane DJ, Fries JF, Cooper NS, et al. The American Rheumatism Association 1987 revised criteria for the classification of rheumatoid arthritis. Arthritis Rheum 1988;31:315–24.
2. Huizinga TW, Amos CI, van der Helm-van Mil AH, Chen W, van Gaalen FA, Jawaheer D, et al. Refining the complex rheumatoid arthritis phenotype based on specificity of the HLA–DRB1 shared epitope for antibodies to citrullinated proteins. Arthritis Rheum 2005;52:3433–8.
3. Feitsma AL, van der Voort EI, Franken KL, el Bannoudi H, Elferink BG, Drijfhout JW, et al. Identification of citrullinated vimentin peptides as T cell epitopes in HLA–DR4–positive patients with rheumatoid arthritis. Arthritis Rheum 2010;62:117–25.
4. Cordova KN, Willis VC, Haskins K, Holers VM. A citrullinated fibrinogen-specific T cell line enhances autoimmune arthritis in a mouse model of rheumatoid arthritis. J Immunol 2013;190:1457–65.
5. Snir O, Rieck M, Gebe JA, Yue BB, Rawlings CA, Nepom G, et al. Identification and functional characterization of T cells reactive to citrullinated vimentin in HLA–DRB1*0401–positive humanized mice and rheumatoid arthritis patients. Arthritis Rheum 2011;63:2873–83.
6. Gerstner C, Dubnovitsky A, Sandin C, Kozhukh G, Uchtenhagen H, James EA, et al. Functional and structural characterization of a novel HLA-DRB1*04:01-restricted α-enolase T cell epitope in rheumatoid arthritis. Front Immunol 2016;7:494.
7. Aggarwal A, Srivastava R, Agrawal S. T cell responses to citrullinated self-peptides in patients with rheumatoid arthritis. Rheumatol Int 2013;33:2359–63.
8. James EA, Rieck M, Pieper J, Gebe JA, Yue BB, Tatum M, et al. Citrulline-specific Th1 cells are increased in rheumatoid arthritis and their frequency is influenced by disease duration and therapy. Arthritis Rheumatol 2014;66:1712–22.
9. Markovics A, Ocsko T, Katz RS, Buzas EI, Glant TT, Mikecz K. Immune recognition of citrullinated proteoglycan aggrecan epitopes in mice with proteoglycan-induced arthritis and in patients with rheumatoid arthritis. PLoS One 2016;11:e0160284.
10. Glant TT, Ocsko T, Markovics A, Szekanecz Z, Katz RS, Rauch TA, et al. Characterization and localization of citrullinated proteoglycan aggrecan in human articular cartilage. PLoS One 2016;11:e0150784.
11. Witter J, Roughley PJ, Webber C, Roberts N, Keystone E, Poole AR. The immunologic detection and characterization of cartilage proteoglycan degradation products in synovial fluids of patients with arthritis. Arthritis Rheum 1987;30:519–29.
12. Holmes MW, Bayliss MT, Muir H. Hyaluronic acid in human articular cartilage: age-related changes in content and size. Biochem J 1988;250:435–41.
13. Glant TT, Radacs M, Nagyeri G, Olasz K, Laszlo A, Boldizsar F, et al. Proteoglycan-induced arthritis and recombinant human proteoglycan aggrecan G1 domain–induced arthritis in BALB/c mice resembling two subtypes of rheumatoid arthritis. Arthritis Rheum 2011;63:1312–21.
14. Von Delwig A, Locke J, Robinson JH, Ng WF. Response of Th17 cells to a citrullinated arthritogenic aggrecan peptide in patients with rheumatoid arthritis. Arthritis Rheum 2010;62:143–9.
15. Buzas EI, Vegvari A, Murad YM, Finnegan A, Mikecz K, Glant TT. T-cell recognition of differentially tolerated epitopes of cartilage proteoglycan aggrecan in arthritis. Cell Immunol 2005;235:98–108.
16. James EA, Moustakas AK, Bui J, Papadopoulos GK, Bondinas G, Buckner JH, et al. HLA–DR1001 presents "altered-self" peptides derived from joint-associated proteins by accepting citulline in three of its binding pockets. Arthritis Rheum 2010;62:2909–18.
17. Ettinger RA, Papadopoulos GK, Moustakas AK, Nepom GT, Kwok WW. Allelic variation in key peptide-binding pockets discriminates between closely related diabetes-protective and diabetes-susceptible HLA-DQB1*06 alleles. J Immunol 2006;176:1988–98.
18. Uchtenhagen H, Rims C, Blahnik G, Chow IT, Kwok WW, Buckner JH, et al. Efficient ex vivo analysis of CD4+ T-cell responses using combinatorial HLA class II tetramer staining. Nat Commun 2016;7:12614.
19. Carmona-Rivera C, Carlucci PM, Moore E, Lingampalli N, Uchtenhagen H, James E, et al. Synovial fibroblast-neutrophil interactions promote pathogenic adaptive immunity in rheumatoid arthritis. Sci Immunol 2017;2:3358.

20. Boots AM, Verheijden GF, Schoningh R, van Staveren CJ, Bos E, Elewaut D, et al. Selection of self-reactive peptides within human aggrecan by use of a HLA-DRB1*0401 peptide binding motif. J Autoimmun 1997;10:569–78.
21. Law SC, Street S, Yu CH, Capini C, Ramnoruth S, Nel HJ, et al. T-cell autoreactivity to citrullinated autoantigenic peptides in rheumatoid arthritis patients carrying HLA-DRB1 shared epitope alleles. Arthritis Res Ther 2012;14:R118.
22. Falconer J, Mahida R, Venkatesh D, Pearson J, Robinson JH. Unconventional T-cell recognition of an arthritogenic epitope of proteoglycan aggrecan released from degrading cartilage. Immunology 2016;147:389–98.

Arthritis & Rheumatology
Vol. 71, No. 4, April 2019, pp 529–541
DOI 10.1002/art.40772

AMERICAN COLLEGE OF RHEUMATOLOGY
EDUCATION • TREATMENT • RESEARCH

Beyond Autoantibodies: Biologic Roles of Human Autoreactive B Cells in Rheumatoid Arthritis Revealed by RNA-Sequencing

Ankit Mahendra,[1] Xingyu Yang,[2] Shaza Abnouf,[1] Jay R. T. Adolacion,[1] Daechan Park,[3] Sanam Soomro,[1] Jason Roszik,[4] Cristian Coarfa,[5] Gabrielle Romain,[1] Keith Wanzeck,[6] S. Louis Bridges Jr.,[6] Amita Aggarwal,[7] Peng Qiu,[2] Sandeep K. Agarwal,[5] Chandra Mohan,[1] and Navin Varadarajan[1]

Objective. To obtain the comprehensive transcriptome profile of human citrulline-specific B cells from patients with rheumatoid arthritis (RA).

Methods. Citrulline- and hemagglutinin-specific B cells were sorted by flow cytometry using peptide–streptavidin conjugates from the peripheral blood of RA patients and healthy individuals. The transcriptome profile of the sorted cells was obtained by RNA-sequencing, and expression of key protein molecules was evaluated by aptamer-based SOMAscan assay and flow cytometry. The ability of these proteins to effect differentiation of osteoclasts and proliferation and migration of synoviocytes was examined by in vitro functional assays.

Results. Citrulline-specific B cells, in comparison to citrulline-negative B cells, from patients with RA differentially expressed the interleukin-15 receptor α (IL-15Rα) gene as well as genes related to protein citrullination and cyclic AMP signaling. In analyses of an independent cohort of cyclic citrullinated peptide–seropositive RA patients, the expression of IL-15Rα protein was enriched in citrulline-specific B cells from the patients' peripheral blood, and surprisingly, all B cells from RA patients were capable of producing the epidermal growth factor ligand amphiregulin (AREG). Production of AREG directly led to increased migration and proliferation of fibroblast-like synoviocytes, and, in combination with anti–citrullinated protein antibodies, led to the increased differentiation of osteoclasts.

Conclusion. To the best of our knowledge, this is the first study to document the whole transcriptome profile of autoreactive B cells in any autoimmune disease. These data identify several genes and pathways that may be targeted by repurposing several US Food and Drug Administration–approved drugs, and could serve as the foundation for the comparative assessment of B cell profiles in other autoimmune diseases.

INTRODUCTION

The identification of citrullination has been a major milestone in the study of rheumatoid arthritis (RA) (1,2). Citrullination is the posttranslational modification of arginine residues to citrulline in proteins, catalyzed by peptidyl arginine deiminase (PAD) enzymes, as one of the key factors mediating the breach in tolerance and eliciting anti–citrullinated protein antibody (ACPA) responses. The appearance of ACPAs in the circulation precedes the onset of clinical disease, and ACPA positivity has a sensitivity of 60–70%, and a specificity of >90%, for the diagnosis of RA (1). ACPAs have been shown to trigger human immune effector functions, including activation of the complement system and the ability to engage activating Fcγ receptors (3). In addition, it has been demonstrated that ACPAs can catalyze the bone erosion commonly seen in RA patients (4).

Although the indispensable role of B cells in autoantibody production is well recognized, their autoantibody-independent

Supported by the Cancer Prevention and Research Institute of Texas (RP130570 and RP180466), the United States Department of Defense (Congressionally Directed Medical Research Program CA160591), the Melanoma Research Alliance (509800), the National Science Foundation (1705464), the NIH (grant R01-CA-174385), the Owens Foundation, the Welch Foundation (E-1774), and the University of Alabama at Birmingham RADAR fund.

[1]Ankit Mahendra, PhD, Shaza Abnouf, BS, Jay R. T. Adolacion, MS, Sanam Soomro, BS, Gabrielle Romain, PhD, Chandra Mohan, MD, PhD, Navin Varadarajan, PhD: University of Houston, Houston, Texas; [2]Xingyu Yang, BS, Peng Qiu, PhD: Georgia Institute of Technology, Atlanta; [3]Daechan Park, PhD: Ajou University, Suwon, Republic of Korea; [4]Jason Roszik, PhD: University of Texas MD Anderson Cancer Center, Houston; [5]Cristian Coarfa, PhD, Sandeep K. Agarwal, MD, PhD: Baylor College of Medicine, Houston, Texas; [6]Keith Wanzeck, MS, S. Louis Bridges Jr., MD, PhD: University of Alabama at Birmingham; [7]Amita Aggarwal, MD: Sanjay Gandhi Postgraduate Institute of Medical Sciences, Lucknow, India.

No potential conflicts of interest relevant to this article were reported.

Address correspondence to Navin Varadarajan, PhD, Department of Chemical & Biomolecular Engineering, University of Houston, 4726 Calhoun Road, Houston, Texas 77204-4005. E-mail: nvaradar@central.uh.edu.

Submitted for publication May 10, 2018; accepted in revised form November 1, 2018.

contributions are not as well-defined. Systemic depletion of B cells using rituximab, a strategy that targets B cells expressing human CD20 (a phenotypic cell surface marker), has been shown to be effective clinically for the treatment of a subset of RA patients (5). Although studies have supported the idea that patients with higher autoantibody titers are likely to respond to rituximab (6), the clinical efficacy of rituximab treatment is not necessarily correlated with a decrease in autoantibody titers (7). This, in turn, implies a more expanded role for B cells in autoimmune pathogenicity beyond antibody production.

Preclinical and clinical data have suggested many different functions of B cells in RA, including 1) a role as antigen-presenting cells (8), 2) direct secretion of proinflammatory cytokines, such as tumor necrosis factor (TNF) and interleukin-6 (IL-6) (9–11), that support the organization of tertiary lymphoid tissues within the inflamed synovium (8,12), and 3) an effect on bone homeostasis through the secretion of RANKL (13). Despite these efforts, a direct interrogation of the roles of the autoreactive B cell compartment, and how they differ from other B cells from the same donor or from B cells from healthy individuals, has not been accomplished.

One of the major challenges in profiling autoreactive B cells within humans is the low frequency of these cells in peripheral blood (<0.1% of all B cells in the circulation) (14). We developed and validated a flow cytometry–based assay for the reliable detection of cyclic citrullinated peptide (CCP)–specific B cells ex vivo. We then performed RNA-sequencing (RNA-seq) on these small numbers of cells with the purpose of comparing the whole transcriptome profile of RA-CCP–specific (RA-CCP^{POS}) B cells to that of RA-CCP–negative (RA-CCP^{NEG}) B cells from the same donor and to that of hemagglutinin-specific (HA^{POS}) B cells from healthy individuals elicited upon vaccination with seasonal influenza virus. We performed a 2-pronged comparison to identify the expression of key genes on all B cells from RA patients that were presumably induced by the systemic proinflammatory environment prevailing in these patients, as well as those genes that were restricted to only autoreactive B cells.

Our data identified a novel role of B cells as an activator of the epidermal growth factor (EGF) pathways by secretion of the EGF receptor ligand amphiregulin (AREG) under proinflammatory conditions, and also identified IL-15 receptor α (IL-15Rα) as a specific biomarker of RA-CCP^{POS} B cells. Overall, our data suggest that besides being a source of autoantibodies, B cells may also play direct roles in the inflammatory cascades and osteoclastogenesis in RA. Significantly, while some of the identified genes and pathways are the targets of approved therapies for RA, our data also illustrate that drugs approved for other indications might be useful in targeting the RA-CCP^{POS} B cell compartment in RA. More broadly, to the best of our knowledge, this is the first comprehensive study on the transcriptome profile of human RA-CCP^{POS} B cells in any autoimmune disease, and these data could serve as a resource to further investigate the role of B cells in autoimmunity.

MATERIALS AND METHODS

Patients. Blood samples were obtained from patients with seropositive RA who provided informed consent for study participation under Institutional Review Board–approved protocols at the Baylor College of Medicine, University of Alabama at Birmingham, and University of Houston. Each blood sample (15 ml) was aspirated into heparin vacutainer tubes (BD Biosciences). Details on the patients' demographic and clinical characteristics are summarized in Supplementary Table 1 (available on the *Arthritis & Rheumatology* web site at http://onlinelibrary.wiley.com/doi/10.1002/art.40772/abstract). All RA patients met the American College of Rheumatology 1987 classification criteria for RA (15), and all were confirmed to be CCP-seropositive.

Flow cytometric sorting of CCP-specific B cells from RA patients' blood. Peripheral blood mononuclear cells (PBMCs), isolated from the blood of RA patients by density centrifugation, were blocked with phosphate buffered saline (PBS)–5% human serum for 20 minutes at 4°C. All subsequent staining steps were performed in PBS containing 2% serum. PBMCs were stained for B cell markers with fluorochrome-labeled antibodies, anti-CD19, IgM, and IgD together with a T cell marker using an anti-CD3 antibody (BioLegend) according to the manufacturer's instructions. Biotinylated CCP-I (Anaspec), a surrogate peptide to capture ACPAs, was then added (1 μg/million PBMCs), followed by labeling with fluorochrome-labeled streptavidin (1 μg/ml). Subsequently, biotinylated cyclic arginine peptide (CAP; Anaspec) was also added (1 μg/million PBMCs) as a control, and then labeled with fluorochrome-labeled streptavidin (1 μg/ml), to exclude B cells cross-reactive to both antigens. Furthermore, CD19^{POS}IgM/IgD^{NEG} B cells (IgG/IgA^{POS}) were gated, and the cell populations CCP^{POS}CAP^{NEG} and CCP^{NEG}CAP^{NEG} were sorted for validation of cell purity.

A total of 125–360 RA-CCP^{POS} B cells were obtained from 10–15 million PBMCs from each patient. The sorted cells were then grown in 96-well tissue culture plates with 1×10^5/well of 3T3 fibroblast cells secreting msCD40L (NIH AIDS reagent program), 100 ng/ml of IL-21 (PeproTech), and 5 μg/ml of anti–APO-1 antibody (eBiosciences) for a period of 14 days, with half of the medium changed once after 7 days. Thereafter, cell purity was assessed by validating the specificity of IgG from the culture supernatants against CCP.

Preparation of the complementary DNA (cDNA) library and RNA-sequencing analyses. Total RNA was obtained by sorting antigen-specific B cells (350–1,000 total cells) ex vivo directly into 100 μl of cell lysis buffer, provided in the RNA-XS RNA isolation kit (Macherey-Nagel). Furthermore, cDNA libraries were synthesized using the commercially available

SMART-Seq Ultra Low Input RNA kit (Clontech), in accordance with the manufacturer's protocols. After preparation of cDNA libraries, they were first tagmented and then barcoded by indexing primers using the Nextra XT kit (Illumina). The libraries were pooled and a 76-bp paired-end sequencing was performed on an Illumina HiSeq3000 sequencer, to yield a minimum of 17.4 million reads per library (range 17.4–37.3 million).

Details on the methods used for RNA-seq bioinformatics analyses (Gene Expression Omnibus RNA-seq data accession no. GSE99006), purification of ACPAs, fibroblast-like synoviocyte (FLS) assays, osteoclastogenesis assays, and SOMAmer assays are described in the Supplementary Materials and Methods (available on the *Arthritis & Rheumatology* web site at http://onlinelibrary.wiley.com/doi/10.1002/art.40772/abstract).

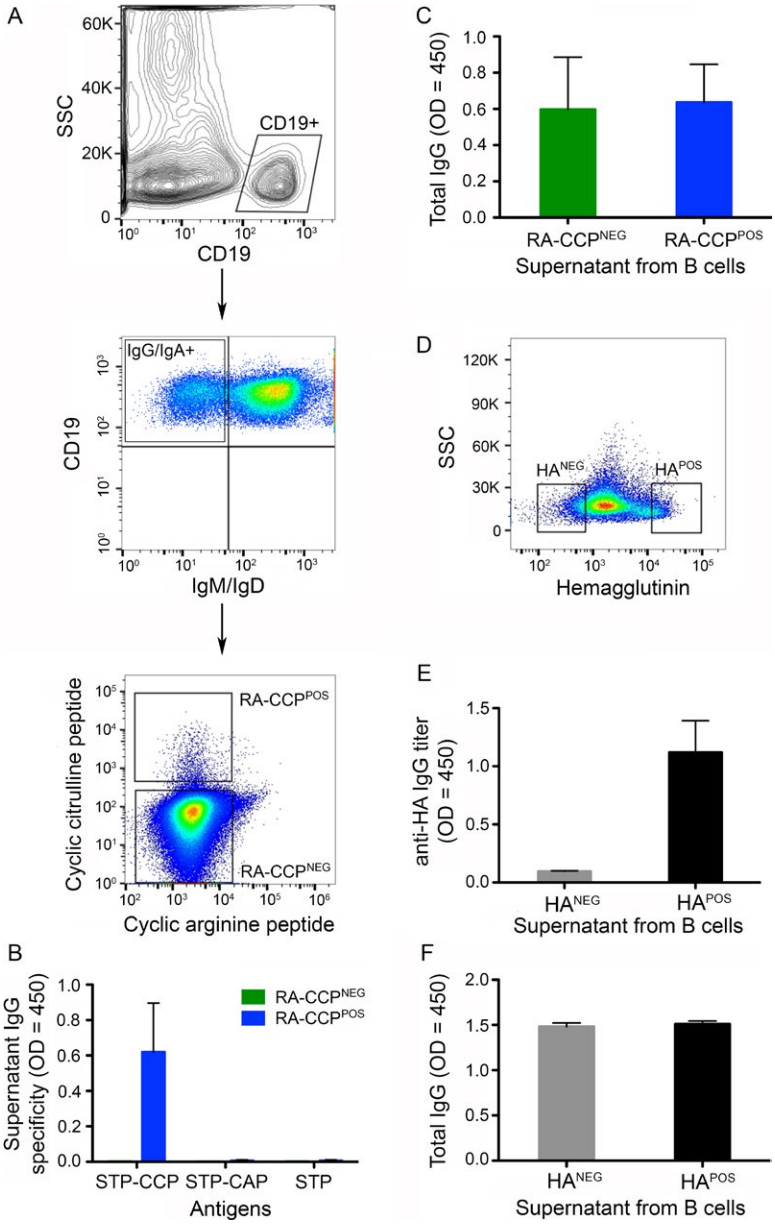

Figure 1. Isolation of an enriched population of rheumatoid arthritis cyclic citrullinated peptide–specific (RA-CCP^{POS}) and hemagglutinin-specific (HA^{POS}) B cells. **A**, Representative flow plots depict the sorting strategy for RA-CCP^{POS} and RA-CCP^{NEG} B cells. Cells were first gated as CD19^{POS}IgM/IgD^{NEG} B cells (IgG/IgA^{POS}); thereafter, RA-CCP^{POS} B cells were sorted by flow cytometry as CCP^{POS}CAP^{NEG} B cells, and RA-CCP^{NEG} cells were sorted as CCP^{NEG}CAP^{NEG} B cells. **B** and **C**, Supernatants (n = 3) were tested by enzyme-linked immunosorbent assay (ELISA) for antigen specificity of RA-CCP^{POS} and RA-CCP^{NEG} B cells (**B**) and for total Ig from RA-CCP^{POS} and RA-CCP^{NEG} B cells (**C**), expanded and differentiated in vitro. **D**, Representative flow plot shows isolation of HA^{POS} and HA^{NEG} B cells, sorted with a similar gating strategy as that described in **A**. **E** and **F**, Supernatants (n = 4) were tested by ELISA for HA reactivity (**E**) and total Ig from HA^{NEG} and HA^{POS} B cell populations (**F**). ELISA results are shown as the mean ± SEM. STP = streptavidin; CAP = cyclic arginine peptide. Color figure can be viewed in the online issue, which is available at http://onlinelibrary.wiley.com/doi/10.1002/art.40772/abstract.

RESULTS

Flow cytometric sorting of antigen-specific B cells. We developed a dual-labeling flow cytometry method of cell sorting using both CCPs and CAPs to isolate RA-CCP^{POS} B cells. In order to verify the purity of our sorting method, an equal number of B cells within the CCP^{POS}CAP^{NEG} population (hereafter referred to as RA-CCP^{POS} B cells) and CCP^{NEG}CAP^{POS} and CCP^{NEG}-CAP^{NEG} populations (hereafter referred to as RA-CCP^{NEG} B cells) (Figure 1A) were sorted in 96-well plates and grown in vitro for 14 days. The purity of our sorting strategy was validated by testing the supernatants after in vitro culture, which confirmed that only the immunoglobulins secreted in B cell cultures established from the RA-CCP^{POS} B cell population demonstrated a specific reactivity toward the CCP, but not toward streptavidin or the control CAP peptide (Figures 1B and C).

After validation of our sorting strategy, a total of 350–1,000 RA-CCP^{POS} B cells (0.01–0.1%) from the peripheral blood of 4 RA patients were used directly for the preparation of cDNA libraries ex vivo, to ensure minimal perturbations to the transcriptional profile. Both RA-CCP^{POS} and RA-CCP^{NEG} B cells were confirmed to be predominantly of the memory phenotype, based on the surface expression of CD27 and IgD (see Supplementary Figure 1A, http://onlinelibrary.wiley.com/doi/10.1002/art.40772/abstract).

For a comparative analysis of the B cell transcriptome profile during autoimmunity compared to that during the normal immune response to vaccination, HA-specific B cells (hereafter referred to as HA^{POS} B cells) were isolated from the peripheral blood of 4 healthy individuals who were vaccinated with the seasonal influenza vaccine. Our ability to enrich for HA^{POS} B cells was validated by the same 3-step procedure as that used for RA-CCP^{POS} B cells: 1) antigen labeling and flow cytometric sorting of a total of 3,500 HA^{POS} and HA^{NEG} cells from PBMCs of these vaccinated donors; 2) in vitro expansion and differentiation; and 3) enzyme-linked immunosorbent assay (ELISA) testing for HA reactivity on the culture supernatants (Figures 1D–F). Similar to the B cells from RA patients, HA^{POS} B cells from healthy individuals also displayed a CD27+ memory phenotype. We did not observe a significant difference in the frequency of memory B cells between different samples of RA-CCP^{POS}, RA-CCP^{NEG}, and HA^{POS} B cells (see Supplementary Figures 1B and C, http://onlinelibrary.wiley.com/doi/10.1002/art.40772/abstract).

Subsequent to validation, 1,000–2,000 HA^{POS} B cells from the same 4 healthy donors were used to construct cDNA libraries ex vivo for RNA-seq analyses. In order to ensure that the differences in the gene expression profile of RA-CCP^{POS} B cells was not attributable to the composition of different isotypes of B cells (IgG versus IgA), we analyzed our RNA-seq data for transcripts associated with IgG and IgA molecules, and confirmed that no significant differences were observed between RA-CCP^{POS}, RA-CCP^{NEG}, and HA^{POS} B cells (see Supplementary Figure 1D, http://onlinelibrary.wiley.com/doi/10.1002/art.40772/abstract).

Distinguishing RA-CCP^{POS}, RA-CCP^{NEG}, and HA^{POS} B cells based on differentially expressed genes (DEGs). The cDNA libraries generated ex vivo from the 12 blood samples (comprising 4 paired RA-CCP^{POS} and RA-CCP^{NEG} B cell populations, and 4 HA^{POS} B cell populations) were barcoded, pooled, and sequenced using 76-bp paired-ends, to yield a minimum of 17 million reads per library. After validation of the RNA-seq populations (see Supplementary Figure 2, http://onlinelibrary.wiley.com/doi/10.1002/art.40772/abstract), differential analyses using the DEseq package revealed that 1,658 genes (false discovery rate [FDR] <0.1) were differentially expressed in RA-CCP^{POS} B cells compared to HA^{POS} B cells, and 431 genes were identified as DEGs in RA-CCP^{POS} B cells compared to RA-CCP^{NEG} B cells (see the complete lists provided in Supplementary Tables 3 and 4, http://onlinelibrary.wiley.com/doi/10.1002/art.40772/abstract).

We utilized t-distributed stochastic neighbor embedding (16) to demonstrate that these identified DEGs could clearly resolve the 3 distinct cellular populations (Figure 2A). As expected, both the number of identified DEGs and their relative change in expression were lower in RA-CCP^{POS} B cells compared to RA-CCP^{NEG} B cells from the same donors, in contrast to comparisons between RA-CCP^{POS} B cells and HA^{POS} B cells (see Supplementary Tables 3 and 4). We evaluated the statistical power of our study to differentiate the RA-CCP^{POS} and RA-CCP^{NEG} B cell subsets. Using powsimR (17), we estimated the statistical power of our study to be 0.86 ± 0.18 (mean ± SEM based on 100 simulations).

Comparisons between RA-CCP^{POS} and HA^{POS} B cells. A number of candidate DEGs whose presence has been well validated in studies of autoimmunity, including the cyclin kinase p21 (*CDKN1A*) (18), ubiquitin ligase *Pell1* (19), and costimulatory molecule *ICOSLG* (20) genes, were identified. The EGF ligand gene *AREG* was identified as the transcript with the largest change in expression (Figure 2B).

By classifying these same DEGs into Gene Ontology categories, we grouped them as being related to B cell activation, genes related to inflammation, and transcription factors. We observed differences in the expression of genes related to B cell activation (Figure 2C), with increased expression of kinase genes such as *PI3KCA* (21) and *MAPK7*/*MAPK8*, which are known to cause autoimmunity under dysregulated activation (22). In addition, several genes related to inflammation, including signaling molecules such as *TNFAIP3* and *IL6ST* and T cell–recruiting chemokine-like *CCL5* and the chemokine receptor gene *CXCR4* (23,24), were up-regulated in RA-CCP^{POS} B cells (Figure 2D).

Analysis of the differentially expressed transcription factors revealed up-regulation of *PRDM1* and *ETV3* and *ETV3L* within RA-CCP^{POS} B cells; these transcription factors are known to inhibit c-Myc and, consequently, hinder cell growth (25), while at the same time

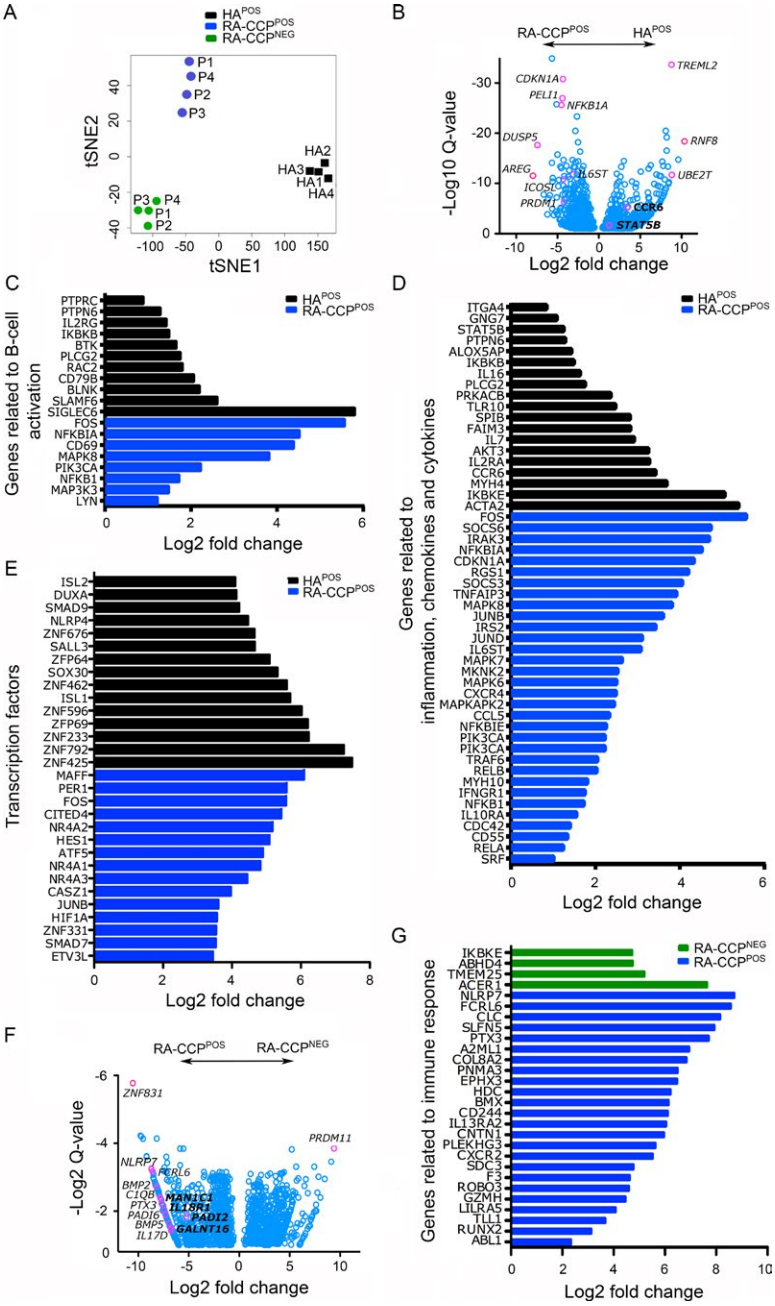

Figure 2. RA-CCP^{POS}, RA-CCP^{NEG}, and HA^{POS} B cells can be differentiated based on differentially expressed genes (DEGs). **A**, For visualization of sample relationships based on differential gene expression, t-distributed stochastic neighbor embedding (t-SNE) was used. P1–4 and HA1–4 represent distinct populations of RA-CCP^{POS} and RA-CCP^{NEG} B cells and HA^{POS} B cells, respectively, based on DEGs. **B**, Volcano plots (generated using the fold change and *q* values of DEGs) show enrichment of genes related to autoimmunity and inflammation in RA-CCP^{POS} B cells compared to HA^{POS} B cells. **C–E**, Gene ontology (GO) plots indicate the fold change in expression of genes related to B cell activation, inflammation, chemokines, and cytokines, and the top 15 transcription factors that were differentially enriched in RA-CCP^{POS} compared to HA^{POS} B cells. **F**, Volcano plots (generated using the fold change and *q* values of DEGs) show differences between RA-CCP^{POS} B cells and RA-CCP^{NEG} B cells from the same donors. **G**, GO plot depicts the fold change in expression of genes related to immune responses that are highly expressed in RA-CCP^{POS} B cells compared to RA-CCP^{NEG} B cells from the same donors. See Figure 1 for other definitions. Color figure can be viewed in the online issue, which is available at http://onlinelibrary.wiley.com/doi/10.1002/art.40772/abstract.

they can promote B cell differentiation and Ig secretion (26). Similarly, the small macrophage-activating factor family of transcription factors (*MAFF* and *MAFG*), which have a direct impact on Ig secretion (27), were enriched in these RA-CCP^{POS} B cells (Figure 2E).

We also sought to determine whether there was a B cell–specific change in expression of genes known to be high-risk loci in RA, as has been documented through large-scale genetic studies (28). Of the known RA-specific loci, 9 genes were also identi-

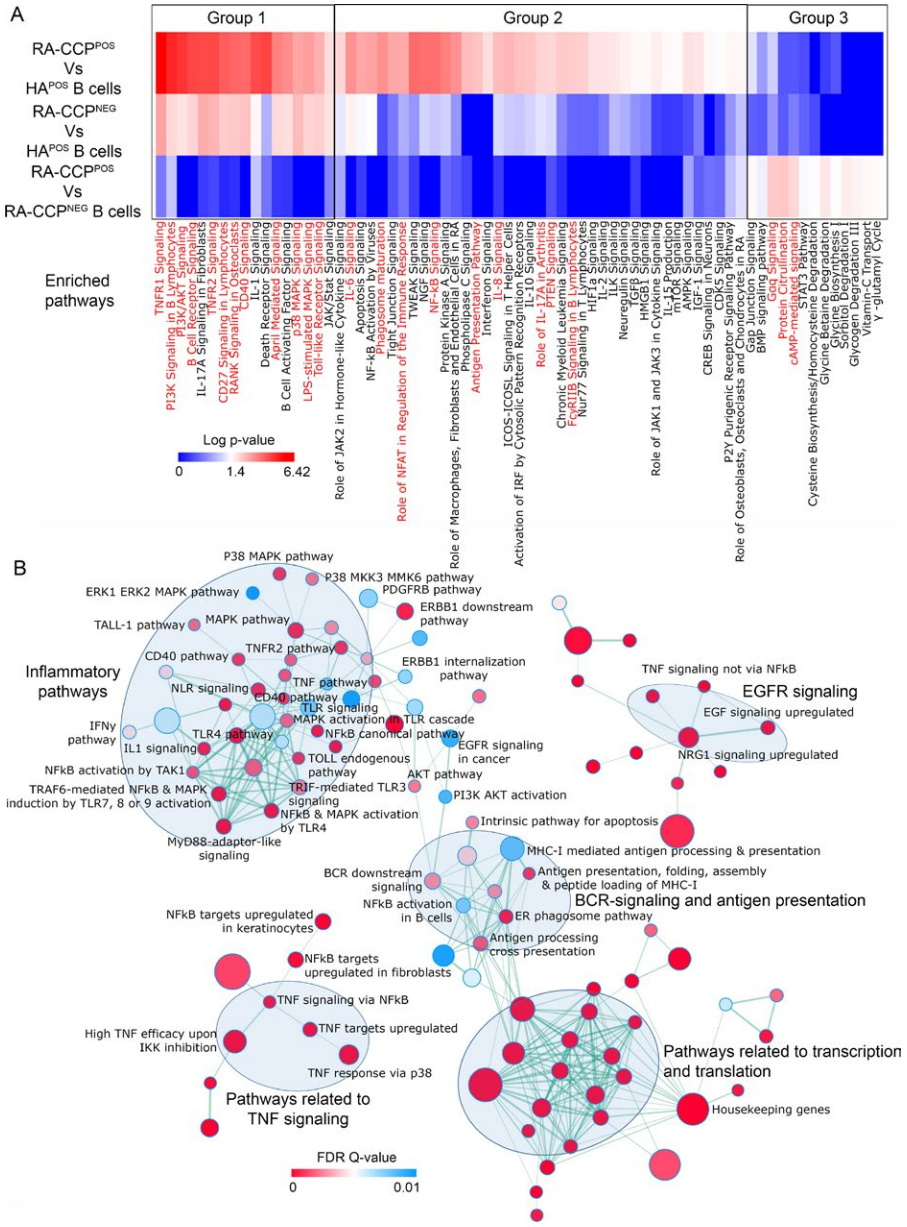

Figure 3. Enrichment maps of pathways enriched in RA-CCP^{POS} B cells compared to HA^{POS} B cells. **A**, Heatmaps were generated using log-transformed *P* values for differentially expressed gene pathways from Ingenuity Pathway Analysis, indicating enrichment of proinflammatory pathways in RA-CCP^{POS} B cells compared to HA^{POS} B cells, and up-regulation of protein citrullination in RA-CCP^{POS} B cells compared to RA-CCP^{NEG} B cells. Highlighted pathways are shown in red. **B**. The gene-set enrichment analysis–derived enriched C2 curated pathways in RA-CCP^{POS} B cells were plotted with the enrichment map application in Cytoscape, using a cutoff false discovery rate (FDR) *q* value of 0.01 and *P* value of 0.005. Nodes (red and blue circles) represent pathways, and the edges (green lines) represent overlapping genes among pathways. The size of nodes represents the number of genes enriched within the pathway, and the thickness of edges represents the number of overlapping genes. The color of nodes was adjusted to an FDR *q* value ranging from 0 to 0.01. Clusters of pathways are labeled as groups with a similar theme. All pathways represented are enriched in RA-CCP^{POS} B cell populations. TNFR1 = tumor necrosis factor receptor 1; PI3K = phosphatidylinositol 3-kinase; IL-17A = interleukin-17A; LPS = lipopolysaccharide; NGF = nerve growth factor; ICOS = inducible costimulator; IRF = interferon regulatory factor; FcγRIIb = Fcγ receptor type IIb; HIF1a = hypoxia-inducible factor 1α; ILK = integrin-linked kinase; TGFβ = transforming growth factor β; HMGB1 = high mobility group box chromosomal protein 1; mTOR = mechanistic target of rapamycin; AMPK = AMP-activated protein kinase; IGF-1 = insulin-like growth factor 1; BMP = bone morphogenetic protein; Gαq = G protein–coupled receptor; PDGFRB = platelet-derived growth factor β receptor; EGFR = endothelial growth factor receptor; TLR = Toll-like receptor; IFNγ = interferon-γ; TAK1 = TGFβ-activated kinase 1; NRG1 = neuregulin 1; TRAF6 = TNFR-associated factor 6; MyD88 = myeloid differentiation factor 88; MHC-I = class I major histocompatibility complex; BCR = B cell receptor; ER = endoplasmic reticulum (see Figure 1 for other definitions).

fied as DEGs (*SH2B3*, *CCR6*, *ILF3*, *TXNDC11*, *PTPRC*, *PRDM1*, *TNFAIP3*, *TRAF6*, and *LBH*) (see Supplementary Figures 3A–C, http://onlinelibrary.wiley.com/doi/10.1002/art.40772/abstract).

Comparisons between RA-CCP^{POS} and RA-CCP^{NEG} B cells. The candidate DEGs that were up-regulated within the RA-CCP^{POS} B cell population, as compared to RA-CCP^{NEG} B cells within these same donors, included the pentraxin gene *PTX3* (Figures 2F and G), which recognizes pathogen-associated molecular patterns, and its binding partner in the complement cascade, *C1QB* (29,30), bone morphogenetic protein genes *BMP2* and *BMP5*, and PAD citrullinating enzyme genes *PADI2* and *PADI6* (31) (Figure 2F). In addition, several immune-related transcripts, such as inflammasome-associated protein gene *NLRP7* (32) and Fc receptor (FcR)–like protein gene *FCRL6* (33), were also up-regulated within RA-CCP^{POS} B cells (Figures 2F and G).

Cytokine and signaling pathways enriched in RA-CCP^{POS} B cells. The differentially expressed pathways were identified by matching the expression data set using Ingenuity Pathway Analysis (IPA), which filtered the pathways directly related to immune cells and their functions, and the results were visualized as a heatmap using the log *P* values (Figure 3A). In order to facilitate comparisons, we identified 3 groups of pathways that were enriched, in which group 1 comprised pathways in both the RA-CCP^{POS} and RA-CCP^{NEG} B cell populations compared to the HA^{POS} B cell population, group 2 comprised pathways enriched only in the RA-CCP^{POS} B cell population but not in the RA-CCP^{NEG} or HA^{POS} B cell populations, and group 3 comprised pathways enriched only in the RA-CCP^{POS} B cell population but not in the RA-CCP^{NEG} B cell population.

The pathways in group 1 were B cell activation pathways (B cell receptor signaling, phosphatidylinositol 3-kinase/AKT, and p38 MAPK), Toll-like receptor (TLR)–based activation pathways (TLR signaling and lipopolysaccharide-stimulated MAPK pathways), and TNF superfamily ligand–mediated signaling pathways (CD40, APRIL signaling) and their receptor signaling pathways (TNFR1, TNFR2, CD27, RANK, and CD40). The pathways in group 2 comprised inflammatory cytokine signaling (IL-6, IL-8, and IL-17A) and RA-specific signatures (role of macrophages, endothelial cells, and osteoclasts in RA), as well as pathways of B cell activation/homeostasis (PTEN, NF-κB, and NFAT activation) and function (phagosome maturation, FcγRIIb signaling, and antigen presentation). Finally, group 3 showed enrichment in pathways for protein citrullination, G protein–coupled receptor (Gαq) signaling and cyclic AMP signaling (Figure 3A). Overall, whereas TNF signaling (group 1) has a global impact on all B cells from RA patients, these data suggest that RA-CCP^{POS} B cells, in comparison to RA-CCP^{NEG} B cells, demonstrate a potential role in protein citrullination and effector functionality.

Based on the substantially larger number of pathways and greater changes in expression identified by IPA in the RA-CCP^{POS} B cells in comparison to the HA^{POS} B cells (groups 1 and 2 combined), we performed gene-set enrichment analysis to compare these 2 populations. We interrogated the changes in these populations against the Molecular Signatures Database (Hallmark and C2 curated gene sets). As shown in Figure 3B, 5 major clusters of pathways were significantly up-regulated (FDR $q < 0.1$) in the RA-CCP^{POS} B cells: 1) transcription and translation; 2) B cell receptor signaling; 3) EGF receptor (EGFR) signaling; 4) TNF signaling; and 5) inflammatory cytokines and chemokines.

Enrichment of *IL15RA* expression in RA-CCP^{POS} B cells from RA patients. As outlined above, there was an abundance of cytokine and inflammation-related pathways found to be enriched in RA-CCP^{POS} B cells. We focused our attention on IL-15 signaling and performed enrichment analyses to compare our different B cell populations against known human IL-15–mediated signaling. RA-CCP^{POS} B cells showed a specific enrichment in IL-15–mediated signaling in comparison to either the HA^{POS} B cells or the RA-CCP^{NEG} B cells (Figures 4A and B).

We next examined the relative abundance of both *IL15* and its specific receptor, *IL15RA*. Indeed, *IL15RA* transcripts were up-regulated within RA-CCP^{POS} B cells relative to either RA-CCP^{NEG} or HA^{POS} B cells (Figure 4C). However, a significant difference in the expression of *IL15* was not observed (see Supplementary Figure 4, http://onlinelibrary.wiley.com/doi/10.1002/art.40772/abstract).

In order to validate the elevated expression of *IL15RA*, we utilized an independent cohort of CCP-seropositive RA patients and performed ex vivo surface staining on B cells by flow cytometry, using the same gating strategy as described earlier. Consistent with the RNA-seq results, there was a distinct subpopulation of RA-CCP^{POS} B cells that expressed IL-15Rα in all of the patients tested, whereas this was clearly absent in either the RA-CCP^{NEG} or HA^{POS} B cell populations (Figure 4D and Supplementary Figure 5 [http://onlinelibrary.wiley.com/doi/10.1002/art.40772/abstract]). Interestingly, within the RA patients, 75–90% of IL-15Rα–expressing IgG/IgA B cells were identified to be RA-CCP^{POS} B cells, thus indicating that IL-15Rα expression was significantly enriched in this population (Figure 4E).

Since IL-15Rα can also be converted to the soluble form by proteolytic cleavage via the TNFα-converting enzyme (TACE) (34), we next investigated the concentrations of soluble IL-15Rα (sIL-15Rα) in the RA patient cohort. Although elevated concentrations of sIL-15Rα in the synovium are known to be associated with increased disease activity, there are no known reports that have documented elevated sIL-15Rα concentrations in the serum of seropositive RA patients (35). To systematically validate a large number of candidate proteins within the RA patients' sera, including sIL-15Rα, we took advantage of the aptamer-based SOMAscan assay, which can detect analytes at picomolar concentrations by utilizing very small volumes of biologic samples (36) (as depicted in Supplementary Figure 6, http://onlinelibrary.wiley.com/doi/10.1002/art.40772/abstract). In a cohort of CCP-seropositive RA patients (11 samples) compared to healthy donors (10 samples), we observed significantly higher

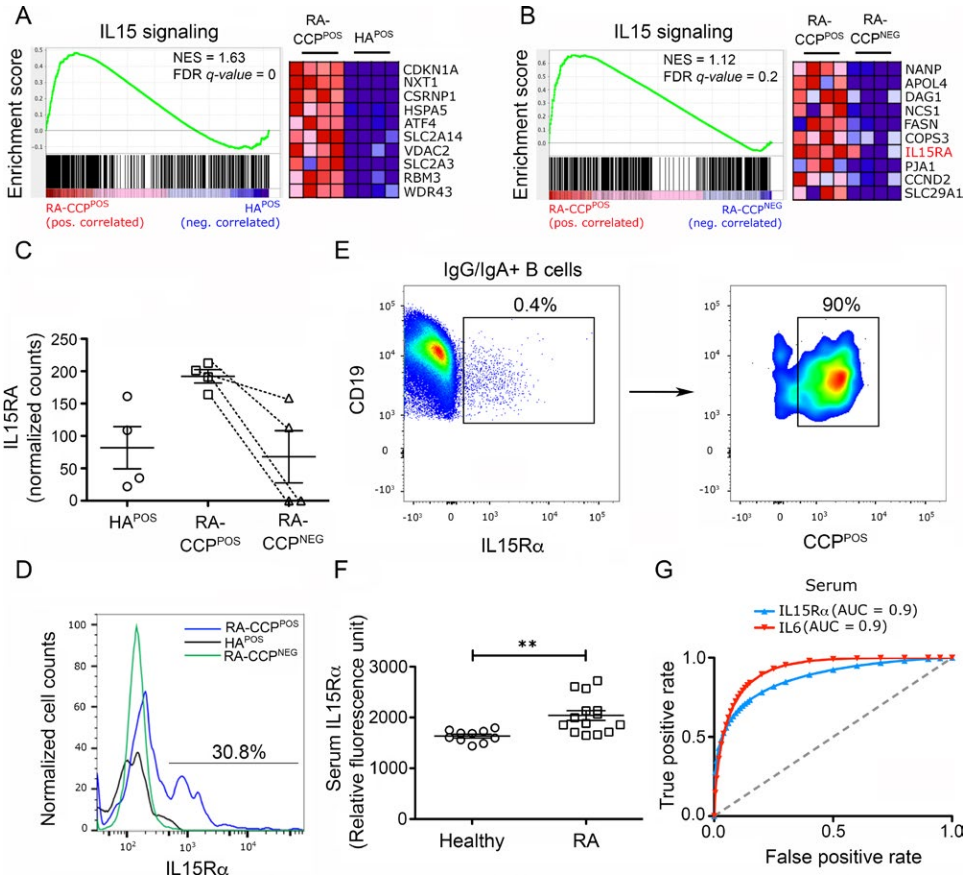

Figure 4. Interleukin-15 receptor α (IL-15Rα) and IL-15 signaling are enriched in RA-CCP^{POS} B cells. **A** and **B**, Left, Gene-set enrichment analysis plots show positive correlations of IL-15 signaling in RA-CCP^{POS} B cells compared to HA^{POS} B cells (**A**) and RA-CCP^{POS} B cells compared to RA-CCP^{NEG} B cells (**B**). Right, Heatmaps show the top 10 genes enriched in the pathway using normalized transcript levels. **C**, Normalized transcript counts of *IL15RA* in RA-CCP^{POS}, RA-CCP^{NEG}, and HA^{POS} B cells are shown. Although nonparametric tests demonstrated significant differences between RA-CCP^{POS} B cells and the other 2 populations, since these would not account for multiple hypothesis testing, we have not shown these results. Horizontal lines with bars show the mean ± SEM. **D**, Representative flow cytometric plots show IL-15Rα expression on RA-CCP^{POS}, RA-CCP^{NEG}, and HA^{POS} B cells (n = 4 each). **E**, Expression of IL-15Rα on RA-CCP^{POS} B cells is shown, gated on IL-15Rα–positive IgG/IgA B cells (n = 3). Cells were sequentially gated as CD19+IgM/IgD–(IgG/IgA^{POS})IL-15Rα^{POS}CCP^{POS}. **F**, Concentrations of IL-15Rα were determined in the serum of RA patients (n = 11) and healthy individuals (n = 10), as evaluated by SOMAscan. Horizontal lines with bars show the mean ± SEM. ** = $P < 0.01$ by Mann-Whitney U test. **G**, Receiver operating characteristic (ROC) curves indicate the predictive value of IL-15Rα and IL-6 serum levels for predicting the occurrence of RA. NES = normalized enrichment score; FDR = false discovery rate; AUC = area under the ROC curve (see Figure 1 for other definitions). Color figure can be viewed in the online issue, which is available at http://onlinelibrary.wiley.com/doi/10.1002/art.40772/abstract.

concentrations of both IL-6 and IL-8 in the RA patients, but no differences were seen in the concentrations of a large panel of other soluble analytes, including IL-1β or IL-17 (see Supplementary Figure 7, http://onlinelibrary.wiley.com/doi/10.1002/art.40772/abstract). When we evaluated sIL-15Rα, we observed significantly higher concentrations in the sera of RA patients in comparison to healthy controls (Figure 4F).

Finally, we also looked at the predictive value of serum sIL-15Rα for the occurrence of CCP-seropositive RA, as determined by the SOMAscan assay, and found that sIL-15Rα displayed both high sensitivity and high specificity for RA compared to healthy controls (Figure 4G). Using pROC, we confirmed the statistical power of sIL-15Rα in this independent cohort of CCP-seropositive RA patients, which yielded a power estimate of 0.88.

EGFR pathways and molecular validation of AREG in RA B cells. AREG is a member of the EGF family of ligands that signal through the EGFRs. It has been previously documented that TNF signaling in conjunction with IL-1β signaling can lead to the up-regulation of AREG (34,37). Our data support a pivotal role of *AREG* in RA-CCP^{POS} B cells (Figure 5A), and also a role of its downstream target pathway, EGF-mediated signaling (Figure 5B).

In order to validate our findings, we used flow cytometry to directly interrogate the expression of AREG within individual B cells from an independent cohort of seropositive RA patients. As expected, we did not observe expression of AREG on RA-CCP^{POS} B cells ex vivo (see Supplementary Figure 8, http://onlinelibrary.wiley.com/doi/10.1002/art.40772/abstract), since AREG is secreted as a soluble protein upon cleavage by TACE (34).

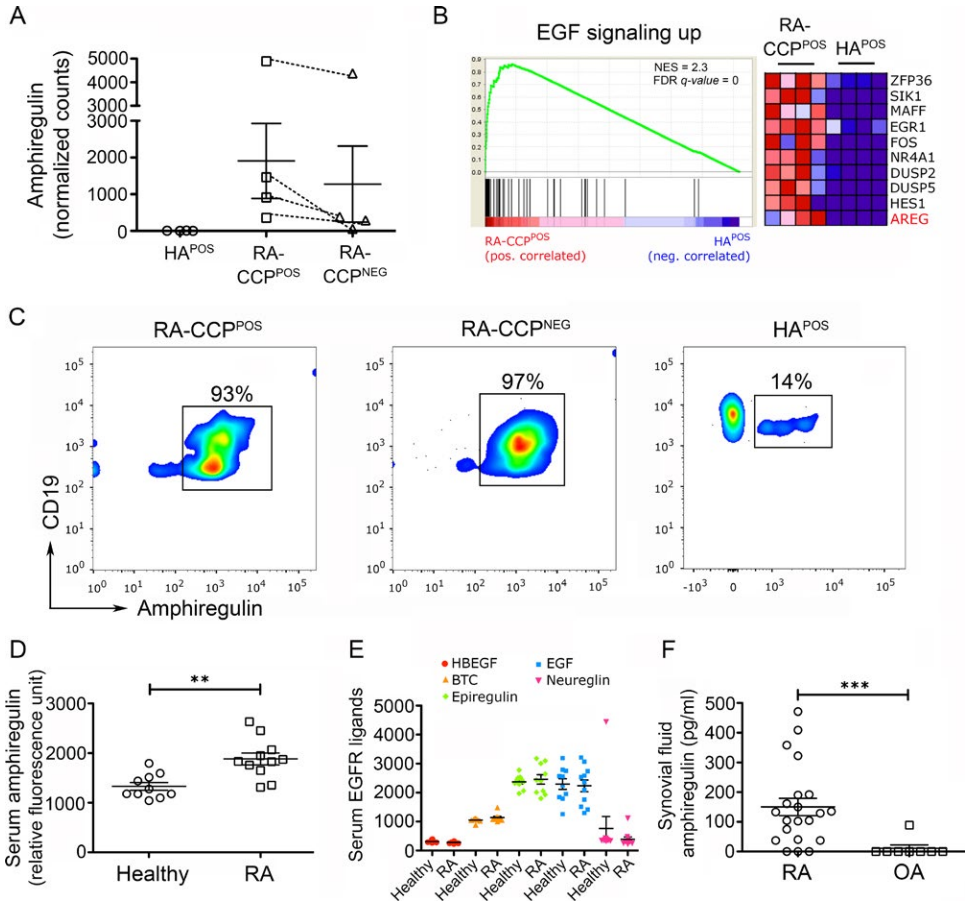

Figure 5. Amphiregulin (AREG) and associated pathways are enriched in RA-CCP^{POS} B cells. **A**, Normalized transcript counts of *AREG* in RA-CCP^{POS}, RA-CCP^{NEG}, and HA^{POS} B cells are shown. Although nonparametric tests demonstrated significant differences between RA-CCP^{POS} B cells and HA^{POS} B cells, since these would not account for multiple hypothesis testing, we have not shown these results. **B**, Left, Gene-set enrichment analysis plot shows the correlation of the epidermal growth factor (EGF) pathway in RA-CCP^{POS} versus HA^{POS} B cells. Right, Heatmap indicates normalized transcript levels of the top 10 genes in the pathway for each sample. **C**, AREG expression was evaluated by flow cytometry on RA-CCP^{POS}, RA-CCP^{NEG}, and HA^{POS} B cells after in vitro expansion (n = 4 each). **D**, Serum concentrations of AREG were determined in RA patients (n = 11) and healthy individuals (n = 10) by SOMAscan aptamer assay. The statistical power of this assay was estimated to be 0.98. **E**, Serum concentrations of all other EGF ligands in RA patients and healthy controls were identified by SOMAscan. **F**, Synovial fluid was assessed for AREG expression by enzyme-linked immunosorbent assay in patients with RA (n = 21) compared to patients with osteoarthritis (OA). In **A** and **D–F**, horizontal lines with bars show the mean ± SEM. ** = $P < 0.01$; *** = $P < 0.001$, by Mann-Whitney U test. NES = normalized enrichment score; FDR = false discovery rate; HBEGF = heparin-binding EGF-like growth factor; BTC = betacellulin (see Figure 1 for other definitions). Color figure can be viewed in the online issue, which is available at http://onlinelibrary.wiley.com/doi/10.1002/art.40772/abstract.

In order to determine whether AREG expression can be induced in vitro in B cells, we sought to mimic the nature of help afforded by T helper cells in vivo in RA (38). Accordingly, populations of RA-CCP^{POS}, RA-CCP^{NEG}, and HA^{POS} B cells were sorted by flow cytometry and incubated with both soluble CD40L and IL-21 for 14 days. Under these conditions, both RA-CCP^{POS} and RA-CCP^{NEG} B cells showed induction of AREG in >80% of cells (Figure 5C), and this was consistent with our RNA-seq data on these populations (Figure 5A). A tendency toward higher expression of AREG was observed in RA-CCP^{POS} B cells compared to HA^{POS} B cells, but owing to the high variance in frequency of AREG-expressing HA^{POS} B cell populations, this change was not significant. Taken together, these findings suggest that under polarizing conditions, at least in vitro, B cells from RA patients act as a source of AREG, a molecule with a known ability to have a global impact on multiple cell types.

Elevated expression of AREG in the serum and synovial fluid of RA patients. Among the different EGF ligands that are known to induce proliferation, growth, and differentiation by signaling through the EGFRs (39), AREG plays a unique role in its ability to induce both cell proliferation and cellular differentiation upon receptor binding (40). Although serum AREG levels in RA have been documented in other reports, these data are contradictory (41–43). We evaluated the concentrations of AREG and the other EGF ligands in the serum of CCP-seropositive RA patients, using the SOMAscan array as outlined above. In this cohort, we observed a significantly higher concentration of

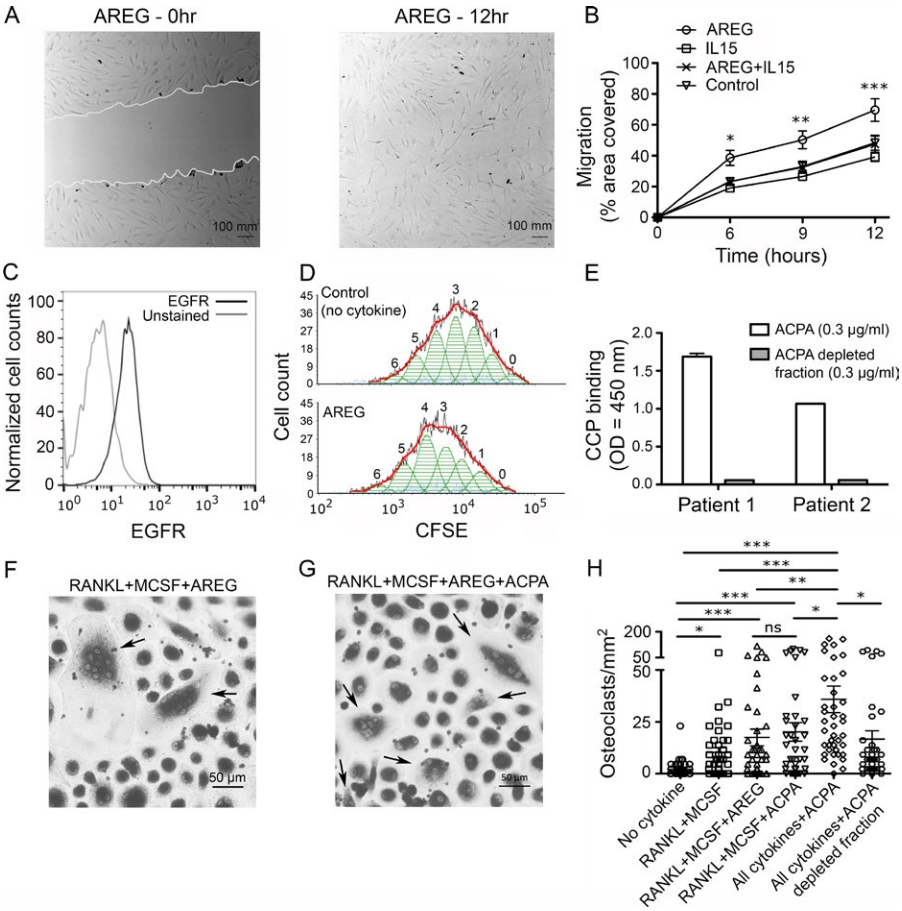

Figure 6. Amphiregulin (AREG) enhances migration and proliferation of fibroblast-like synoviocytes (FLS), and synergizes with anti–citrullinated protein antibodies (ACPAs) in mediating osteoclast differentiation. **A**, Representative scratch assay depicts cell migration at baseline and after 12 hours; experiments were performed twice, in triplicate, on FLS obtained from 1 rheumatoid arthritis (RA) patient. **B**, Migration of RA FLS, in response to AREG, interleukin-15 (IL-15), both AREG and IL-15, or a no cytokine control, is represented as the percentage of scratch area covered. Results are the mean ± SEM. * = $P < 0.05$; ** = $P < 0.01$; *** = $P < 0.001$ versus control, by two-way analysis of variance. **C,** Expression of epidermal growth factor receptor (EGFR) on RA FLS is shown (n = 3 replicates). The light gray line represents unstained cells. **D**, Proliferation of FLS was measured using 5,6-carboxyfluorescein succinimidyl ester (CFSE) dilution (n = 3 replicates). **E**, Enrichment of ACPAs against cyclic citrullinated peptide (CCP) in the plasma of 2 RA patients was assessed by enyzme-linked immunosorbent assay (n = 2 replicates). **F** and **G**, Representative examples of differentiation of osteoclasts from blood monocytes under 2 different conditions are shown. **Arrows** indicate differentiated osteoclasts with ≥3 nuclei. **H**, The number of osteoclasts under different culture conditions is shown. ACPAs from 3 RA patients were used in conjunction with peripheral blood mononuclear cells from 3 healthy individuals (n = 4 replicates); 10 random images per well were obtained at an original magnification of × 20. * = $P < 0.05$; ** = $P < 0.01$; *** = $P < 0.001$, by Kruskal-Wallis test with Dunn's test for multiple comparisons. Horizontal lines with bars show the mean ± SEM in **B** and **H**, and mean ± SD in **E**. MCSF = macrophage colony-stimulating factor; ns = not significant. Color figure can be viewed in the online issue, which is available at http://onlinelibrary.wiley.com/doi/10.1002/art.40772/abstract.

AREG in the serum of RA patients (Figure 5D), but no differences were seen in the concentrations of any of the other EGF ligands investigated, such as heparin-binding EGF-like growth factor, betacellulin, epiregulin, EGF, and neuregulin (Figure 5E).

In addition, we observed a high sensitivity and high specificity of serum AREG in predicting the occurrence of RA (see Supplementary Figure 9, http://onlinelibrary.wiley.com/doi/10.1002/art.40772/abstract). The estimated statistical power of serum AREG concentrations for prediction of RA in our cohort was 0.98.

Since RA is a disease with localized inflammation, we further evaluated the abundance of AREG in the synovial fluid from CCP-seropositive RA patients (21 samples) and compared it with synovial fluid samples from patients with noninflammatory osteoarthritis (OA) (8 samples). Our ELISA results showed that the levels of AREG were significantly higher in RA synovial fluid compared to OA synovial fluid (only 1 OA synovial fluid sample tested positive for AREG) (Figure 5F).

Promotion of migration and proliferation of FLS in vitro by AREG. One of the hallmarks of RA pathogenesis is the activation of FLS, which is characterized by a tumor-like aggressive phenotype within the joints (44). We tested the ability of AREG to increase the invasiveness of human RA FLS,

and observed that AREG promoted the increased migration of FLS, in comparison to controls, in wound-healing assays (Figures 6A and B). We confirmed the expression of EGFR on RA FLS, suggesting that the increased invasiveness was likely attributable to increased AREG-induced EGFR signaling (Figure 6C).

We also observed that RA FLS proliferated more intensely in the presence of AREG in comparison to control FLS (Figure 6D). Taken together, our results thus indicate that high levels of AREG in the peripheral blood and synovial fluid of RA patients could be responsible for the aggressive phenotype of FLS in these patients.

Functional synergy between AREG and ACPAs in mediating osteoclastogenesis. The role of AREG in promoting osteolytic activity has been detailed as one of the mediators of bone metastases in breast cancers (45). Independently, the role of ACPAs in enabling osteoclast differentiation has been described in RA (4). We thus interrogated the functional synergy between these molecules in mediating osteoclastogenesis. First, we purified ACPAs by binding to a CCP-functionalized column (Figure 6E). Next, we evaluated the ability of each of these molecules, either by themselves or in combination, to promote the differentiation of multinucleated tartrate-resistant acid phosphatase–positive osteoclasts from monocyte precursors. Although AREG by itself did not significantly increase the differentiation of osteoclasts, the number of osteoclasts was observed to be higher in cocultures with AREG and ACPAs as compared to all other conditions tested (Figures 6F–H). Our findings thus suggest that AREG can synergize with ACPAs in the differentiation of osteoclasts from blood monocytes.

DISCUSSION

The role of RA-CCP^{POS} B cells as a source of autoantibodies contributing to disease pathology in RA has been extensively studied, but the functional programs that help define the biology of the cell have remained elusive. One of the challenges we encountered was the robust and reliable identification of RA-CCP^{POS} B cells, which accounts for <0.1% of total peripheral B cells in RA patients (14). We successfully designed a sensitive flow cytometric sorting method using peptide–streptavidin conjugates, and sorted both the IgG^{POS} and IgA^{POS} CCP^{POS} B cells, owing to the fact that the antibody response against citrullinated proteins in RA comprises both IgG- and IgA-type immunoglobulins (46).

Based on the RNA-seq data, we confirmed that the expression of the IL-15Rα protein on the cell surface was enriched in the RA-CCP^{POS} B cell population, and also confirmed that increased levels of sIL-15Rα could be detected within the blood of an independent cohort of CCP-seropositive RA patients. IL-15–mediated signaling has been targeted in phase I and phase II clinical trials using HuMax-IL15 (see Supplementary Table 2, http://onlinelibrary.wiley.com/doi/10.1002/art.40772/abstract), a human monoclonal antibody that inhibits the bioactivity of IL-15 and that has produced modest improvements in disease activity (47). Synthetic disease-modifying antirheumatic drugs, including tofacitinib (a JAK inhibitor), can inhibit pathways that are also downstream of IL-15Rα–derived signaling (48). Our data suggest that the targeting of IL-15Rα might provide therapeutic benefit in RA, either by directly targeting the RA-CCP^{POS} B cells or by the elimination of sIL-15Rα in the blood of RA patients. In this regard, it is worth emphasizing that sIL-15Rα is known to increase the potency of IL-15 function by 100-fold when complexed together, and enables signaling in cells that might otherwise lack IL-15Rα (49). As suggested previously, the enrichment of IL-15Rα expression within the RA-CCP^{POS} B cells might be indicative of an altered differentiation state (50).

Our data are the first to reveal the expression of the EGFR ligand AREG on autoreactive B cells, which was also the most differentially expressed gene in RA-CCP^{POS} B cells as compared to HA^{POS} B cells. We confirmed the surface expression of AREG on B cells under inflammatory conditions, identified AREG as a candidate biomarker in CCP-seropositive RA, and evaluated the functional impact of AREG on the cellular effectors of RA. AREG is expressed as a membrane-bound molecule, which is activated upon proteolytic cleavage by TACE (34), thereby acting in an autocrine or paracrine manner and influencing cell survival, proliferation, and motility (51).

Previously reported studies are contradictory with regard to AREG concentrations in the blood of RA patients, with evidence of both significantly increased concentrations and no significant differences in comparison to healthy donors (41–43). One confounding factor in these reports is CCP seropositivity. Consistent with our studies with RA-CCP^{POS} B cells, our results herein demonstrate significant increases in the concentration of AREG in the blood of CCP-seropositive RA patients in comparison to healthy donors. In parallel, immunohistochemistry has confirmed the expression of both AREG and EGFR within the synovial tissue of RA patients (34,42). Investigations using a mouse model of inflammation in RA, in which mice harbored the transgenic IL-6 signal transducer gene, have shown the importance of EGFs, including AREG, in the pathogenesis of arthritis, since targeting AREG either by neutralizing antibodies or by short-hairpin RNA ameliorated the disease severity (43).

The induction of AREG expression is governed by the cytokines transforming growth factor β (TGFβ), TNF, and IL-1β (34,37), which are known to be abundant in RA synovial fluid and plasma (52) (results for TGFβ are shown in Supplementary Figure 10, http://onlinelibrary.wiley.com/doi/10.1002/art.40772/abstract). Our data illustrate that AREG can directly promote the proliferation and invasiveness of FLS. As outlined by elegant studies in breast cancer metastasis models, AREG is

also known to increase the differentiation and activity of osteoclasts from PBMCs in the presence of RANKL and macrophage colony-stimulating factor (45), both of which are abundantly available in the synovial compartment of RA patients. Our in vitro data further highlight the ability of AREG to act in concert with ACPAs to enhance the differentiation of osteoclasts from blood monocytes. Since our RNA-seq data outlined a role for both *IL6ST* and IL-6 signaling in RA-CCP^{POS} B cells, this suggests that IL-6 signaling might facilitate AREG up-regulation. Overall, our results indicate that under proinflammatory conditions, all B cells in RA may contribute to the production of AREG irrespective of antigen specificity, which may potentially affect other cells in the joints.

Through this study, we are reporting for the first time a comprehensive transcriptome profile of RA-CCP^{POS} B cells in RA. To the best of our knowledge, this is also the first study to conduct whole transcriptome profiling of antigen-specific B cells in any human autoimmune disorder. Our results portray B cells not merely as autoantibody producers, but also as a source of diverse molecules that can influence proliferation, differentiation, and activation of other pathogenic cell types. We anticipate that these data will serve as a foundational data set for investigating multiple hypotheses on the roles of B cells in RA and other autoimmune disorders, and will enable drug discovery and validation based on the biology of RA-CCP^{POS} B cells in RA.

We also recognize that although our report represents an important first step, further studies are required to gain a much deeper understanding of autoreactive B cells in autoimmune biology. Comprehensive studies on the relationships between sIL-15Rα and AREG within the synovial compartment, and all of the different cell types that can secrete these molecules and how they influence the expression and secretion of each other and other signaling cascades, need to be performed. Although direct profiling of synovial B cells can reflect their contribution to RA pathophysiology, obtaining these cells is challenging from a clinical perspective. Arthroscopy is considered an invasive procedure and hence not routinely performed in clinical practice. Similarly, although synovial tissue can be accessed from patients undergoing joint replacement, these patients have end-stage disease not reflective of therapeutically relevant disease. Moreover, although single-cell RNA-seq (scRNA-seq) is better suited for studying moderately or highly expressed transcripts, it would be interesting to perform scRNA-seq to document the heterogeneity in autoimmune B cells, to complement our existing results, especially with synovial B cells.

ACKNOWLEDGMENTS

We would like to acknowledge the University of Houston Seq-n-edit core for the RNA-seq data analyses, Intel for the loan of the computing cluster, and the University of Houston Center for Advanced Computing and Data Systems for providing the high-performance computing facilities.

AUTHOR CONTRIBUTIONS

All authors were involved in drafting the article or revising it critically for important intellectual content, and all authors approved the final version to be published. Dr. Varadarajan had full access to all of the data in the study and takes responsibility for the integrity of the data and the accuracy of the data analysis.

Study conception and design. Mahendra, Varadarajan.

Acquisition of data. Mahendra, Abnouf, Soomro, Wanzeck, Bridges, Aggarwal, Agarwal, Mohan, Varadarajan.

Analysis and interpretation of data. Mahendra, Yang, Adolacion, Park, Roszik, Coarfa, Romain, Qiu, Varadarajan.

REFERENCES

1. Van der Linden MP, van der Woude D, Ioan-Facsinay A, Levarht EW, Stoeken-Rijsbergen G, Huizinga TW, et al. Value of anti–modified citrullinated vimentin and third-generation anti–cyclic citrullinated peptide compared with second-generation anti–cyclic citrullinated peptide and rheumatoid factor in predicting disease outcome in undifferentiated arthritis and rheumatoid arthritis. Arthritis Rheum 2009;60:2232–41.
2. Wagner CA, Sokolove J, Lahey LJ, Bengtsson C, Saevarsdottir S, Alfredsson L, et al. Identification of anticitrullinated protein antibody reactivities in a subset of anti-CCP-negative rheumatoid arthritis: association with cigarette smoking and HLA-DRB1 'shared epitope' alleles. Ann Rheum Dis 2015;74:579–86.
3. Boross P, Verbeek JS. The complex role of Fcγ receptors in the pathology of arthritis. Springer Semin Immunopathol 2006;28:339–50.
4. Harre U, Georgess D, Bang H, Bozec A, Axmann R, Ossipova E, et al. Induction of osteoclastogenesis and bone loss by human autoantibodies against citrullinated vimentin. J Clin Invest 2012;122:1791–802.
5. Dorner T, Radbruch A, Burmester GR. B-cell-directed therapies for autoimmune disease. Nat Rev Rheumatol 2009;5:433–41.
6. Lal P, Su Z, Holweg CT, Silverman GJ, Schwartzman S, Kelman A, et al. Inflammation and autoantibody markers identify rheumatoid arthritis patients with enhanced clinical benefit following rituximab treatment. Arthritis Rheum 2011;63:3681–91.
7. Toubi E, Kessel A, Slobodin G, Boulman N, Pavlotzky E, Zisman D, et al. Changes in macrophage function after rituximab treatment in patients with rheumatoid arthritis. Ann Rheum Dis 2007;66:818–20.
8. Takemura S, Klimiuk PA, Braun A, Goronzy JJ, Weyand CM. T cell activation in rheumatoid synovium is B cell dependent. J Immunol 2001;167:4710–8.
9. Barr TA, Shen P, Brown S, Lampropoulou V, Roch T, Lawrie S, et al. B cell depletion therapy ameliorates autoimmune disease through ablation of IL-6-producing B cells. J Exp Med 2012;209:1001–10.
10. McInnes IB, Schett G. Cytokines in the pathogenesis of rheumatoid arthritis. Nat Rev Immunol 2007;7:429–42.
11. Kalliolias GD, Ivashkiv LB. TNF biology, pathogenic mechanisms and emerging therapeutic strategies. Nat Rev Rheumatol 2016;12:49–62.
12. Takemura S, Braun A, Crowson C, Kurtin PJ, Cofield RH, O'Fallon WM, et al. Lymphoid neogenesis in rheumatoid synovitis. J Immunol 2001;167:1072–80.
13. Meednu N, Zhang H, Owen T, Sun W, Wang V, Cistrone C, et al. Production of RANKL by memory B cells: a link between B cells and bone erosion in rheumatoid arthritis. Arthritis Rheumatol 2016;68:805–16.
14. Kerkman PF, Fabre E, van der voort EI, Zaldumbide A, Rombouts Y, Rispens T, et al. Identification and characterisation of citrullinated antigen-specific B cells in peripheral blood of patients with rheumatoid arthritis. Ann Rheum Dis 2016;75:1170–6.
15. Arnett FC, Edworthy SM, Bloch DA, McShane DJ, Fries JF, Cooper NS, et al. The American Rheumatism Association 1987 revised

criteria for the classification of rheumatoid arthritis. Arthritis Rheum 1988;31:315–24.

16. Van der Maaten L, Hinton G. Visualizing data using t-SNE. J Mach Learn Res 2008;9:2579–605.
17. Vieth B, Ziegenhain C, Parekh S, Enard W, Hellmann I. PowsimR: power analysis for bulk and single cell RNA-seq experiments. Bioinformatics 2017;33:3486–8.
18. Santiago-Raber ML, Lawson BR, Dummer W, Barnhouse M, Koundouris S, Wilson CB, et al. Role of cyclin kinase inhibitor p21 in systemic autoimmunity. J Immunol 2001;167:4067–74.
19. Chang M, Jin W, Chang JH, Xiao Y, Brittain GC, Yu J, et al. The ubiquitin ligase Peli1 negatively regulates T cell activation and prevents autoimmunity. Nat Immunol 2011;12:1002–9.
20. Hamel KM, Cao Y, Olalekan SA, Finnegan A. B cell–specific expression of inducible costimulator ligand is necessary for the induction of arthritis in mice. Arthritis Rheumatol 2014;66:60–7.
21. Werner M, Hobeika E, Jumaa H. Role of PI3K in the generation and survival of B cells. Immunol Rev 2010;237:55–71.
22. Thalhamer T, McGrath MA, Harnett MM. MAPKs and their relevance to arthritis and inflammation. Rheumatology (Oxford) 2008;47:409–14.
23. Kurko J, Besenyei T, Laki J, Glant TT, Mikecz K, Szekanecz Z. Genetics of rheumatoid arthritis: a comprehensive review. Clin Rev Allergy Immunol 2013;45:170–9.
24. Nagafuchi Y, Shoda H, Sumitomo S, Nakachi S, Kato R, Tsuchida Y, et al. Immunophenotyping of rheumatoid arthritis reveals a linkage between HLA-DRB1 genotype, CXCR4 expression on memory CD4(+) T cells, and disease activity. Sci Rep 2016;6:29338.
25. Lin Y, Wong K, Calame K. Repression of c-myc transcription by Blimp-1, an inducer of terminal B cell differentiation. Science 1997;276:596–9.
26. Nutt SL, Fairfax KA, Kallies A. BLIMP1 guides the fate of effector B and T cells. Nat Rev Immunol 2007;7:923–7.
27. Muto A, Hoshino H, Madisen L, Yanai N, Obinata M, Karasuyama H, et al. Identification of Bach2 as a B-cell-specific partner for small MAF proteins that negatively regulate the immunoglobulin heavy chain gene 3′ enhancer. EMBO J 1998;17:5734–43.
28. Eyre S, Bowes J, Diogo D, Lee A, Barton A, Martin P, et al. High-density genetic mapping identifies new susceptibility loci for rheumatoid arthritis. Nat Genet 2012;44:1336–40.
29. Moalli F, Jaillon S, Inforzato A, Sironi M, Bottazzi B, Mantovani A, et al. Pathogen recognition by the long pentraxin PTX3. J Biomed Biotechnol 2011;2011:830421.
30. Roumenina LT, Ruseva MM, Zlatarova A, Ghai R, Kolev M, Olova N, et al. Interaction of C1q with IgG1, C-reactive protein and pentraxin 3: mutational studies using recombinant globular head modules of human C1q A, B, and C chains. Biochemistry 2006;45:4093–104.
31. Wang S, Wang Y. Peptidylarginine deiminases in citrullination, gene regulation, health and pathogenesis. Biochim Biophys Acta 2013;1829:1126–35.
32. Khare S, Luc N, Dorfleutner A, Stehlik C. Inflammasomes and their activation. Crit Rev Immunol 2010;30:463–87.
33. Schreeder DM, Cannon JP, Wu J, Li R, Shakhmatov MA, Davis RS. Cutting edge: FcR-like 6 is an MHC class II receptor. J Immunol 2010;185:23–7.
34. Liu FL, Wu CC, Chang DM. TACE-dependent amphiregulin release is induced by IL-1β and promotes cell invasion in fibroblast-like synoviocytes in rheumatoid arthritis. Rheumatology (Oxford) 2014;53:260–9.
35. Santos Savio A, Machado Diaz AC, Chico Capote A, Miranda Navarro J, Rodríguez Alvarez Y, Bringas Pérez R, et al. Differential expression of pro-inflammatory cytokines IL-15Rα, IL-15, IL-6 and TNFα in synovial fluid from rheumatoid arthritis patients. BMC Musculoskelet Disord 2015;16:51.
36. Albaba D, Soomro S, Mohan C. Aptamer-based screens of human body fluids for biomarkers. Microarrays (Basel) 2015;4:424–31.
37. Woodworth CD, McMullin E, Iglesias M, Plowman GD. Interleukin 1 α and tumor necrosis factor α stimulate autocrine amphiregulin expression and proliferation of human papillomavirus-immortalized and carcinoma-derived cervical epithelial cells. Proc Natl Acad Sci U S A 1995;92:2840–4.
38. Rao DA, Gurish MF, Marshall JL, Slowikowski K, Fonseka CY, Liu Y, et al. Pathologically expanded peripheral T helper cell subset drives B cells in rheumatoid arthritis. Nature 2017;542:110–4.
39. Wieduwilt MJ, Moasser MM. The epidermal growth factor receptor family: biology driving targeted therapeutics. Cell Mol Life Sci 2008;65:1566–84.
40. Zaiss DM, Gause WC, Osborne LC, Artis D. Emerging functions of amphiregulin in orchestrating immunity, inflammation, and tissue repair. Immunity 2015;42:216–26.
41. Yamane S, Ishida S, Hanamoto Y, Kumagai K, Masuda R, Tanaka K, et al. Proinflammatory role of amphiregulin, an epidermal growth factor family member whose expression is augmented in rheumatoid arthritis patients. J Inflamm (Lond) 2008;5:5.
42. Swanson CD, Akama-Garren EH, Stein EA, Petralia JD, Ruiz PJ, Edalati A, et al. Inhibition of epidermal growth factor receptor tyrosine kinase ameliorates collagen-induced arthritis. J Immunol 2012;188:3513–21.
43. Harada M, Kamimura D, Arima Y, Kohsaka H, Nakatsuji Y, Nishida M, et al. Temporal expression of growth factors triggered by epiregulin regulates inflammation development. J Immunol 2015;194:1039–46.
44. Bartok B, Firestein GS. Fibroblast-like synoviocytes: key effector cells in rheumatoid arthritis. Immunol Rev 2010;233:233–55.
45. Bolin C, Tawara K, Sutherland C, Redshaw J, Aranda P, Moselhy J, et al. Oncostatin M promotes mammary tumor metastasis to bone and osteolytic bone degradation. Genes Cancer 2012;3:117–30.
46. Kokkonen H, Mullazehi M, Berglin E, Hallmans G, Wadell G, Rönnelid J, et al. Antibodies of IgG, IgA and IgM isotypes against cyclic citrullinated peptide precede the development of rheumatoid arthritis. Arthritis Res Ther 2011;13:R13.
47. Baslund B, Tvede N, Danneskiold-Samsoe B, Larsson P, Panayi G, Petersen J, et al. Targeting interleukin-15 in patients with rheumatoid arthritis: a proof-of-concept study. Arthritis Rheum 2005;52:2686–92.
48. Waldmann TA. The biology of IL-15: implications for cancer therapy and the treatment of autoimmune disorders. J Investig Dermatol Symp Proc 2013;16:S28–30.
49. Machado Diaz AC, Chico Capote A, Arrieta Aguero CA, Rodríguez Alvarez Y, García Del Barco Herrera D, Estévez Del Toro M, et al. Proinflammatory soluble interleukin-15 receptor α is increased in rheumatoid arthritis. Arthritis 2012;2012:943156.
50. Tarte K, Zhan F, De Vos J, Klein B, Shaughnessy J Jr. Gene expression profiling of plasma cells and plasmablasts: toward a better understanding of the late stages of B-cell differentiation. Blood 2003;102:592–600.
51. Berasain C, Avila MA. Amphiregulin. Semin Cell Dev Biol 2014;28:31–41.
52. Tetta C, Camussi G, Modena V, Di Vittorio C, Baglioni C. Tumour necrosis factor in serum and synovial fluid of patients with active and severe rheumatoid arthritis. Ann Rheum Dis 1990;49:665–7.

AMERICAN COLLEGE OF RHEUMATOLOGY
EDUCATION • TREATMENT • RESEARCH

Arthritis & Rheumatology
Vol. 71, No. 4, April 2019, pp 542–549
DOI 10.1002/art.40752

Pain Susceptibility Phenotypes in Those Free of Knee Pain With or at Risk of Knee Osteoarthritis: The Multicenter Osteoarthritis Study

Lisa C. Carlesso,[1] Neil A. Segal,[2] Laura Frey-Law,[3] Yuqing Zhang,[4] Lu Na,[4] Michael Nevitt,[5] Core E. Lewis,[6] and Tuhina Neogi[4]

Objective. It is not clear why some individuals develop pain with knee osteoarthritis (OA). We undertook this study to identify pain susceptibility phenotypes (PSPs) and their relationship to incident persistent knee pain (PKP) 2 years later.

Methods. We identified individuals free of PKP from the Multicenter Osteoarthritis Study, a longitudinal cohort of older adults with or at risk of knee OA. Latent class analysis was used to determine PSPs that may contribute to development of PKP apart from structural pathology. These included widespread pain, poor sleep, and psychological factors as well as pressure pain threshold and temporal summation (TS) as determined by quantitative sensory testing (QST). We used logistic regression to evaluate the association of sociodemographic factors with PSPs and the relationship of PSPs to the development of PKP over 2 years.

Results. A total of 852 participants were included (mean age 67 years, body mass index 29.5 kg/m^2, 55% women). Four PSPs were identified, primarily characterized by varying proportions (low/absent, moderate, or high) of the presence of pressure pain sensitivity and of facilitated TS, reflecting different measures of sensitization. Subjects in the PSP with a high proportion of pressure pain sensitivity and a moderate proportion of facilitated TS were twice as likely to develop incident PKP over 2 years (odds ratio 1.98 [95% confidence interval 1.07–3.68]) compared with subjects in the PSP having a low proportion of sensitization by both measures.

Conclusion. Four PSPs were identified, 3 of which were predominated by QST evidence of sensitization and 1 of which was associated with developing PKP 2 years later. Prevention or amelioration of sensitization may be a novel approach to preventing onset of PKP in OA.

INTRODUCTION

The recognized structure–symptom discordance in knee osteoarthritis (OA) points to the importance of factors other than structural joint pathology in explaining the differences in pain experienced by people with knee OA and, by extension, the susceptibility to developing knee pain in OA (1). It is possible that, independent of structural pathology, multiple characteristics such as psychological factors, sleep, and nervous system sensitization may increase the risk of an individual developing symptoms (2–4). Pain in knee OA has intermittent and constant components, with the former defining the early stages of the disease in which pain, often absent for periods of time, is triggered by activities with high force or loads (5). As the disease progresses, pain becomes more constant or persistent, often punctuated by intense intermittent pain (6). It is not known why the transition from intermittent to constant pain occurs and who may be at risk of developing persistent pain.

Sensitization of the peripheral or central nervous system is a known contributor to pain in people with knee OA (7). Defined as an amplification of neural signaling which manifests as widespread hyperalgesia, spinal hyperexcitability, and impaired descending

The Multicenter Osteoarthritis Study is supported by the NIH (grants U01-AG-18820, U01-AG-18832, U01-AG-18947, and U01-AG-19079). Dr. Carlesso's work was supported by a Canadian Institutes for Health Research Fellowship and an Osteoarthritis Research Society International collaborative scholarship. Dr. Neogi's work was supported by the NIH (grants P60-AR-47785, R01-AR-062506, and K24-AR-070892).

[1]Lisa C. Carlesso, BSc, PT, PhD: Université de Montréal, Hôpital Maisonneuve Rosemont Research Institute, Montreal, Quebec, Canada; [2]Neil A. Segal, MD, MS: University of Kansas Medical Center, Kansas City; [3]Laura Frey-Law, MPT, MS, PhD: University of Iowa, Iowa City; [4]Yuqing Zhang, DSc, Lu Na, MPH, Tuhina Neogi, MD, PhD: Boston University School of Medicine, Boston, Massachusetts; [5]Michael Nevitt, PhD: University of California at San Francisco; [6]Core E. Lewis, MD, MSPH: University of Alabama at Birmingham.

No potential conflicts of interest relevant to this article were reported.

Address correspondence to Lisa C. Carlesso, BSc, PT, PhD, École de réadaptation, Faculté de médecine, Université de Montréal, C.P. 6128, Succursale Centre-ville, Montreal, Quebec H3C 3J7, Canada. E-mail: lisa.carlesso@umontreal.ca.

Submitted for publication February 13, 2018; accepted in revised form October 3, 2018.

modulation, this process allows typically innocuous stimuli to induce and maintain a pain state (8). There is no gold standard to assess sensitization, which has been observed in chronic pain populations, although it is often assessed using quantitative sensory testing (QST) (9–11).

Phenotyping of pain, identified by OA treatment guidelines as a research priority (12,13), is an approach that can account for the multifactorial nature of pain, establish pain prognosis, and enable a rational mechanism-based approach to pain management. Phenotyping of those who are susceptible to the *development* of persistent knee pain (PKP) related to knee OA may provide novel insights into pain mechanisms. Understanding how various risk factors are associated with different pain susceptibility phenotypes (PSPs) would facilitate targeted preventive strategies by helping clinicians identify patients who are at greatest risk of developing persistent pain and likely to benefit from a given treatment.

Initial studies of pain phenotypes in people with knee OA have exclusively examined subjects who are symptomatic in cross-sectional analyses and therefore have not enhanced our understanding of the *development* of pain, particularly the development of PKP or the transition from acute (intermittent) to chronic (persistent) pain. Further, these previous studies differ methodologically in their use of phenotypic variables by including various combinations of psychological factors, surrogate measures of sensitization, and measures of radiographic and pain severity (9,14–18). No studies have included multiple psychological measures and direct QST measures of pain sensitization to define and enable more complete phenotyping in people who have not yet developed PKP but who may be at risk of transitioning to PKP irrespective of structural pathology.

We sought to understand what factors other than structural pathology may be associated with the risk of developing PKP as a first step toward understanding factors that may contribute to the transition from acute activity-related pain to chronic PKP in OA. Thus, the objectives of this study were threefold: 1) to identify PSPs related to psychological factors, measures of sensitization (i.e., QST), widespread pain (WSP), and sleep among persons with or at risk of knee OA who were free of knee pain; 2) to determine risk factors for these identified phenotypes; and 3) to determine the relationship of the PSPs to the development of PKP.

SUBJECTS AND METHODS

Study sample. The Multicenter Osteoarthritis Study (MOST) is a National Institutes of Health–funded longitudinal cohort of community-dwelling adults between the ages of 50 and 79 years who had or were at risk of developing knee OA at baseline. Subjects were recruited from Birmingham, Alabama and Iowa City, Iowa. Details of the cohort have been published elsewhere, and the study was approved by the relevant institutional review boards and was in compliance with the Helsinki Declaration (19). The current sample comprised participants who attended the 60-month visit (baseline for this study; the first visit at which measures of sensitization were obtained) who were free of PKP, defined as those who did not have frequent knee pain (i.e., pain, aching, or stiffness on most days of the past month both at the telephone screen occurring an average of 1 month prior to the clinic visit and at the clinic visit). Thus, some included participants could have experienced intermittent knee pain, although *not* on most days of the month. Participants who screened positive for peripheral neuropathy (20) or who had a prior total knee replacement were excluded from this study.

PSP determination. To determine PSPs related to factors other than structural pathology, we hypothesized that psychological factors (pain catastrophizing, depressive symptoms), sleep, WSP, and QST measures of pain sensitization (pressure pain threshold [PPT], temporal summation [TS]) would identify distinct groups of people based on patterns of grouping by these variables (21–24). As we were seeking to identify pain phenotypes and not overall clinical phenotypes, we based our choice of variables on multidimensional factors known to have a direct relationship with the experience of pain in people with or at risk of knee OA, informed by evidence-based recommendations for pain phenotyping, the relationship of WSP to knee pain, and the availability of variables in the MOST study (21–24). Pain catastrophizing was measured using a single item from the Coping Strategies Questionnaire that has a correlation of 0.74–0.81 with the full scale (25,26). Pain catastrophizing was defined as being present if the score was >1. The Center for Epidemiologic Studies Depression Scale was used as a measure of symptoms of depression, defined as a score of ≥16 (27). WSP was defined using a validated standard homunculus (28). Sleep quality was measured on a 4-point Likert scale, with very bad or bad sleep designated as poor sleep quality.

QST methods have been described elsewhere (11). Briefly, PPT was assessed by applying an algometer (1 cm^2 rubber tip, FDIX25; Wagner) at a rate of 0.5 kg/second on the center of the patellae bilaterally, tibial tuberosities, and distal radioulnar joint (control site; right side unless contraindicated); PPT was defined as the point at which participants indicated the pressure first changed to slight pain. The PPT at each anatomic site was calculated by averaging 3 trials and categorized into sex-specific tertiles. Those in the lowest tertile, demonstrating lower PPTs, represent those with a higher degree of pressure pain sensitivity; they are hereafter referred to as the group that demonstrated evidence of "pressure pain sensitivity." Mechanical TS was assessed using a weighted 60-gram von Frey monofilament (Aalborg University) at the wrist and patellae. Subjects first provided a numerical pain rating in a trial of 4 stimulations. Subsequently, the monofilament was applied repeatedly over the skin of the same site at

a frequency of 1 Hz for 30 seconds. Subjects provided a pain rating at the completion of the train of 30 stimulations and 15 seconds poststimulation. TS was defined as being facilitated when a positive value was found after the pain rating in the initial trial was subtracted from the greater of the pain ratings in the 2 subsequent trials. This group is hereafter referred to as demonstrating evidence of facilitated TS.

Subject characteristics associated with PSPs. Subject characteristics associated with the PSPs were hypothesized to include age, sex, race (Caucasian versus other), education (less than or equal to high school versus postsecondary education or greater), body mass index (BMI), comorbidities (using the Charlson Comorbidity index [29]), and Kellgren/Lawrence (K/L) grade (30). Data on all were collected at the baseline for this study.

Definitions of incident knee pain and PKP. To assess the face validity of the identified PSPs, we sought to examine the relationship of these PSPs with the development of PKP. This was operationalized as PKP and defined as a participant answering "yes" to having knee pain on most days of the past 30 days at both the telephone screen and at the clinic visit (occurring on average 30 days apart), thus spanning a 2-month period. A participant was considered to have incident PKP if either knee met the definition at the 2-year follow-up visit, and the participant had been free of PKP at baseline (the 60-month visit), having answered "no" at that time to having knee pain on most days of the past 30 days both at the telephone screen and at the clinic visit.

Statistical analysis. To identify PSPs, we applied an agnostic approach using latent class analysis (LCA). LCA is a model-based approach that employs fit statistics combined with evidence-based knowledge of the concept being analyzed to decide on the appropriate number of classes. Although the phenotypes are identified in a data-driven approach, we imposed a requirement that each class must have at least 10% of the sample to ensure meaningful interpretation of the classes and to limit possible errors in their estimates. The posterior probability of subgroup membership was generated from the LCA model, and the maximum-probability approach assigned each subject to one of the subgroups. Posterior fit statistics of the Bayesian information criterion (BIC), the adjusted BIC, the Vuong-Lo-Mendell-Rubin (VLMR) test, and the bootstrapped likelihood ratio test (BLRT) were used to determine the optimal number of classes, along with clinical reasoning (31). Once the ideal number of classes was determined, profiles of each class were interpreted using class-specific proportions of each included factor. Sample characteristics were described using class-specific proportions. Next, we ran a separate model using the R3Step method, a 3-step method used to assess the association of latent class predictors with the latent classes (32) (for details of steps, see Supplementary Table 1, available on the *Arthritis & Rheumatology* web site at http://onlinelibrary.wiley.com/doi/10.1002/art.40752/abstract). Finally, we assessed the relationship of the PSPs to incident PKP using the method described by Lanza et al (33). As this method does not allow for covariates to be included in the model (34), we ran adjusted models using logistic regression.

Sensitivity analyses were conducted to assess more parsimonious models, as well as variable contribution to the original model. In 2 sensitivity analyses, we examined one model with fewer QST variables and one using QST variables only. Correlation analysis of the QST variables demonstrated correlations with low-to-high significance (see Supplementary Table 2, http://onlinelibrary.wiley.com/doi/10.1002/art.40752/abstract). We therefore chose to employ a model with one TS variable measured at the wrist, and, to maintain the representation of peripheral and central sensitivity, we retained the variable measuring PPT at the wrist and created one variable that reflected the average patellar PPT from both knees. Those at the tibia were discarded, as it is likely that they represented the same construct given their proximity to the patella. LCA was then performed with a 7-variable model (these limited QST measures plus the other variables originally included). Due to the dominance of the QST variables in our main LCA model (for correlations of remaining indicator variables, see Supplementary Table 3, http://onlinelibrary.wiley.com/doi/10.1002/art.40752/abstract), a second sensitivity analysis was run using a model with only the original QST variables. Analyses were conducted with Mplus version 7.3 (Muthen & Muthen) and SPSS version 22 (IBM).

Table 1. Frequency of indicator variables in the whole sample and each pain susceptibility phenotype*

Class indicator variables	Whole sample (n = 852)
Widespread pain	17.3
Pain catastrophizing	39.6
Symptoms of depression	6.5
Poor sleep	12.9
TS R patella	35.0
TS L patella	36.8
TS wrist	38.4
PPT wrist†	29.1
PPT R tibia†	26.6
PPT L tibia†	27.9
PPT R patella†	28.2
PPT L patella†	27.0

* Values are the percent. TS = temporal summation; R = right; L = left; PPT = pressure pain threshold (in kg/cm^2).
† Refers to the lower tertile of values (i.e., most sensitive) with the referent group being the upper tertile (i.e., least sensitive). The upper limit for the lowest tertile for each anatomic site listed in the table was as follows: 2.76, 4.54, 4.32, 4.22, and 3.97.

RESULTS

There were 852 subjects included in this study (55% female, mean age 67 years, mean BMI 29.5 kg/m^2), all of whom were free of PKP at baseline. We ran models starting with 2 classes to determine the optimal number of classes (i.e., PSPs). With 6 classes, less than 10% of the sample was forming a class, which violated our desire to have each class comprise at least 10% of the sample. Of the 2- to 5-class solutions, the 4- and 5-class solutions were considered superior to the 2- and 3-class solutions. The BIC and adjusted BIC indicated that 5 classes were better, the VLMR suggested that 4 classes were ideal, and the BLRT statistics indicated that either the 4-class solution or the 5-class solution was acceptable. The 4-class solution was chosen because it was more readily interpretable clinically and consistent with our current understanding of contributing mechanisms (i.e., nervous system sensitivity as evidenced in the current literature) (21–24). The model entropy value, an indicator of the quality of classification, was 0.86 (1 = perfect) (see Supplementary Table 4, http://onlinelibrary.wiley.com/doi/10.1002/art.40752/abstract), indicating good quality of classification (35), and the classification probabilities for each class were all ≥0.87.

The 4 PSPs were primarily distinguished by differences in the proportion of sensitization as indicated by demonstration of pressure pain sensitivity (both peripherally and centrally) and/or facilitated TS at each of the anatomic sites tested (proportions of each anatomic site are reported in Table 1). The classes are described in descending order of their sample size. PSP 1, comprising 34% of the sample, had a low-to-moderate proportion of people with both pressure pain sensitivity (~16–26%) and facilitated TS (33–35%). PSP 2, comprising 31% of the sample, had a low proportion to none with pressure pain sensitivity (0–6%) and facilitated TS (2–10%). PSP 3, comprising 23% of the sample, had a high proportion with pressure pain sensitivity (75–89%) and a moderate proportion with facilitated TS (53–58%). Finally, PSP 4 (12% of the sample) had a high proportion with facilitated TS (82–90%) but a very low proportion to none with pressure pain sensitivity (0–4%). The PSPs are presented in Figure 1.

As can be seen in Figure 1, there were few differences in the proportions of other factors examined (e.g., WSP, psychological factors, sleep) among the phenotypes. Specifically, there were no significant differences in the proportions with poor quality sleep across all classes. Statistically significant (although small) differences in pain catastrophizing and WSP were only found between PSP 2 (which had low proportions with both pressure pain sensitivity and facilitated TS) and PSP 3 (which had a high proportion with pressure pain sensitivity and a moderate proportion with facilitated TS). Table 1 shows the frequency of the variables for the whole sample.

Associations of subject characteristics with PSP class membership. Characteristics of subjects in each PSP are presented in Figure 2. The proportion of women was highest in PSP 3 at 74%, in contrast to the proportion of in PSP 4 (26%), which had a low proportion with pressure pain sensitivity and a high proportion with facilitated TS. Proportions of non-Caucasians were greatest in PSP 2 and PSP 4 (22% and 23%, respectively), while the oldest participants were found in PSP 4 (mean age 70 years). Proportions of subjects with K/L grade ≥2, BMI ≥30 kg/m^2, ≥1 comorbidity, and postsecondary education were similar across classes.

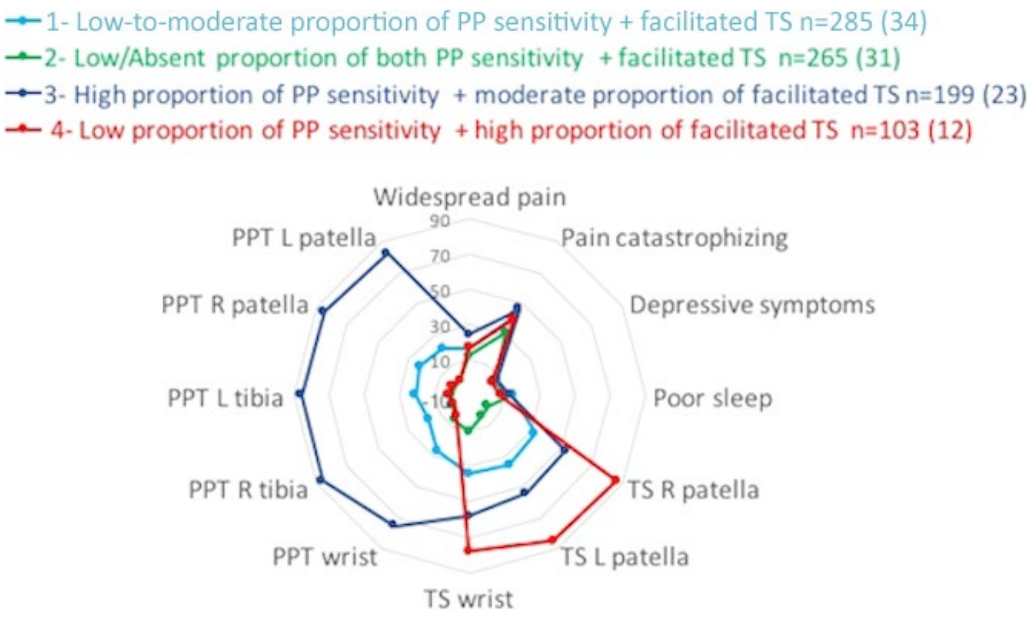

Figure 1. Spidergram plot of identified classes, showing proportions of each indicator variable in each of the respective phenotypes. PP = pressure pain; TS = temporal summation; PPT = pressure pain threshold.

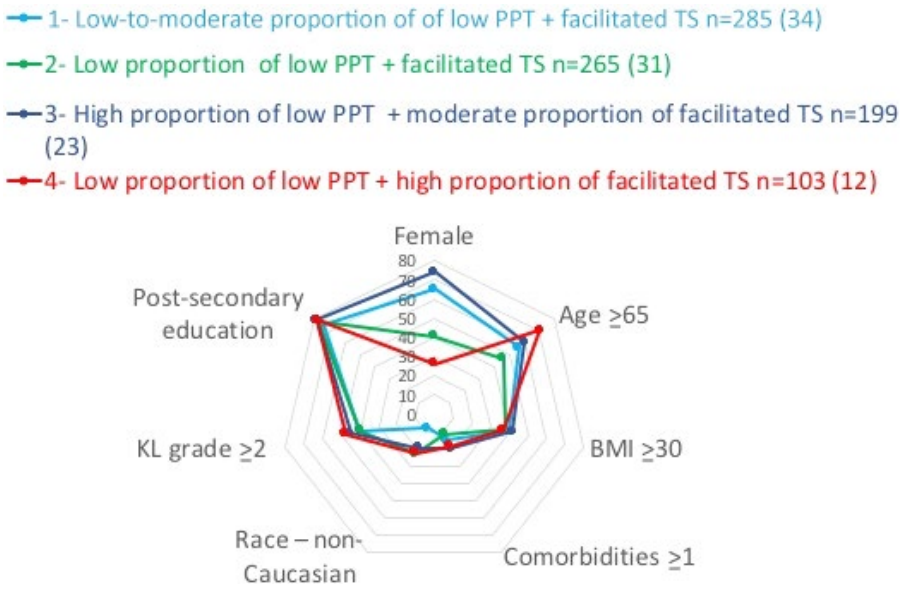

Figure 2. Spidergram plot of subject characteristics, showing proportions of each characteristic in each of the respective phenotypes. PPT = pressure pain threshold; TS = temporal summation; K/L = Kellgren/Lawrence; BMI = body mass index.

The associations of each subject characteristic with PSP membership are presented in Table 2, with PSP 2 (i.e., low proportion to none with both pressure pain sensitivity and facilitated TS) as the referent group. BMI ≥30 kg/m^2, postsecondary education, and K/L grade ≥2 were not significantly associated with membership in any class compared with membership in PSP 2. Female sex was significantly associated with ~3-fold greater odds of being in PSP 1 (moderate proportion with pressure pain sensitivity) and ~4-fold greater odds of being in PSP 3 (high proportion with pressure pain sensitivity), compared with PSP 2, while it was negatively associated with being in PSP 4, which had a low proportion with pressure pain sensitivity but a high proportion with facilitated TS (odds ratio [OR] 0.46 [95% confidence interval {95% CI} 0.27–0.79]). Non-Caucasians and those age ≥65 years had 3.5-fold and 3.0-fold greater odds, respectively, of being in PSP 4 (low proportion with pressure pain sensitivity and high proportion with facilitated TS) and 2.5-fold and 1.9-fold greater odds, respectively, of being in PSP 3 (high proportion with pressure pain sensitivity and moderate proportion with facilitated TS) compared with PSP 2.

Relationship of PSPs to incident PKP outcome. Subjects in PSP 3, which had a high proportion with pressure pain sensitivity and a moderate proportion with facilitated TS, were twice as likely to develop incident PKP over 2 years compared with those in PSP 2, the group with low proportion to none with both pressure pain sensitivity and facilitated TS (OR 1.98 [95% CI 1.07–3.68]). The other classes were not statistically significantly associated with development of PKP (Table 3).

Sensitivity analyses. The models for both sensitivity analyses are presented in Supplementary Figures 1 and 2, http://onlinelibrary.wiley.com/doi/10.1002/art.40752/abstract. The first sensitivity analysis, using a model with fewer QST variables, had a lower overall entropy of 0.835 but improved model fit (BIC = 7,896). Class proportions differed from the original, as did the values for each of the 7 indicator variables (see Supplementary Figure 1). The QST only model (see Supplementary Figure 2), using variables from the original model, resulted in very similar class structure, essentially replicating the pattern of the classes from the original model. Entropy was similar at 0.855 and model fit was lower (BIC = 10,132) (for fit statistics and entropy values, see Supplementary Table 4, http://onlinelibrary.wiley.com/doi/10.1002/art.40752/abstract).

DISCUSSION

We found 4 distinct PSPs among individuals who were free from PKP that were primarily differentiated by measures indicative of sensitization. Other factors traditionally associated with knee pain, such as psychological factors, poor sleep, and WSP, did not differ substantially between the groups. The group with the highest proportion of pressure pain sensitivity at both the knee and the wrist (indicating more sensitization both locally and centrally) had a 2-fold increased risk of developing PKP over a 2-year period. This work lends further support for the importance of sensitization in the knee pain experience of people with symptomatic knee OA (9,36) and provides new insights into the influence of preexisting sensitization on the transition from intermittent to PKP among those who were free of persistent pain initially. Interestingly, subjects in the group with primarily predominant evidence of central sensitization with facilitated TS at either the wrist or the knee were not at increased risk of developing PKP in this sample.

Table 2. Association of subject characteristics with PSP class membership*

Characteristic	Low-to-moderate proportion with both PP sensitivity and facilitated TS (PSP class 1), OR (95% CI)	High proportion with PP sensitivity and moderate proportion with facilitated TS (PSP class 3), OR (95% CI)	Low proportion with PP sensitivity and high proportion with facilitated TS (PSP class 4), OR (95% CI)	Low/absent proportion with both PP sensitivity and facilitated TS (PSP class 2)
Age ≥65 years	1.42 (0.99–2.06)	1.88 (1.24–2.85)†	3.03 (1.78–5.15)†	1 (referent)
Female sex	2.69 (1.87–3.87)†	4.08 (2.68–6.22)†	0.46 (0.27–0.79)†	1 (referent)
BMI ≥30 kg/m^2	1.17 (0.81–1.70)	1.18 (0.78–1.77)	0.99 (0.60–1.64)	1 (referent)
Non-Caucasian	0.80 (0.42–1.52)	2.47 (1.36–4.49)†	3.53 (1.78–6.98)†	1 (referent)
K/L grade ≥2	0.85 (0.59–1.23)	1.15 (0.76–1.73)	1.60 (0.97–2.62)	1 (referent)
Postsecondary education	0.99 (0.65–1.53)	1.33 (0.82–2.17)	1.40 (0.77–2.55)	1 (referent)
One or more comorbidities	1.38 (0.84–2.27)	0.92 (0.51–1.65)	1.32 (0.66–2.63)	1 (referent)

* PP = pressure pain; TS = temporal summation; OR = odds ratio; 95% CI = 95% confidence interval; BMI = body mass index; K/L = Kellgren/Lawrence.
† Significantly different from pain susceptibility phenotype (PSP) class 2.

In contrast to previous phenotyping studies of people with symptomatic knee OA that have concentrated on QST measures or psychological factors (9,15,36), we employed a multifactorial approach similar to that recommended by the Initiative on Methods, Measurement, and Pain Assessment in Clinical Trials (21). This work represents an initial step in helping to more clearly understand symptom persistence and the transition from intermittent to persistent pain. It is noteworthy that the individual entropy values in our LCA model (an indicator of the influence of a variable on class formation; see Supplementary Table 5, http://onlinelibrary.wiley.com/doi/10.1002/art.40752/abstract) for PPT and TS testing were the highest, while minimal between-class differences were noted among the remaining indicator variables. This means that in our community-based cohort, features of pain sensitization had the greatest influence on phenotype formation in those free from PKP, but the psychological constructs (e.g., symptoms of depression, pain catastrophizing), sleep quality, or WSP did not. Our findings indicate that while other studies have highlighted the importance of these latter factors, the presence of sensitization appears to have a far greater influence on the development of persistent pain.

Table 3. Risk of incident PKP*

Class	OR (95% CI)†
Low-to-moderate proportion with both PP sensitivity and facilitated TS (PSP 1) (n = 261)	0.84 (0.43–1.64)
High proportion with PP sensitivity and moderate proportion with facilitated TS (PSP 3) (n = 182)	1.98 (1.07–3.68)‡
Low proportion with PP sensitivity and high proportion with facilitated TS (PSP 4) (n = 96)	0.96 (0.41–2.27)
Low/absent proportion with both PP sensitivity and facilitated TS (PSP 2) (n = 234)	1 (referent)

* Eighty-two of 773 subjects (10.6%) developed incident persistent knee pain (PKP) over 2 years. OR = odds ratio; 95% CI = 95% confidence interval; PP = pressure pain; TS = temporal summation.
† Adjusted for body mass index, race, education, sex, comorbidities, Kellgren/Lawrence grade, and age.
‡ Significantly different from pain susceptibility phenotype (PSP) class 2.

We found female sex, age ≥65 years, and non-Caucasian race to be significant predictors of class membership in PSP 3 compared with PSP 2, with sex and non-Caucasian race having the highest risk estimates of any group. Studies of pain phenotypes in people with symptomatic OA have demonstrated similar associations (9,15,17,36), but others have also shown associations with BMI and education (9,15,36). Few have shown any association with radiographic severity (17,37). In previous studies, female sex has had greater positive associations with facilitated TS as opposed to our finding of an association with greater pressure pain sensitivity and a negative association with facilitated TS (9,36), while reports of the association of non-Caucasian race with increased TS are conflicting (9,36). How these characteristics are related to neurophysiologic test results at different pain stages requires further clarification.

We focused on subjects who were free of persistent pain to evaluate which grouping or cluster of features tended to occur together, as well as their relationship to the development of PKP. In studies of symptomatic groups, there is disagreement as to whether trajectories of pain change or stay stable over periods of 5–6 years (37,38). Our results, while not trajectory based, indicate that the group with the highest proportion with sensitization, as reflected by local, extrasegmental, and distant pressure pain sensitivity, is at higher risk of developing PKP compared with those who have a relative absence of sensitization as reflected by pressure pain sensitivity.

Our first sensitivity analysis revealed that when using fewer QST variables, similar patterns of pain susceptibility groupings among the classes can be found; however, the proportion of individuals found in each respective class changed. By comparison, our second sensitivity analysis, using only the QST measures from our main model provided, yielded almost identical results, thereby demonstrating how these variables drove the model, with psychosocial, WSP, and sleep variables offering little influence in differentiating the groups and the risk of developing PKP. The lack of effect of WSP was further substantiated by a model that we ran without the inclusion of WSP, which did not change the estimates of the remaining variables (see Supplementary Table 6, http://onlinelibrary.wiley.com/doi/10.1002/art.40752/abstract).

Our study has several limitations to consider. While we included variables known to have a direct relationship with the experience of pain in people with or at risk of knee OA and were guided by the availability of variables in the MOST study, the ideal representation and/or combination of variables for pain susceptibility phenotyping may not be fully characterized. Generalizability of our findings is limited in the application to different geographic regions and different racial classes. We used a limited set of QST measures, and our sample may not be representative of the spectrum of OA disease. Finally, as with all latent class models, our findings are exploratory and require external validation. There are equally several strengths to consider. Our study is the first to focus on people with or at risk of knee OA who are free of PKP to understand the development of the clinically relevant entity of PKP in knee OA. This is an important subgroup to consider given the intermittent nature of pain in knee OA that typically evolves to become more persistent over time. We have shown that phenotypes vary according to the degree of sensitization as detected by QST and that specific sociodemographic factors are associated with PSP membership. Compared with other clustering methods, the use of LCA, an agnostic data-driven model-based approach, is less subjective in class formation, creating potentially more valid subgroups.

In conclusion, we identified 4 distinct PSPs in people with or at risk of knee OA who were free of PKP at baseline. We found that the PSP with the highest degree of sensitization, namely the group with the highest proportion of people with pressure pain sensitivity across all sites tested (locally, extrasegmentally, and remotely), was at greatest risk of developing PKP. Understanding the mechanisms that contribute to pain susceptibility and identifying prognostic phenotypes are important steps toward the goal of phenotypic, mechanism-based management of pain.

AUTHOR CONTRIBUTIONS

All authors were involved in drafting the article or revising it critically for important intellectual content, and all authors approved the final version to be published. Dr. Carlesso had full access to all of the data in the study and takes responsibility for the integrity of the data and the accuracy of the data analysis.

Study conception and design. Carlesso, Zhang, Neogi.

Acquisition of data. Carlesso, Segal, Neogi.

Analysis and interpretation of data. Carlesso, Segal, Frey-Law, Zhang, Na, Nevitt, Lewis, Neogi.

REFERENCES

1. Neogi T. The epidemiology and impact of pain in osteoarthritis. Osteoarthritis Cartilage 2013;21:1145–53.
2. Campbell CM, Buenaver LF, Finan P, Bounds SC, Redding M, McCauley L, et al. Sleep, pain catastrophizing, and central sensitization in knee osteoarthritis patients with and without insomnia. Arthritis Care Res (Hoboken) 2015;67:1387–96.
3. Parmelee PA, Tighe CA, Dautovich ND. Sleep disturbance in osteoarthritis: linkages with pain, disability, and depressive symptoms. Arthritis Care Res (Hoboken) 2015;67:358–65.
4. Park SJ, Yoon DM, Yoon KB, Moon JA, Kim SH. Factors associated with higher reported pain levels in patients with chronic musculoskeletal pain: a cross-sectional, correlational analysis. PLoS One 2016;11:e0163132.
5. Maly MR, Cott CA. Being careful: a grounded theory of emergent chronic knee problems. Arthritis Rheum 2009;61:937–43.
6. Hawker GA, Stewart L, French MR, Cibere J, Jordan JM, March L, et al. Understanding the pain experience in hip and knee osteoarthritis: an OARSI/OMERACT initiative. Osteoarthritis Cartilage 2008;16:415–22.
7. Fingleton C, Smart K, Moloney N, Fullen BM, Doody C. Pain sensitization in people with knee osteoarthritis: a systematic review and meta-analysis. Osteoarthritis Cartilage 2015;23:1043–56.
8. Woolf CJ. Central sensitization: implications for the diagnosis and treatment of pain. Pain 2011;152 Suppl:S2–15.
9. Frey-Law LA, Bohr NL, Sluka KA, Herr K, Clark CR, Noiseux NO, et al. Pain sensitivity profiles in patients with advanced knee osteoarthritis. Pain 2016;157:1988–99.
10. Lluch Girbes E, Duenas L, Barbero M, Falla D, Baert IA, Meeus M, et al. Expanded distribution of pain as a sign of central sensitization in individuals with symptomatic knee osteoarthritis. Phys Ther 2016;96:1196–207.
11. Neogi T, Frey-Law L, Scholz J, Niu J, Arendt-Nielsen L, Woolf C, et al. Sensitivity and sensitisation in relation to pain severity in knee osteoarthritis: trait or state? Ann Rheum Dis 2015;74:682–8.
12. Zhang W, Doherty M, Peat G, Bierma-Zeinstra MA, Arden NK, Bresnihan B, et al. EULAR evidence-based recommendations for the diagnosis of knee osteoarthritis. Ann Rheum Dis 2010;69:483–9.
13. McAlindon TE, Bannuru RR, Sullivan MC, Arden NK, Berenbaum F, Bierma-Zeinstra SM, et al. OARSI guidelines for the non-surgical management of knee osteoarthritis. Osteoarthritis Cartilage 2014;22:363–88.
14. Murphy SL, Lyden AK, Phillips K, Clauw DJ, Williams DA. Subgroups of older adults with osteoarthritis based upon differing comorbid symptom presentations and potential underlying pain mechanisms. Arthritis Res Ther 2011;13:R135.
15. Cruz-Almeida Y, King CD, Goodin BR, Sibille KT, Glover TL, Riley JL, et al. Psychological profiles and pain characteristics of older adults with knee osteoarthritis. Arthritis Care Res (Hoboken) 2013;65:1786–94.
16. Finan PH, Buenaver LF, Bounds SC, Hussain S, Park RJ, Haque UJ, et al. Discordance between pain and radiographic severity in knee osteoarthritis: findings from quantitative sensory testing of central sensitization. Arthritis Rheum 2013;65:363–72.
17. Kittelson AJ, Stevens-Lapsley JE, Schmiege SJ. Determination of pain phenotypes in knee osteoarthritis: a latent class analysis using

data from the Osteoarthritis Initiative. Arthritis Care Res (Hoboken) 2015;68:612–20.

18. Egsgaard LL, Eskehave TN, Bay-Jensen AC, Hoeck HC, Arendt-Nielsen L. Identifying specific profiles in patients with different degrees of painful knee osteoarthritis based on serological biochemical and mechanistic pain biomarkers: a diagnostic approach based on cluster analysis. Pain 2015;156:96–107.
19. Segal NA, Nevitt MC, Gross KD, Hietpas J, Glass NA, Lewis CE, et al. The Multicenter Osteoarthritis Study: opportunities for rehabilitation research. PM R 2013;5:647–54.
20. Perkins B, Olaleye D, Zinman B, Bril V. Simple screening tests for peripheral neuropathy in the diabetes clinic. Diabetes Care 2001;24:250–6.
21. Edwards RR, Dworkin RH, Turk DC, Angst MS, Dionne R, Freeman R, et al. Patient phenotyping in clinical trials of chronic pain treatments: IMMPACT recommendations. Pain 2016;157:1851–71.
22. Schiphof D, Kerkhof HJ, Damen J, de Klerk BM, Hofman A, Koes BW, et al. Factors for pain in patients with different grades of knee osteoarthritis. Arthritis Care Res (Hoboken) 2013;65: 695–702.
23. Riddle DL, Stratford PW. Knee pain during daily tasks, knee osteoarthritis severity, and widespread pain. Phys Ther 2014;94:490–8.
24. Neogi T, Nevitt MC, Yang M, Curtis JR, Torner J, Felson DT. Consistency of knee pain: correlates and association with function. Osteoarthritis Cartilage 2010;18:1250–5.
25. Rosenstiel AK, Keefe FJ. The use of coping strategies in low-back patients: relationship to patient characteristics and current adjustment. Pain 1983;17:33–44.
26. Jensen MP, Keefe FJ, Lefebvre JC, Romano JM, Turner JA. One- and two-item measures of pain beliefs and coping strategies. Pain 2003;104:453–69.
27. Radloff L. The CES-D scale: a self-report depression scale for research in the general population. Appl Psychol Meas 1977;1:385–401.
28. Leveille SG, Zhang Y, McMullen W, Kelly-Hayes M, Felson DT. Sex differences in musculoskeletal pain in older adults. Pain 2005;116:332–8.
29. Charlson ME, Pompei P, Ales KL, MacKenzie CR. A new method of classifying prognostic comorbidity in longitudinal studies: development and validation. J Chronic Dis 1987;40:373–83.
30. Kellgren JH, Lawrence JS. Radiological assessment of osteo-arthrosis. Ann Rheum Dis 1957;16:494–502.
31. Nylund K, Asparouhov T, Muthén B. Deciding on the number of classes in LCA and GMM: a Monte Carlo Simulation study. Struct Equ Modeling 2007;14:535–69.
32. Asparouhov T, Muthén B. Auxiliary variables in mixture modeling: 3-step approaches using Mplus. 2014. URL: http://www.statmodel.com/examples/webnote.shtml.
33. Lanza S, Tan X, Bray B. Latent class analysis with distal outcomes: a flexible model-based approach. Struct Equ Modeling 2013;20:1–26.
34. Asparouhov T, Muthén B. Auxiliary variables in mixture modeling: using the BCH method in Mplus to estimate a distal outcome model and an arbitrary second model. 2015. URL: http://www.statmodel.com/examples/webnote.shtml.
35. Celeux G, Soromenho G. An entropy criterion for assessing the number of clusters in a mixture model. J Classif 1996;13:195–212.
36. Cardoso JS, Riley JL III, Glover T, Sibille KT, Bartley EJ, Goodin BR, et al. Experimental pain phenotyping in community-dwelling individuals with knee osteoarthritis. Pain 2016;157:2104–14.
37. Collins JE, Katz JN, Dervan EE, Losina E. Trajectories and risk profiles of pain in persons with radiographic, symptomatic knee osteoarthritis: data from the Osteoarthritis Initiative. Osteoarthritis Cartilage 2014;22:622–30.
38. Bastick AN, Wesseling J, Damen J, Verkleij SP, Emans PJ, Bindels PJ, et al. Defining knee pain trajectories in early symptomatic knee osteoarthritis in primary care: 5-year results from a nationwide prospective cohort study (CHECK). Br J Gen Pract 2016;66:e32–9.

Arthritis & Rheumatology
Vol. 71, No. 4, April 2019, pp 550–560
DOI 10.1002/art.40749

AMERICAN COLLEGE OF RHEUMATOLOGY
EDUCATION • TREATMENT • RESEARCH

Central Sensitization in Knee Osteoarthritis: Relating Presurgical Brainstem Neuroimaging and PainDETECT-Based Patient Stratification to Arthroplasty Outcome

Anushka Soni,[1] Vishvarani Wanigasekera,[1] Melvin Mezue,[1] Cyrus Cooper,[2] Muhammad K. Javaid,[1] Andrew J. Price,[1] and Irene Tracey[1]

Objective. The neural mechanisms of pain in knee osteoarthritis (OA) are not fully understood, and some patients have neuropathic-like pain associated with central sensitization. To address this, we undertook the present study in order to identify central sensitization using neuroimaging and PainDETECT and to relate it to postarthroplasty outcome.

Methods. Patients awaiting arthroplasty underwent quantitative sensory testing, psychological assessment, and functional magnetic resonance imaging (fMRI). Neuroimaging (fMRI) was conducted during punctate stimulation (n = 24) and cold stimulation (n = 20) to the affected knee. The postoperative outcome was measured using the Oxford Knee Score, patient-reported moderate-to-severe long-term pain postarthroplasty, and a range of pain-related questionnaires.

Results. Patients with neuropathic-like pain presurgery (identified using PainDETECT; n = 14) reported significantly higher pain in response to punctate stimuli and cold stimuli near the affected joint ($P < 0.05$). Neural activity in these patients, compared to those without neuropathic-like pain, was significantly lower in the rostral anterior cingulate cortex ($P < 0.05$) and higher in the rostral ventromedial medulla (RVM) during punctate stimulation ($P < 0.05$), with significant functional connectivity between these two areas (r = 0.49, $P = 0.018$). Preoperative neuropathic-like pain and higher neural activity in the RVM were associated with moderate-to-severe long-term pain after arthroplasty ($P = 0.0356$).

Conclusion. The psychophysical and neuroimaging data suggest that a subset of OA patients have centrally mediated pain sensitization. This was likely due to supraspinally mediated reductions in inhibition and increases in facilitation of nociceptive signaling, and was associated with a worse outcome following arthroplasty. The neurobiologic confirmation of central sensitization in patients with features of neuropathic pain, identified using PainDETECT, provides further support for the investigation of such bedside measures for patient stratification, to better predict postsurgical outcomes.

INTRODUCTION

Neuropathic pain is defined as pain caused by a lesion or disease of the somatosensory system (1). In contrast, nociceptive pain is defined as pain that arises from actual or threatened damage to non-neural tissue and is due to the activation of nociceptors (1). Traditionally, pain in osteoarthritis (OA) was thought to be purely nociceptive, but screening tools such as the PainDETECT Questionnaire (PD-Q) (2) have suggested a neuropathic component in some patients (3–5). Animal studies, symptom-based assessments, quantitative sensory testing, and early neuroimaging studies show that central sensitization may be an important mechanism in a subgroup of patients, even in the absence of the structural lesion in the nervous system that is typically required in order to fulfill the definition of neuropathic pain (6–8). This type of pain might be more characteristic of nociplastic pain, a third category recently endorsed by the International Association of the Study of Pain, which acknowledges an abnormal pain state

Dr. Soni's work was supported by the NIHR (grant DRF-2010-03-131). Dr. Wanigasekera's work was supported by the NIHR Oxford Biomedical Research Center. Dr. Tracey's work was supported by the Wellcome Trust.

[1]Anushka Soni, BMBCh, MA, MRCP, DPhil, Vishvarani Wanigasekera, MBBS, MRCP, FRCA, DPhil, Melvin Mezue, BM, DPhil, Muhammad K. Javaid, MBBS, PhD, MRCP, Andrew J. Price, MA, PhD, FRCS, Irene Tracey, MA, DPhil, FRCA, FMedSci: University of Oxford, Oxford, UK; [2]Cyrus Cooper, MA, DM, FRCP, FFPH, FMedSci: University of Oxford, Oxford, UK, and University of Southampton, Southampton, UK.

Dr. Cooper has received consulting fees, speaking fees, and/or honoraria from Amgen, Danone, Eli Lilly, GlaxoSmithKline, Medtronic, Merck, Nestlé, Novartis, Pfizer, Roche, Servier, Shire, Takeda, and UCB (less than $10,000 each). No other disclosures relevant to this article were reported.

Address correspondence to Anushka Soni, BMBCh, MA, MRCP, DPhil, Botnar Research Centre, Institute of Musculoskeletal Sciences, University of Oxford, Oxford OX3 7LD, UK. E-mail: Anushka.soni@ndorms.ox.ac.uk.

Submitted for publication January 22, 2018; accepted in revised form October 2, 2018.

"characterized by clinical and psychophysical findings that suggest altered nociception, despite there being no clear evidence of actual or threatened tissue damage causing the activation of nociceptors or evidence for disease or lesion of the somatosensory system causing the chronic pain" (1,9). However, non-neural tissue is damaged in OA (meaning that the pain is nociceptive), so the nociplastic definition is not ideal either. Nonetheless, as clear lesions of the somatosensory system have not been identified in the context of OA, the term "neuropathic-like pain" is used in the present report to describe patients in whom symptoms suggestive of neuropathic pain have been identified.

Central sensitization is defined as an amplification of neural signaling within the central nervous system that elicits pain hypersensitivity (10). It arises from a wide variety of underlying mechanisms ranging from sensitization within the spinal cord to signal amplification secondary to active descending pain facilitation pathways. The mechanisms by which central sensitization develops in OA and its impact on response to current treatment options remain unclear.

Neuroimaging provides a noninvasive objective method for measuring the central processing of pain in humans. Its utility in furthering our understanding of the pain mechanisms in patient populations and of suitable treatment options is increasingly accepted (11,12). Previous neuroimaging studies in OA patients have demonstrated that both spontaneous and experimentally induced pain are associated with increased neural activity in brain areas involved in sensory discrimination (7,13–16) as well as with the affective and cognitive-evaluative components of nociception (13,14,17). Furthermore, when compared to healthy controls, OA patients exhibited a disruption of the resting state default mode network (15) and a decrease in gray matter volume in areas such as the thalamus (16). Taken together, these findings suggest that both the structure and function of the brain are likely to be affected in patients with knee OA.

In patients with hip OA, neuroimaging results have also demonstrated the involvement of brainstem areas such as the periaqueductal gray (PAG), a component of the descending pain modulatory system (DPMS) (7). In that study, punctate stimulation in an area of referred pain in the OA patients was associated with increased activation in the PAG, when compared to healthy participants. Furthermore, patients with features of neuropathic pain, identified using the PD-Q and psychophysical assessment, showed significantly greater activation within the PAG compared to those with a low PD-Q score. This provided direct evidence of central sensitization in patients with OA, linking activity in the DPMS to neuropathic-like features.

Cortical and subcortical brain areas are known to modulate nociception by interacting with the midbrain and medullary structures that form the DPMS (18). This is a well-characterized network that regulates nociceptive processing in the dorsal horn via inhibitory and facilitatory influences (12,19). The midbrain PAG mainly exerts its effect through the rostral ventromedial medulla (RVM), which is thought to represent the final relay in descending modulation from supraspinal sites (20). The RVM can both inhibit and facilitate pain (21,22), and it is thought that an imbalance between the inhibitory and facilitatory tone of the DPMS may contribute to an abnormal chronic pain state (12). Cortical and subcortical areas of the brain, including the anterior cingulate cortex, amygdala, insula, and hypothalamus, are also involved in pain modulation via the DPMS. This link is likely to explain how other centrally mediated factors such as sleep, cognition, mood, and placebo effects influence the experience of pain (23).

Neuroimaging studies in humans with central sensitization have shown the involvement of the PAG, the adjacent nucleus cuneiformis (NCF), and the mesopontine reticular formation, which are also major sources of input to the RVM (24,25). Furthermore, preclinical work has shown that the central sensitization seen in conjunction with neuropathic features of pain in OA is partly mediated by descending modulation, and that pain relief was achieved by blocking descending pain facilitatory pathways from the RVM (21,22,26). These findings are consistent with a substantial body of work that has demonstrated that central nervous system nociceptive processing is altered in patients with other musculoskeletal conditions such as fibromyalgia (27,28). Interestingly, the coexistence of characteristics of fibromyalgia (suggestive of augmented central nervous system pain processing) in patients with OA has been associated with a poorer outcome following arthroplasty (29).

In this study, we investigated the neural correlates of the features of neuropathic pain (as measured using the modified PD-Q [mPD-Q]), compared to nociceptive pain, in knee OA. Furthermore, we examined the relationship between central sensitization (identified using functional magnetic resonance imaging [fMRI]) and the outcome following knee replacement surgery, a treatment option that only addresses the peripheral nociceptive drive for pain. Based on previous literature and our own work, we chose to specifically examine the PAG, NCF, and RVM. We hypothesized that patients with features of neuropathic pain would show higher activity in response to a painful stimulus in these brainstem regions and have a worse outcome following surgery, compared to those with nociceptive pain.

PATIENTS AND METHODS

Patients. Participants recruited to the Evaluation of Perioperative Pain in Osteoarthritis of the Knee (EPIONE) Study, a prospective cohort study of patients with primary OA who were awaiting primary knee replacement surgery (30), were invited to take part in this neuroimaging substudy. Patients were recruited from the Nuffield Orthopaedic Centre in Oxford, UK. The local ethics committee approved the study (National Research Ethics Service-South Central-Oxford B, 09/H0605/76), and written consent was obtained from each participant. Sample size in our study was based on a previous fMRI study using a similar stimulus paradigm (7). In that study, there was a significant difference in the mean ±

SD percentage of neural activity signal evoked by punctate stimuli between patients with neuropathic pain–like features (0.35 ± 0.25) and those with nociceptive pain (0.98 ± 0.40). Therefore, to detect a statistically significant result with a *P* value of less than 0.05 and a probability of 80%, the estimated sample size per group is 9.

Psychophysical assessment. Validated questionnaires were used to assess psychological characteristics and sleep disturbances. These included the State-Trait Anxiety Inventory (31), the Pain Catastrophizing Scale (32), the Tampa Scale for Kinesiophobia (33), the Hospital Anxiety and Depression Scale (34), and the Pittsburgh Sleep Quality Index (35).

Oxford Knee Score. The primary outcome measure following surgery was the Oxford Knee Score (OKS) (36), which measures 3 symptom domains: pain, stiffness, and functional disability, in relation to the knee. It has been shown that an OKS of ≥37 can be used to identify patients who are more likely to have achieved an acceptable state of postoperative functioning (37). Pain and function subscales, which can be calculated using original data from the OKS, have also been defined and validated (38). These subscales are scored from 0 (best possible score, least severe symptoms) to 100 (worst possible score, most severe symptoms). OKS results at 12 months after surgery were collected as part of a postal questionnaire; participants who did not initially respond were sent 2 postal reminders. The proportion of patients (in each pain group) with moderate-to-severe long-term pain after arthroplasty was used as a secondary outcome measure. Moderate-to-severe long-term postoperative pain was measured 12 months after surgery using the visual analog scale in the short form of the McGill Pain Questionnaire (39,40) and defined by an average pain severity score of ≥3 for the preceding week (41).

Quantitative sensory testing (QST). QST measures including cold detection and cold pain thresholds, as well as mechanical pain threshold in alignment with the standard research protocol for QST (42), were conducted prior to the scan session. Mechanical punctate pain intensity was also measured using a 512-mN punctate probe. For this assessment, a single punctate pain stimulus was delivered over the medial joint line of the affected joint, and the participant was asked to rate the intensity of the pain stimulus on a numeric rating scale (0–10), with 0 indicating that the stimulus was not at all sharp and 10 indicating the sharpest imaginable pain. This was repeated 3 times, and the average pain rating was calculated by taking the arithmetic mean of the 3 readings. Patients were also asked to rate the severity of their current knee pain using a visual analog scale just before commencing the scanning experiment.

Functional MRI scanning protocol. Brain images were acquired using a Siemens Magnetom Verio 3.0T MRI system and a 32-channel head coil. Scan data were acquired during cold stimulation, punctate stimulation, and rest. Participants completed perception ratings at the end of each paradigm (see Supplementary Methods, on the *Arthritis & Rheumatology* web site at http://onlinelibrary.wiley.com/doi/10.1002/art.40749/abstract).

Blood oxygen level–dependent (BOLD) imaging analysis. Prior to analysis, the BOLD fMRI data for those with left-sided knee pain were flipped so that the left–right orientation was comparable across the group. Functional MRI data processing was carried out using an fMRI Expert Analysis Tool, version 6.0 (www.fmrib.ox.ac.uk/fsl). Details on how statistical images were generated to identify significant brain activity evoked by cold pain and punctate paradigms are available in Supplementary Methods and Supplementary Figure 1 (http://onlinelibrary.wiley.com/doi/10.1002/art.40749/abstract). In addition to whole brain analyses, regions of interest analyses were also conducted for the areas in the brainstem, defined a priori (Supplementary Methods).

Post hoc analyses were conducted to further investigate the association of clinical measures of neuropathic pain severity with changes in the BOLD signal in brain areas found to show significantly different levels of activation between the nociceptive and neuropathic-like pain groups. The parameter estimates for these regions were compared to the postoperative outcome OKS and the presence of moderate-to-severe long-term pain at 12 months after arthroplasty (Supplementary Methods).

Seed-based functional connectivity. In order to further extend the findings of the stimulus-evoked fMRI data, resting state data were used to interrogate connectivity between the RVM and the rostral anterior cingulate cortex (rACC). Considering the emerging evidence suggesting that preexisting aberrant connectivity in the reward system, especially involving the nucleus accumbens (NA), may contribute to chronic pain and an inability to derive relief from pain-relieving interventions (43–45), an additional post hoc analysis of connectivity between the RVM and NA was conducted (Supplementary Methods, http://onlinelibrary.wiley.com/doi/10.1002/art.40749/abstract).

Data analysis. The mPD-Q was used to subclassify patients according to established cutoff values for nociceptive pain, unclear pain, and neuropathic pain (2). For the purposes of comparing those with purely nociceptive clinical pain to those with features of neuropathic pain, the unclear pain group was combined with the neuropathic pain group, which is referred to as the neuropathic-like pain group. This approach is consistent with those from previous studies (3,8) and ensures that patients with possible neuropathic pain are included. The differences in psychophysical characteristics between the nociceptive and neuropathic-like pain groups at baseline were investigated using Student's *t*-test for normally distributed data, Wilcoxon-Mann-Whitney test for non-normally distributed data, and Fisher's exact test for categorical data. The Wilcoxon-Mann-Whitney test was used to investigate

Table 1. Preoperative characteristics of participants in the neuroimaging substudy, divided according to the presence or absence of neuropathic pain features*

	Nociceptive pain group (n = 10)	Neuropathic-like pain group (n = 14)
Clinical features		
Age, mean ± SD years	70 ± 7	67 ± 10
Female, no. (%)	3 (30)	8 (57)
Right knee affected, no. (%)	3 (30)	7 (50)
Duration of pain, median (IQR) months	60 (24, 108)	24 (18, 60)
OKS, mean ± SD (range 0–48)	20.5 ± 6.7	17.0 ± 6.5
OKS pain subscale, mean ± SD (range 0–100)	69.2 ± 12.0	74.8 ± 11.2
OKS function subscale, mean ± SD (range 0–100)	61.2 ± 13.1	67.1 ± 11.2
Psychological features		
HAD anxiety, mean ± SD (range 0–21)	6.4 ± 4.5	8.0 ± 3.4
HAD depression, mean ± SD (range 0–21)	6.9 ± 2.3	7.3 ± 3.0
STAI state anxiety, mean ± SD (range 20–80)	31.8 ± 16.2	39.9 ± 13.5
STAI trait anxiety, mean ± SD (range 20–80)	31.6 ± 12.9	38.1 ± 13.7
PCS, median (IQR) (range 0–52)	11 (3, 14)	18 (7, 30)†
TSK, mean ± SD (range 17–68)	33.4 ± 5.3	39.2 ± 4.4†
PSQI, mean ± SD (range 0–21)‡	8.6 ± 1.7	10.7 ± 4.4
QST measures at the knee		
Mechanical pain threshold, median (IQR) mN	96.0 (32.0, 128.0)	32.0 (25.4, 101.6)
Sharpness rating to 512-mN probe, mean ± SD (range 0–10)	4.5 ± 2.4	5.1 ± 2.8
Cold detection threshold, median (IQR) °C	27.7 (27.1, 28.3)	28.7 (27.8, 29.6)
Cold pain threshold, median (IQR) °C	10 (10, 12.0)	20.4 (10, 23.1)†
Stimulus ratings in the scanner		
Unpleasantness of cold stimuli, median (IQR) (range 0–100)	0.0 (0.0, 0.0)	4.5 (0.0, 9.5)
Pain with cold stimuli, median (IQR) (range 0–100)	0.0 (0.0, 24.0)	3.5 (0.0, 24.0)
Sharpness of punctate stimuli, median (IQR) (range 0–100)	0.0 (0.0, 27.0)	17.5 (10.0, 36.0)
Unpleasantness of punctate stimuli, median (IQR) (range 0–100)	0.0 (0.0, 10.0)	11.0 (5.0, 20.0)†
Knee pain ratings in the scanner		
Pain severity immediately prior to experiment, median (IQR) (range 0–100)	0.0 (0.0, 20.0)	20.0 (0.0, 50.0)
Pain severity after cold stimuli, median (IQR) (range 0–100)	3.5 (0.0, 10.5)	3.0 (0.0, 18.5)
Pain severity after punctate stimuli, median (IQR) (range 0–100)	0.0 (0.0, 0.0)	5.5 (0.0, 27.0)†

* The preoperative modified PainDETECT questionnaire score was used to subdivide patients by nociceptive pain (<13) and neuropathic pain (≥13), and the statistical significance of differences between groups was assessed. IQR = interquartile range; OKS = Oxford Knee Score; HAD = Hospital Anxiety and Depression Scale; STAI = State-Trait Anxiety Inventory; PCS = Pain Catastrophizing Score; TSK = Tampa Scale of Kinesiophobia; QST = quantitative sensory testing.
† $P < 0.05$ versus nociceptive pain group.
‡ Measures of the Pittsburgh Sleep Quality Index (PSQI) were only available for 8 and 12 participants in the nociceptive and neuropathic-like pain groups, respectively.

differences in OKS between the 2 groups postoperatively. Fisher's exact test was used to determine differences in the proportion of patients who reported moderate-to-severe long-term pain after arthroplasty and those who achieved patient-acceptable symptom state at 12 months postsurgery.

RESULTS

Twenty-six participants were enrolled in the study. One participant was excluded from all analyses due to excess motion artifact, and a second participant was excluded due to incidental structural abnormality precluding adequate registration. Of the remaining 24 participants, the cold paradigm was not completed in 4 participants due to technical problems with the thermode.

Psychophysical characteristics. Ten patients met the criteria for nociceptive pain, using standard cutoff criteria for the mPD-Q. The remaining 14 patients were included in the neuropathic-like pain group. Although in the neuropathic-like pain group there were trends toward younger age, higher

proportion of female subjects, shorter duration of knee pain, and more severe symptoms prior to surgery, none of these differences reached statistical significance (Table 1). The data on psychological measures demonstrated significant increases in fear of movement and pain catastrophizing in the neuropathic-like pain group compared to the nociceptive group.

For readings obtained with the patient outside the scanner, sensitivity to cold pain was significantly higher in the neuropathic-like pain group compared to the nociceptive pain group ($P < 0.05$). The remaining QST parameters showed a nonsignificant trend toward increased sensitivity in the neuropathic-like pain group compared to the nociceptive pain group.

For readings obtained with the patient inside the scanner, the neuropathic-like pain group reported significantly greater levels of unpleasantness in response to the punctate stimuli ($P < 0.05$). The neuropathic-like pain group also tended to report higher scores for the other ratings, but these did not reach statistical significance. Finally, the neuropathic-like pain group reported significantly greater knee pain immediately after the punctate paradigm, compared to the nociceptive pain group ($P < 0.05$).

Functional MRI results. In the punctate paradigm (n = 24), the stimuli evoked increased brain activity bilaterally in the secondary somatosensory cortex, anterior and posterior insula, and supplementary motor area, as well as in the mid–anterior cingulate cortex (Supplementary Figure 2, http://onlinelibrary.wiley.com/doi/10.1002/art.40749/abstract). Deactivation was seen in the precuneous and contralateral primary motor cortex. The cold paradigm (n = 20) was associated with activation in the following areas bilaterally: secondary somatosensory cortex, caudate, thalamus, cerebellum, and contralateral insula and putamen (Supplementary Figure 2). Deactivation during the cold paradigm was observed in the precuneous and anterior paracingulate gyrus.

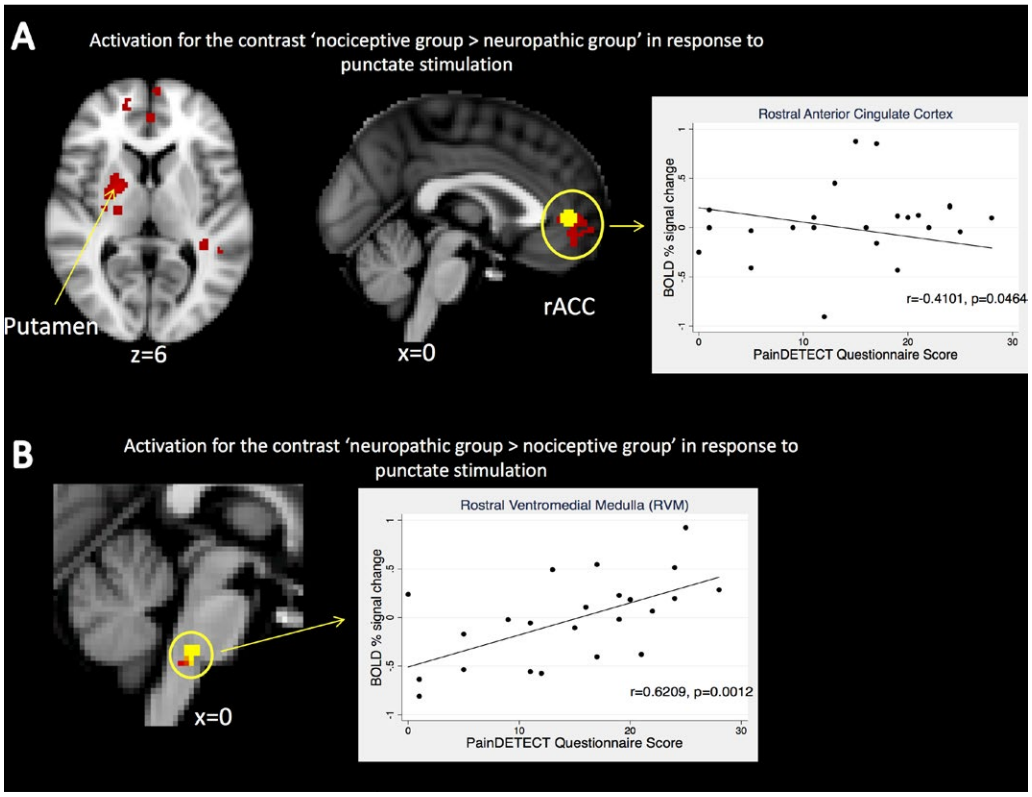

Figure 1. Whole-brain analysis and region of interest analysis results of punctate stimulation. **A**, Mixed-effects, whole-brain analysis comparing responses to punctate stimulation between the neuropathic-like pain group (n = 14) and the nociceptive pain group (n = 10). Correlation between the change in blood oxygen level–dependent (BOLD) signal activity in the rostral anterior cingulate cortex (rACC) and the severity of neuropathic-like pain symptoms is shown. Significantly increased activity in the nociceptive pain group compared to the neuropathic-like pain group is indicated (red), and a functional mask was generated using a 5-mm sphere from the peak voxel of activation in the rACC cluster (yellow). There were no areas in which activation was significantly higher in the neuropathic-like pain group than in the nociceptive pain group. Whole-brain analyses were corrected for multiple comparisons (Z score >2.3, $P < 0.05$). **B**, Region of interest analysis comparing responses (n = 24) to punctate stimulation between the neuropathic-like pain group (n = 14) and the nociceptive pain group (n = 10). Correlation between the change in BOLD signal activity in the rostral ventromedial medulla (RVM) and the severity of neuropathic-like pain symptoms is shown. Region of interest test statistics were generated from a generalized linear model design, thresholded using threshold-free cluster enhancement. $P < 0.05$. Images are displayed in radiologic convention with Montreal Neurological Institute coordinates given.

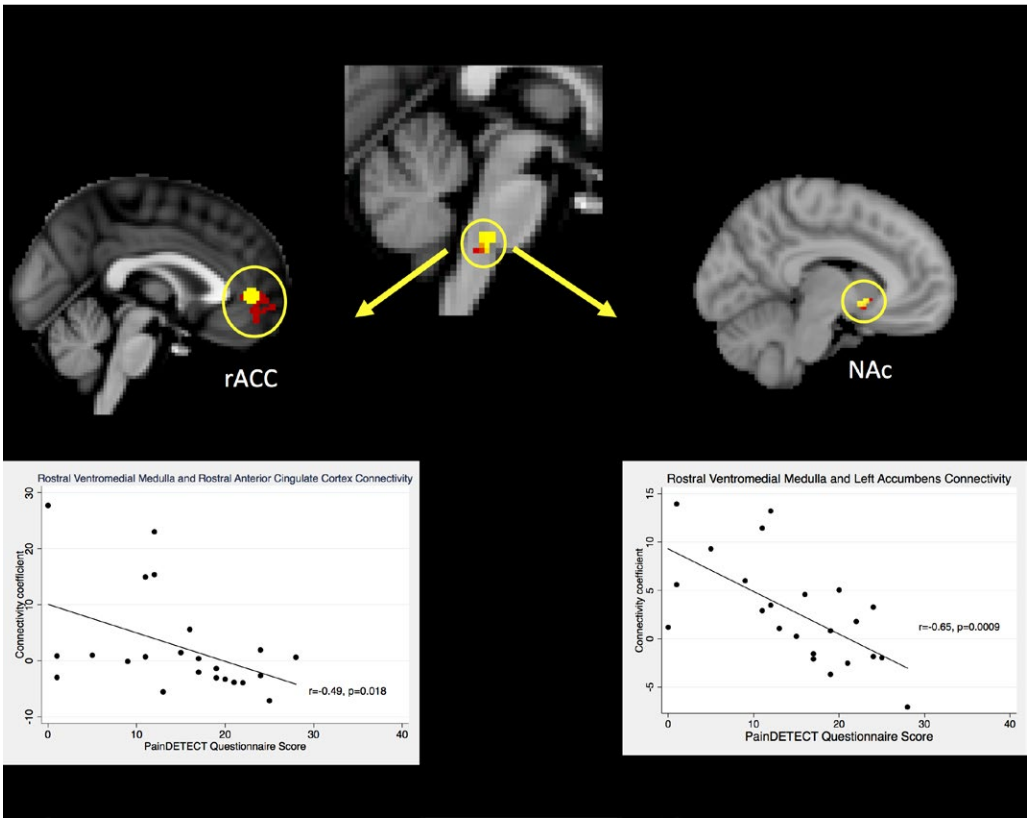

Figure 2. Rostral ventromedial medulla seed-based functional connectivity analysis. Correlation between the connectivity coefficient, for the rACC and NAc, with severity of neuropathic-like pain symptoms (n = 23) is shown. Test statistics were generated from a generalized linear model design and thresholded using threshold-free cluster enhancement. $P < 0.05$. rACC = rostral anterior cingulate cortex; NAc = nucleus accumbens.

For the punctate paradigm, the nociceptive pain group (n = 10) demonstrated significantly higher activation in the rACC and the ipsilateral putamen using whole-brain comparisons, compared to the neuropathic-like pain group (n = 14) (Figure 1A). The change in BOLD activation in the rACC showed a significant inverse relationship with the severity of neuropathic-like pain features, measured using the mPD-Q (r = –0.4101, $P < 0.05$) (Figure 1A). There were no areas in which activation was significantly higher in the neuropathic-like pain group than in the nociceptive pain group. The small sample size (7 patients in the nociceptive pain group and 13 in neuropathic-like pain group) precluded meaningful subgroup analysis for the cold paradigm.

Region of interest analyses revealed increased activation in the ipsilateral NCF ($P < 0.05$) (Supplementary Figure 3, http://onlinelibrary.wiley.com/doi/10.1002/art.40749/abstract) and RVM ($P < 0.05$) (Figure 1B) in the neuropathic-like pain group, compared to the nociceptive pain group, during punctate stimulation. There was no significant difference in activation in the PAG. There was no significant association between BOLD signal change and the mPD-Q score in the NCF (Supplementary Figure 3). The change in BOLD activation in the RVM was significantly and strongly positively correlated with the mPD-Q score (r = 0.6209, $P = 0.0012$) (Figure 1B).

Connectivity results. Whole-brain analysis did not reveal any significant differences in connectivity with the RVM or rACC between the nociceptive pain group and neuropathic-like pain group. Region of interest analysis demonstrated that connectivity between the RVM and the rACC was greater in the nociceptive pain group than in the neuropathic-like pain group with the RVM seed-based analysis only (Figure 2). In addition, region of interest analysis showed increased connectivity between the RVM and contralateral NA in the nociceptive pain group, compared to the neuropathic-like pain group (Figure 2).

Clinical and psychological features 12 months postsurgery. Long-term follow-up data were available for 19 patients. All of the clinical and psychological features showed significant improvement compared to baseline ($P < 0.05$), except for state and trait anxiety, pain catastrophizing, and sleep disturbance. Anxiety and pain catastrophizing were found to be significantly worse in the neuropathic-like pain group, compared to

Table 2. Twelve-month postoperative characteristics of participants in the neuroimaging substudy, divided according to the presence or absence of neuropathic pain features*

	Nociceptive pain group (n = 10)	Neuropathic-like pain group (n = 9)
Clinical features		
OKS, median (IQR) (range 0–48)	46.0 (40.0, 47.0)	40.0 (33.0, 48.0)
OKS pain subscale, median (IQR) (range 0–100)	26.0 (24.0, 32.0)	36.0 (20.0, 52.0)
OKS function subscale, median (IQR) (range 0–100)	20.0 (20.0, 28.6)	31.7 (21.5, 37.2)
Patient-acceptable symptom state, no. (%)	9 (90)	5 (56)
Moderate-to-severe long-term pain after arthroplasty, no. (%)	0 (0)	4 (44)†
Psychological features		
HAD anxiety, median (IQR) (range 0–21)	0.5 (0.0, 2.0)	3.0 (1.0, 7.0)†
HAD depression, median (IQR) (range 0–21)	1.0 (0.0, 3.0)	1.0 (0.0, 7.0)
STAI state anxiety, mean ± SD (range 20–80)	24.0 ± 10.2	33.0 ± 15.8
STAI trait anxiety, mean ± SD (range 20–80)	28.0 ± 5.5	33.9 ± 12.7
PCS, median (IQR) (range 0–52)	5 (0, 6)	14 (2, 17)†
PSQI, mean ± SD (range 0–21)	7.8 ± 2.9	8.7 ± 4.3

* The preoperative PainDETECT questionnaire score was used to subdivide patients by nociceptive pain (<13) and neuropathic pain (≥13), and the statistical significance of differences between groups was assessed. OKS = Oxford Knee Score; IQR = interquartile range; HAD = Hospital Anxiety and Depression Scale; STAI = State-Trait Anxiety Inventory; PCS = Pain Catastrophizing Score; PSQI = Pittsburgh Sleep Quality Index.
† $P < 0.05$ versus nociceptive pain group.

the nociceptive pain group. In the neuropathic-like pain group, there was a nonsignificant trend toward worse clinical symptom severity, which was assessed using the OKS and the proportion of patients achieving a patient-acceptable symptom state. However, the neuropathic-like pain group, as defined presurgically, did have a significantly higher proportion of patients with moderate-to-severe long-term pain after arthroplasty, compared to the nociceptive pain group (Table 2). Furthermore, patients with moderate-to-severe long-term pain after arthroplasty had significantly higher BOLD signal change in the RVM prior to surgery (median –0.38 [interquartile range –0.58, 0.07]), compared to those who did not report long-term pain after arthroplasty (median

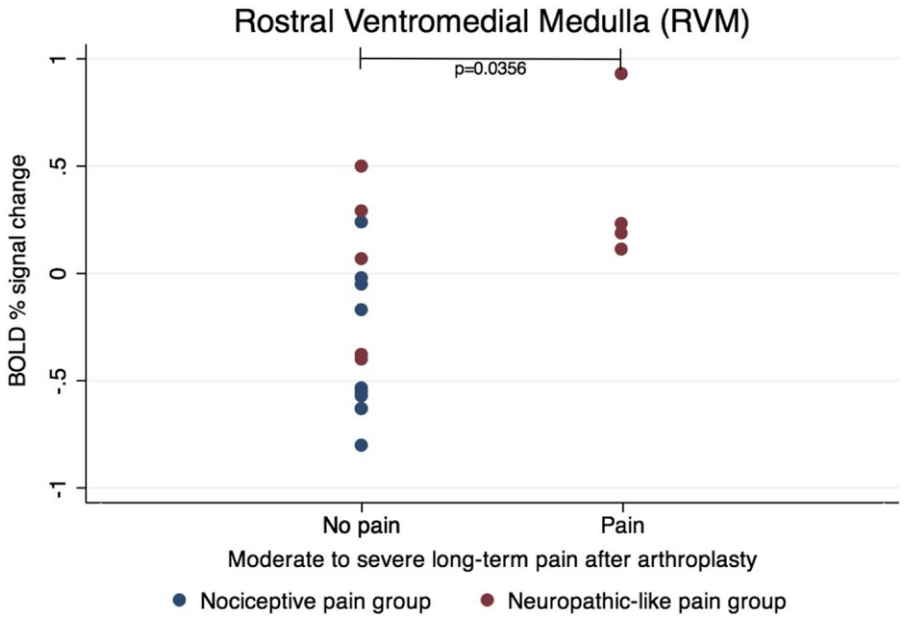

Figure 3. Relationship between functional magnetic resonance imaging activation in the rostral ventromedial medulla prior to surgery and clinical outcome at 12 months (n = 19). BOLD = blood oxygen level–dependent.

0.21 [interquartile range 0.14, 0.58]) ($P = 0.0356$) (Figure 3). There was no significant relationship between BOLD signal change in the rACC and long-term pain after arthroplasty (Supplementary Figure 4, http://onlinelibrary.wiley.com/doi/10.1002/art.40749/abstract), and there was no significant association between BOLD signal change in the RVM or rACC during punctate stimulation and OKS results 12 months postsurgery.

DISCUSSION

The main finding of this preliminary study is that patients awaiting arthroplasty for knee OA who have features of neuropathic pain (identified using the mPD-Q) demonstrated psychophysical and functional imaging evidence of centrally mediated pain sensitization, compared to OA patients with nociceptive pain. The neuropathic-like pain group exhibited significantly lower levels of activation in the rACC (Z score >2.3, $P < 0.05$) and higher levels of activation in the RVM ($P = 0.00182$) and ipsilateral NCF ($P = 0.02962$) in response to punctate stimulation of the affected knee, compared to those with features of nociceptive pain. In addition, the resting state data showed increased connectivity between the RVM and rACC, as well as between the RVM and NA, in the nociceptive pain group compared to the neuropathic-like pain group. Psychophysically, the neuropathic-like pain group had significantly higher sensitivity to cold and punctate stimuli, as well as significantly higher levels of pain catastrophizing and kinesiophobia, prior to surgery.

Following knee replacement surgery, there was a trend toward worse outcomes in the neuropathic-like pain group, with a significantly higher proportion of patients experiencing moderate-to-severe long-term pain after arthroplasty. Moreover, punctate stimuli–evoked RVM activation prior to surgery was significantly higher in patients reporting moderate-to-severe long-term pain after arthroplasty compared to those who did not. These findings may be related to the well-established fact that pain severity prior to surgery is an important predictor of persistent pain after total knee arthroplasty (46). In the current study, patients with neuropathic-like pain reported higher levels of pain and disability prior to surgery but the difference was not statistically significant, possibly due to small sample sizes. The current study, in attempting to stratify patients by different mechanisms for pain, provides additional insight into why some patients, who were also likely to have higher preoperative pain severity, had a higher probability of experiencing unsatisfactory pain relief from arthroplasty.

The rACC is an important cortical area involved in the descending inhibitory control of pain, which works by recruiting an antinociceptive subcortical network, including the amygdalae and PAG (47). Its role in regulating pain has been most extensively investigated in the context of placebo analgesia, where the effect is mediated by the endogenous opioid system via μ-opioid receptor activation in specific brain regions, including the rACC (48). The current study shows that patients with knee OA who demonstrated increased rACC activation in response to punctate stimulation were less likely to report features of neuropathic-like pain with respect to their clinical knee pain. The mechanism underlying the differences in the manifestation of the same clinical condition may therefore be associated with the differential ability to successfully engage the endogenous inhibitory system in patients from the nociceptive pain group, compared to the neuropathic-like pain group. Although the role of the rACC in patients with knee OA had not been previously reported, the current results are consistent with previous observations in fibromyalgia, where reduced structural and functional connectivity in the rACC was demonstrated when compared to control participants (49) and interpreted as a dysfunction in descending inhibition.

The NCF is known to be part of the descending pain modulatory system, and a previous study of experimentally induced central sensitization in healthy participants showed increased activation in the contralateral NCF during hyperalgesia (24). Findings from the current study support a similar involvement of the NCF in the context of clinical pain sensitization secondary to knee OA.

The RVM is known to receive input from the PAG and adjacent NCF and is considered to be the final relay point for the descending supraspinal signals, before modifying incoming nociceptive signals in the dorsal horn of the spinal cord (11). The descending modulation of spinal cord function was originally thought to involve only inhibitory mechanisms, but over time the role of facilitatory effects on nociceptive processing has been recognized, demonstrated in the imaging of humans in injury models, and even shown to be modifiable by analgesics (19,21,22,24,50–52). As such, the RVM is highly likely to be involved in chronic pain development and maintenance (51).

In the current study, increased activation in the RVM in patients with neuropathic-like pain, compared to those with nociceptive pain, may reflect increased activity in RVM on-cells, resulting in descending facilitation similar to what was previously found in hip OA (7) and in our earlier studies that focused on imaging of centrally sensitized states (24,25). Functional MRI data alone do not allow us to distinguish between facilitatory and inhibitory activity in the RVM, and it is possible that the increased activity reflects increased inhibitory drive in response to the greater pain severity associated with the presence of neuropathic-like pain. However, the former hypothesis is somewhat supported by the fact that the mPD-Q score was significantly and positively correlated with the level of RVM activity, as well as by the psychophysical differences that demonstrated heightened fear of movement, pain catastrophizing, punctate unpleasantness score, and joint pain after punctate stimulation in the neuropathic-like pain group compared to the nociceptive group (Table 2). Furthermore, our recent work in diabetic painful peripheral neuropathy emphasizes the facilitatory role of DPMS brainstem nuclei (53).

In accordance with the dual capability of the RVM to inhibit and facilitate pain processing, the higher rate of connectivity between the RVM and rACC in the nociceptive pain group suggests that the RVM in these patients is likely to exert an inhibitory effect on pain. Additionally, before surgery, these patients had higher connectivity between the RVM and NAC (a key structure of the reward processing system), and it was evident that they had better pain relief results postoperatively. This is consistent with the emerging concept that an intact reward system may be important for experiencing pain relief (45). However, this post hoc finding requires further validation in a separate study.

The current study did not demonstrate any significant differences in PAG activation between the 2 patient groups. This is surprising, given the previous findings in patients with hip OA (7) and knowledge about the functional connectivity of the rACC and the descending modulation of pain. It is possible that the involvement of the PAG in more than 1 function and its multiple connections, in conjunction with its relatively small size (54), contributed to a lack of significant difference between the patient groups in this study. Further studies using ultra-high-field imaging or enhanced acquisition sequences to enable functional neuroanatomical dissection of the PAG into its constituent components, as we did for the diabetic painful neuropathy study (53), should also help identify differences in pain-related PAG function that may exist between patient groups.

The main strength of the current study is that it recruited patients with clinically homogeneous disease severity, in that they were all deemed to be appropriate candidates for knee replacement surgery. Moreover, the neuroimaging data were related to behavioral and QST measures. The main limitation of the study was the use of the mPD-Q to stratify patients, as the questionnaire was designed to measure more broadly neuropathic pain rather than specifically and only central sensitization. Since the design of the study, other tools have been developed to specifically identify features of centralized pain, such as the modified 2010 American College of Rheumatology Preliminary Diagnostic Criteria for Fibromyalgia (55) and the Central Sensitization Inventory (56).

It may also be beneficial to compare the responses in the nociceptive pain group to the neuropathic-like pain group without inclusion of the unclear pain group in the latter. Unfortunately, recruitment to a study like this is challenging due to the demographic and the potential for contraindications with MR. The sample size (while adequately powered) was not sufficient to conduct an analysis of arthroplasty outcome data, as only 19 patients returned postsurgery; this is something we would like to address in future studies. The relatively small sample size might also have contributed to the lack of a significant difference in postoperative OKS results between groups, especially as data from 2 larger patient cohorts confirm the difference in outcome between patients stratified by nociceptive pain and neuropathic-like pain as both clinically and statistically significant (30). Nonetheless, the overall proportion of patients with unfavorable long-term pain postarthroplasty, reported here, is reassuringly similar to the data reported in the literature (57).

Finally, what is not clear from this study or previous studies is whether changes in imaging findings are related to the pain or are the consequence of pain-related biomechanical alterations due to musculoskeletal damage causing changes in gait, lifestyle, activity levels, etc. Attempts to decipher this by imaging patients after successful arthroplasty do show normalization of imaging findings (16,58); however, it may be that pain relief facilitated improvement in biomechanics that largely explained the brain imaging changes. A similar line of reasoning supports recent work redefining phantom limb pain (59).

In summary, this preliminary study furthers our understanding of the underlying neurobiologic mechanisms in patients with knee OA who have clinical features suggestive of neuropathic pain. Explorative work has suggested that preoperative PD-Q scores independently predict postoperative pain intensity (60). Current neuroimaging data suggest that this may be due to both reduced descending inhibitory mechanisms and increased supraspinal facilitation of nociceptive signals in the dorsal horn. The neurobiologic suggestion of central sensitization in patients with features of neuropathic pain, identified using the mPD-Q, provides further support for investigation of stratified patient groups in order to better predict the outcome following surgery. Further work is needed to confirm the findings of this small-scale study and to determine the optimal method for identifying the patient group most likely to have more complex underlying pain mechanisms, such as central sensitization. Clarification of the terminology used in this scenario (i.e., in which there is abnormal nociceptive processing in the absence of a structural lesion of the somatosensory system) will also be critical as this body of research progresses, in addition to enabling successful translation to the clinical setting. In the future, it may be possible to use this information to potentially guide the use of drug therapy and behavioral treatments to specifically target this mechanism in order to improve overall arthroplasty-related treatment outcomes.

AUTHOR CONTRIBUTIONS

All authors were involved in drafting the article or revising it critically for important intellectual content, and all authors approved the final version to be published. Dr. Soni had full access to all of the data in the study and takes responsibility for the integrity of the data and the accuracy of the data analysis.

Study conception and design. Soni, Cooper, Javaid, Price, Tracey.
Acquisition of data. Soni, Wanigasekera, Mezue.
Analysis and interpretation of data. Soni, Wanigasekera, Mezue, Javaid, Price, Tracey.

REFERENCES

1. International Association for the Study of Pain. IASP terminology. 2018. URL: http://www.iasp-pain.org/Education/Content.aspx?ItemNumber=1698.

2. Freynhagen R, Baron R, Gockel U, Tolle TR. PainDETECT: a new screening questionnaire to identify neuropathic components in patients with back pain. Curr Med Res Opin 2006;22:1911–20.
3. Soni A, Batra RN, Gwilym SE, Spector TD, Hart DJ, Arden NK, et al. Neuropathic features of joint pain: a community-based study. Arthritis Rheum 2013;65:1942–9.
4. Hochman JR, Gagliese L, Davis AM, Hawker GA. Neuropathic pain symptoms in a community knee OA cohort. Osteoarthritis Cartiledge 2011;19:647–54.
5. Dimitroulas T, Duarte RV, Behura A, Kitas GD, Raphael JH. Neuropathic pain in osteoarthritis: a review of pathophysiological mechanisms and implications for treatment. Semin Arthritis Rheum 2014;44:145–54.
6. Lluch E, Torres R, Nijs J, Van Oosterwijck J. Evidence for central sensitization in patients with osteoarthritis pain: a systematic literature review. Eur J Pain 2014;18:1367–75.
7. Gwilym SE, Keltner JR, Warnaby CE, Carr AJ, Chizh B, Chessell I, et al. Psychophysical and functional imaging evidence supporting the presence of central sensitization in a cohort of osteoarthritis patients. Arthritis Rheum 2009;61:1226–34.
8. Hochman JR, Davis AM, Elkayam J, Gagliese L, Hawker GA. Neuropathic pain symptoms on the modified painDETECT correlate with signs of central sensitization in knee osteoarthritis. Osteoarthritis Cartilage 2013;21:1236–42.
9. Kosek E, Cohen M, Baron R, Gebhart GF, Mico JA, Rice AS, et al. Do we need a third mechanistic descriptor for chronic pain states? Pain 2016;157:1382–6.
10. Woolf CJ. Central sensitization: implications for the diagnosis and treatment of pain. Pain 2011;152 Suppl:S2–15.
11. Lee MC, Tracey I. Imaging pain: a potent means for investigating pain mechanisms in patients. Br J Anaesth 2013;111:64–72.
12. Tracey I. Neuroimaging mechanisms in pain: from discovery to translation. Pain 2017;158 Suppl 1:S115–22.
13. Kulkarni B, Bentley DE, Elliott R, Julyan PJ, Boger E, Watson A, et al. Arthritic pain is processed in brain areas concerned with emotions and fear. Arthritis Rheum 2007;56:1345–54.
14. Parks EL, Geha PY, Baliki MN, Katz J, Schnitzer TJ, Apkarian AV. Brain activity for chronic knee osteoarthritis: dissociating evoked pain from spontaneous pain. Eur J Pain 2011;15:843 e1–14.
15. Baliki MN, Mansour AR, Baria AT, Apkarian AV. Functional reorganization of the default mode network across chronic pain conditions. PLoS One 2014;9:e106133.
16. Gwilym SE, Filippini N, Douaud G, Carr AJ, Tracey I. Thalamic atrophy associated with painful osteoarthritis of the hip is reversible after arthroplasty: a longitudinal voxel-based morphometric study. Arthritis Rheum 2010;62:2930–40.
17. Pujol J, Martinez-Vilavella G, Llorente-Onaindia J, Harrison BJ, Lopez-Sola M, Lopez-Ruiz M, et al. Brain imaging of pain sensitization in patients with knee osteoarthritis. Pain 2017;158:1831–8.
18. Tracey I, Mantyh PW. The cerebral signature for pain perception and its modulation. Neuron 2007;55:377–91.
19. Gebhart GF. Descending modulation of pain. Neurosci Biobehav Rev 2004;27:729–37.
20. Ossipov MH, Dussor GO, Porreca F. Central modulation of pain. J Clin Invest 2010;120:3779–87.
21. De Felice M, Sanoja R, Wang R, Vera-Portocarrero L, Oyarzo J, King T, et al. Engagement of descending inhibition from the rostral ventromedial medulla protects against chronic neuropathic pain. Pain 2011;152:2701–9.
22. Wang R, King T, De Felice M, Guo W, Ossipov MH, Porreca F. Descending facilitation maintains long-term spontaneous neuropathic pain. J Pain 2013;14:845–53.
23. Tracey I, Dickenson A. SnapShot: pain perception. Cell 2012;148:1308.
24. Zambreanu L, Wise RG, Brooks JC, Iannetti GD, Tracey I. A role for the brainstem in central sensitisation in humans: evidence from functional magnetic resonance imaging. Pain 2005;114:397–407.
25. Lee MC, Zambreanu L, Menon DK, Tracey I. Identifying brain activity specifically related to the maintenance and perceptual consequence of central sensitization in humans. J Neurosci 2008;28:11642–9.
26. Havelin J, Imbert I, Cormier J, Allen J, Porreca F, King T. Central Sensitization and neuropathic features of ongoing pain in a rat model of advanced osteoarthritis. J Pain 2016;17:374–82.
27. Phillips K, Clauw DJ. Central pain mechanisms in the rheumatic diseases: future directions. Arthritis Rheum 2013;65:291–302.
28. Sluka KA, Clauw DJ. Neurobiology of fibromyalgia and chronic widespread pain. Neuroscience 2016;338:114–29.
29. Brummett CM, Urquhart AG, Hassett AL, Tsodikov A, Hallstrom BR, Wood NI, et al. Characteristics of fibromyalgia independently predict poorer long-term analgesic outcomes following total knee and hip arthroplasty. Arthritis Rheumatol 2015;67:1386–94.
30. Soni A, The COASt Study Group, Price AJ, Tracey I, Javaid M. Neuropathic pain as a predictor of short and long-term outcome following knee replacement surgery. Osteoarthritis Cartilage 2016;24:S420–1.
31. Spielberger CD, Gorsuch RL, Lushene RE. Self-evaluation questionnaire, STAI form X-1. Palo Alto (CA): Consulting Psychologists Press; 1970.
32. Sullivan MJ, Bishop SR, Pivik J. The Pain Catastrophizing Scale: development and validation. Psychol Assess 1995;7:524–32.
33. Kori SH, Miller RP, Todd DD. Kinesiophobia: a new view of chronic pain behavior. Pain Manage 1990;3:35–43.
34. Zigmond AS, Snaith RP. The Hospital Anxiety and Depression Scale. Acta Psychiatr Scand 1983;67:361–70.
35. Buysse DJ, Reynolds CF III, Monk TH, Berman SR, Kupfer DJ. The Pittsburgh Sleep Quality Index: a new instrument for psychiatric practice and research. Psychiatry Res 1989;28:193–213.
36. Dawson J, Fitzpatrick R, Murray D, Carr A. Questionnaire on the perceptions of patients about total knee replacement. J Bone Joint Surg Br 1998;80:63–9.
37. Keurentjes JC, Van Tol FR, Fiocco M, So-Osman C, Onstenk R, Koopman-Van Gemert AW, et al. Patient acceptable symptom states after total hip or knee replacement at mid-term follow-up: thresholds of the Oxford hip and knee scores. Bone Joint Res 2014;3:7–13.
38. Harris K, Dawson J, Doll H, Field RE, Murray DW, Fitzpatrick R, et al. Can pain and function be distinguished in the Oxford Knee Score in a meaningful way? An exploratory and confirmatory factor analysis. Qual Lif Res 2013;22:2561–8.
39. Melzack R. The short-form McGill Pain Questionnaire. Pain 1987;30:191–7.
40. Melzack R. The McGill pain questionnaire: from description to measurement. Anesthesiology 2005;103:199–202.
41. Petersen KK, Arendt-Nielsen L, Simonsen O, Wilder-Smith O, Laursen MB. Presurgical assessment of temporal summation of pain predicts the development of chronic postoperative pain 12 months after total knee replacement. Pain 2015;156:55–61.
42. Rolke R, Magerl W, Campbell KA, Schalber C, Caspari S, Birklein F, et al. Quantitative sensory testing: a comprehensive protocol for clinical trials. Eur J Pain 2006;10:77–88.
43. Navratilova E, Morimura K, Xie JY, Atcherley CW, Ossipov MH, Porreca F. Positive emotions and brain reward circuits in chronic pain. J Comp Neurol 2016;524:1646–52.

44. Vachon-Presseau E, Tetreault P, Petre B, Huang L, Berger SE, Torbey S, et al. Corticolimbic anatomical characteristics predetermine risk for chronic pain. Brain 2016;139:1958–70.
45. Tracey I. A vulnerability to chronic pain and its interrelationship with resistance to analgesia. Brain 2016;139:1869–72.
46. Lewis GN, Rice DA, McNair PJ, Kluger M. Predictors of persistent pain after total knee arthroplasty: a systematic review and meta-analysis. Br J Anaesth 2015;114:551–61.
47. Bingel U, Lorenz J, Schoell E, Weiller C, Buchel C. Mechanisms of placebo analgesia: rACC recruitment of a subcortical antinociceptive network. Pain 2006;120:8–15.
48. Zubieta JK, Bueller JA, Jackson LR, Scott DJ, Xu Y, Koeppe RA, et al. Placebo effects mediated by endogenous opioid activity on mu-opioid receptors. J Neurosci 2005;25:7754–62.
49. Jensen KB, Srinivasan P, Spaeth R, Tan Y, Kosek E, Petzke F, et al. Overlapping structural and functional brain changes in patients with long-term exposure to fibromyalgia pain. Arthritis Rheum 2013;65:3293–303.
50. Wanigasekera V, Mezue M, Andersson J, Kong Y, Tracey I. Disambiguating pharmacodynamic efficacy from behavior with neuroimaging: implications for analgesic drug development. Anesthesiology 2016;124:159–68.
51. Denk F, McMahon SB, Tracey I. Pain vulnerability: a neurobiological perspective. Nat Neurosci 2014;17:192–200.
52. Bee LA, Dickenson AH. Descending facilitation from the brainstem determines behavioural and neuronal hypersensitivity following nerve injury and efficacy of pregabalin. Pain 2008;140: 209–23.
53. Segerdahl AR, Themistocleous AC, Fido D, Bennett DL, Tracey I. A brain-based pain facilitation mechanism contributes to painful diabetic polyneuropathy. Brain 2018;141:357–64.
54. Hemington KS, Coulombe MA. The periaqueductal gray and descending pain modulation: why should we study them and what role do they play in chronic pain? J Neurophysiol 2015;114:2080–3.
55. Wolfe F, Clauw DJ, Fitzcharles MA, Goldenberg DL, Hauser W, Katz RS, et al. Fibromyalgia criteria and severity scales for clinical and epidemiological studies: a modification of the ACR Preliminary Diagnostic Criteria for Fibromyalgia. J Rheumatol 2011;38:1113–22.
56. Mayer TG, Neblett R, Cohen H, Howard KJ, Choi YH, Williams MJ, et al. The development and psychometric validation of the central sensitization inventory. Pain Pract 2012;12:276–85.
57. Beswick AD, Wylde V, Gooberman-Hill R, Blom A, Dieppe P. What proportion of patients report long-term pain after total hip or knee replacement for osteoarthritis? A systematic review of prospective studies in unselected patients. BMJ Open 2012;2:e000435.
58. Rodriguez-Raecke R, Niemeier A, Ihle K, Ruether W, May A. Brain gray matter decrease in chronic pain is the consequence and not the cause of pain. J Neurosci 2009;29:13746–50.
59. Makin TR, Scholz J, Henderson Slater D, Johansen-Berg H, Tracey I. Reassessing cortical reorganization in the primary sensorimotor cortex following arm amputation. Brain 2015;138:2140–6.
60. Kurien T, Arendt-Nielsen L, Petersen KK, Graven-Nielsen T, Scammell BE. Preoperative neuropathic pain-like symptoms and central pain mechanisms in knee osteoarthritis predicts poor outcome 6 months after total knee replacement surgery. J Pain 2018; 19:1329–41.

Arthritis & Rheumatology
Vol. 71, No. 4, April 2019, pp 561–570
DOI 10.1002/art.40748

AMERICAN COLLEGE OF RHEUMATOLOGY
EDUCATION • TREATMENT • RESEARCH

Annotating Transcriptional Effects of Genetic Variants in Disease-Relevant Tissue: Transcriptome-Wide Allelic Imbalance in Osteoarthritic Cartilage

Wouter den Hollander,[1] Irina Pulyakhina,[2] Cindy Boer,[3] Nils Bomer,[1] Ruud van der Breggen,[1] Wibowo Arindrarto,[1] Rodrigo Couthino de Almeida,[1] Nico Lakenberg,[1] Thom Sentner,[1] Jeroen F. J. Laros,[1] Peter A. C. 't Hoen,[4] Eline P. E. Slagboom,[1] Rob G. H. H. Nelissen,[1] Joyce van Meurs,[3] Yolande F. M. Ramos,[1] and Ingrid Meulenbelt[1]

Objective. Multiple single-nucleotide polymorphisms (SNPs) conferring susceptibility to osteoarthritis (OA) mark imbalanced expression of positional genes in articular cartilage, reflected by unequally expressed alleles among heterozygotes (allelic imbalance [AI]). We undertook this study to explore the articular cartilage transcriptome from OA patients for AI events to identify putative disease-driving genetic variation.

Methods. AI was assessed in 42 preserved and 5 lesioned OA cartilage samples (from the Research Arthritis and Articular Cartilage study) for which RNA sequencing data were available. The count fraction of the alternative alleles among the alternative and reference alleles together (φ) was determined for heterozygous individuals. A meta-analysis was performed to generate a meta-φ and *P* value for each SNP with a false discovery rate (FDR) correction for multiple comparisons. To further validate AI events, we explored them as a function of multiple additional OA features.

Results. We observed a total of 2,070 SNPs that consistently marked AI of 1,031 unique genes in articular cartilage. Of these genes, 49 were found to be significantly differentially expressed (fold change <0.5 or >2, FDR <0.05) between preserved and paired lesioned cartilage, and 18 had previously been reported to confer susceptibility to OA and/or related phenotypes. Moreover, we identified notable highly significant AI SNPs in the *CRLF1*, *WWP2*, and *RPS3* genes that were related to multiple OA features.

Conclusion. We present a framework and resulting data set for researchers in the OA research field to probe for disease-relevant genetic variation that affects gene expression in pivotal disease-affected tissue. This likely includes putative novel compelling OA risk genes such as *CRLF1*, *WWP2*, and *RPS3*.

INTRODUCTION

Due to the increased proportion of elderly persons in the human population, osteoarthritis (OA) has become one of the major musculoskeletal diseases (1). While all joint tissues have been implicated in OA pathology, the disease is characterized primarily by progressive degradation and calcification of articular cartilage (2). Both gene-targeted research (3–5) and genome-wide research (6–9) showed that a multitude of genes are involved in the currently irreversible destruction of articular cartilage that precedes total joint replacement surgery, which is at present the only effective treatment for end-stage OA. In this regard, numerous studies have shown altered regulation of gene expression that reflects, attenuates, and/or stimulates OA-mediated cartilage degradation (10–13). Moreover, multiple OA risk alleles of single-nucleotide polymorphisms (SNPs) were shown to consistently modulate OA pathology by altering transcription of the respective genes in articular cartilage, commonly referred to as an allelic

Supported in part by Treat OA (grant 200800 from the European Commission Seventh Framework Programme), the Dutch Arthritis Society (grant DAA 10-1-402), and the Dutch Scientific Research Council NWO ZonMW VICI (grant 91816631/528). The Research Arthritis and Articular Cartilage study is supported by Leiden University Medical Center.

[1]Wouter den Hollander, PhD, Nils Bomer, PhD, Ruud van der Breggen, BSc, Wibowo Arindrarto, MSc, Rodrigo Couthino de Almeida, PhD, Nico Lakenberg, BSc, Thom Sentner, MSc, Jeroen F. J. Laros, PhD, Eline P. E. Slagboom, PhD, Rob G. H. H. Nelissen, MD, PhD, Yolande F. M. Ramos, PhD, Ingrid Meulenbelt, PhD: Leiden University Medical Center, Leiden, The Netherlands; [2]Irina Pulyakhina, PhD: Radboud University Medical Center Nijmegen, The Netherlands, and Wellcome Trust Centre for Human Genetics, Oxford, UK; [3]Cindy Boer, MSc, Joyce van Meurs, PhD: Erasmus Medical Center, Rotterdam, The Netherlands; [4]Peter A. C. 't Hoen, PhD: Radboud University Medical Center Nijmegen, Nijmegen, The Netherlands.

Drs. van Meurs, Ramos, and Meulenbelt contributed equally to this work.

No potential conflicts of interest relevant to this article were reported.

Address correspondence to Ingrid Meulenbelt, PhD, Department of Medical Statistics and Bioinformatics, Section of Molecular Epidemiology, Leiden University Medical Center, LUMC Post-zone S-05-P, PO Box 9600, 2300 RC Leiden, The Netherlands. E-mail: i.meulenbelt@lumc.nl.

Submitted for publication May 16, 2018; accepted in revised form October 2, 2018.

imbalance (AI) (14–19). Notable recent examples are the genes *ALDH1A2* (18) and *MGP* (20). Hence, it is clear that *in-cis* genetic regulation of transcription plays a substantial role in cartilage homeostasis and, therefore, in OA pathophysiology.

Despite the evidence for *in-cis* genetic regulation of transcription in OA susceptibility, genome-wide association studies (GWAS) have thus far failed to explain the larger part of the hereditary component of OA (21). In this regard, a large number of the tested SNPs in GWAS likely bear no biologic function in relation to the addressed phenotype or disease-relevant tissues (22), resulting in massive inflation of possibly biologically irrelevant statistical tests and thus the multiple testing correction penalty. Consequently, large numbers of SNPs that do bear biologic functionality in the context of OA are missed. Furthermore, SNPs that reside within linkage disequilibrium (LD) blocks are hard to interpret, as association analysis is inherently unable to distinguish disease-relevant alleles from merely statistically associated alleles.

In previous studies, we and others have used targeted approaches to address AI events of putative as well as established OA susceptibility genes (14,16–18,23,24). Given the successful identification of the transcriptional consequences of multiple OA-associated SNPs, we have aimed to characterize, on a transcriptome-wide scale, novel SNPs that tag AI of genes expressed in articular cartilage, and we have subsequently identified those that appear to confer susceptibility to OA. Finally, further using the RNA sequencing data set, we ran analyses to identify AI genes whose expression was additionally modified with severity of OA pathophysiology as reflected by differential expression between preserved and lesioned OA cartilage.

MATERIALS AND METHODS

Cohorts. Ethical approval for the Research Arthritis and Articular Cartilage (RAAK) study was obtained from the medical ethics committee of the Leiden University Medical Center (P08.239), and informed consent was obtained from all patients included. For the current study, RNA sequencing data were available from preserved and lesioned cartilage from 21 patients (6 with hip OA and 15 with knee OA), complemented by an additional 21 preserved samples (from 14 patients with hip OA and 7 patients with knee OA) and 5 lesioned samples (from 2 patients with hip OA and 3 patients with knee OA) (see Supplementary Table 1, available on the *Arthritis & Rheumatology* web site at http://onlinelibrary.wiley.com/doi/10.1002/art.40748/abstract). For cartilage sampling details, see refs. 19 and 25.

RNA sequencing data. After RNA isolation (RNeasy Mini Kit, RNA integrity number >7; Qiagen), paired-end 100-bp RNA library sequencing (Illumina TruSeq RNA Library Prep Kit, Illumina HiSeq 2000) resulted in an average of 10 million clusters. Reads were aligned using GSNAP (an R package within Bioconductor; https://rdrr.io/bioc/gmapR/) against the human (hg19) reference genome, while known Dutch SNPs (Genome of the Netherlands) were masked to aid in preventing potential reference alignment bias. AI events were assessed on SNPs called using SNVMix2 with default settings (26) with minimum coverage of 25 and at least 10 reads (R) per allele. AI is reported as the average fraction (φ) of the alternative allele reads ($R_{alternative}$) among the total number of reads ($R_{total} = R_{alternative} + R_{reference}$) at the position of the respective genetic variation per sample (i):

$$\varphi = \frac{1}{n}\sum_{i=1}^{n}\frac{R_{i,alternative}}{R_{i,reference}}$$

To detect SNPs that robustly mark imbalance, 2 binomial tests were performed per heterozygote and per SNP under the null hypothesis that the amount of imbalance is either greater or smaller than 0.477. A meta-analysis (meta; http://www.r-project.org/) per SNP among heterozygous individuals (null hypothesis median φ = 0.49) was performed to generate a meta-φ and P value per SNP with a false discovery rate (FDR) correction for multiple comparisons. To allow independent samples in the meta-analysis only, the preserved cartilage of each sample pair (n = 21) was used complemented with the individual preserved (n = 21) and lesioned (n = 5) OA samples.

Unfortunately, SNVMix2 discards strand specificity. While in general this does not pose an issue when annotating the AI direction to an effector allele, it does so for A>T, T>A, G>C, and C>G SNPs. Therefore, for these SNPs (n = 119) we supplied (see Supplementary Table 2, http://onlinelibrary.wiley.com/doi/10.1002/art.40748/abstract) minor allele frequencies (MAFs) and SNPs in strong LD for GWAS look-ups. Using the edgeR package, fragments per gene were used to assess the dispersion by quantile-adjusted conditional maximum likelihood (27). Subsequently, differential gene expression analysis was performed pairwise between preserved and lesioned samples for which we had RNA of both (n = 21) (Table 1) followed by FDR correction. Gene Ontology (GO) term enrichment analysis was performed using the tool DAVID available online (28).

Genotype data. Using Illumina HumanOmniExpressExome chips, genome-wide genotyping data were constructed for 216 samples from the RAAK study. SNPs with <95% call rate, Hardy-Weinberg equilibrium $<10^{-4}$, MAF <0.01, or located on the sex chromosomes were removed prior to imputation against the 1000 GenomesV3 March 2012 reference panel (29). We removed SNPs for which the imputation quality of 0.4 was not met (12,30).

TaqMan assay. Conventional TaqMan genotyping was performed on both genomic DNA and articular cartilage complementary DNA (cDNA) (31) from 6 patients (2 females and 4 males) who underwent total joint replacement surgery of the knee due to primary OA. An allele-specific custom TaqMan assay for rs7256319

Table 1. Sample characteristics of preserved and lesioned OA articular cartilage in the Research Arthritis and Articular Cartilage study*

Tissue type	No. of samples	Age, mean ± SD years	No. of men	No. of women	OA articular cartilage		
					Preserved	Lesioned	Preserved–lesioned pairs
Knee	25	69 ± 9	4	21	22	18	15
Hip	22	66 ± 9	5	17	20	8	6
All	47	68 ± 9	9	38	42	26	21

* OA = osteoarthritic.

(ThermoFisher Scientific) was used to quantify the allele ratio in cDNA samples. AI of cDNA was normalized against the genomic DNA ratio (with an inherent 1:1 allele ratio) as a reference.

RESULTS

Transcriptome-wide discovery of articular cartilage AI events. To understand how genetic variation contributes *in-cis* to transcriptional regulation in articular cartilage on a transcriptome-wide scale, we first called heterozygous SNPs (dbSNP144) using RNA sequencing data from articular cartilage derived from patients who underwent total replacement surgery of either the hip joint (n = 22) or knee joint (n = 25) due to primary OA (Table 1; also see Supplementary Table 1, http://onlinelibrary.wiley.com/doi/10.1002/art.40748/abstract). After filtering by the number of read counts per position ($R_{reference}$ ≥10, $R_{alternative}$ ≥10, and R_{total} ≥25), selecting for heterozygous SNPs present in at least 2 individuals, removing SNPs present in multiple or no distinct transcripts, and discarding the HLA locus, we defined φ for 13,853 SNPs as the measure of imbalance (Figure 1A), which denotes the fraction of $R_{alternative}$ among R_{total}. Possibly due to reference bias, a considerable number of SNPs were marked as allelic imbalanced by φ <0.1 or φ >0.9 (n = 418) and were subsequently removed prior to further analyses. As such, in Supplementary Table 2 (http://onlinelibrary.wiley.com/doi/10.1002/art.40748/abstract) we show AI, defined as φ across all individuals heterozygous for the 13,435 SNPs.

Subsequently, a meta-analysis among heterozygous individuals of each SNP (null hypothesis: median φ = 0.49) and subsequent FDR correction for multiple testing revealed 2,070 SNPs that significantly marked AI among 1,031 genes (Figure 1B; also see Supplementary Table 3, http://onlinelibrary.wiley.com/doi/10.1002/art.40748/abstract). To allow unambiguous annotation of the AI direction to a GWAS effector allele, for A>T, T>A, G>C, and C>G SNPs with MAFs surrounding 0.50 (n = 119), we supplied MAFs and SNPs in strong LD.

Intersection of genes subject to AI with those differentially expressed between preserved and paired OA-lesioned cartilage. While articular cartilage genes subject to AI due to genetic variation could contribute to OA pathophysiology in various ways (e.g., in cartilage development or homeostasis), it can be expected that allelic imbalanced genes that additionally mark the articular cartilage's disease state are more likely to contribute to or attenuate disease progression. Therefore, we went back to the original expression data and determined differential expression in patients for whom paired RNA sequencing data of both preserved and OA-lesioned articular cartilage were generated (6 hip joints and 15 knee joints) (Table 1).

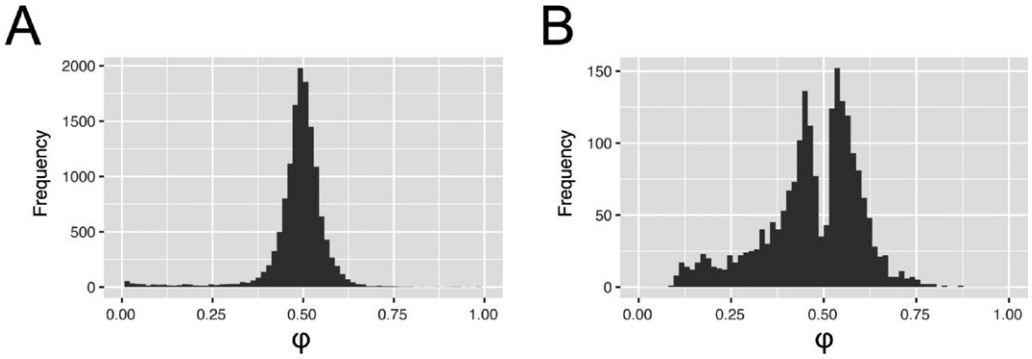

Figure 1. Distribution of allelic imbalance (AI) events in articular cartilage. AI is reported as the average fraction (φ) of the alternative allele reads among the total number of reads. **A**, AI was defined for 13,853 called variants after selecting for at least 2 heterozygotes, selecting single-nucleotide polymorphisms (SNPs) present in only single genes and removing low counts. **B**, After filtering by allelic fraction (0.1<φ<0.9) and meta false discovery rate <0.05, 2,070 SNPs remained that marked significant AI of 1,031 unique genes.

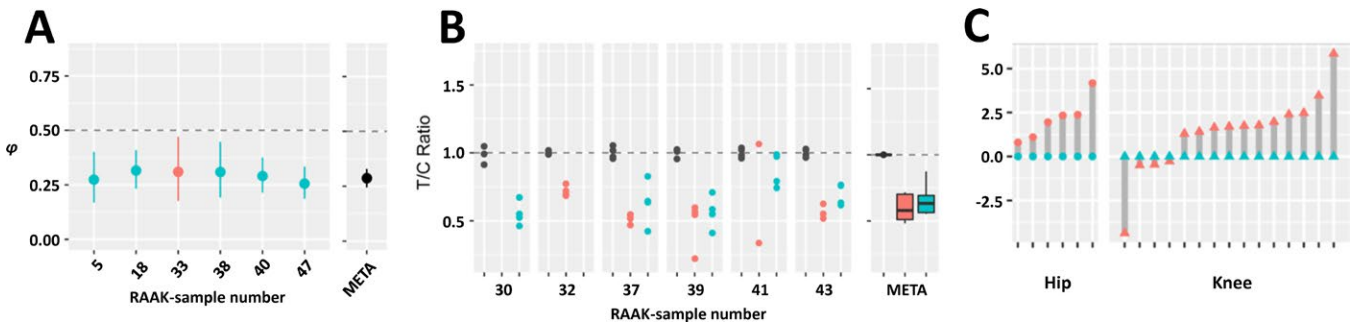

Figure 2. *CRLF1* expression is subject to allelic imbalance (AI) and is modulated in articular cartilage with osteoarthritis (OA)–induced destruction. **A,** AI of rs7256319 in RNA sequencing data set, reported as the average fraction (φ) of the alternative allele reads among the total number of reads with 95% confidence interval, showing decreasing expression of *CRLF1* transcript of the alternative T allele in preserved and lesioned OA cartilage relative to the reference C allele (φ = 0.29, false discovery rate [FDR] = 4.02×10^{-21}). Preserved OA cartilage is depicted in blue, lesioned OA cartilage in red, and meta-φ (META) in black. **B**, Replication of AI expression with rs7256319 by TaqMan genotyping in 6 additional knee samples, confirming the observed lower expression of the alternative allele T relative to the reference allele C of rs7256319 (T:C ratio = 0.63). Preserved OA cartilage is depicted in blue, lesioned OA cartilage in red, and genomic DNA (used as the reference ratio) in black. The meta-φ of genomic DNA, lesioned cartilage complementary DNA (cDNA), and preserved cartilage cDNA is depicted in black, red, and blue, respectively. Data are shown as box plots. Each box represents the 25th to 75th percentiles. Lines inside the boxes represent the median. Lines outside the boxes represent the 10th and 90th percentiles. In **A** and **B**, horizontal dashed lines depict equal ratios of the *CRLF1* rs7256319 alleles. **C**, Differential expression analyses of *CRLF1* showing significantly up-regulated expression in lesioned (red) compared to paired preserved (blue) OA articular cartilage (fold change 4.6, FDR-corrected $P = 3.1 \times 10^{-10}$). RAAK = Research Arthritis and Articular Cartilage (study).

Of the 10,468 Ensembl gene identifiers with at least 5 counts per million, 137 and 86 were observed to be significantly (FDR <0.05) down-regulated (fold change <0.5) and up-regulated (fold change >2), respectively, in lesioned cartilage compared to preserved cartilage (see Supplementary Figure 1A and Supplementary Table 4, http://onlinelibrary.wiley.com/doi/10.1002/art.40748/abstract). As has been shown by microarray studies that have used a similar design, subsequent GO term enrichment analysis (see Supplementary Table 5, http://onlinelibrary.wiley.com/doi/10.1002/art.40748/abstract) revealed significant enrichment for inflammatory pathways (e.g., *SCUBE1*, *CFH*, and *CXCL14*) (see Supplementary Figures 1B–D, http://onlinelibrary.wiley.com/doi/10.1002/art.40748/abstract), pathways of response to wound healing (e.g., *NOTCH3*, *BMP5*, and *SERPINE1*) (see Supplementary Figures 1E–G), and joint development–associated pathways (e.g., *SPP1*, *MMP3*, and *COL9A1*) (see Supplementary Figures 1H–J).

Of the 223 differentially expressed genes, 49 were additionally subject to AI, marked by 128 SNPs (see Supplementary Table 6, http://onlinelibrary.wiley.com/doi/10.1002/art.40748/abstract). A notable example was the *CRLF1* gene, which was subject to highly consistent AI, with the T allele of rs7256319 marking consistently lower expression of *CRLF1* compared to the reference allele C (φ = 0.29, FDR = 4.02×10^{-21}) (Figure 2A). Moreover, as shown in Figure 2B, the AI of *CRLF1* was confirmed by custom TaqMan assay performed in 5 preserved and 5 lesioned articular cartilage samples, originating from 6 independent patients who underwent total knee replacement surgery. In parallel, expression of *CRLF1* in the current data set differed significantly between preserved and OA-lesioned cartilage, with significant up-regulation in OA-affected cartilage (fold change 4.6, FDR = 3.1×10^{-10}) (Figure 2C).

Cartilage AI SNPs that contribute to OA susceptibility. On the basis of the significant AI SNPs in articular cartilage (see Supplementary Table 3, http://onlinelibrary.wiley.com/doi/10.1002/art.40748/abstract), it is to be expected that these SNPs are enriched for those conferring genetic susceptibility to OA. Hence, for 173 AI SNPs with FDR $<5 \times 10^{-8}$, not previously reported as OA risk genes, we went to the genome-wide association catalogs of OA to look for their genetic association signal. We used the GWAS meta-analysis for hip OA performed under the auspices of the Translational Research in Europe Applied Technologies in Osteoarthritis (TreatOA) consortium (32) and the GWAS meta-analysis on cartilage thickness (measured by the OA endophenotype minimal joint space width [JSW]) (8). Given that the entire genome was not being assessed for genetic association, a nominal genetic association ($P < 0.05$) was considered. Moreover, we only checked for genetic association when the AI SNP could be used directly or when a clear proxy SNP was identified.

As shown in Table 2, we observed multiple AI SNPs conferring susceptibility to hip OA and/or minimal JSW. Notable examples in Table 2 are the AI SNP rs3133187 in the *RPS3* gene conferring the most significant susceptibility to hip OA (Figure 3A) and the AI SNP rs1052429 in the *WWP2* gene associated with minimal JSW (Figure 3B). Alternatively, in Supplementary Tables 7 and 8 (http://onlinelibrary.wiley.com/doi/10.1002/art.40748/abstract), we show the intersection of the 65 AI SNPs significantly associated with hip

Table 2. Intersection of highly significant allelic imbalance SNPs with published genome-wide association data sets of minimal JSW and hip OA*

Allelic imbalance						Genome-wide association											
								Minimal JSW					Hip OA				
SNP	Positional gene	AA	AAF	Meta-φ	FDR	SNP	R^2	EA	EAF	Beta	SEM	*P*	EA	EAF	Beta	SEM	*P*
rs4744	*PLA2G2A*	A	0.11	0.46	8.1×10^{-134}	rs11677	1.0	A	0.11	−0.05	0.02	0.0091	A	0.12	0.00	0.04	0.9360
rs4605	*FMOD*	C	0.70	0.49	0.000	rs4605	NA	C	0.52	−0.03	0.01	0.0679	C	0.46	−0.09	0.03	0.0057
rs3190	*PPP1CB*	G	0.56	0.59	6.3×10^{-10}	rs3190	NA	G	0.57	0.03	0.01	0.0076	G	0.57	−0.00	0.02	0.8820
rs1054629	*IBSP*	T	0.18	0.41	1.0×10^{-24}	rs13144371	1.0	A	0.24	0.03	0.01	0.0340	A	0.24	−0.05	0.03	0.0801
rs6546	*C1QTNF3*	G	0.30	0.39	4.8×10^{-13}	rs840385	0.88	C	0.40	−0.03	0.01	0.0168	C	0.39	−0.03	0.03	0.2361
rs3549	*SPARC*	C	0.39	0.45	1.1×10^{-58}	rs1059829	1.0	A	0.53	0.03	0.01	0.0284	A	0.53	−0.02	0.02	0.3896
rs3829078	*CA9*	G	0.05	0.59	2.5×10^{-14}	rs3829078	NA	G	0.11	0.04	0.02	0.0495	G	0.11	−0.04	0.04	0.2710
rs13321	*TNC*	G	0.67	0.53	2.4×10^{-16}	rs12347433	0.1	T	0.72	−0.02	0.01	0.1487	T	0.72	0.06	0.03	0.0256
rs1871452	*CHST3*	A	0.60	0.42	5.4×10^{-25}	rs731027	1.0	T	0.52	0.01	0.01	0.3073	T	0.50	−0.06	0.02	0.0087
rs3133187	*RPS3*	G	0.12	0.42	5.0×10^{-9}	rs3133187	NA	G	0.06	−0.04	0.03	0.1420	G	0.06	0.18	0.05	0.0011
rs1800801	*MGP*	T	0.74	0.41	2.6×10^{-26}	rs4236	0.9	T	0.61	−0.03	0.01	0.0433	T	0.60	0.03	0.03	0.2068
rs3737548	*COL2A1*	T	0.23	0.53	5.1×10^{-72}	rs1635553	0.4	G	0.46	−0.02	0.01	0.2290	G	0.46	−0.06	0.03	0.0161
rs6647	*SERPINA1*	G	0.75	0.41	7.2×10^{-283}	rs6647	NA	G	0.77	−0.03	0.01	0.0848	A	0.76	0.06	0.03	0.0388
rs1052429	*WWP2*	A	0.86	0.56	3.4×10^{-55}	rs1566452	0.9	A	0.73	−0.04	0.01	0.0028	A	0.71	−0.05	0.03	0.0656
rs2646108	*CRISPLD2*	A	0.18	0.63	2.6×10^{-9}	rs2646108	NA	A	0.20	−0.01	0.02	0.7410	A	0.19	0.09	0.03	0.0053
rs6554	*UBA52*	T	0.70	0.43	1.1×10^{-53}	rs6554	NA	T	0.60	0.00	0.01	0.9300	T	0.61	0.05	0.03	0.0416
rs7499	*COL18A1*	A	0.47	0.63	2.0×10^{-11}	rs7499	NA	A	0.40	−0.01	0.01	0.3528	A	0.40	−0.05	0.03	0.0332
rs3088026	*COL6A2*	T	0.07	0.53	5.5×10^{-3}	rs3088026	NA	T	0.09	−0.02	0.02	0.4125	T	0.09	−0.12	0.04	0.0055

* SNPs = single-nucleotide polymorphisms; JSW = joint space width; OA = osteoarthritis; AA = alternative allele; AAF = alternative allele frequency; φ = count fraction of the alternative allele reads among the total number of reads; FDR = false discovery rate relative to median φ = 0.49 as reference; R^2 = measure of linkage disequilibrium of proxy SNP with allelic imbalance SNP; EA = effect allele; EAF = effect allele frequency; NA = not applicable.

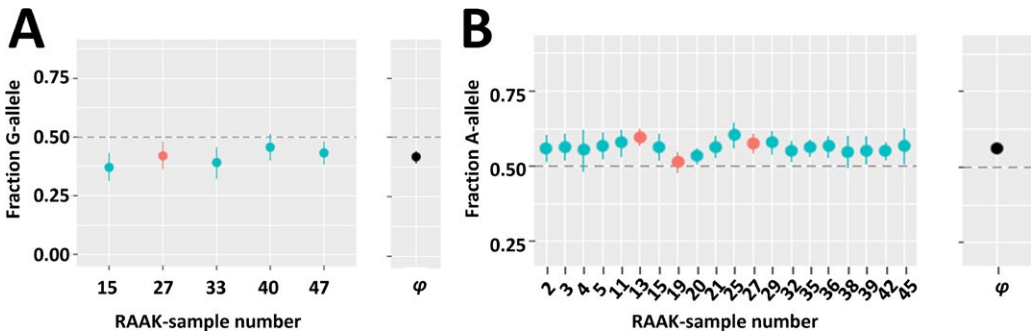

Figure 3. Compelling cartilage-specific allelic imbalance (AI) genes. AI is reported as the average fraction (φ) of the alternative allele reads among the total number of reads with 95% confidence interval. **A**, Significant ($P = 4.97 \times 10^{-9}$) allelic imbalanced expression at rs3133187 with the G allele decreasing expression of *RPS3* transcript in preserved and lesioned osteoarthritic (OA) cartilage relative to the A allele (meta-φ = 0.42). The G allele of rs3133187 additionally confers significant association with hip OA ($P = 1.1 \times 10^{-3}$). **B**, Significant ($P = 3.37 \times 10^{-55}$) allelic imbalanced expression at rs1052429 with the A allele increasing expression of *WWP2* transcript in preserved and lesioned OA cartilage relative to the G allele (meta-φ = 0.56). The A allele of rs1052429, linked to the A allele of rs1566452 ($r^2 = 0.92$, $D' = 1.0$), additionally confers significant association with reduced minimal joint space width ($P = 2.8 \times 10^{-3}$), resulting in cartilage degeneration or OA. Horizontal dashed lines depict equal ratios of alleles. RAAK = Research Arthritis and Articular Cartilage (study).

OA in the TreatOA GWAS meta-analysis (FDR <0.05) and the 63 AI SNPs significantly associated with minimal JSW in the GWAS meta-analysis on cartilage thickness ($P < 0.05$). Among these lists we find SNPs in compelling known (*MGP*, *ALDH1A2*, *FRZB*, *COL11A1*, *PLEC*) and potentially novel (*ACAN*, *MATN*, *TNC*, *VEGFA*, *PLOD2*) OA risk genes.

Cartilage AI SNPs that contribute to expression quantitative trait loci (eQTLs). To provide additional supporting data on the AI findings in the putative OA risk SNPs in Table 2, we combined the RNA sequencing data of the genes with genome-wide SNP data (Illumina HumanOmniExpressExome) of RAAK study samples to extract gene-targeted cartilage eQTLs on the basis of 50 samples that were overlapping. Additionally, we explored eQTL data of the Genotype-Tissue Expression (GTEx) Project. The fact that GTEx data are merely from tissues other than those particularly relevant to OA indicates the generalizability of the identified AI to other tissues. As shown in Supplementary Table 9 (http://onlinelibrary.wiley.com/doi/10.1002/art.40748/abstract), the GTEx eQTL data largely support (the direction of) the identified AI effects also in other tissues.

OA susceptibility SNPs that show AI in cartilage. Since identified OA risk SNPs have been demonstrated to frequently confer risk by modifying expression of positional genes *in-cis*, the aforementioned genome-wide AI data set of articular cartilage (see Supplementary Table 3, http://onlinelibrary.wiley.com/doi/10.1002/art.40748/abstract) can function as a database to assess in silico the direction of effect of such identified susceptibility SNPs. Hence, we reviewed the literature to intersect the list of currently published robust genetic OA association signals with the identified AI SNPs. We included robustly identified susceptibility SNPs and their positional genes associated with knee, hand, and hip OA as well as OA-associated phenotypes such as minimal JSW and markers of cartilage turnover (soluble cartilage oligomeric matrix protein). Of the 46 genes linked to the reported OA risk SNPs, 36 genes were detected in our data set (i.e., had detectable expression levels in cartilage) and were heterozygous carriers of a coding SNP. As shown in Supplementary Table 10 (http://onlinelibrary.wiley.com/doi/10.1002/art.40748/abstract), we found 11 previously identified OA risk genes to contain SNPs that mark AI in articular cartilage. Of these, the respective risk alleles marked lower expression through AI in heterozygotes of *FRZB* (rs7775), *COL11A1* (rs2615977 and rs1676486), *IGFBP3* (rs788748 through double heterozygotes with rs6670), *ALDH1A2* (rs3204689), and *MGP* (rs4764133 in LD with rs1800801). For *SMAD3*, *CDCL5*, *COL12A1*, *BCAP29*, *PIK3R1*, and *COMP*, AI was detected but not in relation to the reported risk alleles.

To provide additional functional data to these previously identified OA risk genes, level and differential expression data between preserved and lesioned OA articular cartilage are depicted in Supplementary Table 11 (http://onlinelibrary.wiley.com/doi/10.1002/art.40748/abstract). For *IGFBP3*, *PIK3R1*, *BCAP29*, *COL12A1*, *FRZB*, *ALDH1A2*, and *MGP,* significant differential expression (FDR <0.05) was observed in addition to AI. Finally, to find supporting data on the AI findings in the OA risk SNPs, we combined the RNA sequencing data of the OA risk genes with genome-wide association data (Illumina HumanOmniExpressExome) of RAAK study samples to extract gene-targeted eQTL data on the basis of 50 cartilage samples that were overlapping. Additionally, to the eQTL data in Supplementary Table 11, we added data from the GTEx Project, although from tissues other than those particularly relevant to OA. For the OA genes *GNL3*, *FTO*, *NCOA3*, *MICAL3*, *IFRD1*, *IGFBP3*, *TGFA*, and *MGP*, we found significant eQTL effects ($P < 0.05$) of risk SNPs that substantiated the respective AI effects.

DISCUSSION

Our approach in the current study comprises a concept framework for complex traits to identify disease-relevant genetic variation, as reflected by allele-associated transcription levels in cartilage, a pivotal tissue in the disease. We have aimed to present the reported observations as a legacy data set for researchers in the field to probe for their gene or SNP of interest. Herein, we highlight notable examples. Among our (highly) significant AI SNPs we confirmed well-known genes that have previously been reported by others to confer robust risk of OA (e.g., *MGP*, *ALDH1A2*, *IGFBP3*, and *FRZB*) (17,33,34). We hypothesize that among our (highly) significant AI SNPs and particularly those that show additional, differential expression between preserved and lesioned OA cartilage (e.g., *CRLF1* [Figure 2; also see Supplementary Table 6, http://onlinelibrary.wiley.com/doi/10.1002/art.40748/abstract]) or genetic association with OA phenotypes (e.g., *WWP2* and *RPS3* [Figure 3 and Table 2; also see Supplementary Tables 7 and 8, http://onlinelibrary.wiley.com/doi/10.1002/art.40748/abstract]) are putative novel compelling OA risk genes.

The *CRLF1* gene, encoding for cytokine receptor–like factor 1 protein, harbors the rs7256319 C>T SNP that has marked imbalanced expression of its respective alleles in articular cartilage, reflected by consistent lower expression of the alternative allele T in comparison with the reference allele C among heterozygotes. As was also reported previously (25,35), *CRLF1* appeared to be significantly up-regulated in lesioned compared to preserved OA articular cartilage (fold change 4.6, FDR = 3.1×10^{-10}), as was its signaling partner *CLCF1* (fold change 2.1, FDR = 1.0×10^{-6}), while the protein complex signaling receptor gene *CNTFR* was significantly down-regulated (fold change 0.3, FDR = 1.9×10^{-8}) (see Supplementary Table 3, http://onlinelibrary.wiley.com/doi/10.1002/art.40748/abstract). Additionally, it was shown by Tsuritani et al (35) that up-regulation of the cytokine receptor–like factor 1/cardiotrophin-like cytokine complex in ATDC5 cells disrupts cartilage homeostasis and promotes progression of OA by enhancing the proliferation of chondrocytes and suppressing the production of cartilage matrix. As such, we hypothesize that the alternative allele T of rs7256319 in heterozygote carriers may be able to mitigate *CRLF1*/*CLCF1* signaling toward ongoing cartilage degradation due to primary OA.

Among the notable novel putative OA genes in Table 2 is *WWP2*, which showed (in addition to multiple coding SNPs marking consistent AI expression of *WWP2* in cartilage) significant differential expression between preserved and lesioned OA cartilage (fold change 0.78, FDR = 0.0053; results not shown) and a signal of genetic association with minimal JSW ($P = 0.0028$) (Figure 3). Based on these data, we hypothesize that allele rs1052429 A located in *WWP2* is an OA susceptibility allele that acts via higher expression of *WWP2* in cartilage, which is associated with lower minimal JSW and thus with degeneration of cartilage. In addition, expression of *WWP2* was previously shown to be consistently modified by methylation at CpG sites (36). The WWP2 protein is a member of the Nedd4 family of E3 ligases, which play an important role in protein ubiquitination (37). Moreover, the encoded protein was shown to physically interact with SOX9, thereby affecting the transcriptional activity of SOX9 via translocation to the nucleus (38).

Similarly, *RPS3*, encoding ribosomal protein S3, is subject to significant AI marked by rs3133187 with the G allele decreasing expression of *RPS3* transcript in cartilage (FDR = 4.97×10^{-9}) and significant association with hip OA ($P = 1.1 \times 10^{-3}$). Ribosomal protein S3 is a multifunctional DNA repair endonuclease and ribosomal protein, yet its role in inducing apoptosis through activation of *CASP8/CASP3* may be relevant to mention with respect to OA (39). It was recently shown by Jeon et al (40) that selective removal of senescent cells may attenuate the development of OA. We hypothesize that decreasing *RPS3* expression by the OA risk allele G of rs3133187 negatively affects removal of senescent chondrocytes by cytokine-induced apoptosis. Nonetheless, functional studies are necessary to verify the exact mechanism by which the AI in *CRLF1*, *WWP2*, and *RPS3* contributes to cartilage degeneration in humans. It would be preferable to investigate this using human in vitro micromass cultures in which the expression of the genes (e.g., by lentiviral induction) is modified in the direction of the risk alleles as previously found with, for example, *GDF5* (15) or *DIO2* (14).

Our RNA sequencing data set consisted of both preserved and lesioned OA samples, as well as knee and hip cartilage. Due to our focus on significant AI effects across our samples, we have ignored possible variation in the AI effects between preserved and lesioned OA cartilage or between knee and hip joints. Such variation could arise, e.g., due to local expression of transcription factors that exaggerate or attenuate the observed AI. By providing AI, defined by φ across all individuals heterozygous for any of the 13,435 SNPs (see Supplementary Table 2, http://onlinelibrary.wiley.com/doi/10.1002/art.40748/abstract), possible differences in AI for preserved/OA or hip/knee cartilage may be explored. It should be mentioned, however, that the current sample size and the variable number of heterozygous individuals likely precludes a robust statement on either analyses and will require additional targeted AI measurements by, for example, TaqMan assay.

By combining reported genetic OA signals with AI SNPs that alter transcription of articular cartilage genes *in-cis*, we also had the opportunity to address functionality of OA risk alleles. For example, the A allele of rs788748, located upstream of *IGFBP3*, is associated with lower odds of hip OA (41). Given that this SNP is not located in an exon, we assessed its potential revelance to AI through rs6670 double heterozygotes, which revealed that the protective rs788748 A allele marks lower expression of *IGFBP3* compared to the G allele. In addition, significant up-regulation of the gene was observed in OA-affected cartilage compared to paired preserved cartilage, as well as a similar eQTL effect of the rs788748 SNP (see Supplementary Table 9, http://onlinelibrary.

wiley.com/doi/10.1002/art.40748/abstract), similar to what has been reported by others (8). These observations solidify the notion of *IGFBP3*'s role in OA, and we propose that the reported protective effect of the rs788748 A allele is mediated through lower expression of the transcript.

For a selected number of comparable (although gene-targeted) studies, we discuss the respective confirmations and/or discrepancies. A number of SNPs are known to mark AI in articular cartilage, as has been shown by gene-targeted approaches. We were able to replicate the earlier observed AI of *ALDH1A2* (18) and *MGP* (20) and to a lesser extent that of *DIO2* (14) and *GDF5* (42). Furthermore, for rs11177 (*GNL3*) (16) and rs6617 (*SPCS1*) (16) in our data set, AI was not as obvious as previously reported, and we did not observe heterozygotes for rs143383 (*GDF5*) (23) or rs3815148 (*HBP1*) (24).

For *COL11A1*, AI was previously thoroughly investigated by Raine et al (17) in view of the OA risk SNP rs2615977 (7) and the lumbar disc herniation SNP rs1676486 (43). They showed that considerable AI of *COL11A1* was correlated with the lumbar disc herniation risk allele of SNP rs1676486, while the observed AI of *COL11A1* was not correlated with the OA risk allele of SNP rs2615977. The latter result was based on the AI effect observed in individuals double heterozygous for rs2615977 and rs9659030. As shown in Supplementary Figure 2 and Supplementary Table 8 (http://onlinelibrary.wiley.com/doi/10.1002/art.40748/abstract), we observed 2 independent *COL11A1* SNPs ($D' = 0.2$, $r^2 = 0.01$) (44) with highly significant meta-φ AI. The first was the abovementioned SNP rs9659030 with meta-φ AI of 0.65 ($P = 1.2 \times 10^{-25}$) and the second was SNP rs2229783 with meta-φ AI of 0.53 ($P = 3.7 \times 10^{-8}$). Notably, and in contrast to the results obtained by Raine et al (17), the extent and consistency of AI for rs9659030 were considerably higher than those for rs2229783 and rs1676486. The suggestive evidence of AI of the lumbar disc herniation risk allele of SNP rs1676486 as well as the AI of its proxy SNP rs2229783 ($D' = 1$, $r^2 = 0.3$) confirm that the lumbar disc herniation risk allele is likely associated with lower *COL11A1* expression. Moreover, the AI of the noncoding OA risk SNP rs2615977, which is not in strong LD with a coding SNP, remains unclear. Yet, based on the proxy SNP rs1031820 ($D' = 0.77$, $r^2 = 0.16$), it may be that the OA risk allele of rs2615977 also acts via lower expression of *COL11A1*.

Taken together, these confirmations and/or discrepancies indicate first and foremost that additional replication to verify AI is required to increase confidence in the observed AI (e.g., by better preselection on heterozygous samples). Second, it stresses the fact that observed AI reflects regulatory properties of the respective LD block and does not per se identify genetic variation that affects respective gene expression levels mechanistically. Furthermore, despite the applied filtering steps and statistics, the list of significant AI SNPs potentially contains a number of false positives, some of which could have originated from alignment bias. While future novel alignment and other bioinformatic approaches (45) might address these issues from a more fundamental perspective, in the present study we have aimed to reduce false-positive AI SNPs by including multiple filtering steps ($0.1<\varphi<0.9$, include SNPs with at least 2 heterozygotes, and null hypothesis adjustment).

While in canonical GWAS a strict genome-wide significance level of 5×10^{-8} is imposed due to the vast amount of SNPs that are tested for, we postulate that providing SNPs that are more likely to affect expression of genes *in-cis* in a disease-relevant tissue could aid the search for the functional susceptibility SNPs and the putative OA risk gene. Nevertheless, among the significant AI SNPs, we did not necessarily obtain a clear enrichment of putative significant OA risk SNPs; among the SNPs for which we had both AI and GWAS data, 6.7% showed significant association with the OA phenotypes, while among the significant AI genes (FDR <0.05), 7.2% showed significant association with the OA phenotypes. Further downstream selection criteria, such as (but not limited to) significant differential expression between preserved and OA-lesioned cartilage and/or trans-eQTL analysis, will help tailor genetic association analyses even more and might attribute SNPs to specific disease facets, such as extent of cartilage degradation, as we have shown in the present study. Of note, inherent to our study design, we might have missed genes that affect joint morphology or cartilage integrity during development and/or that change expression in healthy cartilage or during early-stage OA.

In summary, we present a framework and resulting data set for researchers in the OA research field to probe for disease-relevant genetic variation that affects gene expression in pivotal disease-affected tissue. This likely includes putative novel compelling OA risk genes such as *CRLF1*, *WWP2*, and *RPS3*.

ACKNOWLEDGMENTS

We thank all RAAK study participants. We thank Eka Suchiman for her help in preparing DNA and RNA samples and collection of RAAK study specimens.

AUTHOR CONTRIBUTIONS

All authors were involved in drafting the article or revising it critically for important intellectual content, and all authors approved the final version to be published. Dr. Meulenbelt had full access to all of the data in the study and takes responsibility for the integrity of the data and the accuracy of the data analysis.

Study conception and design. Den Hollander, Couthino de Almeida, Lakenberg, 't Hoen, Ramos, Meulenbelt.

Acquisition of data. Den Hollander, Bomer, Nelissen, Ramos, Meulenbelt.

Analysis and interpretation of data. Den Hollander, Pulyakhina, Boer, van der Breggen, Arindrarto, Couthino de Almeida, Sentner, Laros, 't Hoen, Slagboom, van Meurs, Ramos, Meulenbelt.

REFERENCES

1. Loeser RF, Goldring SR, Scanzello CR, Goldring MB. Osteoarthritis: a disease of the joint as an organ. Arthritis Rheum 2012;64:1697–707.
2. Man GS, Mologhianu G. Osteoarthritis pathogenesis—a complex process that involves the entire joint. J Med Life 2014;7:37–41.
3. Saito T, Fukai AF, Mabuchi AF, Ikeda TF, Yano FF, Ohba S, et al. Transcriptional regulation of endochondral ossification by HIF-2α during skeletal growth and osteoarthritis development. Nat Med 2010;16:678–86.
4. Sherwood J, Bertrand J, Nalesso G, Poulet B, Pitsillides A, Brandolini L, et al. A homeostatic function of CXCR2 signalling in articular cartilage. Ann Rheum Dis 2015;74:2207–15.
5. Van der Kraan PM, Blaney Davidson EN, van den Berg WB. A role for age-related changes in TGFβ signaling in aberrant chondrocyte differentiation and osteoarthritis. Arthritis Res Ther 2010;12:201.
6. Jeffries MA, Donica M, Baker LW, Stevenson ME, Annan AC, Humphrey MB, et al. Genome-wide DNA methylation study identifies significant epigenomic changes in osteoarthritic cartilage. Arthritis Rheumatol 2014;66:2804–15.
7. Zeggini E, Panoutsopoulou K, Southam L, Rayner NW, Day-Williams AG, Lopes MC, et al. Identification of new susceptibility loci for osteoarthritis (arcOGEN): a genome-wide association study. Lancet 2012;380:815–23.
8. Castano-Betancourt MC, Evans DS, Ramos YF, Boer CG, Metrustry S, Liu Y, et al. Novel genetic variants for cartilage thickness and hip osteoarthritis. PLoS Genet 2016;12:e1006260.
9. Meulenbelt I, Min JL, Bos S, Riyazi N, Houwing-Duistermaat JJ, van der Wijk HJ, et al. Identification of DIO2 as a new susceptibility locus for symptomatic osteoarthritis. Hum Mol Genet 2008;17:1867–75.
10. Xu Y, Barter MJ, Swan DC, Rankin KS, Rowan AD, Santibanez-Koref M, et al. Identification of the pathogenic pathways in osteoarthritic hip cartilage: commonality and discord between hip and knee OA. Osteoarthritis Cartilage 2012;20:1029–38.
11. Den Hollander W, Ramos YF, Bomer N, Elzinga S, van der Breggen R, Lakenberg N, et al. Transcriptional associations of osteoarthritis-mediated loss of epigenetic control in articular cartilage. Arthritis Rheumatol 2015;67:2108–16.
12. Ramos YF, Metrustry S, Arden N, Bay-Jensen AC, Beekman M, de Craen AJ, et al. Meta-analysis identifies loci affecting levels of the potential osteoarthritis biomarkers sCOMP and uCTX-II with genome wide significance. J Med Genet 2014;51:596–604.
13. Zhang L, Yang M, Marks P, White LM, Hurtig M, Mi QS, et al. Serum non-coding RNAs as biomarkers for osteoarthritis progression after ACL injury. Osteoarthritis Cartilage 2012;20:1631–7.
14. Bos SD, Bovee JV, Duijnisveld BJ, Raine EV, van Dalen WJ, Ramos YF, et al. Increased type II deiodinase protein in OA-affected cartilage and allelic imbalance of OA risk polymorphism rs225014 at DIO2 in human OA joint tissues. Ann Rheum Dis 2012;71:1254–8.
15. Reynard LN, Bui C, Canty-Laird EG, Young DA, Loughlin J. Expression of the osteoarthritis-associated gene GDF5 is modulated epigenetically by DNA methylation. Hum Mol Genet 2011;20:3450–60.
16. Gee F, Clubbs CF, Raine EV, Reynard LN, Loughlin J. Allelic expression analysis of the osteoarthritis susceptibility locus that maps to chromosome 3p21 reveals cis-acting eQTLs at GNL3 and SPCS1. BMC Med Genet 2014;15:53.
17. Raine EV, Dodd AW, Reynard LN, Loughlin J. Allelic expression analysis of the osteoarthritis susceptibility gene COL11A1 in human joint tissues. BMC Musculoskelet Disord 2013;14:85.
18. Styrkarsdottir U, Thorleifsson G, Helgadottir HT, Bomer N, Metrustry S, Bierma-Zeinstra S, et al. Severe osteoarthritis of the hand associates with common variants within the ALDH1A2 gene and with rare variants at 1p31. Nat Genet 2014;46:498–502.
19. Bomer N, den Hollander W, Ramos YF, Bos SD, van der Breggen R, Lakenberg N, et al. Underlying molecular mechanisms of DIO2 susceptibility in symptomatic osteoarthritis. Ann Rheum Dis 2015;74:1571–9.
20. Den Hollander W, Boer CG, Hart DJ, Yau MS, Ramos YF, Metrustry S, et al. Genome-wide association and functional studies identify a role for matrix Gla protein in osteoarthritis of the hand. Ann Rheum Dis 2017;76:2046–53.
21. Loughlin J. Osteoarthritis: all types of trouble–defining OA in the genomic era. Nat Rev Rheumatol 2011;7:200–1.
22. Panoutsopoulou K, Thiagarajah S, Zengini E, Day-Williams AG, Ramos YF, Meessen JM, et al. Radiographic endophenotyping in hip osteoarthritis improves the precision of genetic association analysis. Ann Rheum Dis 2017;76:1199–1206.
23. Southam L, Rodriguez-Lopez J, Wilkins JM, Pombo-Suarez M, Snelling S, Gomez-Reino JJ, et al. An SNP in the 5′-UTR of GDF5 is associated with osteoarthritis susceptibility in Europeans and with in vivo differences in allelic expression in articular cartilage. Hum Mol Genet 2007;16:2226–32.
24. Raine EV, Wreglesworth N, Dodd AW, Reynard LN, Loughlin J. Gene expression analysis reveals HBP1 as a key target for the osteoarthritis susceptibility locus that maps to chromosome 7q22. Ann Rheum Dis 2012;71:2020–7.
25. Ramos YF, den HW, Bovee JV, Bomer N, van der Breggen R, Lakenberg N, et al. Genes involved in the osteoarthritis process identified through genome wide expression analysis in articular cartilage: the RAAK study. PLoS One 2014;9:e103056.
26. Goya R, Sun MG, Morin RD, Leung G, Ha G, Wiegand KC, et al. SNVMix: predicting single nucleotide variants from next-generation sequencing of tumors. Bioinformatics 2010;26:730–6.
27. Robinson MD, McCarthy DJ, Smyth GK. EdgeR: a Bioconductor package for differential expression analysis of digital gene expression data. Bioinformatics 2010;26:139–40.
28. Huang DW, Sherman BT, Lempicki RA. Systematic and integrative analysis of large gene lists using DAVID bioinformatics resources. Nat Protoc 2009;4:44–57.
29. Schoenmaker M, de Craen AJ, de Meijer PH, Beekman M, Blauw GJ, Slagboom PE, et al. Evidence of genetic enrichment for exceptional survival using a family approach: the Leiden Longevity Study. Eur J Hum Genet 2006;14:79–84.
30. Wood AR, Esko T, Yang J, Vedantam S, Pers TH, Gustafsson S, et al. Defining the role of common variation in the genomic and biological architecture of adult human height. Nat Genet 2014;46:1173–86.
31. Wilkins JM, Southam L, Price AJ, Mustafa Z, Carr A, Loughlin J. Extreme context-specificity in differential allelic expression. Hum Mol Genet 2007;16:537–46.
32. Evangelou E, Kerkhof HJ, Styrkarsdottir U, Ntzani EE, Bos SD, Esko T, et al. A meta-analysis of genome-wide association studies identifies novel variants associated with osteoarthritis of the hip. Ann Rheum Dis 2014;73:2130–6.
33. Raine EV, Reynard LN, van de Laar IM, Bertoli-Avella AM, Loughlin J. Identification and analysis of a SMAD3 cis-acting eQTL operating in primary osteoarthritis and in the aneurysms and osteoarthritis syndrome. Osteoarthritis Cartilage 2014;22:698–705.
34. Gee F, Rushton MD, Loughlin J, Reynard LN. Correlation of the osteoarthritis susceptibility variants that map to chromosome 20q13 with an expression quantitative trait locus operating on NCOA3 and with functional variation at the polymorphism rs116855380. Arthritis Rheumatol 2015;67:2923–32.
35. Tsuritani K, Takeda J, Sakagami J, Ishii A, Eriksson T, Hara T, et al. Cytokine receptor-like factor 1 is highly expressed in damaged

human knee osteoarthritic cartilage and involved in osteoarthritis downstream of TGF-β. Calcif Tissue Int 2010;86:47–57.

36. Reynard LN. Analysis of genetics and DNA methylation in osteoarthritis: what have we learnt about the disease? Semin Cell Dev Biol 2017;62:57–66.
37. Chen W, Jiang X, Luo Z. WWP2: a multifunctional ubiquitin ligase gene. Pathol Oncol Res 2014;20:799–803.
38. Nakamura Y, Yamamoto K, He X, Otsuki B, Kim Y, Murao H, et al. WWP2 is essential for palatogenesis mediated by the interaction between Sox9 and mediator subunit 25. Nat Commun 2011;2:251.
39. Jang CY, Lee JY, Kim J. RpS3, a DNA repair endonuclease and ribosomal protein, is involved in apoptosis. FEBS Lett 2004;560: 81–5.
40. Jeon OH, David N, Campisi J, Elisseeff JH. Senescent cells and osteoarthritis: a painful connection. J Clin Invest 2018;128:1229–37.
41. Evans DS, Cailotto F, Parimi N, Valdes AM, Castano-Betancourt MC, Liu Y, et al. Genome-wide association and functional studies identify a role for IGFBP3 in hip osteoarthritis. Ann Rheum Dis 2015;74:1861–7.
42. Egli RJ, Southam L, Wilkins JM, Lorenzen I, Pombo-Suarez M, Gonzalez A, et al. Functional analysis of the osteoarthritis susceptibility-associated GDF5 regulatory polymorphism. Arthritis Rheum 2009;60:2055–64.
43. Mio F, Chiba K, Hirose Y, Kawaguchi Y, Mikami Y, Oya T, et al. A functional polymorphism in COL11A1, which encodes the α1 chain of type XI collagen, is associated with susceptibility to lumbar disc herniation. Am J Hum Genet 2007;81:1271–7.
44. Machiela MJ, Chanock SJ. LDassoc: an online tool for interactively exploring genome-wide association study results and prioritizing variants for functional investigation. Bioinformatics 2018;34: 887–9.
45. Castel SE, Levy-Moonshine A, Mohammadi P, Banks E, Lappalainen T. Tools and best practices for data processing in allelic expression analysis. Genome Biol 2015;16:195.

Arthritis & Rheumatology
Vol. 71, No. 4, April 2019, pp 571–582
DOI 10.1002/art.40765

AMERICAN COLLEGE OF RHEUMATOLOGY
EDUCATION • TREATMENT • RESEARCH

Targeted Inhibition of Aggrecanases Prevents Articular Cartilage Degradation and Augments Bone Mass in the STR/Ort Mouse Model of Spontaneous Osteoarthritis

Ioannis Kanakis,[1] Ke Liu,[1] Blandine Poulet,[1] Behzad Javaheri,[2] Rob J. van 't Hof,[1] Andrew A. Pitsillides,[2] and George Bou-Gharios[1]

Objective. Cartilage destruction in osteoarthritis (OA) is mediated mainly by matrix metalloproteinases (MMPs) and ADAMTS. The therapeutic candidature of targeting aggrecanases has not yet been defined in joints in which spontaneous OA arises from genetic susceptibility, as in the case of the STR/Ort mouse, without a traumatic or load-induced etiology. In addition, we do not know the long-term effect of aggrecanase inhibition on bone. We undertook this study to assess the potential aggrecanase selectivity of a variant of tissue inhibitor of metalloproteinases 3 (TIMP-3), called [-1A]TIMP-3, on spontaneous OA development and bone formation in STR/Ort mice.

Methods. Using the background of STR/Ort mice, which develop spontaneous OA, we generated transgenic mice that overexpress [-1A]TIMP-3, either ubiquitously or conditionally in chondrocytes. [-1A]TIMP-3 has an extra alanine at the N-terminus that selectively inhibits ADAMTS but not MMPs. We analyzed a range of OA-related measures in all mice at age 40 weeks.

Results. Mice expressing high levels of [-1A]TIMP-3 were protected against development of OA, while those expressing low levels were not. Interestingly, we also found that high levels of [-1A]TIMP-3 transgene overexpression resulted in increased bone mass, particularly in females. This regulation of bone mass was at least partly direct, as adult mouse primary osteoblasts infected with [-1A]TIMP-3 in vitro showed elevated rates of mineralization.

Conclusion. The results provide evidence that [-1A]TIMP-3–mediated inhibition of aggrecanases can protect against cartilage degradation in a naturally occurring mouse model of OA, and they highlight a novel role that aggrecanase inhibition may play in increased bone mass.

INTRODUCTION

Osteoarthritis (OA) is characterized by altered homeostasis of articular cartilage and abnormal bone formation. OA development depends on a balance of extracellular matrix (ECM) production and degradation. Proteolytic enzymes such as ADAMTS as well as matrix metalloproteinases (MMPs) are found to be up-regulated in OA joints (1–5) and are directly involved in OA pathophysiology (6,7). Therefore, inhibition of these metalloproteinases is a potential route for the design of pharmaceutical agents to retard, suppress, and even halt the progression of OA. However, broad-spectrum inhibitors of MMPs, which were shown to be chondroprotective in animal models, raised safety concerns in a clinical trial, pinpointing a need for inhibitors with greater specificity (8). In C57BL/6 mice, loss of activity of key catabolic enzymes, such as ADAMTS-5, protects against OA lesions (9–11) compared with deletion of ADAMTS-1 or ADAMTS-4, which suggests that ADAMTS-5 plays a central role in mouse models of inflammatory- and surgically induced OA (12,13). However, more recent data suggest that another aggrecanase, not yet determined, cleaves aggrecan before its secretion. Moreover, a noncatalytic function of ADAMTS-5 is suggested to have competitive interactions with major endocytic recycling machinery (14).

Investigators using STR/Ort mice as a model of human OA have proved that genetic susceptibility is a solid basis for assessing the protection afforded by novel treatment (15,16). Crucially, OA in STR/Ort mice closely resembles human OA and progresses to cartilage loss, along with similar alterations in bone mass and structure (17–20). Pertinently, it has been shown that the OA-related proteoglycan depletion observed predominantly across

Supported by Versus Arthritis (grants 20039 and 20581).

[1]Ioannis Kanakis, PhD, Ke Liu, PhD, Blandine Poulet, PhD, Rob J. van 't Hof, PhD, George Bou-Gharios, PhD: University of Liverpool, Liverpool, UK; [2]Behzad Javaheri, PhD, Andrew A. Pitsillides, PhD: Royal Veterinary College, London, UK.

No potential conflicts of interest relevant to this article were reported.

Address correspondence to George Bou-Gharios, PhD, Institute of Ageing and Chronic Disease, Faculty of Health & Life Sciences, William Henry Duncan Building, 6 West Derby Street, L7 8TX Liverpool, UK. E-mail: ggharios@liverpool.ac.uk.

Submitted for publication April 10, 2018; accepted in revised form October 25, 2018.

the medial tibial compartment in STR/Ort mouse joints also likely involves both collagenase and aggrecanase activities, as in humans (20,21). Interestingly, compared with C57BL/6 mice, female STR/Ort mice have high bone mass, with bone marrow compression and extramedullary hematopoiesis observed by age 36 weeks (22). Consistently, recent studies from our group showed that this difference is present even in young STR/Ort mice, which have increased cortical and trabecular parameters compared with age-matched CBA mice (23). These characteristics make the STR/Ort strain an intriguing and hitherto unexplored target in which to explore potentially protective transgenic strategies.

Tissue inhibitor of metalloproteinases 3 (TIMP-3) is a native biologic inhibitor of enzyme activity for members of the metzincin family, including collagenases (MMPs 1, 8, and 13), gelatinases (MMPs 2 and 9), and aggrecanases (ADAMTS-4 and ADAMTS-5). Extracellular trafficking of TIMP-3 is regulated by the competition between ECM binding and endocytosis via low-density lipoprotein receptor–related protein 1 (LRP-1) (24–26). It has previously been shown that modifications in TIMP-3 expression could modify joint degeneration (27) and that loss/gain of TIMP-3 function leads to significant alteration in bone structure (28,29). In the present study, we have used a variant of TIMP-3, named [-1A]TIMP-3, which harbors a single alanine addition to the amino-terminal end, which was shown to inhibit aggrecanases, namely ADAMTS-4/5, with much greater selectivity than other MMPs (30,31). This modified activity is driven by conformational changes, in which the active site is tilted and the interaction of Phe^{34} of the inhibitor with MMPs is lost (31).

Our aim was to assess the potential aggrecanase selectivity of [-1A]TIMP-3 on spontaneous OA development and bone formation in STR/Ort mice. We found that high levels of [-1A]TIMP-3 expression in transgenic STR/Ort mice can effectively attenuate cartilage destruction and OA-related subchondral thickening, but, strikingly, can also significantly augment bone mass.

MATERIALS AND METHODS

Generation of lentiviral and plasmid vectors to overexpress [-1A]TIMP-3. The lentivirus vector was constructed by cloning [-1A]TIMP-3 with a FLAG tag into the *Eco* RV–*Sal* I site of the pCCL-expressing vector driven by the elongation factor 1α (EF-1α) promoter. The construct also contained nerve growth factor receptor (NGFR) as a marker (Figure 1A).

We cotransfected 293T17 cells with transfer vector and packaging vectors by electroporation using a Neon transfection system (Invitrogen) to produce the virus. Viral supernatants were harvested 48 and 72 hours after transfection and concentrated by ultracentrifugation at 10,000*g* for 2 hours. The viral pellet was collected and dissolved in phosphate buffered saline (PBS).

A second conditional plasmid was generated using the Col2a1 3-kb promoter and the 3-kb first intron that drives specific expression in chondrocytes (32). The [-1A]TIMP-3 complementary DNA (cDNA) was followed by an internal ribosome entry site and a β-galactosidase reporter gene (Figure 1B).

Transient transduction was performed at 10 multiplicities of infection in 2 cell lines, HEK 293 and HTB94, to test integration efficacy and overexpression capacity. Flow cytometry with allophycocyanin-conjugated anti-NGFR was used to estimate transfection efficiency. Trichloroacetic acid (TCA) protein precipitation and Western blotting were used to test [-1A]TIMP-3 protein levels.

Animals. An STR/Ort mouse colony maintained at Royal Veterinary College, London was used to generate transgenic mice overexpressing [-1A]TIMP-3 on this background. Each fertilized embryo was injected with either Col2a1[-1A]TIMP-3 linearized plasmid in male pro nucleus or by infection using 100 lentiviral particles (EF-1α[-1A]TIMP-3) per embryo. The latter procedure was also used to generate transgenic mice in the control CBA strain (EF-1α[-1A]TIMP-3–transgenic CBA mice). Newborn transgenic mice were routinely genotyped by quantitative polymerase chain reaction (qPCR) using the reporter gene LacZ as well as the [-1A]TIMP-3 insert (see Supplementary Table 1, available on the *Arthritis & Rheumatology* web site at http://onlinelibrary.wiley.com/doi/10.1002/art.40765/abstract). All experimental protocols were performed in compliance with the UK Animals (Scientific Procedures) Act 1986 regulations.

We analyzed hind limb bones and knee joints isolated from STR/Ort mice at age 40 weeks. Age-matched nontransgenic (untreated) STR/Ort mice or transgenic CBA mice, a parental background strain of STR/Ort mice, were used as controls. The exact number of animals used in each analysis is described in Supplementary Table 2, http://onlinelibrary.wiley.com/doi/10.1002/art.40765/abstract.

Western blotting. Cultured media from transfected HEK 293 and HTB94 cells were precipitated with TCA, resuspended in PBS to equal total protein content, resolved by 10% sodium dodecyl sulfate–polyacrylamide gel electrophoresis under reducing conditions, and electrotransferred to Hybond P PVDF membranes (Amersham Biosciences). Membranes were blocked with 5% skim milk and probed overnight at 4°C with rabbit polyclonal anti–TIMP-3 antibody (1:2,000 dilution, AB6000; Millipore), followed by incubation with horseradish peroxidase (HRP)–labeled goat anti-rabbit antibody (1:10,000 dilution; Dako). Analysis was performed using an ECL Advanced Western Blotting Detection Kit (Amersham Biosciences). For Western blots using mouse tails, 250 mg of tissue was boiled at 95°C for 10 minutes in Laemmli buffer, and samples were electrophoresed in 4–12% Bis-Tris precast gels (NuPAGE) at 200V for 35 minutes. Proteins were transferred on PVDF membranes, blocked, and incubated overnight with either anti–TIMP-3 antibody or rabbit anti–β-actin (ab8227; Abcam). Detection was performed using fluorescent

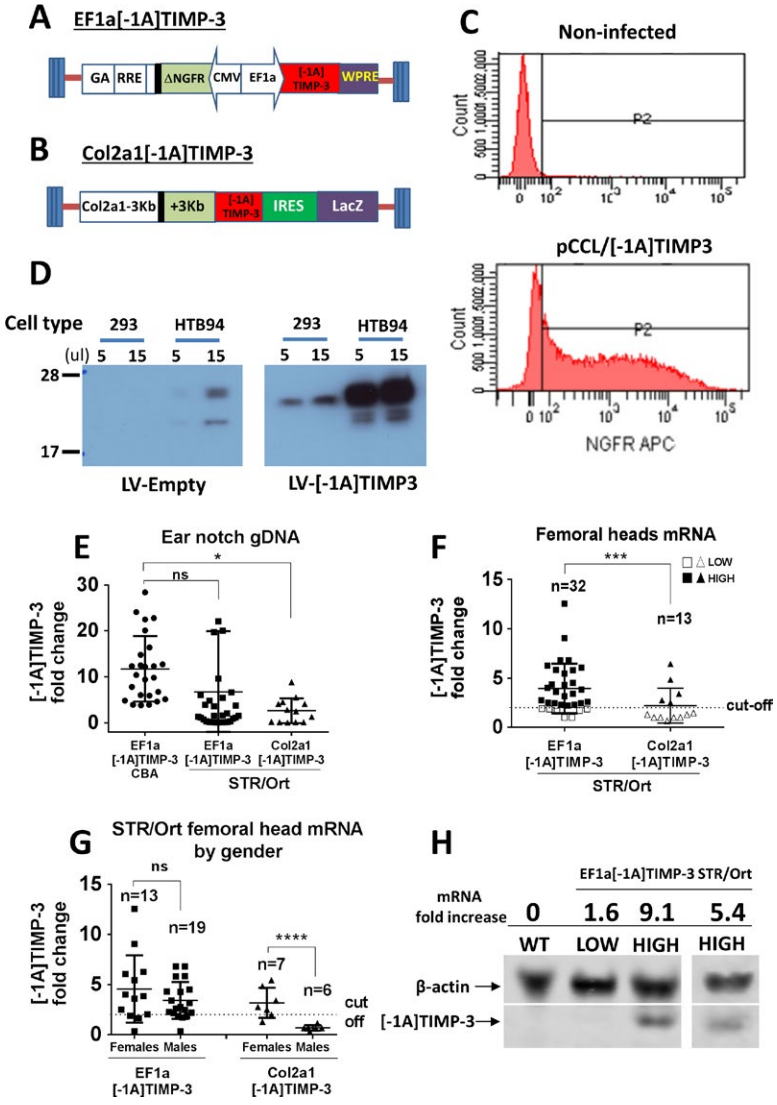

Figure 1. Evaluation of lentiviral expression. **A** and **B**, Illustrations of constructed vectors for overexpression of the tissue inhibitor of metalloproteinases 3 (TIMP-3) variant [-1A]TIMP-3 with lentivirus (LV)–driven elongation factor 1α (EF-1α) promoter (**A**) and conditional Col2a1-driven transductions (**B**) are shown. **C**, Chondrocytic HTB94 cells, analyzed by flow cytometry, show increased expression of nerve growth factor receptor (NGFR) in cells expressing the lentiviral transgene. APC = allophycocyanin. **D**, Western blots of HTB94 cells show small quantities of endogenous TIMP-3 in lentiviral empty vector (LV-empty) compared with high protein levels in both HEK 293 and HTB94 [-1A]TIMP-3–overexpressing cells (LV-[-1A]TIMP-3). **E**, Integration of [-1A]TIMP-3 into genomic DNA (gDNA) extracted from ear notches in all mice was evaluated by quantitative polymerase chain reaction. STR/Ort mice in the Col2a1[-1A]TIMP-3–transgenic group expressed significantly lower levels of [-1A]TIMP-3 compared with EF-1α[-1A]TIMP-3–transgenic CBA control mice. NS = not significant. **F**, Quantification of [-1A]TIMP-3 mRNA in femoral heads of STR/Ort mice showed higher expression in EF-1α[-1A]TIMP-3–transgenic mice. Mice were separated according to high and low levels of [-1A]TIMP-3 mRNA expression, with a cutoff value of 2-fold difference. **G**, Males expressed lower levels of [-1A]TIMP-3 than did females in both transgenic groups, and the difference was significant in Col2a1[-1A]TIMP-3–transgenic mice. **H**, Western blot confirmed increasing levels of [-1A]TIMP-3 protein in STR/Ort mice expressing higher amounts of [-1A]TIMP-3 mRNA compared with STR/Ort mice expressing lower amounts of [-1A]TIMP-3 mRNA and compared with wild-type (WT) mice. In **E–G**, symbols represent individual mice; bars show the mean ± SD. * = $P < 0.05$; *** = $P < 0.001$; **** = $P < 0.0001$.

goat anti-rabbit secondary antibodies (IRDye 680RD for actin and 800CW for TIMP-3; Li-Cor), and relative quantitation was conducted with β-actin as a reference protein.

Quantitative PCR. Integration of [-1A]TIMP-3 cDNA and overexpression were monitored by qPCR at both genomic DNA and messenger RNA (mRNA) levels (for details, see Supplementary Methods, http://onlinelibrary.wiley.com/doi/10.1002/art.40765/abstract).

Micro–computed tomography (micro-CT). Left and right hind limbs of all STR/Ort mice were dissected and immediately

scanned using a Skyscan 1272 micro-CT scanner (Bruker) at 50 kV, 0.5 aluminum filter, 200 mA, voxel size 9.00 μm, and 0.3° rotation angle. Data sets were reconstructed using NRecon reconstruction software, and 3-dimensional volumes of interest were selected using Dataviewer and CTAn software. Morphometric parameters were analyzed for tibial metaphyseal trabecular bone, cortical bone in diaphysis, and subchondral bone in epiphysis as previously described (33,34) (for details, see Supplementary Methods, http://onlinelibrary.wiley.com/doi/10.1002/art.40765/abstract).

In vitro bone cell culture and mineralization assay. STR/Ort and CBA mouse–derived primary osteoblasts were isolated, and their mineralization capacity was assessed by alizarin red S staining after 4 weeks. To assess the in vitro osteoregulatory effect of [-1A]TIMP-3, osteoblasts were isolated from skeletally mature 12-week-old wild-type (WT) C57BL/6 mice and infected with [-1A]TIMP-3 or TIMP-3 lentiviruses, while untreated and lentivirus–mock-infected osteoblasts served as controls. Early mineralization capacity of the infected osteoblasts was evaluated with alizarin red S staining after 21 days (for details, see Supplementary Methods, http://onlinelibrary.wiley.com/doi/10.1002/art.40765/abstract).

Histologic evaluation of cartilage lesions in STR/Ort mice. Following micro-CT, knee joints from all STR/Ort mice were fixed in 4% paraformaldehyde solution for 24 hours, decalcified in 10% EDTA for 3 weeks, and subsequently stored in 70% ethanol until processing. Samples were embedded in paraffin wax and sectioned coronally (5 μm thickness) through the entire joint. Proteoglycan loss was evaluated using Safranin O–fast green staining and a validated scoring system following the Osteoarthritis Research Society International (OARSI) recommendations (35). Joints were scored in a blinded manner by 2 experienced investigators (IK and BP), and scores were averaged using a modification to the methods of Poulet et al (18). To obtain robust results, as OA affects predominantly the medial tibial plateau and medial femoral condyle, the average of the maximum scores at both sites was used for each sample. Mean scores were calculated as the average of the scores recorded at 8 levels at 90-μm intervals across the entire joint.

Immunohistochemistry. For immunohistochemistry experiments, sections were deparaffinized, rehydrated, and probed with selected antibodies. Two percent normal goat serum was used for blocking. For [-1A]TIMP-3 detection, an additional step of antigen retrieval was applied by incubation with chondroitinase ABC (Sigma) at 0.01 units/ml. Rabbit anti-mouse TIMP-3 polyclonal antibody against the C-terminus of TIMP-3 (Millipore) was used at 1:3,000 dilution in normal goat serum. Rabbit anti-mouse anti-NVTEGE antibody (1:850), kindly provided by Dr. J. S. Mort (36), was used for detection of ADAMTS-generated neoepitopes. Nonimmune rabbit serum was used as negative control. Primary antibodies were detected using a Vectastain ABC kit with a secondary goat anti-rabbit biotinylated antibody (Vector) and visualized with HRP-conjugated streptavidin using 3,3′-diaminobenzidine.

Statistical analysis. All data were analyzed with GraphPad Prism 6 software and expressed as the mean ± SD. Data sets were tested for Gaussian distribution with the D'Agostino-Pearson normality test. Comparisons between ≥3 groups were performed by one-way analysis of variance followed by Tukey's multiple comparisons post hoc test. The Mann-Whitney U test or Student's 2-tailed *t*-test was used to compare 2 groups. Correlations were performed with Pearson's test. In all cases, *P* values less than 0.05 were considered significant.

RESULTS

In vitro efficacy of [-1A]TIMP-3 lentiviral transduction. In order to evaluate efficacy of lentiviral transduction, we infected the human embryonic kidney cell line (HEK 293) as well as the chondrosarcoma HTB94 cell line with a lentiviral construct (Figure 1A). Approximately 75% of HTB94 cells transduced with the [-1A]TIMP-3–containing vector expressed the NGFR marker, which is coexpressed by the same vector; in contrast, there was no detectible NGFR marker expression in uninfected control HTB94 cells (Figure 1C).

Western blot analysis showed that control HTB94 cells transduced by empty lentiviral vector secreted a small amount of endogenous TIMP-3 protein into the medium, detected by the anti–TIMP-3 antibody. In contrast, a high level of [-1A]TIMP-3 protein was secreted by HTB94 cells infected with EF-1α[-1A]TIMP-3 lentivirus compared with a lower level of protein from HEK 293 cells (Figure 1D). The data demonstrate effective lentivirus transduction into different types of cells and overexpression of the [-1A]TIMP-3 transgene in chondrocytes.

Transgenic overexpression of [-1A]TIMP-3 in mice. We generated several transgenic lines using 2 different methods. Lentivirus-induced global [-1A]TIMP-3–transgenic mice (EF-1α[-1A]TIMP-3–transgenic mice) were compared with conditional Col2a1[-1A]TIMP-3–transgenic mice. The method of pronuclear injection of fertilized STR/Ort mouse eggs using Col2a1[-1A]TIMP-3 linearized plasmid resulted in a low level of integration of the transgene, as determined by qPCR of genomic DNA from ear notches (Figure 1E). In order to determine mRNA expression levels within STR/Ort transgenic mice, total RNA was extracted from whole mouse femoral heads. Quantitative PCR using a specific primer for FLAG tag at the 3′-end of [-1A]TIMP-3 to distinguish endogenous from transgenic mRNA resulted in a range of mRNA overexpression, ranging between a ≤2-fold and a 13-fold increase (Figure 1F).

Most mice expressing high levels of [-1A]TIMP-3 mRNA were generated from lentiviral infection. [-1A]TIMP-3 mRNA levels were consistent across paired left and right femoral heads in both EF-1α[-1A]TIMP-3– and Col2a1[-1A]TIMP-3–transgenic groups of mice, but lower levels of expression were noted in males compared with females, especially in those of the Col2a1[-1A]TIMP-3–transgenic group, perhaps because of smaller group size (Figure 1G). Western blot showed undetectable [-1A]TIMP-3 protein levels in WT and low expressers but 5–10-fold greater levels in mice deemed high expressers based on an assessment of their [-1A]TIMP-3 mRNA levels (Figure 1H).

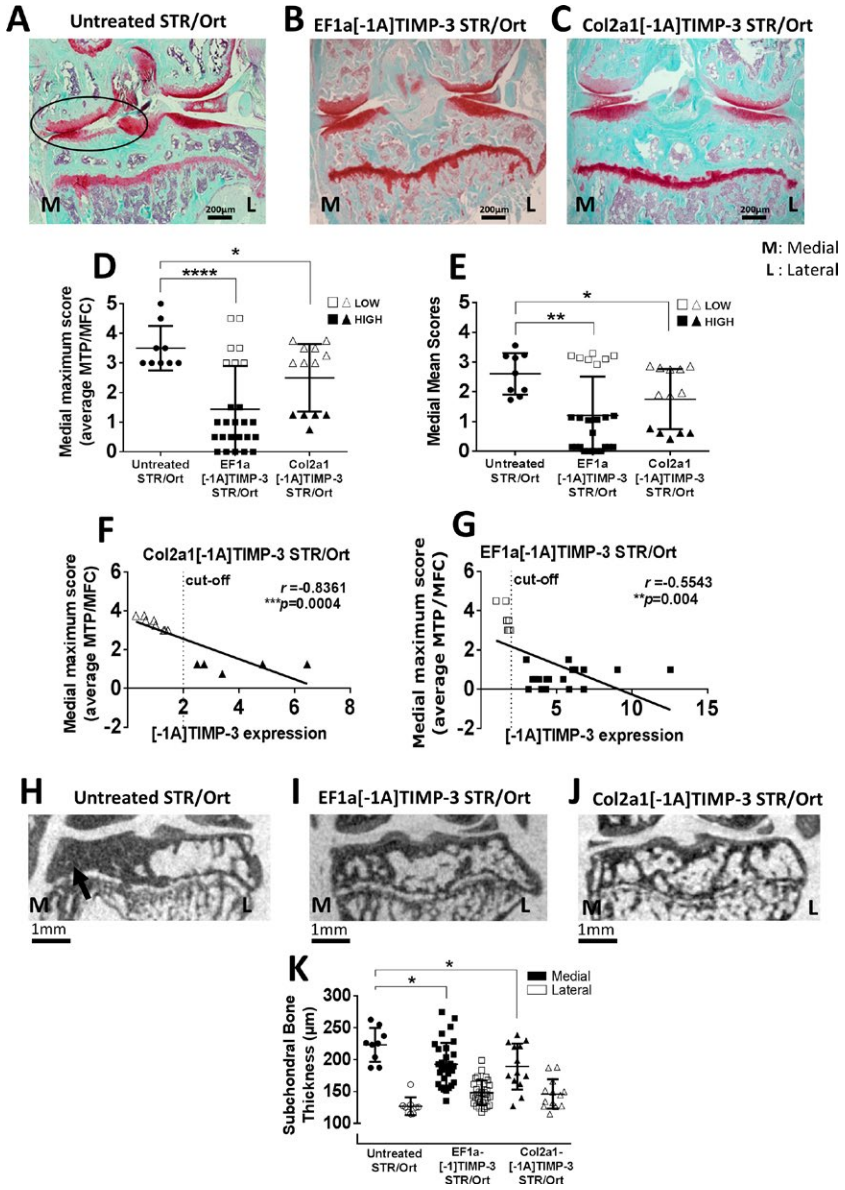

Figure 2. Overexpression of [-1A]TIMP-3 protects against osteoarthritis (OA) cartilage degradation in STR/Ort mice. **A–C**, Untreated STR/Ort mice at age 40 weeks show severe OA erosion in the medial sites of the tibial plateau and femoral condyles (circled in **A**), while both EF-1α[-1A]TIMP-3–transgenic mice (**B**) and Col2a1[-1A]TIMP-3–transgenic mice (**C**) show cartilage protection. **D** and **E**, OA scores of both EF-1α[-1A]TIMP-3–transgenic mice and Col2a1[-1A]TIMP-3–transgenic mice were significantly lower than those of age-matched untreated STR/Ort mice, which had high maximum (**D**) and mean (**E**) OA scores of the knee joints. MTP = medial tibial plateau; MFC = medial femoral condyle. **F** and **G**, Significant negative correlations between [-1A]TIMP-3 expression levels and OA scores were found in Col2a1[-1A]TIMP-3–transgenic mice (**F**) and EF-1α[-1A]TIMP-3–transgenic mice (**G**), which suggests that mice expressing high levels of [-1A]TIMP-3 (solid symbols) were better protected than those expressing low levels of [-1A]TIMP-3 (open symbols). **H–J**, Subchondral bone thickness was assessed by micro–computed tomography, which demonstrated that untreated STR/Ort mice with OA had severe sclerotic lesions (**arrow**) at the medial side of the tibial epiphysis (**H**) compared with EF-1α[-1A]TIMP-3–transgenic mice (**I**) and Col2a1[-1A]TIMP-3–transgenic mice (**J**). **K**, Quantification of subchondral bone thickness showed significant reduction on the medial site, while the lateral site seemed unaffected. In **D**, **E**, and **K**, symbols represent individual mice; bars show the mean ± SD. * = $P < 0.05$; ** = $P < 0.01$; **** = $P < 0.0001$. See Figure 1 for other definitions and explanation of cutoff.

Overall, STR/Ort background transgenic mice were harder to generate by direct pronuclear injection as fewer eggs were fertilized compared with CBA control mice and significant numbers of injected eggs did not survive. Importantly, the various levels of transgene expression achieved allowed us to determine the "threshold" expression level of [-1A]TIMP-3 needed for effective amelioration of the STR/Ort phenotype.

[-1A]TIMP-3 protects against OA cartilage degradation in STR/Ort mice. The main OA features in the STR/Ort mouse knee are cartilage loss on the medial tibial plateau and medial femoral condyle accompanied by osteophyte development and subchondral bone sclerosis (23). Therefore, we investigated these regions in mice age 40 weeks using OARSI maximum and mean OA scores (Figures 2A–E).

We found that while knees of untreated STR/Ort mice at age 40 weeks had severe loss of articular cartilage at the medial tibial plateau and medial femoral condyle (Figure 2A), STR/Ort transgenic mice overexpressing [-1A]TIMP-3 with either EF-1α[-1A]TIMP-3 or Col2a1[-1A]TIMP-3 maintained their articular cartilage (Figures 2B and C). The overall analysis showed a significant reduction or prevention of articular cartilage degradation with a decrease of 57% (mean maximum score 1.4; $P < 0.0001$) for the EF-1α[-1A]TIMP-3–transgenic group and a decrease of 22% (mean maximum score 2.5; $P = 0.0165$) for the Col2a1[-1A]TIMP-3–transgenic group, compared with untreated STR/Ort mice (mean maximum score 3.2) (Figure 2D). Similarly, mean scores at the medial sites for both overexpressing STR/Ort groups were significantly lower than those in the untreated group ($P = 0.005$ for the EF-1α[-1A]TIMP-3–transgenic group and $P = 0.043$ for the Col2a1[-1A]TIMP-3–transgenic group) (Figure 2E). Furthermore, there was a negative correlation between maximum OA score and [-1A]TIMP-3 expression levels, indicating a protective effect of [-1A]TIMP-3 when it is expressed at high levels (Figures 2F and G). A careful examination of stained sections revealed that mice expressing high levels of [-1A]TIMP-3 also showed signs of reduced proteoglycan accumulation in the cruciate ligaments, restored medial collateral ligament physiology, ameliorated osteophyte formation, and abolished synovial activation and inflammatory cell infiltration, which are known hallmarks of OA in this strain (see Supplementary Figure 1, http://onlinelibrary.wiley.com/doi/10.1002/art.40765/abstract).

The micro-CT data showed that untreated STR/Ort controls had severe subchondral sclerosis on the medial side of the knee joint (Figures 2H and K). This subchondral bone thickening was abrogated both in EF-1α[-1A]TIMP-3–transgenic STR/Ort mice and in Col2a1[-1A]TIMP-3–transgenic STR/Ort mice (Figures 2I–K).

Localization of [-1A]TIMP-3 and inhibition of aggrecanases in rescued cartilage. To validate whether the reduction in articular cartilage degradation and diminished aggrecanase cleavage is linked directly to overexpression of [-1A]TIMP-3, immunohistologic labeling for [-1A]TIMP-3 and the aggrecan NVTEGE neoepitope was done on adjacent knee joint sections. Figure 3A shows a representative coronal section of protected knee joint from STR/Ort mice in which [-1A]TIMP-3 immunostaining was seen in the adjacent section; [-1A]TIMP-3 was evident in both menisci and articular cartilage (Figure 3B) and resembled the endogenous TIMP-3 localization with pericellular distribution, as previously described (37).

Immunostaining against the NVTEGE neoepitope, an ADAMTS catabolic product, revealed that the medial side of the joints in OA-prone STR/Ort mice expressing low levels of the transgene (Figure 3F) showed little if any labeling for the NVTEGE neoepitope due to the extensive cartilage damage (verified by Safranin O staining) (Figure 3D) and the likely loss of known matrix binding partners for this antigen. This was consistent with NVTEGE-positive labeling (Figure 3F) in the apparently intact sites directly neighboring this damaged OA cartilage tissue, into which OA development was likely actively advancing. The lateral compartment, which is OA-resistant even in the STR/Ort strain, retained relatively intact cartilage compared with the medial side, yet already exhibited slight proteoglycan loss (evidenced by Safranin O staining) (Figure 3E) that colocalized with NVTEGE-positive labeling (Figure 3G). In contrast, STR/Ort mice expressing high levels of the transgene, which exhibited protection against OA and therefore retention of intact cartilage in both medial (Figure 3I) and lateral (Figure 3J) knee joint compartments, did not show NVTEGE-positive labeling (Figures K–M). This was consistent with [-1A]TIMP-3–related inhibition of ADAMTS-mediated aggrecan degradation.

Selective inhibition of aggrecanases increases bone mass in vivo. Given that STR/Ort mice, especially female mice (22), show increased trabecular bone mass, we examined bone mass (expressed as percentage trabecular bone volume/total tissue volume [%BV/TV]) using micro-CT in the tibial metaphysis of all mice overexpressing the transgene in comparison with untreated STR/Ort mice and EF-1α[-1A]TIMP-3–transgenic CBA control mice. Consistent with previous findings, nontransgenic untreated STR/Ort mice showed significantly increased BV/TV compared with CBA mice (22). Intriguingly, tibial BV/TV was further increased both in EF-1α[-1A]TIMP-3–transgenic mice and in Col2a1[-1A]TIMP-3–transgenic mice compared with untreated STR/Ort mice (Figure 4A) (representative images are shown in Figure 4E), and this was consistent with the other micro-CT trabecular bone parameters (see Supplementary Table 3, http://onlinelibrary.wiley.com/doi/10.1002/art.40765/abstract). The extent of this elevation in BV/TV was greater in EF-1α[-1A]TIMP-3–transgenic mice, presumably due to higher levels of [-1A]TIMP-3 mRNA overexpression. Subgroup analysis of mice expressing low and high levels of [-1A]TIMP-3 showed a statistically significant increase in BV/TV only in STR/Ort mice express-

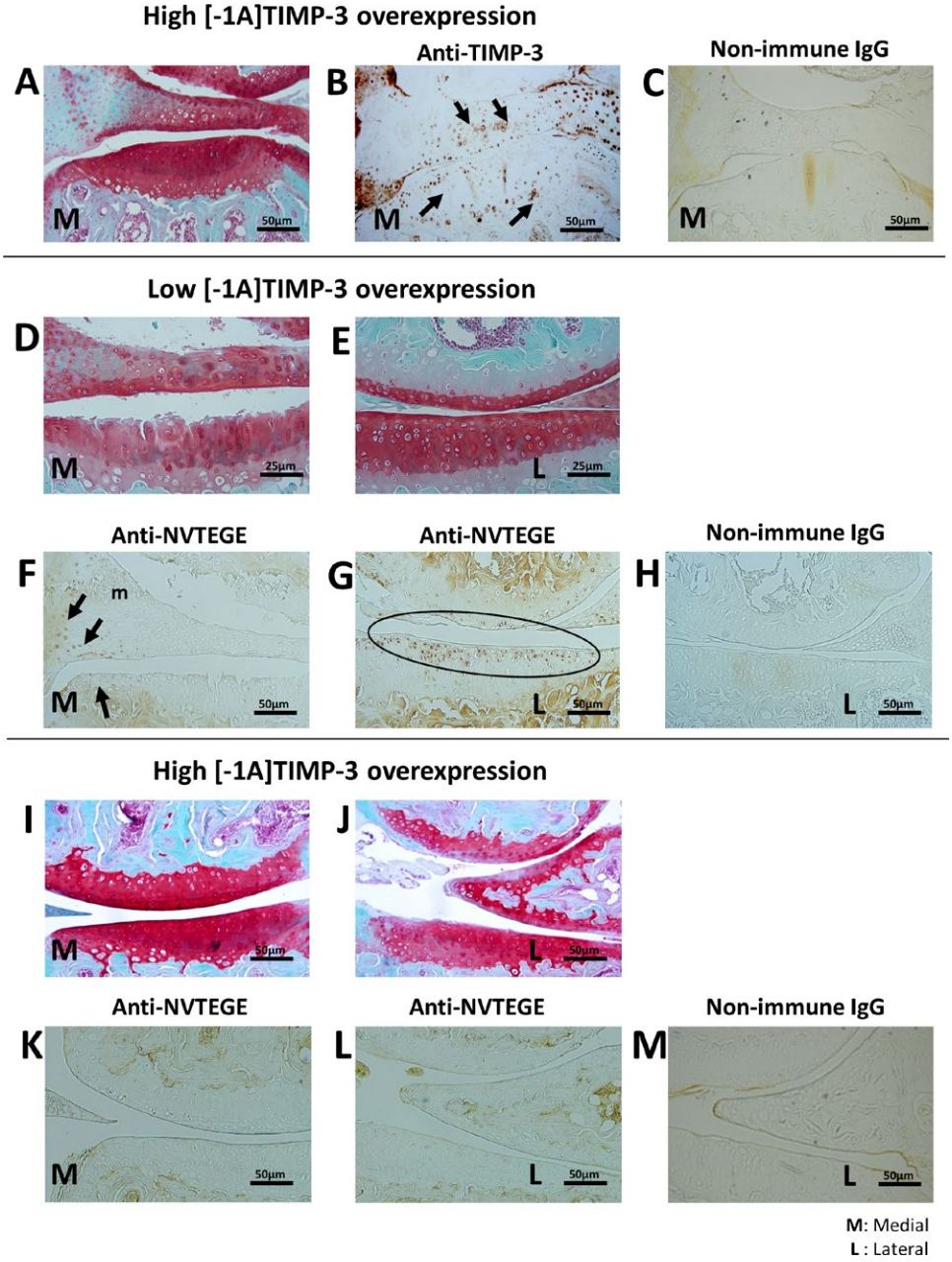

Figure 3. Localization of the tissue inhibitor of metalloproteinases 3 (TIMP-3) variant [-1A]TIMP-3 and inhibition of aggrecanase activity in articular cartilage. **A–C**, Mice expressing high levels of [-1A]TIMP-3, which were protected against osteoarthritis as revealed by Safranin O staining (**A**), showed immunohistochemical staining for anti–TIMP-3 antibody (**arrows** in **B**), which indicated that [-1A]TIMP-3 protein was translated at high levels. Rabbit IgG was used as negative control (**C**). **D** and **F**, STR/Ort mice expressing low levels of the transgene showed cartilage degradation at the medial site (**D**), which was concomitant with a lack of ADAMTS-derived NVTEGE neoepitope in the adjacent section (**F**), where **arrows** indicate peripheral neoepitope staining in meniscus (**m**) and cartilage matrix not yet affected by proteolysis (**F**). **E, G**, and **H**, Safranin O staining of the lateral condyle and plateau shows slight proteoglycan loss (**E**) colocalizing with NVTEGE-positive labeling (circled in **G**). Rabbit IgG was used as negative control (**H**). **I–M**, In contrast, in mice expressing high levels of [-1A]TIMP-3, cartilage matrix integrity was maintained at both medial (**I**) and lateral (**J**) sites, with undetectable levels of NVTEGE at either site (**K** and **L**), which suggests that ADAMTS-4/5 neoepitopes were inhibited by [-1A]TIMP-3. Rabbit IgG was used as negative control (**M**).

ing high levels of [-1A]TIMP-3 (Figure 4B). A similar trend was observed in EF-1α[-1A]TIMP-3–transgenic CBA control mice (Figure 4C).

Data subanalysis based on separation by sex revealed that STR/Ort females of both transgenic mouse lines had substantially higher bone mass than untreated controls (Figure 4D). The difference was greater in female EF-1α[-1A]TIMP-3–transgenic mice expressing high levels of [-1A]TIMP-3. Male STR/Ort mice, which expressed relatively lower overall levels of [-1A]TIMP-3, similarly showed higher bone mass in the EF-1α[-1A]TIMP-3–

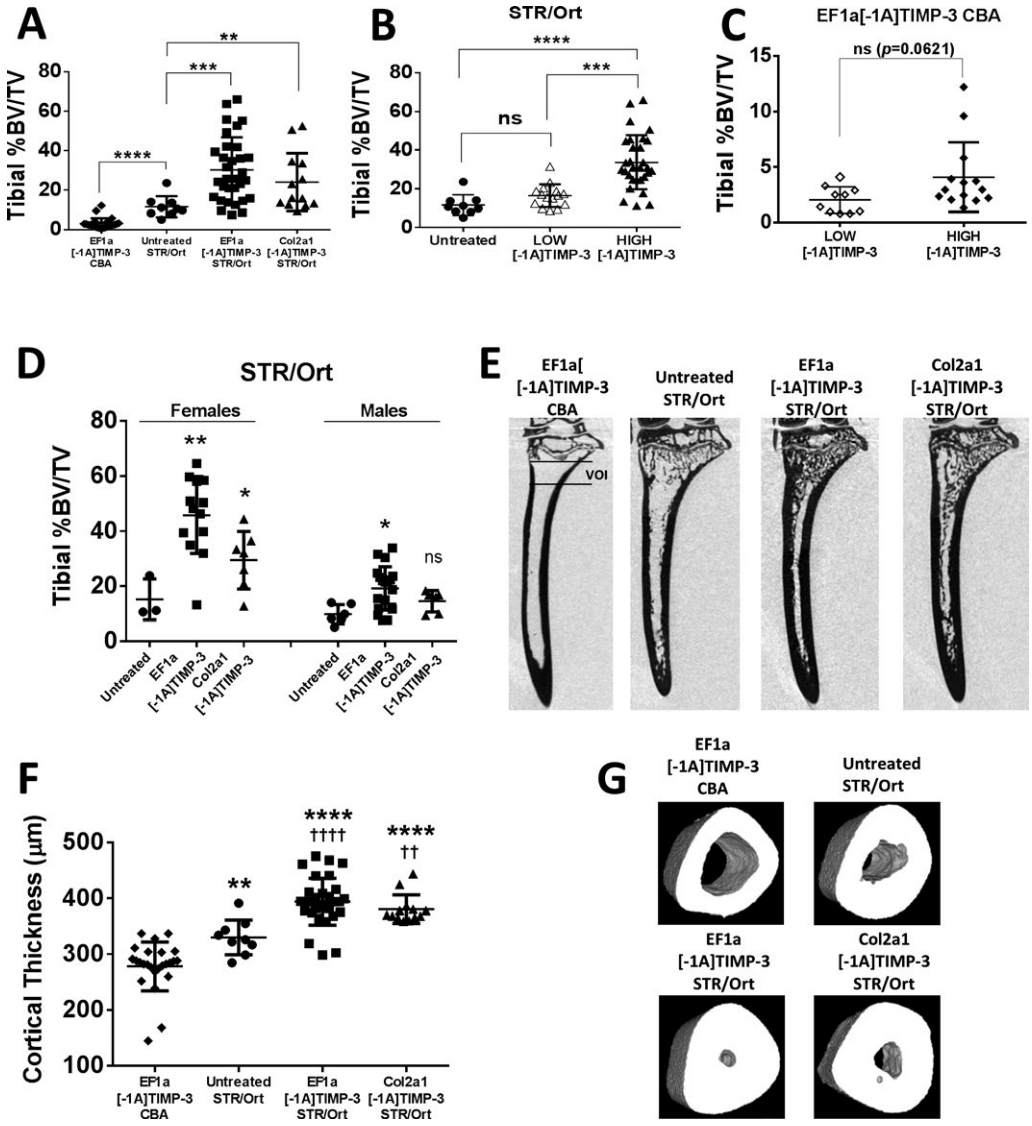

Figure 4. Selective inhibition of aggrecanases by [-1A]TIMP-3 leads to augmented bone mass in vivo. **A**, Micro–computed tomography trabecular analysis showed that untreated STR/Ort mice have significantly increased bone mass compared with EF-1α[-1A]TIMP-3–transgenic CBA mice. EF-1α[-1A]TIMP-3–transgenic mice and Col2a1[-1A]TIMP-3–transgenic mice both had significantly increased bone mass compared with untreated STR/Ort mice. **B**, Elevation of bone volume/total tissue volume (BV/TV) was observed only in STR/Ort mice expressing high levels of [-1A]TIMP-3 (solid symbols), while BV/TV in STR/Ort mice expressing low levels of [-1A]TIMP-3 (open symbols) did not differ from BV/TV in untreated STR/Ort mice. **C**, The increase in BV/TV in EF-1α[-1A]TIMP-3–transgenic CBA mice expressing high levels of [-1A]TIMP-3 was not significant. **D**, Analysis according to sex showed that STR/Ort females overexpressing either transgene had significantly higher bone mass compared with untreated STR/Ort females, while in STR/Ort males an increase in bone mass was observed only in the EF-1α[-1A]TIMP-3–transgenic group. **E**, Representative images from groups of STR/Ort female mice are shown, as well as an image representing a group of female EF-1α[-1A]TIMP-3–transgenic CBA mice. Lines show the bone volume of interest (VOI) that was analyzed in this experiment. **F**, The same results were observed with cortical bone measurements in the same groups of female mice represented in **E**. **G**, Results of cortical bone measurements in **F** are represented visually. In **A–D** and **F**, symbols represent individual mice; bars show the mean ± SD. In **A**–**C**, ** = $P <$ 0.01; *** = $P < 0.001$; **** = $P < 0.0001$. In **D**, * = $P < 0.05$; ** = $P < 0.01$ versus untreated STR/Ort mice. In **F**, ** = $P < 0.01$; **** = $P < 0.0001$ versus EF-1α[-1A]TIMP-3–transgenic CBA mice, and †† = $P < 0.01$; †††† = $P < 0.0001$ versus untreated STR/Ort mice. See Figure 1 for other definitions.

transgenic group compared with untreated STR/Ort mice (Figure 4D). Finally, cortical bone analysis revealed increased mean cortical bone thickness in transgenic STR/Ort mice, demonstrating that the effect of [-1A]TIMP-3 overexpression on bone tissue also extends to cortical bone regions (Figures 4F and G).

[-1A]TIMP-3 enhances in vitro bone formation. The next sets of experiments were devised, first, to determine whether the increase in bone mass is coupled with sustained changes in osteoblasts isolated from CBA and STR/Ort mice with divergent levels of [-1A]TIMP-3 transgene overexpres-

sion, and second, to test whether enhanced bone mass in transgenic mice was related to a developmental program that was abrogated by aggrecanase inhibition, or whether changes in isolated adult osteoblasts correspond to greater bone formation observed in [-1A]TIMP-3–overexpressing mice. Primary osteoblasts were isolated from long bones of CBA and STR/Ort EF-1α[-1A]TIMP-3–overexpressing mice, and the level of mineralization was assessed using alizarin red S staining. Results showed that the level of mineralization in isolated osteoblasts depended on the level of [-1A]TIMP-3 expression (Figures 5A and B); higher [-1A]TIMP-3 expression levels in both STR/Ort and CBA mice were associated with a greater extent of mineralization, with osteoblasts from these mice forming larger and more numerous bone nodules compared

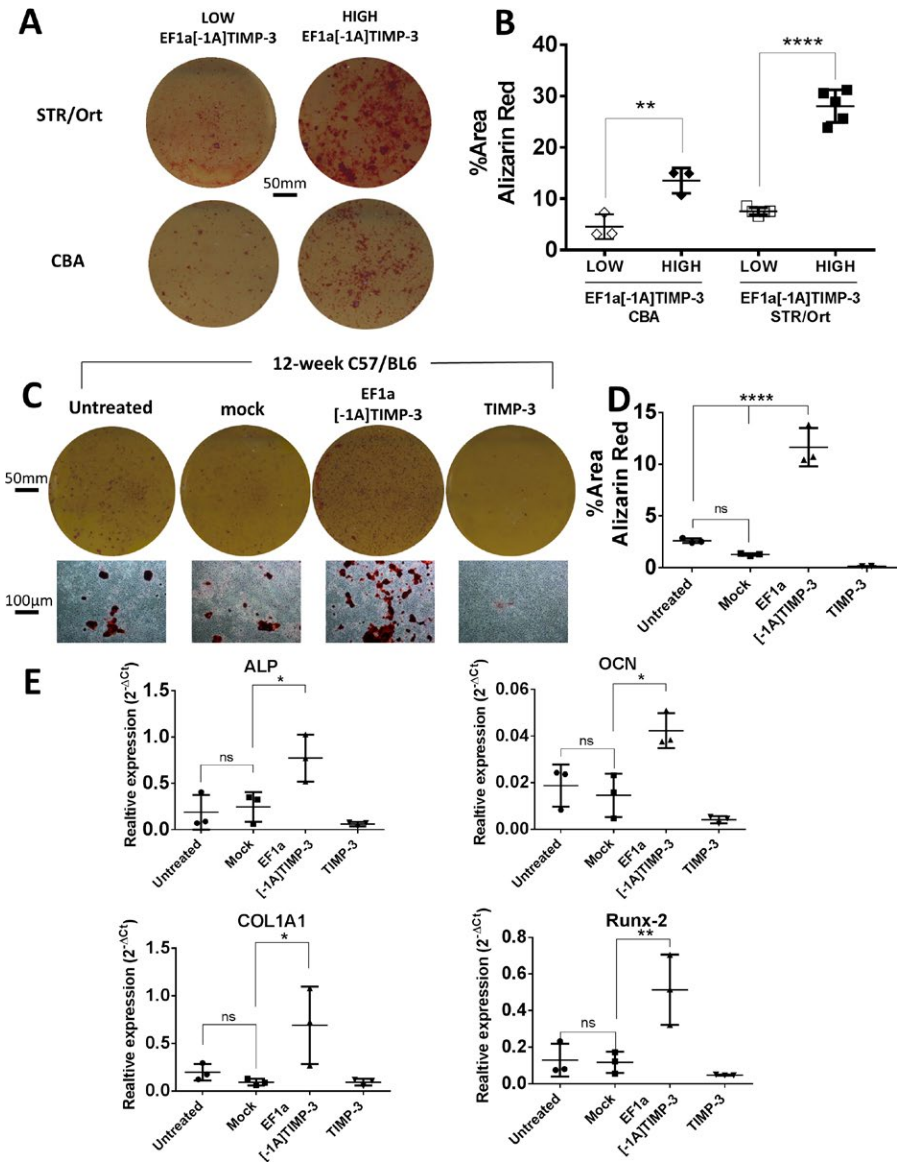

Figure 5. Overexpression of [-1A]TIMP-3 increases bone formation both in transgenic mouse–derived and newly infected primary osteoblasts. **A** and **B**, In vitro bone mineralization assay using alizarin red S staining indicated that long bone osteoblasts derived from EF-1α[-1A]TIMP-3–transgenic STR/Ort and CBA mice expressing high levels of [-1A]TIMP-3 had greater bone-forming capacity than osteoblasts derived from mice in these groups expressing low levels of [-1A]TIMP-3 (**A**), forming more and larger bone nodules with a significantly greater percentage of stained area (**B**) at 28 days of mineralization. **C** and **D**, Mature osteoblasts isolated from 12-week-old C57BL/6 mice were left untreated, mock-infected, or infected with lentiviral [-1A]TIMP-3 or native TIMP-3 and assessed for the extent of mineralization at 21 days (**C**); osteoblasts infected with lentiviral [-1A]TIMP-3 showed a significantly greater rate of mineralization compared with untreated or mock-infected osteoblasts (**D**). **C–E**, In contrast, overexpression of native TIMP-3 completely stopped mineralization of bone matrix. **E**, Osteoblasts infected with lentiviral [-1A]TIMP-3 also showed significantly increased expression of osteogenic gene markers such as alkaline phosphatase (AP), osteocalcin (OC), type I collagen (COL1A1), and the transcription factor Runx-2 compared with untreated or mock-infected osteoblasts. In **B**, **D**, and **E**, symbols represent individual mice; bars show the mean ± SD. * = $P < 0.05$; ** = $P < 0.01$; **** = $P < 0.0001$. See Figure 1 for other definitions.

with osteoblasts derived from mice expressing low levels of [-1A]TIMP-3.

To further determine whether [-1A]TIMP-3 directly affects osteoblastic bone formation and mineralization in cells that were not previously exposed to the [-1A]TIMP-3 transgene in vivo, we performed in vitro transduction of adult osteoblasts isolated from the long bones of 3-month-old WT mice. We found that [-1A]TIMP-3–transduced osteoblasts formed a significantly increased number of mineralized bone nodules compared with untreated or mock-infected cells (Figures 5C and D). In order to verify that [-1A]TIMP-3 exerts different effects compared with native, endogenous TIMP-3, we extended the experiments to include native TIMP-3. In contrast to transduction with [-1A]TIMP-3, native TIMP-3 completely abrogated bone formation, consistent with our previous in vivo findings, in which overexpression of Col2a1-driven TIMP-3 resulted in significant reduction in bone mass (28). Similarly, expression of mRNA for alkaline phosphatase, osteocalcin, type I collagen, and RUNX-2, reflecting osteogenic stimulation, was found to be elevated in [-1A]TIMP-3–transduced osteoblasts and suppressed by TIMP-3 (Figure 5E).

DISCUSSION

The primary aim of our study was to evaluate whether OA that arises spontaneously in STR/Ort mice can be ameliorated by an aggrecanase inhibitor. We used [-1A]TIMP-3, a modified TIMP-3 that was shown to be a "selective" but not a "specific" inhibitor against aggrecanases in vitro (30).

We compared knee joints of untreated STR/Ort mice with STR/Ort mice that were genetically modified to overexpress [-1A]TIMP-3 either specifically in chondrocytes using the Col2a1 promoter/enhancer Col2a1[-1A]TIMP-3 or ubiquitously through lentiviral transduction using EF-1α[-1A]TIMP-3. The results clearly showed that mice overexpressing [-1A]TIMP-3 had protected articular cartilage or reduced severity of cartilage degradation compared with age-matched, untreated STR/Ort control mice. This protection was dependent on expression levels of [-1A]TIMP-3. Maximum and mean OA scores were lower in mice expressing high levels of [-1A]TIMP-3 and higher in mice expressing low levels of [-1A]TIMP-3, irrespective of lentiviral or Col2a1-selective delivery. Our findings demonstrate the critical roles of aggrecanases in OA pathophysiology in STR/Ort mice, and they highlight that [-1A]TIMP-3 can restrict cartilage aggrecan degradation by blocking aggrecanase activity, and not only that of ADAMTS-4 and ADAMTS-5.

Furthermore, our findings indicate that the characteristic subchondral bone sclerosis observed in the medial site of epiphysis (19,38) was also significantly reduced in response to [-1A]TIMP-3 overexpression. This suggests that [-1A]TIMP-3 may regulate communication between chondrocytes and bone cells, or may indeed have a direct effect on bone through chondrocyte transdifferentiation into osteoblasts (39). Alternatively, we need to explore the possibility that the primary effect of [-1A]TIMP-3 could be the reduction in subchondral bone sclerosis, which in turn improves cartilage stability.

It should be noted that catabolic enzymes such as ADAMTS-4 and ADAMTS-5 are endocytosed by chondrocytes via LRP-1 (25,40) which potentially provides protection for cartilage. It is also notable that LRP-1–mediated endocytic clearance of TIMP-3 (37,41) and [-1A]TIMP-3 is likely to be regulated by LRP-1 (42). This was evident when sulfated glycans (37) inhibited binding of TIMP-3 to LRP-1 or when mutants of LRP-1 binding inhibited metalloproteinase-mediated degradation of cartilage at lower concentrations and for longer periods of time than WT TIMP-3, indicating that their increased half-lives improved their ability to protect cartilage (42).

The fact that the endogenous level of TIMP-3 could be very tightly regulated by LRP-1 at steady state requires an overexpression system rather than knockout to investigate the role of TIMP-3 in vivo, as in the present study in which a significant amount of [-1A]TIMP-3 protein in mice expressing high levels of the transgene was evident by Western blot, compared with endogenous (WT) TIMP-3. This indicates that the overexpression system overcomes LRP-1–mediated endocytic clearance. However, in OA cartilage and under inflammatory conditions this clearance system is impaired due to increased shedding of LRP-1 (26). It is plausible that LRP-1 shedding, defective LRP-1 clearance, or the apparent role of glucose transporter 4/LRP-1 interaction (14) may be important contributors to the many defects that increase the chances of OA development in STR/Ort mice, but we have not investigated this process. Nonetheless, the selective aggrecanase inhibitor [-1A]TIMP-3 is able to ameliorate the cartilage pathology of these mice.

Another major and surprising finding is related to the effect of [-1A]TIMP-3–mediated aggrecanase inhibition on bone mass. STR/Ort mice have an inherent high bone mass phenotype, which is linked to increased osteoblast numbers and bone formation and reduced osteoclast activity (22). Moreover, STR/Ort females exhibit higher bone mass than males, underlying the reported sexual dimorphism in this strain (19,43). Evidence presented herein shows that STR/Ort mice expressing high levels of [-1A]TIMP-3, especially females, had significantly increased trabecular parameters and cortical bone thickness, compared with control mice and mice expressing low levels of [-1A]TIMP-3. We expected the opposite effect, since our previous studies demonstrated that high levels of WT TIMP-3 overexpression in mouse cartilage led to lack of secondary ossification, and mice with intermediate levels of TIMP-3 had reduced bone mass (28). It has already been shown that MMP deficiency (e.g., deficiencies of MMP-9 and membrane type 1 MMP) can lead to developmental skeletal abnormalities (44,45). The increased bone mass in STR/Ort mice was mirrored in CBA control mice, which suggests that bone augmentation by [-1A]TIMP-3 is not specific to the STR/Ort strain. Taken together, the data suggest that there might be a unique involvement of

aggrecanases in bone metabolism, and they highlight that maintaining skeletal homeostasis depends on balanced matrix remodeling by aggrecanases and collagenases.

The findings from in vitro primary osteoblast mineralization assays show that osteoblasts isolated from STR/Ort mice highly overexpressing [-1A]TIMP-3 had a greater bone-forming capacity. This suggests that bone formation is positively influenced by inhibition of aggrecanases, which warrants further investigation. Most important, this observation was not strain-specific, as in vitro infection of WT osteoblasts from young C57BL/6 mice also resulted in enhanced bone mineralization and induction of osteogenic pathways when transduced by lentivirus overexpressing [-1A]TIMP-3 compared with TIMP-3. Our data suggest that [-1A]TIMP-3 may serve as a novel therapeutic agent in osteoporotic bone loss. This notion is supported by findings indicating that conditional overexpression of bone-specific TIMP-1, an MMP-only inhibitor, in osteoblasts leads to low bone turnover only in females (46).

In conclusion, the spontaneous OA that develops over time in STR/Ort mice is driven by aggrecanases, and [-1A]TIMP-3 overexpression can protect against cartilage damage and subchondral bone thickening in this mouse model. In addition, high levels of [-1A]TIMP-3 overexpression also led to a significant increase in bone mass, which highlights a possible dual role of this molecule as a regulator of cartilage and bone homeostasis. In the absence of an effective OA treatment, our novel data show that [-1A]TIMP-3 or other similar molecules exhibiting selective affinity for aggrecanases could be strong candidates for treatment of OA and osteoporosis.

ACKNOWLEDGMENT

The authors are grateful to Professor Hideaki Nagase for providing the cDNA for the [-1A]TIMP-3.

AUTHOR CONTRIBUTIONS

All authors were involved in drafting the article or revising it critically for important intellectual content, and all authors approved the final version to be published. Dr. Bou-Gharios had full access to all of the data in the study and takes responsibility for the integrity of the data and the accuracy of the data analysis.

Study conception and design. Kanakis, Pitsillides, Bou-Gharios.
Acquisition of data. Kanakis, Liu, Javaheri.
Analysis and interpretation of data. Kanakis, Liu, Poulet, Javaheri, van 't Hof.

REFERENCES

1. Neuhold LA, Killar L, Zhao W, Sung ML, Warner L, Kulik J, et al. Postnatal expression in hyaline cartilage of constitutively active human collagenase-3 (MMP-13) induces osteoarthritis in mice. J Clin Invest 2001;107:35–44.
2. Fuchs S, Skwara A, Bloch M, Dankbar B. Differential induction and regulation of matrix metalloproteinases in osteoarthritic tissue and fluid synovial fibroblasts. Osteoarthritis Cartilage 2004;12:409–18.
3. Yang CY, Chanalaris A, Troeberg L. ADAMTS and ADAM metalloproteinases in osteoarthritis—looking beyond the 'usual suspects'. Osteoarthritis Cartilage 2017;25:1000–9.
4. Verma P, Dalal K. ADAMTS-4 and ADAMTS-5: key enzymes in osteoarthritis. J Cell Biochem 2011;112:3507–14.
5. Echtermeyer F, Bertrand J, Dreier R, Meinecke I, Neugebauer K, Fuerst M, et al. Syndecan-4 regulates ADAMTS-5 activation and cartilage breakdown in osteoarthritis. Nat Med 2009;15:1072–6.
6. Glyn-Jones S, Palmer AJ, Agricola R, Price AJ, Vincent TL, Weinans H, et al. Osteoarthritis. Lancet 2015;386:376–87.
7. Nagase H, Kashiwagi M. Aggrecanases and cartilage matrix degradation. Arthritis Res Ther 2003;5:94–103.
8. Nemunaitis J, Poole C, Primrose J, Rosemurgy A, Malfetano J, Brown P, et al. Combined analysis of studies of the effects of the matrix metalloproteinase inhibitor marimastat on serum tumor markers in advanced cancer: selection of a biologically active and tolerable dose for longer-term studies. Clin Cancer Res 1998;4:1101–9.
9. Glasson SS, Askew R, Sheppard B, Carito B, Blanchet T, Ma HL, et al. Deletion of active ADAMTS5 prevents cartilage degradation in a murine model of osteoarthritis. Nature 2005;434:644–8.
10. Stanton H, Rogerson FM, East CJ, Golub SB, Lawlor KE, Meeker CT, et al. ADAMTS5 is the major aggrecanase in mouse cartilage in vivo and in vitro. Nature 2005;434:648–52.
11. Botter SM, Glasson SS, Hopkins B, Clockaerts S, Weinans H, van Leeuwen JP, et al. ADAMTS5-/- mice have less subchondral bone changes after induction of osteoarthritis through surgical instability: implications for a link between cartilage and subchondral bone changes. Osteoarthritis Cartilage 2009;17:636–45.
12. Glasson SS, Askew R, Sheppard B, Carito BA, Blanchet T, Ma HL, et al. Characterization of and osteoarthritis susceptibility in ADAMTS-4–knockout mice. Arthritis Rheum 2004;50:2547–58.
13. Little CB, Mittaz L, Belluoccio D, Rogerson FM, Campbell IK, Meeker CT, et al. ADAMTS-1–knockout mice do not exhibit abnormalities in aggrecan turnover in vitro or in vivo. Arthritis Rheum 2005;52:1461–72.
14. Gorski DJ, Xiao W, Li J, Luo W, Lauer M, Kisiday J, et al. Deletion of ADAMTS5 does not affect aggrecan or versican degradation but promotes glucose uptake and proteoglycan synthesis in murine adipose derived stromal cells. Matrix Biol 2015;47:66–84.
15. Brewster M, Lewis EJ, Wilson KL, Greenham AK, Bottomley KM. Ro 32-3555, an orally active collagenase selective inhibitor, prevents structural damage in the STR/ORT mouse model of osteoarthritis. Arthritis Rheum 1998;41:1639–44.
16. Chiusaroli R, Visentini M, Galimberti C, Casseler C, Mennuni L, Covaceuszach S, et al. Targeting of ADAMTS5's ancillary domain with the recombinant mAb CRB0017 ameliorates disease progression in a spontaneous murine model of osteoarthritis. Osteoarthritis Cartilage 2013;21:1807–10.
17. Mason RM, Chambers MG, Flannelly J, Gaffen JD, Dudhia J, Bayliss MT. The STR/ort mouse and its use as a model of osteoarthritis. Osteoarthritis Cartilage 2001;9:85–91.
18. Poulet B, Ulici V, Stone TC, Pead M, Gburcik V, Constantinou E, et al. Time-series transcriptional profiling yields new perspectives on susceptibility to murine osteoarthritis. Arthritis Rheum 2012;64:3256–66.
19. Staines KA, Poulet B, Wentworth DN, Pitsillides AA. The STR/Ort mouse model of spontaneous osteoarthritis: an update. Osteoarthritis Cartilage 2017;25:802–8.
20. Chambers MG, Cox L, Chong L, Suri N, Cover P, Bayliss MT, et al. Matrix metalloproteinases and aggrecanases cleave aggrecan in different zones of normal cartilage but colocalize in the development of osteoarthritic lesions in STR/Ort mice. Arthritis Rheum 2001;44:1455–65.

21. Flannelly J, Chambers MG, Dudhia J, Hembry RM, Murphy G, Mason RM, et al. Metalloproteinase and tissue inhibitor of metalloproteinase expression in the murine STR/Ort model of osteoarthritis. Osteoarthritis Cartilage 2002;10:722–33.
22. Pasold J, Engelmann R, Keller J, Joost S, Marshall RP, Frerich B, et al. High bone mass in the STR/Ort mouse results from increased bone formation and impaired bone resorption and is associated with extramedullary hematopoiesis. J Bone Miner Metab 2013;31:71–81.
23. Staines KA, Madi K, Mirczuk SM, Parker S, Burleigh A, Poulet B, et al. Endochondral growth defect and deployment of transient chondrocyte behaviors underlie osteoarthritis onset in a natural murine model. Arthritis Rheumatol 2016;68:880–91.
24. Scilabra SD, Yamamoto K, Pigoni M, Sakamoto K, Muller SA, Papadopoulou A, et al. Dissecting the interaction between tissue inhibitor of metalloproteinases-3 (TIMP-3) and low density lipoprotein receptor-related protein-1 (LRP-1): development of a "TRAP" to increase levels of TIMP-3 in the tissue. Matrix Biol 2017;59:69–79.
25. Yamamoto K, Troeberg L, Scilabra SD, Pelosi M, Murphy CL, Strickland DK, et al. LRP-1-mediated endocytosis regulates extracellular activity of ADAMTS-5 in articular cartilage. FASEB J 2013;27:511–21.
26. Yamamoto K, Santamaria S, Botkjaer KA, Dudhia J, Troeberg L, Itoh Y, et al. Inhibition of shedding of low-density lipoprotein receptor–related protein 1 reverses cartilage matrix degradation in osteoarthritis. Arthritis Rheumatol 2017;69:1246–56.
27. Sahebjam S, Khokha R, Mort JS. Increased collagen and aggrecan degradation with age in the joints of Timp3$^{-/-}$ mice. Arthritis Rheum 2007;56:905–9.
28. Poulet B, Liu K, Plumb D, Vo P, Shah M, Staines K, et al. Over-expression of TIMP-3 in chondrocytes produces transient reduction in growth plate length but permanently reduces adult bone quality and quantity. PLoS One 2016;11:e0167971.
29. Javaheri B, Hopkinson M, Poulet B, Pollard AS, Shefelbine SJ, Chang YM, et al. Deficiency and also transgenic overexpression of Timp-3 both lead to compromised bone mass and architecture in vivo. PLoS One 2016;11:e0159657.
30. Wei S, Kashiwagi M, Kota S, Xie Z, Nagase H, Brew K. Reactive site mutations in tissue inhibitor of metalloproteinase-3 disrupt inhibition of matrix metalloproteinases but not tumor necrosis factor-α-converting enzyme. J Biol Chem 2005;280:32877–82.
31. Lim NH, Kashiwagi M, Visse R, Jones J, Enghild JJ, Brew K, et al. Reactive-site mutants of N-TIMP-3 that selectively inhibit ADAMTS-4 and ADAMTS-5: biological and structural implications. Biochem J 2010;431:113–22.
32. Zhou G, Garofalo S, Mukhopadhyay K, Lefebvre V, Smith CN, Eberspaecher H, et al. A 182 bp fragment of the mouse pro α 1(II) collagen gene is sufficient to direct chondrocyte expression in transgenic mice. J Cell Sci 1995;108:3677–84.
33. Van 't Hof RJ. Analysis of bone architecture in rodents using microcomputed tomography. Methods Mol Biol 2012;816:461–76.
34. Huesa C, Ortiz AC, Dunning L, McGavin L, Bennett L, McIntosh K, et al. Proteinase-activated receptor 2 modulates OA-related pain, cartilage and bone pathology. Ann Rheum Dis 2016;75:1989–97.
35. Glasson SS, Chambers MG, Van Den Berg WB, Little CB. The OARSI histopathology initiative: recommendations for histological assessments of osteoarthritis in the mouse. Osteoarthritis Cartilage 2010;18 Suppl 3:S17–23.
36. Mort JS, Roughley PJ. Production of antibodies against degradative neoepitopes in aggrecan. Methods Mol Med 2004;100:237–50.
37. Troeberg L, Lazenbatt C, Anower EK, Freeman C, Federov O, Habuchi H, et al. Sulfated glycosaminoglycans control the extracellular trafficking and the activity of the metalloprotease inhibitor TIMP-3. Chem Biol 2014;21:1300–9.
38. Stok KS, Pelled G, Zilberman Y, Kallai I, Goldhahn J, Gazit D, et al. Revealing the interplay of bone and cartilage in osteoarthritis through multimodal imaging of murine joints. Bone 2009;45:414–22.
39. Javaheri B, Caetano-Silva SP, Kanakis I, Bou-Gharios G, Pitsillides AA. The chondro-osseous continuum: is it possible to unlock the potential assigned within? Front Bioeng Biotechnol 2018;6:28.
40. Yamamoto K, Owen K, Parker AE, Scilabra SD, Dudhia J, Strickland DK, et al. Low density lipoprotein receptor-related protein 1 (LRP1)-mediated endocytic clearance of a disintegrin and metalloproteinase with thrombospondin motifs-4 (ADAMTS-4): functional differences of non-catalytic domains of ADAMTS-4 and ADAMTS-5 in LRP1 binding. J Biol Chem 2014;289:6462–74.
41. Rother S, Samsonov SA, Hempel U, Vogel S, Moeller S, Blaszkiewicz J, et al. Sulfated hyaluronan alters the interaction profile of TIMP-3 with the endocytic receptor LRP-1 clusters II and IV and increases the extracellular TIMP-3 level of human bone marrow stromal cells. Biomacromolecules 2016;17:3252–61.
42. Doherty CM, Visse R, Dinakarpandian D, Strickland DK, Nagase H, Troeberg L. Engineered tissue inhibitor of metalloproteinases-3 variants resistant to endocytosis have prolonged chondroprotective activity. J Biol Chem 2016;291:22160–72.
43. Mahr S, Menard J, Krenn V, Muller B. Sexual dimorphism in the osteoarthritis of STR/Ort mice may be linked to articular cytokines. Ann Rheum Dis 2003;62:1234–7.
44. Engsig MT, Chen QJ, Vu TH, Pedersen AC, Therkidsen B, Lund LR, et al. Matrix metalloproteinase 9 and vascular endothelial growth factor are essential for osteoclast recruitment into developing long bones. J Cell Biol 2000;151:879–89.
45. Holmbeck K, Bianco P, Caterina J, Yamada S, Kromer M, Kuznetsov SA, et al. MT1-MMP-deficient mice develop dwarfism, osteopenia, arthritis, and connective tissue disease due to inadequate collagen turnover. Cell 1999;99:81–92.
46. Geoffroy V, Marty-Morieux C, Le Goupil N, Clement-Lacroix P, Terraz C, Frain M, et al. In vivo inhibition of osteoblastic metalloproteinases leads to increased trabecular bone mass. J Bone Miner Res 2004;19: 811–22.

Arthritis & Rheumatology
Vol. 71, No. 4, April 2019, pp 583–593
DOI 10.1002/art.40751

AMERICAN COLLEGE OF RHEUMATOLOGY
EDUCATION • TREATMENT • RESEARCH

Genetic Inactivation of ZCCHC6 Suppresses Interleukin-6 Expression and Reduces the Severity of Experimental Osteoarthritis in Mice

Mohammad Y. Ansari,[1] Nazir M. Khan,[1] Nashrah Ahmad,[2] Jonathan Green,[1] Kimberly Novak,[1] and Tariq M. Haqqi[1]

Objective. Cytokine expression is tightly regulated posttranscriptionally, but high levels of interleukin-6 (IL-6) in patients with osteoarthritis (OA) indicate that regulatory mechanisms are disrupted in this disorder. The enzyme ZCCHC6 (zinc-finger CCHC domain–containing protein 6; TUT-7) has been implicated in posttranscriptional regulation of inflammatory cytokine expression, but its role in OA pathogenesis is unknown. The present study was undertaken to investigate whether ZCCHC6 directs the expression of IL-6 and influences OA pathogenesis in vivo.

Methods. Human and mouse chondrocytes were stimulated with recombinant IL-1β. Expression of ZCCHC6 in human chondrocytes was knocked down using small interfering RNAs. IL-6 transcript stability was determined by actinomycin D chase, and 3′-uridylation of microRNAs was determined by deep sequencing. Zcchc6$^{-/-}$ mice were produced by gene targeting. OA was surgically induced in the knee joints of mice, and disease severity was scored using a semiquantitative grading system.

Results. ZCCHC6 was markedly up-regulated in damaged cartilage from human OA patients and from wild-type mice with surgically induced OA. Overexpression of ZCCHC6 induced the expression of IL-6, and its knockdown reduced IL-6 transcript stability and IL-1β–induced IL-6 expression in chondrocytes. Reintroduction of Zcchc6 in Zcchc6$^{-/-}$ mouse chondrocytes rescued the IL-1β–induced IL-6 expression. Knockdown of ZCCHC6 reduced the population of micro-RNA 26b (miR-26b) with 3′-uridylation by 60%. Zcchc6$^{-/-}$ mice with surgically induced OA produced low levels of IL-6 and exhibited reduced cartilage damage and synovitis in the joints.

Conclusion. These findings indicate that ZCCHC6 enhances IL-6 expression in chondrocytes through transcript stabilization and by uridylating miR-26b, which abrogates repression of IL-6. Inhibition of IL-6 expression and significantly reduced OA severity in Zcchc6$^{-/-}$ mice identify ZCCHC6 as a novel therapeutic target to inhibit disease pathogenesis.

INTRODUCTION

Osteoarthritis (OA) is the most common form of arthritis, affecting diarthrodial joints and causing pain and disability (1). OA pathology is now being recognized as driven by a proinflammatory component, as high levels of interleukin-6 (IL-6) and other cytokines are present in the synovial fluid of OA patients and also seen in animal models of OA (2–5). A prospective study of a population-based cohort of British women showed a correlation of higher body mass index and elevated serum levels of IL-6 with development of radiographic knee OA (6). IL-6 has also been shown to act as a crucial mediator of matrix metalloproteinase 13 expression in hypoxia-inducible factor 2α–induced experimental OA in mice (7) and affects anabolic processes in cartilage, such as down-regulation of type II collagen expression (8). It has been reported that IL-6 increases the severity of OA, and inhibition of IL-6/STAT3 signaling slows the progression of experimental OA (9,10). However, regulation of IL-6 expression in OA is still not fully understood.

Expression of cytokine genes is a tightly regulated process to control tissue inflammation. Cytokine gene expression is regulated by various factors at the transcriptional, posttranscrip-

Supported in part by the NIH (grants R01-AT-005520, R01-AT-007373, and R01-AR-067056). Dr. Haqqi's work was supported in part by Northeast Ohio Medical University.

[1]Mohammad Y. Ansari, PhD, Nazir M. Khan, PhD (current address: Emory University, Atlanta, Georgia), Jonathan Green, PhD, Kimberly Novak, MS, Tariq M. Haqqi, PhD: Northeast Ohio Medical University, Rootstown; [2]Nashrah Ahmad, MS: Northeast Ohio Medical University, Rootstown, and Kent State University, Kent, Ohio.

No potential conflicts of interest relevant to this article were reported.

Address correspondence to Tariq M. Haqqi, PhD, Department of Anatomy and Neurobiology, RGE-238, Northeast Ohio Medical University, 4209 Street Route 44, Rootstown, OH 44272. E-mail: thaqqi@neomed.edu.

Submitted for publication April 11, 2018; accepted in revised form October 3, 2018.

tional, and translational levels (11), and microRNAs (miRNAs) have been found to play a critical role in the regulation of cytokine gene expression (12). Recent work has shown the presence of nontemplated uridine residues, added by terminal uridylyltransferases (TUTases), on pre-miRNAs, miRNAs, and messenger RNAs (mRNAs) (13–16). ZCCHC6 (zinc-finger CCHC domain–containing protein 6; TUT-7) is a noncanonical poly(A) polymerase and a member of the nucleotidyltransferase superfamily that has been shown to uridylate the 3′ end of miRNAs and modulate the biogenesis and stability of mRNAs and miRNAs (17,18). It was found that knockdown of ZCCHC11 expression in A549 cells suppressed the expression of IL-6 by altering the 3′-uridylation of miRNAs involved in the regulation of IL-6 expression (19). ZCCHC6, a homolog of ZCCHC11, has recently been shown to be involved in the regulation of inflammatory cytokines in mouse macrophages (20), but its role in chondrocytes or in OA pathogenesis has not previously been investigated.

In this study, we used human OA cartilage and a mouse model of surgically induced OA to investigate the expression of ZCCHC6 and examine whether it regulates IL-6 expression in chondrocytes and affects OA pathogenesis in vivo. Herein we report that ZCCHC6 expression was highly up-regulated in human and mouse OA cartilage and chondrocytes and was also modulated by IL-1β in vitro. Human chondrocytes transfected with ZCCHC6-targeting small interfering RNAs (siRNAs) expressed low levels of IL-6, while its overexpression enhanced the production of IL-6. ZCCHC6 modulated both the stability and the expression of IL-6 mRNAs in chondrocytes. Knockdown of ZCCHC6 had no effect on the overall expression level of miRNAs but reduced the population of 3′-uridylated miRNA 26b (miR-26b), which targets IL-6 mRNA in human chondrocytes. Zcchc6$^{-/-}$ mice with surgically induced OA expressed low levels of IL-6 in the joints and showed reduced synovitis, significantly reduced cartilage damage, and loss of proteoglycans compared to wild-type (WT) littermates. Taken together, our gain-of-function and loss-of-function studies clearly demonstrated that ZCCHC6 acts as a novel regulator of IL-6 expression and disease pathogenesis in a mouse model of OA.

MATERIALS AND METHODS

Chondrocyte preparation and culture. Experiments involving the use of discarded, deidentified human cartilage samples were approved as non–human subject study under 45 CFR, Exemption 4, by the Summa Health System/Northeast Ohio Medical University Institutional Review Board. Chondrocytes from OA cartilage were prepared by enzymatic digestion and cultured as described previously (21). Chondrocytes from mouse joints using femoral condyles and tibial plateaus were prepared as described (22). When 80% confluent, chondrocyte cultures were serum starved overnight and then stimulated for various amounts of time with 5 ng/ml human IL-1β or mouse IL-1β (nos. 201-LB-025 and 401-ML-005, respectively; R&D Systems). Culture supernatants were centrifuged for 5 minutes at 20,000*g* to remove debris prior to use in enzyme-linked immunosorbent assays (ELISAs) and cytokine multiplex assays. Chondrocyte phenotype was analyzed using a polymerase chain reaction (PCR) array for chondrocyte-specific genes (no. GK064; ScienCell Research Laboratories).

Experimental OA and histologic analyses of mouse knee joints. All animal studies were approved by the Institutional Animal Use and Care Committee of the Northeast Ohio Medical University. Zcchc6$^{+/-}$ mice were generated by gene targeting (SIGTR ES cell line AE0325; Mutant Mouse Regional Resource Center, University of California, Davis), and Zcchc6$^{-/-}$ mice were produced by breeding Zcchc6$^{+/-}$ × Zcchc6$^{+/-}$ mice and then Zcchc6$^{-/-}$ × Zcchc6$^{-/-}$ mice. Experimental OA was induced in the right knee of 12-week-old male Zcchc6$^{-/-}$ mice and WT littermates (n = 10 per group) by surgical destabilization of the medial meniscus (DMM) as previously described (23). Sham surgery was performed on the left knee, which served as a control. Mice were killed 8 weeks postsurgery, and the joints were used for histologic assessment of disease severity and scored according to the semiquantitative Osteoarthritis Research Society International (OARSI) grading system (24). Synovitis was determined by Safranin O and hematoxylin staining, and the degree of synovial inflammation was scored on a scale of 0–3 as previously described (25).

Knockdown and overexpression of ZCCHC6. Human OA chondrocytes were transfected with 100 nmoles of scrambled or ZCCHC6-targeting siRNAs (On-Target Plus SMARTpool; Dharmacon) or ZCCHC6 expression plasmid (26) (generously provided by Dr. Chris Norbury, University of Oxford, Oxford, UK) using a 4D Nucleofector System (Lonza) and P3 Primary Cell 4D Nucleofection kit (Amaxa) and were cultured as described above. Gene expression analyses were performed 48 hours after transfection.

Total RNA isolation from cartilage and chondrocytes and gene expression analysis by TaqMan assay. Human cartilage samples were stained with India ink and cartilage from damaged and undamaged areas was resected, frozen in liquid nitrogen, and pulverized to powder using a freezer mill (no. 6770; Spex). The pulverized cartilage was then used to extract DNA-free total RNA using an miRNeasy kit (no. 217004; Qiagen). Total RNA from human or mouse chondrocytes was also prepared as above. Integrity of RNA preparations was determined using TapeStation 4200 (Agilent), and 1 μg of total RNA was used to synthesize complementary DNA (cDNA) (cDNA synthesis kit, no. 4368814; Applied Biosystems); mRNA expression was determined by TaqMan assay.

Messenger RNA decay experiments. The stability of IL-6 mRNA transcripts in human OA chondrocytes with knockdown of ZCCHC6 expression or in Zcchc6$^{-/-}$ and Zcchc6$^{+/+}$ mouse chondrocytes was determined by actinomycin D chase experiments as described previously (27).

RNA immunoprecipitation assay (RIPA). RIPA was performed as described earlier (27). Briefly, chondrocytes (5×10^6 cells per 100-mm dish, total of 10 dishes) were stimulated with IL-1β for 6 hours, harvested, and washed with ice-cold phosphate buffered saline followed by lysis in Polysomes lysis buffer (100 m*M* KCl, 5 m*M* $MgCL_2$, 10 m*M* HEPES, 0.5% Nonidet P40, 1 m*M* dithiothreitol, 100 units/ml RNasin, 400 μ*M* vanadyl ribonucleoside complex, and protease inhibitor cocktail). The lysate was incubated with anti-ZCCHC6 antibody (or rabbit IgG as control) overnight at 4°C. The antibody–lysate mix was incubated with protein A–agarose beads for pulldown, and RNA was prepared from the immunoprecipitate using the TRIzol–chloroform method, followed by TaqMan assay for IL-6 mRNA quantification.

Western immunoblotting. Protein expression was determined by Western blotting as described (28). Briefly, chondrocytes were lysed in RIPA buffer containing complete protease inhibitor cocktail (no. 11697498001; Roche), and the protein concentration was estimated by Bradford dye assay. Lysates were resolved by sodium dodecyl sulfate–polyacrylamide gel electrophoresis and transferred to PVDF membrane (no. 1704156; Bio-Rad). Membranes were probed with primary polyclonal antibodies specific for ZCCHC6 (validated by siRNA-mediated knockdown of ZCCHC6) (no. sc-137947; Santa Cruz Biotechnology) or an anti–β-actin monoclonal antibody (no. sc-47778; Santa Cruz Biotechnology) followed by appropriate horseradish peroxidase (HRP)–conjugated secondary antibodies (Cell Signaling Technology). Images were acquired using a *Pxi*-Imaging System (Syngene), and band intensities were quantified with ImageJ software (National Institutes of Health).

IL-6 ELISA. IL-6 concentrations in the culture supernatants were determined using a human IL-6 ELISA kit according to the instructions of the manufacturer (R&D Systems). Plates were read with a Synergy H1 Hybrid Plate Reader (BioTek Instruments). The sensitivity of the assay was 0.7 pg IL-6/ml.

Cytokine multiplex immunoassay. Levels of secreted cytokines and chemokines in the culture supernatants were determined using a Procarta Plex 65-plex immunoassay for human chondrocytes and 36-plex immunoassay for mouse chondrocytes (both from ThermoFisher Scientific). Human chondrocytes with knockdown of ZCCHC6 expression or chondrocytes isolated from $Zcchc6^{-/-}$ mice and WT littermates were stimulated with IL-1β for 6 hours, and 50-μl aliquots of the supernatants in duplicate were assayed for secreted molecules using a Luminex 200 System and analyzed with ProcartaPlex Analyst 1.0 (Luminex).

Cytokine PCR array analyses. Human OA chondrocytes with knockdown of ZCCHC6 expression were stimulated with IL-1β for 6 hours, and total RNA was extracted for cDNA synthesis as described above. Gene expression was analyzed using a panel of 88 genes involved in immune cell response, inflammation, and cellular signaling and 8 housekeeping genes as normalization control (no. HAIIR-I; Realtimeprimers.com).

Immunohistochemistry analysis. Full-thickness human cartilage pieces were obtained from the tibial plateau and were fixed in 4% paraformaldehyde for 48 hours. Samples were dehydrated, embedded in paraffin, and 5-μ*M*–thick serial sections were cut for immunohistochemistry. To analyze the expression of ZCCHC6, sections were probed with anti-ZCCHC6 antibody and appropriate HRP-conjugated secondary antibody. The sections were developed with DAB substrate (Pierce), and images were captured with an Olympus VS120 scanning microscope.

Deep sequencing of small RNAs and miRNA 3′ end uridylation analyses. Total RNA from control and ZCCHC6-depleted chondrocytes from 3 different donors was prepared using a miRNeasy kit as described above. RNA samples with RNA integrity numbers of ≥8 were used for deep sequencing. The small RNA library was prepared using a TruSeq small RNA Library Prep Kit according to the instructions of the manufacturer (Illumina), and sequencing was performed on an Illumina MiSeq system using an MiSeq reagent kit. The miRNA 3′-uridylation analysis was performed using Chimira (29).

Transfection of human OA chondrocytes with WT and modified miR-26a/26b mimetics. Standard miR-26a and miR-26b oligos and oligos with addition of 1 or 2 nontemplate uridines were purchased from IDT Inc. Oligo-transfected and mock-transfected human OA chondrocytes were treated with IL-1β for 6 hours, and IL-6 mRNA expression was determined by TaqMan assay.

Statistical analysis. All statistical analyses were performed using GraphPad Prism version 7.04. The significance of differences between groups was calculated by Student's 2-tailed *t*-test for comparisons of 2 groups and by one-way analysis of variance followed by Tukey's post hoc test for comparisons of >2 groups. *P* values less than or equal to 0.05 were considered significant.

RESULTS

Up-regulation of ZCCHC6 in human and mouse OA cartilage and chondrocytes treated with IL-1β. To explore the role of TUTases in OA pathogenesis, we first analyzed the expression profile of ZCCHC6 (TUT-7) and ZCCHC11 (TUT-4) in human OA cartilage. Our data showed that expression levels of both ZCCHC6 and ZCCHC11 were high in damaged cartilage compared to undamaged cartilage from the same patient (Figure 1A). Importantly, the expression of ZCCHC6 was significantly higher than that of ZCCHC11 ($P = 0.02$) (Figure 1A). Consistent with the increased mRNA

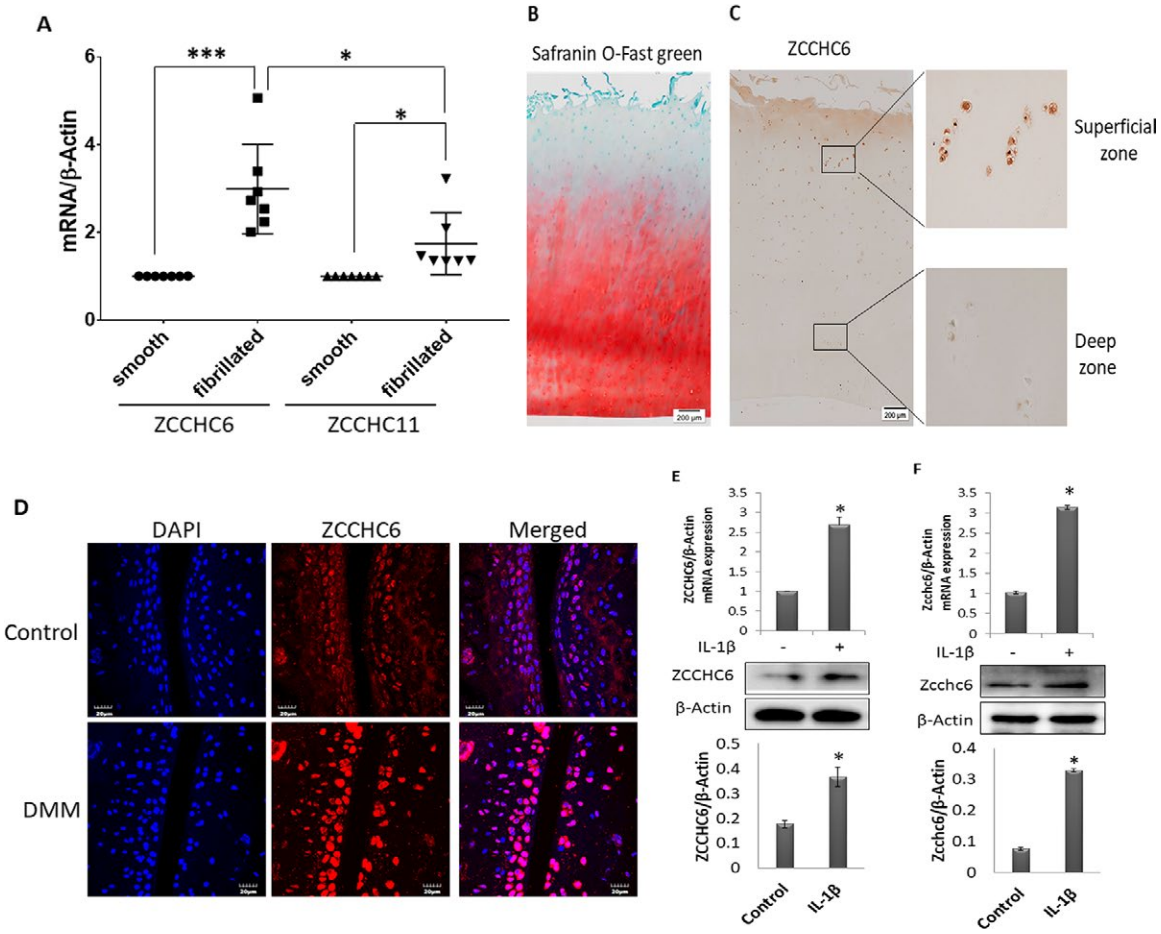

Figure 1. High levels of ZCCHC6 (zinc-finger CCHC domain–containing protein 6) expression in the damaged areas of human and mouse osteoarthritic (OA) cartilage. **A**, Total RNA was prepared from damaged (fibrillated) and undamaged (smooth) areas of human OA cartilage (n = 7), and the expression of ZCCHC6 and ZCCHC11 was determined by TaqMan assay. The data were normalized to β-actin and are represented as the fold change relative to the expression level in smooth cartilage. Symbols represent individual samples; bars show the mean ± SD. **B**, Human OA cartilage sections (n = 5) were stained with Safranin O–fast green. Representative image shows the superficial zone, with excessive loss of proteoglycans compared to the deep zone. Bar = 200 μm. **C**, ZCCHC6 protein expression in human OA cartilage was determined by immunohistochemistry. Bar = 200 μm. The superficial damaged area showed increased expression of ZCCHC6 protein in comparison to the deep zone. Boxed areas in the left panels are shown at higher magnification in the right panels. **D**, OA was induced in the knee joints of male C57BL/6 mice by destabilization of the medial meniscus (DMM), and expression of Zcchc6 was visualized by immunofluorescence staining. The staining showed enhanced expression of Zcchc6 in mouse knee joints with DMM surgery compared to controls. Bars = 20 μm. **E** and **F**, Human (**E**) and mouse (**F**) OA chondrocytes were treated with interleukin-1β (IL-1β), and the expression of ZCCHC6 mRNA and protein was assessed. Values are the mean ± SD (3 independent Western blot experiments in the protein analyses). * = $P < 0.05$; *** = $P < 0.0005$.

expression, immunohistochemistry analysis showed increased numbers of ZCCHC6-positive chondrocytes in the damaged OA cartilage (Figures 1B and C). Similarly, the number of Zcchc6-positive chondrocytes was significantly increased in the cartilage of mice with surgically induced OA (Figure 1D). Additionally, stimulation of both human and mouse chondrocytes with IL-1β caused significant up-regulation of ZCCHC6 mRNA and protein expression (Figures 1E and F).

ZCCHC6 regulation of IL-6 expression in chondrocytes under pathologic conditions. To delineate the target(s) of ZCCHC6 in chondrocytes, a systematic and comprehensive analysis was performed to define the common cytokine(s)/chemokine(s) affected by ZCCHC6 depletion in both human and mouse chondrocytes. A Venn diagram analysis (Figure 2A) of the data derived from cytokine PCR array and multiplex assays (Supplementary Table 1, on the *Arthritis & Rheumatology* web site at http://onlinelibrary.wiley.com/doi/10.1002/art.40751/abstract) from human and mouse chondrocytes indicated that IL-6 is the major cytokine regulated by ZCCHC6. Based on the above analysis and published reports on the role of IL-6 in OA pathogenesis (7,8), we chose to study the regulation of IL-6 by ZCCHC6 in human and mouse chondrocytes by using loss-of-function and gain-of-function approaches. Chondrocytes with siRNA-mediated knockdown of ZCCHC6 (Figure 2B) significantly suppressed

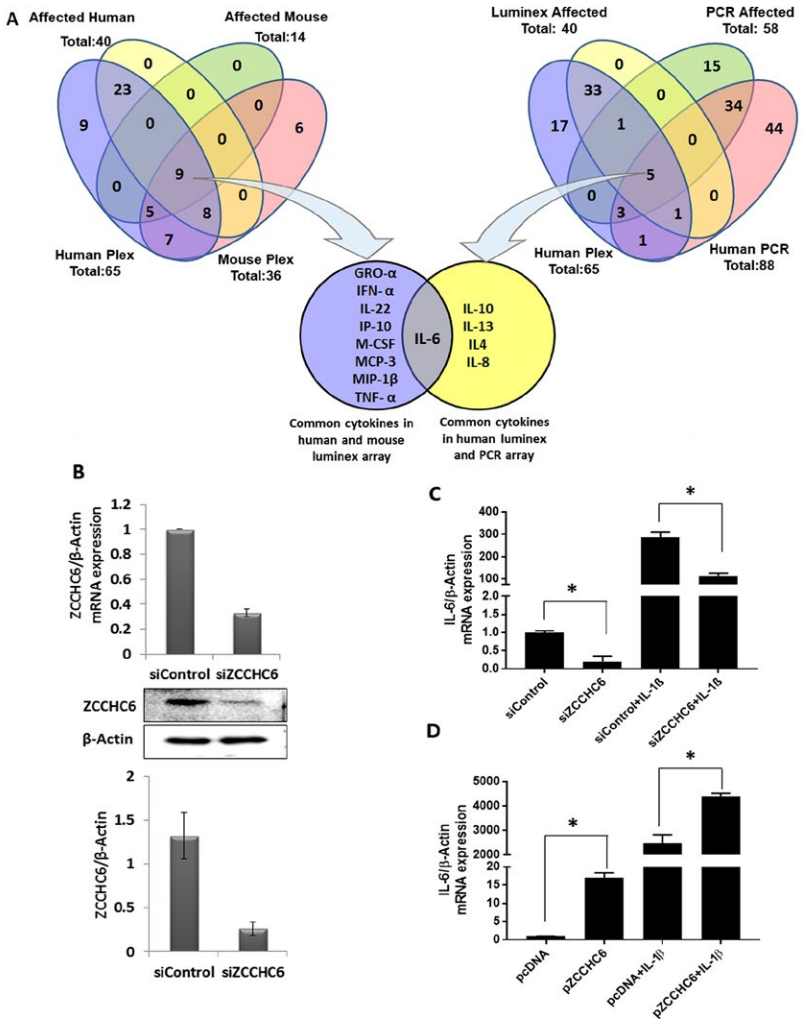

Figure 2. ZCCHC6 regulates IL-6 expression in chondrocytes. **A**, Cytokine multiplex assay (Plex) and quantitative polymerase chain reaction (qPCR) were performed with culture supernatant from ZCCHC6-depleted human chondrocytes and Zcchc6$^{-/-}$ mouse chondrocytes, and total RNA prepared from ZCCHC6-depleted human chondrocytes and their respective controls. Cytokine expression in the 3 different experiments was compared. As seen in the Venn diagrams, IL-6 was the common cytokine down-regulated in both human and mouse chondrocytes. **B**, Small interfering RNA (siRNA)–mediated knockdown of ZCCHC6 at the mRNA and protein levels was confirmed by qPCR and Western blotting, respectively. **C**, Human OA chondrocytes with siRNA-mediated knockdown of ZCCHC6 expressed low levels of constitutive and IL-1β–induced IL-6 compared to controls. **D**, Overexpression of ZCCHC6 in human OA chondrocytes increased constitutive and IL-1β–induced expression of IL-6. Values are the mean ± SD. * = $P < 0.05$. GROα = growth-related oncogene α; IFNα = interferon-α; IP-10 = interferon-γ–inducible 10-kd protein; M-CSF = macrophage colony-stimulating factor; MCP-3 = monocyte chemotactic protein 3; MIP-1β = macrophage inflammatory protein 1β; TNF = tumor necrosis factor (see Figure 1 for other definitions). Color figure can be viewed in the online issue, which is available at http://onlinelibrary.wiley.com/doi/10.1002/art.40751/abstract.

the expression of constitutive and IL-1β–induced IL-6 mRNA and protein expression (Figure 2C and Supplementary Figure 1, http://onlinelibrary.wiley.com/doi/10.1002/art.40751/abstract). Furthermore, human OA chondrocytes with overexpression of ZCCHC6 (Supplementary Figure 2, http://onlinelibrary.wiley.com/doi/10.1002/art.40751/abstract) showed significantly increased constitutive expression of IL-6, which was further increased by severalfold upon stimulation with IL-1β (Figure 2D).

To determine whether the observed effect of ZCCHC6 knockdown and overexpression is specific to ZCCHC6 or if other TUTases also regulate IL-6 expression, we knocked down the expression of TUT-1 and TUT-2 in human OA chondrocytes using siRNAs and examined the expression of IL-6 mRNA. Interestingly knockdown of TUT-1 and TUT-2 expression did not suppress the expression of IL-6 (Supplementary Figure 3, http://onlinelibrary.wiley.com/doi/10.1002/art.40751/abstract), demonstrating that the observed effect in chondrocytes with knockdown of ZCCHC6 expression was ZCCHC6 specific. Of importance is our finding that knockdown of ZCCHC6 did not alter the expression of ZCCHC11 (Supplementary Figure 4, http://onlinelibrary.wiley.com/doi/10.1002/art.40751/abstract). Taken together, the above data demonstrated that ZCCHC6 plays an essential role in the regulation of IL-6 expression in OA chondrocytes under pathologic conditions.

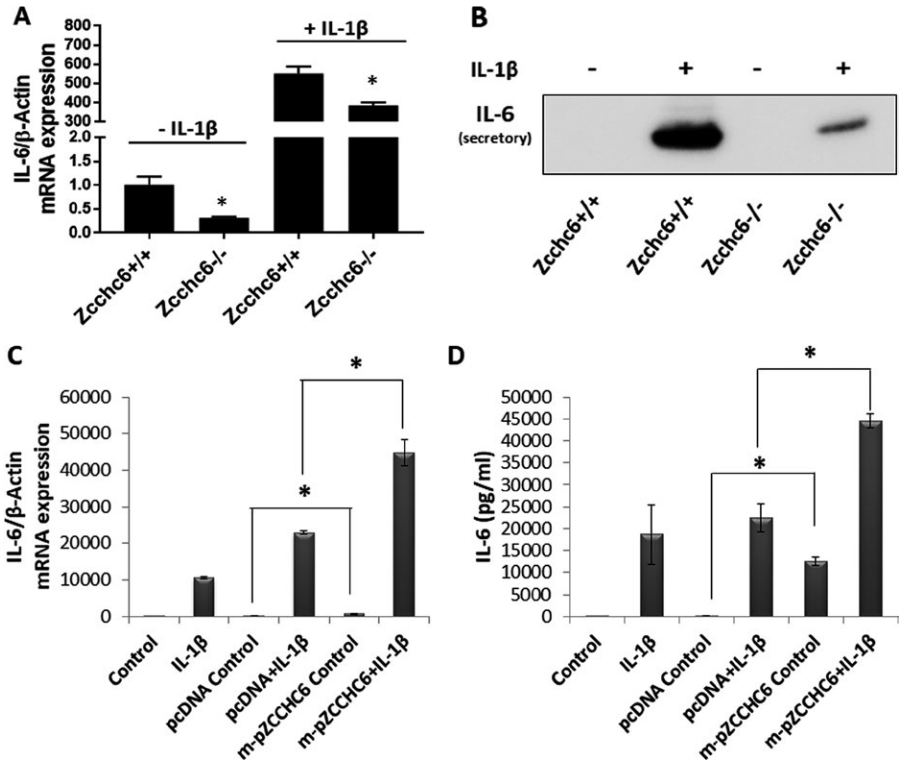

Figure 3. Zcchc6$^{-/-}$ mouse chondrocytes express low levels of IL-6 upon stimulation with interleukin-1β (IL-1β). **A**, Chondrocytes from the knee joints of Zcchc6$^{-/-}$ mice and Zcchc6$^{+/+}$ littermates were either left untreated or treated with IL-1β. Expression of IL-6 mRNA was downregulated in Zcchc6$^{-/-}$ mouse chondrocytes compared to Zcchc6$^{+/+}$ mouse chondrocytes, in both the presence and the absence of IL-1β. **B**, IL-6 protein expression in the culture supernatant was determined by Western blotting. The results showed reduced levels of IL-6 protein in Zcchc6$^{-/-}$ mouse chondrocyte culture supernatant. **C** and **D,** Zcchc6$^{-/-}$ mouse chondrocytes were transfected with mouse (m) Zcchc6 overexpression plasmid, followed by stimulation with IL-1β; pcDNA was used as control. Zcchc6 expression restored constitutive and induced expression of IL-6 mRNA (**C**) and protein (**D**) in Zcchc6$^{-/-}$ mouse chondrocytes. Experiments were repeated at least 3 times. Values are the mean ± SD. * = $P < 0.05$.

To investigate whether ZCCHC6 also regulates the expression of IL-6 in mouse chondrocytes, we prepared articular cartilage chondrocytes from Zcchc6$^{-/-}$ mice and corresponding WT (Zcchc6$^{+/+}$) littermates and assessed the expression of IL-6 as described above. Similar to the data obtained with human chondrocytes, expression of IL-6 in Zcchc6$^{-/-}$ mouse chondrocyte was significantly reduced in comparison to the levels detected in Zcchc6$^{+/+}$ mouse chondrocytes (Figure 3A). Stimulation of mouse chondrocytes with IL-1β resulted in significant increases in the expression of IL-6 mRNA and protein in both Zcchc6$^{+/+}$ and Zcchc6$^{-/-}$ mouse chondrocytes; however, IL-6 expression in Zcchc6$^{-/-}$ mouse chondrocytes remained significantly low compared to the levels in Zcchc6$^{+/+}$ mouse chondrocytes (Figures 3A and B). To confirm that the observed effect on IL-6 expression was due to depletion of Zcchc6, chondrocytes prepared from Zcchc6$^{-/-}$ mice were transfected with Zcchc6 expression plasmid, and expression of IL-6 was determined. Restoration of Zcchc6 expression in Zcchc6$^{-/-}$ mouse chondrocytes not only rescued, but also increased, the constitutive and IL-1β–induced expression of IL-6 (Figures 3C and D), indicating that Zcchc6 is an important regulator of IL-6 expression in chondrocytes.

ZCCHC6 binds IL-6 mRNA transcripts in chondrocytes. Zinc-finger–containing proteins, such as ZCCHC6, are known to bind to RNA (30), but the binding of ZCCHC6 to IL-6 mRNA has not been reported. We performed an RNA immunoprecipitation assay and found significant enrichment of IL-6 mRNA in the anti-ZCCHC6 antibody pulldown fractions compared to control IgG pulldown fractions (Figure 4A). We further confirmed the binding of ZCCHC6 protein with IL-6 mRNA in colocalization studies using immunofluorescence staining of ZCCHC6 protein and fluorescence in situ hybridization of IL-6 mRNA. In these experiments we found that IL-6 mRNA colocalized with the ZCCHC6 protein in human chondrocytes (Supplementary Figure 5, on the *Arthritis & Rheumatology* web site at http://onlinelibrary.wiley.com/doi/10.1002/art.40751/abstract).

Essential role of ZCCHC6 in maintaining the poly(A) tail lengths and stability of IL-6 mRNA transcripts in chondrocytes. Poly(A) tail length of mammalian mRNA functions as an important determinant of mRNA stability and translation (31). Since ZCCHC6 is a noncanonical poly(A) polymerase and our data demonstrated its binding with IL-6 mRNA (Fig-

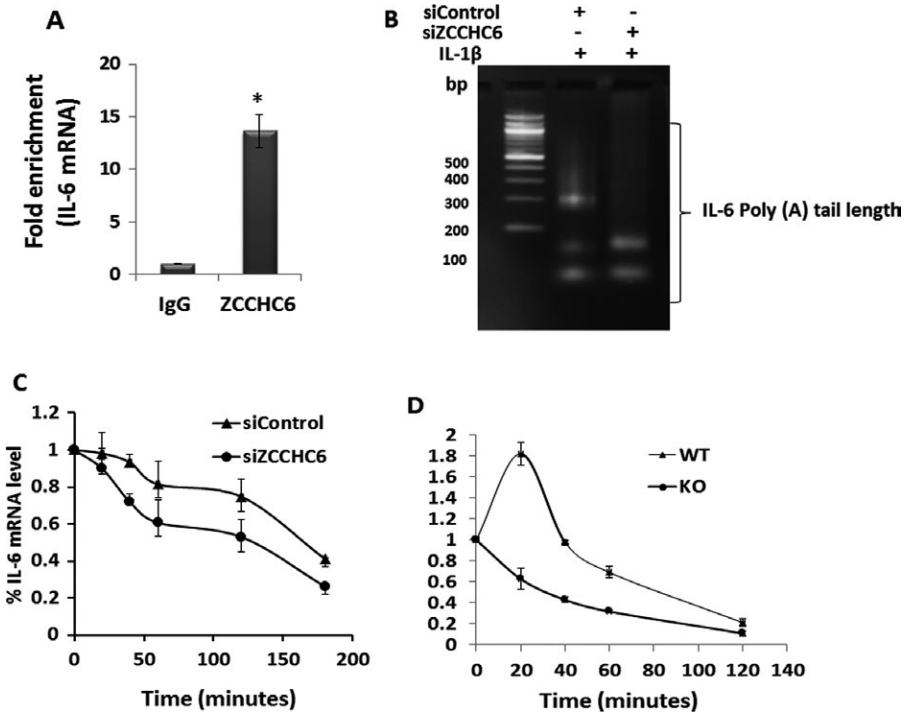

Figure 4. ZCCHC6 binds to IL-6 mRNA and regulates its stability. **A**, Human OA chondrocytes were stimulated with IL-1β for 6 hours and harvested for RNA immunoprecipitation assay (RIPA) using anti-ZCCHC6 antibody. RIPA showed significant enrichment of IL-6 mRNA with anti-ZCCHC6 antibody compared to IgG (negative control). * = $P < 0.05$. **B**, Poly(A) tail length of IL-6 mRNA was reduced in ZCCHC6-depleted human OA chondrocytes. **C**, ZCCHC6-depleted human OA chondrocytes showed a significantly reduced half-life of IL-6 mRNA ($t_{½}$ 83.18 ± 10.29 minutes with ZCCHC6 small interfering RNA [siRNA], versus 157.74 ± 5.33 minutes with control siRNA; $P < 0.05$). **D**, Zcchc6$^{-/-}$ mouse chondrocytes also showed a significantly reduced half-life of IL-6 mRNA ($t_{½}$ 28.68 ± 1.5 minutes in chondrocytes from Zcchc6$^{-/-}$ mice, versus 55.37 ± 5.4 minutes in chondrocytes from Zcchc6$^{+/+}$ mice; $P < 0.05$). Experiments were repeated at least 3 times. Values are the mean ± SD. WT = wild-type; KO = knockout (see Figure 1 for other definitions).

ure 4A), we investigated whether it plays a role in maintaining the poly(A) tail length of IL-6 mRNA in human chondrocytes, using a loss-of-function approach. In human chondrocytes with knockdown of ZCCHC6 expression, the poly(A) tail length of IL-6 mRNA was decreased (Figure 4B). This suggested that in the absence of ZCCHC6, IL-6 mRNA may not be stable and may have a shorter half-life. To test this, human OA chondrocytes with siRNA-mediated knockdown of ZCCHC6 were stimulated with IL-1β, after which actinomycin D chase experiments were performed. The mean ± SD half-life ($t_{½}$) of IL-6 mRNA in control chondrocytes was found to be 157.74 ± 5.33 minutes; this was reduced to 83.18 ± 10.29 minutes in chondrocytes with siRNA-mediated knockdown of ZCCHC6 (Figure 4C). In accordance with these findings, Zcchc6$^{-/-}$ mouse chondrocytes that were stimulated with IL-1β also showed almost a 50% reduction in the half-life of IL-6 mRNA ($t_{½}$ 28.68 ± 1.5 minutes, versus 55.37 ± 5.4 minutes in WT mouse chondrocytes) (Figure 4D). In summary, our experiments showed that absence of ZCCHC6 negatively affects the poly(A) tail length and the stability of IL-6 mRNA in chondrocytes, suggesting that maintaining the poly(A) tail length is a step through which ZCCHC6 regulates IL-6 expression.

ZCCHC6 knockdown reduces the 3′-uridylation of IL-6–targeting miRNAs. Previous studies have demonstrated that the closely homologous enzyme ZCCHC11 regulates the expression of IL-6 by 3′-uridylation of miRNAs (19). Since ZCCHC6 has been shown to uridylate RNAs (31), we investigated whether it plays a role in maintaining high levels of IL-6 expression through the inactivation of miRNAs that repress IL-6 expression via nontemplate additions of uridines at the 3′ ends. We analyzed the 3′-uridylation of miRNAs at a global level in ZCCHC6-depleted chondrocytes by deep sequencing. Data analyses using the online miRNA modification analysis tool Chimira (29) showed that ZCCHC6 depletion in human OA chondrocytes resulted in a global reduction of 3′– mono- and di-uridylation of miRNAs (Supplementary Figure 6, http://onlinelibrary.wiley.com/doi/10.1002/art.40751/abstract).

Since our aim was to investigate the regulation of IL-6 expression, we chose miR-26a and miR-26b, which are known to repress IL-6 expression (19) by binding to the highly conserved "seed sequence" present in the 3′-UTR of IL-6 mRNA (Figure 5A). We first determined the expression levels of miR-26a and miR-26b miRNAs in human chondrocytes with depleted expression of ZCCHC6 and found that these levels were not affected (Figure 5B).

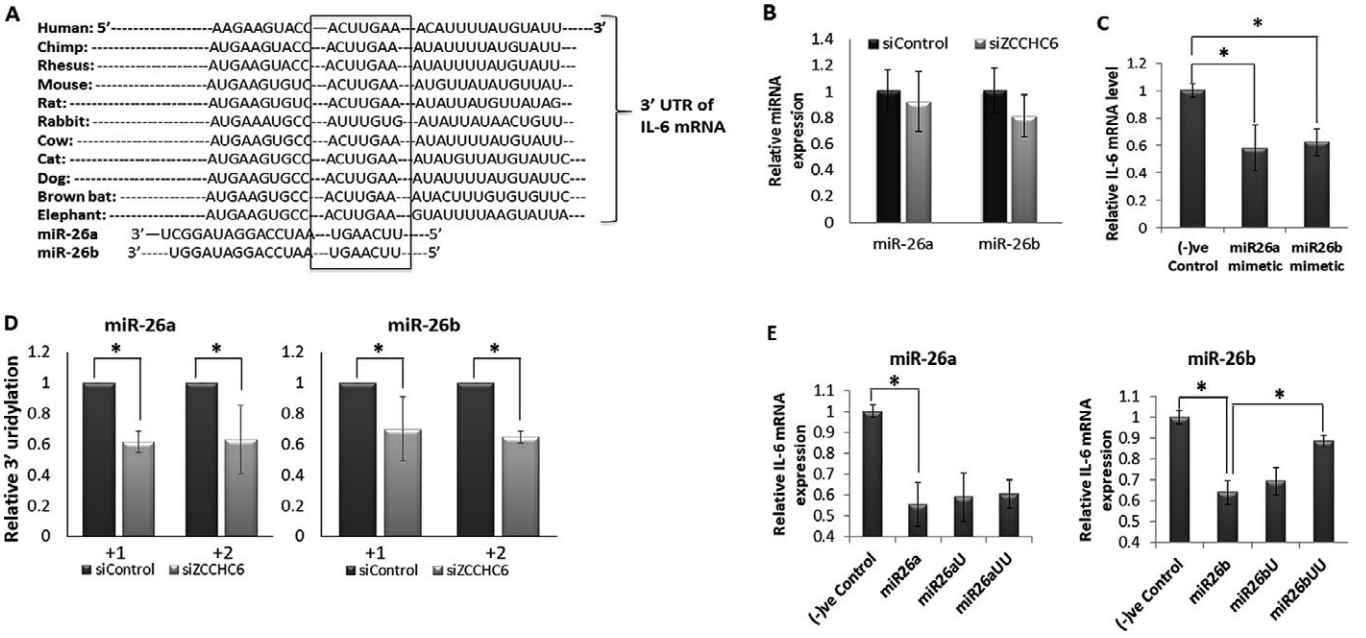

Figure 5. IL-6 mRNA expression in chondrocytes is regulated by the 26a/b family of microRNAs (miR26a/b). **A**, Targetscan prediction showed a conserved site for miR26a/b in the 3′-untranslated region (3′-UTR) of IL-6 mRNA. **B**, The expression levels of miR26a and miR26b were not altered in human chondrocytes with knockdown of ZCCHC6 (via small interfering RNA [siZCCHC6]). **C**, Expression of miR26a and miR26b suppressed the IL-1β–induced expression of IL-6 in human OA chondrocytes. **D**, 3′-uridylation analyses of miR26a and miR26b by deep sequencing showed decreased uridylation at the +1 and +2 positions. **E**, Human OA chondrocytes were transfected with miR26a or miR26b mimetics and with miR26a and miR26b mimetics with additional mono- or di-uridines (U or UU) at the 3′ ends, followed by treatment with IL-1β for 6 hours. Scrambled oligo was used as a negative control. Quantitative polymerase chain reaction analysis showed that miR26b mimetics with di-uridine at the 3′ end (UU) failed to suppress IL-1β–induced expression of IL-6 mRNA. Experiments were repeated with chondrocytes from at least 3 OA donors. Values are the mean ± SD. * = $P < 0.05$. See Figure 1 for other definitions.

Further, overexpression of miR-26a and miR-26b suppressed the IL-1β–induced expression of IL-6 in human OA chondrocytes (Figure 5C). We next analyzed the deep sequencing data to investigate the 3′-uridylation of miR-26a and miR-26b miRNAs and discovered that the 3′-uridylation of miR-26a/26b miRNAs at the +1 and +2 positions was significantly decreased in ZCCHC6-depleted chondrocytes (Figure 5D). To test whether 3′-uridylation of miR-26a and miR-26b abrogates their suppressive effects in chondrocytes, we used miR-26a and miR-26b mimetics with additional mono-uridines (U) or di-uridines (UU) at their 3′ end and determined their ability to suppress IL-1β–induced expression of IL-6 in human chondrocytes. Interestingly, we observed that addition of uridines at the 3′ end of miR-26b, but not of miR-26a, abrogated the suppression of IL-1β–induced IL-6 expression in human OA chondrocytes (Figure 5E). Taken together, these findings suggest that the increased expression of IL-6 may result from inactivation of miR-26b by 3′-uridylation due to increased expression and activity of ZCCHC6 in chondrocytes under pathologic conditions.

Genetic inactivation of Zcchc6 abrogates OA pathogenesis. We used Zcchc6$^{-/-}$ mice to investigate the role of Zcchc6 in regulating IL-6 expression and OA pathogenesis in vivo. Zcchc6$^{-/-}$ mice were born in Mendelian ratios without any overt abnormalities. Since female mice are resistant to the development of OA (32), we performed DMM surgery on 12-week-old male Zcchc6$^{+/+}$ and Zcchc6$^{-/-}$ mice and assessed the effect of Zcchc6 inactivation on the severity of OA 8 weeks post-DMM. We used serial sections of frontally embedded knee joints, harvested at 80-μ*M* intervals, for histologic scoring, and intervening sections were used to analyze the expression of IL-6 by immunohistochemistry. Our results showed that compared to WT littermates, Zcchc6$^{-/-}$ mice exhibited low levels of IL-6 in the joints with DMM-induced OA (Figure 6A). Additionally, cartilage erosion was significantly reduced in Zcchc6$^{-/-}$ mice compared to WT littermates (Figure 6B). OARSI scoring further confirmed a significant reduction in cartilage damage in Zcchc6$^{-/-}$ mice (Figure 6C). We additionally found that synovitis was reduced in these mice (Figures 6D and E), and IL-6 expression in the synovium was decreased (Figure 6F). There was also a significant reduction in osteophyte thickness (Figure 6G). Overall, these results support the conclusion that Zcchc6 plays a critical role in disease pathogenesis through up-regulated expression of IL-6 in mice with DMM-induced OA.

DISCUSSION

A hallmark of OA is the progressive and irreversible cartilage degradation due to enhanced production of inflammatory

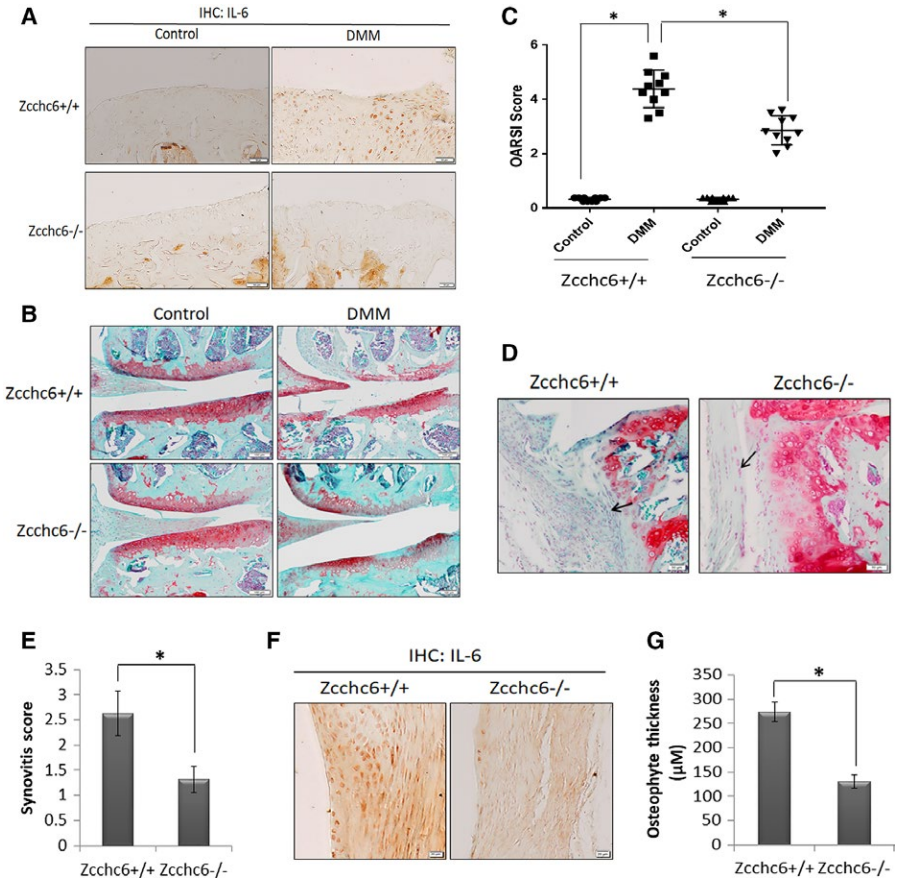

Figure 6. Zcchc6 inactivation reduces the severity of experimental OA in mice. **A**, Twelve-week-old male Zcchc6$^{-/-}$ or Zcchc6$^{+/+}$ C57BL/6 mice (n = 10 per group) were subjected to DMM surgery of the right knee to induce OA, with the left knee used as a control. Mice were killed 8 weeks after DMM surgery, and joints were collected and processed for histologic analysis. Immunohistochemistry (IHC) studies with anti–IL-6 antibody showed decreased expression of IL-6 protein in the operated joints from Zcchc6$^{-/-}$ mice compared to Zcchc6$^{+/+}$ mice. Bars = 50 μm. **B**, Loss of proteoglycans in the knee joints with surgically induced OA was analyzed by Safranin O–fast green staining. The results showed less of a decrease in proteoglycan staining in the joints of Zcchc6$^{-/-}$ with DMM compared to those of Zcchc6$^{+/+}$ mice with DMM. Bars = 100 μm. **C**, OA was scored according to the Osteoarthritis Research Society International (OARSI) grading system. Zcchc6 deletion exhibited a protective effect on cartilage degeneration in mice with surgically induced OA. **D** and **E**, Synovium from Zcchc6$^{-/-}$ and Zcchc6$^{+/+}$ littermates with surgically induced OA was analyzed by staining with Safranin O–hematoxylin (**D**) (bars = 50 μm), and the results were quantified (**E**). Synovial thickness and synovitis were significantly reduced in Zcchc6$^{-/-}$ mice. **F**, Immunohistochemistry analysis of Zcchc6$^{-/-}$and Zcchc6$^{+/+}$ mouse joints with surgically induced OA showed reduced expression of IL-6 in the synovium of Zcchc6$^{-/-}$ mice. Bars = 20 μm. **G**, Osteophyte thickness was significantly reduced in the operated joints from Zcchc6$^{-/-}$ mice compared to Zcchc6$^{+/+}$ mice. In **C**, symbols represent individual samples; bars show the mean ± SD. In **E** and **G**, values are the mean ± SD. * = $P < 0.005$. See Figure 1 for other definitions.

cytokines, such as IL-6, by activated chondrocytes, which in turn amplifies the inflammatory effect in the involved joints and induces expression of several cartilage extracellular matrix–degrading enzymes. The overall cytokine repertoire of OA synovial fluid has been shown to be primarily dependent on the extent of disease (5). Importantly, our results showed that human chondrocyte cultures derived from pathologic cartilage samples produced a cytokine repertoire that included elevated levels of IL-6 (Supplementary Table 1, on the *Arthritis & Rheumatology* web site at http://onlinelibrary.wiley.com/doi/10.1002/art.40751/abstract), mirroring the cytokine repertoire in OA synovial fluid (2). Highly elevated levels of IL-6 were also detected in knee cartilage from OA patients (3) and were found to positively correlate with the degree of radiographic damage (4).

Cytokines are central mediators of tissue inflammation and their expression is tightly regulated at various levels, including transcriptional, posttranscriptional, and translational levels. Our group has demonstrated previously that various transcription factors, including NF-κB and activator protein 1, regulate the expression of IL-6 at the transcriptional level in human chondrocytes (33,34). Posttranscriptional regulation by RNA binding proteins and miRNAs has been shown to play a vital role in controlling the expression of cytokines by modulating mRNA stability and translation (12). ZCCHC6 and its homolog, ZCCHC11, have been

reported to uridylate and alter the stability of mRNAs in HeLa cells (18). It was also found that ZCCHC11 knockdown in A549 cells down-regulated the expression of IL-6 (19). However; the involvement of ZCCHC6 or any other TUTase in regulating IL-6 gene expression in chondrocytes and its role in OA pathogenesis have not been reported.

In the present study, we used loss-of-function and gain-of-function approaches to investigate the potential role of ZCCHC6 in the posttranscriptional regulation of IL-6 expression. Our data showed that ZCCHC6 down-regulation in human OA chondrocytes significantly reduced the expression of IL-6 mRNA and protein. This is similar to the effect of ZCCHC11 depletion in A549 cells (19). We further found that, in accordance with the observations in human OA chondrocytes, the expression of IL-6 in Zcchc6-deficient mouse chondrocytes was also down-regulated in both in vitro and in vivo studies (Figure 3). In contrast to the results reported here, a recent study showed increased expression of IL-6 in Zcchc6-deficient mouse macrophages (20), indicating cell type– and context-specific regulation of IL-6 expression by Zcchc6 in vivo.

The poly(A) tail length of eukaryotic mRNA is a critical determinant of transcript stability and translational efficiency (35). We found that IL-6 mRNA had a shorter poly(A) tail length in chondrocytes with ZCCHC6 depletion, indicating that ZCCHC6 functions in maintaining IL-6 transcript stability and translation. This is supported by our demonstration that overexpression of ZCCHC6 in human chondrocytes up-regulated the expression of IL-6 mRNA and protein. To our knowledge, this has not been shown in any cell type before. This activity of ZCCHC6 in maintaining the poly(A) tail lengths of IL-6 mRNA in chondrocytes mimics that of ZCCHC11 in immune cells (19). Since ZCCHC11 expression was not altered in chondrocytes with knockdown of ZCCHC6, and knockdown of TUT-1 and TUT-2 did not affect IL-6 mRNA expression, the down-regulation of IL-6 expression appears to be specific to ZCCHC6 knockdown in chondrocytes. We postulate that these enzymes may have cell-specific nonredundant functions as well.

Cytokine expression is tightly regulated by miRNAs (12), and ZCCHC6 and ZCCHC11 both have been shown to regulate the expression of various cytokines by altering miRNA biogenesis and stability (17). ZCCHC6 has been found to selectively uridylate miRNAs and modulate their stability and mRNA-repressive activity (36,37). Interestingly, we found that ZCCHC6 knockdown in human OA chondrocytes decreased the 3′-uridylation of miRNAs, with significant reduction in the population of 3′-uridylated miR-26b. Furthermore, we showed that a miR-26b mimetic with additional UU (di-uridines) at the 3′ end did not suppress the expression of IL-6 mRNA. This indicates that the miR-26b with 2 uridines at the 3′ end found in our RNA-Seq analyses represents the miR-26b population that is incapable of suppressing IL-6 expression and identifies a mechanism through which increased ZCCHC6 activity contributes to increased IL-6 expression in chondrocytes under pathologic conditions.

Our results are consistent with those of another study in which it was found that 3′-uridylation of miR-26b abrogated IL-6 mRNA–repressive activity in A549 cells (19). As IL-6 plays an important role in the OA pathogenesis, we also investigated whether its inhibition may prevent cartilage damage in OA. Indeed, we found that the expression of IL-6 and damage to cartilage were both significantly reduced in Zcchc6$^{-/-}$ mice that had undergone DMM surgery. These results strongly support the hypothesis that Zcchc6 contributes to OA pathogenesis by facilitating increased expression of IL-6 in chondrocytes. However; our data on IL-6 do not rule out the possibility that ZCCHC6 regulates other OA-related genes as well, and this will be investigated in future studies.

In summary, the present study is the first in vivo analysis of the effects of ZCCHC6 on IL-6 expression in articular cartilage chondrocytes and its role in OA pathogenesis. We demonstrated that genetic inactivation of Zcchc6 reduced IL-6 expression and cartilage damage in a mouse model of OA. Additionally, we found that the expression patterns of ZCCHC6 and IL-6 were similar in human and mouse OA cartilage. Taken together, these data demonstrate a previously unknown function of ZCCHC6 in regulating IL-6 expression in chondrocytes and thus a potential role of this enzyme in OA pathogenesis and identify a potential therapeutic target for the management of OA.

AUTHOR CONTRIBUTIONS

All authors were involved in drafting the article or revising it critically for important intellectual content, and all authors approved the final version to be published. Dr. Haqqi had full access to all of the data in the study and takes responsibility for the integrity of the data and the accuracy of the data analysis.

Study conception and design. Ansari, Khan, Ahmad, Green, Novak, Haqqi.

Acquisition of data. Ansari, Khan, Haqqi.

Analysis and interpretation of data. Ansari, Khan, Ahmad, Green, Novak, Haqqi.

REFERENCES

1. Loeser RF, Collins JA, Diekman BO. Aging and the pathogenesis of osteoarthritis. Nat Rev Rheumatol 2016;12:412–20.
2. Malemud CJ. Biologic basis of osteoarthritis: state of the evidence. Curr Opin Rheumatol 2015;27:289–94.
3. Moktar NM, Yusof HM, Yahaya NH, Muhamad R, Das S. The transcript level of interleukin-6 in the cartilage of idiopathic osteoarthritis of knee. Clin Ter 2010;161:25–8.
4. Orita S, Koshi T, Mitsuka T, Miyagi M, Inoue G, Arai G, et al. Associations between proinflammatory cytokines in the synovial fluid and radiographic grading and pain-related scores in 47 consecutive patients with osteoarthritis of the knee. BMC Musculoskelet Disord 2011;12:144.
5. Tsuchida AI, Beekhuizen M, 't Hart MC, Radstake TR, Dhert WJ, Saris DB, et al. Cytokine profiles in the joint depend on pathology, but are different between synovial fluid, cartilage tissue and cultured chondrocytes. Arthritis Res Ther 2014;16:441.

6. Livshits G, Zhai G, Hart DJ, Kato BS, Wang H, Williams FM, et al. Interleukin-6 is a significant predictor of radiographic knee osteoarthritis: the Chingford Study. Arthritis Rheum 2009;60: 2037–45.
7. Ryu JH, Yang S, Shin Y, Rhee J, Chun CH, Chun JS. Interleukin-6 plays an essential role in hypoxia-inducible factor 2α–induced experimental osteoarthritic cartilage destruction in mice. Arthritis Rheum 2011;63:2732–43.
8. Poree B, Kypriotou M, Chadjichristos C, Beauchef G, Renard E, Legendre F, et al. Interleukin-6 (IL-6) and/or soluble IL-6 receptor down-regulation of human type II collagen gene expression in articular chondrocytes requires a decrease of Sp1.Sp3 ratio and of the binding activity of both factors to the COL2A1 promoter. J Biol Chem 2008;283:4850–65.
9. Latourte A, Cherifi C, Maillet J, Ea HK, Bouaziz W, Funck-Brentano T, et al. Systemic inhibition of IL-6/Stat3 signalling protects against experimental osteoarthritis. Ann Rheum Dis 2017;76:748–55.
10. Nasi S, So A, Combes C, Daudon M, Busso N. Interleukin-6 and chondrocyte mineralisation act in tandem to promote experimental osteoarthritis. Ann Rheum Dis 2016;75:1372–9.
11. Kovarik P, Ebner F, Sedlyarov V. Posttranscriptional regulation of cytokine expression. Cytokine 2017;89:21–6.
12. Palanisamy V, Jakymiw A, van Tubergen EA, D'Silva NJ, Kirkwood KL. Control of cytokine mRNA expression by RNA-binding proteins and microRNAs. J Dent Res 2012;91:651–8.
13. Mullen TE, Marzluff WF. Degradation of histone mRNA requires oligouridylation followed by decapping and simultaneous degradation of the mRNA both 5′ to 3′ and 3′ to 5′. Genes Dev 2008;22:50–65.
14. Rissland OS, Norbury CJ. Decapping is preceded by 3′ uridylation in a novel pathway of bulk mRNA turnover. Nat Struct Mol Biol 2009;16:616–23.
15. Shen B, Goodman HM. Uridine addition after microRNA-directed cleavage. Science 2004;306:997.
16. Thornton JE, Chang HM, Piskounova E, Gregory RI. Lin28-mediated control of let-7 microRNA expression by alternative TUTases Zcchc11 (TUT4) and Zcchc6 (TUT7). RNA 2012;18:1875–85.
17. Kim B, Ha M, Loeff L, Chang H, Simanshu DK, Li S, et al. TUT7 controls the fate of precursor microRNAs by using three different uridylation mechanisms. EMBO J 2015;34:1801–15.
18. Lim J, Ha M, Chang H, Kwon SC, Simanshu DK, Patel DJ, et al. Uridylation by TUT4 and TUT7 marks mRNA for degradation. Cell 2014;159:1365–76.
19. Jones MR, Quinton LJ, Blahna MT, Neilson JR, Fu S, Ivanov AR, et al. Zcchc11-dependent uridylation of microRNA directs cytokine expression. Nat Cell Biol 2009;11:1157–63.
20. Kozlowski E, Wasserman GA, Morgan M, O'Carroll D, Ramirez NP, Gummuluru S, et al. The RNA uridyltransferase Zcchc6 is expressed in macrophages and impacts innate immune responses. PLoS One 2017;12:e0179797.
21. Ansari MY, Khan NM, Ahmad I, Haqqi TM. Parkin clearance of dysfunctional mitochondria regulates ROS levels and increases survival of human chondrocytes. Osteoarthritis Cartilage 2018;26: 1087–97.
22. Gosset M, Berenbaum F, Thirion S, Jacques C. Primary culture and phenotyping of murine chondrocytes. Nat Prot 2008;3:1253–60.
23. Glasson SS, Blanchet TJ, Morris EA. The surgical destabilization of the medial meniscus (DMM) model of osteoarthritis in the 129/SvEv mouse. Osteoarthritis Cartilage 2007;15:1061–9.
24. Glasson SS, Chambers MG, van den Berg WB, Little CB. The OARSI histopathology initiative: recommendations for histological assessments of osteoarthritis in the mouse. Osteoarthritis Cartilage 2010;18 Suppl 3:S17–23.
25. Kim JH, Jeon J, Shin M, Won Y, Lee M, Kwak JS, et al. Regulation of the catabolic cascade in osteoarthritis by the zinc-ZIP8-MTF1 axis. Cell 2014;156:730–43.
26. Rissland OS, Mikulasova A, Norbury CJ. Efficient RNA polyuridylation by noncanonical poly(A) polymerases. Mol Cell Biol 2007;27:3612–24.
27. Ansari MY, Haqqi TM. Interleukin-1β induced stress granules sequester COX-2 mRNA and regulates its stability and translation in human OA chondrocytes. Sci Rep 2016;6:27611.
28. Ansari MY, Khan NM, Haqqi TM. A standardized extract of Butea monosperma (Lam.) flowers suppresses the IL-1β-induced expression of IL-6 and matrix-metalloproteases by activating autophagy in human osteoarthritis chondrocytes. Biomed Pharmacother 2017;96:198–207.
29. Vitsios DM, Enright AJ. Chimira: analysis of small RNA sequencing data and microRNA modifications. Bioinformatics 2015;31:3365–7.
30. Brown RS. Zinc finger proteins: getting a grip on RNA. Curr Opin Struct Biol 2005;15:94–8.
31. Norbury CJ. Cytoplasmic RNA: a case of the tail wagging the dog. Nat Rev Mol Cell Biol 2013;14:643–53.
32. Ma HL, Blanchet TJ, Peluso D, Hopkins B, Morris EA, Glasson SS. Osteoarthritis severity is sex dependent in a surgical mouse model. Osteoarthritis Cartilage 2007;15:695–700.
33. Haseeb A, Ansari MY, Haqqi TM. Harpagoside suppresses IL-6 expression in primary human osteoarthritis chondrocytes. J Orthop Res 2017;35:311–20.
34. Rasheed Z, Akhtar N, Haqqi TM. Advanced glycation end products induce the expression of interleukin-6 and interleukin-8 by receptor for advanced glycation end product-mediated activation of mitogen-activated protein kinases and nuclear factor-κB in human osteoarthritis chondrocytes. Rheumatology (Oxford) 2011;50:838–51.
35. Meyer S, Temme C, Wahle E. Messenger RNA turnover in eukaryotes: pathways and enzymes. Crit Rev Biochem Mol Biol 2004;39:197–216.
36. Thornton JE, Du P, Jing L, Sjekloca L, Lin S, Grossi E, et al. Selective microRNA uridylation by Zcchc6 (TUT7) and Zcchc11 (TUT4). Nucleic Acids Res 2014;42:11777–91.
37. Jones MR, Blahna MT, Kozlowski E, Matsuura KY, Ferrari JD, Morris SA, et al. Zcchc11 uridylates mature miRNAs to enhance neonatal IGF-1 expression, growth, and survival. PLoS Genet 2012;8:e1003105.

Arthritis & Rheumatology
Vol. 71, No. 4, April 2019, pp 594–598
DOI 10.1002/art.40750

AMERICAN COLLEGE OF RHEUMATOLOGY
EDUCATION • TREATMENT • RESEARCH

BRIEF REPORT

Sacroiliac Joint Ankylosis in Young Spondyloarthritis Patients Receiving Biologic Therapy: Observation of Serial Magnetic Resonance Imaging Scans

Timothy J. P. Bray, Andre Lopes, Corinne Fisher, Coziana Ciurtin, Debajit Sen, and Margaret A. Hall-Craggs

Objective. To assess the temporal relationship between initiating biologic therapy and magnetic resonance imaging (MRI) scores of inflammation and structural damage in young patients with spondyloarthritis.

Methods. A local adolescent/young adult patient rheumatology database was searched for patients ages 12–24 years who had evidence of sacroiliitis on MRI and a clinical diagnosis of enthesitis-related arthritis (ERA) with axial involvement or nonradiographic axial spondyloarthritis. Patients treated with tumor necrosis factor inhibitor (TNFi) therapy who had undergone a minimum of 1 MRI scan before and 2 MRI scans after starting TNFi therapy (over ≥2 years) were included. Images of the sacroiliac joints were scored for inflammation and structural abnormalities (including erosions, fat metaplasia, and fusion). The effects of TNFi therapy and of time since initiation of TNFi therapy on inflammation and structural abnormalities were assessed using a mixed-effects regression analysis.

Results. Twenty-nine patients (ages 12–23 years) with ERA or nonradiographic axial spondyloarthritis who underwent TNFi therapy were included. Inflammation scores were significantly lower in patients receiving TNFi treatment ($P = 0.013$), but there was no significant effect of time from TNFi initiation on inflammation ($P = 0.125$). Conversely, there was no significant effect of active TNFi treatment on fusion scores ($P = 0.308$), but fusion scores significantly increased with time from TNFi initiation ($P < 0.001$); a similar positive relationship between time since biologic start and fat metaplasia scores was observed.

Conclusion. TNFi therapy failed to prevent the eventual development of joint ankylosis in this cohort of young patients with spondyloarthritis, despite a substantial reduction in inflammation with TNFi therapy.

INTRODUCTION

The spondyloarthritides are a group of immune-mediated inflammatory disorders that are characterized by inflammation of the spine, entheses, and peripheral joints. Ankylosing spondylitis (AS) is the "prototypic" spondyloarthritis and causes ankylosis (fusion) of the axial skeleton with subsequent disability, morbidity, and impaired quality of life (1). However, ankylosis may be less severe or absent in other spondyloarthritis subgroups, suggesting that these groups represent a milder or earlier form of the disease (1). For example, patients with nonradiographic axial spondyloarthritis have little or no structural damage, and pediatric patients with spondyloarthritis—who are typically diagnosed as having enthesitis-related arthritis (ERA)—may have a similar phenotype (2,3). However, it remains unclear whether the disease in these patients represents an early form of AS or a fundamentally different subtype of spondyloarthritis. Furthermore, it is not known whether treating these patients early in their disease might prevent ankylosis.

Evidence from the preclinical literature suggests that new bone formation may be initiated by an initial inflammatory trigger (4,5), and data from cohorts of adult patients with spondyloarthri-

The views expressed in this publication are those of the authors and not necessarily those of the UK Department of Health.

Dr. Bray's work was supported by Arthritis Research UK (grant 21369). Ms Fisher's work was supported by Arthritis Research UK. Dr. Hall-Craggs' work was supported by the NIHR University College London Hospital Biomedical Research Center.

Timothy J. P. Bray, MBBChir, PhD, Andre Lopes, MSc, Corinne Fisher, MBBCh, Coziana Ciurtin, MMedSc, PhD, Debajit Sen, MBBS, Margaret A. Hall-Craggs, MBBS, MD: University College London, London, UK.

No potential conflicts of interest relevant to this article were reported.

Address correspondence to Timothy J. P. Bray, MBBChir, PhD, or Margaret A. Hall-Craggs, MBBS, MD, Centre for Medical Imaging, Charles Bell House, 43-45 Foley Street, Fitzrovia, London W1W 7TS, UK. E-mail: t.bray@ucl.ac.uk or margaret.hall-craggs@nhs.net.

Submitted for publication April 4, 2018; accepted in revised form October 2, 2018.

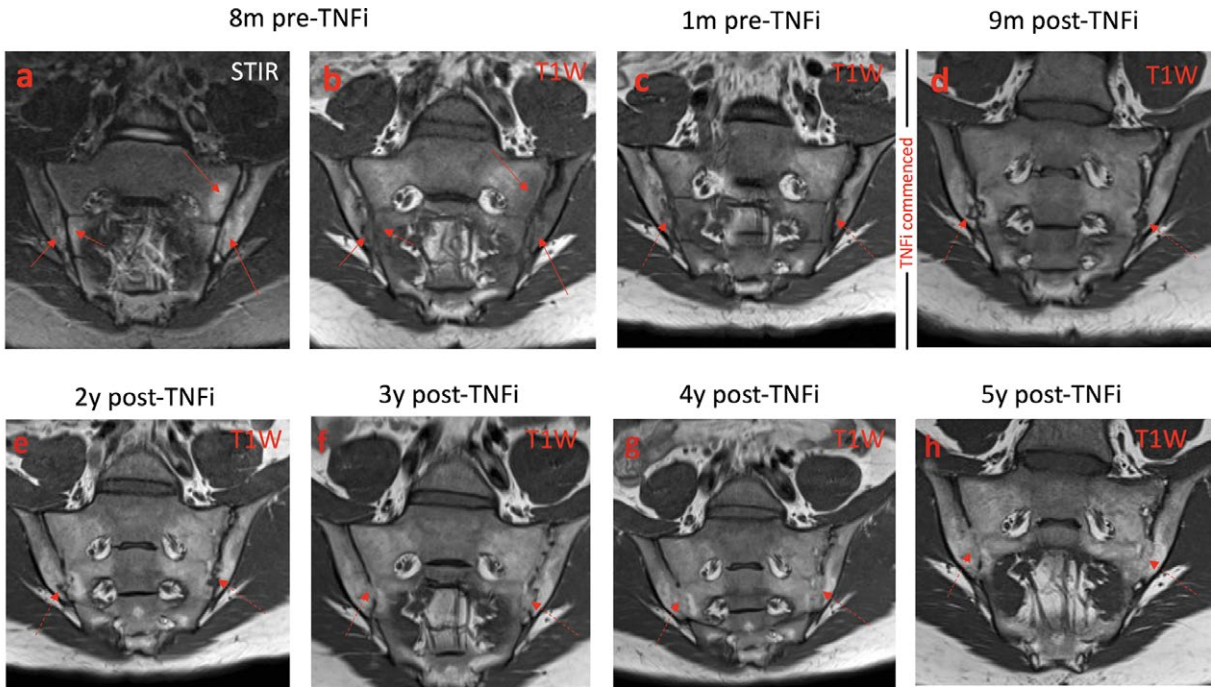

Figure 1. Magnetic resonance images from a representative patient showing the progression of ankylosis over a 5-year period. **a**–**c**, Before the initiation of tumor necrosis factor inhibitor (TNFi) therapy, bilateral bone marrow edema is evident on the STIR image (**a**) and T1-weighted (T1W) images (**b** and **c**). **d**–**h**, After TNFi therapy, the joint erosions gradually become less distinct, and the joints ultimately fuse in anatomic locations similar to those in which the initial edema was found. **Arrows** indicate the areas of edema (on STIR images) and fat metaplasia (on T1W images).

tis suggest that structural damage is often preceded by inflammation (6,7). These findings suggest that early, aggressive treatment of spondyloarthritis might reduce the stimulus for subsequent ankylosis (8). However, studies of animal models of the spondyloarthritides have unravelled alternative pathways, suggesting that an uncoupling of inflammation and bone formation, each involving different molecular mechanisms, may take place, with bone morphogenetic protein and Wnt signaling involved in the bone formation pathway (9). In adults with established AS, clinical trials of tumor necrosis factor inhibitor (TNFi) therapy have produced mixed results, but have not shown a clear reduction in spinal radiographic progression when compared to historical cohorts of patients who have never been treated with a TNFi (10,11).

Despite their well-recognized efficacy in controlling inflammation, the debate about the role of TNFi as disease modifiers in spondyloarthritis continues. In this study, we assessed serial magnetic resonance imaging (MRI) scans in young patients with axial spondyloarthritis undergoing biologic therapy, in order to describe the changes in inflammation and structural damage occurring over time.

MATERIALS AND METHODS

This retrospective study was covered by Institutional Review Board approval from the National Research Ethics Service Committee London (Bentham, UK) (reference no. 11/LO/0330). Informed consent was waived because of the retrospective nature of the study.

A local rheumatology database containing clinical data from adolescents and young adults was used to identify patients ages 12–24 years who had evidence of sacroiliitis on MRI, and who had a clinical diagnosis of ERA with axial involvement or nonradiographic axial spondyloarthritis (2,3). A subsequent search of the picture-archiving and communication system was used to identify all patients who had undergone at least 3 MRI scans of the sacroiliac joints over at least a 2-year period, with at least 1 scan conducted before or at the time of starting the TNFi (adalimumab, etanercept, or infliximab) therapy, and at least 2 scans conducted after the start of the TNFi therapy. Posttreatment scans were performed either due to clinical need or as a part of routine imaging in the follow-up period, according to a previously described protocol (12).

The posttreatment protocol was as follows: MRI scans were acquired on a 1.5-Tesla MRI system with integrated posterior and anterior surface coils, using a specified protocol that included STIR, T1-weighted turbo spin-echo (T1WSE), and post–gadolinium-enhanced fat-saturated images of the sacroiliac joints and thoracolumbar spine. Sequence parameters included the following: for STIR images, repetition time (TR) 4,340–6,070 msec, echo time (TE) 83 msec, and inversion time (TI) 150 msec; for T1WSE images, TR 475–610 msec and TE 11 msec; and for T1WSE images with fat saturation, TR 619–715 msec and TE 11

msec. Sacroiliac joint images were acquired in both para-coronal (angled parallel to the sacrum) and para-axial (angled perpendicular to the sacrum) planes, and thoracolumbar spine images were acquired in the sagittal plane with extended lateral coverage. Only the sacroiliac joint images were used for the current analyses. Representative MR images demonstrating the progression of ankylosis in a young patient over a 5-year period, before and after TNFi therapy, are shown in Figure 1.

MR images of the sacroiliac joints were scored independently by 2 readers (TJPB and MHC) with specific expertise in musculoskeletal imaging and in the assessment of spondyloarthritis. The extent of inflammation was assessed on STIR images using the Spondyloarthritis Research Consortium of Canada scoring system (13), taking care to differentiate between areas of high signal due to skeletal immaturity and bone marrow edema. Chronic inflammatory (structural) abnormalities were assessed on T1-weighted images using a recently proposed structural score, which measures the extent of erosions, fat metaplasia, and joint fusion (14). For each subject, the images were scored in temporal order to enable comparison with previous scans. Readers were blinded with regard to the biologic start dates and to the clinical status at the time of each scan.

The statistical analysis plan was designed to evaluate the effect of the biologic treatment as well as the effect of time from biologic initiation on 4 outcomes, which were measured using MRI scores. The outcomes assessed were MRI scores of inflammation, fat metaplasia, erosions, and fusion. For each outcome, we took the mean of the 2 observers' measurements for the statistical analysis. A mixed-effects model was used for each outcome and included, as explanatory variables, treatment (receving biologic therapy versus not receiving biologic therapy) and time from biologic start, and accounted for repeated measurements in each patient. Assuming a quadratic, cubic, and categorical relationship between time and the outcome measures based on likelihood ratio testing, the linear model was compared to more complex models. If this analysis did not reveal a significant improvement with any of the more complex models over the linear model at a 5% significance level, then the reference results were derived from the linear model. For completeness, the fluctuations over time in each of the MRI scores were summarized from the results derived from the saturated model, where time was included as a categorical variable.

We also tested for relationships between inflammation and fusion, between fat metaplasia and fusion, between erosions and fusion, and between inflammation and fat metaplasia, using random intercept and slope models for each of the relationships in question. For example, in order to assess whether, adjusting for time, inflammation scores have an effect on fusion, a random intercept and slope model was implemented in which we included fusion as the outcome variable and time and inflammation scores as the explanatory variables.

RESULTS

Twenty-nine patients (23 male and 6 female) were included in the study. The mean age at biologic start was 17 years 2 months (range 12 years 3 months to 22 years 10 months). Twenty-three patients were HLA–B27 positive, 2 were negative for HLA–B27, and 4 had not been tested. The mean symptom duration in patients at the time of biologic therapy start was 5 years 3 months (range 4 months to 11 years). In total, 18 patients were treated with etanercept, 8 with adalimumab, and 3 with infliximab. Five patients switched biologics during the follow-up period of the study (due to side effects in 3 cases, and due to inefficacy in 2 cases). The mean number of MRI scans performed per patient was 4.5 (range 3–7), and the mean interval between the first and last scans was 5 years 2 months (range 1 year 9 months to 9 years 11 months).

Our analysis of the mixed-effects model did not reveal a significant improvement with any of the more complex models over the linear model. Therefore, the linear model was selected for the main analysis.

Estimates of inflammation, erosions, fat metaplasia, and fusion scores in the 29 patients over time, derived from the saturated model for the purposes of illustration, are shown in Figures 2A–D. Inflammation scores were significantly lower in patients receiving TNFi treatment than in those not receiving TNFi treatment (β = –6.94, 95% confidence interval [95% CI] –12.4 to –1.44; P = 0.013), but there was no significant effect of time since biologic initiation on inflammation scores (β = –0.90, 95% CI –2.04 to 0.35; P = 0.125) (Figure 2A).

Conversely, there was no significant effect of active TNFi treatment on fusion scores (β = –0.74, 95% CI –2.17 to 0.69; P = 0.308), but there was a significant positive relationship between time since biologic start and fusion scores (β = 1.55, 95% CI 1.02 to 2.09; P < 0.001).

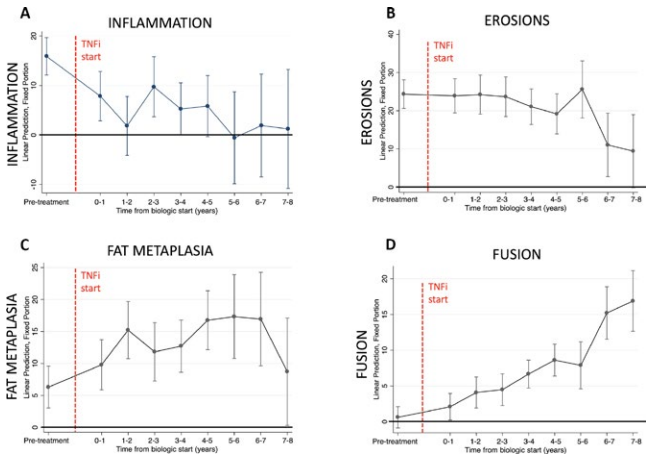

Figure 2. Scores of inflammation (**A**), erosions (**B**), fat metaplasia (**C**), and fusion (**D**) over time before and after the start of tumor necrosis factor inhibitor (TNFi) therapy, in the linear mixed-effects model. Bars show the estimate for each time point ± 95% confidence interval.

Similarly, there was no significant effect of active TNFi treatment on fat metaplasia scores (β = 1.66, 95% CI –1.38 to 4.70; *P* = 0.285), but time since biologic start was significantly associated with fat metaplasia scores (β = 1.53, 95% CI 0.57 to 2.50; *P* = 0.002) (Figure 2C). There was no significant effect of TNFi treatment (β = 0.12 –3.83 to 4.06; *P* = 0.954) or time since biologic initiation (β = –0.82, 95% CI –1.91 to 0.27; *P* = 0.139) on erosion scores (Figure 2B).

When the effects of time and treatment were accounted for, there was a significant negative relationship between inflammation and fat metaplasia scores (β = –0.25, 95% CI –0.34 to –0.17; *P* < 0.001). However, there was no significant relationship between inflammation and fusion scores (β = –0.02, 95% CI –0.06 to 0.03); *P* = 0.443), fat metaplasia and fusion scores (β = 0.04, 95% CI –0.04 to 0.12; *P* = 0.305), or erosions and fusion scores (β = –0.05, 95% CI –0.11 to 0.01; *P* = 0.104).

DISCUSSION

The spondyloarthritides encompass a wide range of disease phenotypes, each of which varies in terms of disease severity, the presence of structural damage, and age at presentation. Spondyloarthritis patients who present early might offer a unique opportunity to study the disease course, and to characterize the evolution of inflammatory and structural damage over time. In addition, it has been suggested that early intervention might help to avoid structural complications and thereby improve long-term outcomes (8). However, we observed that TNFi therapy did not prevent the eventual fusion of the sacroiliac joints in patients with ERA, despite there being relatively little structural damage (particularly fusion) at presentation and despite the fact that inflammation was substantially reduced by TNFi treatment. Although sacroiliac joint ankylosis in itself may have a relatively small effect on disability, it is possible that the effect of treatment on inflammation and structural damage would be similar in the remainder of the spine.

The results of our study do not enable us to comment on the specific cause of fusion in these patients; we do not know whether fusion is a consequence of inflammation itself, or whether it is related to the TNFi therapy. Although the levels of inflammation were substantially reduced after treatment, it is possible that low levels of inflammation persist and drive joint ankylosis. Alternatively, joint fusion may be triggered by the initial inflammatory insult and then proceed independently, as other authors have suggested (4,5). Either way, these results suggest that more research is needed into strategies for preventing structural damage, either through a reduction in inflammation or the inhibition of bone-forming pathways.

Some limitations have arisen due to the retrospective nature of the study. Since the number of MRI scans was an inclusion criterion, it is likely that our cohort includes patients with more severe disease. However, the severity of the disease in this cohort of patients with "definite" spondyloarthritis probably also increased the size of the effects in question, which may have actually strengthened the analysis.

An additional issue is that scans were acquired at irregular intervals (as determined by clinical need), meaning that the data were not evenly distributed in the posttreatment period. Nonetheless, our regression model accounted for the clustered nature of the data, reducing any potential effect on the final analysis. It should be emphasized that spondyloarthritis in young people is comparatively rare, and it would have been very difficult to acquire data over such a long time period in a prospective manner.

The development of imaging methods that could identify new bone formation before the development of overt ankylosis might reduce the follow-up period needed to assess the effect of novel therapies on new bone formation. Several groups have begun to explore MRI methods that can derive signal directly from mineralized bone or quantify bone mineral density indirectly (15), and it is likely that these techniques will become more widely applicable in the years to come.

In conclusion, we found that TNFi therapy in young patients with spondyloarthritis failed to prevent the eventual development of joint ankylosis, despite a substantial reduction in inflammation with TNFi therapy.

AUTHOR CONTRIBUTIONS

All authors were involved in drafting the article or revising it critically for important intellectual content, and all authors approved the final version to be published. Drs. Bray and Hall-Craggs had full access to all of the data in the study and take responsibility for the integrity of the data and the accuracy of the data analysis.

Study conception and design. Bray, Hall-Craggs.
Acquisition of data. Bray, Fisher, Ciurtin, Sen, Hall-Craggs.
Analysis and interpretation of data. Bray, Lopes, Hall-Craggs.

REFERENCES

1. Sieper J, Poddubnyy D. Axial spondyloarthritis. Lancet 2017;390:73–84.
2. Petty RE, Southwood TR, Manners P, Baum J, Glass DN, Goldenberg J, et al. International League of Associations for Rheumatology classification of juvenile idiopathic arthritis: second revision, Edmonton, 2001. J Rheumatol 2004;31:390–2.
3. Rudwaleit M, Landewé R, van der Heijde D, Listing J, Brandt J, Braun J, et al. The development of Assessment of SpondyloArthritis international Society classification criteria for axial spondyloarthritis (part I): classification of paper patients by expert opinion including uncertainty appraisal. Ann Rheum Dis 2009;68:770–6.
4. Lories RJ, Matthys P, de Vlam K, Derese I, Luyten FP. Ankylosing enthesitis, dactylitis, and onychoperiostitis in male DBA/1 mice: a model of psoriatic arthritis. Ann Rheum Dis 2004;63:595–8.
5. Schett G, Stolina M, Dwyer D, Zack D, Uderhardt S, Krönke G, et al. Tumor necrosis factor α and RANKL blockade cannot halt bony spur formation in experimental inflammatory arthritis. Arthritis Rheum 2009;60:2644–54.

6. Van der Heijde D, Salonen D, Weissman BN, Landewé R, Maksymowych WP, Kupper H, et al. Assessment of radiographic progression in the spines of patients with ankylosing spondylitis treated with adalimumab for up to 2 years. Arthritis Res Ther 2009;11:R127.
7. Chiowchanwisawakit P, Lambert RG, Conner-Spady B, Maksymowych WP. Focal fat lesions at vertebral corners on magnetic resonance imaging predict the development of new syndesmophytes in ankylosing spondylitis. Arthritis Rheum 2011;63:2215–25.
8. Fisher C, Ioannou Y, Hall-Craggs M, Sen D. Enthesitis related arthritis: a new era of understanding. Ann Paediatr Rheumatol 2012;1:8–16.
9. Lories RJ, Luyten FP. Bone morphogenetic proteins in destructive and remodeling arthritis. Arthritis Res Ther 2007;9:207.
10. Van Der Heijde D, Landewé R, Baraliakos X, Houben H, Van Tubergen A, Williamson P, et al. Radiographic findings following two years of infliximab therapy in patients with ankylosing spondylitis. Arthritis Rheum 2008;58:3063–70.
11. Van der Heijde D, Dijkmans B, Geusens P, Sieper J, DeWoody K, Williamson P, et al. Efficacy and safety of infliximab in patients with ankylosing spondylitis: results of a randomized, placebo-controlled trial (ASSERT). Arthritis Rheum 2005;52:582–91.
12. Fisher C, Ioannou Y, Hall-Craggs MA, Sen D. Enthesitis-related arthritis: a new era of understanding. Ann Paediatr Rheumatol 2012;1:8–16.
13. Maksymowych WP, Inman RD, Salonen D, Dhillon SS, Williams M, Stone M, et al. Spondyloarthritis Research Consortium of Canada magnetic resonance imaging index for assessment of sacroiliac joint inflammation in ankylosing spondylitis. Arthritis Rheum 2005;53:703–9.
14. Maksymowych WP, Wichuk S, Chiowchanwisawakit P, Lambert RG, Pedersen SJ. Development and preliminary validation of the Spondyloarthritis Research Consortium of Canada magnetic resonance imaging sacroiliac joint structural score. J Rheumatol 2015;42:79–86.
15. Bray TJP, Bainbridge A, Punwani S, Ioannou Y, Hall-Craggs MA. Simultaneous quantification of bone edema/adiposity and structure in inflamed bone using chemical shift-encoded MRI in spondyloarthritis. Magn Reson Med 2018;79:1031–42.

Arthritis & Rheumatology
Vol. 71, No. 4, April 2019, pp 599–611
DOI 10.1002/art.40753

AMERICAN COLLEGE OF RHEUMATOLOGY
EDUCATION • TREATMENT • RESEARCH

Efficacy and Safety of Ixekizumab in the Treatment of Radiographic Axial Spondyloarthritis: Sixteen-Week Results From a Phase III Randomized, Double-Blind, Placebo-Controlled Trial in Patients With Prior Inadequate Response to or Intolerance of Tumor Necrosis Factor Inhibitors

Atul Deodhar,[1] Denis Poddubnyy,[2] Cesar Pacheco-Tena,[3] Carlo Salvarani,[4] Eric Lespessailles,[5] Proton Rahman,[6] Pentti Järvinen,[7] Juan Sanchez-Burson,[8] Karl Gaffney,[9] Eun Bong Lee,[10] Eswar Krishnan,[11] Silvia Santisteban,[11] Xiaoqi Li,[11] Fangyi Zhao,[11] Hilde Carlier,[11] and John D. Reveille,[12] for the COAST-W Study Group

Objective. To investigate the efficacy and safety of ixekizumab in patients with active radiographic axial spondyloarthritis (SpA) and prior inadequate response to or intolerance of 1 or 2 tumor necrosis factor inhibitors (TNFi).

Methods. In this phase III randomized, double-blind, placebo-controlled trial, adult patients with an inadequate response to or intolerance of 1 or 2 TNFi and an established diagnosis of axial SpA (according to the Assessment of SpondyloArthritis international Society [ASAS] criteria for radiographic axial SpA, with radiographic sacroiliitis defined according to the modified New York criteria and ≥1 feature of SpA) were recruited and randomized 1:1:1 to receive placebo or 80-mg subcutaneous ixekizumab every 2 weeks (IXEQ2W) or 4 weeks (IXEQ4W), with an 80-mg or 160-mg starting dose. The primary end point was 40% improvement in disease activity according to the ASAS criteria (ASAS40) at week 16. Secondary outcomes and safety were also assessed.

Results. A total of 316 patients were randomized to receive placebo (n = 104), IXEQ2W (n = 98), or IXEQ4W (n = 114). At week 16, significantly higher proportions of IXEQ2W patients (n = 30 [30.6%]; $P = 0.003$) or IXEQ4W patients (n = 29 [25.4%]; $P = 0.017$) had achieved an ASAS40 response versus the placebo group (n = 13 [12.5%]), with statistically significant differences reported as early as week 1 with ixekizumab treatment. Statistically significant improvements in disease activity, function, quality of life, and spinal magnetic resonance imaging–evident inflammation were observed after 16 weeks of ixekizumab treatment versus placebo. Treatment-emergent adverse events (AEs) with ixekizumab treatment were more frequent than with placebo. Serious AEs were similar across treatment arms. One death was reported (IXEQ2W group).

Conclusion. Ixekizumab treatment for 16 weeks in patients with active radiographic axial SpA and previous inadequate response to or intolerance of 1 or 2 TNFi yields rapid and significant improvements in the signs and symptoms of radiographic axial SpA versus placebo.

ClinicalTrials.gov identifier: NCT02696798.
Supported by Eli Lilly and Company.

[1]Atul Deodhar, MD: Oregon Health & Science University, Portland; [2]Denis Poddubnyy, MD: Universitätsmedizin Berlin and German Rheumatism Research Centre, Berlin, Germany; [3]Cesar Pacheco-Tena, MD, PhD: Universidad Autónoma de Chihuahua, Chihuahua, Mexico; [4]Carlo Salvarani, MD: Azienda USL-IRCCS di Reggio Emilia and Universita' di Modena e Reggio Emilia, Reggio Emilia, Italy; [5]Eric Lespessailles, MD, PhD: University of Orléans, Orléans, France; [6]Proton Rahman, MD: Memorial University, St. John's, Newfoundland, Canada; [7]Pentti Järvinen, MD, PhD: Kiljava Medical Research, Hyvinkää, Finland; [8]Juan Sanchez-Burson, MD, PhD: Hospital Infanta Luisa, Seville, Spain; [9]Karl Gaffney, MB, BCH: Norfolk and Norwich Hospital NHS Foundation Trust and University of East Anglia, Norwich, UK; [10]Eun Bong Lee, MD, PhD: Seoul National University College of Medicine, Seoul, Republic of Korea; [11]Eswar Krishnan, MD, Silvia Santisteban, MD, Xiaoqi Li, PhD, Fangyi Zhao, PhD, Hilde Carlier, MD: Eli Lilly and Company, Indianapolis, Indiana; [12]John D. Reveille, MD: University of Texas–McGovern Medical School, Houston.

Dr. Deodhar has received consulting fees from AbbVie, Pfizer, UCB, and Bristol-Myers Squibb (less than $10,000 each) and from Eli Lilly and Company, Janssen, and Novartis (more than $10,000 each), and research support from AbbVie, Eli Lilly and Company, Janssen, Novartis, Pfizer, and UCB. Dr. Poddubnyy has received consulting and/or speaking fees from AbbVie, Bristol-Myers Squibb, Janssen, MSD, Novartis, Pfizer, Roche, and UCB (less than $10,000 each) and research support from AbbVie, MSD, Novartis, Pfizer, and Eli Lilly and Company. Drs. Pacheco-Tena, Salvarani, Lespessailles, and Sanchez-Burson have received research support from Eli Lilly and Company. Dr. Rahman has received consulting fees and/or speaking fees from AbbVie, Amgen, Bristol-Myers Squibb, Celgene, Pfizer, Merck, and UCB (less than $10,000 each) and from Eli Lilly and Company, Janssen, and Novartis (more than $10,000 each), and research support from Janssen. Dr. Järvinen has received consulting fees from Pfizer (less than $10,000) and research support from AbbVie, Eli Lilly and Company, Novartis, and Pfizer. Dr. Gaffney has received consulting and speaking fees from AbbVie, Eli Lilly and Company, Pfizer, Novartis, and UCB Pharma (less than $10,000

INTRODUCTION

Axial spondyloarthritis (SpA) is a chronic inflammatory disease that is estimated to affect 0.9–1.4% of adults in the US and encompasses both nonradiographic axial SpA and radiographic axial SpA (1,2). Radiographic axial SpA is also referred to as ankylosing spondylitis (AS). The disease is typically characterized by inflammatory back pain and radiographically defined sacroiliac (SI) joint structural damage (2,3). Patients with axial SpA may also exhibit peripheral musculoskeletal (inflammatory arthritis, enthesitis, and dactylitis) and extraarticular (uveitis, psoriasis, and inflammatory bowel disease [IBD]) involvement.

Currently, the American College of Rheumatology/Spondylitis Association of America/Spondyloarthritis Research and Treatment Network, the Assessment of SpondyloArthritis international Society (ASAS)/European League Against Rheumatism, and the National Institute for Health and Care Excellence guidelines for the management of axial SpA recommend treatment with tumor necrosis factor inhibitors (TNFi) in patients with axial SpA who do not respond or tolerate nonsteroidal antiinflammatory drugs (NSAIDs) (4–6). Approximately 30–40% of patients with AS do not achieve adequate disease control or symptom relief according to clinical trials of TNFi (7–12). In addition, some patients may not be eligible to receive TNFi due to relative contraindications (13).

The interleukin-17 (IL-17) axis has been linked to the immunopathology of axial SpA (14,15). IL-17 inhibition has demonstrated efficacy in patients with AS; however, an IL-17 antagonist has not been evaluated in a population that exclusively consisted of patients with prior inadequate response to or intolerance of TNFi in a clinical trial setting (16). This is an important population on which to focus, given that it has been shown to be difficult to treat, with treatment responses lower in magnitude than observed in biologics-naive populations (17,18).

Ixekizumab is a high-affinity monoclonal antibody that selectively targets IL-17A (19). Here we present the 16-week results of COAST-W, a phase III clinical trial investigating the efficacy and safety of ixekizumab in patients with active radiographic axial SpA and previous inadequate response to or intolerance of 1 or 2 TNFi.

PATIENTS AND METHODS

Trial design. COAST-W is a multicenter, phase III, randomized, double-blind, placebo-controlled, parallel-group, outpatient clinical trial of 1 year's duration, followed by an optional 2-year extension trial (COAST-Y) (see Supplementary Figure 1, available on the *Arthritis & Rheumatology* web site at http://onlinelibrary.wiley.com/doi/10.1002/art.40753/abstract). Patient enrollment and data collection occurred at 106 sites located in 15 countries across North America, South America, Europe, and Asia (for a list of investigators and sites, see Supplementary Appendix A, available at http://onlinelibrary.wiley.com/doi/10.1002/art.40753/abstract). This trial was conducted in accordance with the ethical principles of the Declaration of Helsinki and in compliance with local laws and regulations. All participants provided informed consent. COAST-W protocol and consent forms were approved by each site's institutional review board or ethics committee. The trial was registered with ClinicalTrials.gov (NCT02696798) and the European Union Clinical Trials Register (2015-003937-84).

Trial participants. Complete inclusion and exclusion criteria are provided in Supplementary Appendix B (available at http://onlinelibrary.wiley.com/doi/10.1002/art.40753/abstract). Eligible subjects were age ≥18 years, required to have an established diagnosis of axial SpA and fulfillment of ASAS classification criteria for radiographic axial SpA (i.e., radiographic evidence of sacroiliitis according to the modified New York criteria and having ≥1 SpA feature), and required to have a history of back pain for ≥3 months with an age at onset of <45 years (20–22). SI joint radiographs were scored by central readers. All patients fulfilling ASAS criteria for radiographic axial SpA (20) also fulfilled the modified New York criteria for AS (21).

Additional inclusion criteria included a baseline Bath Ankylosing Spondylitis Disease Activity Index (BASDAI) score (23) of ≥4, a baseline total back pain numeric rating scale score of ≥4, and a history of therapy for axial SpA of at least 12 weeks' duration prior to screening. Patients were required to have discontinued at least 1 TNFi, but no more than 2 TNFi, either due to intolerance or due to an inadequate response (in the opinion of the investigator) to treatment with a single TNFi for at least 12 weeks at an adequate dose. The required TNFi washout periods are described in Supplementary Appendix B and were based upon the half-lives of the respective TNFi.

The exclusion criteria included total spinal ankylosis (according to the site investigator's opinion), active or recent infections, current or history of lymphoproliferative or malignant disease (<5 years prior to baseline) or other medical conditions (e.g., systemic inflammatory diseases or chronic pain conditions such as fibromyalgia), other non-TNF biologic or other immunomodulatory agent treatments, or surgical procedures that could pose an unacceptable risk to patients or that could confound interpretation of trial results. Patients with IBD (Crohn's disease or ulcerative colitis) were eligible if no disease

each) and research support from those companies. Dr. Lee has received research support from GC Pharm and Eli Lilly and Company. Drs. Krishnan, Santisteban, Li, Zhao, and Carlier own stock or stock options in Eli Lilly and Company. Dr. Reveille has received consulting fees from Janssen, Eli Lilly and Company, UCB, and Novartis (less than $10,000 each). See Appendix A for members of the COAST-W Study Group.

Address correspondence to Atul Deodhar, MD, Division of Arthritis & Rheumatic Diseases (OP09), Oregon Health & Science University, 3181 SW Sam Jackson Park Road, Portland, OR 97239. E-mail: deodhara@ohsu.edu.

Submitted for publication August 21, 2018; accepted in revised form October 3, 2018.

exacerbations had occurred for ≥6 months (stable treatment allowed). Patients with anterior uveitis were eligible if no exacerbations had occurred for ≥4 weeks.

Patients could continue to receive the following medications at a stable dose: sulfasalazine (≤3 gm/day), methotrexate (≤25 mg/week), prednisone or equivalent (≤10 mg/day), and NSAIDs. No changes to these medications were allowed during the blinded treatment dosing period, except for safety reasons. Analgesics were also allowed according to the eligibility criteria (see Supplementary Appendix B, available at http://onlinelibrary.wiley.com/doi/10.1002/art.40753/abstract).

Randomization and blinding. Patients were randomly assigned (1:1:1) to receive subcutaneous administration of ixekizumab 80 mg every 2 weeks (IXEQ2W group), ixekizumab 80 mg every 4 weeks (IXEQ4W group), or matched placebo from week 0 to week 16. Patients randomized to the ixekizumab treatment regimens were randomized (1:1) to receive either an 80-mg or 160-mg starting dose of ixekizumab at week 0. The 2 starting doses were included in order to assess the impact of starting dose on week 16 responses, following regulatory agency feedback. All patients received the same frequency and number of injections regardless of treatment arm or assigned starting dose.

During the double-blinded treatment period (weeks 0–16), site personnel, patients, and the sponsor trial team were blinded with regard to treatment. Randomization to treatment groups was determined using a computer-generated, random-sequence, interactive web-response system with follow-up confirmation by site personnel using the confirmation number present on the investigational product packaging. Randomization of treatment assignment (including starting dose) was stratified by country, high-sensitivity C-reactive protein (CRP) level (≤5 or >5 mg/liter) at screening, and the number of prior TNFi taken (1 or 2) to achieve between-group comparability.

At week 16, patients entered the extended treatment period (weeks 16–52). Patients who were initially assigned to the placebo arm were, for the extended treatment period, randomly reassigned at week 16 to IXEQ4W or IXEQ2W with a 160-mg starting dose. Patients already receiving ixekizumab remained on their assigned treatment regimens through week 52.

Procedures of product administration. The investigational product was supplied in prefilled manual syringes for subcutaneous administration, with trial-specific labels. Ixekizumab and its matching placebo were visually indistinguishable from each other. To maintain blinding, all patients received 2 injections at week 0 and 1 injection every 2 weeks. Placebo patients received a placebo injection every 2 weeks and IXEQ4W patients received a placebo injection every other 2 weeks to maintain blinding. Patients assigned to an ixekizumab treatment regimen received their starting dose (either 80-mg ixekizumab [1 80-mg injection and 1 placebo injection] or ixekizumab 160 mg [2 80-mg injections]) at week 0. Trial visits and data collection occurred at baseline (week 0) and at weeks 1, 2, 4, 8, 12, and 16 during the blinded treatment dosing period. The primary end point was assessed at week 16.

Efficacy and safety assessments. The primary end point of the trial was the proportion of patients achieving an ASAS 40% improvement in disease activity (ASAS40) (22) at week 16, with comparison of each ixekizumab dosing regimen to placebo. Major secondary end points assessed at week 16 were ASAS20, an Ankylosing Spondylitis Disease Activity Score (ASDAS) of <2.1 (inactive or low disease activity) (24), and changes from baseline in the ASDAS, BASDAI, Bath Ankylosing Spondylitis Functional Index (BASFI) (25), Medical Outcomes Study Short Form 36 (SF-36) health survey physical component score (PCS) (26), ASAS Health Index (ASAS-HI) (27,28), and Spondyloarthritis Research Consortium of Canada (SPARCC) magnetic resonance imaging (MRI) index for the spine (MRI protocol addendum only) (29). These end points were assessed at every visit (i.e., screening, baseline, weeks 1, 2, 4, 8, 12, and 16) except for the SF-36 PCS and ASAS-HI (collected at baseline, weeks 4, 8, and 16) and MRI (collected at baseline and week 16). Additionally, CRP level was assessed at every visit. All listed end points are described in Supplementary Appendix C, available on the *Arthritis & Rheumatology* web site at http://onlinelibrary.wiley.com/doi/10.1002/art.40753/abstract.

Safety outcomes were assessed at every visit. Data on terms related to cerebrocardiovascular events and suspected IBD were adjudicated by external clinical event committees. Details on adjudication criteria are provided in Supplementary Appendix C.

Statistical analysis. The sample size of COAST-W was estimated to have 96% power for testing the superiority of IXEQ2W to placebo for an ASAS40 response at week 16 (for details on power analysis assumptions, see Supplementary Appendix C).

Efficacy analyses for the blinded treatment dosing period included all randomized patients according to the treatment to which they were assigned. Analyses of the IXEQ2W and IXEQ4W treatment groups were performed without regard to the starting dose. Missing values (including for those patients who discontinued trial treatment) were imputed as nonresponders using nonresponder imputation for categorical variables; continuous variables were analyzed using a mixed-effects model of repeated measures (MMRM) without imputation for missing values.

The primary analysis method for categorical outcome variables was logistic regression with treatment, geographic region, baseline CRP status (≤5 versus >5 mg/liter), and the number of prior TNFi taken included in the model. Secondary analysis of categorical outcomes was performed using Fisher's exact test when the logistic model did not converge due to sparse data.

The primary analysis method for continuous outcomes, except SPARCC MRI index scores, was MMRM with treatment, geographic region, baseline CRP level, the number of prior TNFi

taken, baseline value, visit, baseline value–by-visit, and treatment-by-visit interaction as fixed factors. The primary analysis method for SPARCC MRI index scores was analysis of covariance (ANCOVA) with observed case analysis, with inclusion only of patients with both baseline (between 42 days prior to and 14 days after the first injection) and week 16 (injection date at week 16 [±14 days]) SPARCC MRI index scores. The ANCOVA included treatment, geographic region, baseline CRP level, number of prior TNFi taken, and baseline value.

A graphical multiple testing strategy was implemented for primary and major secondary objectives to control the overall family-wise Type I error rate at a 2-sided alpha level of 0.05 (see Supplementary Figures 2–4, available on the *Arthritis & Rheumatology* web site at http://onlinelibrary.wiley.com/doi/10.1002/art.40753/abstract). There was no adjustment for multiple comparisons for any other analyses. The analyses investigating efficacy prior to week 16 were not included in the multiple testing strategy.

Descriptive analyses (with no prespecified hypothesis testing) were performed using the safety population, which was defined as all randomized patients who received ≥1 dose of the trial drug, according to assigned treatments. Safety data were summarized as the frequency of events occurring in each treatment group during the blinded treatment dosing period.

RESULTS

Patient disposition and baseline characteristics. The Consolidated Standards of Reporting Trials (CONSORT) diagram is provided in Figure 1. Of the 610 patients assessed for trial eligibility, 316 were randomly assigned to either placebo (n = 104), IXEQ2W (n = 98), or IXEQ4W (n =114), and 294 patients were designated as ineligible at screening or were discontinued prior to randomization. The predominant reason for ineligibility at screening was the lack of definitive sacroiliitis according to centrally read SI joint radiographs (n = 217 [35.6%]) (see Supplementary Table 1, available at http://onlinelibrary.wiley.com/doi/10.1002/art.40753/abstract). The number of patients screened and enrolled for each country is shown in Supplementary Table 2 (available at http://onlinelibrary.wiley.com/doi/10.1002/art.40753/abstract). The 16-week blinded treatment dosing period was completed by 93 patients (89.4%) receiving placebo, 90 patients (91.8%) receiving IXEQ2W, and 99 patients (86.8%) receiving IXEQ4W. Overall, 282 patients (89.2%) completed week 16.

Treatment arms were generally balanced for baseline demographic and clinical characteristics (Table 1). Baseline spondyloarthritis features are listed in Supplementary Table 3 (available at

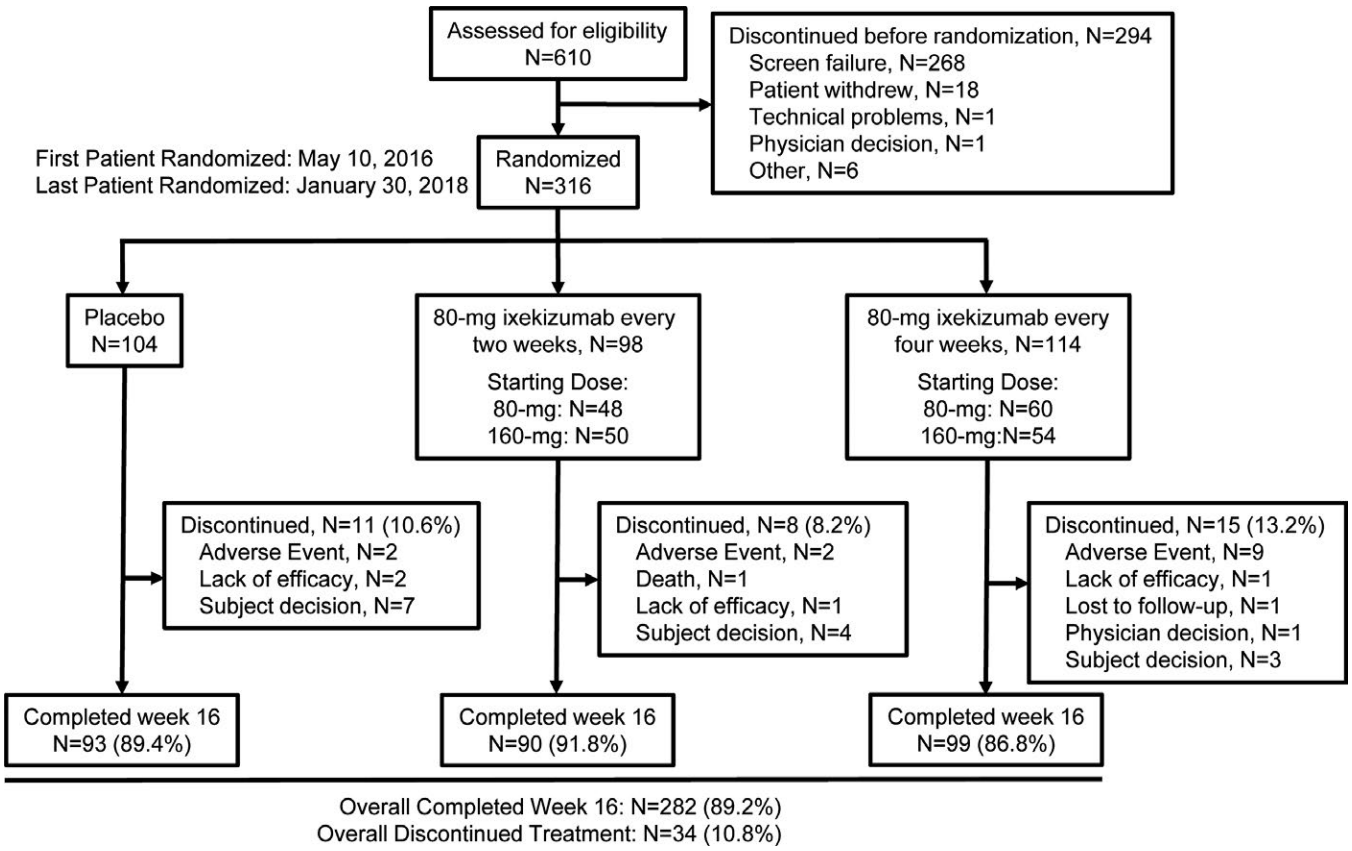

Figure 1. Disposition of the patients. Details are given according to the Consolidated Standards of Reporting Trials (CONSORT) statement for reporting randomized controlled trials.

Table 1. Patient demographic and clinical characteristics for the intent-to-treat population in the COAST-W study*

	Placebo group (n = 104)	IXEQ2W group (n = 98)	IXEQ4W group (n = 114)
Age, mean ± SD years	46.6 ± 12.7	44.2 ± 10.8	47.4 ± 13.4
Male sex	87 (83.7)	75 (76.5)	91 (79.8)
Race			
White	85 (81.7)	78 (79.6)	91 (80.5)
Asian	13 (12.5)	13 (13.3)	14 (12.4)
Weight, mean ± SD kg	84.3 ± 17.9	79.3 ± 17.3	85.5 ± 20.2
<70 kg	21 (20.2)	25 (25.5)	24 (21.1)
≥70 kg	83 (79.8)	73 (74.5)	90 (78.9)
Body mass index, mean ± SD kg/m^2	28.9 ± 5.6	27.5 ± 5.4	29.4 ± 7.3
Age at onset of axial SpA, mean ± SD years	27.1 ± 8.8	28.1 ± 10	28.9 ± 9.6
Duration of symptoms since axial SpA onset, mean ± SD years	19.9 ± 11.6	16.5 ± 9.6	18.8 ± 11.6
Duration of disease since axial SpA diagnosis, mean ± SD years	13.0 ± 10.5	11.7 ± 8.8	10.1 ± 7.8
Use of DMARDs			
Methotrexate	20 (19.2)	9 (9.2)	12 (10.5)
Sulfasalazine	13 (12.5)	16 (16.3)	17 (14.9)
Use of oral corticosteroid	14 (13.5)	11 (11.2)	11 (9.6)
Use of NSAIDs	84 (80.8)	71 (72.4)	86 (75.4)
Prior TNFi experience†			
1 prior TNFi	62 (59.6)	66 (68.0)	70 (61.4)
2 prior TNFi	42 (40.4)	31 (32.0)	44 (38.6)
Reason for failing prior TNFi‡			
Inadequate response to 1 TNFi	64 (61.5)	66 (68.0)	75 (65.8)
Inadequate response to 2 TNFi	32 (30.8)	20 (20.6)	26 (22.8)
Intolerance of TNFi	8 (7.7)	11 (11.3)	13 (11.4)
TNFi washout period, median (minimum–maximum) days§	123.5 (31.0–4,053.0)	143.0 (32.0–3,851.0)	153.5 (29.0–4,639.0)
Baseline C-reactive protein, mean ± SD mg/liter	16.0 ± 22.3	16.9 ± 19.8	20.2 ± 34.3
≤5.00 mg/liter	39 (37.5)	26 (26.5)	44 (38.6)
>5.00 mg/liter	65 (62.6)	72 (73.5)	70 (61.4)
ASDAS, mean ± SD	4.1 ± 0.8	4.2 ± 0.8	4.2 ± 0.9
BASDAI score, mean ± SD	7.3 ± 1.3	7.5 ± 1.3	7.5 ± 1.3
BASFI score, mean ± SD	7.0 ± 1.7	7.4 ± 1.4	7.4 ± 1.8
ASAS-HI score, mean ± SD	9.0 ± 3.5	10.1 ± 3.6	10.0 ± 3.7
SF-36 PCS, mean ± SD	30.6 ± 7.8	27.9 ± 7.3	27.5 ± 8.3
SPARCC MRI spine score, mean ± SD¶	6.4 ± 10.2	11.1 ± 20.3	8.3 ± 16
SPARCC MRI spine score ≥2¶	25 (49.0)	24 (45.3)	31 (53.4)

* Except where indicated otherwise, values are the number (%) of patients in the analysis population. IXEQ2W = 80-mg subcutaneous ixekizumab every 2 weeks; IXEQ4W = 80-mg subcutaneous ixekizumab every 4 weeks; SpA = spondyloarthritis; DMARDs = disease-modifying antirheumatic drugs; NSAIDs = nonsteroidal antiinflammatory drugs; ASDAS = Ankylosing Spondylitis Disease Activity Score; BASDAI = Bath Ankylosing Spondylitis Disease Activity Index; BASFI = Bath Ankylosing Spondylitis Functional Index; ASAS-HI = Assessment of Spondyloarthritis international Society Health Index; SF-36 = Medical Outcomes Study Short Form 36 health survey; PCS = physical component score; SPARCC = Spondyloarthritis Research Consortium of Canada.

† Patients were included regardless of whether they were inadequate responders to or intolerant of tumor necrosis factor inhibitors (TNFi).

‡ If a patient had both an inadequate response to 1 TNFi and an intolerance of another TNFi, that patient was classified as having had an inadequate response to 1 TNFi. Patients in the intolerance category discontinued prior TNFi (1 or 2) due to intolerance only.

§ Washout period for the last TNFi taken. Data were available for all but 1 IXEQ2W patient.

¶ Data were available for the magnetic resonance imaging (MRI) addendum population only (n = 51 for the placebo group, n = 58 for the IXEQ2W group, and n = 53 for the IXEQ4W group).

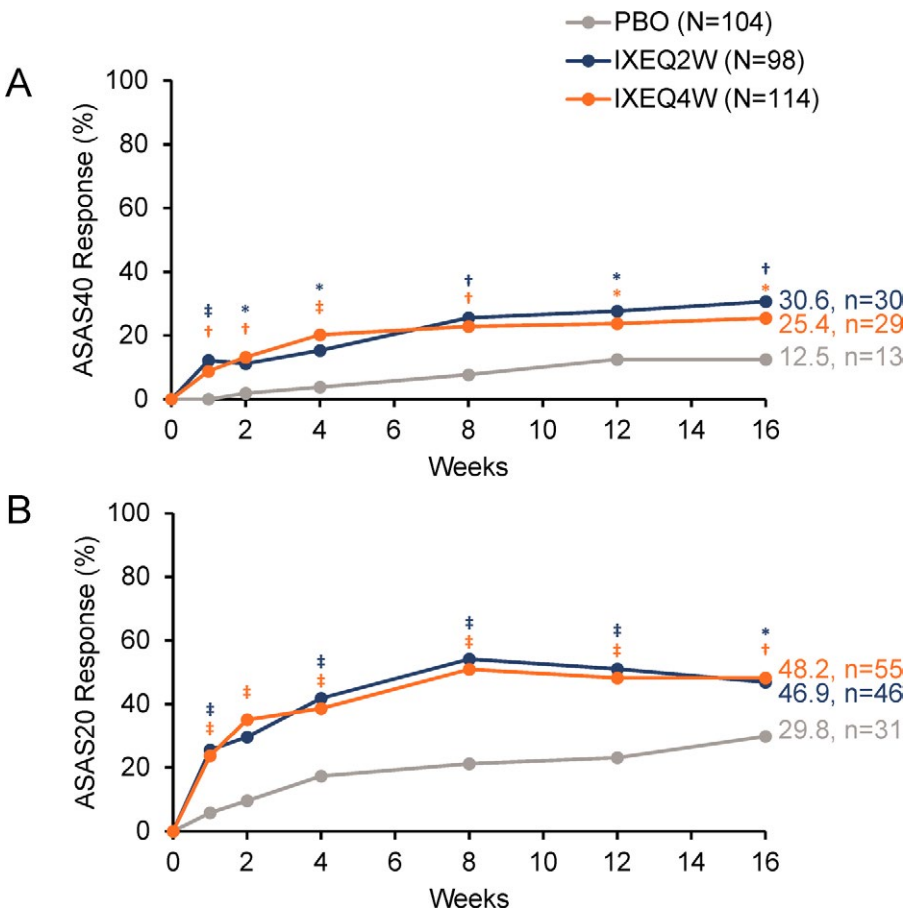

Figure 2. Proportion of patients achieving **A**, 40% improvement in disease activity according to the Assessment of SpondyloArthritis international Society criteria (ASAS40) or **B**, ASAS20 responses through week 16 when treated with placebo (PBO), ixekizumab every 2 weeks (IXEQ2W), or ixekizumab every 4 weeks (IXEQ4W). * = $P < 0.05$; † = $P < 0.01$; ‡ = $P < 0.001$, all versus placebo by logistic regression analysis, except for week 1 with ASAS40, for which Fisher's exact test was used due to model nonconvergence. Only analyses at week 16 were included in the prespecified multiple testing strategy. n = number of patients in the analysis category; N = number of patients in the analysis population.

http://onlinelibrary.wiley.com/doi/10.1002/art.40753/abstract). Overall, 315 patients had prior TNFi experience; 205 patients (65.1%) had an inadequate response to 1 TNFi, 78 patients (24.8%) had an inadequate response to 2 TNFi, and 32 patients (10.2%) were intolerant of TNFi. One patient was inadvertently enrolled without prior TNFi experience. Reasons for the discontinuation of previous biologic therapies are provided in Supplementary Table 4 (available at http://onlinelibrary.wiley.com/doi/10.1002/art.40753/abstract). The median washout period for TNFi prior to study entry was 5 months (minimum 1 month, maximum 155 months). At baseline, 86 patients (27.2%) were receiving concomitant conventional synthetic disease-modifying antirheumatic drugs (DMARDs; sulfasalazine or methotrexate).

Clinical end points. Ixekizumab was found to be superior to placebo for the primary and all major secondary end points at week 16 with both ixekizumab treatment regimens, except for ASAS-HI scores with IXEQ2W (Figures 2–4 and Supplementary Table 5, available at http://onlinelibrary.wiley.com/doi/10.1002/art.40753/abstract). The proportion of patients who achieved the primary end point of an ASAS40 response at week 16 was significantly higher among patients treated with either IXEQ2W (n = 30 [30.6%]; $P = 0.003$) or IXEQ4W (n = 29 [25.4%]; $P = 0.017$) than among patients treated with placebo (n = 13 [12.5%]), with a significant response observed as early as week 1 for both ixekizumab regimens (Figure 2A). The proportion of patients who achieved an ASAS20 response at week 16 was also significantly higher among patients treated with either IXEQ2W (n = 46 [46.9%]) or IXEQ4W (n = 55 [48.2%]) than among patients treated with placebo (n = 31 [29.8%]), with a significant response as early as week 1 for both dosing regimens (Figure 2B). The starting dose of 160 mg versus 80 mg at week 0 did not lead to a significant improvement of the results observed at week 16 (Supplementary Figure 5, available at http://onlinelibrary.wiley.com/doi/10.1002/art.40753/abstract). Further analyses are required in order to evaluate the effect of starting dose on speed of onset.

Statistically significant improvements in measures of disease activity were observed among patients treated with IXEQ2W or IXEQ4W relative to placebo at week 16, as measured by a change from baseline in ASDAS and BASDAI scores, as well as achieve-

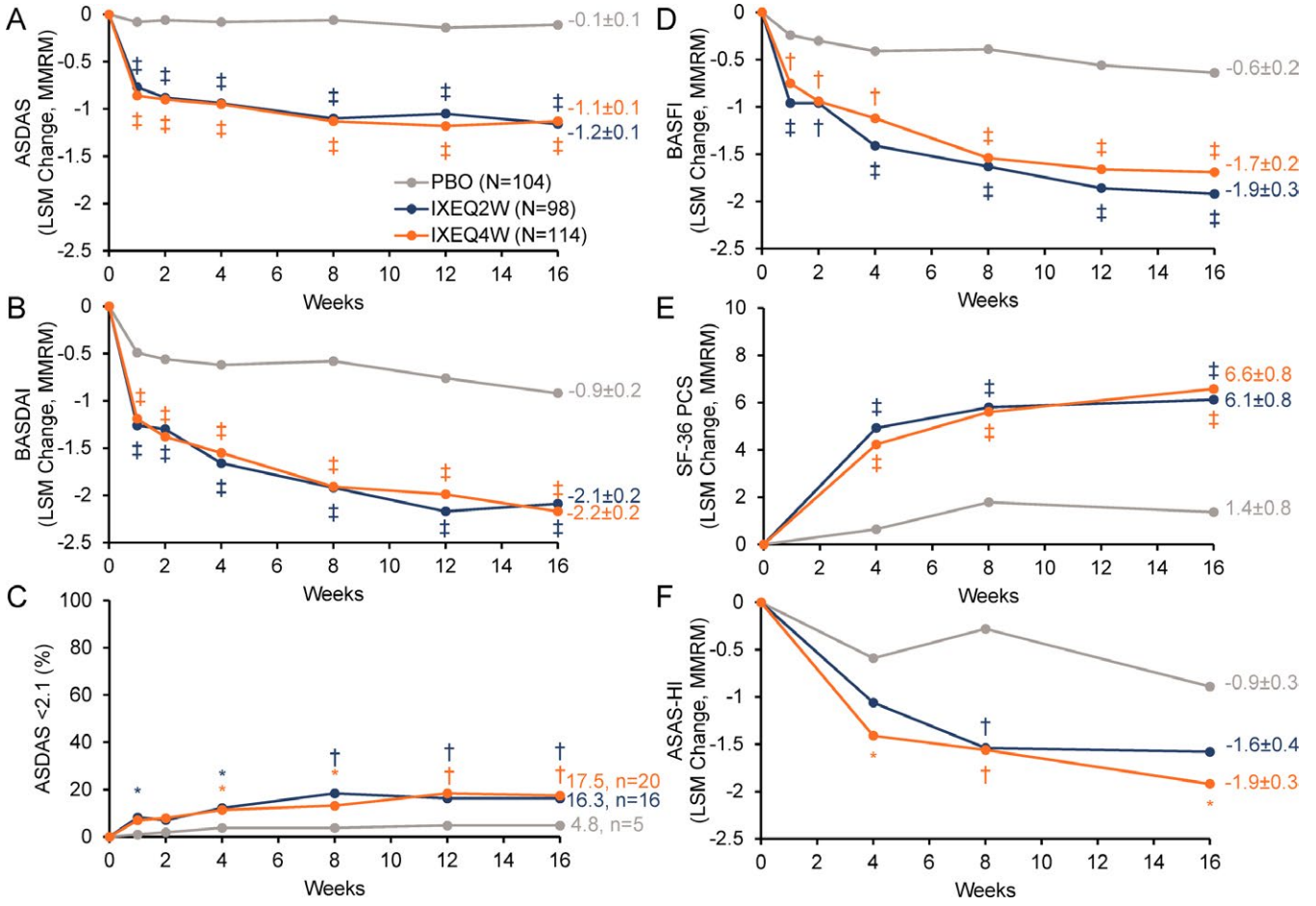

Figure 3. Major secondary outcomes investigating disease activity, function, and quality of life among patients treated with placebo (PBO), ixekizumab every 2 weeks (IXEQ2W), or ixekizumab every 4 weeks (IXEQ4W) for 16 weeks. **A–D**, Ankylosing Spondylitis Disease Activity Score (ASDAS) (**A**), Bath Ankylosing Spondylitis Disease Activity Index (BASDAI) (**B**), ASDAS score <2.1 (**C**), and Bath Ankylosing Spondylitis Functional Index (BASFI) (**D**). **E** and **F**, Medical Outcomes Study Short Form 36 (SF-36) health survey, physical component score (PCS) (**E**) and Assessment of Spondyloarthritis international Society Health Index (ASAS-HI) (**F**). * = $P < 0.05$; † = $P < 0.01$; ‡ = $P < 0.001$, all versus placebo by mixed-effects model of repeated measures (MMRM) or logistic regression analysis (**C** only). Only analyses at week 16 were included in the prespecified multiple testing strategy. Values shown at week 16 for all measures (except **C**) are the least squares mean (LSM) ± SE.

ment of ASDAS <2.1 (inactive or low disease activity) (Figures 3A–C). Patient function was also significantly improved at week 16 in patients treated with IXEQ2W or IXEQ4W relative to placebo, as measured by a change from baseline in BASFI scores (Figure 3D).

Quality of life end points. Statistically significant improvements in quality of life, as measured by mean change from baseline in the SF-36 PCS, were reported at week 16 for patients treated with IXEQ2W and IXEQ4W versus placebo (Figure 3E). Similarly, statistically significant improvements in health functioning, as measured by mean change from baseline in ASAS-HI scores, were reported at week 16 among patients treated with IXEQ4W versus placebo (Figure 3F).

Spinal MRI and systemic inflammation. Spinal MRI and systemic inflammation significantly improved in patients treated with IXEQ2W or IXEQ4W, as demonstrated by the mean change from baseline in SPARCC MRI index spine scores and in mean change from serum baseline CRP levels, respectively, at week 16 versus placebo (Figures 4A and B).

Safety. Safety outcomes reported in COAST-W during the blinded treatment dosing period are summarized in Table 2. Overall mean ± SD exposure was 109.1 ± 19.6 days or a total of 94.4 patient-years. The proportions of patients in each ixekizumab treatment regimen who reported treatment-emergent adverse events (TEAEs) were higher than those for placebo patients and were similar between ixekizumab treatment regimens. Most reported TEAEs were mild or moderate in severity. Severe TEAEs occurred in 7 placebo patients (6.7%), 4 IXEQ2W patients (4.1%), and 4 IXEQ4W patients (3.5%). The most frequently reported TEAEs (occurring in ≥5% of patients receiving ixekizumab overall) were upper respiratory tract infections and injection site reactions. AEs leading to discontinuation

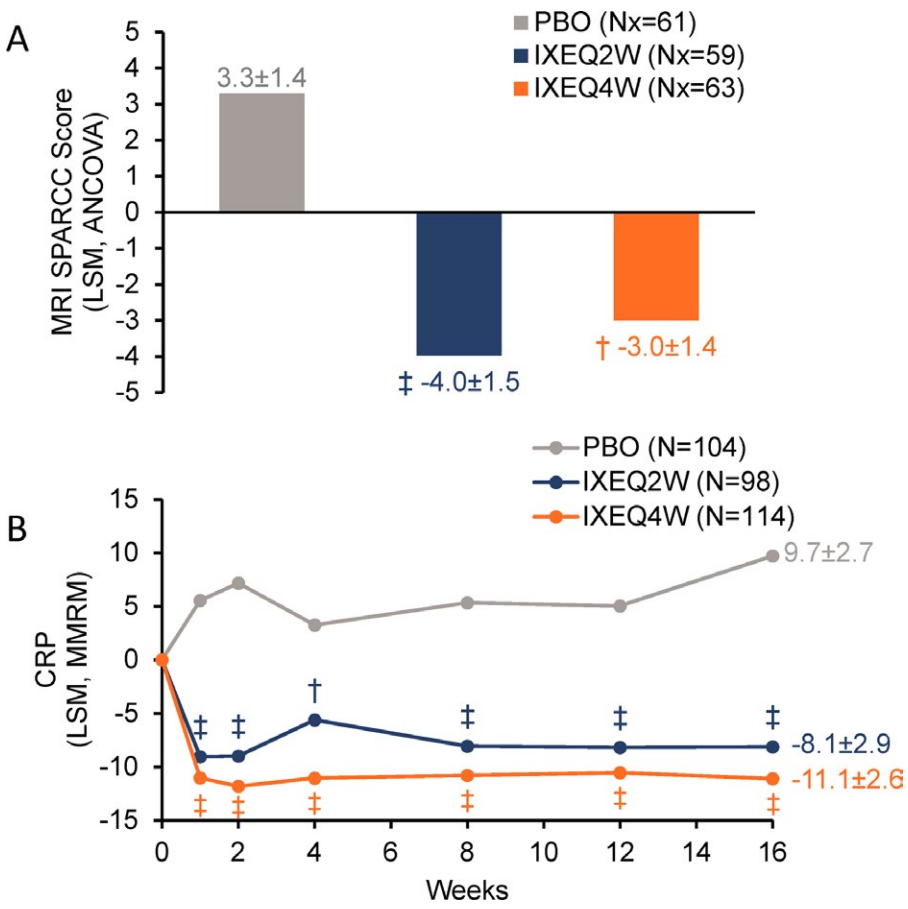

Figure 4. Spondyloarthritis Research Consortium of Canada (SPARCC) magnetic resonance imaging (MRI) index spine scores (**A**) and serum C-reactive protein (CRP) levels (**B**) among patients treated with placebo (PBO), ixekizumab every 2 weeks (IXEQ2W), or ixekizumab every 4 weeks (IXEQ4W) through 16 weeks. † = $P < 0.01$; ‡ = $P < 0.001$, all versus placebo by analysis of covariance (ANCOVA) and least squares mean (LSM) (**A**) or mixed-effects model of repeated measures (MMRM) and LSM (**B**). Only SPARCC MRI spine score analyses at week 16 were included in the prespecified multiple testing strategy. Values shown are the LSM ± SE. N = number of patients in the analysis population; Nx = number of patients in the MRI addendum population.

were reported for 2 placebo patients (1.9%), 3 IXEQ2W patients (3.1%), and 10 IXEQ4W patients (8.8%) (for specific AEs, see Supplementary Table 6, available on the *Arthritis & Rheumatology* web site at http://onlinelibrary.wiley.com/doi/10.1002/art.40753/abstract). Few serious AEs were reported, with similar rates across treatment arms: n = 5 (4.8%) for placebo patients, n = 3 (3.1%) for IXEQ2W patients, and n = 4 (3.5%) for IXEQ4W patients. One death (suicide) occurred in the IXEQ2W treatment arm, in a patient with a documented prior history of depression of ~1 year (reported as mild at study entry), and was judged by the blinded principal investigator to be unrelated to the investigational product.

The incidence of infections was higher for ixekizumab than for placebo, with most infections being mild or moderate (Table 2). Two *Candida* infections were reported in the IXEQ2W study arm (1 esophageal and 1 genital candidiasis), 1 herpes zoster infection was reported in the IXEQ4W study arm, and no infections were reported in the placebo group. Serious infections were reported in 2 patients in the IXEQ4W group (1 peritonitis and 1 pharyngitis; both patients continued the trial). No new cases of tuberculosis or reactivation were reported during the trial.

Reported injection site reactions were all mild or moderate in severity, occurred across all treatment arms (n = 6 [5.8%] for placebo, n = 16 [16.3%] for IXEQ2W, and n = 9 [7.9%] for IXEQ4W), and led to treatment discontinuation in only 2 patients (1 each in the IXEQ2W and IXEQ4W groups).

Mild neutropenia (grade 1) occurred more frequently in the ixekizumab arms than in the placebo arm, was transient in nature, and resolved spontaneously while ixekizumab treatment continued. A single case of grade 2 neutropenia was reported in each ixekizumab treatment arm; 1 of these cases existed before treatment began. One malignancy (acute promyelocytic leukemia [PML]) was reported 4 weeks postbaseline in the IXEQ4W treatment arm. The single report of grade 4 neutropenia was in this same patient. A post hoc analysis of a serum sample collected prior to investigational product exposure revealed that this patient had a genetic risk factor for acute PML (PML/retinoic acid receptor α mutation) prior to trial entry. Treatment was discontinued in this patient.

Table 2. Adverse events (AEs) and treatment-emergent adverse events (TEAEs) during the 16-week blinded treatment dosing period of the COAST-W study*

	Placebo group (n = 104)	IXEQ2W group (n = 98)	IXEQ4W group (n = 114)
TEAE	51 (49.0)	59 (60.2)	73 (64.0)
Mild	18 (17.3)	23 (23.5)	34 (29.8)
Moderate	26 (25.0)	32 (32.7)	35 (30.7)
Severe	7 (6.7)	4 (4.1)	4 (3.5)
Discontinuation due to AE	2 (1.9)	3 (3.1)	10 (8.8)
Serious AE	5 (4.8)	3 (3.1)	4 (3.5)
Death	0	1 (1.0)	0
Common TEAEs†			
Upper respiratory tract infection	3 (2.9)	4 (4.1)	9 (7.9)
Injection site reaction	1 (1.0)	8 (8.2)	3 (2.6)
TEAEs of special interest			
Hepatic	2 (1.9)	1 (1.0)	5 (4.4)
Cytopenia	0	2 (2.0)	0
Grade 1 neutropenia (≥1.5 to <2.0 × 10^9 cells/liter)	1 (1.0)	8 (8.2)	10 (8.8)
Grade 2 neutropenia (≥1.0 to <1.5 × 10^9 cells/liter)	0	1 (1.0)	1 (0.9)
Grade 3 neutropenia (≥0.5 to <1.0 × 10^9 cells/liter)	0	0	0
Grade 4 neutropenia (<0.5 × 10^9 cells/liter)	0	0	1 (0.9)
Infections	10 (9.6)	23 (23.5)	34 (29.8)
Mild	5 (4.8)	14 (14.3)	20 (17.5)
Moderate	5 (4.8)	9 (9.2)	13 (11.4)
Severe	0	0	1 (0.9)
Serious	0	0	2 (1.8)
Candida (genital)	0	1 (1.0)	0
Candida (esophageal)	0	1 (1.0)	0
Herpes zoster	0	0	1 (0.9)
Reactivated tuberculosis	0	0	0
Allergic reactions/hypersensitivities	1 (1.0)	6 (6.1)	3 (2.6)
Potential anaphylaxis	0	0	0
Injection site reactions‡	6 (5.8)	16 (16.3)	9 (7.9)
Cerebrocardiovascular events§	1 (1.0)	1 (1.0)	0
Malignancies	0	0	1 (0.9)
Depression	5 (4.8)	2 (2.0)	0
Anterior uveitis¶	0	3 (3.1)	2 (1.8)
Inflammatory bowel disease	1 (1.0)	0	3 (2.6)
Interstitial lung disease	0	0	0

* Values are the number (%) of patients in the analysis population. IXEQ2W = 80-mg subcutaneous ixekizumab every 2 weeks; IXEQ4W = 80-mg subcutaneous ixekizumab every 4 weeks.
† Common TEAEs are defined as those that occurred at a frequency of ≥5% for patients receiving ixekizumab (both treatment regimen populations combined).
‡ Injection site reaction high-level terms include injection site, pain, erythema, dermatitis, hypersensitivity, pruritus, bruising, rash, and paresthesia or reaction (unspecified).
§ Confirmed cerebrocardiovascular events only.
¶ Anterior uveitis was not a prespecified AE of special interest but was included in the prespecified analyses.

Single adjudicated cerebrocardiovascular events were reported in the placebo and IXEQ2W treatment arms. The cerebrocardiovascular events were confirmed as stent placement (placebo group) and atrial fibrillation (IXEQ2W group), respectively. Both of these patients continued treatment through week 16. No major adverse cerebrocardiovascular events were reported dur-

ing the blinded treatment dosing period. Depression was reported more often in patients taking placebo (n = 5 [4.8%]) than in patients taking IXEQ2W (n = 2 [2.0%]) and IXEQ4W (n = 0).

IBD was reported in 1 patient (1.0%) in the placebo arm (colitis), no patients in the IXEQ2W arm, and in 3 patients (2.6%) in the IXEQ4W arm (1 colitis, 1 ulcerative colitis, and 1 Crohn's disease). Two cases (1 in the placebo group and 1 in the IXEQ4W group) were flares in patients with a preexisting diagnosis of IBD. Of the other 2 IBD cases (IXEQ4W group), 1 case was in a current smoker (smoking since 1994) with a perianal cyst reported in 2010 and accompanying intermittent abdominal pain since that time. The other case was in a long-term smoker (since 2009), who stopped smoking 3 months prior to trial entry, with a prior history of anemia (2012–2014) and intermittent diarrhea since 2011 (ongoing but mild at time of trial entry). All reported cases of IBD were adjudicated as "probable." Anterior uveitis was reported in 3 IXEQ2W patients (3.1%) and 2 IXEQ4W patients (1.8%); 3 of these 5 patients (2 in the IXEQ2W group and 1 in the IXEQ4W group) were documented to have a preexisting history of anterior uveitis; 4 of the 5 patients were HLA–B27 positive, and all had longstanding disease (experiencing symptoms for at least 7 years and up to 28 years). Psoriasis was reported in 2 patients with a previous medical history of psoriasis (1 in the placebo group and 1 in the IXEQ4W group).

Treatment-emergent antidrug antibodies were observed in 3 placebo patients (2.9%), 4 IXEQ2W patients (4.1%), and 8 IXEQ4W patients (7.1%). Most of the reported antidrug antibodies were classified as being low titer, 2 IXEQ2W patients (2.0%) and 1 IXEQ4W patient (0.9%) were reported as having moderate titers, and 1 IXEQ2W patient (0.9%) was reported with high titers. Neutralizing antidrug antibodies were detected in 3 IXEQ4W patients (2.7%). No associations were identified between treatment-emergent antidrug antibody status and ASAS40 response, injection site reactions, or potential allergic/hypersensitivity events with either ixekizumab treatment regimen.

DISCUSSION

The COAST-W trial is the first large, randomized, controlled trial focusing exclusively on radiographic axial SpA patients with prior treatment failure (inadequate response to or intolerance of 1 or 2 TNFi). In that respect, this study differs from other reported phase III studies of radiographic axial SpA that enrolled exclusively or predominantly biologic DMARD (bDMARD)–naive patients. Ixekizumab was superior to placebo in reducing the signs and symptoms of radiographic axial SpA in this population of patients with longstanding disease and very high disease activity. For the primary end point (ASAS40 response), both IXEQ2W and IXEQ4W were superior to placebo at week 16. Statistically significant and clinically meaningful improvements over placebo were also observed at week 16 for all major secondary end points, including measures of disease activity, function, and quality of life for IXEQ4W and for all but 1 (ASAS-HI) major secondary end points for IXEQ2W. Statistically significant improvements over placebo were reported early in the trial for all of these end points. In addition, and despite baseline levels of spinal inflammation being relatively low, thereby hampering the ability to show improvement, a statistically significant and objective effect on spinal inflammation was observed for IXEQ2W and IXEQ4W, as measured by the SPARCC MRI index score, which was supported by parallel improvements in CRP levels. The spinal MRI data are the first to be reported in a large subset of patients with prior intolerance of or inadequate response to TNFi in the context of a placebo-controlled registration study.

Despite the greater exposure with the IXEQ2W regimen, IXEQ2W did not show a clinically meaningful incremental increase in observed efficacy relative to the IXEQ4W regimen. Similarly, the week 0 starting dose of ixekizumab 160 mg did not reveal a clinically meaningful incremental improvement in week 16 response rates relative to the 80-mg starting dose for either ixekizumab regimen. The impact of starting dose on speed of onset requires further analysis.

Ixekizumab showed an acceptable safety profile in this patient population with longstanding and very active disease. The frequency of TEAEs in this population (patients with prior inadequate response to or intolerance of TNFi) was higher across all treatment arms, including placebo, than those reported in a bDMARD-naive population with radiographic axial SpA from another phase III ixekizumab study (COAST-V, NCT02696785) (30). TEAEs occurred more often with ixekizumab than with placebo, mostly driven by upper respiratory tract infections and injection site reactions. Serious AEs occurred at similar rates across ixekizumab and placebo treatment arms. The reported frequencies for total TEAEs and serious AEs are consistent with those reported among patients with psoriasis and psoriatic arthritis (PsA) treated with ixekizumab (31–34). Discontinuations due to AEs were similar for IXEQ2W relative to placebo but higher for IXEQ4W relative to placebo, with no particular AE driving the difference. The explanation for this discrepancy is unclear, given that there were no discontinuations due to AEs in the IXEQ4W treatment arm in the study of ixekizumab treatment in bDMARD-naive patients with radiographic axial SpA (30).

Infection frequencies were higher in patients treated with ixekizumab relative to placebo. The majority of infections were mild, with the most commonly reported being upper respiratory tract infections and nasopharyngitis. Serious infections were uncommon (n = 2). Reported infection frequencies were higher than those reported in COAST-V, but consistent with or lower than those reported in trials of ixekizumab for PsA and psoriasis (30).

Injection site reactions (high-level terms) were higher in patients treated with ixekizumab relative to placebo, and similar to or lower than previously observed in trials of ixekizumab for PsA and psoriasis (33,34). One case of grade 4 neutropenia was reported in the IXEQ4W treatment arm in a patient with treatment-

emergent acute PML who had a genetic risk factor for this disease. In the IXEQ2W treatment arm, one patient with a documented prior history of depression committed suicide, which was judged by the blinded investigator to be unrelated to the investigational product.

The incidences of IBD and acute anterior uveitis in the current study involving patients with prior inadequate response to or intolerance of 1 or 2 TNFi, and longstanding (mean ± SD symptom duration 18.4 ± 11.1 years) and very active disease, were higher than reported among bDMARD-naive patients with radiographic axial SpA treated with ixekizumab (30). Certain comorbidities in axial SpA, especially IBD and acute anterior uveitis, have been reported to be associated with longer disease duration (35). Integrated data from the ixekizumab axial SpA studies, as well as longer-term data, are needed to better understand whether the IBD events observed in the current study reflect the recruited patient population, study treatment, other factors (such as discontinuation of prior TNFi), or a combination of the above (36).

The incidence of ixekizumab antidrug antibodies was low and consistent with previous reports in patients with PsA and prior inadequate response to or intolerance of 1 or 2 TNFi (34). Ixekizumab antidrug antibodies were not associated with immune reactions or reductions in efficacy.

TNFi and 1 IL-17A antagonist (secukinumab) are the only approved biologic agents for treatment of AS. The ixekizumab results reported here for patients with inadequate response to or intolerance of 1 or 2 TNFi are consistent with those previously reported for secukinumab in patients with inadequate response to or intolerance of 1 TNFi (subset of 85 patients from the MEASURE-2 study) (18). However, given that other baseline characteristics may also differ between these 2 studies, direct comparisons should not be made between the trial results. Both MEASURE-2 and COAST-W demonstrate that IL-17A antagonists are efficacious and well-tolerated in patients with prior intolerance of or inadequate response to TNFi.

The COAST-W trial has several strengths. It is the first large, randomized, controlled trial to focus exclusively on patients with radiographic axial SpA with a prior inadequate response to or intolerance of 1 or 2 TNFi. This focus allowed for a comprehensive evaluation of the baseline characteristics, burden of disease, and treatment efficacy and safety in this population. COAST-W also used the ASAS40 response as the primary end point, reflecting major improvement and representing a more stringent end point than the commonly used ASAS20. In addition, COAST-W is the first placebo-controlled trial to generate spinal MRI data in a TNFi-intolerant or inadequate responder population. Conversely, the current data set is limited to a 16-week treatment period. Longer-term data, which are being collected through 1 year of treatment in the present trial, as well as during an optional 2-year extension trial, will provide further information on the long-term efficacy and safety of ixekizumab.

In conclusion, the findings of this study demonstrate that the ixekizumab treatment regimens yield rapid and significant improvements in the signs and symptoms of radiographic axial SpA, as well as a significant reduction in inflammation of the spine as measured by MRI, when compared to placebo. The current results support ixekizumab as a treatment option for patients with radiographic axial SpA and prior inadequate response to or intolerance of TNFi.

AUTHOR CONTRIBUTIONS

All authors were involved in drafting the article or revising it critically for important intellectual content, and all authors approved the final version to be submitted for publication. Dr. Deodhar had full access to all of the data in the study and takes responsibility for the integrity of the data and the accuracy of the data analysis.

Study conception and design. Deodhar, Zhao, Carlier.

Acquisition of data. Deodhar, Poddubnyy, Pacheco-Tena, Salvarani, Lespessailles, Rahman, Järvinen, Sanchez-Burson, Gaffney, Lee, Santisteban, Li, Zhao, Carlier, Reveille.

Analysis and interpretation of data. Deodhar, Poddubnyy, Krishnan, Santisteban, Li, Zhao, Carlier.

ROLE OF THE STUDY SPONSOR

An academic advisory committee was involved in the study design and data interpretation, together with authors from Eli Lilly and Company. Authors had full access to all the data in the study and had final responsibility for the decision to submit for publication. Eli Lilly and Company contributed to study design, data collection, data analysis, data interpretation, manuscript preparation, and publication decisions. Dr. Krishnan was responsible for the overall conduct of the study. Medical writing support was provided by Brian S. Comer, PhD. Editorial support was provided by P. Vidhyasagar Arya, PhD. Statistical analysis and programming support was provided by Emily Seem, MS, and Lingling Xie, MS. All are employees of Eli Lilly and Company. Publication of this article was not contingent upon approval by Eli Lilly and Company.

REFERENCES

1. Reveille JD, Witter JP, Weisman MH. Prevalence of axial spondylarthritis in the United States: estimates from a cross-sectional survey. Arthritis Care Res (Hoboken) 2012;64:905–10.
2. Sieper J, Poddubnyy D. Axial spondyloarthritis. Lancet 2017;390: 73–84.
3. Braun J, Sieper J. Ankylosing spondylitis. Lancet 2007;369:1379–90.
4. Van der Heijde D, Ramiro S, Landewe R, Baraliakos X, van den Bosch F, Sepriano A, et al. 2016 update of the ASAS-EULAR management recommendations for axial spondyloarthritis. Ann Rheum Dis 2017;76:978–91.
5. Ward MM, Deodhar A, Akl EA, Lui A, Ermann J, Gensler LS, et al. American College of Rheumatology/Spondylitis Association of America/Spondyloarthritis Research and Treatment Network 2015 recommendations for the treatment of ankylosing spondylitis and nonradiographic axial spondyloarthritis. Arthritis Rheumatol 2016;68:282–98.
6. National Institute for Health and Care Excellence. TA383: TNF-α inhibitors for ankylosing spondylitis and non-radiographic axial spondyloarthritis. 2016. URL: https://www.nice.org.uk/guidance/ta383.
7. Van der Heijde D, Kivitz A, Schiff MH, Sieper J, Dijkmans BA, Braun J, et al. Efficacy and safety of adalimumab in patients with ankylosing spondylitis: results of a multicenter, randomized, double-blind, placebo-controlled trial. Arthritis Rheum 2006;54:2136–46.

8. Inman RD, Davis JC Jr, van der Heijde D, Diekman L, Sieper J, Kim SI, et al. Efficacy and safety of golimumab in patients with ankylosing spondylitis: results of a randomized, double-blind, placebo-controlled, phase III trial. Arthritis Rheum 2008;58:3402–12.
9. Van den Bosch F, Deodhar A. Treatment of spondyloarthritis beyond TNF-α blockade. Best Pract Res Clin Rheumatol 2014;28: 819–27.
10. Deodhar A, Reveille JD, Harrison DD, Kim L, Lo KH, Leu JH, et al. Safety and efficacy of golimumab administered intravenously in adults with ankylosing spondylitis: results through week 28 of the GO-ALIVE study. J Rheumatol 2018;45:341–8.
11. Heiberg MS, Koldingsnes W, Mikkelsen K, Rodevand E, Kaufmann C, Mowinckel P, et al. The comparative one-year performance of anti–tumor necrosis factor α drugs in patients with rheumatoid arthritis, psoriatic arthritis, and ankylosing spondylitis: results from a longitudinal, observational, multicenter study. Arthritis Rheum 2008;59:234–40.
12. Glintborg B, Ostergaard M, Krogh NS, Dreyer L, Kristensen HL, Hetland ML. Predictors of treatment response and drug continuation in 842 patients with ankylosing spondylitis treated with anti-tumour necrosis factor: results from 8 years' surveillance in the Danish nationwide DANBIO registry. Ann Rheum Dis 2010;69:2002–8.
13. D'Angelo S, Carriero A, Gilio M, Ursini F, Leccese P, Palazzi C. Safety of treatment options for spondyloarthritis: a narrative review. Expert Opin Drug Saf 2018;17:475–86.
14. Kenna TJ, Davidson SI, Duan R, Bradbury LA, McFarlane J, Smith M, et al. Enrichment of circulating interleukin-17–secreting interleukin-23 receptor–positive γ/δ T cells in patients with active ankylosing spondylitis. Arthritis Rheum 2012;64:1420–9.
15. Shen H, Goodall JC, Hill Gaston JS. Frequency and phenotype of peripheral blood Th17 cells in ankylosing spondylitis and rheumatoid arthritis. Arthritis Rheum 2009;60:1647–56.
16. Baeten D, Sieper J, Braun J, Baraliakos X, Dougados M, Emery P, et al. Secukinumab, an interleukin-17A inhibitor, in ankylosing spondylitis. N Engl J Med 2015;373:2534–48.
17. Pavelka K, Kivitz A, Dokoupilova E, Blanco R, Maradiaga M, Tahir H, et al. Efficacy, safety, and tolerability of secukinumab in patients with active ankylosing spondylitis: a randomized, double-blind phase 3 study, MEASURE 3. Arthritis Res Ther 2017;19:285.
18. Sieper J, Deodhar A, Marzo-Ortega H, Aelion JA, Blanco R, Jui-Cheng T, et al. Secukinumab efficacy in anti-TNF-naive and anti-TNF-experienced subjects with active ankylosing spondylitis: results from the MEASURE 2 Study. Ann Rheum Dis 2017;76:571–92.
19. Liu L, Lu J, Allan BW, Tang Y, Tetreault J, Chow CK, et al. Generation and characterization of ixekizumab, a humanized monoclonal antibody that neutralizes interleukin-17A. J Inflamm Res 2016;9:39–50.
20. Rudwaleit M, van der Heijde D, Landewe R, Listing J, Akkoc N, Brandt J, et al. The development of Assessment of SpondyloArthritis international Society classification criteria for axial spondyloarthritis (part II): validation and final selection. Ann Rheum Dis 2009;68:777–83.
21. Van der Linden S, Valkenburg HA, Cats A. Evaluation of diagnostic criteria for ankylosing spondylitis: a proposal for modification of the New York criteria. Arthritis Rheum 1984;27:361–8.
22. Sieper J, Rudwaleit M, Baraliakos X, Brandt J, Braun J, Burgos-Vargas R, et al. The Assessment of SpondyloArthritis international Society (ASAS) handbook: a guide to assess spondyloarthritis. Ann Rheum Dis 2009;68 Suppl 2:ii1–44.
23. Garrett S, Jenkinson T, Kennedy LG, Whitelock H, Gaisford P, Calin A. A new approach to defining disease status in ankylosing spondylitis: the Bath Ankylosing Spondylitis Disease Activity Index. J Rheumatol 1994;21:2286–91.
24. Machado PM, Landewe RB, van der Heijde DM. Endorsement of definitions of disease activity states and improvement scores for the Ankylosing Spondylitis Disease Activity Score: results from OMERACT 10. J Rheumatol 2011;38:1502–6.
25. Calin A, Garrett S, Whitelock H, Kennedy LG, O'Hea J, Mallorie P, et al. A new approach to defining functional ability in ankylosing spondylitis: the development of the Bath Ankylosing Spondylitis Functional Index. J Rheumatol 1994;21:2281–5.
26. Ware JE Jr, Snow KK, Kosinski M, Gandek B. SF-36 health survey: manual and interpretation guide. 2nd ed. Lincoln (RI): QualityMetric; 2000.
27. Kiltz U, van der Heijde D, Boonen A, Braun J. The ASAS Health Index (ASAS HI): a new tool to assess the health status of patients with spondyloarthritis. Clin Exp Rheumatol 2014;32 Suppl 85:S105–8.
28. Kiltz U, van der Heijde D, Boonen A, Cieza A, Stucki G, Khan MA, et al. Development of a health index in patients with ankylosing spondylitis (ASAS HI): final result of a global initiative based on the ICF guided by ASAS. Ann Rheum Dis 2015;74:830–5.
29. Maksymowych WP, Inman RD, Salonen D, Dhillon SS, Krishnananthan R, Stone M, et al. Spondyloarthritis Research Consortium of Canada magnetic resonance imaging index for assessment of spinal inflammation in ankylosing spondylitis. Arthritis Rheum 2005;53:502–9.
30. Van der Heijde D, Wei J, Dougados M, Mease PJ, Deodhar A, Maksymowych W, et al. Ixekizumab significantly improves signs, symptoms, and spinal inflammation of active ankylosing spondylitis/radiographic axial spondyloarthritis: 16-week results of a phase 3 randomized, active and placebo-controlled trial [abstract]. Arthritis Rheumatol 2018;70 Suppl 10. URL: https://acrabstracts.org/abstract/ixekizumab-significantly-improves-signs-symptoms-and-spinal-inflammation-of-active-ankylosing-spondylitis-radiographic-axial-spondyloarthritis-16-week-results-of-a-phase-3-randomized-active-a/.
31. Gordon KB, Blauvelt A, Papp KA, Langley RG, Luger T, Ohtsuki M, et al. Phase 3 trials of ixekizumab in moderate-to-severe plaque psoriasis. N Engl J Med 2016;375:345–56.
32. Griffiths CE, Reich K, Lebwohl M, van de Kerkhof P, Paul C, Menter A, et al. Comparison of ixekizumab with etanercept or placebo in moderate-to-severe psoriasis (UNCOVER-2 and UNCOVER-3): results from two phase 3 randomised trials. Lancet 2015;386:541–51.
33. Mease PJ, van der Heijde D, Ritchlin CT, Okada M, Cuchacovich RS, Shuler CL, et al. Ixekizumab, an interleukin-17A specific monoclonal antibody, for the treatment of biologic-naive patients with active psoriatic arthritis: results from the 24-week randomised, double-blind, placebo-controlled and active (adalimumab)-controlled period of the phase III trial SPIRIT-P1. Ann Rheum Dis 2017;76:79–87.
34. Nash P, Kirkham B, Okada M, Rahman P, Combe B, Burmester GR, et al. Ixekizumab for the treatment of patients with active psoriatic arthritis and an inadequate response to tumour necrosis factor inhibitors: results from the 24-week randomised, double-blind, placebo-controlled period of the SPIRIT-P2 phase 3 trial. Lancet 2017;389:2317–27.
35. Varkas G, Vastesaeger N, Cypers H, Colman R, Renson T, van Praet L, et al. Association of inflammatory bowel disease and acute anterior uveitis, but not psoriasis, with disease duration in axial spondyloarthritis: results from two Belgian nationwide axial spondyloarthritis cohorts. Arthritis Rheumatol 2018;70:1588–96.
36. Kennedy NA, Warner B, Johnston EL, Flanders L, Hendy P, Ding NS, et al. Relapse after withdrawal from anti-TNF therapy for inflammatory bowel disease: an observational study, plus systematic review and meta-analysis. Aliment Pharmacol Ther 2016;43:910–23.

APPENDIX A: MEMBERS OF THE COAST-W STUDY GROUP

Members of the COAST-W Study Group are as follows: Christopher Antolini, Valderilio Azevedo, Magnus Barkham, Aaron Alejandro Barrera Rodriguez, Alberto Berman, Tomasz Blicharski, Jan Brzezicki, Gerd Burmester, Judith Carrio, Eduardo Collantes, Bernard Combe, Fidencio Cons-Molina, Gregorio Cortes-Maisonet, Anna Dudek, Sergio Duran Barragan, Ori Elkayam, Kathleen Flint, Mauro Galeazzi, Norman Gaylis, David Goddard, Carlos Gonzalez Fernandez, Philippe Goupille, Jordi Gratacos Masmitja, Maria Greenwald, Elisa Gremese, Seung Jae Hong, Mary Howell, Pawel Hrycaj, Akgun Ince, Ji Hyeon Ju, Jeffrey Kaine, Seong Wook Kang, Mauro Keiserman, Tae-Hwan Kim, Alan Kivitz, Steven Klein, Joel Kremer, Chang Keun Lee, Sang Heon Lee, Sang-Hoon Lee, Roger Lidman, James Loveless, Eleonora Lucero, Jose Maldonado Cocco, Flora Marcolino, Xavier Mariette, Daksha Mehta, Frederic Morin, Yolanda Moscovici, Eric Mueller, Eduardo Mysler, Francisco Navarro Blasco, Minh Nguyen, Carlos Pantojas, Min-Chan Park, Amarilis Perez-De Jesus, Eric Peters, Rafal Plebanski, Roel Querubin, Cesar Ramos Remus, Tatiana Reitblat, Tania Rivera, Juan Cruz Rizo Rodriguez, Michael Sayers, Antonio Scotton, Craig Scoville, David Shaw, Kichul Shin, Atul Singhal, Cassandra Skinner, Oscar Soto-Raices, Martin Soubrier, Malgorzata Szymanska, Christine Thai, Marleen van de Sande, Alvin Wells, Rafal Wojciechowski, Ricardo Xavier, Antonio Ximenes, and Devy Zisman.

AMERICAN COLLEGE OF RHEUMATOLOGY
EDUCATION • TREATMENT • RESEARCH

Arthritis & Rheumatology
Vol. 71, No. 4, April 2019, pp 612–625
DOI 10.1002/art.40770

Interleukin-17A Inhibition Diminishes Inflammation and New Bone Formation in Experimental Spondyloarthritis

Melissa N. van Tok,[1] Leonie M. van Duivenvoorde,[1] Ina Kramer,[2] Peter Ingold,[2] Sabina Pfister,[2] Lukas Roth,[2] Iris C. Blijdorp,[1] Marleen G. H. van de Sande,[1] Joel D. Taurog,[3] Frank Kolbinger,[2] and Dominique L. Baeten[4]

Objective. It remains unclear if and how inflammation and new bone formation in spondyloarthritis (SpA) are coupled. We undertook this study to assess the hypothesis that interleukin-17A (IL-17A) is a pivotal driver of both processes.

Methods. The effect of tumor necrosis factor (TNF) and IL-17A on osteogenesis was tested in an osteoblastic differentiation assay using SpA fibroblast-like synoviocytes (FLS) differentiated with dexamethasone, β-glycophosphatase, and ascorbic acid. IL-17A blockade was performed in HLA–B27/human β_2-microglobulin (hβ_2m)–transgenic rats, which served as a model for SpA in both prophylactic and therapeutic settings. Inflammation and new bone formation were evaluated by micro–computed tomography imaging, histologic analysis, and gene expression profiling.

Results. TNF and IL-17A significantly increased in vitro osteoblastic differentiation. In vivo, prophylactic blockade of IL-17A significantly delayed spondylitis and arthritis development and decreased arthritis severity. Anti–IL-17A treatment was also associated with prevention of bone loss and periosteal new bone formation. Therapeutic targeting of IL-17A after the initial inflammatory insult also significantly reduced axial and peripheral joint inflammation. This treatment was again associated with a marked reduction in spinal and peripheral structural damage, including new bone formation. RNA sequencing of target tissue confirmed that IL-17A is a key driver of the molecular signature of disease in this model and that therapeutic anti–IL-17A treatment reversed the inflammatory signature and the selected gene expression related to bone damage.

Conclusion. Both prophylactic and therapeutic inhibition of IL-17A diminished inflammation and new bone formation in HLA-B27/hβ_2m–transgenic rats. Taken together with the ability of IL-17A to promote osteoblastic differentiation of human SpA FLS, these data suggest a direct link between IL-17A–driven inflammation and pathologic new bone formation in SpA.

INTRODUCTION

The structural hallmark of spondyloarthritis (SpA) is excessive new bone formation, which in some cases progresses to complete spinal ankylosis. The mechanism behind new bone formation in SpA remains poorly understood. The fact that tumor necrosis factor (TNF) inhibition, which potently suppresses inflammation and focal bone destruction in both axial and peripheral SpA, has little to no impact on new bone formation (1–5) suggests an uncoupling of inflammation and osteoproliferation. This uncoupling could be explained either by reparative bone formation after resolution of inflammation (i.e., the TNF-brake hypothesis) (6) or by the existence of 2 parallel but independent processes of inflammation and structural remodeling initiated by a common trigger (i.e., the entheseal stress hypothesis) (7). The notion that inflammation and new bone formation are uncoupled is, however, challenged by a couple of key observations. In the HLA–B27/human β_2-microglobulin (B27/hβ_2m)–transgenic rat model of SpA, new

Dr. Baeten's work was supported by the Netherlands Scientific Organization (NWO Vici grant) and the European Research Council (ERC Consolidator grant).

[1]Melissa N. van Tok, PhD, Leonie M. van Duivenvoorde, PhD, Iris C. Blijdorp, BS, Marleen G. H. van de Sande, MD, PhD: Amsterdam UMC, University of Amsterdam, Amsterdam, The Netherlands; [2]Ina Kramer, PhD, Peter Ingold, Sabina Pfister, PhD, Lukas Roth, PhD, Frank Kolbinger, PhD: Novartis Institutes for BioMedical Research, Basel, Switzerland; [3]Joel D. Taurog, MD: University of Texas Southwestern Medical Center, Dallas; [4]Dominique L. Baeten, MD, PhD: Academic Medical Centre/University of Amsterdam, Amsterdam, The Netherlands, and UCB Pharma, Slough, UK.

Mr. Ingold and Drs. Kramer, Pfister, and Roth own stock or stock options in Novartis Pharma. Dr. van de Sande has received consulting fees from AbbVie, Eli Lilly, Janssen, and Novartis (less than $10,000 each) and research grants from those companies. Dr. Taurog holds license agreements with AbbVie, AnGes, Celgene, and Novartis and has received research support from AbbVie. Dr. Baeten owns stock or stock options in UCB. No other disclosures relevant to this article were reported.

Address correspondence to Dominique L. Baeten, MD, PhD, Amsterdam UMC, University of Amsterdam, Meibergdreef 9, 1105 AZ Amsterdam, The Netherlands. E-mail: d.l.baeten@amc.uva.nl.

Submitted for publication January 29, 2018; accepted in revised form October 30, 2018.

bone formation is never observed in the absence of inflammation. Both processes exist simultaneously at distinct anatomic sites of the joint (8,9). In human axial SpA, high disease activity is associated with accelerated spinal progression (10). Accordingly, in this report we propose an alternative hypothesis: that chronic tissue inflammation and new bone formation in SpA are directly linked by inflammatory mediators distinct from soluble TNF (11). We have previously provided direct evidence for this concept by demonstrating that overexpression of transmembrane (but not soluble) TNF in mice leads to axial and peripheral inflammation and new bone formation, reminiscent of human SpA (van Duivenvoorde LM, et al: submitted for publication).

One of the key inflammatory mediators in SpA is interleukin-17A (IL-17A) (12). Animal studies, translational research, and clinical trials have demonstrated that IL-17A plays a central role in inflammation in both axial and peripheral SpA (12–16). However, its potential role in new bone formation remains incompletely understood. Beyond the well-established effect of IL-17A on osteoclasts (17,18), 2 recent studies demonstrated in vitro and in vivo that IL-17A has an inhibitory effect on mature osteoblasts through the Wnt signaling pathway (19,20). In contrast, IL-17A promoted new bone formation and fracture healing in a drill-hole model by stimulating proliferation and osteoblastic differentiation of mesenchymal precursors (21). Accordingly, IL-17A was shown to promote osteoblastic differentiation of human stromal precursor cells, including bone marrow mesenchymal stem cells (22,23) and fibroblast-like synoviocytes (FLS) (24). These conflicting results may be explained by differences in cell origin, state of differentiation, and/or microenvironment, which suggests the necessity of a detailed analysis of the role of IL-17A in new bone formation in SpA-relevant in vitro and/or in vivo models. We hypothesized that IL-17A is a key mediator linking inflammation to new bone formation in SpA. To test this hypothesis, we performed in vitro human osteoblastic differentiation assays and in vivo IL-17A blockade in *Mycobacterium tuberculosis*–induced disease in B27/hβ_2m–transgenic rats (9,25).

MATERIALS AND METHODS

In vitro osteoblastic differentiation. Primary human FLS cultures were generated from synovial biopsy samples from 8 SpA patients, according to standardized protocol (26). Periosteal cells were derived (with written informed consent) from waste material from nonarthritic patients undergoing total knee replacement surgery. StemXVivo osteogenic/adipogenic base medium (no. CCM007; R&D Systems) supplemented with 100 n*M* dexamethasone, 50 μ*M* ascorbic acid, and 10 m*M* β-glycophosphatase was used for differentiation in the presence or absence of 50 ng/ml recombinant IL-17A (R&D Systems), 1 ng/ml recombinant TNF (R&D Systems), or a combination of both. Half of the medium was replaced twice weekly. After 14 days and 21 days, wells were stained for alizarin red or alkaline phosphatase (AP); cells were fixed with 4% formalin, washed with phosphate buffered saline, and incubated with 2% alizarin red S or AP dye. After the drying of the wells, 2 independent observers scored the percentage of staining.

RNA was extracted using RNeasy Micro Columns (no. 74004; Qiagen), and complementary DNA (cDNA) was synthesized using a RevertAid First Strand cDNA Synthesis Kit (no. K1622; ThermoFisher), both according to the manufacturer's protocol, after 7 days and 14 days of differentiation. Quantitative polymerase chain reaction (qPCR) analyses were performed using TaqMan assays (Life Technologies) for *ALPL* (assay ID Hs01029144_m1), *RUNX2* (assay ID Hs00231692_m1), *BGLAP* (assay ID Hs01587814_g1), *IBSP* (assay ID Hs00173720_m1), and *GAPDH* (no. 4310884E) as a housekeeping gene. The expression of all indicated genes was measured at several time points (3 days, 7 days, 14 days, and 21 days after differentiation) to identify the peak expression. For *ALPL*, *RUNX2*, and *IBSP*, the peak was on day 7, and for *BGLAP* it was on day 14 (data not shown). All qPCR data were analyzed using the $2^{-\Delta\Delta Ct}$ method (27).

Rats. The transgenic 21-3 (B27/hβ_2m) Reh and 283-2 (B27/hβ_2m) Reh rat lines (26) on Lewis background were bred and housed (4 per cage) in open or individually ventilated cages at the animal research facility at Amsterdam Medical Center (AMC). Orchiectomized and *M tuberculosis*–immunized [21-3 × 283-2] F1 male rats were used for all experiments (9,26). All experiments were approved by the AMC Animal Ethics Committee.

Orchiectomy and immunization. To prevent epididymoorchitis, orchiectomy on 4-week-old male rats was performed using standard methods (9,28). Briefly, orchiectomy was performed under isoflurane anesthesia via the abdominal cavity. Fifteen minutes prior to surgery, all rats received 1 ml/kg carprofen as a painkiller. After a washout period of 2 weeks, rats were immunized with 45–60 μg of pulverized heat-inactivated *M tuberculosis* (Difco) in 100 μl Freund's incomplete adjuvant (Chondrex), as previously described (9). Rats received an intradermal injection at the tail base under isoflurane anesthesia. The *M tuberculosis* dose was dependent on housing conditions (45 μg for animals in open-cage housing and 60 μg for animals in individually ventilated cage housing).

Anti–IL-17A treatment. Rats were treated once weekly via intraperitoneal injection with 15 mg/kg mouse anti–mouse/rat IL-17A antibody (BZN035) or with mouse IgG2a isotype control antibody (both from Novartis). Prophylactic treatment (n = 6 rats per group) started 1 week after immunization. Therapeutic treatment (n = 12 rats per group) started 1 week after the arthritis incidence reached 50%. At the start of therapeutic treatment, randomization was performed based on arthritis scores. Treatment continued for 5 weeks, and rats were killed 1 week after the final injection. The therapeutic intervention was performed in duplicate, and data were pooled for analysis.

Clinical scoring. The presence and severity of arthritis in the paws were determined macroscopically (0–3 score) as previously described (9), and digital swelling was measured by plethysmometry. Cumulative clinical scores were calculated for severity analysis. Swelling (in cm^3) was normalized to the day before disease onset (for the prophylactic treatment experiment) or to the day of treatment initiation (for the therapeutic treatment experiment). Spondylitis (presence of swelling and bumps in the tail) was determined macroscopically and severity was scored (0–3 score) at the end of the therapeutic treatment experiment.

Clinical scoring during the therapeutic treatment experiment was performed by 1 observer (MNvT) who was blinded with regard to treatment details. Humane end points were defined as 15% body weight loss or 2 completely swollen paws (in the prophylactic treatment group), and 20% body weight loss or 2 completely swollen front paws (in the therapeutic treatment group). In the prophylactic treatment experiment, 4 of 6 IgG2a-treated controls were killed 13 days prior to the end of the experiment due to severe disease that resulted in >15% body weight loss; in these cases, the last observation was carried forward. In the therapeutic treatment experiment, no rats reached the humane end points. Additionally, rats in this group that did not have arthritis at the start of treatment were excluded from further analysis (except for incidence analysis). Among the 12 rats in each therapeutic treatment group, 3 rats per group had no arthritis at the start of treatment (resulting in a total of 9 rats per group). During the therapeutic treatment experiment, age-matched healthy control rats were included only for ex vivo experiments and analyses. These HLA–B27–transgenic rats were orchiectomized to prevent epididymoorchitis but were not immunized.

Ex vivo micro–computed tomography (micro-CT) analysis. Hind paws, lumbar spines, and tails of IgG2a-treated and anti–IL-17A–treated rats (and age-matched healthy controls, only in the therapeutic treatment experiment) were fixed in 4% formalin, transferred to 70% ethanol, and imaged with a micro-CT scanner. Hind paws and lumbar spines were measured using a μCT 40 instrument, and tail vertebrae were imaged with a vivaCT 40 instrument (both from Scanco Medical). The following scan parameters were employed: energy/intensity 70 kV, 114 μA, 4 W; sample time 150 msec for hind paws, 190 msec for caudal vertebrae, and 300 msec for lumbar vertebrae; matrix 1,024 × 1,024 pixels for hind paws and caudal spine, and 2,048 × 2,048 pixels for lumbar spine; and voxel size 20 μm for hind paws, 25 μm for caudal vertebrae, and 10 μm for lumbar vertebrae. Structural vertebral bone parameters were calculated from 60 slices of L4, applying a segmentation threshold of 620 mg of hydroxyapatite (HA)/cm^3. Segmentation thresholds of 400–750 mg of HA/cm^3 (hind paws) or 200–500 mg of HA/cm^3 (caudal vertebrae) were used to identify the newly formed bone anticipated to have a lower material bone mineral density (BMD). Segmentation thresholds of 800–3,000 mg of HA/cm^3 (hind paws) or 550–3,000 mg of HA/cm^3 (caudal vertebrae) were applied in order to measure the normal mature bone with higher BMD. In addition, a Gaussian filter (σ = 0.8, support of 1 voxel) was applied, and 1 surface voxel was removed with a morphologic erosion operation to compensate for the partial volume effect.

Histology. After micro-CT analysis, hind paws and tails of IgG2a-treated and anti–IL-17A–treated rats (and age-matched healthy controls, only in the therapeutic experiment) were decalcified in OsteoSoft decalcifier solution (no. 101728; Merck) and embedded in paraffin. Five-micrometer sections were stained for hematoxylin and eosin (H&E) or Safranin O. Briefly, sections were deparaffinized and, for H&E staining, incubated in Mayer's hematoxylin (no. MHS16) and Eosin Y solution (no. HT110116) (both from Sigma). For Safranin O staining, sections were incubated in Weigert's iron hematoxylin (no. HT1079), 0.1% fast green FCF (no. F7252), and 0.1% Safranin O solution (no. HT90432) (all from Sigma). Sections were dehydrated, embedded in Entellan (no. 1.07961.0100; Merck), and semiquantitatively scored by 2 separate observers (MNvT, LMvD), both blinded with regard to treatment details, as previously described (8).

RNA sequencing library preparation and analysis. RNA samples were obtained from the 2 most severely swollen metacarpophalangeal (MCP) joints in 1 front paw (n = 5 IgG2a-treated rats and 5 anti–IL-17A–treated rats) and both front paws from age-matched healthy control rats (n = 3), using previously described methods for total RNA extraction from frozen bone tissue (29). From each sample of RNA, Illumina mRNA-Seq libraries were prepared using a TruSeq Ribozero RNA kit (Illumina) according to the manufacturer's instructions. Libraries were pooled and sequenced on a HiSeq 2000 sequencing system at ~30 million reads. Of 16 samples, 4 were excluded from further analysis (1 in the healthy control group and 3 in the IgG2a-treated group) due to an insufficient total library size evident by hierarchical clustering analysis. RNA sequencing reads for each library were mapped using Spliced Transcripts Alignment to a Reference software against the National Center for Biotechnology Information rat genome version 5.0. Read counts were aggregated at gene level using featureCounts. Finally, gene differential expression was calculated with the edgeR analysis pipeline package. Briefly, library sizes were normalized using voom factor size estimation, and cross-replicate variability of gene counts was estimated by fitting a generalized linear model (Limma). The following comparisons were computed: IgG2a versus healthy control, anti–IL-17A versus healthy control, and anti–IL-17A versus IgG2a. False discovery rate was controlled by adjusting differential gene expression *P* values using the Benjamini-Hochberg method (30), and differentially

expressed genes were defined as having a $\log_2$ fold change of >1 and an adjusted *P* value of <0.01.

RNA sequencing gene enrichment analysis. Univariate analysis of gene expression is often not enough to understand the function of regulated genes and their roles in biologic processes. Therefore, differentially expressed genes were mapped to known biologic pathways using Ingenuity Pathway Analysis. With this measure, the top enriched canonical pathways that were up-regulated (versus healthy controls) by IgG2a treatment and/or down-regulated upon anti–IL-17A treatment were determined using an adjusted *P* value of <0.01. Additionally, we compiled an IL-17A gene signature by selecting genes that were dysregulated (based on IL-17A stimulation and inhibition in different cell types, i.e., whole blood, keratinocytes, and/or synoviocytes) in at least 3 of 22 data sets (Roth L, et al:

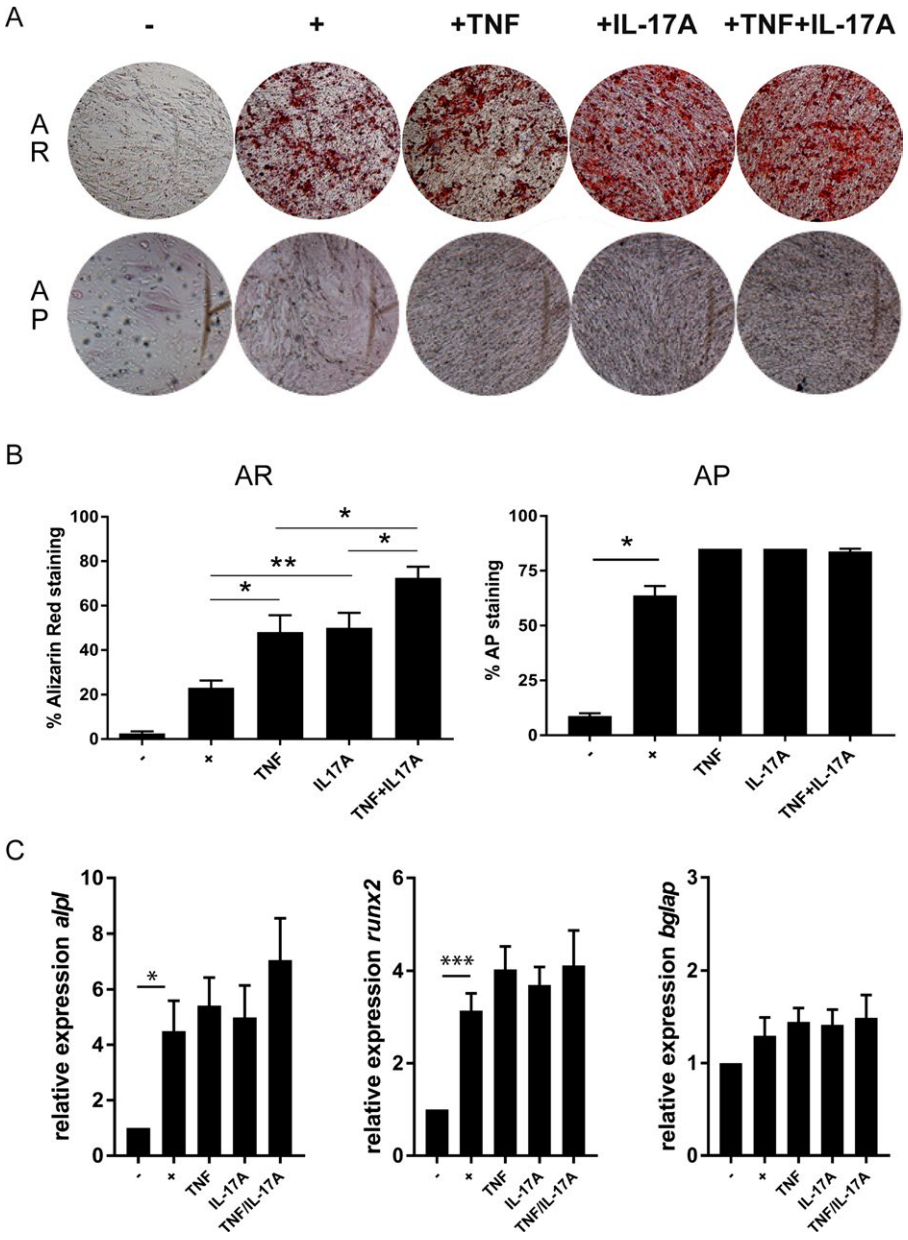

Figure 1. In vitro differentiation of spondyloarthritis (SpA) fibroblast-like synoviocytes (FLS) to osteoblasts is accelerated in the presence of tumor necrosis factor (TNF) and interleukin-17A (IL-17A). SpA FLS (n = 8) were differentiated to osteoblasts, and on day 14 and 21, alizarin red (AR) staining was performed. StemXvivo osteogenic/adipogenic medium was used in all experiments, either without differentiation factors (–), with differentiation factors (+), or with differentiation factors in the presence of IL-17A, TNF, or the combination of TNF and IL-17A. **A**, Representative images of alizarin red and alkaline phosphatase (AP) staining. Original magnification × 100. **B**, Quantification of alizarin red and AP staining on day 21, after the start of differentiation. **C**, Relative expression of *ALPL*, *RUNX2*, and *BGLAP* after 7 days or 14 days of differentiation. Values in **B** and **C** are the mean ± SEM. * = $P < 0.05$; ** = $P < 0.01$; *** = $P < 0.001$. Color figure can be viewed in the online issue, which is available at http://onlinelibrary.wiley.com/doi/10.1002/art.40770/abstract.

unpublished observations). These 132 genes downstream of IL-17A were assessed by Fisher's exact test for enrichment (versus healthy controls) with IgG2a and with anti–IL-17A versus IgG2a treatment with a $\log_2$ fold change cutoff of >1 and an adjusted *P* value of <0.01 for each individual gene.

Statistical analysis. Data were analyzed using GraphPad Prism 6 and IBM SPSS Statistics 23 software. Student's *t*-test or one-way analysis of variance (for multiple comparisons) was performed on all metric data; for clinical scores and hind paw swelling, the area under the curve was calculated first. All categorical data (semiquantitative scores) were analyzed by a Mann-Whitney U test.

RESULTS

IL-17A promotion of in vitro osteogenesis. It was previously shown that IL-17A promotes osteoblastic differentiation of FLS in osteoarthritis (but not rheumatoid arthritis) (24). We hypothesized that IL-17A and other inflammatory mediators would also promote osteoblastic differentiation of FLS in SpA. FLS derived from the synovium (a major target lesion of the disease) of patients with active SpA were differentiated toward osteoblasts. Mineralization and differentiation were determined by alizarin red or AP staining after 14 days and 21 days of differentiation. Alizarin red staining was absent in undifferentiated FLS, which were treated with osteogenic medium alone, and mild background staining was observed for AP. Osteogenic medium supplemented with differentiation factors in the absence or presence of TNF or IL-17A induced clear alizarin red and AP staining, indicating the differentiation toward osteoblasts (Figure 1A). Dose dependent effects of recombinant IL-17A could be observed for alizarin red staining (see Supplementary Figure 1, on the *Arthritis & Rheumatology* web site at http://onlinelibrary.wiley.com/doi/10.1002/art.40770/abstract).

Quantification of staining indicated that combined IL-17A and TNF significantly increased mineralization at both time points. IL-17A and TNF (Figure 1B), but not IL-22 and IL-17F (data not shown), increased differentiation on day 21. AP staining did not further increase with the addition of cytokines to the differentiation cocktail (Figure 1B). Gene expression analysis on day 7 and day 14 indicated increased expression of osteogenesis-relevant genes, including *ALPL* and *RUNX2*, but not *BGLAP*, under all differentiation conditions (Figure 1C). These data indicate that TNF and IL-17A promoted the differentiation of SpA FLS toward osteoblasts.

Reduction in joint inflammation with prophylactic IL-17A blockade. To test whether IL-17A is an important driver of experimental SpA, we treated HLA–B27–transgenic rats with an anti–IL-17A antibody or IgG2a as a control, in a prophylactic treatment experiment (Figure 2A). Clinical disease development was monitored over time, and inflammation was analyzed histologically at the end of the study. All control rats developed clinical spondylitis and arthritis, with a mean onset time of 14 days. In contrast, the development of spondylitis and arthritis were significantly delayed in the anti–IL-17A–treated rats, with a mean onset time of 28 days ($P = 0.037$) and 27 days ($P = 0.015$), respectively (Figure 2B). Similarly, arthritis score and hind paw swelling were significantly decreased in the rats treated with anti–IL-17A (Figure 2C). Finally, there was a trend toward less histologically evident inflammation and destruction in the axial joints of anti–IL-17A–treated rats. Peripheral inflammation and destruction were significantly reduced in anti–IL-17A–treated ankle joints (Figure 2D). Taken together, these data indicate that spondylitis and arthritis in HLA–B27–transgenic rats is at least partially IL-17A–dependent.

Decreased structural damage with prophylactic IL-17A blockade. To assess the effect of IL-17A blockade on new bone formation, spine and ankle tissues were analyzed by micro-CT imaging and histology. We hypothesized that the decrease in inflammation would partially prevent the development of new bone formation. Histologic analysis of the spine indicated a trend toward less new bone formation and no difference in the presence of hypertrophic chondrocytes. We observed a significant decrease in histologically evident new bone formation in the ankle joints after anti–IL-17A treatment. The presence of ectopic foci of hypertrophic chondrocytes was similar in both groups (Figure 3A). Micro-CT analysis of the ankle joints revealed loss of cortical bone and the distinct presence of low-density bone (used as a measure for new bone formation) in the control group. Both bone loss and new bone formation were less pronounced in the ankles of anti–IL-17A–treated rats (Figure 3B and Supplementary Figure 2, http://onlinelibrary.wiley.com/doi/10.1002/art.40770/abstract). Quantification of normal-density bone (>800 mg of HA/cm^3) revealed that rats receiving anti–IL-17A treatment had significantly increased bone volume, suggesting reduced bone loss (Figure 3C). Moreover, anti–IL-17A–treated rats exhibited significantly less low-density bone tissue than IgG2a-treated rats, suggesting less new bone formation (Figure 3D). Accordingly, these data suggest that prophylactic inhibition of inflammation by anti–IL-17A treatment prevents structural damage including periosteal new bone formation.

Reduction in spondylitis and arthritis after therapeutic IL-17A blockade. After demonstrating that this model is IL-17A–dependent, we next assessed whether blockade of IL-17A under conditions of established pathology can impact inflammation and new bone formation. HLA–B27–transgenic rats were treated with anti–IL-17A or IgG2a antibodies after disease onset, and clinical arthritis and spondylitis were monitored over time. Axial and peripheral joints were analyzed by micro-CT and histologic assessment at the end of the study (Figure 4A). Whereas spondylitis and arthritis developed simi-

larly in both groups prior to the initiation of treatment, at the end of the study, spondylitis was observed in 6 of 12 anti–IL-17A–treated rats versus 10 of 12 IgG2a-treated controls, and arthritis was present in 7 of 12 anti–IL-17A–treated rats versus 11 of 12 IgG2a-treated controls (Figure 4B). Spondylitis severity was significantly reduced in rats that received anti–IL-17A treatment (Figure 4C). In rats that developed arthritis (n = 9 in each group), the arthritis score significantly decreased and swelling of the hind paws stabilized, resulting in significantly less severe arthritis in anti–IL-17A–treated rats compared to controls (Figure 4D). Histologically evident inflammation and destruction tended to be reduced in the spines of rats treated with anti–IL-17A. Ankle joints showed significantly less inflammation and destruction upon anti–IL-17A treatment (Figure 4E). Collectively, these data demonstrate that therapeutic anti–IL-17A treatment decreased axial and peripheral joint inflammation.

Reduced periosteal new bone formation after therapeutic IL-17A blockade. To assess whether IL-17A inhibition after the initial inflammatory insult can reduce structural damage, axial and peripheral joints were analyzed by micro-CT and histologic assessment at the end of therapeutic treatment. Age-matched healthy controls (nonimmunized HLA–B27–transgenic rats) were included in this analysis to indicate normal levels of low- and normal-density bone. Bone loss, destruction, new bone formation, and ectopic foci of hypertrophic chondrocytes were assessed.

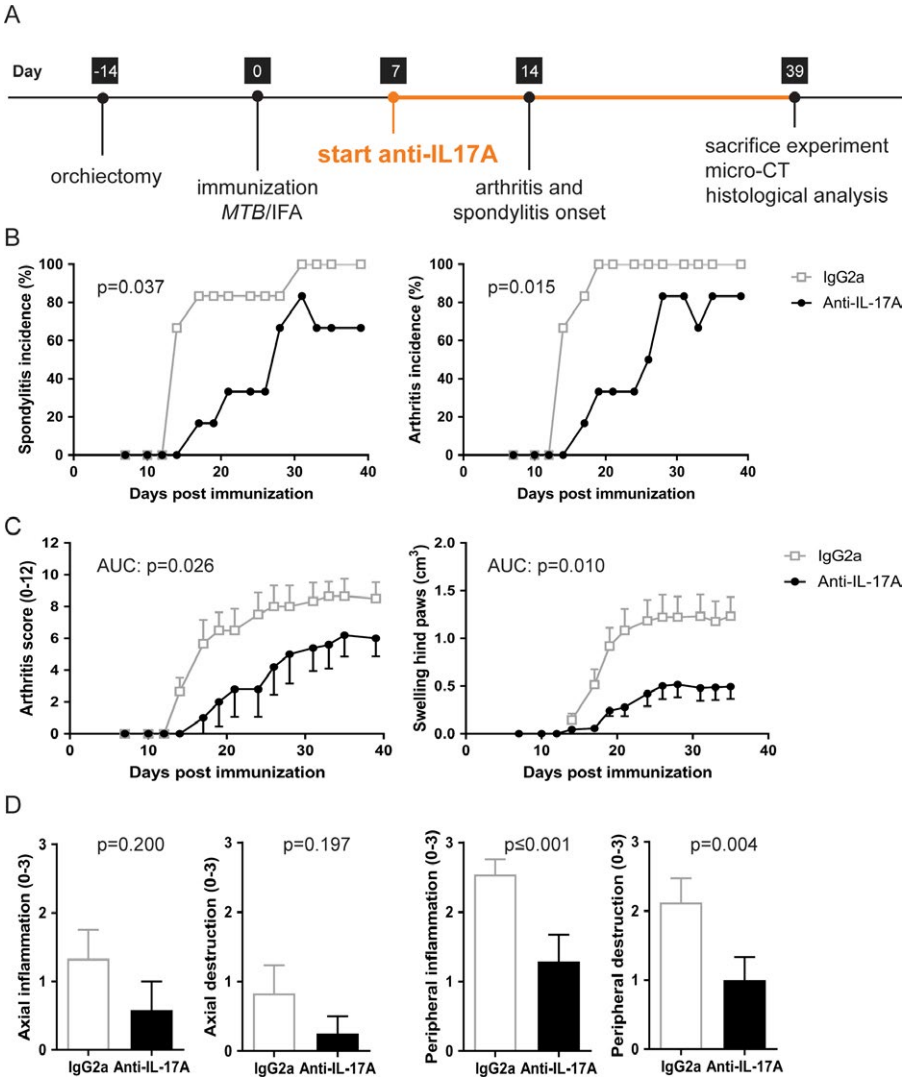

Figure 2. Prophylactic treatment with anti–interleukin-17A (anti–IL-17A) reduces clinical symptom development and histologically evident inflammation in HLA–B27–transgenic rats. **A**, Timeline of HLA–B27–transgenic rat immunizations and prophylactic treatment with anti–IL-17A or IgG2a (n = 6 rats per group) for 5 weeks. **B**, Spondylitis and arthritis incidence. **C**, Arthritis severity in diseased rats as measured by arthritis score and swelling of hind paws. **D**, Inflammation and destruction of axial and peripheral joints from all rats, quantified following histologic staining. Values in **C** and **D** are the mean ± SEM. MTB = *Mycobacterium tuberculosis*; IFA = Freund's incomplete adjuvant; micro-CT = micro–computed tomography; AUC = area under the curve. Color figure can be viewed in the online issue, which is available at http://onlinelibrary.wiley.com/doi/10.1002/art.40770/abstract.

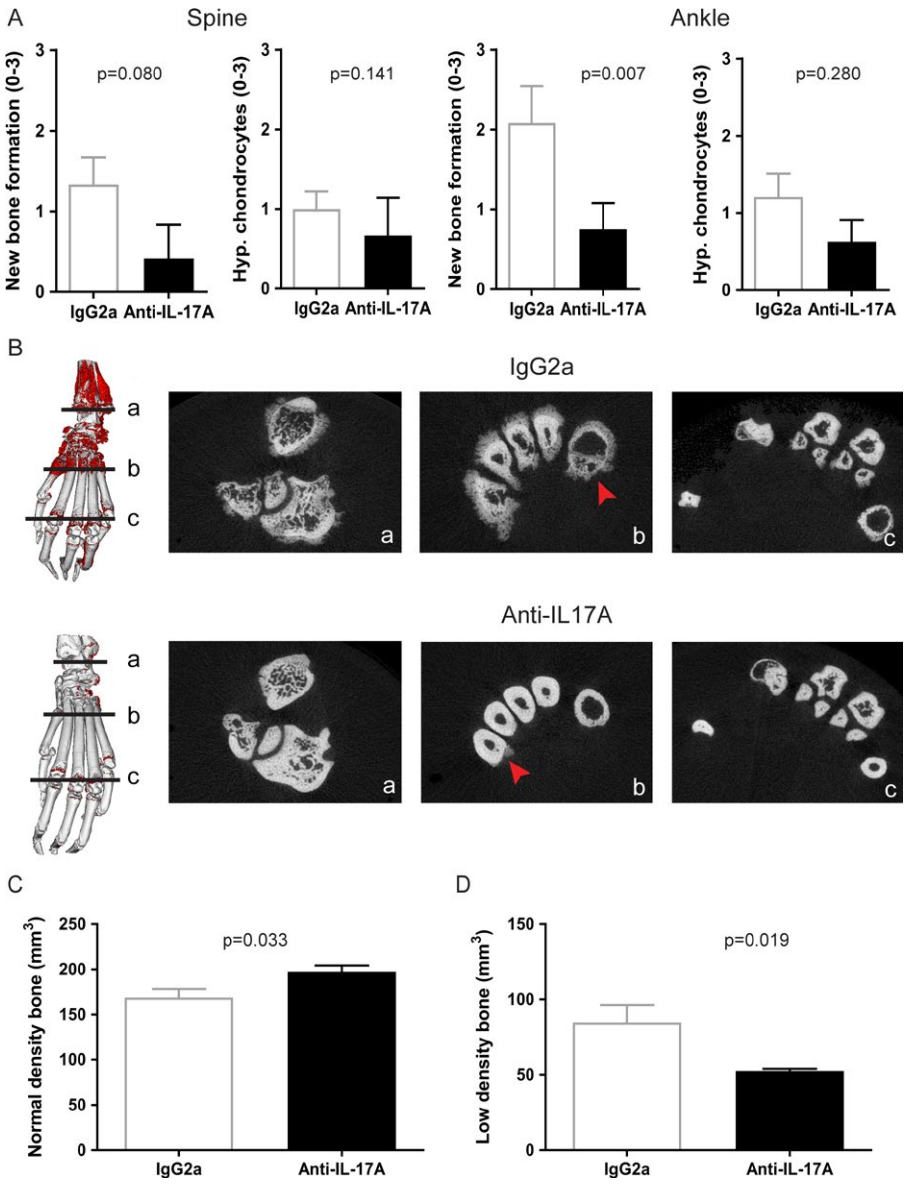

Figure 3. Reduction in structural damage with prophylactic anti–interleukin-17A (anti–IL-17A) treatment. In addition to clinical and histologic examination of inflammation, structural damage was assessed by micro–computed tomography (micro-CT) (n = 6 rats per group). **A**, Histologic quantification of new bone formation and ectopic foci of hypertrophic (Hyp.) chondrocytes in axial and peripheral joints. **B**, Micro-CT analysis revealing normal-density/cortical bone and low-density/newly formed bone in IgG2a-treated controls and anti–IL-17A–treated rats. Red coloring in the 3-dimensional models and **arrowheads** in the 2-dimensional cross-sections indicate low-density bone. **C** and **D**, Quantification of normal-density bone (**C**) and low-density bone (**D**). Values in **A**, **C**, and **D** are the mean ± SEM.

Histologic analysis of the axial joints showed numerical (albeit not statistically significant) differences in new bone formation and hypertrophic chondrocytes in the spines of anti–IL-17A–treated rats (n = 9) (Figure 5A). Reconstructed 3-dimensional (3-D) images of caudal vertebrae were analyzed for new bone formation (Figure 5B). In the IgG2a-treated rat group (n = 9), 11 vertebrae from 5 rats were affected by new bone formation, and in the anti–IL-17A–treated rat group (n = 9), 9 vertebrae from 3 rats were affected (Figure 5C). In addition, classic micro-CT analysis revealed trends toward a mild positive effect of anti–IL-17A treatment on ameliorating osteopenia in the lumbar spine by preserving cancellous bone volume/total volume, BMD, and trabecular thickness, but not trabecular number (Supplementary Figure 3, http://onlinelibrary.wiley.com/doi/10.1002/art.40770/abstract).

Histologic analysis of the peripheral joints showed significantly less new bone formation and ectopic foci of hypertrophic chondrocytes in the ankles of anti–IL-17A–treated rats (Figure 5D). Similar to our observations after prophylactic treatment, micro-CT imaging revealed loss of cortical bone and distinct presence of low-density bone in IgG2a-treated rats, while this was strongly reduced in anti–IL-17A–treated rats (Figure 5E and Supplementary Figure 4, http://onlinelibrary.wiley.com/doi/10.1002/art.40770/abstract).

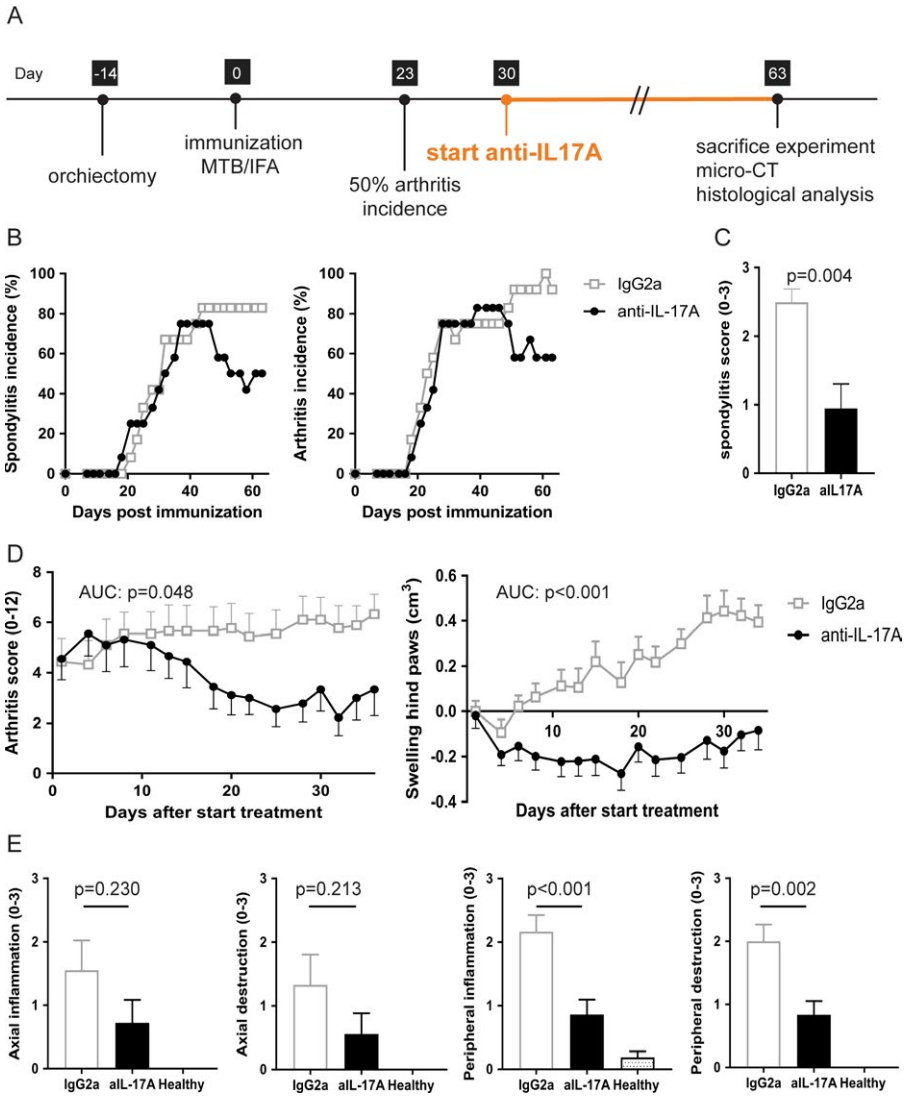

Figure 4. Therapeutic treatment with anti–IL-17A reduces clinical symptom development and histologically evident inflammation in HLA–B27–transgenic rats. **A**, Timeline of HLA–B27–transgenic rat immunizations and therapeutic treatment with anti–IL-17A or IgG2a (n = 12 rats per group) for 5 weeks. **B**, Spondylitis and arthritis incidence. **C**, Spondylitis score of rats that had arthritis at start of treatment (n = 9 rats per group). **D**, Arthritis severity in rats that had arthritis at the start of treatment, as measured by arthritis score and hind paw swelling. **E**, Inflammation and destruction of axial and peripheral joints from rats that had arthritis at the start of treatment, quantified following histologic staining. Values in **C**, **D**, and **E** are the mean ± SEM. See Figure 2 for definitions. Color figure can be viewed in the online issue, which is available at http://onlinelibrary.wiley.com/doi/10.1002/art.40770/abstract.

Accordingly, normal-density bone tissue was increased by 8% in anti–IL-17A–treated rats compared to IgG2a-treated rats, although the difference was not significant (Figure 5F). Low-density bone volume, reflecting newly formed bone, in anti–IL-17A–treated rats was significantly lower than in IgG2a-treated rats and was even similar to that in age-matched, nonimmunized healthy controls (Figure 5G). Taken together, these data confirm that therapeutic IL-17A blockade reduced not only inflammation but structural damage, including new bone formation.

IL-17A as major driver of molecular signature of disease. To confirm and extend the above findings at the molecular level, RNA was extracted from the front paw MCP joints of age-matched healthy controls, IgG2a-treated rats, and anti–IL-17A–treated rats from the therapeutic experiment for RNA sequencing analysis. Principal component analysis identified all groups as separate clusters (Supplementary Figure 5, http://onlinelibrary.wiley.com/doi/10.1002/art.40770/abstract). Nine hundred twenty-two identified genes were up-regulated in disease; 323 of these genes were consistently down-regulated after anti–IL-17A treatment (Supplementary Figure 6). Pathway enrichment analysis indicated that the majority of the differentially expressed genes were related to cell cycle control, granulocyte adhesion, cytotoxic T cell signaling, and the IL-17A pathway (Supplementary Figure 6). The top 20 significantly up-regulated transcripts in IgG2a-treated

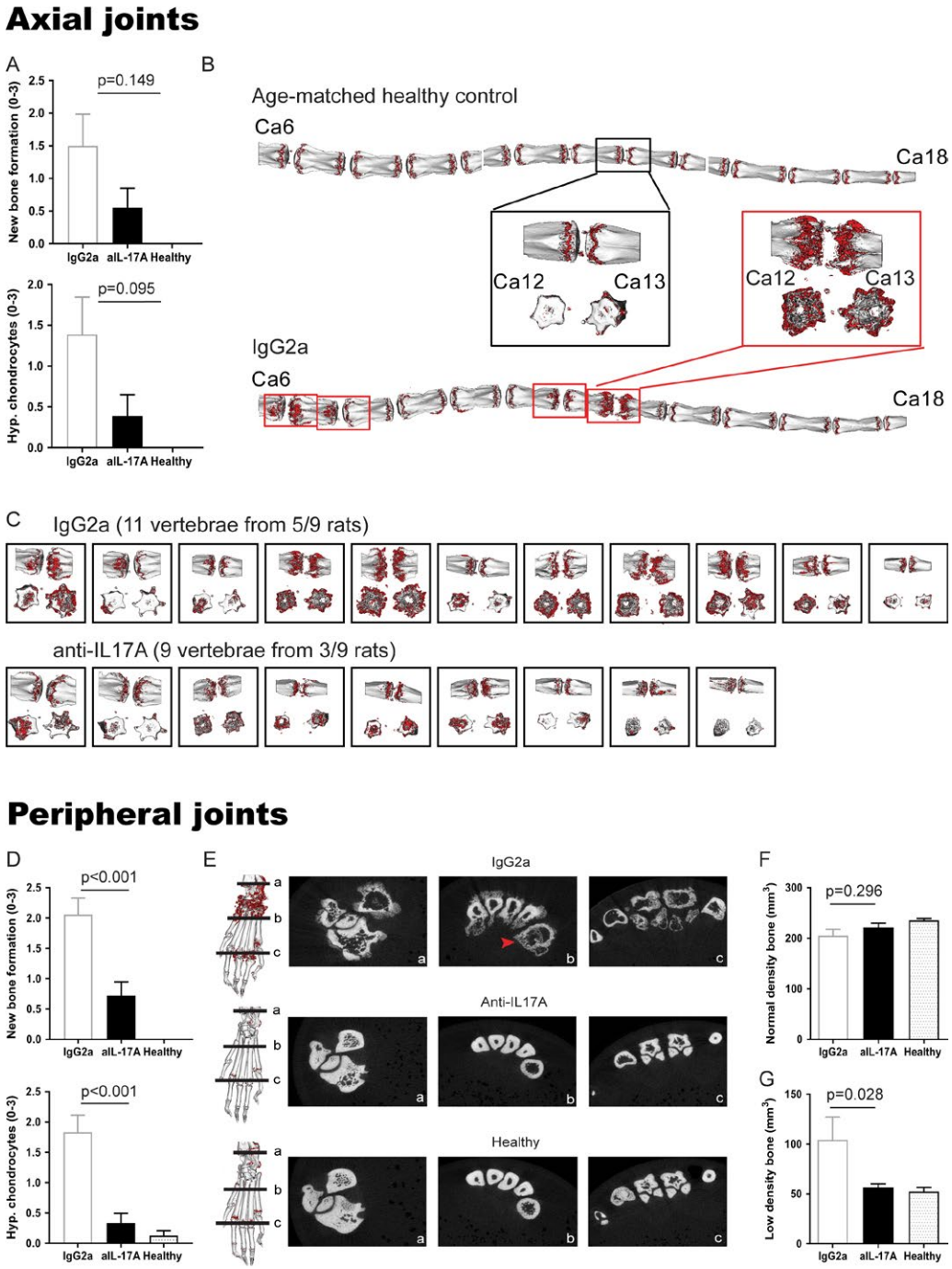

Figure 5. Therapeutic treatment with anti–IL-17A reduces structural damage. Structural damage was assessed by micro-CT analysis and histologic assessment (n = 9 rats per group). **A**, Histologic quantification of new bone formation and presence of hypertrophic (Hyp.) chondrocytes in the spine of IgG2a-treated rats, anti–IL-17A–treated rats, and healthy control rats. **B**, Overview of the caudal spine of 1 healthy rat and 1 IgG2-treated rat with arthritis. Red coloring indicates low-density bone. **C**, Overview of all vertebrae affected by new bone formation as indicated by red staining of low-density bone in IgG2a- and anti–IL-17A–treated rats. **D**, Histologic quantification of new bone formation and presence of hypertrophic chondrocytes in the ankles of IgG2a-treated rats, anti–IL-17A–treated rats, and healthy control rats. **E**, Micro-CT analysis showing normal-density/cortical bone and low-density/newly formed bone. Red coloring in the 3-dimensional models and **arrowheads** in the 2-dimensional cross-sections indicate low-density bone. **F** and **G**, Quantification of normal-density bone (**F**) and low-density bone (**G**). Values in **A**, **D**, and **F** are the mean ± SEM. See Figure 2 for other definitions.

rats versus healthy controls (Table 1) revealed genes related to neutrophils (such as defensins, elastase, and myeloid peroxidase) and erythrocytes. Strikingly, 35% of the total number of up-regulated genes were markedly suppressed by treatment with anti–IL-17A. Analysis of all genes that were significantly down-regulated upon anti–IL-17A treatment showed

Table 1. Top 20 up-regulated genes in front paw bone of IgG2a-treated rats*

Gene	Log_2 fold change, IgG2a-treated rats versus healthy control rats	Log_2 fold change, anti–IL-17A–treated rats versus IgG2a-treated rats	Expression value in healthy controls, mean ± SD FPKM	Expression value in IgG2a-treated rats, mean ± SD FPKM	Expression value in anti–IL-17A–treated rats, mean ± SD FPKM
Defa5	7.07	−3.68	13.70 ± 4.68	980.27 ± 331.68	132.07 ± 59.93
RatNP-3b	6.94	−3.64	10.52 ± 3.46	749.07 ± 264.79	94.05 ± 48.43
Defa11	6.94	−3.88	0.60 ± 0.27	49.49 ± 20.49	4.87 ± 2.60
Prtn3	6.72	−4.35	0.44 ± 0.21	17.72 ± 9.81	1.46 ± 0.83
Np4	6.66	−3.47	17.26 ± 5.74	950.18 ± 313.53	145.71 ± 77.36
Ms4a3	6.4	−3.41	0.74 ± 0.16	30.91 ± 12.83	5.58 ± 3.26
Elane	6.3	−3.99	3.25 ± 1.17	88.95 ± 46.32	11.48 ± 6.83
Ngp	5.99	−2.87	12.08 ± 5.14	374.43 ± 55.68	75.06 ± 25.10
Ctsg	5.97	−3.91	2.97 ± 0.97	88.07 ± 46.79	10.52 ± 6.13
Camp	5.77	−2.72	15.03 ± 4.77	591.79 ± 128.84	108.98 ± 35.32
Mpo	5.76	−3.27	3.84 ± 1.12	88.41 ± 40.76	17.69 ± 10.22
Rhag	5.16	−3.14	1.04 ± 0.30	23.59 ± 6.81	2.70 ± 0.58
Spta1	5.11	−2.76	0.61 ± 0.15	14.09 ± 4.17	2.20 ± 0.57
Slc4a1	5.06	−2.86	3.32 ± 0.65	79.77 ± 25.51	11.54 ± 3.11
Mcpt9	4.99	−3.33	0.63 ± 0.22	14.55 ± 3.92	1.81 ± 0.73
Rhd	4.95	−3.04	1.67 ± 0.38	37.81 ± 11.97	4.55 ± 0.95
Ermap	4.89	−2.7	0.67 ± 0.15	13.80 ± 3.93	2.14 ± 0.50
Kel	4.88	−2.83	0.54 ± 0.14	10.11 ± 2.68	1.42 ± 0.33
Gypa	4.81	−3.04	4.02 ± 0.80	91.33 ± 30.59	11.11 ± 2.81
S100a9	4.79	−2.59	137.19 ± 32.77	2,902.75 ± 762.68	547.33 ± 117.62

* Anti–IL-17A = anti–interleukin-17A; FPKM = fragments per kilobase million.

significant down-regulation of the IL-17 gene signature, including *Lcn2* (Supplementary Table 1 and Supplementary Figure 7, http://onlinelibrary.wiley.com/doi/10.1002/art.40770/abstract). These data indicate that IL-17A is a major driver of the molecular disease signature in this experimental SpA model. A subanalysis of genes related to molecular mechanisms of new bone formation failed to reveal any specifically up-regulated pathway. However, a similar analysis of genes that were down-regulated by anti–IL-17A treatment revealed strong suppression of carbonic anhydrase (*CA*) 1 and 2, which are genes involved in bone metabolism, and specifically, calcification (Supplementary Table 1).

DISCUSSION

While clinical trials with anti–IL-17A antibodies demonstrated the importance of this cytokine in axial and peripheral joint inflammation in the context of human SpA (13–16), the exact manner in which IL-17A exerts proinflammatory functions in this disease remains poorly understood. In psoriasis, studies of target tissues (30) and animal models (31,32) have elucidated the cellular and molecular immunopathology driven by IL-17A. In contrast, SpA studies of target tissues (33,34) are currently scarce, and animal models do not seem to recapitulate human disease. IL-17A minicircle DNA overexpression, as well as IL-17A blockade in mice overexpressing IL-23 minicircle DNA, failed to reveal a prominent role of this cytokine in these models (35). In curdlan-induced arthritis in SKG mice, the effect of IL-17A deficiency is small (36), and therapeutic blockade has not been assessed. Moreover, some of these models poorly replicate key features of human SpA, including pathologic new bone formation (37).

Here we show that IL-17A plays a pivotal role in the HLA–B27–transgenic rat model of SpA, which is driven by overexpression of the major human susceptibility gene associated with the disease and shows all major clinical and pathologic features of the human disease, with the exception of extraarticular manifestations (8,9). The notion that IL-17A has a central role in this model is supported by the prophylactic and therapeutic effect of anti–IL-17A on axial and peripheral joint inflammation, and by RNA sequencing analysis of the target tissues, which indicated that the molecular signature of the disease is driven in part by IL-17A. Regarding axial disease, it is important to understand that not all vertebrae are affected by spondylitis. Thus, quantification of axial pathology is rather difficult. Assessment of clinical spondylitis at the end of therapeutic treatment indicated a significant reduction in spondylitis severity upon anti–IL-17A treatment. Both histologic analysis and micro-CT imaging showed a trend toward less new bone for-

mation in the spine. To confirm these findings, we performed a second independent experiment with IL-17A blockade. In this follow-up experiment, we observed similar results: severity of spondylitis and levels of histologically evident inflammation were significantly decreased. Moreover, histologic analysis of spinal tissue indicated significantly less new bone formation upon treatment with anti–IL-17A as compared to the isotype control. Micro-CT analysis indicated similar results, although the findings were not statistically significant. The results presented in this report provide evidence of a diminished presence of inflammation and new bone formation in the spine.

One of the most enigmatic aspects of SpA is the link between inflammation and new bone formation. In contrast to bone destruction, which can be driven by both TNF and IL-17A (15,16,38), the failure of TNF inhibition to profoundly impact new bone formation in ankylosing spondylitis (AS) raises the possibility that inflammation and new bone formation may be uncoupled. The first hypothesis on this uncoupling proposes that new bone formation in SpA is an excessive form of physiologic repair that, initiated by inflammation and bone destruction, occurs only after the resolution of the inflammatory process (6). According to this hypothesis, late antiinflammatory treatment would not affect new bone formation, as the repair process would already have been triggered. However, this hypothesis is inconsistent with observations that inhibition of osteoclasts does not inhibit new bone formation in experimental arthritis (39) and that TNF blockade does not accelerate osteoproliferation in human AS (1). In the present study, we further invalidated this concept by showing that therapeutic suppression of inflammation by IL-17A blockade after the initial insult does not promote or stabilize new bone formation but instead significantly inhibits this process.

The second hypothesis on uncoupling of inflammation and new bone formation proposes that an unknown trigger, presumably entheseal stress, induces simultaneous inflammation and activation of stromal progenitor cells, resulting in inflammation-independent tissue remodeling, new bone formation, and ankylosis (7). According to this hypothesis, progression of structural damage after the initial phase of the disease would not be reduced by antiinflammatory treatment and would require specific targeting of stromal remodeling pathways. While our observations on the prophylactic impact of anti–IL-17A on both inflammation and new bone formation are consistent with this hypothesis, the therapeutic effect of IL-17A blockade on structural damage that was demonstrated in our study clearly indicates that progression of new bone formation is dependent on ongoing, IL-17A–driven inflammation.

Regarding the question of whether anti–IL-17A treatment affects osteoblasts directly or through the resolution of inflammation, we can only speculate. The finding that inflammation correlated with new bone formation in the anti–IL-17A–treated rats (data not shown) does not prove a direct effect of anti–IL-17A treatment on osteoblasts or new bone formation. However, in vitro differentiation experiments indicate that IL-17A is capable of directly stimulating osteoblastic differentiation. Moreover, exploratory experiments with in vitro differentiation of FLS indicate that in the absence of inflammation, IL-17A can stimulate osteoblastic differentiation (Supplementary Figures 8B and C, http://onlinelibrary.wiley.com/doi/10.1002/art.40770/abstract). These data suggest that IL-17A does have the ability to directly regulate new bone formation.

A key question raised by our current findings relates to the mechanism by which IL-17A exerts its function on bone. The mechanism of action of IL-17A in bone appears similar to that in peripheral and axial joints. Additionally, micro-CT analysis reveals a paradoxical effect with the simultaneous improvement of the quality of the cortical bone and inhibition of periosteal new bone formation. Two mechanisms could, either separately or together, contribute to the improvement in cortical bone quality: first, a decrease in bone resorption, and second, an increase in osteoblastic activity. In the analysis of bone metabolism, we observed a clear decreasing effect of anti–IL-17A on pathologic new bone formation. Based on in vitro assays, histologic assessment, and micro-CT, we concluded that osteoblasts could be less active. We also analyzed cortical bone, as this mechanism could apply to it as well; however, micro-CT analysis of the cortical bone indicated no difference in cortical bone density upon anti–IL-17A treatment. These data imply that different cells or mechanisms are important for the formation of normal/cortical bone versus pathological/syndesmophyte bone.

Use of some additional methods, such as the measurement of bone metabolism/turnover markers in the serum, would not contribute to the understanding of ongoing processes. We believe that micro-CT imaging and histologic analysis give a more accurate overview of ongoing processes, as they indicate the location of the processes. While quantitative analysis of micro-CT results is based on bone density (in which low-density bone could contribute to levels of bone loss and levels of bone formation), histologic quantification is specific to either bone destruction or formation. Both methods used in this study indicate that levels of bone loss as well as pathologic bone formation are decreased upon anti–IL-17A treatment.

It has yet to be established if the effect of IL-17A on in vitro differentiation corresponds to the inhibitory effect of IL-17A on mature osteoblasts (19,20) or to the stimulatory effect of IL-17A on osteoblastic differentiation of mesenchymal precursors (22–24). In support of the latter, we demonstrated that IL-17A directly promotes osteoblastic differentiation of human FLS in SpA. Furthermore, RNA expression of bone sialoprotein, a major structural matrix protein, was increased after the addition of IL-17A during differentiation (data not shown). RNA sequencing demonstrated that IL-17A blockade down-regulated a number of gene products related to bone calcification, including *CA1* and *CA2*; *CA2* was previously shown to be directly induced by IL-17A (40). Unfortunately, our approach failed to reveal specific new bone formation pathways activated by disease; genes involved in osteoblastic differentiation or function were not differentially regulated upon

anti–IL-17A treatment. More approaches to elucidate the precise molecular pathways and provide insight into relevant mechanisms are needed. In particular, the temporal aspects of IL-17A–mediated disease progression and anti–IL-17A therapy must be addressed, as our detailed analyses focused only on 1 time point following 5 weeks of treatment.

The in vitro differentiation assays raised another important question: is IL-17A unique in its ability to drive osteoblastic differentiation and new bone formation? This question is difficult to answer using in vitro assays, as they yield conflicting results depending on the exact model. For example, the osteoblastic differentiation assay for FLS that we and others used (24) shows a positive effect of IL-17A and of TNF, either alone or combined with IL-17A (24), but not of IL-17F (data not shown). In an exploratory experiment, we obtained similar results using human periosteum-derived cells (Supplementary Figure 8A, http://onlinelibrary.wiley.com/doi/10.1002/art.40770/abstract). However, in studies involving differentiation of periosteal cells using another differentiation medium, others have demonstrated promotion of bone formation by IL-17A and IL-17F, but not TNF (41).

The above data indicate that the ability to drive osteogenic differentiation is not unique to IL-17A. Further research is needed to determine differences in cell origin and the relationship to differentiation capacity. Other cytokines, either related to IL-17A (e.g., IL-17F) or unrelated (e.g., TNF), might have the same osteogenic potential as IL-17A in vitro. In vivo, in the classic TNF overexpression models that lead to high levels of soluble TNF, there are no signs of new bone formation (42,43). Moreover, TNF blockade with etanercept in a therapeutic setting failed to suppress pathology (including inflammation and new bone formation) in an HLA–B27–transgenic rat model (9). We recently discovered that selective overexpression of the transmembrane form of TNF in mice induces SpA-like arthritis, tendinitis, and spondylitis with prominent new bone formation and ankylosis (van Duivenvoorde LM, et al: submitted for publication). These findings warrant further direct comparisons of anti–IL-17A and anti-TNF (which may be more potent than soluble TNF receptor to block transmembrane TNF) in our HLA–B27–transgenic rats, as well as further research into the specific interactions between transmembrane TNF and IL-17A.

Another important aspect of this study, as highlighted by the ongoing debate on the role of TNF in osteoproliferation, is the relevance and applicability of these findings to human SpA. In vitro differentiation using a cocktail of dexamethasone, β-glycophosphatase, and ascorbic acid indicated that IL-17A can accelerate osteogenesis. Similar results were achieved in the absence of antiinflammatory dexamethasone (Supplementary Figure 8C, http://onlinelibrary.wiley.com/doi/10.1002/art.40770/abstract). Others have shown that IL-17A can exert similar osteogenesis-stimulating effects during osteoblastic differentiation of primary periosteal cells (41). In vivo models, including the HLA–B27–transgenic rat model, show both periosteal and endochondral new bone formation. In the spine, the site of new bone formation lesions is similar to the site of syndesmophyte formation in humans (8). The current human in vitro assays and rat in vivo experiments provide a clear biologic basis, but no definitive proof, that IL-17A plays a role in new bone formation or syndesmophyte formation in human SpA. However, it is notable that magnetic resonance imaging evaluation of the spine in AS patients treated with the anti–IL-17A monoclonal antibody secukinumab showed a low number of vertebral units with new fatty lesions, a feature that has been associated with subsequent new bone formation (44). Accordingly, data after 2 years and 4 years of continuous treatment with secukinumab indicated low progression rates of new bone formation, as assessed by the modified Stoke Ankylosing Spondylitis Spinal Score (45–47).

While the present study has obvious limitations including the absence of a control group, preliminary observations in human patients, taken together with the biologic rationale presented by the current results, provide sufficient justification to proceed with well-controlled, long-term, head-to-head studies to assess whether blocking of IL-17A–driven inflammation could not only suppress inflammation but also halt progression of structural damage in SpA.

ACKNOWLEDGMENTS

The authors would like to thank Antje Huppertz, Christine Halleux, Tanja Grabenstaetter, Charles Moes, and Christine Henninger (Novartis Pharma) and Desirée Pots and Veronique Knaup (Academic Medical Center) for technical support, and Edward J. Oakeley, Mevion Oertli, and Ulrike Naumann (Novartis Pharma) for RNA sequencing and data curation.

AUTHOR CONTRIBUTIONS

All authors were involved in drafting the article or revising it critically for important intellectual content, and all authors approved the final version to be published. Ms van Tok had full access to all of the data in the study and takes responsibility for the integrity of the data and the accuracy of the data analysis.

Study conception and design. van Tok, van Duivenvoorde, Kramer, van de Sande, Kolbinger, Baeten.

Acquisition of data. van Tok, van Duivenvoorde, Kramer, Ingold, Pfister, Roth, Blijdorp.

Analysis and interpretation of data. van Tok, van Duivenvoorde, Kramer, Ingold, Pfister, Roth, Taurog, Kolbinger, Baeten.

ADDITIONAL DISCLOSURES

Authors Kramer, Ingold, Pfister, Roth, and Kolbinger are employees of Novartis. Author Baeten is an employee of UCB Pharma.

REFERENCES

1. Baraliakos X, Heldmann F, Callhoff J, Listing J, Appelboom T, Brandt J, et al. Which spinal lesions are associated with new bone formation in patients with ankylosing spondylitis treated with anti-TNF agents? A long-term observational study using MRI and conventional radiography. Ann Rheum Dis 2014;73:1819–25.

2. Van der Heijde D, Landewe R, Baraliakos X, Houben H, van Tubergen A, Williamson P, et al. Radiographic findings following two years of infliximab therapy in patients with ankylosing spondylitis. Arthritis Rheum 2008;58:3063–70.
3. Van der Heijde D, Landewe R, Einstein S, Ory P, Vosse D, Ni L, et al. Radiographic progression of ankylosing spondylitis after up to two years of treatment with etanercept. Arthritis Rheum 2008;58:1324–31.
4. Finzel S, Kraus S, Schmidt S, Hueber A, Rech J, Engelke K, et al. Bone anabolic changes progress in psoriatic arthritis patients despite treatment with methotrexate or tumour necrosis factor inhibitors. Ann Rheum Dis 2013;72:1176–81.
5. Maas F, Arends S, Brouwer E, Essers I, van der Veer E, Efde M, et al. Reduction in spinal radiographic progression in ankylosing spondylitis patients receiving prolonged treatment with tumor necrosis factor inhibitors. Arthritis Care Res (Hoboken) 2017;69:1011–9.
6. Sieper J, Appel H, Braun J, Rudwaleit M. Critical appraisal of assessment of structural damage in ankylosing spondylitis: implications for treatment outcomes. Arthritis Rheum 2008;58:649–56.
7. Lories RJ, Luyten FP, de Vlam K. Progress in spondylarthritis: mechanisms of new bone formation in spondyloarthritis. Arthritis Res Ther 2009;11:221.
8. Van Duivenvoorde LM, Dorris ML, Satumtira N, van Tok MN, Redlich K, Tak PP, et al. Relationship between inflammation, bone destruction, and osteoproliferation in the HLA–B27/human β2 -microglobulin–transgenic rat model of spondylarthritis. Arthritis Rheum 2012;64:3210–9.
9. Van Tok MN, Satumtira N, Dorris M, Pots D, Slobodin G, van de Sande MG, et al. Innate immune activation can trigger experimental spondyloarthritis in HLA-B27/Huβ2m transgenic rats. Front Immunol 2017;8:920.
10. Poddubnyy D, Protopopov M, Haibel H, Braun J, Rudwaleit M, Sieper J. High disease activity according to the Ankylosing Spondylitis Disease Activity Score is associated with accelerated radiographic spinal progression in patients with early axial spondyloarthritis: results from the GErman SPondyloarthritis Inception Cohort. Ann Rheum Dis 2016;75:2114–8.
11. Hreggvidsdottir HS, Noordenbos T, Baeten DL. Inflammatory pathways in spondyloarthritis. Mol Immunol 2014;57:28–37.
12. Yeremenko N, Paramarta JE, Baeten D. The interleukin-23/interleukin-17 immune axis as a promising new target in the treatment of spondyloarthritis. Curr Opin Rheumatol 2014;26:361–70.
13. Baeten D, Baraliakos X, Braun J, Sieper J, Emery P, van der Heijde D, et al. Anti-interleukin-17A monoclonal antibody secukinumab in treatment of ankylosing spondylitis: a randomized, double-blind, placebo-controlled trial. Lancet 2013;382:1705–13.
14. Baeten D, Sieper J, Braun J, Baraliakos X, Dougados M, Emery P, et al. Secukinumab, an interleukin-17A inhibitor, in ankylosing spondylitis. N Engl J Med 2015;373:2534–48.
15. Mease PJ, McInnes IB, Kirkham B, Kavanaugh A, Rahman P, van der Heijde D, et al. Secukinumab inhibition of interleukin-17A in patients with psoriatic arthritis. N Engl J Med 2015;373:1329–39.
16. Mease PJ, van der Heijde D, Ritchlin CT, Okada M, Cuchacovich RS, Shuler CL, et al. Ixekizumab, an interleukin-17A specific monoclonal antibody, for the treatment of biologic-naive patients with active psoriatic arthritis: results from the 24-week randomized, double-blind, placebo-controlled and active (adalimumab)-controlled period of the phase III trial SPIRIT-P1. Ann Rheum Dis 2017;76:79–87.
17. Lubberts E, van den Bersselaar L, Oppers-Walgreen B, Schwarzenberger P, Coenen-de Roo CJ, Kolls JK, et al. IL-17 promotes bone erosion in murine collagen-induced arthritis through loss of the receptor activator of NF-κ B ligand/osteoprotegerin balance. J Immunol 2003;170:2655–62.
18. Adamopoulos IE, Suzuki E, Chao CC, Gorman D, Adda S, Maverakis E, et al. IL-17A gene transfer induces bone loss and epidermal hyperplasia associated with psoriatic arthritis. Ann Rheum Dis 2015;74:1284–92.
19. Shaw AT, Maeda Y, Gravallese EM. IL-17A deficiency promotes periosteal bone formation in a model of inflammatory arthritis. Arthritis Res Ther 2016;18:104.
20. Uluckan O, Jimenez M, Karbach S, Jeschke A, Grana O, Keller J, et al. Chronic skin inflammation leads to bone loss by IL-17-mediated inhibition of Wnt signaling in osteoblasts. Sci Transl Med 2016;8:330ra37.
21. Ono T, Okamoto K, Nakashima T, Nitta T, Hori S, Iwakura Y, et al. IL-17-producing γδ T cells enhance bone regeneration. Nat Commun 2016;7:10928.
22. Croes M, Oner FC, van Neerven D, Sabir E, Kruyt MC, Blokhuis TJ, et al. Proinflammatory T cells and IL-17 stimulate osteoblast differentiation. Bone 2016;84:262–70.
23. Osta B, Lavocat F, Eljaafari A, Miossec P. Effects of interleukin-17A on osteogenic differentiation of isolated human mesenchymal stem cells. Front Immunol 2014;5:425.
24. Osta B, Roux JP, Lavocat F, Pierre M, Ndongo-Thiam N, Boivin G, et al. Differential effects of IL-17A and TNF-α on osteoblastic differentiation of isolated synoviocytes and on bone explants from arthritis patients. Front Immunol 2015;6:151.
25. Tran TM, Dorris ML, Satumtira N, Richardson JA, Hammer RE, Shang J, et al. Additional human β2-microglobulin curbs HLA–B27 misfolding and promotes arthritis and spondylitis without colitis in male HLA–B27–transgenic rats. Arthritis Rheum 2006;54:1317–27.
26. Gerlag DM, Tak PP. How to perform and analyse synovial biopsies. Best Pract Res Clin Rheumatol 2009;23:221–32.
27. Livak KJ, Schmittgen TD. Analysis of relative gene expression data using real-time quantitative PCR and the 2-ΔΔCt Method. Methods 2001;25:402–8.
28. Taurog JD. Autoimmune epididymoorchitis is essential to the pathogenesis of male-specific spondyloarthritis in HLA–B27–transgenic rats. Arthritis Rheum 2012;64:2518–28.
29. Keller H, Kneissel M. SOST is a target gene for PTF in bone. Bone 2005;37:148–58.
30. Hawkes JE, Chan TC, Krueger JG. Psoriasis pathogenesis and the development of novel targeted immune therapies. J Allergy Clin Immunol 2017;140:645–53.
31. Takaishi M, Ishizaki M, Suzuki K, Isobe T, Shimozato T, Sano S. Oral administration of a novel RORγt antagonist attenuates psoriasis-like skin lesion of two independent mouse models through neutralization of IL-17. J Dermatol Sci 2017;85:12–9.
32. Van der Fits L, Mourits S, Voerman JS, Kant M, Boon L, Laman JD, et al. Imiquimod-induced psoriasis-like skin inflammation in mice is mediated via the IL-23/IL-17 axis. J Immunol 2009;182:5836–45.
33. Noordenbos T, Yeremenko N, Gofita I, van de Sande M, Tak PP, Canete JD, et al. Interleukin-17–positive mast cells contribute to synovial inflammation in spondylarthritis. Arthritis Rheum 2012;64:99–109.
34. Appel H, Maier R, Wu P, Scheer R, Hempfing A, Kayser R, et al. Analysis of IL-17$^+$ cells in facet joints of patients with spondyloarthritis suggests that the innate immune pathway might be of greater relevance than the Th17-mediated adaptive immune response. Arthritis Res Ther 2011;13:R95.
35. Sherlock JP, Joyce-Shaikh B, Turner SP, Chao CC, Sathe M, Grein J, et al. IL-23 induces spondyloarthropathy by acting on ROR-γt+ CD3+CD4-CD8- entheseal resident T cells. Nat Med 2012;18:1069–76.
36. Benham H, Rehaume LM, Hasnain SZ, Velasco J, Baillet AC, Ruutu M, et al. Interleukin-23 mediates the intestinal response to microbial β-1,3-glucan and the development of spondyloarthritis pathology in SKG mice. Arthritis Rheumatol 2014;66:1755–67.

37. Vieira-Sousa E, van Duivenvoorde LM, Fonseca JE, Lories RJ, Baeten DL. Animal models as a tool to dissect pivotal pathways driving spondyloarthritis. Arthritis Rheumatol 2015;67:2813–27.
38. Koenders MI, Marijnissen RJ, Devesa I, Lubberts E, Joosten LA, Roth J, et al. Tumor necrosis factor–interleukin-17 interplay induces S100A8, interleukin-1β, and matrix metalloproteinases, and drives irreversible cartilage destruction in murine arthritis: rationale for combination treatment during arthritis. Arthritis Rheum 2011;63:2329–39.
39. Lories RJ, Derese I, Luyten FP. Inhibition of osteoclasts does not prevent joint ankylosis in a mouse model of spondyloarthritis. Rheumatology (Oxford) 2008;47:605–8.
40. Kitami S, Tanaka H, Kawato T, Tanabe N, Katono-Tani T, Zhang F, et al. IL-17A suppresses the expression of bone resorption-related proteinases and osteoclast differentiation via IL-17RA or IL-17RC receptors in RAW264.7 cells. Biochimie 2010;92:398–404.
41. Shah M, Maroof A, Al-Hosni R, Gikas P, Gozzard N, Shaw S, et al. T cell-derived IL-17A and IL-17F drive bone formation from human periosteal stem cells: implications for enthesophyte formation. Ann Rheum Dis 2017;76 Suppl 2:221.
42. Redlich K, Gortz B, Hayer S, Zwerina J, Kollias G, Steiner G, et al. Overexpression of tumor necrosis factor causes bilateral sacroiliitis. Arthritis Rheum 2004;50:1001–5.
43. Kontoyiannis D, Pasparakis M, Pizarro TT, Cominelli F, Kollias G. Impaired on/off regulation of TNF biosynthesis in mice lacking TNF AU-rich elements: implications for joint and gut-associated immunopathologies. Immunity 1999;10:387–98.
44. Baraliakos X, Borah B, Braun J, Baeten D, Laurent D, Sieper J, et al. Long-term effects of secukinumab on MRI findings in relation to clinical efficacy in subjects with active ankylosing spondylitis: an observational study. Ann Rheum Dis 2016;75:408–12.
45. Braun J, Baraliakos X, Deodhar A, Baeten D, Sieper J, Emery P, et al. Effect of secukinumab on clinical and radiographic outcomes in ankylosing spondylitis: 2-year results from the randomized phase III MEASURE 1 study. Ann Rheum Dis 2017;76:1070–7.
46. Braun J, Baraliakos X, Deodhar AA, Poddubnyy D, Emery P, Delicha EM, et al. Secukinumab demonstrates low radiographic progression and sustained efficacy through 4 years in patients with active ankylosing spondylitis [abstract]. Arthritis Rheumatol 2017;69 Suppl 10. URL: https://acrabstracts.org/abstract/secukinumab-demonstrates-low-radiographic-progression-and-sustained-efficacy-through-4-years-in-patients-with-active-ankylosing-spondylitis/.
47. Creemers MC, Franssen MJ, van't Hof MA, Gribnau FW, van de Putte LB, van Riel PL. Assessment of outcome in ankylosing spondylitis: an extended radiographic scoring system. Ann Rheum Dis 2005;64:127–9.

DOI 10.1002/art.40887

Errata

In the article by Eder et al in the March 2017 issue of *Arthritis & Rheumatology* (The Development of Psoriatic Arthritis in Patients With Psoriasis Is Preceded by a Period of Nonspecific Musculoskeletal Symptoms: A Prospective Cohort Study [pages 622–629]), one of the institutional affiliations of the second author was inadvertently omitted. Dr. Ari Polachek's affiliations should have read: "University Health Network, Toronto, Ontario, Canada, and Tel Aviv Sourasky Medical Center, Sackler Faculty of Medicine, Tel Aviv University, Tel Aviv, Israel."

In the article by Polachek et al in the May 2018 issue of *Arthritis & Rheumatology* (The Association Between HLA Genetic Susceptibility Markers and Sonographic Enthesitis in Psoriatic Arthritis [pages 756–762]), the name of one of the institutions of the first author was worded incorrectly. Dr. Ari Polachek's affiliations should have read: "Toronto Western Hospital, Toronto, Ontario, Canada, and Tel Aviv Sourasky Medical Center, Sackler Faculty of Medicine, Tel Aviv University, Tel Aviv, Israel."

We regret the errors.

American College of Rheumatology
Education • Treatment • Research

Arthritis & Rheumatology
Vol. 71, No. 4, April 2019, pp 626–631
DOI 10.1002/art.40778

BRIEF REPORT

Regression of Peripheral Subclinical Enthesopathy in Therapy-Naive Patients Treated With Ustekinumab for Moderate-to-Severe Chronic Plaque Psoriasis: A Fifty-Two–Week, Prospective, Open-Label Feasibility Study

Laura Savage,[1] Mark Goodfield,[2] Laura Horton,[1] Abdulla Watad,[3] Elizabeth Hensor,[1] Paul Emery,[1] Richard Wakefield,[1] Miriam Wittmann,[4] and Dennis McGonagle[1]

Objective. To investigate whether sonographically determined subclinical enthesopathy in patients with moderate-to-severe psoriasis regresses with the use of ustekinumab therapy for skin disease.

Methods. Seventy-three patients with moderate-to-severe psoriasis, who were not treated with systemic therapy and did not have symptoms of psoriatic arthritis (PsA), and 23 healthy volunteers were screened by ultrasound for subclinical enthesitis. Subsequently, 23 patients with psoriasis whose ultrasound results showed inflammatory changes were treated with ustekinumab for 52 weeks. The evolution of sonographic abnormalities of the upper and lower limb entheses was assessed using an extensive gray-scale and power Doppler (PD) ultrasound protocol at weeks 0, 12, 24, and 52. For each parameter, a gray-scale or PD ultrasound score of >0 was determined to be abnormal, and a summative score based on the Glasgow Ultrasound Enthesitis Scoring System was calculated.

Results. Of all the patients with psoriasis screened using ultrasound, 49.3% had at least 1 inflammatory entheseal abnormality. Mean ± SD inflammation scores were higher in the patients with psoriasis compared with the healthy volunteers (9.9 ± 6.6 versus 1.0 ± 1.4). With treatment, the mean inflammation scores decreased significantly by 42.2% from week 0 to week 24 (–4.2 [95% confidence interval –6.3, –2.1]; $P < 0.001$) and by 47.5% by week 42 (–4.7 [95% confidence interval –7.1, –2.3]; $P = 0.001$). Entheseal structural abnormalities did not change significantly during treatment.

Conclusion. Within 12 weeks of treatment, interleukin-12 (IL-12)/IL-23 inhibition for psoriasis appears to suppress subclinical enthesopathy, and the suppression is maintained through week 52. Further longitudinal studies are needed to determine whether therapy initiated for skin disease may prevent the development of PsA.

INTRODUCTION

The recognition that psoriatic arthritis (PsA) can quickly lead to irreversible joint damage, functional limitation, and quality-of-life impairment has prompted a shift in disease management toward earlier diagnosis and treatment (1). Given that 70% of PsA patients have antecedent psoriasis, dermatologists are ideally positioned to identify joint abnormalities earlier. In some psoriasis

ISRCTN: 18043449; EudraCT database no. 2012-002640-25.

Supported by the Leeds Foundation for Dermatology Research and an unrestricted educational grant from Janssen-Cilag Pharmaceuticals.

[1]Laura Savage, PhD, Laura Horton, PhD, Elizabeth Hensor, PhD, Paul Emery, MD, Richard Wakefield, MD, Dennis McGonagle, FRCPI, PhD, MD: Leeds Institute of Rheumatic and Musculoskeletal Medicine, University of Leeds, NIHR Leeds Biomedical Research Centre, Leeds Teaching Hospitals NHS Trust, Leeds, UK; [2]Mark Goodfield, MD: Leeds Teaching Hospitals NHS Trust, Leeds, UK; [3]Abdulla Watad, MD: Leeds Institute of Rheumatic and Musculoskeletal Medicine, University of Leeds, NIHR Leeds Biomedical Research Centre, Leeds Teaching Hospitals NHS Trust, Leeds, UK, Sheba Medical Center, Ramat-Gan, Israel, and Tel-Aviv University, Tel-Aviv, Israel; [4]Miriam Wittmann, PhD, MD: Leeds Teaching Hospitals NHS Trust, Leeds, UK, and University of Bradford, Bradford, UK.

Dr. Savage has received honoraria from Pfizer and Janssen-Cilag (more than $10,000 each) and research support from these companies. Dr. Goodfield has received honoraria from AbbVie, Amgen, Biogen, Celgene, Galderma, Janssen, Leo Pharma, Lilly, Novartis, and Pfizer (more than $10,000 each). Dr. Emery has received consulting fees, speaking fees, and/or honoraria from Bristol-Myers Squibb, Abbott, Pfizer, MSD, Novartis, Roche, and UCB (more than $10,000 each) and research support from Abbott, Bristol-Myers Squibb, Pfizer, MSD, and Roche. Dr. Wakefield has received consulting fees, speaking fees, and/or honoraria from AbbVie and General Electric (less than $10,000 each). Dr. Wittmann has received consulting fees, speaking fees, and/or honoraria from AbbVie, Novartis, Biogen, L'Oreal, Leo, and Janssen (less than $10,000 each). Dr. McGonagle has received consulting fees, speaking fees, and/or honoraria from AbbVie, Celgene, Eli Lilly, Janssen, Merck, Novartis, Pfizer, and UCB (more than $10,000 each) and research support from AbbVie, Celgene, Janssen, Merck, Novartis, and Pfizer. No other disclosures relevant to this article were reported.

Address correspondence to Dennis McGonagle, FRCPI, PhD, MD, Section of Musculoskeletal Disease, Leeds Institute of Molecular Medicine, University of Leeds, NIHR Leeds Musculoskeletal Biomedical Research Unit, Chapel Allerton Hospital, Leeds, UK. E-mail: d.g.mcgonagle@leeds.ac.uk.

Submitted for publication August 12, 2018; accepted in revised form November 6, 2018.

populations, ~2% of patients develop PsA each year (1). However, despite dermatologists' increasing awareness of the development of PsA and the support of screening for PsA in psoriasis patients, the prevalence of undiagnosed musculoskeletal disease remains high, with undiagnosed PsA reported in up to 29% of patients presenting to dermatology clinics (2).

Enthesitis is believed to be the primary abnormality in PsA (3). Trials investigating the efficacy of biologic agents in PsA have shown improvements in clinical enthesitis as a secondary outcome measure (4). However, the presence of subclinical enthesopathy and associated osteitis, for which clinical examination is ineffective, has been reported in patients with psoriasis but no arthritis (5). The sonographic response to biologic drugs used in psoriasis and established PsA in subclinical enthesopathy is not well studied. One small observational study (6) showed a decrease in morphologic sonographic abnormalities in psoriasis patients who had enthesitis treated with methotrexate or tumor necrosis factor (TNF) inhibitors for 6 months, although some of these patients fulfilled the Classification of Psoriatic Arthritis (CASPAR) Study Group criteria for PsA (6,7).

Systemic interleukin-23 (IL-23) overexpression leads to a psoriatic-like spondyloarthritis (SpA) phenotype that begins in the enthesis (8). Given the clear role of IL-23 in the development of a SpA-based, entheseal-driven pathology, a therapeutic strategy aimed at blocking the IL-23/IL-17 axis would be a logical option for the treatment of subclinical enthesopathy in early PsA. Therefore, we investigated the effect of IL-12/IL-23 inhibition on the sonographic features of subclinical enthesopathy in patients with moderate-to-severe psoriasis treated with ustekinumab, a fully humanized monoclonal antibody directed against IL-12/IL-23p40.

PATIENTS AND METHODS

Patient groups. Seventy-three consecutive new adult patients with moderate-to-severe chronic plaque psoriasis (Psoriasis Area and Severity Index [PASI] score >10) (9) and no PsA (defined as the absence of clinically evident signs/symptoms of inflammatory arthritis according to the CASPAR criteria and a Psoriasis Epidemiology Screening Tool score of <3) and 23 healthy volunteers were screened for subclinical enthesitis by ultrasound.

Exclusion criteria for both cohorts included any known rheumatologic disease, positive rheumatoid factor or anti–citrullinated protein antibody, and prior treatment with any disease-modifying antirheumatic drug for any condition. The only prior antipsoriatic therapies permitted were emollients, topical medications, and narrowband ultraviolet phototherapy, since prior systemic therapies may affect subclinical enthesopathy. Patients with psoriasis were eligible for inclusion if they exhibited sonographic inflammatory changes that fulfilled the Outcome Measures in Rheumatology (OMERACT) definition of enthesopathy in at least 1 peripheral enthesis (10). Eligible patients with contraindications to treatment with ustekinumab were excluded.

Ultrasonography. Gray-scale and power Doppler (PD) ultrasound examinations were performed by 2 research sonographers (1 of whom was an author of this report [LH]) who are fully trained in entheseal ultrasonography using a General Electric Logiq E9 machine. The sonographers were aware of the patients' psoriasis diagnosis, and it was not possible for them to be blinded with regard to other findings at study visits due to the fact that they performed the previous scans and the number of participants in the trial was small. The psoriasis patients underwent initial ultrasonography of the upper and lower limb entheses and adjacent bursae to screen for the presence of subclinical inflammation, and were eligible for further participation in the study if they exhibited thickening, hypoechoic change, and/or a PD signal in at least 1 enthesis.

An ultrasound was performed on eligible patients at baseline (day of first ustekinumab dose) and after 12, 24, and 52 weeks of therapy. The entheseal sites examined were identical to those examined on the screening ultrasound with the exception of the third, fourth, and fifth fingers, as they exhibited little or no enthesitis at screening. The healthy volunteers had only 1 ultrasound. Entheses of the flexor and extensor pollicus longus, flexor digitorum profundus, extensor digitorum, common extensor and flexor, distal brachial triceps, quadriceps, proximal and distal patellar, Achilles, plantar aponeurosis, and peroneal brevis tendons were assessed.

Ultrasound image interpretation. The OMERACT definition of enthesopathy was used to interpret ultrasound images. Each entheseal site was assessed for thickening, hypoechogenicity, PD signal and calcification, and adjacent enthesophytes, bone erosions, and cortex irregularities. Cortex irregularity and bursal involvement were included in the assessment, since cortex irregularity may reflect cumulative damage from previous inflammation and bursal involvement indicates synovio–entheseal complex involvement, a key lesion that may be involved in the transition from subclinical enthesopathy to PsA. Gray-scale and PD bursal hypertrophy were also assessed at the entheseal sites.

Entheseal thickening was assessed at the widest point of the entheseal insertion on longitudinal scans. A previously published quantitative scoring system was applied to the measurements and, where available, normal values were accepted as reported in the literature (10,11). Where information on normal values was unavailable, the method of Gibbon and Long (12) was used, which informed the published plantar fascia threshold used in the Glasgow Ultrasound Enthesitis Scoring System (GUESS) (11). The upper limit of tendon thickness in our healthy volunteer cohort was used as the threshold for designating increased tendon thickness in the psoriasis patients.

Drug therapy. Ustekinumab was administered at the licensed dose by the clinician (weight <100 kg: 45 mg; weight ≥100 kg: 90 mg) at weeks 0, 4, 16, 28, 40, and 52; subcutaneous administration was performed by the clinician to ensure compliance. Some concomitant topical psoriasis therapies were permitted (emollients, topical corticosteroids, coal tar preparations, and vitamin D analogs). Glucocorticoids, regular use of nonsteroidal antiinflammatory drugs, systemic immunosuppressants, and any experimental drugs were prohibited.

Clinical assessment. Clinical assessments were performed prior to each ultrasound by a dermatologist (LS) who is trained in musculoskeletal examination, with an additional safety visit at week 4. Assessments included the PASI score, percentage body surface area (BSA), modified Nail Psoriasis Severity Index (mNAPSI) score, documentation of anatomic sites with psoriasis, and assessments for enthesitis (30 sites), dactylitis, and peripheral joint swelling and/or tenderness (66/68 joints).

Statistical analysis. This study was designed as a pilot to inform a larger randomized controlled trial. The sample size for the treatment phase was based on the published standards, suggesting that between 12 and 30 patients should be recruited for pilot studies. We aimed to recruit at least 12 (up to 30) depending on the recruitment rate, which was a feasibility outcome of the trial. Group mean ± SD or median and interquartile range (IQR) values were calculated, with 95% confidence intervals (95% CIs).

RESULTS

Participant characteristics. Seventy-three patients (45 male and 28 female) with moderate-to-severe plaque psoriasis (median PASI score 17.6 [IQR 11.9, 25.4]) were screened by ultrasound. Thirty-six patients (49.3%) had ≥1 sonographic inflammatory abnormality that fulfilled the OMERACT definition of enthesopathy. Of the 36 patients, 30 met the trial eligibility criteria, of whom 6 chose conventional therapy and 1 was lost to follow-up. Twenty-three patients consented to trial participation and were treated with ustekinumab. Attempts were made to recruit healthy volunteers with similar characteristics (age, sex, body mass index [BMI]) to the group of psoriasis patients, although specific case matching was not performed (Table 1).

Table 1. Descriptive characteristics of the 2 cohort populations*

	Psoriasis patients (n = 23)	Healthy volunteers (n = 23)
Sex		
Male	12 (52.2)	12 (52.2)
Female	11 (47.8)	11 (47.8)
Age, mean ± SD (range) years	44.1 ± 13.9 (20–74)	39.3 ± 8.3 (22–59)
Fitzpatrick skin type (phototype)		
I	3 (13.0)	4 (17.4)
II	11 (47.8)	14 (60.9)
III	8 (34.8)	4 (17.4)
IV	0 (0)	1 (4.3)
V	1 (4.3)	0 (0)
VI	0 (0)	0 (0)
BMI, median (IQR) kg/m^2	29.6 (27.6, 29.6)	26.8 (24.6, 31.5)
Smoking status		
Never	8 (34.8)	18 (78.3)
Current	7 (30.4)	1 (4.3)
Previous	8 (34.8)	4 (17.4)
Ever	15 (65.2)	5 (21.7)
Cigarette pack-years in current/ex-smokers, median (IQR) years	20 (7, 32)	7.9 (4, 12)
Alcohol consumption in drinkers, median (IQR) units/week	10 (10, 20)	10 (10, 20)
Positive family history of psoriasis	13 (56.5)	2 (8.7)
Positive family history of psoriatic arthritis	2 (8.7)	0 (0)
Positive family history of other rheumatologic disorder	4 (17.4)	10 (43.5)
Positive family history of autoimmune disease	2 (8.7)	6 (26.1)

* Except where indicated otherwise, values are the number (%) of subjects. BMI = body mass index; IQR = interquartile range

There were no meaningful clinical differences in age (mean difference 4.8 years [95% CI –2.0, 11.6]) and BMI (median difference 3.3 kg/m^2 [95% CI 0.1, 6.7]).

Pretreatment ultrasonographic abnormalities in patients with psoriasis compared with healthy volunteers. *Entheseal inflammation*. Of the 598 entheses scanned in psoriasis patients at week 0 (median 6 [of 26] per patient [IQR 4, 9]), 24.2% had at least 1 inflammatory entheseal abnormality (thickening, hypoechogenicity, and/or PD signal) with a score of >0, compared with 4.5% in healthy volunteers (median 1 [of 26] per volunteer [IQR 0, 1]). In total, 187 inflammatory abnormalities were shown in patients with psoriasis (mean ± SD 8.7 ± 4.7 abnormalities per patient), compared with 24 shown in healthy volunteers (1.0 ± 1.4 abnormalities per healthy volunteer). Mean ± SD inflammation scores were higher in patients with psoriasis (9.9 ± 6.6 of a possible 294, compared with 1.0 ± 1.4 in the healthy volunteer group). In both groups, abnormalities were seen with the greatest frequency in knee tendons (distal patellar more frequently than quadriceps), followed by the common extensor and flexor tendons of the elbow and large entheses of the ankle. Bursitis was infrequent; 1 patient had gray-scale hypertrophy in 1 superficial infrapatellar bursa and the contralateral deep infrapatellar bursa, and 1 volunteer had gray-scale hypertrophy in 1 retrocalcaneal bursa at week 0. At clinical assessment, 29 tender enthesis sites from the 736 examined in all 23 patients were identified (3.9%), and 4 patients had asymptomatic toe swelling consistent with low-grade dactylitis.

Chronic entheseal damage. At week 0, 15.9% of the 598 entheses examined (median 5 [of 26] per patient [IQR 2, 8]) had at least 1 chronic abnormality indicative of structural damage

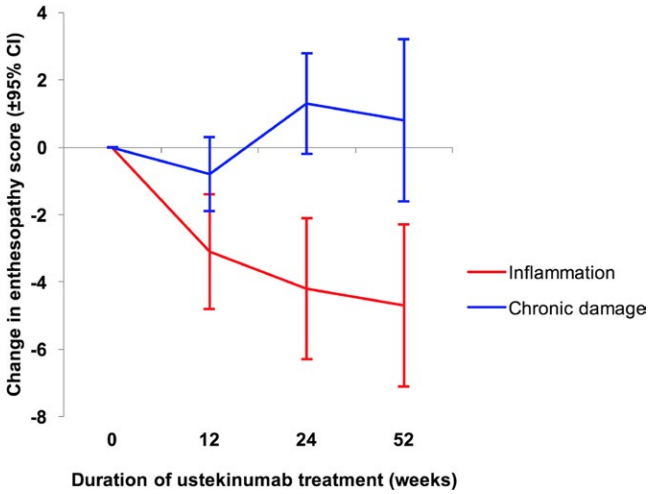

Figure 1. Mean change (with 95% confidence interval [95% CI]) in total enthesopathy scores for inflammatory and chronic damage abnormalities over time in patients treated with ustekinumab. Progressive improvement of lesions shown to be potentially inflammatory was evident, but chronic changes showed no significant differences.

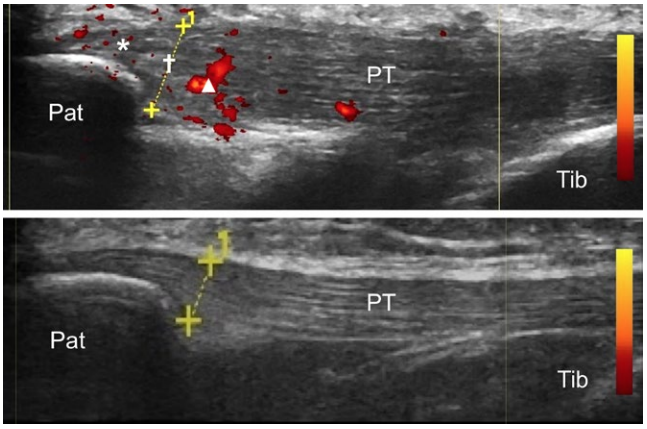

Figure 2. Ultrasound images showing resolution of subclinical enthesopathy. Reductions in entheseal thickness from grade 2 to grade 0 (†), in hypoechogenicity from grade 1 to grade 0 (*), and in power Doppler signal from grade 3 to grade 0 (△) within the left proximal patellar tendon enthesis were seen between week 0 (top) and week 52 of ustekinumab therapy (bottom). **Pat** = patella; **PT** = patellar tendon; **Tib** = tibia.

with a score of >0, compared with 6.0% in the healthy volunteer group (median 1 [of 26] per participant [IQR 0, 3]). In total, 137 abnormalities were identified in the psoriasis group (mean ± SD 6.0 ± 4.7 abnormalities per patient), compared with 36 in healthy volunteers (1.6 ± 1.6 abnormalities per volunteer). Mean ± SD chronicity scores were higher in patients with psoriasis (7.9 ± 5.7 of a possible 312, compared with 2.0 ± 1.9 in the healthy volunteer group).

Cutaneous responses to ustekinumab in participants with psoriasis. The median duration of psoriasis was 11 years (IQR 7, 25). Median baseline PASI score and BSA were 18.0 and 30%, respectively. Twenty-one patients (91.3%) achieved a ≥75% reduction in PASI scores (PASI75) response, 17 patients (73.9%) achieved a PASI90 response, and 11 patients (47.8%) achieved a PASI100 response by week 24 (primary end point of the study of ustekinumab efficacy for psoriasis), and responses were generally maintained through week 52. Seventeen patients had nail involvement at baseline (median mNAPSI 28/140). Median mNAPSI scores decreased significantly (by 15 points and 22 points) at weeks 24 and 52, respectively.

Ultrasonographic musculoskeletal responses to ustekinumab in patients with psoriasis. *Entheseal inflammation*. Mean entheseal inflammation scores decreased by 42.2% from week 0 to week 24 (–4.2 [95% CI –6.3, –2.1]; Cohen's d effect size [*d*] = 1.2, $P < 0.001$) and by 47.5% by week 52 (–4.7 [95% CI –7.1, –2.3]); $d = 1.3$, $P = 0.001$) (Figure 1). The percentage of entheses with at least 1 inflammatory abnormality decreased from 24.2% to 14.0% by week 24, and to 10.4% by week 52. Of the 187 inflammatory abnormalities found at baseline, 116 (62.0%) resolved, 14 (7.5%) improved,

55 (29.4%) remained unchanged, and 2 (1.1%) worsened by week 24. An example of resolution of subclinical enthesopathy is shown in Figure 2. During treatment, 38 new abnormalities developed by week 24. The mean ± SD total number of abnormalities per patient decreased from 8.1 ± 4.7 at week 0 to 5.7 ± 3.8 lesions (difference –2.5 [95% CI –3.6, –1.3]) at week 12, to 4.7 ± 4.2 (difference –3.4 [95% CI –4.9, –1.9]) at week 24, and to 3.5 ± 2.7 (difference –4.7 [95% CI –6.6, –2.7]) at week 52. Bursitis had resolved at week 24 in the patient who had 2 affected areas at baseline. Three patients developed transient unilateral bursal synovial hypertrophy in 1 area during the study, with resolution occurring by the following scan in all cases. At all time points assessed, there were no substantive differences in inflammatory enthesopathy scores according to age, sex, BMI, smoking status, alcohol consumption, duration of psoriasis, anatomic location of psoriatic plaques, family history, or HLA–Cw06 status.

Chronic entheseal damage. Structural abnormalities remained static or marginally worsened over time. Mean entheseal chronic damage scores increased by 16.5% between weeks 0 and 24 (mean increase 1.3 [95% CI –0.2, 2.7]; $d = 0.5$, $P < 0.082$), and by 10% between weeks 0 and 52 (mean increase 0.8 [95% CI –1.6, 3.1]; $d = 0.2$, $P = 0.512$) (Figure 1). The percentage of entheses with at least 1 chronic damage abnormality increased from 15.9% at week 0 to 18.6% at week 24 and 20.0% at week 52. Of the 137 chronic damage abnormalities shown at week 0, 35 (25.5%) resolved, 14 (10.2%) improved, 75 (54.7%) remained unchanged, and 13 (9.5%) worsened by week 24. Sixty-eight new abnormalities developed during treatment. The mean ± SD total number of abnormalities per patient changed from 6.0 ± 4.7 at week 0 to 5.6 ± 5.0, 7.4 ± 5.7, and 7.6 ± 6.1 at weeks 12, 24, and 52, respectively.

Adverse events occurred in a similar frequency to that reported in phase III studies and registry data for ustekinumab. The adverse events were not serious (3 cases of upper respiratory infection, 1 case of gastroenteritis, and 2 follicular abnormalities).

DISCUSSION

Our findings confirm that subclinical enthesopathy in patients with psoriasis is not uncommon, with 49.3% of the 73 patients with moderate-to-severe psoriasis having at least 1 potentially modifiable inflammatory abnormality at first presentation to a dermatologist. This percentage is broadly consistent with recent magnetic resonance imaging findings in psoriasis patients but is higher than previously reported from more limited ultrasound protocols (13,14). We determined that targeted treatment of psoriasis with a therapeutic agent independently shown to work in PsA, namely anti–IL-12/23p40, can be associated with regression of subclinical inflammatory entheseal and synovial abnormalities. Ultrasonography-determined chronic damage abnormalities did not significantly improve. Our findings support the concept that therapies that suppress subclinical enthesopathy may have the potential to prevent the development of arthritis, at least in a subset of cases, but this needs formal testing in longitudinal studies.

To evaluate the effect of therapy on subclinical skeletal abnormalities in psoriasis, we used a more comprehensive ultrasound scoring system based on the GUESS. We chose the GUESS as it is an easily reproducible, standardized measure of sonographic lower limb entheseal abnormalities. However, it excludes several accessible entheses that have not been reliably investigated in patients with subclinical disease (notably those in the upper limbs), and parameters such as hypoechogenicity, PD signal, and bone cortex irregularities that are fundamental parts of the OMERACT definition of enthesopathy. Though important to include, PD signal was a rare finding, with only 0.2% of entheses exhibiting signals in patients with psoriasis prior to treatment. This is less than the 1–7.4% previously reported in other psoriasis cohorts (5,14), which may be due to a dilutional effect from the inclusion of many more entheseal sites and the investigation of asymptomatic patients. As in previous studies, patients in our study exhibited the most abnormalities in the larger entheses, such as the quadriceps, proximal and distal patella, common extensor, and Achilles tendon insertions. However, reflecting the heterogeneous nature of PsA, abnormalities in the smaller entheses were not infrequent (10–20%), especially in the extensor and flexor pollicis longus tendon insertions of the thumb, the peroneal brevis enthesis, and the flexor digitorum profundus enthesis of the index finger.

In our cohort, there were no significant changes in chronic damage abnormalities with ustekinumab therapy. While some structural lesions worsened, some appeared to decrease in severity or resolve (primarily bone erosions), which is a recognized phenomenon in rheumatoid arthritis (15) and in PsA (16). The rate of progression of structural lesions without ustekinumab therapy is unknown. Inclusion of an untreated group may have helped determine whether ustekinumab slowed the development of damage. However, this limitation is difficult to overcome, as it would be unethical to not treat a group of psoriasis patients. In our study, we attempted to recruit control patients with psoriasis undergoing narrowband ultraviolet B phototherapy for comparison, but this proved unfeasible. Similarly, it may have been helpful to rescan the healthy volunteers after 24 weeks to indicate the rate of progression in the normal population. High rates of structural damage in the Achilles tendon enthesis were shown in our healthy volunteer cohort (30.4%, compared with 17.4% in psoriasis patients), but the opposite was shown for inflammatory abnormalities (4.3% in the healthy volunteers and 15.2% in psoriasis patients). This suggests that structural changes in the healthy volunteers were caused by trauma and natural degeneration rather than an inflammatory process.

To the best of our knowledge, this is the first study to evaluate the alteration in sonographic features of subclinical enthesitis with an IL-12/IL-23p40 inhibitor and the first study to investigate sonographic treatment responses in patients with asymptomatic psoriasis who are naive to systemic therapy. However, a recent

study demonstrated that downstream inhibition of IL-17 may have a similar effect on subclinical PsA (17).

The relatively small number of patients investigated in this pilot study prevents any definite conclusions regarding the effectiveness of ustekinumab in treating subclinical enthesitis and bursitis, although the identified trends are encouraging. Since this was an open-label study, there is a possibility of bias in the longitudinal imaging assessments, although the imaging was performed in a dark room with limited verbal interaction and with other patients in different studies also undergoing sonographic assessments.

These data are consistent with recently published reports regarding good sonographic responses of entheseal abnormalities after treatment with TNF inhibitors in patients with psoriasis (6) and SpA (18). The results of our proof-of-concept study support the notion that IL-12/IL-23 has a role in entheseal-driven pathology in the early stages of PsA and promote the need for larger trials to determine whether the regression of subclinical arthropathy is associated with PsA prevention.

ACKNOWLEDGMENT

We would like to thank Dr. Alwyn Jackson for his help in performing the ultrasonography assessment.

AUTHOR CONTRIBUTIONS

All authors were involved in drafting the article or revising it critically for important intellectual content, and all authors approved the final version to be published. Dr. McGonagle had full access to all of the data in the study and takes responsibility for the integrity of the data and the accuracy of the data analysis.

Study conception and design. Savage, Wakefield, McGonagle.
Acquisition of data. Savage, Horton, Hensor, Wakefield, McGonagle.
Analysis and interpretation of data. Savage, Goodfield, Watad, Hensor, Emery, Wittmann.

REFERENCES

1. Eder L, Haddad A, Rosen CF, Lee KA, Chandran V, Cook R, et al. The incidence and risk factors for psoriatic arthritis in patients with psoriasis: a prospective cohort study. Arthritis Rheumatol 2016;68:915–23.
2. Haroon M, Kirby B, FitzGerald O. High prevalence of psoriatic arthritis in patients with severe psoriasis with suboptimal performance of screening questionnaires. Ann Rheum Dis 2013;72:736–40.
3. McGonagle D, Gibbon W, Emery P. Classification of inflammatory arthritis by enthesitis. Lancet 1998;352:1137–40.
4. Ramiro S, Smolen JS, Landewé R, Heijde DV, Gossec L. How are enthesitis, dactylitis and nail involvement measured and reported in recent clinical trials of psoriatic arthritis? A systematic literature review. Ann Rheum Dis 2018;77:782–3.
5. Naredo E, Moller I, de Miguel E, Batlle-Gualda E, Acebes C, Brito E, et al. High prevalence of ultrasonographic synovitis and enthesopathy in patients with psoriasis without psoriatic arthritis: a prospective case-control study. Rheumatology (Oxford) 2011;50:1838–48.
6. Acquacalda E, Albert C, Montaudie H, Fontas E, Danre A, Roux CH, et al. Ultrasound study of entheses in psoriasis patients with or without musculoskeletal symptoms: a prospective study. Joint Bone Spine 2015;82:267–71.
7. Taylor W, Gladman D, Helliwell P, Marchesoni A, Mease P, Mielants H, and the CASPAR Study Group. Classification criteria for psoriatic arthritis: development of new criteria from a large international study. Arthritis Rheum 2006;54:2665–73
8. Sherlock JP, Joyce-Shaikh B, Turner SP, Chao CC, Sathe M, Grein J, et al. IL-23 induces spondyloarthropathy by acting on ROR-γt+ CD3+CD4-CD8- entheseal resident T cells. Nat Med 2012;18:1069–76.
9. Fredriksson T, Pettersson U. Severe psoriasis—oral therapy with a new retinoid. Dermatologica 1978;157:238–44.
10. Wakefield RJ, Balint PV, Szkudlarek M, Filippucci E, Backhaus M, D'Agostino MA, et al. Musculoskeletal ultrasound including definitions for ultrasonographic pathology. J Rheumatol 2005;32:2485–7.
11. Balint PV, Kane D, Wilson H, McInnes IB, Sturrock RD. Ultrasonography of entheseal insertions in the lower limb in spondyloarthropathy. Ann Rheum Dis 2002;61:905–10.
12. Gibbon WW, Long G. Ultrasound of the plantar aponeurosis (fascia). Skeletal Radiol 1999;28:21–6.
13. Faustini F, Simon D, Oliveira I, Kleyer A, Haschka J, Englbrecht M, et al. Subclinical joint inflammation in patients with psoriasis without concomitant psoriatic arthritis: a cross-sectional and longitudinal analysis. Ann Rheum Dis 2016;75:2068–74.
14. Gutierrez M, Filippucci E, De Angelis R, Salaffi F, Filosa G, Ruta S, et al. Subclinical entheseal involvement in patients with psoriasis: an ultrasound study. Semin Arthritis Rheum 2011;40: 407–12.
15. Ideguchi H, Ohno S, Hattori H, Senuma A, Ishigatsubo Y. Bone erosions in rheumatoid arthritis can be repaired through reduction in disease activity with conventional disease-modifying antirheumatic drugs. Arthritis Res Ther 2006;8:R76.
16. Finzel S, Kraus S, Schmidt S, Hueber A, Rech J, Engelke K, et al. Bone anabolic changes progress in psoriatic arthritis patients despite treatment with methotrexate or tumour necrosis factor inhibitors. Ann Rheum Dis 2013;72:1176–81.
17. Kampylafka E, d Oliveira I, Linz C, Lerchen V, Englbrecht M, Simon D, et al. Disease interception in psoriasis patients with subclinical joint inflammation by interleukin 17 inhibition with secukinumab: data from a prospective open label study [abstract]. Ann Rheum Dis 2018;77 Suppl 2:199
18. Aydin SZ, Karadag O, Filippucci E, Atagunduz P, Akdogan A, Kalyoncu U, et al. Monitoring Achilles enthesitis in ankylosing spondylitis during TNF-α antagonist therapy: an ultrasound study. Rheumatology (Oxford) 2010;49:578–82.

AMERICAN COLLEGE OF RHEUMATOLOGY
EDUCATION • TREATMENT • RESEARCH

Arthritis & Rheumatology
Vol. 71, No. 4, April 2019, pp 632–640
DOI 10.1002/art.40773

Suppression of Murine Lupus by CD4+ and CD8+ Treg Cells Induced by T Cell–Targeted Nanoparticles Loaded With Interleukin-2 and Transforming Growth Factor β

David A. Horwitz,[1] Sean Bickerton,[2] Michael Koss,[3] Tarek M. Fahmy,[2] and Antonio La Cava[4]

Objective. To develop a nanoparticle (NP) platform that can expand both CD4+ and CD8+ Treg cells in vivo for the suppression of autoimmune responses in systemic lupus erythematosus (SLE).

Methods. Poly(lactic-co-glycolic acid) (PLGA) NPs encapsulating interleukin-2 (IL-2) and transforming growth factor β (TGFβ) were coated with anti-CD2/CD4 antibodies and administered to mice with lupus-like disease induced by the transfer of DBA/2 T cells into (C57BL/6 × DBA/2)F_1 (BDF1) mice. The peripheral frequency of Treg cells was monitored ex vivo by flow cytometry. Disease progression was assessed by measuring serum anti–double-stranded DNA antibody levels by enzyme-linked immunosorbent assay. Kidney disease was defined as the presence of proteinuria or renal histopathologic features.

Results. Anti-CD2/CD4 antibody–coated, but not noncoated, NPs encapsulating IL-2 and TGFβ induced CD4+ and CD8+ FoxP3+ Treg cells in vitro. The optimal dosing regimen of NPs for expansion of CD4+ and CD8+ Treg cells was determined in in vivo studies in mice without lupus and then tested in BDF1 mice with lupus. The administration of anti-CD2/CD4 antibody–coated NPs encapsulating IL-2 and TGFβ resulted in the expansion of CD4+ and CD8+ Treg cells, a marked suppression of anti-DNA antibody production, and reduced renal disease.

Conclusion. This study shows for the first time that T cell–targeted PLGA NPs encapsulating IL-2 and TGFβ can expand both CD4+ and CD8+ Treg cells in vivo and suppress murine lupus. This approach, which enables the expansion of Treg cells in vivo and inhibits pathogenic immune responses in SLE, could represent a potential new therapeutic modality in autoimmune conditions characterized by impaired Treg cell function associated with IL-2 deficiency.

INTRODUCTION

Systemic lupus erythematosus (SLE) is a disorder of immune regulation in which genetic and environmental factors contribute to the disruption of immune homeostasis. In SLE, normally quiescent self-reactive T and B cells become activated and are no longer held in check by the mechanisms of peripheral tolerance, including suppression by Treg cells, which are specialized cells that have an impaired function in SLE (1).

Since the levels of interleukin-2 (IL-2) and transforming growth factor β (TGFβ) that are required for the induction, expansion, and function of Treg cells are compromised in SLE (1), and because IL-2 and TGFβ help induce both CD4+ and CD8+ Treg cells (in normal and disease settings), it has been proposed that these cytokines could be manipulated for the possible restoration of Treg cell deficits (2). For example, low-dose IL-2 therapy has been used to correct defects in Treg cells and to improve clinical disease in SLE patients (3,4), supporting the concept that the functional impairment of Treg cells in SLE that is attributable to cytokine deficiency can be corrected by selective cytokine modulation.

We recently reported that nanoparticles (NPs) composed of the biocompatible FDA-approved biodegradable polymer poly(lactic-co-glycolic acid) (PLGA) coated with anti-CD4 antibody (for the targeting of CD4+ T cells) that encapsulate IL-2 and TGFβ can induce ex vivo functional, stable CD4+CD25+FoxP3+ Treg

Supported by the NIH (grants GM-007205 and AI-109677 to Mr. Bickerton and Dr. La Cava, respectively).

[1]David A. Horwitz, MD: Keck School of Medicine of the University of Southern California, Los Angeles and General Nanotherapeutics, Santa Monica, California; [2]Sean Bickerton, MS, Tarek M. Fahmy, PhD: Yale University, New Haven, Connecticut; [3]Michael Koss, MD: Keck School of Medicine at the University of Southern California, Los Angeles; [4]Antonio La Cava, MD, PhD: David Geffen School of Medicine at the University of California, Los Angeles.

Dr. Horwitz and Mr. Bickerton contributed equally to this work.

Dr. Horwitz is Chief Executive Officer of General Nanotherapeutics, LLC. Dr. Fahmy owns stock or stock options in Toralgen. No other disclosures relevant to this article were reported.

Address correspondence to Antonio La Cava, MD, PhD, University of California, Los Angeles, 1000 Veteran Avenue 32-59, Los Angeles, CA 90095 (e-mail: alacava@mednet.ucla.edu); or to David A. Horwitz, MD, 566 Latimer Road, Santa Monica, CA 90402 (e-mail: dhorwitz@usc.edu).

Submitted for publication May 3, 2018; accepted in revised form November 1, 2018.

cells (5). In this study, we extend those findings by exploring the therapeutic effects of targeted delivery of IL-2 and TGFβ to T cells for the induction of Treg cells in vivo. In addition to targeting CD4+ T cells by coating NPs with anti-CD4 antibody, we co-coated NPs with anti-CD2 antibody to target CD8+ T cells (2) and induce CD8+ Treg cells ex vivo (because of the protective effects of CD8+ Treg cells in SLE) (6,7).

Specifically, the effects of NPs encapsulating IL-2 and TGFβ were investigated in a murine lupus model where donor CD4+ T cells from DBA/2 mice injected into (C57BL/6 × DBA/2)F_1 (BDF1) mice recognize the host major histocompatibility complex (MHC) antigens, become activated, and drive B cell hyperactivity (8,9). In this model, the outcome of the cell transfer is lymphoid hyperplasia, polyclonal B cell activation, and anti–double-stranded DNA (anti-dsDNA) antibody production within 2 weeks and immune complex glomerulonephritis within 4–6 weeks (8,9). Of note, an advantage of this model is that a single transfer of DBA/2 CD4+ and CD8+ Treg cells generated ex vivo with IL-2 and TGFβ is sufficient to block B cell activation, autoantibody production, and immune complex nephritis (10), allowing the testing of the therapeutic potential of targeted delivery of IL-2 and TGFβ to T cells for the induction of Treg cells in vivo. Our results indicate that NPs encapsulating IL-2 and TGFβ induced both CD4+ and CD8+ Treg cells in vivo, with subsequent reduced lupus disease manifestations.

MATERIALS AND METHODS

NP preparation and characterization. Cytokine-encapsulating PLGA NPs were prepared according to a previously described water/oil/water double emulsion protocol (5). Briefly, 60 mg PLGA (50:50; Durect) were dissolved in 3 ml of chloroform in a glass test tube. A primary emulsion was generated by adding 200 μl of an aqueous solution containing 2.5 μg carrier-free TGFβ and 1.25 μg IL-2 (PeproTech). Addition was carried out dropwise while continuously vortexing the chloroform polymer solution. The resulting primary emulsion was sonicated using an Ultrasonic Processor GEX600 model probe at 38% amplitude for a 10-second pulse, and added dropwise to a continuously vortexed glass test tube containing 4 ml of 4.7% polyvinyl alcohol (PVA) and 0.625 mg/ml avidin–palmitate conjugate, as previously described (11). The resulting double emulsion was sonicated with three 10-second pulses with 20-second breaks in an ice bath in between before transfer to a beaker containing 200 ml of 0.25% PVA. Particles were allowed to harden by stirring for 3 hours at room temperature. Hardened NPs were washed 3 times by cycles of pelleting at 18,000*g* and resuspension in Milli-Q water. Washed NPs were flash-frozen in liquid nitrogen and lyophilized for multiple days to enable long-term storage. NPs were stored at –20°C until used and prepared from lyophilized stocks for each experiment.

For cell targeting, NPs were freshly prepared in phosphate buffered saline (PBS) at the target concentration and reacted with the biotinylated targeting antibody at a concentration ratio of 2 μg antibody to 1 mg NPs 10 minutes prior to use. NP size was quantified using dynamic light scattering with a Malvern Zetasizer Nano. Cytokine encapsulation and release were measured by BD OptEIA enzyme-linked immunosorbent assay (ELISA) kits, either after disrupting particles in DMSO or by supernatant analysis of release study aliquots. For the release assay, a 1% weight/volume solution of Pluronic F-127 in PBS was used as release buffer, to help stabilize released cytokine and prevent binding to the tube surface and loss of capture/detection antibody binding ability.

Mice. C57BL/6, DBA/2, and BALB/c mice (including DO11.10, $H2^d$) were purchased from The Jackson Laboratory. Female C57BL/6 mice and male DBA/2 mice were bred for the generation of (C57BL/6 × DBA/2)F_1 (BDF1) mice. Disease was induced in BDF1 mice at 8 weeks of age by the transfer of parent DBA/2 cells according to standard protocols (10). BDF1 mice were then given an intraperitoneal (IP) injection of vehicle as control or PLGA NPs encapsulating IL-2 and TGFβ and left uncoated (control) or coated with anti-CD2 and anti-CD4 antibody (BD Biosciences). Mice were monitored biweekly for the frequency of circulating Treg cells by flow cytometric analysis. Serum samples were obtained via retroorbital bleeding. Proteinuria was measured using Albustix strips (Siemens). Mice were maintained in specific pathogen–free facilities at the University of California, Los Angeles. Experiments were approved by the Institutional Animal Research Committee.

In vitro assays. For T cell proliferation, splenocytes were incubated at 37°C at a concentration of 2×10^5 cells/well in 96-well plates (Corning) in complete RPMI medium (100 units/ml penicillin, 100 μg/ml streptomycin, and 10% heat-inactivated fetal calf serum) for 72 hours in the absence (control) or presence of plate-bound anti-CD3 antibody (1 μg/ml) and soluble anti-CD28 antibody (1 μg/ml) (BD Biosciences). In some experiments, ovalbumin 323–339 peptide (ThermoFisher Scientific) was added, with or without NPs, with paired control without peptide. ^{3}H-thymidine was added during the last 16 hours before cell harvesting on a Tomtec Harvester 96. The stimulation index was calculated as the mean counts per minute of antigen-stimulated wells/mean cpm of wells with medium only.

ELISA. ELISA measurement of anti-dsDNA antibody levels was performed using kits from Alpha Diagnostics International, according to the manufacturer's instructions. Optical density was measured at 450 nm.

Flow cytometric analysis. Peripheral blood mononuclear cells (PBMCs) or splenocytes were isolated according to standard procedures, and single-cell suspensions were used for phenotype analyses using combinations of fluorochrome-conjugated antibodies. After Fc blocking, fluorochrome-conjugated anti-

mouse antibodies to CD4, CD8, CD25, CD19, CD11b, CD11c, and Gr-1 (all from eBioscience) or isotype control antibodies were used for staining prior to acquisition on a FACSCalibur flow cytometer (BD Biosciences) and subsequent analysis using FlowJo software (Tree Star). For intracellular staining of FoxP3, cells were first stained for the expression of cell surface markers before fixation/permeabilization and FoxP3 staining using an eBioscience FoxP3 Staining Kit, according to the manufacturer's instructions. The gating strategy used for the different immune cell populations is shown in Supplementary Figure 1 (available on the *Arthritis & Rheumatology* web site at http://onlinelibrary.wiley.com/doi/10.1002/art.40773/abstract).

Histologic analysis. Kidney sections (4 μm thick) were stained with hematoxylin and eosin according to standard procedures (12). For assessment of pathologic changes by glomerular activity score and tubulointerstitial activity score, sections were scored in a blinded manner, on a scale of 0–3, where 0 = no lesions, 1 = lesions in <30% of glomeruli, 2 = lesions in 30–60% of glomeruli, and 3 = lesions in >60% of glomeruli. The glomerular activity score includes glomerular proliferation, karyorrhexis, fibrinoid necrosis, inflammatory cells, cellular crescents, and hyaline deposits. The tubulointerstitial activity score includes interstitial inflammation, tubular cell necrosis and/or flattening, and epithelial cells or macrophages in the tubular lumen. The raw scores were averaged to obtain a mean score for each feature, and the mean scores were summed to obtain an average score from which a composite kidney biopsy score was obtained (13). For indirect immunofluorescence studies, sections were fixed in cold acetone for 5 minutes, washed, and blocked with 2% bovine serum albumin for 1 hour before staining with rabbit anti-mouse IgG (Fisher Scientific).

Statistical analysis. Statistical analyses were performed using GraphPad Prism software version 5.0. Parametric testing was done using the unpaired *t*-test; nonparametric testing was used when data were not normally distributed. *P* values less than 0.05 were considered significant.

RESULTS

Preparation of NPs. The prepared cytokine-encapsulating NPs were characterized through examination of physical properties, encapsulation metrics, and release kinetics (Figure 1), as previously described (5,14). By dynamic light scattering, NPs were found to have a mean ± SD hydrodynamic diameter of 245.3 ± 2.2 nm with a low polydispersity index (mean ± SD 0.06 ± 0.01), indicative of a uniform NP population with a relatively tight size distribution (Figure 1B). Cytokine encapsulation was measured by ELISA after NPs were disrupted using DMSO. Standard curves were generated using cytokine standards, but all wells were supplemented to contain 5% volume/volume DMSO and the appropriate concentration of empty NPs. Using this method, NPs were found to contain a mean ± SD of 7.4 ± 0.4 ng TGFβ and 1.9 ± 0.1 ng IL-2 per mg NP. For TGFβ, the percent encapsulation efficiency was 17.8 ± 1.1; for IL-2, it was 9.1 ± 0.4.

The release assay was performed using 1 mg/ml aliquots of particles in release buffer. At each time point, aliquots were spun down in a microcentrifuge and supernatant was isolated from the particle pellet. The pellet was then resuspended in fresh release buffer until the next time point. Supernatant samples were frozen until the end of the study, at which point ELISA analysis was performed. As seen in Figure 1C, release of TGFβ and IL-2 from the NP system occurred in a burst during the first 24 hours, followed by a slower, more sustained release profile over the course of the 14-day period.

Establishment of conditions for the induction of CD4+ and CD8+ Treg cells. To induce CD4+ and CD8+ Treg cells simultaneously, we used PLGA NPs encapsulating IL-2

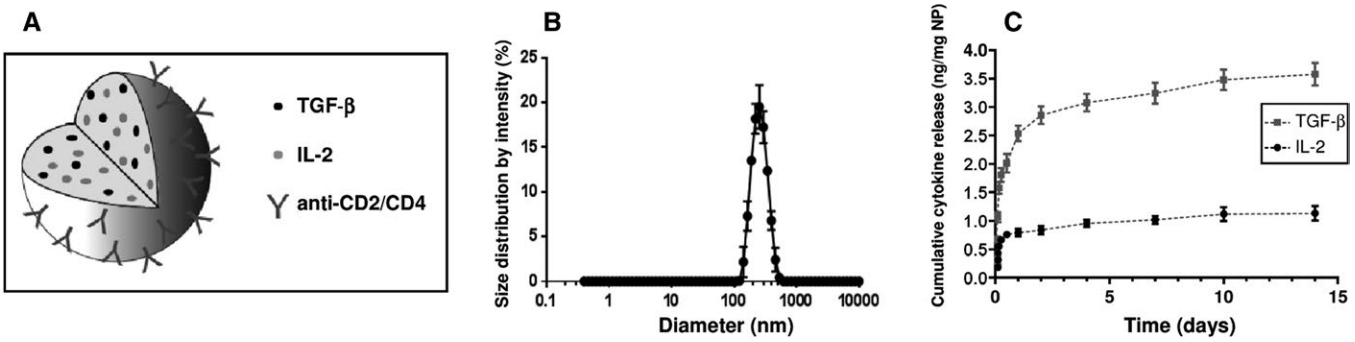

Figure 1. Characterization of the cytokine-encapsulating poly(lactic-co-glycolic acid) (PLGA) nanoparticles (NPs). **A**, Schematic representation of the PLGA NP system showing co-encapsulation of interleukin-2 (IL-2) and transforming growth factor β (TGFβ) and surface coating with targeting anti-CD2 and anti-CD4 antibodies. **B**, Size distribution of the IL-2/TGFβ-encapsulating NP population. Physical characterization of NP size was performed using dynamic light scattering. NPs had a negative surface charge as measured by zeta potential (mean ± SD −15.1 ± 0.5 mV) in Milli-Q water. **C**, Loading and release of the 2 encapsulated cytokines quantified by enzyme-linked immunosorbent assay. Results are the mean ± SD.

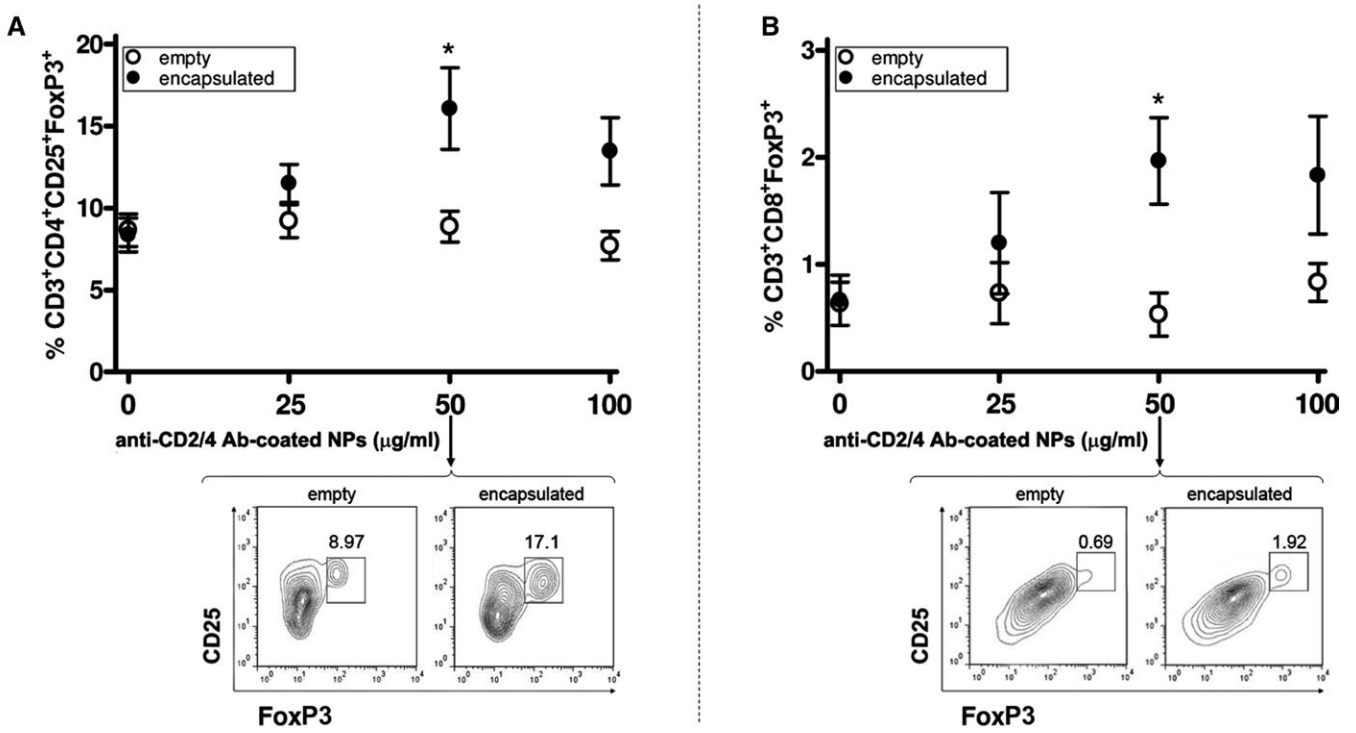

Figure 2. Establishment of conditions for the in vitro induction of CD4+ and CD8+ Treg cells with anti-CD2/CD4 antibody (anti-CD2/4 Ab)–coated PLGA NPs encapsulating IL-2 and TGFβ. Sorted CD3+ T cells (negatively selected with magnetic beads) from 12-week-old BALB/c mouse splenocytes were cultured in the presence of anti-CD3/CD28 antibodies and the indicated doses of anti-CD2/CD4–coated cytokine-encapsulating NPs (2 μg of each antibody per mg NP). After 3 days, flow cytometric analysis was performed. Top panels show the percentage of CD4+ (**A**) and CD8+ (**B**) Treg cells in cultures with cytokine-encapsulating NPs and cultures with empty NPs. Significant differences were observed at a dose of 50 μg/ml NP. Circles and error bars show the mean ± SEM. Bottom panels show representative flow cytometry plots for pregated CD4+ (**A**) and CD8+ (**B**) cells induced with the 50 μg/ml NP dose. Results are representative of 4 experiments using 3 mice per group. * = $P < 0.05$ versus empty NPs. See Figure 1 for definitions.

and TGFβ in amounts that had been used previously (5). Scalar doses of NPs coated with anti-CD2/CD4 antibodies (Figure 1A) were added in culture to mouse purified CD3+ cells for delivery to T cells, in a paracrine manner, of IL-2 and TGFβ that induce Treg cells in vitro. Since anti-CD3/CD28 antibody stimulation with 50 μg/ml NPs promoted a significant increase in the frequency of both CD4+ and CD8+ Treg cells (Figures 2A and B), we proceeded to study the conditions for generation of Treg cells in vivo.

Establishment of in vivo conditions for the induction of CD4+ and CD8+ Treg cells in mice without lupus. Treatment with anti-CD2/CD4 antibody–coated NPs was compared with treatment with NPs coated with anti-CD2 antibody only or anti-CD4 antibody only, keeping constant the total amount of NPs (all encapsulating IL-2 and TGFβ) (Figures 3A and B). After a loading dose, 1.5 mg NPs were injected into BALB/c mice every 3 days or every 6 days for the first 12 days. One week later, both groups of mice received another 1.5 mg NPs. Analysis of Treg cells among circulating PBMCs on day 21 revealed that only those animals that had received NPs every 3 days had significant increases in Treg cells (Figure 3B and Supplementary Figure 2, available on the *Arthritis & Rheumatology* web site at http://onlinelibrary.wiley.com/doi/10.1002/art.40773/abstract).

Importantly, the coating antibodies needed to be attached to the same NP (co-coated), since coating of anti-CD2 and anti-CD4 antibodies on NPs independently was not effective in expanding Treg cells. Anti-CD2 antibody coating expanded CD8+FoxP3+ cells (Figure 3B), and the percentage of CD8+-FoxP3+ cells induced by anti-CD2 antibody–coated NPs was higher than that induced by anti-CD2/CD4 antibody–coated NPs (likely due to lower per-NP coating of anti-CD2 antibody in the co-coated system and increased competitive binding to CD4+ T cells). In view of the superiority of the anti-CD2/CD4 antibody–coated NPs in inducing Treg cells as compared to NPs coated with each antibody alone, we performed the subsequent experiments in mice with lupus using anti-CD2/CD4 antibody–coated NPs encapsulating IL-2 and TGFβ. This treatment for the expansion of Treg cells did not affect T cell responsiveness to antigenic stimulation (Supplementary Figure 3, available on the *Arthritis & Rheumatology* web site at http://onlinelibrary.wiley.com/doi/10.1002/art.40773/abstract), suggesting that the binding of NPs to CD2 or CD4 co-receptors did not impede activation through the T cell receptor.

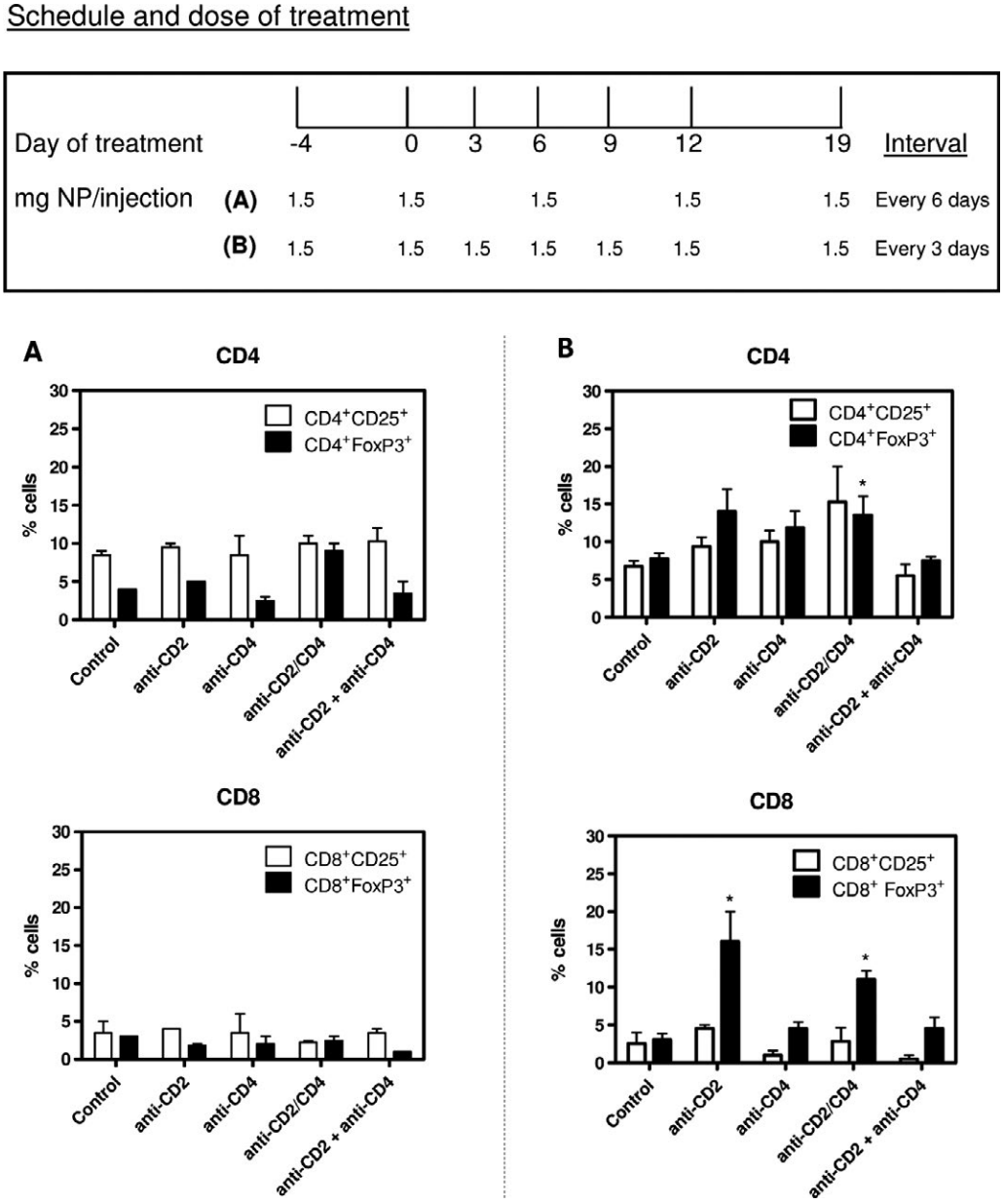

Figure 3. Protocol for PLGA NP administration in BALB/c mice for the identification of an optimal dose for the expansion of Treg cells in vivo. Mice were treated with noncoated NPs (control) or with NPs coated with anti-CD2 antibody alone, NPs coated with anti-CD4 antibody alone, NPs co-coated with anti-CD2 and anti-CD4 antibodies (anti-CD2/CD4; both antibodies attached to the same NP), or a combination of NPs coated with anti-CD2 antibodies and NPs coated with anti-CD4 antibodies. All NPs encapsulated IL-2 and TGFβ. **A**, Percentages of CD4+ (top) and CD8+ (bottom) Treg cells in mice injected every 6 days with 1.5 mg of NPs coated as indicated (treatment protocol A in the top panel). **B**, Percentages of CD4+ (top) and CD8+ (bottom) Treg cells in mice injected every 3 days with 1.5 mg of NPs coated as indicated (treatment protocol B in the top panel). Bars show the mean ± SEM (n = 4 mice per group). Results are representative of 2 experiments. * = $P < 0.05$ versus controls, by Mann-Whitney U test. See Figure 1 for definitions.

In vivo studies in BDF1 mice with lupus. When the treatment protocol shown in Figure 4 was followed in BDF1 mice with lupus, treatment with anti-CD2/CD4 antibody–coated NPs encapsulating IL-2 and TGFβ resulted in increased numbers of circulating CD4+ and CD8+ Treg cells (Figure 4A and Supplementary Figure 4, available on the *Arthritis & Rheumatology* web site at http://onlinelibrary.wiley.com/doi/10.1002/art.40773/abstract). Protection against lupus disease manifestations was observed when high doses of NPs were used (Figures 4B and C).

In BDF1 mice, disease onset after the transfer of DBA/2 cells is rapid, with anti-DNA autoantibodies appearing by 2 weeks and proteinuria due to immune complex glomerulonephritis by 6 weeks after transfer (8–10). Figure 4 shows that a total dose of 7.5 mg NPs was superior to that of 4.5 mg in inducing tolerogenic

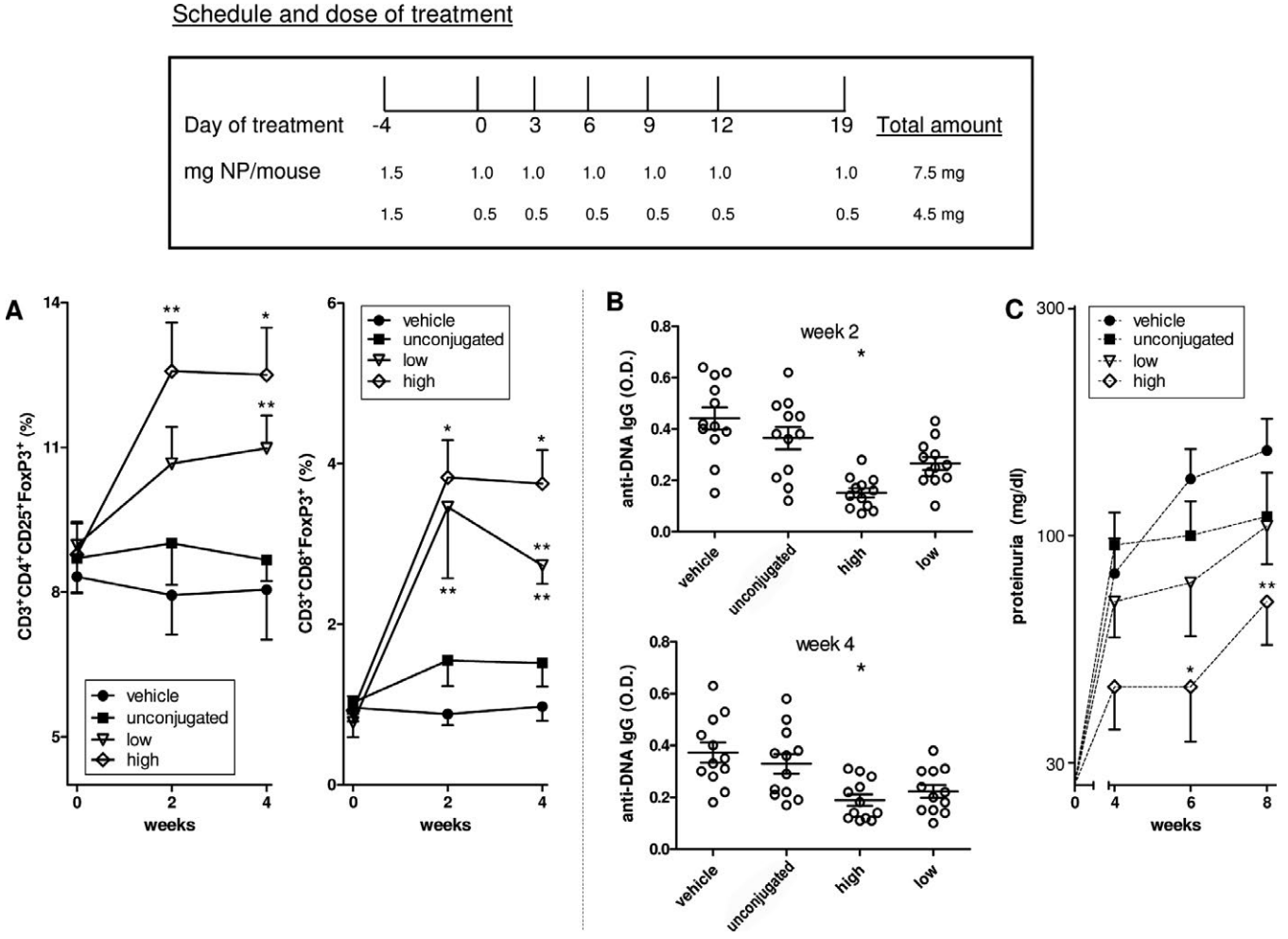

Figure 4. Reduced lupus manifestations in BDF1 mice with expansion of Treg cells after treatment with T cell–targeted PLGA NPs encapsulating IL-2 and TGFβ. Mice were treated with vehicle, noncoated (unconjugated) NPs, a low dose (4.5 mg total) of anti-CD2/CD4–coated NPs (treatment protocol shown in the top panel), or a high dose (7.5 mg total) of anti-CD2/CD4–coated NPs (treatment protocol shown in the top panel). **A**, Percentages of peripheral CD4+ (left) and CD8+ (right) Treg cells at the indicated time points after treatment. **B**, Enzyme-linked immunosorbent assay measurements of anti–double-stranded DNA antibody levels in mouse sera obtained at the indicated time points after treatment. Symbols represent individual mice (n = 12 per group); horizontal lines and error bars show the mean ± SEM. **C**, Proteinuria at the indicated time points after treatment in the same group of mice as in **A**. In **A** and **C**, symbols and error bars show the mean ± SEM (n = 12 mice per group). * = $P < 0.05$;** = $P < 0.005$, versus unconjugated NPs. See Figure 1 for definitions.

effects. This higher dose was associated with an increase in CD4+ Treg cells of ~2-fold and an increase in CD8+ Treg cells of ~4-fold, but not with changes in the frequency of other immune cell populations (Supplementary Figure 5, available on the *Arthritis & Rheumatology* web site at http://onlinelibrary.wiley.com/doi/10.1002/art.40773/abstract), and with a significant decrease in the production of anti-dsDNA autoantibodies (Figure 4B) and reduction in proteinuria (Figure 4C).

We previously reported that PLGA NPs needed to be targeted to induce and expand CD4+ Treg cells (5). In the present study, NPs also needed to be targeted for the expansion of CD4+ and CD8+ FoxP3-expressing Treg cells and protection against the development of anti-DNA autoantibodies and proteinuria in mice. Indeed, noncoated NPs containing IL-2 and TGFβ administered at equivalent doses had none of these effects (Figure 4). Of note, the decreased proteinuria in mice treated with T cell–targeted NPs encapsulating IL-2 and TGFβ was reflected by histopathologic kidney changes that indicated preserved glomeruli and reduced IgG precipitation (Figure 5). Conversely, control mice (including those treated with untargeted NPs) displayed glomerular hypercellularity and proliferative changes characteristic of lupus nephritis and IgG precipitation that were associated with worse renal disease scores (Figure 5).

DISCUSSION

We describe for the first time a biodegradable formulation of NPs that can expand both CD4+ and CD8+ Treg cells in vivo sufficiently to suppress lupus manifestations in mice. The coating with anti-CD2/CD4 antibody enabled NPs to bind both CD4+ and

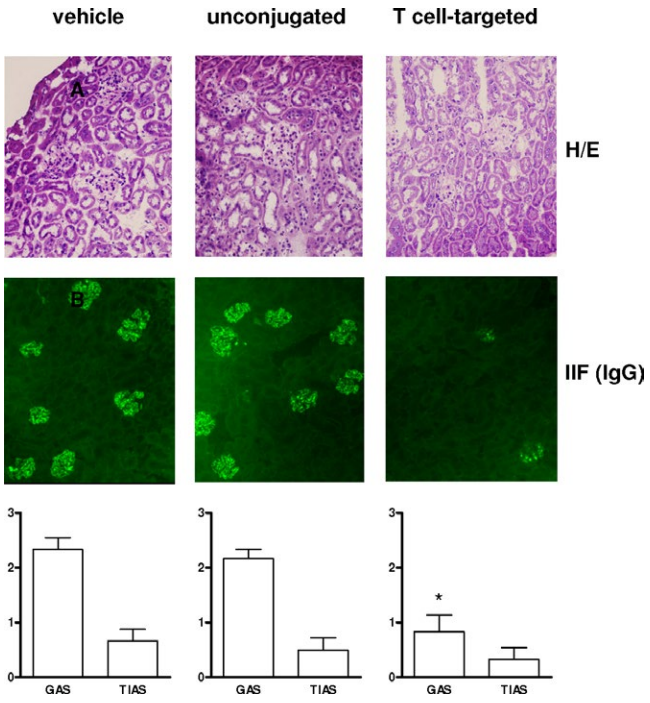

Figure 5. Renal histopathologic features of BDF1 mice with lupus after treatment with NPs encapsulating IL-2 and TGFβ and coated with anti-CD2/CD4 antibody. Top and middle, Hematoxylin and eosin (H&E) staining (top) and indirect immunofluorescence for IgG (middle) in kidney sections (4 μm) from a mouse treated with vehicle, a mouse treated with noncoated (unconjugated) NPs, and a mouse treated with anti-CD2/CD4–antibody coated (T cell–targeted) NPs. Results are representative of 6 mice per group. Original magnification × 20. Bottom, Cumulative kidney glomerular activity score (GAS) and tubulointerstitial activity score (TIAS) in mice treated with vehicle, unconjugated NPs, or T cell–targeted NPs. Bars show the mean ± SEM (n = 6 mice per group). Kidney sections were scored 6 weeks after the start of treatment. * = $P < 0.001$ versus vehicle. See Figure 1 for other definitions.

CD8+ T cells for the expansion of both cell types in vivo, in mice without lupus and in BDF1 mice with lupus, with resulting reduction of anti-dsDNA autoantibody levels and immune complex glomerulonephritis in the latter.

Several tolerogenic strategies enhance the ability of lupus Treg cells to suppress the production of pathogenic autoantibodies, including anti-DNA. These include an induction and expansion of Treg cells or the administration of tolerogenic peptides that induce both CD4+ and CD8+ Treg cells (10,15–19). Regarding the latter, the immunotherapeutic potential of CD8+ Treg cells in SLE has not been examined thoroughly, although it is known that improved function of CD8+ Treg cells in human SLE is associated with disease remission (20,21). We have previously shown that IL-2 and TGFβ can induce CD8+ cells to become Treg cells (22), with a protective effect in humanized mice (23). Notably, when we used both CD4+ and CD8+ Treg cells induced ex vivo with IL-2 and TGFβ to suppress lupus-like disease in BDF1 mice, the therapeutic effects were much stronger than when the mice were treated with CD4+ Treg cells alone, suggesting an important role of CD8+ Treg cells in suppressing lupus autoimmunity (10).

In the present study, anti-CD2 antibody targeted CD8+ cells in vivo and induced FoxP3+ Treg cells, as is known to happen with this stimulus together with CD3 stimulation (24) and consistent with the notion that anti-CD2 antibody and the CD2-specific fusion protein alefacept have immunosuppressive effects in patients with autoimmune disease (25,26). Mechanistically, the observed synergy of anti-CD2 and anti-CD4 antibodies could underscore 2 potential non–mutually exclusive possibilities: 1) antibody administration to target cells with nanoscale reagents could afford multivalency (i.e., multiple copies of antibodies binding the targets would increase avidity, and thus pharmacologic effects), and 2) targeted proximal release of IL-2 and TGFβ could promote local expansion of Treg cells. In this context, the encapsulant released from NPs is known to be most effective within nanoscale distances from the target cell.

We previously modeled mathematically the "flattening" of the cell interface as it interacts with the particle, identifying a significantly enhanced magnitude of cytokine accumulation at the cell–particle interface (27–29). This phenomenon of "paracrine effect post release" suggests that targeting, and therefore ligation, via anti-CD2 and anti-CD4 antibodies could bring particles and T cells within nanoscale ligand–receptor distances, increasing the local concentration of cytokines available to cells with great efficacy (5). This phenomenon occurs in systems of artificial antigen presentation, where IL-2 encapsulated in NPs has an equivalent T cell stimulatory effect to soluble IL-2 at a 1,000-fold higher concentration (27–29). NPs also create a local acidic microenvironment that can convert endogenous latent TGFβ to its active form, and this could synergize with IL-2 in extending Treg cell expansion—even after the TGFβ stores in the NPs are depleted. Taken together, these features suggest an advantage in the use of NP delivery systems to afford cytokine delivery at local levels in minute doses, mitigating high dose–related toxicity while retaining high bioactivity.

Presently, the treatment of SLE (and other autoimmune diseases) includes agents that target proinflammatory cytokines, effector cells, or signaling pathways (30). Although those agents can block disease progression, they rarely induce remission because they also target the compensatory regulatory pathways that are required to stop disease. Other attempts to treat SLE have tried to "reset" the immune system to cause remission. For example, lymphoid cell depletion followed by autologous stem cell transplantation resulted in extended disease remission in SLE, but this strategy—while valid as proof of concept—was associated with postoperative patient mortality (31).

Multiple approaches that use ex vivo expanded CD4+ Treg cells in autoimmune diseases are under investigation, especially in type 1 diabetes (32), but carry problems such as the need for autologous Treg cells that remain functionally stable in vivo, in addition to requiring technically cumbersome procedures to prepare Treg cells in large numbers. Given these considerations, the use of

NPs can represent a new therapeutic possibility for the targeting of T cells (or antigen-presenting cells [APCs]) in the induction of immune tolerance. PLGA NPs encapsulating tolerogenic peptides or peptides and rapamycin that targeted APCs prevented or reversed disease in animal models of autoimmune diabetes and multiple sclerosis through TGFβ-dependent induction of Treg cells (33,34). Moreover, NP-mediated delivery of the immunosuppressive drug Ca^{2+}/calmodulin-dependent protein kinase IV inhibitor ameliorated murine SLE (35–37).

Additionally, a recent study showed that iron oxide NPs coated with MHC peptides could convert interferon-γ–producing Th1 cells into IL-10–producing Tr1 cells, affording therapeutic effects in mouse models of autoimmune disease (38). Although CD4+ Treg cells induced DCs to become tolerogenic and protect secondary hosts (39), that system had limitations. It did not permit encapsulation/sustained release of multiple therapeutic agents, and different MHC-specific peptides would be needed to match the MHC diversity encountered in human autoimmune diseases. Also, extended iron oxide accumulation is toxic. Conversely, biodegradable PLGA NPs—unlike the iron oxide NPs that act on differentiated Th1 cells—act upstream at the level of T cells that differentiate to become suppressor cells.

Before concluding, we acknowledge that our study raises questions to address in future experiments. For example, we expanded both CD4+ and CD8+ Treg cells but do not know the precise relative contribution of each subset on the timing of the response and possible reciprocal cell interactions in the suppression of lupus manifestations. Another unexplored aspect is that anti-CD2 antibody can also bind natural killer (NK) cells (2), and the contribution of this interaction might be important (since CD8–NK cell interactions induce NK cells to produce TGFβ) (2,22). In this sense, NPs loaded with IL-2 and a TGFβ inhibitor greatly impacted cancer cells and the tumor microenvironment by primarily affecting NK cells (40). We will also need to address whether the induced Treg cells could transfer suppressive activity to conventional T cells through "infectious tolerance" (41), and whether the combination of TGFβ and IL-2 protected T cells against apoptosis, e.g., via a modulation of the antiapoptotic protein Bcl-x_L (42). Notwithstanding these considerations, our findings suggest that NPs that carry cytokines that are deficient in SLE (43) could represent a novel strategy to restore tolerogenic responses in the disease, and that targeting CD2 and CD4 simultaneously might facilitate synergistic therapeutic effects.

AUTHOR CONTRIBUTIONS

All authors were involved in drafting the article or revising it critically for important intellectual content, and all authors approved the final version to be published. Dr. La Cava had full access to all of the data in the study and takes responsibility for the integrity of the data and the accuracy of the data analysis.

Study conception and design. Horwitz, Fahmy, La Cava.

Acquisition of data. Bickerton, La Cava.

Analysis and interpretation of data. Horwitz, Bickerton, Koss, Fahmy, La Cava.

ADDITIONAL DISCLOSURES

Author Horwitz is an employee of General Nanotherapeutics.

REFERENCES

1. Ferretti C, La Cava A. Overview of the pathogenesis of systemic lupus erythematosus. In: Tsokos GC, editor. Systemic lupus erythematosus—basic, applied and clinical aspects. Cambridge: Academic Press; 2016. p. 55–62.
2. Gray JD, Hirokawa M, Ohtsuka K, Horwitz DA. Generation of an inhibitory circuit involving CD8+ T cells, IL-2, and NK cell-derived TGF-β: contrasting effects of anti-CD2 and anti-CD3. J Immunol 1998;160:2248–54.
3. Von Spee-Mayer C, Siegert E, Abdirama D, Rose A, Klaus A, Alexander T, et al. Low-dose interleukin-2 selectively corrects regulatory T cell defects in patients with systemic lupus erythematosus. Ann Rheum Dis 2016;75:1407–15.
4. He J, Zhang X, Wei Y, Sun X, Chen Y, Deng J, et al. Low-dose interleukin-2 treatment selectively modulates $CD4^+$ T cell subsets in patients with systemic lupus erythematosus. Nat Med 2016;22:991–3.
5. McHugh MD, Park J, Uhrich R, Gao W, Horwitz DA, Fahmy TM. Paracrine co-delivery of TGF-β and IL-2 using CD4-targeted nanoparticles for induction and maintenance of regulatory T cells. Biomaterials 2015;59:172–81.
6. Dinesh RK, Skaggs BJ, La Cava A, Hahn BH, Singh RP. $CD8^+$ Tregs in lupus, autoimmunity, and beyond. Autoimmun Rev 2010;9:560–8.
7. Hahn BH, Singh RP, La Cava A, Ebling FM. Tolerogenic treatment of lupus mice with consensus peptide induces Foxp3-expressing, apoptosis-resistant, TGFβ-secreting $CD8^+$ T cell suppressors. J Immunol 2005;175:7728–37.
8. Via CS, Shearer GM. T-cell interactions in autoimmunity: insights from a murine model of graft-versus-host disease. Immunol Today 1988;9:207–13.
9. Rus VA, Svetic A, Nguyen P, Gausen WC, Via CS. Kinetics of Th1 and Th2 cytokine production during the early course of acute and chronic murine graft-versus-host disease: regulatory role of donor $CD8^+$ T cells. J Immunol 1995;155:2396–406.
10. Zheng SG, Wang JH, Koss MN, Quismorio F Jr, Gray JD, Horwitz DA. $CD4^+$ and $CD8^+$ regulatory T cells generated ex vivo with IL-2 and TGF-β suppress a stimulatory graft-versus-host disease with a lupus-like syndrome. J Immunol 2004;172:1531–9.
11. Fahmy TM, Samstein RM, Harness CC, Saltzman MW. Surface modification of biodegradable polyesters with fatty acid conjugates for improved drug targeting. Biomaterials 2005;26:5727–36.
12. Lourenço EV, Liu A, Matarese G, La Cava A. Leptin promotes systemic lupus erythematosus by increasing autoantibody production and inhibiting immune regulation. Proc Natl Acad Sci U S A 2016;113:10637–42.
13. Ferrera F, Hahn BH, Rizzi M, Anderson M, FitzGerald J, Millo E, et al. Protection against renal disease in (NZB × NZW)F_1 lupus-prone mice after somatic B cell gene vaccination with anti-DNA immunoglobulin consensus peptide. Arthritis Rheum 2007;56:1945–53.
14. Park J, Gao W, Whiston R, Strom TB, Metcalfe S, Fahmy TM. Modulation of $CD4^+$ T cell lineage outcomes with targeted nanoparticle mediated cytokine delivery. Mol Pharm 2011;8:143–52.
15. La Cava A, Ebling FM, Hahn BH. Ig-reactive $CD4^+CD25^+$ T cells from tolerized (New Zealand Black × New Zealand White)F_1 mice

suppress in vitro production of antibodies to DNA. J Immunol 2004;173:3542–8.

16. Singh RP, La Cava A, Wong M, Ebling F, Hahn BH. $CD8^+$ T cell-mediated suppression of autoimmunity in a murine lupus model of peptide-induced immune tolerance depends on Foxp3 expression. J Immunol 2007;178:7649–57.
17. Kang HK, Michaels MA, Berner BR, Datta SK. Very low-dose tolerance with nucleosomal peptides controls lupus and induces potent regulatory T cell subsets. J Immunol 2005;174:3247–55.
18. Sharabi A, Mozes E. The suppression of murine lupus by a tolerogenic peptide involves foxp3-expressing CD8 cells that are required for the optimal induction and function of foxp3-expressing CD4 cells. J Immunol 2008;181:3243–51.
19. Scalapino KJ, Daikh DI. Suppression of glomerulonephritis in NZB/NZW lupus prone mice by adoptive transfer of ex vivo expanded regulatory T cells. PLoS One 2009;24:e6031.
20. Suzuki M, Jagger AL, Konya C, Shimojima Y, Pryshchep S, Goronzy JJ, et al. $CD8^+CD45RA^+CCR7^+FOXP3^+$ T cells with immunosuppressive properties: a novel subset of inducible human regulatory T cells. J Immunol 2012;189:2118–30.
21. Zhang L, Bertucci AM, Ramsey-Goldman R, Burt RK, Datta SK. Regulatory T cell (Treg) subsets return in patients with refractory lupus following stem cell transplantation, and TGF-β-producing $CD8^+$ Treg cells are associated with immunological remission of lupus. J Immunol 2009;183:6346–58.
22. Hirokawa M, Horwitz DA. The role of transforming growth factor β in the generation of suppression: an interaction between $CD8^+$ T and NK cells. J Exp Med 1994;180:1937–42.
23. Horwitz DA, Pan S, Ou JN, Wang J, Chen M, Gray JD, et al. Therapeutic polyclonal human $CD8^+CD25^+FoxP3^+TNFR2^+PD\text{-}L1^+$ regulatory cells induced ex vivo. Clin Immunol 2013;149:450–63.
24. Ochando JC, Yopp AC, Yang Y, Garin A, Li Y, Boros P, et al. Lymph node occupancy is required for the peripheral development of alloantigen-specific Foxp3+ regulatory T cells. J Immunol 2005;174:6993–7005.
25. Hafler DA, Ritz J, Schlossman SF, Weiner HL. Anti-CD4 and anti-CD2 monoclonal antibody infusions in subjects with multiple sclerosis. Immunosuppressive effects and human anti-mouse responses. J Immunol 1988;141:131–8.
26. Rigby MR, Harris KM, Pinckney A, DiMeglio LA, Rendell MS, Felner EI, et al. Alefacept provides sustained clinical and immunological effects in new-onset type 1 diabetes patients. J Clin Invest 2015;125:3285–96.
27. Labowsky M, Lowenthal J, Fahmy TM. An in silico analysis of nanoparticle/cell diffusive transfer: application to nano-artificial antigen-presenting cell—T-cell interaction. Nanomedicine 2015;11:1019–28.
28. Labowsky M, Fahmy TM. Diffusive transfer between two intensely interacting cells with limited surface kinetics. Chem Eng Sci 2012;74:114–23.
29. Steenblock ER, Fadel T, Labowsky M, Pober JS, Fahmy TM. An artificial antigen-presenting cell with paracrine delivery of IL-2 impacts the magnitude and direction of the T cell response. J Biol Chem 2011;286:34883–92.
30. Wong M, La Cava A. Lupus, the current therapeutic approaches. Drugs Today (Barc) 2011;47:289–302.
31. Burt RK, Traynor A, Statkute L, Barr WG, Rosa R, Schroeder J, et al. Nonmyeloablative hematopoietic stem cell transplantation for systemic lupus erythematosus. JAMA 2006;295:527–35.
32. Gitelman SE, Bluestone JA. Regulatory T cell therapy for type 1 diabetes: may the force be with you. J Autoimmun 2016;71:78–87.
33. Hunter Z, McCarthy DP, Yap WT, Harp CT, Getts DR, Shea LD, et al. A biodegradable nanoparticle platform for the induction of antigen-specific tolerance for treatment of autoimmune disease. ACS Nano 2014;25:2148–60.
34. Maldonado RA, LaMothe RA, Ferrari JD, Zhang AH, Rossi RJ, Kolte PN, et al. Polymeric synthetic nanoparticles for the induction of antigen-specific immunological tolerance. Proc Natl Acad Sci U S A 2015;112:156–65.
35. Look M, Stern E, Wang QA, DiPlacido LD, Kashgarian M, Craft J, et al. Nanogel-based delivery of mycophenolic acid ameliorates systemic lupus erythematosus in mice. J Clin Invest 2013;123:1741–9.
36. Otomo K, Koga T, Mizui M, Yoshida N, Kriegel C, Bickerton S, et al. Cutting edge: nanogel-based delivery of an inhibitor of CaMK4 to $CD4^+$ T cells suppresses experimental autoimmune encephalomyelitis and lupus-like disease in mice. J Immunol 2015;195:5533–7.
37. Maeda K, Otomo K, Yoshida N, Abu-Asab MS, Ichinose K, Nishino T, et al. CaMK4 compromises podocyte function in autoimmune and nonautoimmune kidney disease. J Clin Invest 2018;128:3445–59.
38. Clemente-Casares X, Blanco J, Ambalavanan P, Yamanouchi J, Singha S, Fandos C, et al. Expanding antigen-specific regulatory networks to treat autoimmunity. Nature 2016;530:434–40.
39. Lan Q, Zhou X, Fan H, Chen M, Wang J, Ryffel B, et al. Polyclonal CD4+Foxp3+ Treg cells induce TGF-β-dependent tolerogenic dendritic cells that suppress the murine lupus-like syndrome. J Mol Cell Biol 2012;4:409–19.
40. Park J, Wrzesinski SH, Stern E, Look M, Criscione J, Ragheb R, et al. Combination delivery of TGF-β inhibitor and IL-2 by nanoscale liposomal polymeric gels enhances tumour immunotherapy. Nat Mater 2012;11:895–905.
41. Andersson J, Tran DQ, Pesu M, Davidson TS, Ramsey H, O'Shea JJ, et al. $CD4^+$ $FoxP3^+$ regulatory T cells confer infectious tolerance in a TGF-β-dependent manner. J Exp Med 2008;205:1975–81.
42. Ben-David H, Sharabi A, Dayan M, Sela M, Mozes E. The role of $CD8^+CD28^-$ regulatory cells in suppressing myasthenia gravis-associated responses by a dual altered peptide ligand. Proc Natl Acad Sci U S A 2007;104:17459–64.
43. Moulton VR, Tsokos GC. T cell signaling abnormalities contribute to aberrant immune cell function and autoimmunity. J Clin Invest 2015;125:2220–7.

Arthritis & Rheumatology
Vol. 71, No. 4, April 2019, pp 641–650
DOI 10.1002/art.40766

AMERICAN COLLEGE OF RHEUMATOLOGY
EDUCATION • TREATMENT • RESEARCH

Dampening of CD8+ T Cell Response by B Cell Depletion Therapy in Antineutrophil Cytoplasmic Antibody–Associated Vasculitis

Antoine Néel,[1] Marie Bucchia,[1] Mélanie Néel,[1] Gaelle Tilly,[1] Aurélie Caristan,[1] Michele Yap,[2] Marie Rimbert,[1] Sarah Bruneau,[1] Marion Cadoux,[1] Christian Agard,[3] Maryvonne Hourmant,[4] Pascal Godmer,[5] Sophie Brouard,[1] Céline Bressollette,[1] Mohamed Hamidou,[1] Regis Josien,[1] Fadi Fakhouri,[1] and Nicolas Degauque[1]

Objective. To compare the effects of rituximab (RTX) and conventional immunosuppressants (CIs) on CD4+ T cells, Treg cells, and CD8+ T cells in antineutrophil cytoplasmic antibody–associated vasculitis (AAV).

Methods. A thorough immunophenotype analysis of CD4+, Treg, and CD8+ cells from 51 patients with AAV was performed. The production of cytokines and chemokines by CD8+ T cells stimulated in vitro was assessed using a multiplex immunoassay. The impact of AAV B cells on CD8+ T cell response was assessed using autologous and heterologous cocultures.

Results. CD4+ and Treg cell subsets were comparable among RTX-treated and CI-treated patients. In contrast, within the CD8+ T cell compartment, RTX, but not CIS, reduced CD45RA+CCR7– (TEMRA) cell frequency (from a median of 39% before RTX treatment to 10% after RTX treatment [$P < 0.01$]) and efficiently dampened cytokine/chemokine production (e.g., the median macrophage inflammatory protein 1α level was 815 pg/ml in patients treated with RTX versus 985 pg/ml in patients treated with CIs versus 970 pg/ml in those with active untreated AAV [$P < 0.01$]). CD8+ T cell subsets cocultured with autologous B cells produced more proinflammatory cytokines in AAV patients than in controls (e.g., for tumor necrosis factor–producing effector memory CD8+ T cells: 14% in AAV patients versus 9.2% in controls [$P < 0.05$]). In vitro disruption of AAV B cell–CD8+ T cell cross-talk reduced CD8+ T cell cytokine production, mirroring the reduced CD8+ response observed ex vivo after RTX treatment.

Conclusion. The disruption of a pathogenic B cell/CD8+ T cell axis may contribute to the efficacy of RTX in AAV. Further studies are needed to determine the value of CD8+ T cell immunomonitoring in B cell–targeted therapies.

INTRODUCTION

Antineutrophil cytoplasmic antibody (ANCA)–associated vasculitides (AAV) are autoimmune diseases characterized by small vessel and/or extravascular inflammation. Pathogenesis involves both the innate and adaptive immune systems (1,2), including ANCA-producing B cells, CD4+ T cells, and Treg cells (3,4). Analyses of the leukocyte transcriptome of patients with AAV and of mouse models suggest that CD8+ T cells are also involved (5,6). How this complex autoimmune response is orchestrated remains unclear. In 2010 and 2014, two randomized trials demonstrated the efficacy of rituximab (RTX) in AAV, and thus the central role of B cells (7,8). The initial rationale for targeting B cells was that antimyeloperoxidase ANCAs are pathogenic (3). However, T cells likely contribute to tissue damage (3). B cells can present antigens, produce various cytokines, and engage bidirectional cross-talk with

The FP7 VISICORT project was supported by the European Union's Seventh Framework Programme for Research, Technological Development and Demonstration (grant 602470). The IHU-Cesti project was supported by the Nantes Metropole and Pays de la Loire Region as well as the Investments for the Future program (ANR-10-IBHU-005) from the Agence Nationale de la Recherche. The LabEX IGO program was supported by the Investments for the Future program (ANR-11-LABX-0016-01) from the Agence Nationale de la Recherche. Dr. Antoine Néel's work was supported by the Groupama Loire Bretagne/Fondation Groupama pour la santé. Dr. Caristan's work was supported by the French Internal Medicine Society. Dr. Yap's work was supported by the ProGreffe Foundation (International Fellowship grant).

[1]Antoine Néel, MD, PhD, Marie Bucchia, MD, Mélanie Néel, Gaelle Tilly, Aurélie Caristan, MD, Marie Rimbert, PharmD, PhD, Sarah Bruneau, PhD, Marion Cadoux, Sophie Brouard, DVM, PhD, Céline Bressollette, MD, PhD, Mohamed Hamidou, MD, PhD, Regis Josien, MD, PhD, Fadi Fakhouri, MD, PhD, Nicolas Degauque, PhD: INSERM UMR1064, Université de Nantes and CHU Nantes, Nantes, France; [2]Michele Yap, PhD: CHU Nantes, Nantes, France; [3]Christian Agard, MD, PhD: CHU Nantes and CIC biothérapie, Nantes, France; [4]Maryvonne Hourmant, MD, PhD: INSERM UMR1064, Université de Nantes and CHU Nantes, Nantes France, and Centre Hospitalier Bretagne Atlantique, Vannes, France; [5]Pascal Godmer, MD: Centre Hospitalier Bretagne Atlantique, Vannes, France.

No potential conflicts of interest relevant to this article were reported.

Address correspondence to Antoine Néel, MD, PhD, Service de Médecine Interne, Centre Hospitalier Universitaire de Nantes, Hôtel Dieu, 1 Place Alexis Ricordeau, 44093 Nantes, France. E-mail: antoine.neel@chu-nantes.fr.

Submitted for publication February 22, 2018; accepted in revised form October 25, 2018.

other immune cells, including T cells. Their antibody-independent pathogenic role in autoimmunity was demonstrated years ago (9). In experimental encephalitis, the efficacy of RTX has been linked to the suppression of interleukin-6 (IL-6)–producing B cells (10). In human diseases, most investigators have focused on the impact of RTX on CD4+ T cells, with conflicting results (11). How RTX impacts the T cell response in AAV patients has not been fully investigated (12).

In 2010–2014 AAV maintenance treatment shifted from conventional immunosuppressants (CIs) to RTX in France. We viewed this transitional period as a unique opportunity to compare the effects of RTX and CIs on T cells and improve our understanding of the remarkable efficacy of RTX.

PATIENTS AND METHODS

Inclusion criteria and blood samples. Inclusion criteria were a diagnosis of ANCA-associated microscopic polyangiitis or granulomatosis with polyangiitis (GPA). Patients with eosinophilic granulomatosis with polyangiitis and those receiving dialysis were excluded. Patients with active disease were not receiving treatment (including steroids). Remission was defined as a Birmingham Vasculitis Activity Score of 0 for 3 months with no evidence of systemic inflammation, which allowed stable or tapered maintenance treatment. Patients with disease in remission received either no treatment, maintenance RTX (500 mg every 6 months) with or without low-dose corticosteroids (<10 mg/day), or oral CIs (azathioprine [AZA], mycophenolate mofetil, or methotrexate [MTX]) with or without low-dose corticosteroids (<10 mg/day) for >3 months. The study was performed in accordance with the Declaration of Helsinki, with participants' written informed consent. Peripheral blood mononuclear cells (PBMCs) were separated on a Ficoll gradient layer and frozen in 10% DMSO autologous serum. The presence of anti-cytomegalovirus (anti-CMV) IgG was determined by chemiluminescence immunoassay (DiaSorin) on frozen sera.

Polychromatic flow cytometric analysis. Detailed phenotyping of T cell subsets was performed using the following 4 monoclonal antibody (mAb) panels analyzed with an LSRII flow cytometer (BD Immunocytometry Systems). The CD4+ T cell panel consisted of Brilliant Violet 605–conjugated CD3 (OKT3), PerCP–Cy5.5–conjugated CD4 (L200), allophycocyanin [APC]–Vio770–conjugated CD45RA (T6D11), phycoerythrin (PE)–Cy7–conjugated CCR7 (3D12), PE-conjugated CCR4 (1G1), fluorescein isothiocyanate (FITC)–conjugated CCR5 (2D7/CCR5), and PE-Vio770–conjugated CD161 (191B8). The Treg cell panel consisted of Brilliant Violet 605–conjugated CD3 (OKT3), Pacific Blue–conjugated CD4 (RPA-T4), Brilliant Violet 421–conjugated CD25 (BC96), PE-conjugated CD127 (A019D5), Alexa Fluor 647–conjugated FoxP3 (236A/E7), Alexa Fluor 488–conjugated Helios (22F6), APC-Vio770–conjugated CD45RA (T6D11), and PE-Vio770–conjugated CD161 (191B8). CD8+ T cell panel number 1 consisted of VioBlue–conjugated CD3 (BW264/56), VioGreen–conjugated CD8 (BW135/80), APC–Vio770–conjugated CD45RA (T6D11), PE–Cy7–conjugated CCR7 (3D12), Brilliant Violet 605–conjugated CD27 (L128), PE–CF594–conjugated CD28 (CD28.2), FITC-conjugated CD57 (TB03), and PE-conjugated T-bet (O4–46). CD8+ T cell panel number 2 consisted of VioBlue-conjugated CD3 (BW264/56), VioGreen-conjugated CD8 (BW135/80), APC–Vio770–conjugated CD45RA (T6D11), PE–Cy7–conjugated CCR7 (3D12), Brilliant Violet 605–conjugated CD27 (L128), PE–CF594–conjugated CD28 (CD28.2), Alexa Fluor 700–conjugated granzyme B (GB11), and PE-conjugated perforin (B-D48). Intracellular cytokine staining was performed using a fixation/permeabilization solution kit (BD Biosciences) and mAb PE-conjugated IL-2 (5344.111) and FITC-conjugated tumor necrosis factor (TNF) (6401.1111).

A Live/Dead Fixable Yellow Dead Cell Stain kit (Invitrogen) was used to exclude dead cells from the analysis. BD CompBeads stained separately with individual mAb were used to define the compensation matrix. Data were analyzed using FlowJo version 9.0.1 (Tree Star). All antibodies were purchased from BD Biosciences, except for anti-CD3, anti-CD8, anti-CD45RA, anti-CD161, and anti-CD57 mAb (all from Miltenyi Biotec), anti-Helios, Brilliant Violet–conjugated anti-CD3 and anti-CD25 (all from BioLegend), anti-FoxP3 (eBioscience), and antiperforin (Diaclone).

CCR7 and CD45RA expression were used to identify naive (CD45RA+CCR7+), central memory (CD45RA–CCR7+), effector memory (CD45RA–CCR7–), and late differentiated effector memory (CD45RA+CCR7– [TEMRA]) CD4+ or CD8+ T cells.

Fluorescence-activated cell sorting (FACS), cell culture, and measurement of multiplex cytokine production. PBMCs were thawed, rested overnight in TexMACS medium (Miltenyi Biotec), and stained with anti-CD3, anti-CD4, and anti-CD8 mAb. CD3+CD4–CD8+ cells were FACS-sorted (FACSAria; BD Biosciences) (purity >95%) and then stimulated for 4 hours with phorbol myristate acetate (PMA) (100 ng/ml; Sigma) and ionomycin (1 μg/ml; Sigma) in 96-well round-bottomed plates (5×10^5 cells/well) at 37°C in 5% CO_2. The production of 34 cytokines and chemokines was measured in CD8+ T cell culture supernatant using a multiplex Luminex immunoassay (ProcartaPlex Human Cytokine & Chemokine Panel 1A; Affymetrix).

B cell–CD8+ T cell cocultures. B cells (CD19+), naive (CD45RA+CD28+) CD8+ T cells, and effector memory (CD45RA–CD28+) CD8+ T cells were purified by FACS (FACSAria; BD Biosciences) (purity >95%). B cells were cultured with naive or effector memory CD8+ T cells (1:1 ratio, 10^6 cells/ml in round-bottomed plates) in TexMACS medium with staphylococcal enterotoxin B (SEB; 10 mg/ml). After 72 hours, brefeldin A (10 mg/ml; Sigma)

was added for 4 hours. IL-2 and TNF production of CD8+ T cells was then assessed by intracellular flow cytometry. All AAV patients (n = 15) had untreated active disease (had not received steroids, immunosuppressants, or previous RTX).

Statistical analysis. Quantitative variables are presented as the median (interquartile range [IQR]). Unpaired group comparisons were performed using the Mann-Whitney test (for 2 groups) or the Kruskal-Wallis test with Dunn's post hoc test (for ≥3 groups). Paired data were compared using Wilcoxon's signed rank test.

RESULTS

Cohort characteristics. A total of 51 patients were included. Clinical data are reported in Table 1. Of the 63 samples obtained, 20 were from patients with untreated active disease (at diagnosis in 18 cases) and 43 were from patients with disease in remission while receiving maintenance treatment with either RTX (n = 20) or CIs (n = 14 [AZA in 10, MTX in 2, and mycophenolate mofetil in 2]), or with disease in drug-free remission (n = 9). Twelve patients were analyzed at 2 time points, first while untreated (active disease) and then with disease in remission while receiving RTX (n = 8) or CIs (n = 4). All RTX-treated patients had received a 500 mg infusion 6 months before sampling and had undetectable B cells (<5/mm^3). The median B cell count in patients receiving CIs was 42/mm^3 (IQR 10–56). The median CD4+ T cell count was 292/mm^3 (IQR 255–343) in patients receiving CIs versus 344/mm^3 (IQR 211–644) in patients receiving RTX. The median CD8+ T cell count was 199/mm^3 (IQR 160–308) in patients receiving CIs versus 238/mm^3 (IQR 145–324) in patients receiving RTX (nonsignificant difference).

Most key clinical data were comparable between patients treated with RTX and those treated with CIs, including demographic characteristics, disease and ANCA type, past exposure to cyclophosphamide, and renal function (Table 1). Patients treated with RTX tended to have had more relapses than patients treated with CIs (nonsignificant difference). In contrast, drug-free patients had a more prolonged duration of remission than CI-treated or RTX-treated patients (median 46 months versus 10 and 6 months, respectively; $P = 0.01$ and $P = 0.002$). Furthermore, most of these 9 patients with disease in long-term remission off therapy had had a single disease flare before entering remission, whereas more patients treated with CIs or RTX experienced more than one relapse (65% for RTX and 12% for long-term remission; $P = 0.01$).

Similar distributions of CD4+ and Treg cell subsets in patients with disease in remission receiving CIs and those receiving RTX. We first assessed whether disease activity and/or maintenance therapy affected the distribution of the different CD4+ and Treg cell subsets. Patients with disease in remission had a decreased proportion of naive (CD45RA+CCR7+) CD4+ T cells ($P = 0.002$) (Figure 1A) and an increased proportion of effector memory (CD45RA–CCR7–) T cells (Figure 1A) ($P = 0.001$) compared to patients with active disease. When the analysis was narrowed to patients with disease in remission, we found that patients treated with RTX, patients treated with CIs, and patients with disease in long-term remission off therapy had comparable distributions of

Table 1. Characteristics of the patients with AAV*

		Patients with AAV in remission		
	Patients with untreated active AAV (n = 20)	B cell depletion therapy (RTX) (n = 20)	CIs (n =14)	Long-term remission off therapy (n = 9)
Sex, no. (%) male	13 (65)	14 (70)	5 (36)	2 (22)
Age, years	67 (55–79)	65 (56–75)	68 (59–82)	63 (62–73)
GPA, no (%)	11 (55)	14 (70)	7 (50)	6 (66)
Anti-MPO, no. (%)	11 (55)	7 (35)	7 (50)	4 (44)
eGFR, ml/minute/1.73m^2	53 (17–92)	58 (34–86)	67 (44–93)	59 (34–82)
Disease duration, months	0.6 (0.3–0.9)	20 (10–108)	19 (13–53)	58 (13–86)
Past CYC exposure, no. (%)	2 (10)	17 (85)	11 (79)	7 (78)
Remission duration, months	NA	6 (5–8)	10 (6–17)	46 (20–73)†
Single flare, no. (%)	18 (90)	7 (35)	8 (57)	8 (88)‡
Previous flares	0 (0–0)	2 (1–4.5)	1 (1–2)	1 (1–1)§

* Except where indicated otherwise, values are the median (interquartile range). AAV = antineutrophil cytoplasmic antibody–associated vasculitis; CIs = conventional immunosuppressants; GPA = granulomatosis with polyangiitis; anti-MPO = antimyeloperoxidase; eGFR = estimated glomerular filtration rate; CYC = cyclophosphamide; NA = not applicable.
† $P = 0.002$ versus rituximab (RTX).
‡ $P = 0.01$ versus RTX.
§ $P = 0.008$ versus RTX.

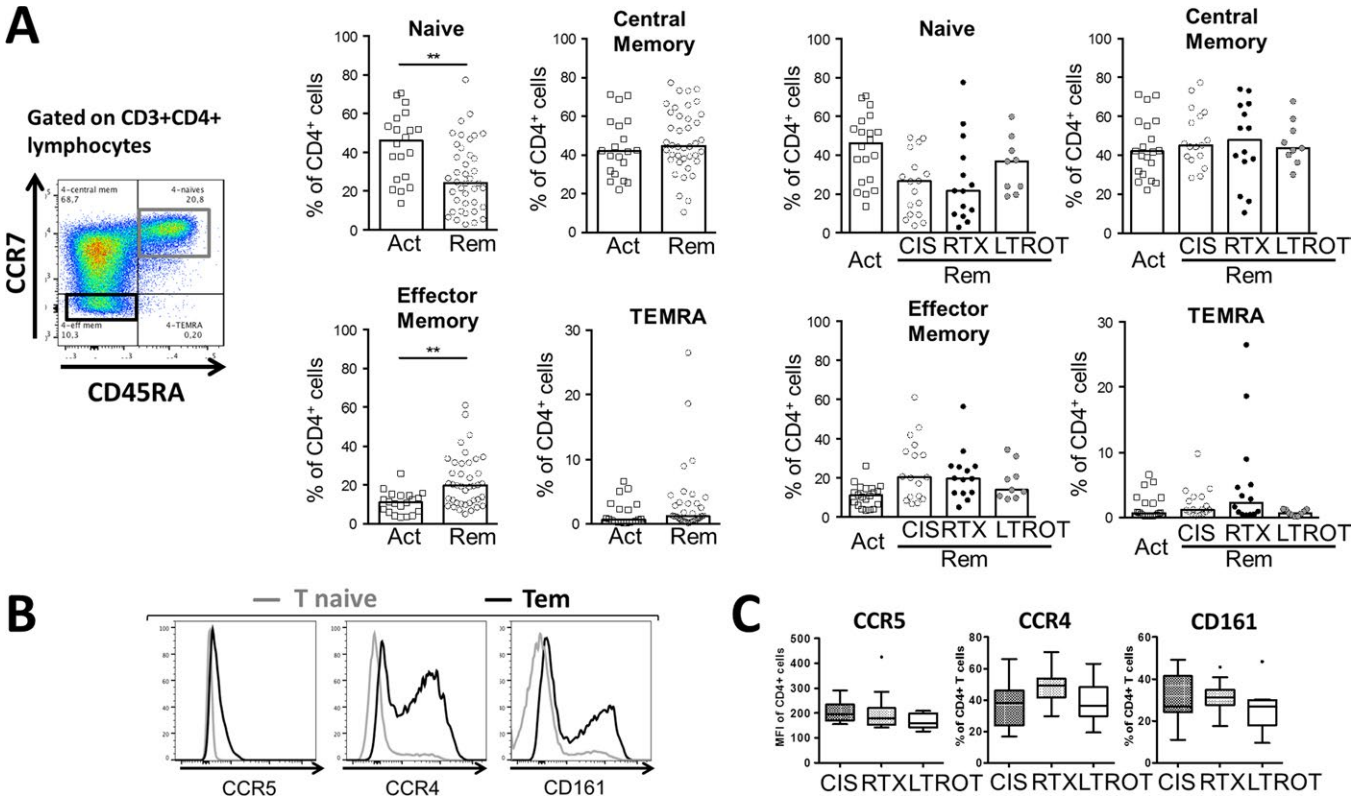

Figure 1. Lack of a significant impact of maintenance treatment type on CD4+ T cell subsets or CD4+ T helper cell markers during remission of antineutrophil cytoplasmic antibody–associated vasculitis (AAV). **A**, Frequency of naive, central memory, effector memory, and TEMRA CD4+ T cell subsets according to the expression of CD45RA and CCR7 in patients with AAV. Left, Gating strategy for CCR7 and CD45RA. Middle, Frequencies of T cell subsets in patients with active AAV (Act) and patients with AAV in remission (Rem). Right, Frequencies of T cell subsets in patients with active AAV, patients with AAV in remission treated with conventional immunosuppressants (CIs), patients with AAV in remission treated with rituximab (RTX), and patients with AAV in long-term remission off therapy (LTROT). The frequencies of CD4+ T cell subsets correlated with disease activity but not with type of maintenance treatment received during remission. Bars show the median; symbols represent individual patients. ** = $P < 0.01$ by Mann-Whitney test. **B**, CD4+ T cell surface expression of CCR5, CCR4, and CD161, used as surrogates for Th1, Th2, and Th17 response, respectively. The expression of these markers was compared between naive T cells and effector memory T (Tem) cells. **C**, Expression of CCR5, CCR4, and CD161 in patients with AAV in remission treated with CIs, patients with AAV in remission treated with RTX, and patients with AAV in long-term remission off therapy. Data are shown as box plots. Lines inside the boxes represent the median. Circles indicate outliers. Box plots were constructed using Tukey's method**.** MFI = mean fluorescence intensity. Color figure can be viewed in the online issue, which is available at http://onlinelibrary.wiley.com/doi/10.1002/art.40766/abstract.

CD4+ T cell subsets. The expression levels of CCR5, CCR4, and CD161 were then monitored as surrogate markers for Th1, Th2, and Th17 cells, respectively. As expected, CCR5, CCR4, and CD161 were mainly expressed on effector memory T cells (Figure 1B). Their level of expression was analyzed on total CD4+ cells as well as on naive T cell, central memory T cell, effector memory T cell, and TEMRA subsets. No difference was observed between patients treated with CIs, patients treated with RTX, and patients with disease in long-term remission off therapy (Figure 1C).

Several groups, including ours, have reported on quantitative and/or functional Treg cell deficiency in AAV (4), and a recent study suggested that RTX increased Treg cell frequency in patients with GPA (11). In our cohort, the frequency of $CD25^{high}CD127^{low}FoxP3+$ Treg cells was not significantly different in patients treated with CIs, patients treated with RTX, and patients with disease in long-term remission off therapy ($P = 0.195$) (Figure 2B). We hypothesized that RTX could target some Treg cell subsets that have been identified in recent years, including resting (CD45RA+) Treg cells, memory ($CD45RA–FoxP3^{high}$) Treg cells, or Treg cell subsets that reportedly exhibit proinflammatory potential, i.e., CD161+ Treg cells (13,14) or Treg cells lacking Helios expression (15–17). We thus analyzed these markers (gating strategy shown in Figure 2A) but did not find any difference between RTX-treated and CI-treated patients (Figure 2C). Overall, RTX had no distinctive impact on CD4+ and Treg cell subset distribution as compared to CIs.

Opposite distributions of CD8+ T cell subsets in patients with disease in remission receiving CIs versus those receiving RTX. In contrast to the CD4+ and Treg cell compartments, we observed significant differences in the

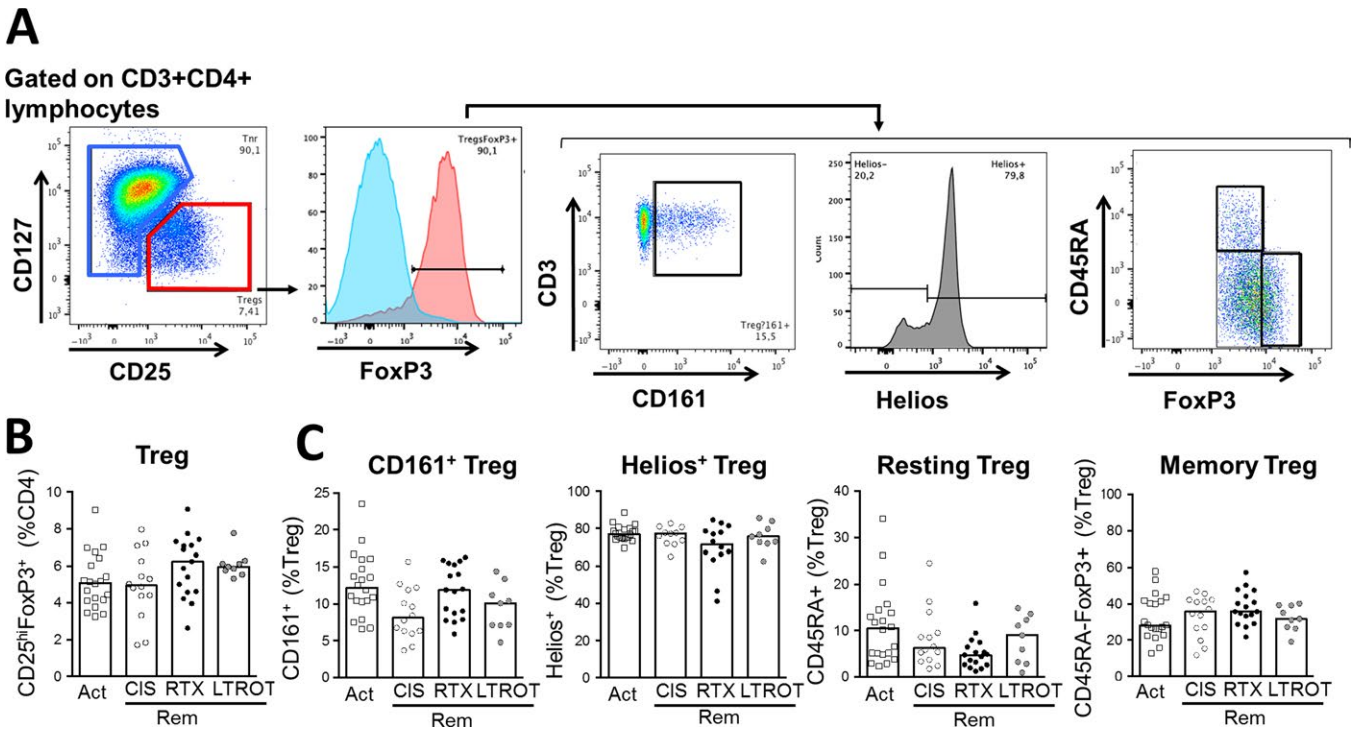

Figure 2. Lack of a significant impact of maintenance treatment type on total Treg cells or Treg cell subsets during remission of AAV. **A**, Gating strategy for the identification of Treg (CD3+CD4+CD25^{high}CD127^{low}FoxP3+) cells and Treg cell subsets. Resting and memory Treg cells were defined as CD45RA+ and CD45RA–FoxP3^{high} Treg cells, respectively. **B** and **C**, Frequencies of total Treg cells (**B**) and frequencies of CD161+ Treg cells, Helios+ Treg cells, resting (CD45RA+) Treg cells, and memory (CD45RA–FoxP3^{high}) Treg cells (**C**) in patients with active AAV, patients with AAV in remission treated with CIs, patients with AAV in remission treated with RTX, and patients with AAV in long-term remission off therapy. No significant differences were found (all $P > 0.05$ by Kruskal-Wallis test). Bars show the median; symbols represent individual patients. See Figure 1 for definitions. Color figure can be viewed in the online issue, which is available at http://onlinelibrary.wiley.com/doi/10.1002/art.40766/abstract.

distribution of CD8+ T cell subsets in patients treated with CIs, patients treated with RTX, and patients with disease in long-term remission off therapy (Figure 3A). RTX-treated patients and patients with disease in long-term remission off therapy had fewer CD45RA+CCR7–CD8+ (TEMRA) cells and more CD45RA–CCR7–CD8+ (effector memory) T cells than CI-treated patients. We then assessed whether the phenotypic features of TEMRA CD8+ cells were different across these 3 groups. As expected, TEMRA CD8+ T cells were predominantly CD28–CD27– with a high expression of perforin, granzyme B, and CD57 (Figure 3B). No significant differences among treatment groups were seen for the expression of these markers on TEMRA CD8+ cells (Figure 3C).

Given that the decision to use RTX or CIs was left to the discretion of the clinician, we assessed whether any confounding clinical parameter correlated with TEMRA frequency. Renal function, disease type, ANCA specificity, disease duration, and the number of past disease flares did not correlate with the frequency of TEMRA CD8+ T cells (Figure 3D). Recent studies have revealed that TEMRA CD4+ and CD8+ cell frequency is critically influenced by latent CMV infection in AAV (18,19). Accordingly, we found that latent CMV infection was associated with an increased proportion of TEMRA cells. Among the entire cohort, the frequency of TEMRA CD8+ cells was 20.5% and 48.5% in CMV-negative patients and CMV-positive patients, respectively ($P < 0.001$). In order to confirm the opposite effect of RTX and CIs on CD8+ memory cells and to rule out any confounding effect of CMV status, we analyzed the CD8+ T cell phenotype of 12 patients before and 6–12 months after the initiation of treatment with RTX or CIs. This analysis confirmed that, regardless of CMV status, RTX reduced the frequency of TEMRA CD8+ T cells (from a median of 39% before treatment to 10% after treatment [$P < 0.01$]), whereas CIs tended to have the opposite effect (Figure 3E). We then investigated whether cytotoxic CD8+ T cells were present in vasculitis lesions using diagnostic muscle biopsy specimens from 3 patients with untreated active AAV. CD8+ T cells infiltrating inflamed small vessels were observed in all cases and expressed the cytotoxic marker T cell intracellular antigen 1. Representative results are shown in Figure 3F.

B cell depletion dampens ex vivo CD8+ T cell cytokine production. In order to determine whether the opposite effect of RTX and CIs on the CD8+ T cell compartment had functional consequences in AAV patients, we compared their impact on in vitro production of cytokines and chemokines by purified CD8+ T cells stimulated with PMA and ionomycin.

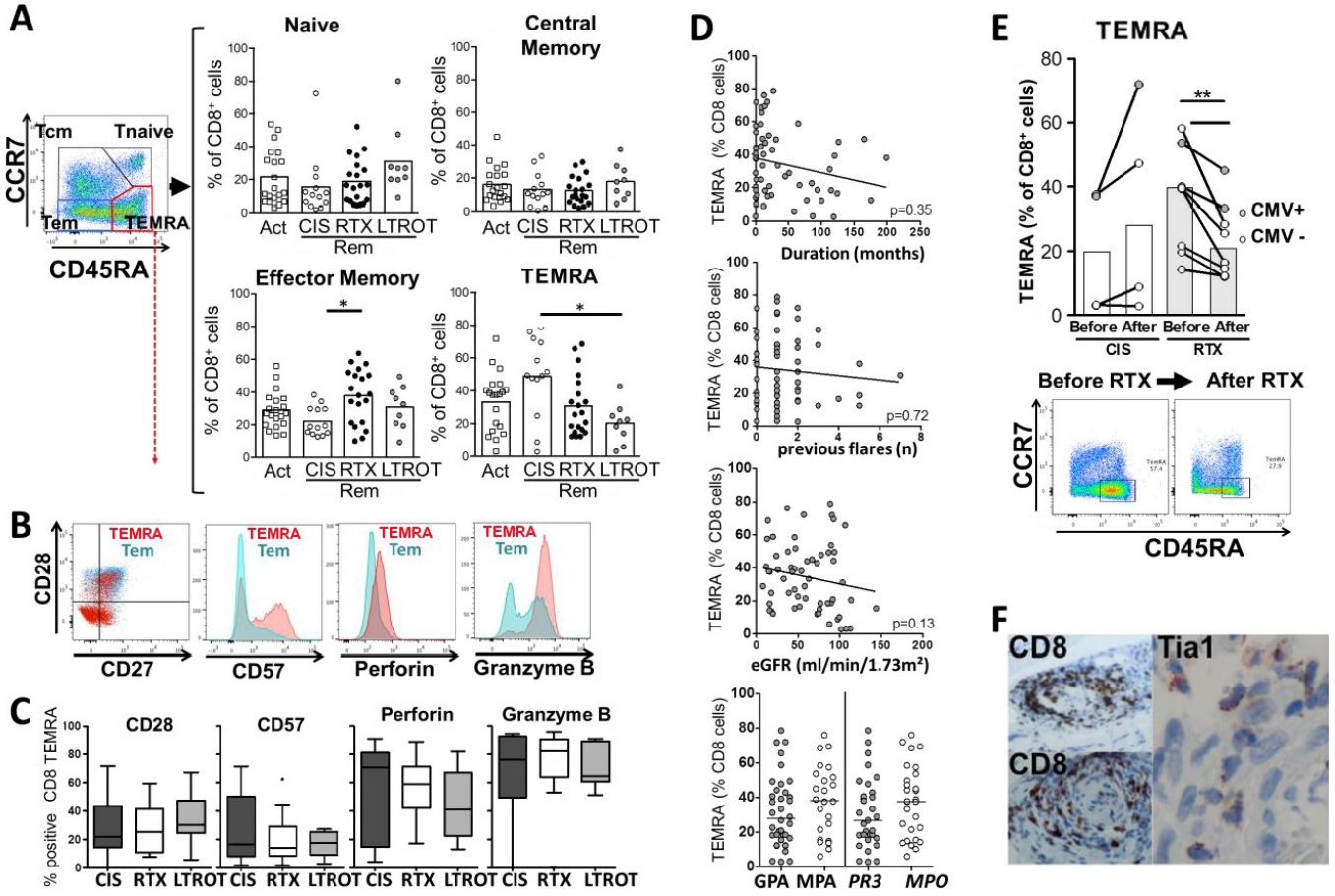

Figure 3. Opposite effects of RTX and CIs on memory CD8+ T cells in AAV patients. **A**, Frequency of naive, central memory (Tcm), effector memory (Tem), and TEMRA CD8+ T cell subsets according to the expression of CD45RA and CCR7 in patients with active AAV, patients with AAV in remission treated with CIs, patients with AAV in remission treated with RTX, and patients with AAV in long-term remission off therapy. Representative flow cytometry data are shown. Bars show the median; symbols represent individual patients. * = $P < 0.05$ across remission groups, by Kruskal-Wallis test with Dunn's post hoc test. **B**, Representative flow cytometry data of phenotype characterization of TEMRA and effector memory T cells. **C,** Lack of modification of TEMRA phenotype by maintenance treatment in AAV patients. Data are shown as box plots. Lines inside the boxes represent the median. The circle indicates an outlier (n = 13 patients treated with CIs, n = 15 patients treated with RTX, and n = 9 patients with AAV in long-term remission off therapy). Box plots were constructed using Tukey's method. **D**, Lack of correlation between TEMRA frequency and disease duration, previous flares, renal function, or disease phenotype. Circles represent individual patients; horizontal lines show the median. eGFR = estimated glomerular filtration rate; GPA = granulomatosis with polyangiitis; MPA = microscopic polyangiitis; PR3 = proteinase 3; MPO = myeloperoxidase. **E,** Longitudinal analysis of TEMRA frequency in AAV patients before and after treatment with RTX (n = 8) or CIs (n = 4) and according to cytomegalovirus (CMV) status (CMV positive [open circles] or CMV negative [closed circles]). Bars show the median; circles connected by a line represent samples taken from the same patient before and after treatment.** = $P < 0.01$ by paired *t*-test. **F,** Immunohistochemical staining for CD8 and T cell intracellular antigen 1 (TIA-1) in diagnostic muscle biopsy specimens from 3 patients with untreated active AAV. Original magnification × 40. See Figure 1 for other definitions.

We found that CD8+ T cells from patients with disease in remission while receiving CIs produced similar levels of cytokines and chemokines as those from patients with untreated active disease. Conversely, CD8+ T cells from patients receiving RTX produced lower levels of proinflammatory cytokines and chemokines compared to the 2 other groups (Figure 4A). Differentially expressed cytokines and chemokines included interferon-γ (IFNγ), macrophage inflammatory protein 1α (MIP-1α)/CCL3, MIP-1β/CCL4, RANTES/CCL5, IFNγ–inducible 10-kd protein/CXCL10, stromal cell–derived factor 1α/CXCL12a, and eotaxin. For MIP-1α, for example, the median level was 815 pg/ml in patients treated with RTX versus 985 pg/ml in patients treated with CIs versus 970 pg/ml in those with active untreated AAV ($P < 0.01$). Similar trends were observed for TNF and granulocyte–macrophage colony-stimulating factor. Low amounts of IL-4, IL-5, IL-8, IL-10, IL-12p70, IL-13, IL-18, IL-21, IL-22, IL-27, monocyte chemotactic protein 1 (MCP-1), and growth-related oncogene α were also detectable, without any difference across groups. Levels of IL-1α, IL-1β, IL-1 receptor antagonist, IL-6, IL-7, IL-9, IL-15, IL-17A, IL-23, IL-31, IFNα, and lymphotoxin were below the detection threshold. IL-2 production was too high to be confidently quantified.

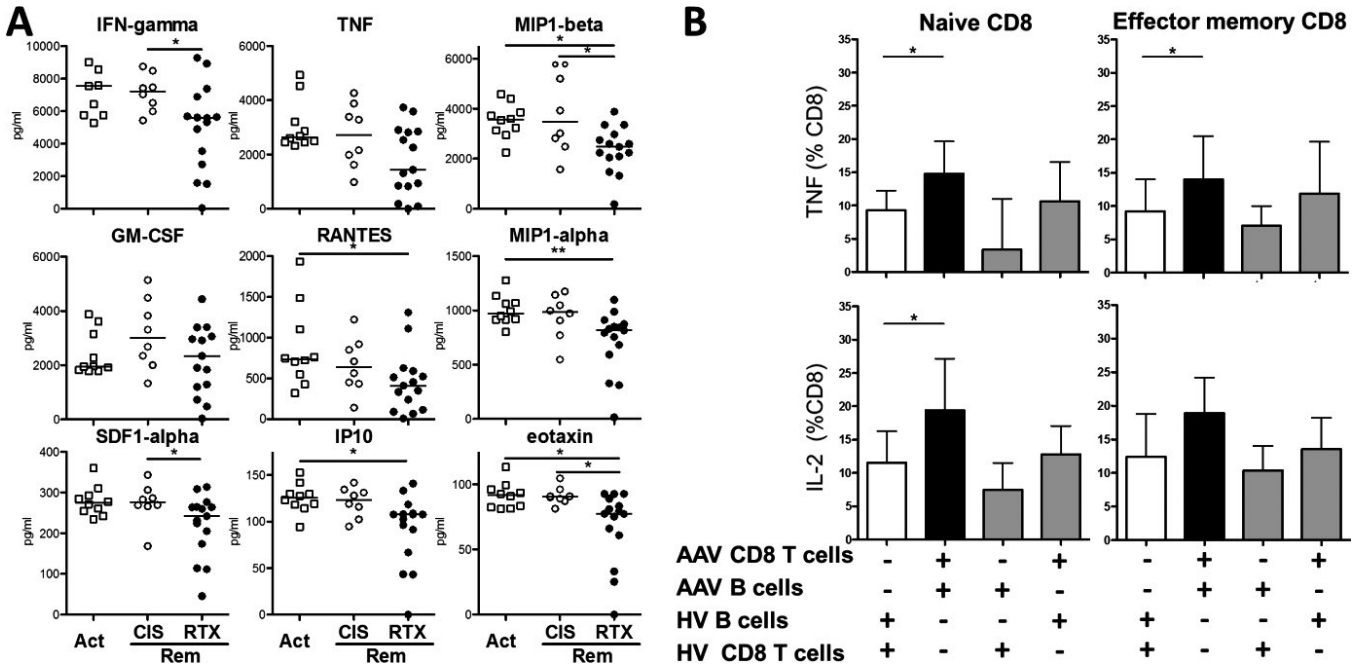

Figure 4. Diminished ex vivo production of cytokines and chemokines by CD8+ T cells in RTX-treated AAV patients and propensity of B cells from AAV patients to promote CD8+ T cell cytokine production in vitro. **A**, Decrease in the levels of cytokines and chemokines secreted by CD8+ T cells purified from AAV patients treated with RTX. Levels of interferon-γ (IFNγ), tumor necrosis factor (TNF), macrophage inflammatory protein 1β (MIP-1β), granulocyte–macrophage colony-stimulating factor (GM-CSF), RANTES, MIP-1α, stromal cell–derived factor 1α (SDF-1α), IFNγ–inducible 10-kd protein (IP-10), and eotaxin were quantified in the supernatants of purified CD8+ T cells after 4 hours of polyclonal stimulation using a 34-plex immunoassay. CD8+ T cells from RTX-treated patients produced lower levels of proinflammatory cytokines and chemokines than those from CI-treated patients and patients with untreated active disease. Symbols represent individual patients; horizontal lines show the median. * = $P < 0.05$; ** = $P < 0.01$, by Kruskal-Wallis test with Dunn's post hoc test. **B**, Production of TNF and interleukin-2 (IL-2) by CD8+ T cells purified from patients with untreated active AAV or aged-matched healthy volunteers (HV). Purified naive or effector memory CD8+ T cells were cocultured with B cells in the presence of staphylococcal enterotoxin B superantigen for 72 hours. Autologous cocultures of CD8+ T cells and B cells from healthy volunteers (n = 29), autologous cocultures of CD8+ T cells and B cells from AAV patients (n = 11), cocultures of B cells from AAV patients (n = 15) and CD8+ T cells from healthy volunteers (n = 15), and cocultures of CD8+ T cells from AAV patients (n = 15) and B cells from healthy volunteers (n = 15) were performed. Bars show the median ± interquartile range. * = $P < 0.005$. See Figure 1 for other definitions.

Thus, B cell depletion therapy appears to be more effective than a pleiotropic CI in suppressing the proinflammatory potential of CD8+ T cells. Of note, the production of proinflammatory cytokines and chemokines did not correlate with the frequency of TEMRA CD8+ T cells, suggesting that RTX had a broad effect on the CD8+ T cell compartment, beyond its impact on the distribution of memory CD8+ T cell subsets.

Promotion of CD8+ T cell activation by AAV B cells in vitro. Having shown that B cell depletion reduced TEMRA frequency and CD8+ T cell cytokine production ex vivo, we then assessed whether B cells from patients with untreated active AAV could promote CD8+ T cell activation in vitro. FACS-sorted naive or effector memory CD8+ T cells were cocultured with B cells for 72 hours in the presence of SEB superantigen. Cytokine production of CD8+ T cells was then assessed by flow cytometry with intracellular staining. Preliminary experiments performed in healthy volunteers confirmed that in B cell–CD8+ T cell cocultures, the addition of SEB induced a B cell–dependent CD8+ T cell activation (data available upon request from the corresponding author).

We found that CD8+ T cells cocultured with autologous B cells produced more proinflammatory cytokines in patients with untreated active AAV than in age-matched healthy volunteers (e.g., the median percent of TNF-producing effector memory CD8+ T cells was 14% in AAV patients versus 9.2% in controls [$P < 0.05$]) (Figure 4B). Of note, cytokine production was lower when CD8+ T cell subsets from patients were stimulated with B cells from healthy volunteers or vice versa (Figure 4B). Taken together, these results demonstrate the cross-talk between B cells and CD8+ T cells in AAV patients, leading to CD8+ T cell hyperactivation.

DISCUSSION

The main objective of this study was to compare the impact of RTX and CIs on CD4+ T cells, Treg cells, and CD8+ T cells in AAV. The first finding of our study was that patients receiving

RTX and those receiving CIs had similar distributions of CD4+ T cell and Treg cell subsets. CD4+ T helper cells, including Th1, Th2, Th17, and follicular helper T cells, are believed to play a key role in AAV (3). Whether B cell depletion differentially affects these populations remains unclear. Stasi et al reported an increase in Th2 cell frequency in patients with autoimmune thrombocytopenia who responded to B cell depletion treatment (20). It has been suggested that in rheumatoid arthritis (RA), B cell depletion reduces the Th17 cell but not the Th1 cell response (21). Recently, Verstappen et al reported that patients with primary Sjögren's syndrome exhibited an increased frequency of follicular helper T cells, which decreased upon B cell depletion, whereas the Th1 and Th2 cell populations remained stable. A subtle decrease in Th17 cells was also noticed (22). How RTX affects distinct CD4+ T cell lineages probably varies according to the underlying disease and remains to be fully investigated (11). However, when we compared the expression of Th1, Th2, and Th17 markers on CD4+ T cells from patients with AAV in remission, we found no significant difference between patients receiving RTX and those receiving CIs.

Several investigators have reported that Treg cells from AAV patients had a decreased suppressive function (4,23–25), even in remission and in the absence of any immunosuppressant (4). With regard to the effects of B cell depletion therapy on Treg cells, contradictory data have been reported in studies performed in various settings such as cryoglobulinemic vasculitis (26), RA (27,28), systemic lupus erythematosus (SLE) (29,30), and autoimmune thrombocytopenia (16). Importantly, most of those data were from uncontrolled longitudinal studies using simple staining strategies for Treg cell identification. Herein, we report the results of an in-depth phenotype analysis of Treg cells from AAV patients. Treg cells expressing CD161+ or lacking Helios have been reported to be more prone to producing proinflammatory cytokines (13–17). We found no clear impact of B cell depletion therapy on these subsets as compared to CIs.

Recently, Zhao et al (12) compared the frequency of Treg cells and CD45RA/CD25 expression–defined subsets in GPA patients under various conditions (active disease versus inactive disease; CI-treated versus RTX-treated). They found that the frequency of Treg cells in GPA patients after RTX treatment was similar to that in healthy controls, while GPA patients receiving CIs had a reduced frequency of Treg cells (12). They also found a trend for Treg cell frequencies to increase after RTX treatment. In contrast, we found no significant difference in Treg cell frequency in patients receiving RTX versus those receiving CIs. Of note, the increase in Treg cells (CD4+CD25+CD127− T cells) noticed by Zhao et al was mainly driven by CD45RA−CD25+ cells, which are probably not bona fide Treg cells (31). We also assessed the frequencies of resting (CD45RA+) Treg cells and memory (CD45RA−FoxP3^{high}) Treg cells and found no difference between RTX-treated and CI-treated patients. Interestingly, a recent study demonstrated that in tumor-bearing mice, RTX could even dampen Treg cell expansion (32). Further studies are needed to determine whether RTX impacts the Treg cell compartment in patients with autoimmune diseases.

Our main finding was that RTX and CIs had clear opposite effects on CD8+ T cells. TEMRA cells were expanded by CIs but decreased by RTX. These cells had a typical TEMRA phenotype with a high cytotoxic potential reflected by the strong expression of perforin and granzyme B, which may be implicated in tissue damage. In a murine model of pauci-immune glomerulonephritis, both anti-CD8 and antiperforin antibody therapies have been shown to reduce glomerular lesions (33,34). In AAV patients, CD8+ T cells are present in granulomatous and renal lesions. However, little data were available regarding the role of CD8+ T cells in AAV until recently. In 2010, McKinney et al analyzed the prognostic value of transcription profiling of neutrophils, monocytes, CD8+ T cells, CD4+ T cells, and B cells in AAV (5). Unexpectedly, they found that the CD8+ T cell transcriptome identified 2 subject groups and predicted relapse risk. They identified a CD8+ T cell exhaustion signature that predicted a favorable outcome in a wide range of autoimmune diseases. These findings suggest that CD8+ T cell effector functions have a deleterious role in AAV and other autoimmune diseases.

Interestingly, we found that B cell depletion therapy reduced cytokine production by CD8+ T cells in AAV patients, whereas CIs did not. In other words, a B cell–targeted therapy had more impact on cytokine production by CD8+ T cells than an immunosuppressant that directly impacts T cell biology. This paradoxical finding suggests that B cells play a key role in the CD8+ T cell response, which may contribute to the high efficacy of RTX in AAV. However, since viral and/or opportunistic infections are not a usual feature of the absence of B cells in humans (i.e., X-linked agammaglobulinemia), one may cast doubt over the role of B cells in the CD8+ response in humans. In fact, protective and autoimmune humoral and cellular responses may not be equally sensitive to B cell depletion. For instance, RTX has been shown to reduce autoreactive but not tetanus toxoid–specific CD4+ cells in pemphigus vulgaris (35).

Unfortunately, AAV relapses remain a key issue in the era of B cell depletion therapy. Several teams have shown that highly sensitive B cell immunophenotyping could help estimate the relapse risk following B cell depletion in SLE (36) or RA (37) and more recently AAV (38–40). However, this B cell–focused approach poses technical difficulties due to the rarity of B cells following RTX, and does not assess the pleiotropic effects of B cell repopulation. Our results suggest that the analysis of CD8+ T cells during and after RTX maintenance treatment may help identify new immunomonitoring readouts.

In conclusion, the disruption of B cell help to a pathogenic CD8+ T cell response could contribute to the dramatic efficacy of RTX. Further studies are needed to determine how B cells impact CD8+ T cell responses and to assess the value of CD8+ T cell immunomonitoring in patients receiving B cell–targeted therapies.

AUTHOR CONTRIBUTIONS

All authors were involved in drafting the article or revising it critically for important intellectual content, and all authors approved the final version to be published. Dr. A. Néel had full access to all of the data in the study and takes responsibility for the integrity of the data and the accuracy of the data analysis.

Study conception and design. A. Néel, Rimbert, Bruneau, Brouard, Josien, Fakhouri, Degauque.

Acquisition of data. A. Néel, Bucchia, M. Néel, Tilly, Caristan, Yap, Cadoux, Agard, Hourmant, Godmer, Bressollette, Hamidou, Degauque.

Analysis and interpretation of data. A. Néel, Josien, Fakhouri, Degauque.

REFERENCES

1. Braudeau C, Néel A, Amouriaux K, Martin JC, Rimbert M, Besançon A, et al. Dysregulated responsiveness of circulating dendritic cells to Toll-like receptors in ANCA-associated vasculitis. Front Immunol 2017;8:102.
2. Braudeau C, Amouriaux K, Néel A, Herbreteau G, Salabert N, Rimbert M, et al. Persistent deficiency of circulating mucosal-associated invariant T (MAIT) cells in ANCA-associated vasculitis. J Autoimmun 2016;70:73–9.
3. Kallenberg CG, Stegeman CA, Abdulahad WH, Heeringa P. Pathogenesis of ANCA-associated vasculitis: new possibilities for intervention. Am J Kidney Dis 2013;62:1176–87.
4. Rimbert M, Hamidou M, Braudeau C, Puéchal X, Teixeira L, Caillon H, et al. Decreased numbers of blood dendritic cells and defective function of regulatory T cells in antineutrophil cytoplasmic antibody-associated vasculitis. PLoS One 2011;6:e18734.
5. McKinney EF, Lyons PA, Carr EJ, Hollis JL, Jayne DR, Willcocks LC, et al. A CD8+ T cell transcription signature predicts prognosis in autoimmune disease. Nat Med 2010;16:586–91.
6. Chang J, Eggenhuizen P, O'Sullivan KM, Alikhan MA, Holdsworth SR, Ooi JD, et al. CD8+ T cells effect glomerular injury in experimental anti-myeloperoxidase GN. J Am Soc Nephrol 2017;28:47–55.
7. Guillevin L, Pagnoux C, Karras A, Khouatra C, Aumaître O, Cohen P, et al, for the French Vasculitis Study Group. Rituximab versus azathioprine for maintenance in ANCA-associated vasculitis. N Engl J Med 2014;371:1771–80.
8. Stone JH, Merkel PA, Spiera R, Seo P, Langford CA, Hoffman GS, et al. Rituximab versus cyclophosphamide for ANCA-associated vasculitis. N Engl J Med 2010;363:221–32.
9. Chan OT, Hannum LG, Haberman AM, Liu Z, Zhao M, Aratani Y, et al. A novel mouse with B cells but lacking serum antibody reveals an antibody-independent role for B cells in murine lupus. J Exp Med 1999;189:1639–48.
10. Barr TA, Shen P, Brown S, Lampropoulou V, Roch T, Lawrie S, et al. B cell depletion therapy ameliorates autoimmune disease through ablation of IL-6-producing B cells. J Exp Med 2012;209:1001–10.
11. Lund FE, Randall TD. Effector and regulatory B cells: modulators of CD4+ T cell immunity. Nat Rev Immunol 2010;10:236–47.
12. Zhao Y, Lutalo PM, Thomas JE, Sangle S, Choong LM, Tyler JR, et al. Circulating T follicular helper cell and regulatory T cell frequencies are influenced by B cell depletion in patients with granulomatosis with polyangiitis. Rheumatology (Oxford) 2014;53:621–30.
13. Afzali B, Mitchell PJ, Edozie FC, Povoleri GA, Dowson SE, Demandt L, et al. CD161 expression characterizes a subpopulation of human regulatory T cells that produces IL-17 in a STAT3-dependent manner. Eur J Immunol 2013;43:2043–54.
14. Pesenacker AM, Bending D, Ursu S, Wu Q, Nistala K, Wedderburn LR. CD161 defines the subset of FoxP3+ T cells capable of producing proinflammatory cytokines. Blood 2013;121:2647–58.
15. Verhagen J, Wraith DC. Comment on "Expression of Helios, an Ikaros transcription factor family member, differentiates thymic-derived from peripherally induced Foxp3+ T regulatory cells". J Immunol 2010;185:7129.
16. Takatori H, Kawashima H, Matsuki A, Meguro K, Tanaka S, Iwamoto T, et al. Helios enhances Treg cell function in cooperation with FoxP3. Arthritis Rheumatol 2015;67:1491–502.
17. Thornton AM, Korty PE, Tran DQ, Wohlfert EA, Murray PE, Belkaid Y, et al. Expression of Helios, an Ikaros transcription factor family member, differentiates thymic-derived from peripherally induced Foxp3+ T regulatory cells. J Immunol 2010;184:3433–41.
18. Morgan MD, Pachnio A, Begum J, Roberts D, Rasmussen N, Neil DA, et al. CD4+CD28– T cell expansion in granulomatosis with polyangiitis (Wegener's) is driven by latent cytomegalovirus infection and is associated with an increased risk of infection and mortality. Arthritis Rheum 2011;63:2127–37.
19. Eriksson P, Sandell C, Backteman K, Ernerudh J. Expansions of CD4+CD28– and CD8+CD28– T cells in granulomatosis with polyangiitis and microscopic polyangiitis are associated with cytomegalovirus infection but not with disease activity. J Rheumatol 2012;39:1840–3.
20. Stasi R, Cooper N, Del Poeta G, Stipa E, Evangelista ML, Abruzzese E, et al. Analysis of regulatory T-cell changes in patients with idiopathic thrombocytopenic purpura receiving B cell-depleting therapy with rituximab. Blood 2008;112:1147–50.
21. Van de Veerdonk FL, Lauwerys B, Marijnissen RJ, Timmermans K, Di Padova F, Koenders MI, et al. The anti-CD20 antibody rituximab reduces the Th17 cell response. Arthritis Rheum 2011;63:1507–16.
22. Verstappen GM, Kroese FG, Meiners PM, Corneth OB, Huitema MG, Haacke EA, et al. B cell depletion therapy normalizes circulating follicular Th cells in primary Sjögren syndrome. J Rheumatol 2017;44:49–58.
23. Abdulahad WH, Stegeman CA, van der Geld YM, Doornbos-van der Meer B, Limburg PC, Kallenberg CG. Functional defect of circulating regulatory CD4+ T cells in patients with Wegener's granulomatosis in remission. Arthritis Rheum 2007;56:2080–91.
24. Morgan MD, Day CJ, Piper KP, Khan N, Harper L, Moss PA, et al. Patients with Wegener's granulomatosis demonstrate a relative deficiency and functional impairment of T-regulatory cells. Immunology 2010;130:64–73.
25. Free ME, Bunch DO, McGregor JA, Jones BE, Berg EA, Hogan SL, et al. Patients with antineutrophil cytoplasmic antibody-associated vasculitis have defective Treg cell function exacerbated by the presence of a suppression-resistant effector cell population. Arthritis Rheum 2013;65:1922–33.
26. Saadoun D, Rosenzwajg M, Landau D, Piette JC, Klatzmann D, Cacoub P. Restoration of peripheral immune homeostasis after rituximab in mixed cryoglobulinemia vasculitis. Blood 2008;111:5334–41.
27. Feuchtenberger M, Müller S, Roll P, Waschbisch A, Schäfer A, Kneitz C, et al. Frequency of regulatory T cells is not affected by transient B cell depletion using anti-CD20 antibodies in rheumatoid arthritis. Open Rheumatol J 2008;2:81–8.
28. Díaz-Torné C, Ortiz de Juana MA, Geli C, Cantó E, Laiz A, Corominas H, et al. Rituximab-induced interleukin-15 reduction associated with clinical improvement in rheumatoid arthritis. Immunology 2014;142:354–62.
29. Vigna-Perez M, Hernández-Castro B, Paredes-Saharopulos O, Portales-Pérez D, Baranda L, Abud-Mendoza C, et al. Clinical and immunological effects of rituximab in patients with lupus nephritis refractory to conventional therapy: a pilot study. Arthritis Res Ther 2006;8:R83.

30. Vallerskog T, Gunnarsson I, Widhe M, Risselada A, Klareskog L, van Vollenhoven R, et al. Treatment with rituximab affects both the cellular and the humoral arm of the immune system in patients with SLE. Clin Immunol 2007;122:62–74.
31. Miyara M, Yoshioka Y, Kitoh A, Shima T, Wing K, Niwa A, et al. Functional delineation and differentiation dynamics of human CD4+ T cells expressing the FoxP3 transcription factor. Immunity 2009;30:899–911.
32. Deligne C, Metidji A, Fridman WH, Teillaud JL. Anti-CD20 therapy induces a memory Th1 response through the IFN-γ/IL-12 axis and prevents protumor regulatory T-cell expansion in mice. Leukemia 2015;29:947–57.
33. Fujinaka H, Yamamoto T, Feng L, Nameta M, Garcia G, Chen S, et al. Anti-perforin antibody treatment ameliorates experimental crescentic glomerulonephritis in WKY rats. Kidney Int 2007;72:823–30.
34. Reynolds J, Norgan VA, Bhambra U, Smith J, Cook HT, Pusey CD. Anti-CD8 monoclonal antibody therapy is effective in the prevention and treatment of experimental autoimmune glomerulonephritis. J Am Soc Nephrol 2002;13:359–69.
35. Eming R, Nagel A, Wolff-Franke S, Podstawa E, Debus D, Hertl M. Rituximab exerts a dual effect in pemphigus vulgaris. J Invest Dermatol 2008;128:2850–8.
36. Vital EM, Dass S, Buch MH, Henshaw K, Pease CT, Martin MF, et al. B cell biomarkers of rituximab responses in systemic lupus erythematosus. Arthritis Rheum 2011;63:3038–47.
37. Dass S, Rawstron AC, Vital EM, Henshaw K, McGonagle D, Emery P. Highly sensitive B cell analysis predicts response to rituximab therapy in rheumatoid arthritis. Arthritis Rheum 2008;58:2993–9.
38. Md Yusof MY, Vital EM, Das S, Dass S, Arumugakani G, Savic S, et al. Repeat cycles of rituximab on clinical relapse in ANCA-associated vasculitis: identifying B cell biomarkers for relapse to guide retreatment decisions. Ann Rheum Dis 2015;74:1734–8.
39. Bunch DO, McGregor JG, Khandoobhai NB, Aybar LT, Burkart ME, Hu Y, et al. Decreased $CD5^+$ B cells in active ANCA vasculitis and relapse after rituximab. Clin J Am Soc Nephrol 2013;8:382–91.
40. Bunch DO, Mendoza CE, Aybar LT, Kotzen ES, Colby KR, Hu Y, et al. Gleaning relapse risk from B cell phenotype: decreased CD5+ B cells portend a shorter time to relapse after B cell depletion in patients with ANCA-associated vasculitis. Ann Rheum Dis 2015;74:1784–6.

DOI 10.1002/art.40888

Applications Invited for *Arthritis & Rheumatology* Editor-in-Chief (2020–2025 Term)

The American College of Rheumatology Committee on Journal Publications announces the search for the position of Editor, *Arthritis & Rheumatology*. The official term of the next *Arthritis & Rheumatology* editorship is July 1, 2020–June 30, 2025; however, some of the duties of the new Editor will begin during a transition period starting April 1, 2020. ACR members who are considering applying should submit a nonbinding letter of intent by May 1, 2019 to the Managing Editor, Jane Diamond, at jdiamond@rheumatology.org, and are also encouraged to contact the current Editor-in-Chief, Dr. Richard Bucala, to discuss details; initial contact should be made via e-mail to richard.bucala@yale.edu. Applications will be due June 21, 2019 and will be reviewed during the summer of 2019. Application materials are available on the ACR web site at https://www.rheumatology.org/Learning-Center/Publications-Communications/Journals/A-R.

Arthritis & Rheumatology
Vol. 71, No. 4, April 2019, pp 651–658

AMERICAN COLLEGE OF RHEUMATOLOGY
EDUCATION • TREATMENT • RESEARCH

LETTERS

DOI 10.1002/art.40783

Diagnostic pitfalls and treatment challenges in interstitial pneumonia with autoimmune features: comment on the article by Wilfong et al

To the Editor:

We read with interest the article by Wilfong et al which reviewed the diagnostic challenges in and treatment options for patients with interstitial pneumonia with autoimmune features (IPAF) (1). This term was used by the American Thoracic Society (ATS) and European Respiratory Society (ERS) to describe patients with idiopathic interstitial pneumonia who do not meet classification criteria for a connective tissue disease (CTD) but have features of autoimmunity (2). From a rheumatologist's perspective, IPAF, particularly with extrathoracic clinical manifestations or specific autoantibodies, represents an early manifestation of a probable autoimmune disease and may precede the involvement of other organs. The latter may be masked or prevented by immunosuppressive therapy. In a study by Ito et al, 12% of 98 patients with IPAF developed a definite CTD (i.e., rheumatoid arthritis, systemic sclerosis [SSc]) within a median follow-up of 4.5 years (3). In another study by Hu et al, 32% of patients with CTD-associated interstitial lung disease (ILD) did not receive an accurate initial diagnosis (4). Therefore, classification criteria for IPAF should evolve along with criteria for the early diagnosis of rheumatic diseases, such as the Very Early Diagnosis of Systemic Sclerosis approach (5).

The current IPAF criteria give substantial weight to various autoantibodies. Antineutrophil cytoplasmic antibody (ANCA) positivity has been reported in patients with interstitial pneumonia and may indicate microscopic polyangiitis. In our cohort, ILD was found in 11 of 102 patients (11.8%) with microscopic polyangiitis who tested positive for ANCA. In 6 patients, interstitial pneumonia was the first and only manifestation that preceded the overt clinical development of systemic vasculitis. The radiologic patterns included nonspecific interstitial pneumonia, usual interstitial pneumonia, or unclassifiable interstitial pneumonia. In the official ATS/ERS research statement, ANCAs were not included in the serologic domain because they are associated with the vasculitides, rather than the CTD-associated ILD spectrum of disorders (2). We believe ANCA (particularly myeloperoxidase) should be included in this domain given the fine line between CTD and systemic vasculitides.

Evidence supporting the choice of treatment in patients with IPAF is scarce. Unlike in idiopathic pulmonary fibrosis, corticosteroids and/or immunosuppressive agents are frequently given as first-line therapy in IPAF. Wilfong et al stated that mycophenolate mofetil and azathioprine are likely first-line agents, while rituximab and calcineurin inhibitors may play a role in refractory disease. Cyclophosphamide is another possible option, given its established efficacy in patients with lung disease related to SSc or ANCA-associated vasculitis. In a recent retrospective cohort study, Wiertz et al found that patients with steroid-resistant unclassifiable idiopathic interstitial pneumonia, particularly those with IPAF, could respond to induction treatment with intravenous cyclophosphamide (6). Unlike Wilfong and colleagues, we would not overestimate the potential role of calcineurin inhibitors in patients with refractory ILD, given their limited use in the practice of rheumatologists and pulmonologists. In contrast, the value of rituximab was established in patients with autoimmune diseases (rheumatoid arthritis, lupus nephritis, or ANCA-associated vasculitis), and its administration in more severe forms of IPAF may be justified.

We agree with Wilfong et al that careful prospective clinical and immunologic phenotyping is essential in identifying various subtypes of IPAF that may have different responses to treatment. The results of several studies suggested that certain autoantibodies may predict worse prognosis (anti–Scl-70 and anti-CADM/MDA-5 antibodies) or better prognosis (antinuclear antibody) in patients with IPAF (7,8). Testing for specific autoantibodies seems to be a promising approach to predict progression and response to treatment in patients with IPAF. However, the implication of the humoral immune response with regard to disease behavior and management remains unknown. In rheumatology, step-up immunosuppressive therapy has been partly replaced by a more personalized approach that tailors treatment decisions to the characteristics of the disease and individual patient. It is tempting to extrapolate the data on treatment for specific CTDs to their IPAF counterparts, which is defined by the presence of respective autoantibodies. This claim lacks supportive evidence, though the "absence of evidence is not evidence of absence."

In conclusion, there is a wide knowledge gap regarding the efficacy of immunosuppressive treatment in patients with IPAF. We need prospective trials so that the efficacy and safety of disease-modifying antirheumatic drugs, biologic agents (rituximab), and antifibrotic agents (nintedanib and pirfenidone) can be investigated. Notably, nintedanib and pirfenidone are currently under investigation in multicenter, double-blind, randomized, placebo-controlled trials in patients with unclassifiable progressive fibrosing ILD. Future progress in the field will be impossible without close collaboration between pulmonologists and rheumatologists.

Supported by the Russian Academic Excellence Project 5-100.

Pavel Novikov, MD
Elena Shchegoleva, MD
Larisa Akulkina, MD
Nikolai Bulanov, MD
Sechenov First Moscow State Medical University
Ekaterina Vinogradova, MD
Sergey Moiseev, MD
Sechenov First Moscow State Medical University and Lomonosov Moscow State University
Moscow, Russia

1. Wilfong EM, Lentz RJ, Guttentag A, Tolle JJ, Johnson JE, Kropski JA, et al. Interstitial pneumonia with autoimmune features: an emerging challenge at the intersection of rheumatology and pulmonology [review]. Arthritis Rheumatol 2018;70:1901–13.
2. Fischer A, Antoniou KM, Brown KK, Cadranel J, Corte TJ, du Bois RM, et al. An official European Respiratory Society/American Thoracic Society research statement: interstitial pneumonia with autoimmune features. Eur Respir J 2015;46:976–87.
3. Ito Y, Arita M, Kumagai S, Takei R, Noyama M, Tokioka F, et al. Serological and morphological prognostic factors in patients with interstitial pneumonia with autoimmune features. BMC Pulm Med 2017;17:111.
4. Hu Y, Wang LS, Wei YR, Du SS, Du YK, He X, et al. Clinical characteristics of connective tissue disease–associated interstitial lung disease in 1,044 Chinese patients. Chest 2016;149:201–8.
5. Minier T, Guiducci S, Bellando-Randone S, Bruni C, Lepri G, Czirják L, et al. Preliminary analysis of the very early diagnosis of systemic sclerosis (VEDOSS) EUSTAR multicentre study: evidence for puffy fingers as a pivotal sign for suspicion of systemic sclerosis. Ann Rheum Dis 2014;73:2087–93.
6. Wiertz IA, van Moorsel CH, Vorselaars AD, Quanjel MJ, Grutters JC. Cyclophosphamide in steroid refractory unclassifiable idiopathic interstitial pneumonia and interstitial pneumonia with autoimmune features (IPAF). Eur Respir J 2018;51:1702519.
7. Vij R, Noth I, Strek ME. Autoimmune-featured interstitial lung disease: a distinct entity. Chest 2011;140:1292–9.
8. Jee A, Adelstein S, Bleasel J, Keir GJ, Nguyen M, Sahhar J, et al. Role of autoantibodies in the diagnosis of connective-tissue disease ILD (CTD-ILD) and interstitial pneumonia with autoimmune features (IPAF). J Clin Med 2017;6:E51.

DOI 10.1002/art.40782

Reply

To the Editor:

We thank Dr. Novikov and colleagues for their comments on our recent review. We agree that the ATS/ERS classification criteria for patients with IPAF (1) will need to be reviewed, revised, and validated moving forward. We also agree that collaboration between rheumatologists and pulmonologists in the management of these cases is critical. In our ongoing prospective longitudinal cohort, >93% of cases are co-managed by rheumatology and pulmonology clinicians. We strongly advocate this approach worldwide to provide accurate classification and diagnosis at the time of presentation, and to monitor for the emergence of a clearly defined CTD.

We concur that ANCA testing should occur in the setting of new ILD, although ANCA testing was not universally recommended in the 2018 idiopathic pulmonary fibrosis diagnostic guidelines (2). However, whether or not a patient with ILD and a positive ANCA has undifferentiated disease or is better classified as having ANCA-associated vasculitis is under debate. In 2014, Comarmond and coworkers conducted a retrospective review of patients with pulmonary fibrosis and ANCA-associated vasculitis (AAV), with myeloperoxidase antibody specificity being more common than proteinase 3 specificity (3). They reported that ~40% of patients had evidence of pulmonary fibrosis before clinically apparent vasculitis, and another 40% of patients presented with pulmonary fibrosis and evidence of systemic vasculitis (usually microscopic polyangiitis). A variety of radiographic patterns were present. Interestingly, patients with pulmonary fibrosis had poor prognosis with a global mortality of 56%, which was somewhat improved by induction therapy consisting of glucocorticoids and either cyclophosphamide or rituximab versus glucocorticoids alone (3). The induction treatment regimens for AAV differ from the initial treatment of other CTD-associated ILDs, so these patients would likely benefit from targeted vasculitis therapy. Draft American College of Rheumatology/European League Against Rheumatism classification criteria for AAV would classify these patients as having AAV (4), which would exclude them from the IPAF algorithm should those criteria be ultimately ratified.

We also agree that there is significant ambiguity in treatment algorithms. In refractory disease, it is reasonable to try a variety of immunosuppressive agents, and an order in which to try various therapies may not be clear. We concur with using a personalized approach, depending on the exact clinical picture and patient preferences. We believe that calcineurin inhibitors are an emerging therapy for myositis-related ILD as highlighted in other recent reviews (5,6), and its efficacy in the treatment of rheumatoid arthritis has been previously documented (7). It may be less ideal in SSc, given the risk of renal adverse events. Furthermore, for patients with severe ILD in whom lung transplantation may be necessary, some transplant centers may have considerable reluctance to transplant after administration of either cyclophosphamide or rituximab. Calcineurin inhibitors, in contrast, are routinely used posttransplant, and these medications may be viewed differently by some transplant pulmonologists and may preserve transplant candidacy.

In conclusion, we welcome the ongoing discussion regarding these criteria, diagnostic approaches, and management strategies. We believe that patients with ANCA-associated ILD likely have AAV rather than IPAF based on the most recent draft AAV criteria. We also welcome ongoing collaborations and multicenter cohort studies to validate these criteria and determine the best treatment options.

The content herein is solely the responsibility of the authors and do not necessarily represent official views of the National Center for Advancing Translational Sciences or the National Institutes of Health. Supported by award UL1-TR000445 from the National Center for Advancing Translational Sciences, NIH, to Drs. Wilfong and Crofford. Dr. Wilfong's work was also supported by grant T32-AR-007304 from the National Institute of Arthritis and Musculoskeletal and Skin Diseases and grant T32-HL-087738 from the National Heart, Lung, and Blood Institute, NIH. Dr. Byram's work was supported by the Vasculitis Clinical Research Consortium and the Vasculitis Foundation. Dr. Crofford has received research support from EMD Serono, Boehringer Ingelheim, and Cumberland Pharmaceuticals unrelated to this work. No other disclosures relevant to this article were reported.

Erin M. Wilfong, MD, PhD
Vanderbilt University Medical Center Nashville, TN and University of California San Francisco
Kevin W. Bayram, MD
Leslie J. Crofford, MD
Vanderbilt University Medical Center Nashville, TN

1. Fischer A, Antoniou KM, Brown KK, Cadranel J, Corte TJ, du Bois RM, et al. An official European Respiratory Society/American Thoracic Society research statement: interstitial pneumonia with autoimmune features. Eur Respir J 2015;46:976–87.
2. Raghu G, Remy-Jardin M, Myers JL, Richeldi L, Ryerson CJ, Lederer DJ, et al. Diagnosis of idiopathic pulmonary fibrosis: an official ATS/ERS/JRS/ALAT clinical practice guideline. Am J Respir Crit Care Med 2018;198:e44–68.
3. Comarmond C, Crestani B, Tazi A, Hervier B, Adam-Marchand S, Nunes H, et al. Pulmonary fibrosis in antineutrophil cytoplasmic antibodies (ANCA)-associated vasculitis: a series of 49 patients and review of the literature. Medicine (Baltimore) 2014;93:340–9.
4. Robson JC, Grayson PC, Ponte C, Suppiah R, Craven A, Khalid S, et al. Draft classification criteria for the ANCA-associated vasculitides [abstract]. Ann Rheum Dis 2018;Suppl 2:60–1.
5. Mecoli CA, Christopher-Stine L. Management of interstitial lung disease in patients with myositis specific autoantibodies. Curr Rheumatol Rep 2018;20:27.
6. Oddis CV, Aggarwal R. Treatment in myositis. Nat Rev Rheumatol 2018;14:279–89.
7. Furst DE, Saag K, Fleischmann MR, Sherrer Y, Block JA, Schnitzer T, et al. Efficacy of tacrolimus in rheumatoid arthritis patients who have been treated unsuccessfully with methotrexate: a six-month, double-blind, randomized, dose-ranging study. Arthritis Rheum 2002;46:2020–8.

DOI 10.1002/art.40743

Questions regarding the value of CCL21 as a potential biomarker for pulmonary arterial hypertension in systemic sclerosis: comment on the article by Hoffmann-Vold et al

To the Editor:

We read with great interest the recent article by Hoffmann-Vold et al (1), in which they report that serum levels of CCL21 were significantly higher in systemic sclerosis (SSc) patients than controls, and were elevated prior to pulmonary arterial hypertension (PAH) diagnosis. Moreover, concentrations of CCL21 were positively correlated with PAH development and occurrence of PAH-related events, which suggested that CCL21 has potential as a biomarker for SSc-related PAH risk prediction and disease progression. However, we have some concerns regarding the use of serum CCL21 levels as a biomarker for this condition.

First, in a large case–control association study of a cohort consisting of 1,031 European Caucasian SSc patients and 1,014 healthy controls, Coustet et al (2) showed that the rs2812378 polymorphism of CCL21 did not contribute to SSc susceptibility. Their results did not support implication of the CCL21 gene in the pathogenesis of SSc, although more single-nucleotide polymorphism (SNP) markers at CCL21 loci should be investigated before definitely ruling out association with SSc. It would be interesting to explore possible associations of functional SNPs with susceptibility/resistance to the development of SSc in different populations.

Second, studies have shown that CCL21 concentrations are also elevated in other rheumatic diseases, such as rheumatoid arthritis (RA) and systemic lupus erythematosus (3,4). Moreover, SSc sometimes occurs concurrently with other diseases, including RA. Therefore, it must be elucidated whether the SSc patients in Hoffman-Vold and colleagues' study concomitantly had other immune-related diseases and if so, whether the specificity and sensitivity of CCL21 could reach the standards for clinical application. In addition, serum levels of CCL21 would have to be measured both before and after treatment in patients with SSc-associated PAH to ascertain whether these levels are reduced after treatment.

Third, Qu et al (5) have reported that higher glucose levels and older age were each correlated with higher CCL21 expression in NOD mice, and CCL21 was highly expressed and increased in an age-dependent manner in NOD mice compared with normal controls. Although age and sex were taken into account in Hoffman-Vold et al's study, the patients' history of diabetes and alcohol intake should also be considered. In addition,

In conclusion, we welcome the ongoing discussion regarding these criteria, diagnostic approaches, and management strategies. We believe that patients with ANCA-associated ILD likely have AAV rather than IPAF based on the most recent draft AAV criteria. We also welcome ongoing collaborations and multicenter cohort studies to validate these criteria and determine the best treatment options.

The content herein is solely the responsibility of the authors and do not necessarily represent official views of the National Center for Advancing Translational Sciences or the National Institutes of Health. Supported by award UL1-TR000445 from the National Center for Advancing Translational Sciences, NIH, to Drs. Wilfong and Crofford. Dr. Wilfong's work was also supported by grant T32-AR-007304 from the National Institute of Arthritis and Musculoskeletal and Skin Diseases and grant T32-HL-087738 from the National Heart, Lung, and Blood Institute, NIH. Dr. Byram's work was supported by the Vasculitis Clinical Research Consortium and the Vasculitis Foundation. Dr. Crofford has received research support from EMD Serono, Boehringer Ingelheim, and Cumberland Pharmaceuticals unrelated to this work. No other disclosures relevant to this article were reported.

Erin M. Wilfong, MD, PhD
Vanderbilt University Medical Center Nashville, TN and University of California San Francisco
Kevin W. Bayram, MD
Leslie J. Crofford, MD
Vanderbilt University Medical Center Nashville, TN

1. Fischer A, Antoniou KM, Brown KK, Cadranel J, Corte TJ, du Bois RM, et al. An official European Respiratory Society/American Thoracic Society research statement: interstitial pneumonia with autoimmune features. Eur Respir J 2015;46:976–87.
2. Raghu G, Remy-Jardin M, Myers JL, Richeldi L, Ryerson CJ, Lederer DJ, et al. Diagnosis of idiopathic pulmonary fibrosis: an official ATS/ERS/JRS/ALAT clinical practice guideline. Am J Respir Crit Care Med 2018;198:e44–68.
3. Comarmond C, Crestani B, Tazi A, Hervier B, Adam-Marchand S, Nunes H, et al. Pulmonary fibrosis in antineutrophil cytoplasmic antibodies (ANCA)-associated vasculitis: a series of 49 patients and review of the literature. Medicine (Baltimore) 2014;93:340–9.
4. Robson JC, Grayson PC, Ponte C, Suppiah R, Craven A, Khalid S, et al. Draft classification criteria for the ANCA-associated vasculitides [abstract]. Ann Rheum Dis 2018;Suppl 2:60–1.
5. Mecoli CA, Christopher-Stine L. Management of interstitial lung disease in patients with myositis specific autoantibodies. Curr Rheumatol Rep 2018;20:27.
6. Oddis CV, Aggarwal R. Treatment in myositis. Nat Rev Rheumatol 2018;14:279–89.
7. Furst DE, Saag K, Fleischmann MR, Sherrer Y, Block JA, Schnitzer T, et al. Efficacy of tacrolimus in rheumatoid arthritis patients who have been treated unsuccessfully with methotrexate: a six-month, double-blind, randomized, dose-ranging study. Arthritis Rheum 2002;46:2020–8.

DOI 10.1002/art.40743

Questions regarding the value of CCL21 as a potential biomarker for pulmonary arterial hypertension in systemic sclerosis: comment on the article by Hoffmann-Vold et al

To the Editor:

We read with great interest the recent article by Hoffmann-Vold et al (1), in which they report that serum levels of CCL21 were significantly higher in systemic sclerosis (SSc) patients than controls, and were elevated prior to pulmonary arterial hypertension (PAH) diagnosis. Moreover, concentrations of CCL21 were positively correlated with PAH development and occurrence of PAH-related events, which suggested that CCL21 has potential as a biomarker for SSc-related PAH risk prediction and disease progression. However, we have some concerns regarding the use of serum CCL21 levels as a biomarker for this condition.

First, in a large case–control association study of a cohort consisting of 1,031 European Caucasian SSc patients and 1,014 healthy controls, Coustet et al (2) showed that the rs2812378 polymorphism of CCL21 did not contribute to SSc susceptibility. Their results did not support implication of the CCL21 gene in the pathogenesis of SSc, although more single-nucleotide polymorphism (SNP) markers at CCL21 loci should be investigated before definitely ruling out association with SSc. It would be interesting to explore possible associations of functional SNPs with susceptibility/resistance to the development of SSc in different populations.

Second, studies have shown that CCL21 concentrations are also elevated in other rheumatic diseases, such as rheumatoid arthritis (RA) and systemic lupus erythematosus (3,4). Moreover, SSc sometimes occurs concurrently with other diseases, including RA. Therefore, it must be elucidated whether the SSc patients in Hoffman-Vold and colleagues' study concomitantly had other immune-related diseases and if so, whether the specificity and sensitivity of CCL21 could reach the standards for clinical application. In addition, serum levels of CCL21 would have to be measured both before and after treatment in patients with SSc-associated PAH to ascertain whether these levels are reduced after treatment.

Third, Qu et al (5) have reported that higher glucose levels and older age were each correlated with higher CCL21 expression in NOD mice, and CCL21 was highly expressed and increased in an age-dependent manner in NOD mice compared with normal controls. Although age and sex were taken into account in Hoffman-Vold et al's study, the patients' history of diabetes and alcohol intake should also be considered. In addition,

serum CCL21 levels were compared between patients with diffuse cutaneous SSc and those with limited cutaneous SSc and were also classified as high (>0.4 ng/ml) or low, but whether there was a relationship between CCL21 level and SSc type was not addressed.

The precise role of CCL21 in SSc and the relationship between serum CCL21 levels and the severity of SSc-related PAH are still unclear and require further study. Although CCL21 might serve as a useful biomarker for SSc-related PAH, clinical trials with a larger sample size are needed to confirm this.

Ren-Peng Zhou, MD, PhD
Xin Wei, MD
Gang-Gang Ma, MD
Second Hospital of Anhui Medical University
Fei Zhu, MD
Fei-Hu Chen, MD, PhD
Anhui Medical University
Wei Hu, MD, PhD
Second Hospital of Anhui Medical University
Hefei, China

1. Hoffmann-Vold AM, Hesselstrand R, Fretheim H, Ueland T, Andreassen AK, Brunborg C, et al. CCL21 as a potential serum biomarker for pulmonary arterial hypertension in systemic sclerosis. Arthritis Rheumatol 2018;70:1644–53.
2. Coustet B, Dieude P, Wipft J, Avouac J, Hachulla E, Diot E, et al. Association study of 3 rheumatoid arthritis risk loci in systemic sclerosis in European Caucasian population. Clin Exp Rheumatol 2011;29 Suppl 65:S6–9.
3. Pickens SR, Chamberlain ND, Volin MV, Pope RM, Talarico NE, Mandelin AM II, et al. Role of the CCL21 and CCR7 pathways in rheumatoid arthritis angiogenesis. Arthritis Rheum 2012;64: 2471–81.
4. Odler B, Bikov A, Streizig J, Balogh C, Kiss E, Vincze K, et al. CCL21 and IP-10 as blood biomarkers for pulmonary involvement in systemic lupus erythematosus patients. Lupus 2017;26: 572–9.
5. Qu P, Ji RC, Kato S. Expression of CCL21 and 5′-nase on pancreatic lymphatics in nonobese diabetic mice. Pancreas 2005;31: 148–55.

DOI 10.1002/art.40819

Insufficient evidence to consider CCL21 a potential serum biomarker for pulmonary arterial hypertension in systemic sclerosis: comment on the article by Hoffmann-Vold et al

To the Editor:

Systemic sclerosis (SSc) is a chronic connective tissue disease (CTD) with an autoimmune pattern characterized by inflammation, fibrosis, and microcirculation changes leading to internal organ malfunctions. It is the most severe CTD, associated with high mortality risk. Available evidence suggests that immunity and genetic factors may correlate with the pathogenesis of this complex disease (1). However, the etiology of SSc and biomarkers for its diagnosis have not been clearly elucidated to date.

We read with interest the report by Hoffmann-Vold et al (2), who showed that serum levels of the chemokine CCL21 were elevated in SSc patients compared with healthy controls, and elevated prior to pulmonary arterial hypertension (PAH) diagnosis. PAH was more frequent in patients with high CCL21 levels than in those with low CCL21 levels. In addition, CCL21 was related to PAH and occurrence of PAH-associated events. Risk stratification at PAH diagnosis alone did not predict PAH-related events, but when combined with assessment of CCL21 levels, stratification was predictive. The authors concluded that CCL21 may be a promising marker for SSc-related PAH risk prediction and PAH progression. Interestingly, another CTD, systemic lupus erythematosus (SLE), sometimes occurs in combination with SSc, including in some patients with SSc-related PAH. Odler et al (3) reported that SLE patients with pulmonary involvement showed significant decreases in lung function parameters, such as forced vital capacity, total lung capacity, diffusing capacity for carbon monoxide (DLco), and diffusion of CO corrected for lung volume, as compared with SLE patients without pulmonary involvement. Serum levels of CCL21 were significantly higher in patients with pulmonary involvement than in patients without pulmonary manifestations, and were negatively correlated with DLco and diffusion of CO corrected for lung volume. Moreover, receiver operating characteristics analysis confirmed high sensitivity and specificity for distinguishing SLE patients with and those without pulmonary involvement according to concentrations of CCL21 (area under the curve 0.85, sensitivity 88.90%, specificity 75.00%) (3). Collectively, these findings suggested that CCL21 has potential as a biomarker for lung involvement, especially SSc-related PAH.

In our opinion, however, it is premature to come to this conclusion, for a variety of reasons. First, in a study of CCL21 gene polymorphism rs2812378 in a cohort of 1,031 SSc patients and 1,014 controls of European Caucasian origin (4), Coustet et al demonstrated that allelic and genotypic frequencies of this polymorphism were similar in SSc patients and controls. Subphenotype analyses, in particular analyses in subgroups with the diffuse cutaneous SSc subtype, specific autoantibodies, or fibrosing alveolitis, did not reveal any difference between SSc patients and controls. Indeed, this was an important study with a large sample size to potentially confirm the correlation between CCL21 and SSc, but the results did not show a significant relationship. Therefore, the implication of the CCL21 gene in the pathogenesis of SSc requires further investigation, for instance, by studying more single-nucleotide

polymorphism (SNP) markers in this gene or exploring possible functional SNPs to determine how the gene contributes to or inhibits SSc development, especially with PAH, in populations of different ethnicities.

Second, to determine whether serum CCL21 can be a biomarker for SSc or SSc-related PAH, preclinical disease, early disease, and longstanding disease should be major focuses of investigation, and serum levels of CCL21 should be evaluated at these different stages of disease. The results of studies based on this design could lead to a full understanding of the significance of this molecule. However, Hoffmann-Vold and colleagues' study was not performed using this design. Therefore, we suggest that the authors conduct additional studies in which CCL21 is evaluated at all stages of SSc in order to assess its potential as a marker for SSc-related PAH.

Third, CCL21 treatment can increase the expression of vascular endothelial growth factor (VEGF) in human lung cancer cells, through ERK1/2 and Akt phosphorylation (5). Interestingly, CCL21 suppression has been shown to correlate with inhibition of pulmonary vascular smooth muscle cell proliferation, prevention of thickening of the vessel walls and luminal occlusion of pulmonary arteries, and blocking of pulmonary fibrosis (6). Thus, whether CCL21 can regulate the VEGF signaling pathway and in turn play an important role in SSc-related PAH is still a topic for investigation.

In conclusion, current evidence is not sufficient to confirm CCL21 as a biomarker for SSc or SSc-related PAH. Further studies are needed to elucidate the above questions.

Supported by the National Natural Science Foundation of China (grant 81701606).

Wang-Dong Xu, MD
Southwest Medical University
Luzhou, China
Lin-Chong Su, MD
Affiliated Minda Hospital of Hubei Institute for Nationalities
Hubei, China
An-Fang Huang, MD
Affiliated Hospital of Southwest Medical University
Luzhou, China

1. Denton CP, Khanna D. Systemic sclerosis. Lancet 2017;390:1685–99.
2. Hoffmann-Vold AM, Hesselstrand R, Fretheim H, Ueland T, Andreassen AK, Brunborg C, et al. CCL21 as a potential serum biomarker for pulmonary arterial hypertension in systemic sclerosis. Arthritis Rheumatol 2018;70:1644–53.
3. Odler B, Bikov A, Streizig J, Balogh C, Kiss E, Vincze K, et al. CCL21 and IP-10 as blood biomarkers for pulmonary involvement in systemic lupus erythematosus patients. Lupus 2017;26:572–9.
4. Coustet B, Dieude P, Wipft J, Avouac J, Hachulla E, Diot E, et al. Association study of 3 rheumatoid arthritis risk loci in systemic sclerosis in European Caucasian population. Clin Exp Rheumatol 2011;29 Suppl 65:S6–9.
5. Sun L, Zhang Q, Li Y, Tang N, Qiu X. CCL21/CCR7 up-regulate vascular endothelial growth factor-D expression via ERK pathway in human non-small cell lung cancer cells. Int J Clin Exp Pathol 2015;8:15729–38.
6. Huang J, Maier C, Zhang Y, Soare A, Dees C, Beyer C, et al. Nintedanib inhibits macrophage activation and ameliorates vascular and fibrotic manifestations in the Fra2 mouse model of systemic sclerosis. Ann Rheum Dis 2017;76:1941–8.

DOI 10.1002/art.40816

Reply

To the Editor:

We thank Dr. Zhou and coworkers for their interest in our study on the role of CCL21 in PAH associated with SSc, and we wish to respond to the concerns they raise. Genome-wide association studies (GWAS) represent a major advance in biomedical discovery, revealing many robust associations with complex diseases. However, although polymorphisms associated with SSc have been identified, to date there are no known genetic loci for SSc-related PAH. Second, despite this success, GWAS have been met with considerable skepticism regarding their clinical applicability, mainly arising from unclear functional consequences. Until functional variants are known, caution should be applied in the interpretation of genetic risk for complex diseases, including SSc-related PAH, based on studies using tag SNPs.

We agree that CCL21 is not a specific biomarker for SSc, as we also pointed out in the article. Its association with atherosclerosis has also been shown previously, by our colleagues at Oslo University Hospital (1). In the recent study published in *Arthritis & Rheumatology*, we showed that CCL21 is specific for PAH within the SSc population and may help to distinguish SSc patients who are likely to develop PAH from those who are not. Patients with SSc overlap with another condition were excluded from the study cohort, and the frequency of diabetes mellitus was very low (<2.5%) and was therefore not adjusted for.

Last, we have since analyzed sera from a partly overlapping SSc cohort from the Oslo University Hospital in a different laboratory (University of California, Los Angeles) applying a different technique (Luminex). The correlation between the CCL21 measurements was good ($r > 0.5$, $P < 0.001$) and the data reproducible in the new population, indicating the robustness of CCL21 as a potential biomarker for PAH prediction

and prognostication. However, further clinical and mechanistic studies are warranted to elucidate the roles of the CCR7/CCL21 axis in SSc.

We also thank Xu and coworkers for their interest in the study and wish to address their concerns as well. We agree that the 2011 study by Coustet et al (2), which did not demonstrate any significant association between CCL21 SNP rs2812378 and SSc, is relevant when considering the potential role of CCL21 in disease pathogenesis. However, that study assessed only a single SNP, and it did not address associations with SSc-related PAH. Additionally, the functional consequences of polymorphisms identified by GWAS have generally been unclear. As noted above, we fully agree that CCL21 is not a specific biomarker for SSc but is also associated with several other conditions.

Recently, we have conducted further analyses of sera from 123 SSc patients without interstitial lung disease, segregated by mean pulmonary artery pressure (mPAP) assessed by right heart catheterization. We assessed 3 groups of SSc patients: 50 patients with normal mPAP (<20 mm Hg), 45 patients with borderline mPAP (20–24 mm Hg) (as an expression of preclinical or early PAH), and 28 patients with elevated mPAP (>25 mm Hg) (consistent with manifest PAH). These data were presented at the 2018 American College of Rheumatology Annual Meeting (3). Interestingly, we found significantly increased CCL21 levels in patients with elevated mPAP (mean ± SD 0.52 ± 0.25 ng/ml), patients with borderline mPAP (0.44 ± 0.33 ng/ml), and patients with normal mPAP (0.37 ± 0.31 ng/ml) compared with healthy controls (0.28 ± 0.14 ng/ml) (all $P < 0.0001$) (Figure 1), supporting the notion of an increasingly dysregulated immune pathway linked to the development of lung vascular damage in SSc.

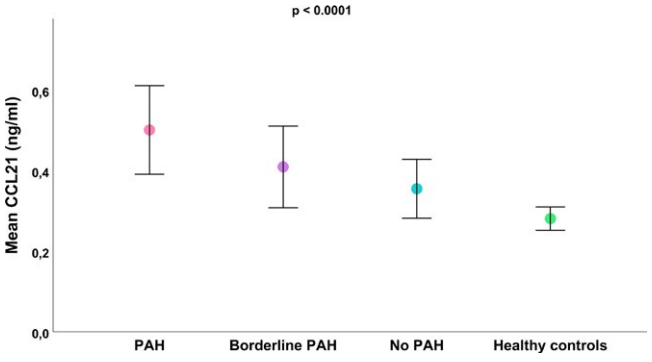

Figure 1. CCL21 levels in systemic sclerosis (SSc) patients according to right heart catheterization–verified mean pulmonary arterial pressure (mPAP). Mean ± SD CCL21 levels in 100 healthy controls, 50 SSc patients with normal mPAP (<20 mm Hg), 45 SSc patients with borderline mPAP (20–24 mm Hg) (as an expression of preclinical or early pulmonary artery hypertension [PAH]), and 28 SSc patients with elevated mPAP (>25 mm Hg) (consistent with manifest PAH) are shown. *P* value is for each SSc group versus controls.

Of note, previous work has demonstrated lymphatic vessel abnormalities in SSc. VEGF-C is a major growth factor for lymphatic vessels, and it has been shown that VEGF-C and its cognate receptor VEGF-R3 are down-regulated in PAH (4). CCL21 has a key role in inflammation leading to PAH and is expressed in lymphatic endothelial cells (5). Based on these observations we also assessed characteristics of VEGF-C and the correlation between VEGF-C and CCL21 in SSc-related PAH. We found that VEGF-C and CCL21 levels were negatively correlated in SSc patients with PAH, while they were positively correlated in patients without pulmonary hypertension and in healthy controls (data not shown). Based on this observation, we speculate that the increased levels of CCL21 in patients with SSc-related PAH may reflect lymphatic vessel abnormalities in this disorder. To further address this possibility, studies with mechanistic approaches are needed.

Anna-Maria Hoffmann-Vold, MD, PhD
Henriette Didriksen, MS
Øyvind Molberg, MD, PhD
Oslo University Hospital Rikshospitalet and University of Oslo
Oslo, Norway

1. Halvorsen B, Dahl TB, Smedbakken LM, Singh A, Michelsen AE, Skjelland M, et al. Increased levels of CCR7 ligands in carotid atherosclerosis: different effects in macrophages and smooth muscle cells. Cardiovasc Res 2014;102:148–56.
2. Coustet B, Dieude P, Wipft J, Avouac J, Hachulla E, Diot E, et al. Association study of 3 rheumatoid arthritis risk loci in systemic sclerosis in European Caucasian population. Clin Exp Rheumatol 2011;29 Suppl 65:S6–9.
3. Didriksen H, Fretheim H, Palchevskiy V, Andreassen AK, Garen T, Midtvedt O, et al. The lymphangiogenetic factors VEGF-C, CCL21, and Ang-2 are associated with pulmonary arterial hypertension in systemic sclerosis [abstract]. Arthritis Rheumatol 2018;70 Suppl 9. URL: https://acrabstracts.org/abstract/the-lymphangiogenetic-factors-vegf-c-ccl21-and-ang-2-are-associated-with-pulmonary-arterial-hypertension-in-systemic-sclerosis/.
4. Hwangbo C, Lee HW, Kang H, Ju H, Wiley DS, Papangeli I, et al. Modulation of endothelial bone morphogenetic protein receptor type 2 activity by vascular endothelial growth factor receptor 3 in pulmonary arterial hypertension. Circulation 2017;135:2288–98.
5. Larsen KO, Yndestad A, Sjaastad I, Løberg EM, Goverud IL, Halvorsen B, et al. Lack of CCR7 induces pulmonary hypertension involving perivascular leukocyte infiltration and inflammation. Am J Physiol Lung Cell Mol Physiol 2011;301:L50–9.

DOI 10.1002/art.40795

Adalimumab as treatment for venous thrombosis in Behçet's syndrome: comment on the article by Emmi et al

To the Editor:

We read with interest the article by Emmi et al (1) regarding the effect of adalimumab (ADA)–based treatment versus disease-modifying antirheumatic drug (DMARD) therapy for venous thrombosis in Behçet's syndrome (BS). Their findings add important data to help answer the difficult questions on the treatment of BS. However, there are some concerns.

The age at BS onset is usually in the third or fourth decade, and there is a male predominance in severe BS (2). However, after several years, disease burnout may occur, and if there is major organ/system involvement, it usually occurs within the first 5 years (3). In the article by Emmi and colleagues, the patient age at disease onset and disease duration were not described in detail. The mean ± SD age at treatment initiation was 42.8 ± 11.2 years for ADA-based regimens and 53.8 ± 32.1 years for DMARD therapy. The timing of venous thrombosis occurrence also should have been reported to better define the course of disease in the patients. Nineteen men and 16 women were treated with DMARDs alone, and 18 men and 17 women were treated with ADA-based regimens. There were no differences in clinical characteristics between the sexes, and the mean age of the 2 groups at ADA or DMARD initiation was quite high. Comparing the effectiveness of ADA and DMARDS in groups that are not homogenous in terms of disease manifestations may not reflect the real picture in a disease with an expanded clinical spectrum like BS.

In the intervention group that received ADA-based regimens, 8 of the 35 patients were also treated with DMARDs. We question whether the authors excluded these patients in their data analysis. If not, this could have confounded the assessment of the effectiveness of ADA.

Additionally, venous thrombosis can vary from superficial thrombosis to very severe superior/inferior vena cava thrombosis. Postthrombotic syndrome is a major problem in patients with BS (4). Emmi and colleagues' report includes no quantification of the severity of thrombosis. We believe this is an important consideration in treatment choices. Further, we do not understand why postthrombotic syndrome was not taken into account in the evaluation of vascular outcomes.

We thank Dr. Emmi et al for this important and useful study and look forward to clarification of some of these questions.

Dr. Karadag has received speaking fees and honoraria from AbbVie, Roche, and UCB Pharma (less than $10,000 each). No other disclosures relevant to this article were reported.

Bayram Farisogullari, MD
Alper Sari, MD
Sefika Nur Ayar, MD
Levent Kilic, MD
Berkan Armagan, MD
Omer Karadag, MD
Hacettepe University
Ankara, Turkey

1. Emmi G, Vitale A, Silvestri E, Boddi M, Becatti M, Fiorillo C, et al. Adalimumab-based treatment versus disease-modifying antirheumatic drugs for venous thrombosis in Behçet's syndrome: a retrospective study of seventy patients with vascular involvement. Arthritis Rheumatol 2018;70:1500–7.
2. Seyahi E. Behçet's disease: how to diagnose and treat vascular involvement. Best Pract Res Clin Rheumatol 2016;30:279–95.
3. Kural-Seyahi E, Fresko I, Seyahi N, Ozyazgan Y, Mat C, Hamuryudan V, et al. The long-term mortality and morbidity of Behçet syndrome: a 2-decade outcome survey of 387 patients followed at a dedicated center. Medicine (Baltimore) 2003;82:60–76.
4. Yazici H, Seyahi E, Hatemi G, Yazici Y. Behçet syndrome: a contemporary view. Nat Rev Rheumatol 2018;14:119.

DOI 10.1002/art.40794

Reply

To the Editor:

We thank Dr. Farisogullari and colleagues for their comments on our article reporting on how an ADA-based regimen is more effective and rapid than DMARD therapy in inducing resolution of venous thrombosis in patients with BS, allowing significant reduction of steroid exposure. Farisogullari et al suggested that our results may have been influenced by the heterogeneity between the ADA group and the DMARD group, specifically considering age (mean ± SD age at treatment initiation was 42.8 ± 11.2 years in the ADA group and 53.8 ± 32.1 years in the DMARD group). However, we are confident this difference had a minor impact on our results. In fact, the 2 groups were similar in terms of disease duration from the time of BS diagnosis to the time the considered venous events occurred and the subsequent start of ADA or DMARD treatment (mean ± SD 82.3 ± 17.3 months in the ADA group versus 89.6 ± 15.6 months in the DMARD group; $P = 0.753$). Thus, the results were obtained from groups that were homogeneous with similar disease duration.

Farisogullari and colleagues' major concern was that 8 patients within the ADA group were cotreated with DMARDs, suggesting that this cotreatment may have influenced the reported effectiveness of ADA. This concern has a clear pharmacologic rationale, considering the potential synergic action of the 2 treatments. However, in our cohort, stratified results confirmed the direct role of ADA in inducing vascular response. In fact, the number of patients with effective vascular control was 96.3% in the ADA-only group (26 of 27) and 100% among the 8 patients treated with ADA plus DMARDs. Furthermore, the mean ± SD time to achieve a vascular response was 3.6 ± 1.9 weeks in the ADA-only group and 3.9 ± 1.2 weeks in the ADA plus DMARD group ($P = 0.735$). As we reported in our article, the mean ± SD time to achieve a vascular response in the DMARDs-only group was 6.3 ± 1.2 weeks, which is significantly longer compared to patients treated with ADA only ($P = 0.0002$) and those treated with ADA plus DMARDs ($P = 0.0005$).

Overall, the results from our study provided strong evidence in support of the use of ADA in the treatment of venous thrombosis in typical sites. In the article, we detailed the reasons for limiting our analysis to acute and typical manifestations. However, as correctly emphasized by Farisogullari et al, the occurrence of venous thrombosis in atypical sites and the occurrence of postthrombotic syndrome represent major problems in patients with BS. Additional studies investigating the influence of tumor necrosis factor inhibitors in such manifestations would be of clinical help.

Giacomo Emmi, MD, PhD
Alessandra Bettiol, MD
University of Florence
Florence, Italy

ACR Announcements

AMERICAN COLLEGE OF RHEUMATOLOGY
2200 Lake Boulevard NE, Atlanta, Georgia 30319-5312
www.rheumatology.org

ACR Meetings

Annual Meetings
November 8–13, 2019, Atlanta
November 6–11, 2020, Washington, DC

State-of-the-Art Clinical Symposium
April 5–7, 2019, Chicago

For additional information, contact the ACR office.

Applications Invited for *Arthritis & Rheumatology* Editor-in-Chief (2020–2025 Term)

The American College of Rheumatology Committee on Journal Publications announces the search for the position of Editor, *Arthritis & Rheumatology*. The official term of the next *Arthritis & Rheumatology* editorship is July 1, 2020–June 30, 2025; however, some of the duties of the new Editor will begin during a transition period starting April 1, 2020. ACR members who are considering applying should submit a nonbinding letter of intent by May 1, 2019 to the Managing Editor, Jane Diamond, at jdiamond@rheumatology.org, and are also encouraged to contact the current Editor-in-Chief, Dr. Richard Bucala, to discuss details; initial contact should be made via e-mail to richard.bucala@yale.edu. Applications are due by June 21, 2019 and will be reviewed during the summer of 2019. Application materials are available on the ACR web site at https://www.rheumatology.org/Learning-Center/Publications-Communications/Journals/A-R.

Nominations for ACR Awards of Distinction and Masters Due May 15

The ACR has many Awards of Distinction, including the Presidential Gold Medal. Members who wish to nominate a colleague or mentor for an Award of Distinction must complete the online form at www.rheumatology.org. The nomination process includes a letter of nomination, 2 additional letters of recommendation, and a copy of the nominee's curriculum vitae. Recognition as a Master of the American College of Rheumatology is one of the highest honors the ACR bestows. The designation of Master is conferred on ACR members age 65 or older who have made outstanding contributions to the field of rheumatology through scholarly achievements and/or service to their patients, students, and the profession. To nominate someone for a Master designation, members must complete the online nomination form at www.rheumatology.org and include a letter of nomination, 2 supporting letters from voting members of the ACR, and the nominee's curriculum vitae. Nominees for ACR Master must have reached the age of 65 before October 1, 2019.

ACR Invites Nominations for Volunteer Positions

The ACR encourages all members to participate in forming policy and conducting activities by assuming positions of leadership in the organization. Positions are available in all areas of the work of the American College of Rheumatology and the Rheumatology Research Foundation. Please visit www.rheumatology.org for information about nominating yourself or a colleague for a volunteer position with the College. The deadline for volunteer nominations is June 1, 2019. Letters of recommendation are not required but are preferred.

New Division Name

Rheumatology is truly a people specialty: We often develop lifelong relationships with our patients as well as our colleagues. We increasingly recognize that providing the best rheumatologic care requires a team effort. The collegial nature of our specialty is reflected in the ACR's mission statement: To empower rheumatology professionals to excel in their specialty.

In keeping with this mission, we are pleased to announce that our health professionals' membership division is changing its name to Association of Rheumatology Professionals (ARP). This name change highlights the dedication of the ACR to serve the entire rheumatology community. It also reflects our broadened base of interprofessional members (administrators, advanced practice nurses, health educators, nurses, occupational therapists, pharmacists, physical therapists, physician assistants, research teams, and more).

The name is new, but our commitment and promise remain the same: We are here for you, so you can be there for your patients.